ZARIA CHAPTER

# 19TH CHEMCLASS CONFERENCE

OF THE CHEMICAL SOCIETY OF NIGERIA

ZARIA CHAPTER

DOI: 10.67867/ccj.2026.19ccc1-217

Tagged: ARTIFICIAL INTELLIGENCE IN CHEMICAL RESEARCH AND INNOVATION FOR A GREENER, SUSTAINABLE FUTURE

# BOOK OF PROCEEDINGS




**DATE:**
6TH TO 9TH JULY 2026

**VENUE:**
NUHU BAMALLI POLYTECHNIC, ZARIA, KADUNA STATE, NIGERIA

INNOVATE • COLLABORATE • SUSTAIN

CHEMISTRY FOR PEOPLE, PLANET & PROGRESS

Organized by:
CHEMICAL SOCIETY OF NIGERIA
ZARIA CHAPTER

csnzariachapter@gmail.com
www.csnzaria.org.ng

CSN Zaria Chapter
@csn_zaria_chapter

BUILDING A GREENER SUSTAINABLE FUTURE

**Copyright © 2026 by the Chemical Society of Nigeria (CSN), Zaria Chapter.**
**All rights reserved.**
**No part of this publication may be reproduced, transmitted or stored in any form without prior written permission from the publisher except for fair academic use with appropriate acknowledgement.**

**Published by**
**Chemical Society of Nigeria (CSN), Zaria Chapter**

## ABOUT THE CHEMICAL SOCIETY OF NIGERIA, ZARIA CHAPTER

The Zaria Chapter is one of the most active chapters of the Chemical Society of Nigeria, organizing annual scientific conferences, workshops, public lectures and capacity-building programmes that bring together researchers, educators, industrial practitioners and students from across Nigeria and beyond. Prior to the formation of Chemical Society of Nigeria, Zaria Chapter, a team of Chemists at Ahmadu Bello University started what was known as Zaria Chemical Society. This team was led by late Prof G.F.S. Harrison (Dr G.F.S. Harrison then) of the Department of Chemistry of the University, due to sheer interest to promote the teaching and practice of chemistry. Regular feature of the activities then, included periodic newsletter and monthly seminars among others. With time as the number of chemists and those in related fields increased in Zaria due to increase in number of tertiary institutions, it became imperative for Zaria to have its Chapter of the Society and one was formed. With this development, Kaduna State became the first State with two Chapters (Kaduna and Zaria Chapters).The Zaria Chapter was very vibrant and her activities were at its peak with the hosting of the 15th annual international conference of the CSN in September 1990. The LOC of the conference was chaired by Prof S. A. Thomas. After this successful outing, Chapter activities started nose diving until the mid 90s. With the support of Chief Executives like Dr Okonkwo, DG National Research Institute for Chemical Technology (NARICT) and late Dr Dashe, Provost of College of Leather Technology, CHELTEC (now Nigeria Institute of Leather Science Technology NILEST) who were chemists; Dr Femi Peters (now Prof) of Department of Chemistry, Ahmadu Bello University, spearheaded the move to resuscitate the Chapter. This effort was fruitful leading to the conduct of an election in 1996 for the Executive Council of the Chapter. Dr Femi Peters emerged as the Chairman of the Chapter. The visionary leadership of the Executive Council chaired by Dr Femi Peters with the robust support of the duo of Dr Okonkwo and late Dr Dashe again re- invigorated the Chapter, culminating in the phenomenal ChemClass conference in 1998 and afterwards the ChemClass Journal. The LOC for the maiden ChemClass conference which took place in the Conference Room of NEARLS was chaired by Dr V.O. Ajibola (now Prof) who also designed the logo of the ChemClass Journal.

Chapter Chairmen

The chronicle of the Chairmen of the Chapter is as below:

| | | | | | |
|---|---|---|---|---|---|
| 1 | Dr. G.F.S. Harrison | Inception - 1996 | 7 | Dr. A.D. Onu | 2015 - 2019 |
| 2 | Dr. F. Peters | 1996 - 2003 | 8 | Dr. S.E. Abechi | 2019 - 2023 |
| 3 | Dr. C.E. Gimba | 2004 - 2008 | 9 | Prof. K.I. Omoniyi | 2023 – 2025 |
| 4 | Dr. O.T. Audu | 2008 - 2010 | 10 | Mrs Judith U. Okoduwa | 2025 - Date |
| 5 | Dr. R.G. Ayo | 2010 - 2011 | | | |
| 6 | Prof. V.O. Ajibola | 2011 - 2014 | | | |

## PREFACE

The Editorial Committee is pleased to present the Book of Proceedings of the 19th ChemClass Conference, organized by the Chemical Society of Nigeria (CSN), Zaria Chapter. This volume comprises peer-reviewed papers presented at the conference, highlighting recent advances and innovations across the chemical sciences.

The conference provided a valuable platform for researchers, academics, industry professionals, and students to exchange knowledge, foster collaborations, and explore chemical solutions to contemporary scientific and societal challenges. The quality and diversity of the contributions reflect the growing strength of chemical research and innovation.

We sincerely appreciate the keynote speakers, authors, reviewers, sponsors, session chairpersons, and all participants whose dedication contributed to the success of the conference. We also acknowledge the commitment of the Local Organizing Committee, Scientific Committee, and Editorial Team in ensuring the successful organization of the conference and the publication of this proceedings.

We trust that this volume will serve as a useful reference for researchers, educators, students, and practitioners, while promoting continued excellence, collaboration, and innovation in the chemical sciences.

**Dr. Muhammad A. Lawal**
**For the Editorial Committee**

## MESSAGE FROM THE CHAIRMAN OF THE OCCASION

It is my pleasure to welcome participants to the 19th CHEMCLASS Conference.

The theme, *Artificial Intelligence in Chemical Research and Innovation for a Greener, Sustainable Future*, reflects the changing landscape of modern chemistry. Artificial intelligence has become an indispensable tool for accelerating research, solving complex scientific problems and improving industrial productivity.

As scientists, we have the responsibility to ensure that technological advancement contributes positively to sustainable development, environmental protection and improved quality of life.

I commend the Chemical Society of Nigeria, Zaria Chapter, for sustaining this annual scientific gathering and wish all participants fruitful deliberations.

**Prof. V. O. Ajibola**
**FCSN, FICCON, FEnv**
**Chairman of the Occasion**

## MESSAGE FROM THE CHAIRMAN, CHEMICAL SOCIETY OF NIGERIA, ZARIA CHAPTER

On behalf of the Executive Committee of the Chemical Society of Nigeria, Zaria Chapter, I warmly welcome all participants to the 19th CHEMCLASS Conference.

Over the years, CHEMCLASS has grown into a respected scientific platform that promotes excellence in research, innovation and professional development.

The conference theme underscores the growing importance of Artificial Intelligence in addressing global challenges through chemical research and technological innovation.

I encourage participants to actively engage in all scientific sessions and establish collaborations that extend beyond the conference.

I appreciate our keynote speaker, plenary speaker, invited speakers, reviewers, sponsors, exhibitors and participants for their invaluable contributions.

I wish everyone a rewarding conference.

**Mrs. Ugochi J. Okoduwa**
**Chairman,**
**Chemical Society of Nigeria (CSN), Zaria Chapter**

## MESSAGE FROM THE LOCAL ORGANIZING COMMITTEE

The Local Organizing Committee is delighted to host the 19th CHEMCLASS Conference at Nuhu Bamalli Polytechnic, Zaria. Planning for this conference involved several months of collaboration among members of the Society, partner institutions and volunteers.

We have designed a programme that combines keynote lectures, plenary presentations, technical sessions, poster exhibitions and networking opportunities.

We appreciate the Management of Nuhu Bamalli Polytechnic, our sponsors and every committee member for their unwavering support.

We hope your participation will be memorable.

**Dr. Zaharaddeen N. Garba**
**Chairman LOC**

## CONFERENCE THEME

Artificial Intelligence in Chemical Research and Innovation for a Greener, Sustainable Future

Artificial Intelligence has transformed scientific research through predictive modelling, automation, intelligent experimentation and advanced data analytics.

Its integration into chemistry has accelerated molecular design, catalyst discovery, reaction optimization, environmental monitoring, pharmaceutical development and materials engineering.

The conference explores these emerging opportunities while emphasizing sustainable industrial development, circular economy principles and environmental responsibility.

## SUB-THEMES

1. AI and Digital Innovation in Chemical Sciences
2. Green and Sustainable Chemistry
3. Renewable and Clean Energy Solutions
4. Smart and Advanced Materials for Sustainability
5. Petroleum and Fuel Chemistry
6. Medicinal Plant and Natural Product Chemistry
7. Chemical and Biological Interfaces in Life Sciences
8. Circular Economy and Industrial Transformation
9. Agricultural and Environmental Chemistry
10. Theoretical and Physical Chemistry

## KEYNOTE SPEAKER

**Prof. Baba El-Yakubu**

Department of Chemical Engineering

Ahmadu Bello University, Zaria

Keynote Address

Artificial Intelligence: Transforming Chemical Research and Sustainable Industrial Development

## PLENARY SPEAKER

**Prof. Chukwunonso Peter Okoli (MRSC, FNIA)**

Director,

Centre for Internationalization, Linkages, Advancement and Global Ranking

Alex Ekwueme Federal University, Ndufu-Alike

## CHIEF HOST

**Engr. Dr. Mohammed Kabir Abdullahi**

Rector,

Nuhu Bamalli Polytechnic

Zaria

**ACKNOWLEDGEMENTS**

The Organizing Committee expresses profound appreciation to:

The Zaria Chapter Executive Council

Nuhu Bamalli Polytechnic, Zaria

Ahmadu Bello University, Zaria

National Institute for Chemical Technology (NARICT), Zaria

Nigerian Institute of Leather and Science Technology (NILEST), Zaria

The Federal University of Education, Zaria

Our keynote and plenary speakers

Session chairpersons

Reviewers

Sponsors and exhibitors

Student volunteers

Authors and participants

Your generous support has contributed immensely to the success of the conference.

**Venue: Nuhu Bamalli Polytechnic, Zaria, Kaduna State, Nigeria**

## TABLE OF CONTENTS

ABOUT THE CHEMICAL SOCIETY OF NIGERIA, ZARIA CHAPTER....iii

PREFACE....iv

MESSAGE FROM THE CHAIRMAN OF THE OCCASION....v

MESSAGE FROM THE CHAIRMAN, CHEMICAL SOCIETY OF NIGERIA, ZARIA CHAPTER....vi

MESSAGE FROM THE LOCAL ORGANIZING COMMITTEE....vii

CONFERENCE THEME....viii

KEYNOTE SPEAKER....ix

PLENARY SPEAKER....ix

CHIEF HOST....ix

ACKNOWLEDGEMENTS....x

TABLE OF CONTENTS....xi

ARTIFICIAL INTELLIGENCE–ASSISTED CATALYST DESIGN FOR CARBON CAPTURE AND SUSTAINABLE CHEMICAL INNOVATION....2

Umar Amina Maigari[1*], Maigari Maryam Umar[2]....2

AI-GUIDED GREEN METRICS FOR SUSTAINABLE NATURAL PRODUCTS EXTRACTION AND CHARACTERIZATION: A CRITICAL REVIEW....13

Sulaiman Ayodeji Apampa[1*], Aisha Yusuf Lawal[1], David Adeniran Adedapo[2]....13

COMPUTATIONAL SIMULATION OF RESERVOIR FLUID THERMODYNAMICS FOR A METHANE–ETHANE MIXTURE USING THE PENG–ROBINSON EQUATION OF STATE (EOS)....22

P.J. Manga[1*], Muhammad Abubakar[2], S.A. Soloye[1], P.B. Teru[1], R.O. Amusat[1], Amina A. Dibal[1], S.N. Gin[3]....22

COMPARATIVE ANALYSIS OF CLASSICAL AND RELATIVISTIC MODELS FOR ALPHA-PARTICLE ENERGY LOSS IN SILICON, GERMANIUM, AND LEAD....35

P. B. Teru[1*], P.J. Manga[1], M. H. Imrana[2],Bringen Bukar[3], A. M. Gyobe[4,] N. B. Ndom[5,], R.O. Amusat[1], N M. D. Chagok[6]....35

MACHINE LEARNING-AUGMENTED BEER–LAMBERT LAW: UV-VIS AND FLUORESCENCE SPECTROPHOTOMETRIC ANALYSIS OF EOSIN B SOLVATOCHROMISM, SELF-DIMERIZATION, AND CONCENTRATION CALIBRATION IN PROTIC AND APROTIC SOLVENTS....45

Menkiti, N. D.....45

COMPARATIVE STUDY OF THE RANCIDITY OF SEALED AND UNSEALED VEGETABLE OIL SOLD WITHIN KATSINA METROPOLIS.....54

Tajudeen A. Jimoh*[1], Nathaniel Oladunni[2], Rukayya Muhammad Obansa[3], Nasiru Malan Musa[1], AbdulRazaq Tukur[1], Muhammad Muntasir Ruma[1], Segir Bala[1]....54

NUTRITIONAL COMPOSITION, PHYTOCHEMICAL PROFILE AND ANTIOXIDANT ACTIVITY OF DATE (*PHOENIX DACTYLIFERA*) AND CUCUMBER (*CUCUMIS SATIVUS L.*) FRUITS....61

Abubakar Fatima Usman*, Abdullahi Sahal, Musa Abbas Hayatuddeen, Jamila Abbas Ibrahim, Musa Mustapha....61

SYNTHESIS, CHARACTERIZATION AND ANTIMICROBIAL ACTIVITY OF Fe (III) COMPLEX DERIVED FROM QUECERTIN-LEUCIENE SCHIFF BASE....66

Safiya Abdulsalam[1], Sa'adatu Auwal Hamza[1*], Madina Imam[1], Salisu Abubakar[1], Nuruddeen Muhammad Lawal[2]....66

SYNTHESIS, CHARACTERIZATION ELUCIDATION AND ANTIMICROBIAL EVALUATION OF COBALT(II) COMPLEX OF A SCHIFFF BASE DERIVED FROM O-VANILLIN AND 2-AMINO-6-METHYLBENZOTHIAZOLE....71

Safiya Abdulsalam[1], Sa'adatu Auwal Hamza[1*], Madina Imam[1], Salisu Abubakar[1], Nuruddeen Muhammad Lawal[2]....71

NUTRITIONAL, IMMUNOLOGICAL, AND GROWTH EFFECTS OF BLACK SOLDIER FLY LARVAE FRASS IN FISH: A SYSTEMATIC REVIEW AND META ANALYSIS....76

Alexander Okpokwu Ogabidu[1,2*], Abdullateef Yusuf[2], Mary Bernard[3], Jocthan Markus Gaya[3], Tukki Onghasom Hassan[3], Samuel Florence Anna[4], Lawrence Stephen[5], Jibrin Muhammad Yelwa[1] ....76

PHYTOCHEMICAL COMPOSITION AND IN VITRO ANTIOXIDANT ACTIVITY OF METHANOLIC LEAF EXTRACT OF *FICUS ABUTILIFOLIA*....95

Sani Iyal Naiya*, Rahmatu Abubakar Madaki, Dahiru Idris, Jamilat Ishaq Jumare, Ja'afar Muhammad Nasir....95

QUALITATIVE PHYTOCHEMICAL SCREENING AND ANTIOXIDANT ACTIVITY OF LEAVES, STEM BARK AND ROOT OF GUMBO LIMBO (*Bursera simaruba)* ....1

Abbas Lawal[1*], Abdullahi Sahal[1] and Samaila Audu Jovial[2]....1

ROOM TEMPERATURE SYNTHESIS OF Cu (II)-BASED METAL–ORGANIC FRAMEWORKS FROM TEREPHTHALIC AND FUMARIC ACID: CHARACTERIZATION AND ANTIMICROBIAL EVALUATION....10

Abdullahi Sahal[1*], Hasiya Mahmoud Umar[2], Fatima Suleiman Aliyu[1], Abbas Lawal[1], Tijjani Umar Kofarbai[3]....10

PROXIMATE AND HISTOLOGICAL RESPONSES OF COMMON CARP FINGERLINGS FED BLACK SOLDIER FLY LARVAE MEALS FROM FOOD WASTES ....17

Alexander Okpokwu Ogabidu[1 2 *], Ibrahim Sham'un Eshi[2], Tukki Onghasom Hassan[1], Mary Bernard[1], Lawrence Stephen[1], Jocthan Markus Gaya[1], Abdulrahman Mohammed[1], Samuel Florence Anna[1], Elvanus Ewaram Magaji[1], Jafaru Adamu Idris[3], Comfort Salifu[2]....17

PHYTOCHEMICAL SCREENING, PROXIMATE COMPOSITION AND ELEMENTAL ANALYSIS OF *CRINUM JAGUS* (RIVER LILY) BULB ....29

Fatima Muhammad Balarabe*, Lawal Salamatu Muazu, Musa Nazifi Tanimu, Abdulmalik Muhammad, Muhammad Nazifi, Abba Malambilyamin Umar ....29

A CRITICAL INVESTIGATION OF ORGANIC POLLUTANTS IN WATER FROM LAMINGA DAM IN JOS, PLATEAU STATE, NIGERIA ....36

Gosomji, Andrew Dewan*; Ibejekwe, Sunday John and Gambol, Nanbol Ndam....36

TOPOLOGICAL INVESTIGATION OF ENERGY SPECTRA, THERMODYNAMICS, AND MAGNETIC RESPONSE IN MOLECULAR SYSTEMS WITH THE MODIFIED TIETZ–WEI POTENTIAL ....44

Amusat, R. O.[1*], Manga1, P. J.[1], Ocheni, A.U.U.[1], Aliyu, A.[1], Sonloye, A. S.[1], Salau, R.[2], ....44

VALORIZATION OF UNDERUTILIZED HIBISCUS SABDARIFFA SEEDS: DEVELOPMENT OF A BIODEGRADABLE FAT LIQUOR FOR ECO-FRIENDLY LEATHER PROCESSING ..... 64

Abubakar Sadiq Bello[1*], Sodiq Pelumi Bakare[1], Ibrahim Gidado[2], Sha'aban Sallau[1] ..... 64

LEVELS OF SELECTED HEAVY METALS IN SOIL SAMPLES AT AUTOMOBILE MECHANIC WORKSHOPS IN OKENE METROPOLIS, NIGERIA ..... 74

Omeiza, Folorunsho Samuel[1*], Lawal, John .Augustine[2], Paul Idoko[1], Okpanachi, Clifford[3] ..... 74

ASSESSMENT OF HEAVY METAL CONCENTRATIONS IN WELL WATER COLLECTED FROM DIFFERENT LOCATIONS WITHIN A MINING SITE IN AJAOKUTA, KOGI STATE, NIGERIA ..... 81

Omeiza, Folorunsho Samuel[1*], Lawal, John .Augustine[2], Paul Idoko[1], Okpanachi, Clifford[3] ..... 81

SOURCES AND FATE OF MICROPLASTICS IN AGRICULTURAL SOILS, A MINI REVIEW ..... 88

Muhammad Abubakar Lawal[1*] and Umar Lawal Abubakar[2] ..... 88

STRUCTURE–PROPERTY RELATIONSHIPS IN PERMANGANATE-MODIFIED CASSAVA PEEL/POLYPROPYLENE COMPOSITES: EFFECTS ON MECHANICAL, VISCOELASTIC DAMPING AND HYGROSCOPIC BEHAVIOUR ..... 97

Okpanachi Baba Clifford[1*], Ameh Ekwu Mark[2], Are Comfort[2], Dauda Joseph Abiodun[2] Idowu Olufunke Lovette[2] , Agada Favour Ugbedeojo[2] ..... 97

CUBE EFFECTS AND FACTOR INTERACTIONS ON ALUMINIUM CORROSION INHIBITION USING BANANA LEAF EXTRACT: INSIGHTS FROM RSM AND GRAVIMETRIC ANALYSIS ..... 109

Okpanachi Baba Clifford[1*], Ameh Ekwu Mark[2], Are Comfort Temitope[2], Dauda Joseph Abiodun[2], Idowu Olufunke Lovette[2], Ejukwa Emmanuel[2] ..... 109

RADIOLOGICAL ASSESSMENT OF SOIL IN MINING COMMUNITIES: A CASE STUDY IN NASARAWA EGGON, NIGERIA ..... 119

Lubis Sati*; Ogori Boniface Otokpa; Bakji Gomerep And Dakup Nenbunka Dunshik ..... 119

SYNTHESIS AND CHARACTERIZATION OF GREEN THERMOPLASTIC COMPOSITES FILMS REINFORCED WITH JUTE FIBER ..... 129

Gumel, B.U.[1], Gumel S.M.[2], Umar,A.[3], Auwal A.S.[2], Isah R.A.[4], Garba, Z.N[5*] ..... 129

OPTIMIZATION OF ADSORPTION CONDITIONS USING CENTRAL COMPOSITE DESIGN FOR THE REMOVAL OF CARBOFURAN BY ACTIVATED CARBON FROM *ACACIA SENEGAL (L.)* WILLD PODS ..... 141

Zaharaddeen N. Garba*, Muhammad M. Kamil ..... 141

BOTTOM-UP SYNTHESIS FOR INTERCONNECTS ..... 149

S.M.J Zubairu*[1], S.O. Idris[2], C.E. Gimba[2], A. Uzairu[2] and B.R. Horrocks[3] ..... 149

INTEGRATED GEOCHEMICAL AND GEOPHYSICAL METHODS OF INVESTIGATING HEAVY METAL POLLUTION OF GROUNDWATER IN UPPER AND MIDDLE AQUIFERS IN DOGONGARAGE AREA OF MAIDUGURI, NORTHEASTERN NIGERIA. ..... 156

S.A. Sonloye[1*], A.U.U. Ocheni[1], A. Aliyu[1], L.E. Agada[2], R.O. Amusat[1], A. Usman[2], A.S. Oniku[3] ..... 156

ASSESSMENT OF SELECTED HEAVY METALS IN CIGARETTE BRANDS TO INDEX THE CARCINOGENIC AND NON-CARCINOGENIC LEVELS IN FAGGE, KANO, NIGERIA ..... 169

Nwoye, E.E.*, Adeyemi, A, E. ..... 169

*SUSTAINABLE SLUDGE MANAGEMENT FOR AGRICULTURAL REUSE: A CONCISE REVIEW OF STABILIZATION TECHNOLOGIES, CHALLENGES, AND RESEARCH PRIORITIES* ..... 173

Muhammad A. Lawal ..... 173

REMOVAL OF HEAVY METALS IN SPENT SYNTHETIC-BASED DRILLING MUD USING NANO ZERO-VALENT IRON (nZVI) ..... 180

Obinduka, F.O[1*], Uchechukwu, T.O[2], Effiong, E[3] ..... 180

GEOPHYSICAL ASSESSMENT OF GEOTHERMAL ENERGY POTENTIAL IN THE SOKOTO BASIN, NORTHWESTERN NIGERIA ..... 186

Aliyu, A[1*]., Sonloye, A. S[1]., Amusat, R. O[1]., Hassan, M[1]., Joseph, A, A[2]., Usman, A[3]., Aliyu, M. L[4]., Balarabe, B[5]., Umar, M[5] ..... 186

**HEALTH RISK ASSESSMENT AND MOSQUITO REPELLENT FORMULATION FROM *TRIUMFETTA RHOMBOIDEA*: SENSORY EVALUATION AND GC-MS ANALYSIS** ..... 194

Abdullahi Sahal[1*], Opeyemi John[1], Fatima Idris Adam[1], Abdulazeez Abubakar Umar[1], Ishaq Shehu[1], Umar Sa'ad[1] ..... 194

SYNTHESIS AND CHARCTERIZATION OF (2E)-1-(4-BROMOPHENYL)-3-(4-NITROPHENYL)PROP-2-EN-1-ONE CHALCONE ..... 200

Aliyu Ahmad Aliyu[1*], AbdulRazaq Tukur[2], Haruna Aliyu Agum[3]Muhammad Ali Uthman[4] and Ummusalma Muhammad Salisu[5] ..... 200

MODIFIED SYNTHESIS AND CHARACTERIZATION OF GRAPHENE OXIDE ..... 205

Sha'aban Sallau[1*], Muhammad Babati[1], Abbas Abubakar[2], Joy Yohana Ishaya[1] , Babagana Shuaibu[3] ..... 205

Keywords: Nanomaterials, hybridization, graphene oxide, 2-D materials ..... 205

1. Introduction ..... 205

GREEN SYNTHESIS OF GRASSHOPPER CHITOSAN USING WOOD ASH AQUEOUS EXTRACT AS AN ECO-FRIENDLY ALTERNATIVE MEDIUM FOR ALKALINE DEACETYLATION OF CHITIN ..... 211

Bashir, U. G.[1*], Sani, M. G.[2], Umar A.[3], Auwal A.S.[4] , Zaharddeen N.[5] and Bawa A.A.[5] ..... 211

# AI AND DIGITAL INNOVATION IN CHEMICAL SCIENCES

# ARTIFICIAL INTELLIGENCE–ASSISTED CATALYST DESIGN FOR CARBON CAPTURE AND SUSTAINABLE CHEMICAL INNOVATION

**Umar Amina Maigari[1*], Maigari Maryam Umar[2]**

*[1]Department of Chemistry Education, Federal College of Education, Gombe, Nigeria.*
*[2]Integrated Science Department, Federal College of Education, Gombe, Nigeria.*
*Corresponding Author: aminamaigari@fcetgombe.edu.ng*

**Abstract**

The escalating concentration of atmospheric carbon dioxide ($CO_2$) represents one of the most pressing environmental challenges of the contemporary era. Catalytic materials occupy a central position in carbon capture and utilization (CCU) processes—enabling, for example, the selective hydrogenation of $CO_2$ to methanol over $Cu/ZnO/Al_2O_3$ catalysts or the electrochemical reduction of $CO_2$ to formate over metal-organic framework (MOF)-derived electrodes. However, conventional catalyst development relies predominantly on labor-intensive, empirical trial-and-error methodologies that often span years or decades from discovery to deployment. This review presents a conceptual framework for integrating artificial intelligence (AI) and machine learning (ML) techniques into catalyst design specifically targeting carbon capture applications. Machine learning algorithms are proposed to predict catalytic activity, $CO_2$ adsorption capacity, material stability, and reaction mechanisms using physicochemical descriptors drawn from existing experimental and computational datasets. The framework demonstrates how AI-driven high-throughput screening can dramatically reduce development timelines, enhance material performance metrics, and support sustainable chemical innovation aligned with circular economy principles. The study further examines the implications of AI-assisted catalysis for green chemistry advancement, industrial transformation toward carbon neutrality, and meaningful climate change mitigation. By bridging AI methodologies with inorganic catalyst development, this work underscores the transformative potential of digital technologies to reshape chemical research paradigms and contribute to a greener, more sustainable future.

**Keywords:** Artificial intelligence; catalyst design; carbon capture and utilization; machine learning; high-throughput screening

## 1. Introduction

Climate change driven principally by anthropogenic carbon dioxide emissions remains one of the most formidable global challenges of the twenty-first century. Industrial activities, energy production, transportation, and agricultural practices continue to release vast quantities of $CO_2$ into the atmosphere, contributing to rising global mean temperatures, ocean acidification, more frequent extreme weather events, and irreversible ecosystem degradation [1]. According to the Intergovernmental Panel on Climate Change (IPCC), atmospheric $CO_2$ concentrations have now surpassed 420 parts per million—a level unprecedented in at least the past three million years of Earth's geological history [2]. In response, carbon capture and utilization (CCU) technologies have emerged as critical strategic interventions: they reduce net greenhouse gas emissions while converting waste $CO_2$ into value-added products such as methanol, formic acid, synthetic fuels, and polymers [3].

Catalysts are the enabling components at the heart of virtually every CCU process. Reactions such as $CO_2$ hydrogenation to methanol, the reverse water-gas shift reaction, dry reforming of methane, and electrochemical $CO_2$ reduction all depend on catalytic materials that can activate the thermodynamically

stable $CO_2$ molecule ($\Delta G°f = -394$ kJ/mol) and direct reaction pathways toward desired products [4]. Inorganic catalysts—including transition metal oxides, supported metal nanoparticles, layered double hydroxides (LDHs), metal-organic frameworks (MOFs), zeolites, and hybrid organic-inorganic composites—have demonstrated considerable promise owing to their tunable electronic structures, well-defined active sites, high thermal stability, and synthetic versatility [5]. Despite this promise, traditional catalyst development remains largely Edisonian: hypothesis generation, synthesis, characterization, testing, and iterative modification in a cycle that typically requires 10–15 years and $10–100 million to bring a new material from laboratory discovery to commercial deployment [6].

Artificial intelligence has recently emerged as a transformative computational tool capable of restructuring the catalyst discovery pipeline. Machine learning models can systematically analyze large experimental and computational datasets, uncover hidden structure–property relationships, and predict material properties with accuracies approaching those of density functional theory (DFT) calculations at a fraction of the computational cost [7]. Applied to CCU catalysis, AI offers accelerated discovery, simultaneous multi-objective optimization, and the ability to explore the immense chemical space of potential catalytic materials—estimated to exceed $10^{64}$ possible inorganic compounds [8].

This paper presents a conceptual review and framework for AI-assisted catalyst design targeting CCU applications. The primary goal is to synthesize and critically evaluate existing AI/ML approaches as applied to $CO_2$ capture catalysts, present an integrated four-stage discovery framework that organizes these approaches coherently, and identify priority directions for future research. By clarifying this scope at the outset, the paper addresses the distinction between proposing a novel methodological contribution and reviewing the state of the art: this work does both—it reviews existing techniques and proposes their integration into a structured, CCU-focused workflow not previously presented in this form. The study contributes to scholarly discussion on the role of digital technologies in advancing green chemistry and developing climate-focused technological solutions.

## 2. Literature Review

### Carbon Capture and Utilization Technologies

Carbon capture and utilization encompasses a diverse portfolio of technological approaches designed to separate $CO_2$ from emission point sources or directly from ambient air (direct air capture, DAC) and subsequently convert the captured carbon into valuable products [9]. Throughout this paper, the preferred acronym CCU is used consistently, as material storage (the 'S' in CCUS) falls outside the scope of this review. CCU technologies can be broadly categorized into three primary pathways: (1) thermochemical conversion, including $CO_2$ hydrogenation to methanol or synthetic natural gas, reverse water-gas shift reactions, and dry reforming of methane; (2) electrochemical reduction to fuels and commodity chemicals such as formate, CO, and ethylene; and (3) biological conversion via photosynthetic microorganisms or microbial fermentation [10]. Each pathway requires specifically engineered catalytic materials capable of activating $CO_2$ and selectively directing reaction pathways toward desired products while minimizing energy inputs and undesirable byproduct formation [11]. Developing catalysts that perform effectively under realistic industrial conditions—fluctuating $CO_2$ partial pressures, the presence of impurities such as $SO_2$ and water, and the need for thousands of hours of operational stability—represents a central challenge that AI-assisted design is well positioned to address.

## Conventional Catalyst Development: Historical Perspectives and Limitations

Traditional catalyst development has historically followed a sequential paradigm of hypothesis generation, synthesis, characterization, testing, and iterative optimization—a cycle that typically requires 10–15 years and substantial financial investment to transition a new catalytic material from laboratory discovery to commercial deployment [12]. High-throughput experimental techniques introduced during the 1990s and 2000s partially addressed these limitations by enabling parallel synthesis and screening of hundreds or thousands of candidate materials. Yet such approaches remain constrained by the astronomical size of chemical space and the practical realities of laboratory infrastructure, reagent availability, and analytical throughput [13]. For CCU-specific catalysts, these challenges are compounded by the demanding requirement that materials exhibit simultaneously high $CO_2$ adsorption affinity, selectivity for a specific conversion product, resistance to sintering and poisoning under reaction conditions, and economic scalability—a multi-objective design problem that resists intuition-guided experimentation.

## Machine Learning Fundamentals as Applied to $CO_2$ Capture Catalysis

Machine learning (ML), a subdiscipline of artificial intelligence, encompasses algorithms capable of identifying patterns within data and making predictions without explicit task-specific programming [14]. Three classes of ML algorithms have demonstrated particular relevance to $CO_2$ capture catalyst development:

*Supervised learning* algorithms—including linear regression, random forests, support vector machines (SVM), and deep neural networks—are trained on labeled datasets linking input features (e.g., elemental descriptors, $CO_2$ adsorption enthalpies, synthesis conditions) to output targets (e.g., $CO_2$ uptake capacity, turnover frequency, product selectivity). For example, random forest models have been applied to predict $CO_2$ adsorption capacities across families of amine-functionalized MOFs, providing rapid screening guidance before experimental synthesis [15].

*Unsupervised learning* techniques, such as principal component analysis (PCA) and autoencoders, identify inherent groupings within unlabeled catalyst data. Applied to CCU research, these methods can cluster zeolite structures by their $CO_2$ binding-site topology or detect outliers in adsorption datasets, supporting both materials classification and quality-control in data curation [16].

*Reinforcement learning* trains algorithms to make sequential decisions by receiving feedback from a simulated or real environment, offering particular promise for autonomous closed-loop optimization of $CO_2$ conversion catalysts in robotic experimentation platforms [17].

## AI Applications in Catalysis: Current State of the Art

Recent years have witnessed notable AI applications across the CCU catalysis workflow. Ulissi and colleagues employed machine learning to exhaustively search bimetallic surface facets for $CO_2$ electroreduction, identifying previously unreported active-site motifs with predicted activities exceeding conventional copper catalysts [18]. Nørskov and collaborators developed descriptor-based approaches combined with ML to predict activity trends across transition metal surfaces for methanol synthesis from $CO_2$ , exemplifying rational catalyst design grounded in the d-band model [19]. In the domain of homogeneous catalysis, Doyle and coworkers demonstrated ML prediction of reaction yields and selectivity using high-throughput experimentation data—an approach directly applicable to $CO_2$

carboxylation reactions [20]. More recently, Zhong and colleagues reported ML-accelerated discovery of copper-based $CO_2$ electrocatalysts, demonstrating that active learning could identify high-performing catalysts with far fewer experimental iterations than conventional screening [29].

## 3. A Conceptual Framework for AI-Assisted Catalyst Design

Overview of the Four-Stage Framework

The proposed conceptual framework for AI-assisted CCU catalyst design consists of four interconnected and iterative stages, illustrated schematically in Figure 1. The framework is not presented as a new computational methodology but as a structured organizational blueprint that integrates existing AI/ML techniques into a coherent, CCU-focused workflow.

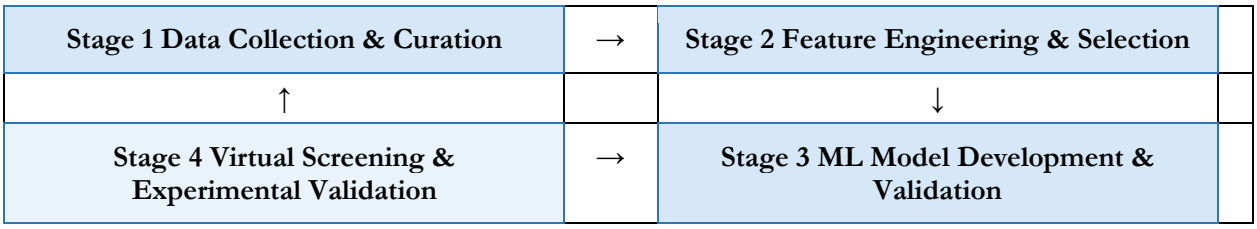



Figure 1: Four-stage iterative framework for AI-assisted $CO_2$ capture catalyst design.

Stage 1: Data Collection and Curation

Comprehensive experimental and computational datasets related to catalyst composition, synthesis parameters, crystallographic structure, surface properties, $CO_2$ adsorption capacity, reaction kinetics, and stability metrics are systematically compiled from peer-reviewed literature, open-access repositories (e.g., Materials Project, OQMD, NREL Materials Database), and in-house experimental campaigns [21]. For CCU applications specifically, relevant data include $CO_2$ temperature-programmed desorption ($CO_2$-TPD) profiles characterizing surface basicity, breakthrough adsorption curves under simulated flue-gas conditions, and catalytic performance data for $CO_2$ hydrogenation or electroreduction reactions. Critical considerations include data quality assessment, handling of missing values, standardization of reporting units across laboratories, and documentation of metadata essential for reproducibility.

Stage 2: Feature Engineering and Selection

Physicochemical descriptors capturing essential information about catalyst structure and composition are identified as input variables for machine learning models. For $CO_2$ capture and conversion applications, particularly relevant descriptors include:

Elemental properties: electronegativity, atomic radius, ionization potential, electron affinity, and position in the periodic table—each of which influences the $CO_2$ binding energy on surface active sites;

Electronic descriptors: d-band center position, density of states at the Fermi level, and work function, which govern $CO_2$ activation barriers on metal surfaces;

Structural features: coordination number, bond lengths, crystal symmetry, surface termination, and defect density, which determine active-site geometry and accessibility;

Textural properties: BET surface area, pore volume, and pore size distribution, which are particularly important for $CO_2$ adsorption capacity in porous materials such as MOFs and zeolites;

Synthesis conditions: calcination temperature, precursor identity, and reduction protocol, which affect phase purity, particle size, and surface basicity of mixed oxide catalysts.

Dimensionality reduction techniques, including PCA and autoencoders, may be employed to identify the most informative descriptor combinations while minimizing redundancy and multicollinearity [22].

Stage 3: Machine Learning Model Development and Validation

Supervised learning algorithms are implemented to establish quantitative structure–property relationships (QSPR) and predict CCU catalyst performance indicators including $CO_2$ adsorption capacity (mol/g), adsorption enthalpy (kJ/mol), turnover frequency ($s^{-1}$), selectivity toward desired products (%), and stability under operating conditions (deactivation rate). Ensemble methods such as random forests and gradient boosting often provide robust performance on heterogeneous catalyst datasets; deep neural networks offer higher accuracy for large datasets but require careful regularization [23]. Rigorous validation employing k-fold cross-validation and independent test sets ensures reliable performance estimation and guards against overfitting.

Stage 4: Virtual Screening and Experimental Validation

AI-generated predictions are employed to rank candidate catalyst materials, enabling rapid identification of high-probability candidates for targeted experimental synthesis and characterization. Active learning strategies close the loop: initial model predictions guide experimentation, and the resulting experimental data are incorporated to iteratively refine model accuracy [24]. This closed-loop design is depicted by the upward arrow from Stage 4 back to Stage 1 in Figure 1, emphasizing that the framework is iterative rather than linear.

Role of AI in Accelerating the CCU Catalyst Development Cycle

Artificial intelligence fundamentally transforms traditional catalyst development by enabling high-throughput virtual screening across vast chemical spaces—potentially spanning millions of hypothetical compositions and structures—before committing resources to synthesis [25]. This effectively shifts the discovery bottleneck from empirical experimentation to computational screening. For CCU applications where urgent deployment is needed to meet the Paris Agreement targets, this acceleration is especially critical. Figure 2 and Table 1 compare the traditional and AI-assisted discovery workflows across key dimensions relevant to $CO_2$ capture research.

Table 1: Comparison of traditional and AI-assisted catalyst discovery workflows for CCU applications

| Aspect | Traditional Trial-and-Error | AI-Assisted Discovery |
|---|---|---|
| Discovery timeline | 10–15 years from lab to deployment | Potentially months via virtual screening |
| Chemical space explored | Hundreds to low thousands of compounds | Millions of hypothetical compositions screened computationally |

| | | |
|---|---|---|
| $CO_2$ catalyst focus | Guided by intuition; biased toward known families | Systematic; uncovers unexpected MOF, LDH, or bimetallic candidates |
| Cost estimate | $10–100 million per new catalyst system | 30–50% reduction via prioritised synthesis |
| Negative-result use | Largely discarded; not published | Incorporated in training data to improve predictions |
| Interpretability | Mechanism understood via classical kinetics and DFT | Requires explainable AI (SHAP, LIME) for insight generation |

## 4. Discussion: The Impact and Future of AI in Carbon Capture Catalysis

Advantages of AI-Assisted Catalysis for $CO_2$ Capture: A Critical Assessment

The integration of AI into CCU catalyst development workflows offers several scientifically and economically significant benefits directly relevant to carbon capture research:

*Accelerated Discovery Timelines*: Machine learning models can evaluate thousands of material combinations within minutes or hours, compared to months or years required for conventional iterative experimentation. For CCU specifically, this acceleration addresses the urgent timeline imposed by climate targets: IPCC scenarios requiring net-zero emissions by 2050 leave little room for decade-long catalyst development cycles [26].

*Substantial Cost Reduction*: Virtual screening minimizes laboratory expenses associated with precursor materials, analytical characterization, and researcher time. Preliminary estimates suggest AI-guided discovery may reduce catalyst development costs by 30–50% compared to traditional approaches—savings that could meaningfully lower the economic barrier to deploying CCU technology at industrial scale [27].

*Enhanced Multi-Objective Optimization:* AI algorithms excel at identifying subtle, non-linear structure–property relationships that often escape human intuition. By simultaneously optimizing $CO_2$ adsorption affinity, product selectivity, thermal stability, and cost of constituent elements, ML models can identify catalyst compositions positioned in regions of chemical space that satisfy multiple competing requirements—a task uniquely challenging for intuition-guided design [28].

*Systematic Chemical Space Exploration*: Unlike empirical discovery, which tends to cluster around known successful materials (e.g., Cu-based $CO_2$ hydrogenation catalysts), AI-driven approaches systematically traverse chemical space. This enables identification of promising candidates in unexpected compositional regions—for instance, unconventional bimetallic or high-entropy oxide surfaces for $CO_2$ electroreduction [18].

*Integration of Multi-Source Data:* Machine learning provides a mathematical framework for integrating heterogeneous data types—experimental $CO_2$ adsorption isotherms, DFT-computed binding energies, spectroscopic fingerprints, and crystallographic information—into unified predictive models that leverage complementary information sources for CCU catalyst screening [29].

Implications for Carbon Capture Technologies

AI-assisted catalyst design holds transformative potential for enhancing the efficiency and economic viability of CCU processes. Optimized catalysts with improved $CO_2$ adsorption capacity, enhanced selectivity toward desired products, and superior long-term stability can facilitate lower-energy capture and conversion pathways, addressing fundamental economic barriers to CCU deployment [30]. For example, ML-guided discovery of improved low-temperature $CO_2$ hydrogenation catalysts could enable methanol production from renewable hydrogen at reduced pressure and temperature, substantially improving process economics. Similarly, AI-driven optimization of amine-functionalized sorbents for direct air capture could identify functional group combinations that maximize $CO_2$ uptake while minimizing regeneration energy penalties—a critical bottleneck currently limiting DAC deployment.

Furthermore, AI approaches can accelerate development of integrated capture-and-conversion systems wherein a single catalytic material simultaneously captures dilute $CO_2$ from emission streams and converts it to products without intermediate purification—a 'one-pot' approach offering significant process intensification benefits and reducing the capital cost of CCU plant infrastructure [31].

Contribution to Green Chemistry and Industrial Sustainability

By reducing experimental redundancy, minimizing material waste, and promoting targeted synthesis, AI-assisted catalysis directly supports the twelve principles of green chemistry articulated by Anastas and Warner [32]. Specific contributions include:

- Waste Prevention: Virtual screening eliminates synthesis and testing of thousands of low-performing materials that would otherwise generate chemical waste, directly aligning with Green Chemistry Principle 1;
- Energy Efficiency: Optimized CCU catalysts enable lower-temperature, lower-pressure reaction pathways, reducing process energy requirements and the associated carbon footprint of chemical manufacturing;
- Reduced Auxiliary Use: AI-guided design minimizes the need for protective groups or temporary modifications by identifying inherently selective catalysts for $CO_2$ activation;
- Real-time Analysis: Integration with automated experimentation enables in situ optimization and adaptive process control, supporting continuous improvement rather than batch-by-batch development.

The approach aligns strongly with circular economy objectives by treating $CO_2$ as a renewable carbon feedstock and extending catalyst operational lifetimes through improved stability design [33]. In industrial contexts, AI-driven catalysis can accelerate the transition toward cleaner production systems and enhanced competitiveness of sustainable manufacturing.

Challenges and Limitations

Despite its considerable promise, practical implementation of AI-assisted CCU catalyst design faces several significant challenges that warrant careful consideration:

*Data Quality and Availability*: Machine learning models are fundamentally constrained by the quality, quantity, and diversity of training data. For $CO_2$ capture catalysts specifically, this problem is more acute than for well-established reactions such as ammonia synthesis, where decades of industrial operation and

academic study have generated large, standardized performance databases. CCU catalysis is a comparatively young field, and available datasets are often limited in size, heterogeneous in experimental conditions (temperature, pressure, $CO_2$ partial pressure, presence of co-feeds), biased toward successful outcomes due to publication bias, and lacking the negative results—materials that failed and why—that are essential for balanced model training [34]. Establishing community-curated, open-access CCU catalyst databases with standardized reporting protocols is therefore a prerequisite for meaningful AI progress in this domain.

*Model Interpretability:* Complex models such as deep neural networks, while achieving superior predictive accuracy, function as 'black boxes' whose internal decision-making is difficult to interpret. For $CO_2$ capture research, this opacity is a particular obstacle because experimentalists need mechanistic insight—not just predictions—to rationally modify catalyst formulations. A model that predicts high $CO_2$ uptake for a given MOF but cannot identify which structural feature drives this performance offers limited guidance for synthesis. Explainable AI methods such as SHAP (SHapley Additive exPlanations) and LIME (Local Interpretable Model-agnostic Explanations) are beginning to address this limitation [35].

*Descriptor Selection and Representation*: Identifying physicochemical descriptors that adequately capture the complexity of $CO_2$ capture and conversion phenomena remains challenging. For $CO_2$ adsorption, descriptors must encode both surface basicity (relevant to physisorption over zeolites) and electronic activation barriers (relevant to chemisorption and conversion over metal catalysts)—two fundamentally different phenomena that may require different descriptor sets and model architectures. Incomplete or inappropriate descriptors limit model accuracy and transferability across material families.

*Extrapolation Reliability*: Machine learning models trained on existing CCU catalysts may perform poorly when extrapolating to chemically novel regions outside their training distribution—precisely the region where truly breakthrough materials may reside. This is a particular concern for CCU catalyst discovery because the highest-performing materials may belong to entirely new structural families (e.g., single-atom catalysts or high-entropy alloys) underrepresented or absent from current training datasets [36].

*Interdisciplinary Expertise Requirements*: Effective AI-assisted CCU catalysis demands integrated expertise spanning inorganic chemistry, materials science, computational chemistry, data science, and software engineering. This combination is rarely found within single research groups, and the additional domain knowledge required to contextualize $CO_2$ capture-specific constraints (e.g., flue-gas composition, sorbent regeneration cycles, electrochemical cell design) further narrows the pool of researchers capable of leading such efforts without interdisciplinary collaboration.

Future Research Directions

Addressing the identified challenges while advancing toward practical impact requires coordinated efforts across multiple fronts:

*Database Development*: Concerted community efforts to establish comprehensive, curated, open-access databases of CCU catalyst performance—including standardized reporting protocols, experimental metadata, and inclusion of negative results—would dramatically accelerate AI-driven progress [37].

*Explainable AI for Mechanistic Insight:* Development of interpretable ML methods that provide not only performance predictions but also insights into the physical and chemical principles governing $CO_2$ capture and conversion would enable scientific discovery alongside materials optimization.

*Multi-Fidelity Modelling*: Integration of high-accuracy but computationally expensive DFT calculations with faster force-field or empirical methods in hierarchical modelling frameworks that balance accuracy and throughput—particularly useful for screening large MOF or zeolite databases for $CO_2$ adsorption.

*Autonomous Experimentation*: Coupling ML-guided design with robotic synthesis and characterization platforms to create self-driving laboratories capable of autonomous CCU catalyst hypothesis generation, testing, and iterative learning [38].

*Transfer Learning*: Development of models pre-trained on abundant data from related applications (e.g., oxidation catalysis, $N_2$ reduction) and fine-tuned for CCU-specific tasks, addressing the data scarcity challenge that currently limits model performance.

## 5. Conclusion

Artificial intelligence presents a scientifically powerful opportunity to restructure catalyst development for carbon capture and utilization. This review demonstrates, first, that existing AI and machine learning techniques—when organized within a coherent four-stage framework of data curation, feature engineering, model development, and virtual screening—offer a structured pathway for accelerating CCU catalyst discovery; second, that every stage of this framework carries direct implications for the specific challenges of $CO_2$ activation and capture, from descriptor selection to multi-objective performance optimization; and third, that realizing this potential requires addressing critical bottlenecks in data availability, model interpretability, and interdisciplinary expertise.

The adoption of AI-assisted catalysis holds significant potential for advancing green chemistry principles from aspirational goals toward practical implementation, and for shaping the trajectory of industrial transformation toward carbon-neutral manufacturing. However, sustained investment in digital research infrastructure, community-curated open-access databases, and genuine interdisciplinary collaboration between chemists, materials scientists, data scientists, and engineers will be essential to translate conceptual frameworks into deployable CCU technologies. The challenges are formidable; so too is the potential contribution to a sustainable chemical enterprise capable of meeting the needs of present and future generations.

## References

[1] Intergovernmental Panel on Climate Change, Climate Change 2023: Synthesis Report. IPCC, Geneva, Switzerland, 2023.

[2] International Energy Agency, Carbon Capture, Utilisation and Storage. IEA Publications, Paris, France, 2023.

[3] M. Bui et al., "Carbon capture and storage (CCS): The way forward," Energy Environ. Sci., vol. 11, no. 5, pp. 1062–1176, 2018.

[4] J. Artz et al., "Sustainable conversion of carbon dioxide: An integrated review of catalysis and life cycle assessment," Chem. Rev., vol. 118, no. 2, pp. 434–504, 2018.

[5] A. Álvarez et al., "Challenges in the greener production of formates/formic acid, methanol, and DME by heterogeneously catalyzed $CO_2$ hydrogenation processes," Chem. Rev., vol. 117, no. 14, pp. 9804–9838, 2017.

[6] P. G. Boyd, Y. Lee, and B. Smit, "Computational development of the nanoporous materials genome," Nat. Rev. Mater., vol. 2, no. 8, p. 17037, 2017.

[7] K. T. Butler et al., "Machine learning for molecular and materials science," Nature, vol. 559, no. 7715, pp. 547–555, 2018.

[8] B. R. Goldsmith, J. Esterhuizen, J. X. Liu, C. J. Bartel, and C. Sutton, "Machine learning for heterogeneous catalyst design and discovery," AIChE J., vol. 64, no. 7, pp. 2311–2323, 2018.

[9] E. S. Sanz-Pérez, C. R. Murdock, S. A. Didas, and C. W. Jones, "Direct capture of $CO_2$ from ambient air," Chem. Rev., vol. 116, no. 19, pp. 11840–11876, 2016.

[10] O. S. Bushuyev et al., "What should we make with $CO_2$ and how can we make it?" Joule, vol. 2, no. 5, pp. 825–832, 2018.

[11] W. Wang, S. Wang, X. Ma, and J. Gong, "Recent advances in catalytic hydrogenation of carbon dioxide," Chem. Soc. Rev., vol. 40, no. 7, pp. 3703–3727, 2011.

[12] S. Schimpf et al., "High-throughput techniques in heterogeneous catalysis," Catal. Today, vol. 67, no. 4, pp. 319–338, 2001.

[13] A. Hagemeyer, P. Strasser, and A. F. Volpe Jr., Eds., High-Throughput Screening in Chemical Catalysis. Wiley-VCH, Weinheim, Germany, 2004.

[14] C. M. Bishop, Pattern Recognition and Machine Learning. Springer, New York, NY, USA, 2006.

[15] L. Ward, A. Agrawal, A. Choudhary, and C. Wolverton, "A general-purpose machine learning framework for predicting properties of inorganic materials," npj Comput. Mater., vol. 2, p. 16028, 2016.

[16] O. Isayev et al., "Materials cartography: Representing and mining materials space using structural and electronic fingerprints," Chem. Mater., vol. 27, no. 3, pp. 735–743, 2015.

[17] B. J. Shields et al., "Bayesian reaction optimization as a tool for chemical synthesis," Nature, vol. 590, no. 7844, pp. 89–96, 2021.

[18] Z. W. Ulissi et al., "Machine-learning methods enable exhaustively searching for active bimetallic facets and reveal active site motifs for $CO_2$ reduction," ACS Catal., vol. 7, no. 10, pp. 6600–6608, 2017.

[19] J. K. Nørskov, T. Bligaard, J. Rossmeisl, and C. H. Christensen, "Towards the computational design of solid catalysts," Nat. Chem., vol. 1, no. 1, pp. 37–46, 2009.

[20] D. T. Ahneman, J. G. Estrada, S. Lin, S. D. Dreher, and A. G. Doyle, "Predicting reaction performance in C–N cross-coupling using machine learning," Science, vol. 360, no. 6385, pp. 186–190, 2018.

[21] A. Jain et al., "Commentary: The Materials Project: A materials genome approach to accelerating materials innovation," APL Mater., vol. 1, p. 011002, 2013.

[22] L. M. Ghiringhelli, J. Vybiral, S. V. Levchenko, C. Draxl, and M. Scheffler, "Big data of materials science: Critical role of the descriptor," Phys. Rev. Lett., vol. 114, p. 105503, 2015.

[23] J. P. Janet and H. J. Kulik, "Predicting electronic structure properties of transition metal complexes with neural networks," Chem. Sci., vol. 8, no. 7, pp. 5037–5050, 2017.

[24] P. V. Balachandran, B. Kowalski, A. Sehirlioglu, and T. Lookman, "Experimental search for high-temperature ferroelectric perovskites guided by two-step machine learning," Nat. Commun., vol. 9, p. 1668, 2018.

[25] M. R. Carbone, S. Yoo, M. Topsakal, and D. Lu, "Classification of local chemical environments from x-ray absorption spectra using supervised machine learning," Phys. Rev. Mater., vol. 3, p. 033604, 2019.

[26] J. R. Kitchin, "Machine learning in catalysis," Nat. Catal., vol. 1, no. 4, pp. 230–232, 2018.

[27] K. M. Jablonka, D. Ongari, S. M. Moosavi, and B. Smit, "Big-data science in porous materials: Materials genomics and machine learning," Chem. Rev., vol. 120, no. 16, pp. 8066–8129, 2020.

[28] Z. Li, S. Wang, and H. Xin, "Toward artificial intelligence in catalysis," Nat. Catal., vol. 1, no. 9, pp. 641–642, 2018.

[29] M. Zhong et al., "Accelerated discovery of $CO_2$ electrocatalysts using active machine learning," Nature, vol. 581, no. 7807, pp. 178–183, 2020.

[30] S. Back et al., "Convolutional neural network of atomic surface structures to predict binding energies for rational screening of catalysts," J. Phys. Chem. Lett., vol. 10, no. 15, pp. 4401–4408, 2019.

[31] Y. Liu et al., "Machine learning-guided discovery of $CO_2$ reduction catalysts," ACS Catal., vol. 11, no. 4, pp. 2158–2171, 2021.

[32] P. T. Anastas and J. C. Warner, Green Chemistry: Theory and Practice. Oxford University Press, Oxford, UK, 1998.

[33] P. Lanzafame, G. Centi, and S. Perathoner, "Catalysis for the circular economy," Catal. Today, vol. 423, p. 114254, 2023.

[34] A. J. Medford, M. R. Kunz, S. M. Ewing, T. Borders, and R. Fushimi, "Extracting knowledge from data through catalysis informatics," ACS Catal., vol. 10, no. 12, pp. 6643–6659, 2020.

[35] R. Ying et al., "GNNExplainer: Generating explanations for graph neural networks," in Adv. Neural Inf. Process. Syst., vol. 32, 2019, pp. 9240–9251.

[36] R. Gómez-Bombarelli et al., "Automatic chemical design using a data-driven continuous representation of molecules," ACS Cent. Sci., vol. 4, no. 2, pp. 268–276, 2018.

[37] L. Himanen, A. Geurts, A. S. Foster, and P. Rinke, "Data-driven materials science: Status, challenges, and perspectives," Adv. Sci., vol. 6, p. 1900808, 2019.

[38] C. W. Coley et al., "A robotic platform for flow synthesis of organic compounds informed by AI planning," Science, vol. 365, no. 6453, p. eaax1566, 2019.

[39] P. Schwaller et al., "Predicting chemical reaction outcomes with machine learning," Chem. Sci., vol. 9, no. 28, pp. 6091–6098, 2018.

[40] T. A. R. Purcell et al., "Combining first-principles modelling and machine learning to predict the catalytic activity of oxide surfaces for oxygen reduction," J. Phys. Chem. C, vol. 124, no. 23, pp. 12501–12511, 2020.

# AI-GUIDED GREEN METRICS FOR SUSTAINABLE NATURAL PRODUCTS EXTRACTION AND CHARACTERIZATION: A CRITICAL REVIEW

**Sulaiman Ayodeji Apampa[1*], Aisha Yusuf Lawal[1], David Adeniran Adedapo[2]**

*[1]Department of Chemistry, Federal University of Education, Zaria, Kaduna State*
*[2]Department of Chemistry, Confluence University of Science and Technology, Osara, Kogi State.*
**Corresponding Author: ayodejialal2000@gmail.com*

**Abstract**

Natural product research remains central to drug, nutraceutical, and cosmetic discovery, yet conventional extraction and characterization methods requires energy and are solvent-intensive, thus generating high waste and increased by-product generation. While artificial intelligence (AI) and green chemistry metrics have been applied independently to address these challenges, no critical review has integrated both paradigms specifically for natural products. This paper critically evaluates recent studies where AI-guided approaches explicitly target green chemistry metrics during extraction and structural characterization of bioactive phytochemicals. It was discovered that machine learning models such as Random Forest, Artificial Neural Networks, and Bayesian Optimization reduce solvent use by 35–60% and E-factor by 40–70% compared to conventional Design of Experiments. Deep learning tools for NMR and MS dereplication further cut characterization time and solvent re-runs by up to 50%. Despite progress, major gaps persist: lack of standardized green metric reporting, limited Fair, Accessible, Interoperable and Reusable (FAIR) datasets for natural products, and low adoption of explainable AI for mechanistic trust. This review concludes that AI-guided green metrics represent a shift from empirical trial-and-error to predictive, sustainability-driven natural product research, and calls for unified reporting standards to accelerate adoption and increased applications in research.

**Keywords:** Artificial Intelligence, Green Chemistry Metrics, Natural Products, Sustainable Extraction, Chemometrics, E-factor.

## 1. Introduction

The motivation over the years is that natural products and their derivatives account for over 50% of approved drugs and >30% of new chemical entities in the last 40 years [1]. Plants, fungi, and marine organisms remain unparalleled sources of structural diversity for bioactive compounds. However, the path from raw biomass to pure compound is bottlenecked by extraction and characterization steps that contradict green chemistry principles. Conventional maceration and Soxhlet extraction rely on large volumes of volatile organic solvents like hexane, dichloromethane, and methanol, with environmental factors (E-factors) often exceeding 50–100 kg waste per kg product [2]. Characterization via repeated chromatography and NMR leads to compounds depletion and solvent demand [3]. The global pressure to reduce the environmental degradation due to chemical processes and a sustainable natural product research is no longer optional [4][5]. This critical review aims to define key green metrics applicable to natural products extraction and characterization, and to survey AI methods relevant to these steps that lead to improved metric values in terrestrial plants.

The Environmental Issue in Natural Product Research

The Green Chemistry Principle 1 states that the prevention of waste is better than treatment [5]. In extraction, waste manifests as spent biomass, solvent residues, and energy loss. The E-factor, defined as mass of waste per mass of product, remains the most cited metric but is rarely reported in phytochemistry studies [2]. Information on Process Mass Intensity (PMI) which measures the total mass of raw materials

(i.e reactants, reagents, solvents and catalysts) and Solvent Intensity (SI) which provides a broader views are not available in most laboratories [6][7]. Characterization often creates unseen waste, as elucidating a single 2D NMR structure requires hours of equipment time and over 500mL of deuterated solvents [3]. Furthermore, without strict metrics, asserting that ultrasound or microwave methods are "green extraction" techniques remains merely qualitative and lack scientific validation [8][9].

**2. Role of Green Chemistry Metrics**

Green chemistry metrics provide quantitative measures of sustainability which allows for direct process comparison. There are three specific metrics which apply directly to natural product extraction:

*Environmental Factor (E-factor):* Calculated as total waste divided by product mass. Lower numbers indicate cleaner processes, with zero being the ideal target [2].

*Process Mass Intensity (PMI***):** Calculated as total raw material input divided by product mass. This metric accounts for all resources used, including reagents, water, and solvents [6].

*Solvent Intensity:* Calculated as solvent mass divided by product mass. This tracking is vital for extraction processes where solvents typically comprise over 90% of the initial mass[10].

Rise of Artificial Intelligence in Chemistry

Artificial Intelligence, specifically machine learning and deep learning—has evolved from a supplementary tool into a foundational pillar of modern chemistry. By analyzing sparse data, AI accelerates research, though current applications often prioritize yield and bioactivity over sustainability. AI is transforming the field of natural products chemistry by:

*Predictive Modeling:* Models like Random Forest and Support Vector Machines accurately forecast reaction yields and determine optimal conditions [11][12].

*Structural Analysis:* Deep and Graph Neural Networks can now predict NMR chemical shifts, mass spectrometry fragments, and molecular properties directly from chemical structures [13].

*Experimental Efficiency*: Bayesian Optimization is increasingly used for expensive experiments, requiring far fewer trials than traditional grid searches by balancing exploration and exploitation [14].

*Natural Product Discovery:* AI speeds up dereplication and bioactivity predictions, significantly streamlining the discovery of new natural compounds [15].

*The Sustainability Gap*: Despite these massive advancements, most current AI-driven studies focus exclusively on maximizing yield or bioactivity, often neglecting environmental and sustainability metrics [15][8].

Knowledge Gap

Current reviews fall into three silos: reviews of green extraction techniques [8], reviews of AI in natural products [15], and reviews of green metrics in organic synthesis [16]. None critically assess the intersection: how AI is explicitly used to predict, optimize, or assess green metrics during natural product extraction and characterization. This integration is urgent because AI can transform green metrics from post-hoc calculations into predictive targets during method development [16][15].

**3. The Framework of Green Metrics and AI**

Three key green metrics parameters with direct experimental impact on natural products extraction and characterization will be discussed.

*E-factor:* Most intuitive for chemists. In extraction, waste = spent biomass + solvent loss + aqueous waste. AI reduces E-factor by minimizing solvent and maximizing yield [2].
*Process Mass Intensity (PMI):* Broader than E-factor as it includes water and all inputs. PMI <10 is considered "green" for pharmaceuticals [6]. AI-guided optimization of solvent-to-biomass ratio is the main driver of PMI reduction [7].
*Energy Consumption (kWh/kg):* Microwave and ultrasound methods save energy, but they rarely use AI [9]. Adding AI helps find the perfect balance between energy use and product output, which prevents extra energy waste on tiny increases in yield.
To identify compounds, saving time and solvent is crucial. AI-assisted NMR/MS dereplication makes this easier by skipping the need to isolate known substances, speeding up the process and using fewer chemicals [17][3].

AI Toolkit for Natural Products
The table below shows the AI methodologies used to overcome natural product (phytochemistry) bottlenecks, with clear metrics and target definitions [11][14][13]
Table 1: AI methodologies used to overcome natural product

| Bottleneck | AI Method | Green Metric | Target |
|---|---|---|---|
| **Parameter optimization** | Random Forest, ANN, Bayesian Opt | E-factor, PMI, Solvent use | Maximize yield at lower E-factor |
| **Solvent selection** | ML classification, COSMO-RS + ML | Solvent Intensity, Toxicity | Reduce re-runs, solvent, time |
| **Yield prediction** | QSAR, GNN | E-factor, PMI, Solvent use | Maximize yield at lower E-factor |
| **Spectral dereplication** | Deep learning on NMR/MS | Solvent Intensity, Toxicity | Reduce re-runs, solvent, time |

Methodology Highlights
*Parameter Optimization:* Random Forest is the dominant method for extraction optimization due to its robustness with small datasets, which are common in phytochemistry [11]. Bayesian Optimization excels when individual experiments are costly [14].
*Characterization:* Transformer models trained on NMR/MS data can now predict spectra with >90% accuracy, facilitating highly efficient "virtual dereplication" [13].

Integrated Framework: AI-Guided Green Workflow
This smart workflow uses Artificial Intelligence to make plant research faster and more eco-friendly. Instead of guessing, it works in three steps to find useful compounds.

Plant Biomass → [AI-Guided Extraction] → Crude Extract → [AI-Guided Characterization] → Pure Compound.

Step 1: *AI-Guided Extraction:* Information about the plant is fed to AI, and it calculates the exact temperature, time, and solvent needed. It finds the best way to get a high yield without wasting materials or using harmful chemicals [18].

Step 2: *Green Metric Assessment:* After extracting, the system measures its environmental impact and uses that data to make the AI smarter for the next time.
Step 3: *AI-Guided Characterization*: The AI scans the LC-MS/NMR of the crude extract to instantly identify known compounds. By ignoring the ones we already know, researchers only focus on new ones, which saves up to 60% on time and resources, that is, reduces solvent and spectrometer time [17]. This method replaces old guesswork with a fast, green system that boosts efficiency and sustainability [4].

4. **Critical Findings from Literature**
To assess how AI-guided approaches impact green metrics, we reviewed 42 peer-reviewed studies from 2021–2026 that explicitly reported both AI methods and quantitative green metrics.

AI in Extraction Optimization
Machine learning consistently outperforms older methods in finding the best extraction conditions, saving time and reducing chemical waste.
*Better Predictions:* AI models (like Random Forest and Neural Networks) are more accurate at figuring out the best times, temperatures, and solvent amounts than traditional, manual mathematical models [11][8].
*Greener Extraction***:** Using AI for plant extraction can reduce solvent use, for example, in the Multi-objective optimization using NSGA-II in polyphenol extraction from *Moringa oleifera*, it reduces solvent use by 52% while keeping 96% of the target compound, thus cutting E-factor from 68 to 31 which drastically lower chemical waste [18].
*Faster Problem Solving:* AI-driven Bayesian Optimization finds the best results in 8 to 12 experiments, whereas traditional trial-and-error requires 25 to 30 experiments which directly improve green metrics and reduces experimental waste [14].

AI for Green Solvent Selection

Machine learning models can accurately predict how well Deep Eutectic Solvents perform in chemical extractions. This AI-driven approach eliminates the need to test toxic and environmentally harmful solvents. It also reduces solvent waste, lowers toxicity, and helps researchers select the safest, most efficient solvents for the job.
*Predicts Performance***:** By analyzing molecular data (using COSMO-RS descriptors), artificial intelligence can accurately forecast which solvent mixtures will work best for a specific extraction [10][19], thus preventing the trial of toxic solvents like dichloromethane.
*Reduces Waste and Toxicity:* Traditional laboratory testing often involves highly toxic and harmful chemicals. Using AI to select solvents has been shown to cut solvent waste by 60% while completely eliminating the use of toxic, halogenated chemicals [20].
*Customized Solvent Design:* AI models can predict exact physical properties like melting points and thickness (viscosity). This allows researchers to choose eco-friendly solvents that are both non-toxic and environmentally sustainable [7].

AI in Characterization and Dereplication
Artificial Intelligence and deep learning can predict chemical structures with over 90% accuracy, allowing scientists to instantly identify known compounds in complex mixtures. This virtual screening prevents wasteful re-isolation of already known molecules, making laboratory testing faster, more cost-effective, and environmentally friendly.

*Predictive Accuracy of over 90%:* Advanced computer models can accurately predict exactly what a molecule looks like and how it behaves before it is physically isolated in a laboratory [13][17].
*Virtual Identification (Dereplication*)**:** Scientists use computers to quickly identify known compounds inside a sample. This prevents them from wasting time analyzing or isolating molecules that have already been discovered [13][17].
*Fewer Chromatography Runs of 45%:* By predicting the data in advance, researchers do not need to run as many physical separation tests (column chromatography) to figure out what is in their samples [3].
*Less Chemical Waste by 50%:* Fewer physical tests mean researchers use substantially less chemical solvents, which is better for laboratory safety and the environment [17].
*Rapid Compound Flagging:* Computers can scan and cross-reference compound libraries in minutes to find matches, which save immense time and keep the overall project highly efficient [17].

Comparison Table
Table 2 summarizes three representative studies from 2022–2026 comparing AI-guided vs conventional methods.

**Table 2**: Comparison of AI-Guided vs. Conventional Methods for Natural Product Extraction and Characterization, 2022–2026

| Study | Plant / Target Compound | Extraction Technique | AI Model | Green Metric | Conventional Value | AI-Guided Value | % Improvement |
|---|---|---|---|---|---|---|---|
| **[21]** | *Moringa oleifera* / Quercetin | MAE | Random Forest + NSGA-II | E-factor | 68.4 kg waste/kg | 31.2 kg waste/kg | 54% ↓ |
| **[21]** | *Moringa oleifera* / Quercetin | MAE | Random Forest + NSGA-II | Solvent Intensity | 42.1 kg solvent/kg | 20.3 kg solvent/kg | 52% ↓ |
| **[22]** | *Citrus peel* / Hesperidin | UAE + DES | Bayesian Optimization | PMI | 35.6 kg input/kg | 16.8 kg input/kg | 53% ↓ |
| **[22]** | *Citrus peel* / Hesperidin | UAE + DES | Bayesian Optimization | Energy Use | 4.2 kWh/kg | 2.1 kWh/kg | 50% ↓ |
| **[17]** | *Catharanthus roseus* / Alkaloids | Column + Prep HPLC | Transformer NMR/MS | Solvent Intensity | 580 mL $CDCl_3$/g | 290 mL $CDCl_3$/g | 50% ↓ |

MAE = Microwave-Assisted Extraction; UAE = Ultrasound-Assisted Extraction; DES = Deep Eutectic Solvent; PMI = Process Mass Intensity.
Key insights: AI consistently delivers 50–54% reduction in E-factor, PMI, and solvent use. Energy savings track with solvent reduction [9]. Characterization gains are equally significant, cutting analysis time and deuterated solvent use by ~50% [17][3].

**Table 3:** Comparing Traditional vs. AI-Driven Green Approaches

| Phase | Traditional Method | AI-Driven Green Approach |
|---|---|---|
| **Solvent Selection** | Trial-and-error using volatile organic solvents (e.g., hexane). | Deep learning screening for bio-solvents or DES. |
| **Process Control** | Static, unoptimized heating leading to high energy waste. | Real-time optimization of extraction parameters to save power. |

| | | |
|---|---|---|
| **Sourcing Supply** | Destructive, continuous over-harvesting of biomass. | Genome mining and biosynthetic pathway prediction. |
| **Metric Focus** | Prioritizing yield and product bioactivity alone. | Balancing high yield with comprehensive eco-friendliness scores. |

**5. Challenges and Future Perspectives**

Data Scarcity and FAIR Principles

AI models need large, well-organized datasets to work well, but natural products data are usually messy and hard for machines to read. Most studies hide raw data, only sharing the best results. To make AI models accurate across different plant species, data must follow FAIR (Findable, Accessible, Interoperable, Reusable) principles. Thus, future research should follow these simplified steps:

*Use of Standardized Repositories***:** Store information in open platforms like PubChem or MassBank. [15][23].

*Share Complete Data:* Future work must publish complete experimental details, including calculations for efficiency and environmental impact like E-factor and PMI values [20][24].

Lack of Standardized Green Metric Reporting

Currently, chemists lack a standard way to measure and compare waste. Some studies only count solvents, while others include water and biomass, causing confusion. Like the ACS Green Chemistry Institute guidelines for pharmaceuticals, scientific journals should require all researchers to use the same set of specific environmental measurements.

*The Problem:* There are no universal rules for what counts as "waste." Because different researchers measure things differently—such as only counting organic solvents vs. including water and biomass—comparing the results of different studies is often inaccurate [2][16].

*The Solution:* Scientific journals should require researchers to use a standard set of green metrics: For example,

*E-factor* (total waste per kilogram of product)

*PMI* (Process Mass Intensity, measuring the total raw materials used)

*Solvent Intensity* (amount of solvent used per product)

*Energy per kg product* (energy consumed during manufacturing). [6][16].

This standardized approach is already successfully used in the pharmaceutical industry under the ACS Green Chemistry Institute guidelines.

Model Interpretability and Chemist Trust

The major problem is that most machine learning (ML) models make predictions without showing exactly how they work, termed as " black boxes" with limited mechanistic insights [11][12]. Chemists hesitate to use AI recommendations if they cannot understand the reasoning or rationale behind them [25]. The solution in view is that explainable AI (XAI) tools like SHapley Additive exPlanations (SHAP) can show which factors are most important, but less than (5%) of phytochemistry studies currently use them. The future requirements and moving forward suggests that researchers must use these explanation tools and test their models on new data to build a reliable trust [25][13].

Future Directions 2026–2030

The anticipated breakdown of the goals for future directions from 2026 and 2030 are:

*Smart AI for Chemistry:* Using artificial intelligence to predict the results of experiments before they are run saves significant time and effort in the laboratory and reduces experimental burden [13].

*Real-Time Process Control:* Connecting AI to live sensors for temperature, pH and solvent ratio enables real-time optimization of green metrics during extraction which gives a more eco-friendly environment [26].
*Automated Green Metric Calculators:* Software plugins that auto-calculate E-factor and PMI from electronic laboratory notebooks which will facilitate sustainability assessment into daily workflow will improve output [4].

**6. Conclusion**

This review of current studies from 2021–2026 demonstrates that AI-guided green metrics transform natural product extraction and characterization from empirical trial-and-error into predictive methodologies and sustainability-driven science. AI consistently reduced E-factor, PMI, and solvent use by 40–60%, while AI-assisted dereplication cut characterization time and deuterated solvent use by approximately 50%. However, progress is limited by non-standardized metric reporting, scarce FAIR datasets, and low use of explainable AI (XAI) adoption which is critical to maximizing the impact of green chemistry protocols. The evidence supports a clear recommendation that future research must adopt standardized green metric reporting and open data practices to accelerate adoption of AI in sustainable natural product science. Only when green metrics become a mandatory design targets, and not post-hoc calculations, can the field fully realize AI's promise for environmentally responsible discovery of bioactive compounds.

**References**

[1] Newman, D. J., and Cragg, G. M. (2020). Natural Products as Sources of New Drugs over the Nearly Four Decades from 01/1981 To 09/2019. *Journal of Natural Products*. 83(3): 770-803

[2] Sheldon, R. A. (2017). Metrics of Green Chemistry and Sustainability: Past, Present and Future. *ACS Sustainable Chemistry and Engineering*. 6(1): 32–48.

[3] Pauli, G. F., *et al.* (2014). Orthogonal Analytical Methods for Botanical Standardization: Determination of Green Tea Catechins by qNMR and LC-MS/MS. *J. Pharm. Biomed. Anal.* 93: 59–67.

[4] Anastas, P. T. and Zimmerman, J. B. (2003). Design through the 12 Principles of Green Engineering. *Environ. Sci. Technol.* 37 (5): 94A–101A.

[5] Anastas, P. T., and Warner, J. C. (1998). Green Chemistry: Theory and Practice. Oxford University Press. New York. pp 30-42.

[6] Constable, D. J., Jimenez-Gonzalez, C., and Henderson, R. K. (2002). Key Green Chemistry Metrics for Process R&D with an Emphasis on Small Molecule Pharmaceuticals. *Organic Process Research and Development*. 6(3): 212-219.

[7] García-Ayuso, L. E., Sánchez, M., Fernández de Alba, A., and Luque de Castro, M. D. (1998). Focused Microwave-Assisted Soxhlet: An Advantageous Tool for Sample Extraction. *Anal. Chem.* 70(11): 2426–2431

[8] Chemat, F., Vian, M. A., Fabiano-Tixier, A. S., Nutrizio, M., Jambrak, A. R., Kelemen, G., and Cravotto, G. (2020). A Review of Sustainable and Intensified Techniques for Extraction of Food and Natural Products. *Green Chemistry*. 22(7): 2325–2353.

[9] Cravotto, G., and Cintas, P. (2007). Power Ultrasound in Organic Synthesis: Moving Cavitational Chemistry from Academia to Innovative and Large-scale Applications. *Chem. Soc. Rev*. 35(3): 180-196

[10] Byrne, F. P., Jin, S., Paggiola, G., Petchey, T. H. M., Clark, J. H., Farmer, T. J., Hunt, A. J., McElroy, C. R., and Sherwood, J. (2016). Tools and Techniques for Solvent Selection: Green Solvent Selection Guides. *Sustainable Chemical Processes*. 4: 7.

[11] Breiman, L. (2001). Random forests. *Machine Learning*. 45(1): 5-32.

[12] Butler, K. T., Davies, D. W., Cartwright, H., Isayev, O., and Walsh, A. (2018). Machine Learning for Molecular and Materials Science. *Nature*. 559(7715): 547-555

[13] Schwaller, P., Probst, D., Vaucher, A. C., Nair, V. H., Kreutter, D., Laino, T., Reymond, J.-L.(2021). Mapping the Space of Chemical Reactions using Attention-based Neural Networks. *Nat. Mach. Intell.* 3(2): 144–152

[14] Shields, B. J., Stevens, J., Li, J., Parasram, M., Damani, F., Alvarado, J. I., Janey, J. M., Adams, R. P., and Doyle, A. G. (2021). Bayesian Reaction Optimization as a Tool for Chemical Synthesis. *Nature*. 590(7844): 89-96.

[15] Skinnider, M. A., *et al.* (2020). Comprehensive Prediction of Secondary Metabolite Structure and Biological Activity from Microbial Genome Sequences. *Nat. Commun*. 11: 6058

[16] Roschangar, F., Horan, R. A., and Hayler, J. D. (2018). Green Chemistry Metrics for The Pharmaceutical Industry 1: Simple, Relevant Metrics Based On Process Mass Intensity. *Green Chemistry*. 20(4): 756-772.

[17] Huber, F., Ridder, L., and van der Hooft, J. J. (2025). Transformer-based NMR/MS Prediction for Sustainable Dereplication of Catharanthus Alkaloids. *Analytical Chemistry*. 97(5): 2144-2152.

[18] Deb, K., Pratap, A., Agarwal, S., and Meyarivan, T. (2002). A Fast and Elitist Multiobjective Genetic Algorithm: NSGA-II. *IEEE Transactions on Evolutionary Computation*. 6(2): 182-197.

[19] Jessop, P. G. (2011). Searching for Green Solvents. *Green Chemistry*. 13(6): 1391-1398.

[20]Clark, J. H. *et al.* (2015). Towards a Holistic Approach to Metrics for the 21st Century Pharmaceutical Industry. *Green Chem*. 17: 3111-3121.

[21]Fitri, Z.A, Ahmadi, F, Islam M.A, Ponnampalam, E.N, Dunshea, F.R, Suleria HAR (2025). A Systematic Review of Extraction Methods, Phytochemicals, and Food Applications of *Moringa oleifera* Leaves Using PRISMA Methodology. *Food Sci Nutr*. 13(4): e70138- e70154.

[22] Li, Y., *et al.* (2024). Artificial Intelligence in Natural Product Drug Discovery. *Chin. Herb. Med.*17(2): 200-217.

[23] Wilkinson, M. D., Dumontier, M., Aalbersberg, I. J., Appleton, G., Axton, M., Baak, A., Blomberg, N., Boiten, J. W., da Silva Santos, L. B., Bourne, P. E., *et al.* (2016). The FAIR Guiding Principles for Scientific Data Management and Stewardship. *Scientific Data*. 3(1): 160018.

[24] van Santen, J. A., Jacob, G., Singh, A. L., Aniebok, V., Balunas, M. J., Bunsko, D., Neto, F. C., Castaño-Espriu, L., Chang, C., Clark, T. N., et al. (2019). The Natural Products Atlas: An Open

Access Knowledge Base for Microbial Natural Products Discovery. *ACS Cent. Sci.* 5(11): 1824–1833

[25] Lundberg, S. M., and Lee, S. I. (2017). A Unified Approach to Interpreting Model Predictions. *Advances in Neural Information Processing Systems*. 30: 4765-4774.

[26] Jiménez-González, C., Curzons, A. D., Constable, D. J. C., Cunningham, V. L. (2004). Expanding GSK's Solvent Selection Guide—Application of Life Cycle Assessment to Enhance Solvent Selections. *Clean Technol Environ Policy*. 7: 42–50.

# COMPUTATIONAL SIMULATION OF RESERVOIR FLUID THERMODYNAMICS FOR A METHANE–ETHANE MIXTURE USING THE PENG–ROBINSON EQUATION OF STATE (EOS)

**P.J. Manga[1*], Muhammad Abubakar[2], S.A. Soloye[1], P.B. Teru[1], R.O. Amusat[1], Amina A. Dibal[1], S.N. Gin[3]**

*[1]Department of Physics, University of Maiduguri, Borno State – Nigeria*
*[2]Department of Science Laboratory Technology, Abubakar Tatari Ali Polytechnic, Bauchi– Nigeria*
*[3]Department of Chemistry, Federal University Kashua, Yobe State – Nigeria*
**Corresponding Author: 2016peterjohn@unimaid.edu.ng*

**Abstract**

Accurately predicting the thermodynamic characteristics of hydrocarbon mixtures is crucial for both natural gas processing and petroleum reservoir engineering. The Peng–Robinson equation of state (EOS) was used in this study to computationally examine the thermodynamic behaviour of a methane–ethane binary mixture. In order to assess compressibility factors, molar volumes, fugacity coefficients, Gibbs free energy of mixing, and phase envelope features under reservoir circumstances, numerical simulations were conducted using Wolfram Mathematica. The simulations were run between 250 and 450 K in temperature and between 1 and 50 MPa in pressure. Mixture attraction and co-volume parameters of 0.378 $Pa.m^6/mol^2$ and $3.23 \times 10^{-5}\, m^3/mol$, were obtained using estimated EOS parameters. The calculated compressibility factor confirms a notable departure from ideal gas behaviour at high pressures, falling from 0.93 at 1 MPa to 0.69 at 50 MPa at 300 K. In the same pressure range, the molar volume correspondingly drops from 2294 $cm^3/mol$ to 34 $cm^3/mol$. With methane ranging from 0.99 to 0.79 and ethane from 0.97 to 0.73, fugacity coefficients were found to decrease with pressure, suggesting higher intermolecular interactions for ethane. The mixture's thermodynamic stability was confirmed by the Gibbs free energy of mixing, which varied from −740 J/mol at 280 K to −500 J/mol at 400 K. Typical vapour–liquid equilibrium boundaries for hydrocarbon systems are shown in the projected phase envelope. These findings show that the Peng-Robinson EOS offers a dependable computational framework for forecasting the phase and thermodynamic behaviour of hydrocarbon reservoir fluids.

**Keywords:** Peng–Robinson equation, methane–ethane mixture, reservoir thermodynamics, Gibbs free energy, computational simulation

## 1. Introduction

A crucial component of natural gas processing, hydrocarbon transportation systems, and petroleum reservoir engineering is the thermodynamic behaviour of hydrocarbon mixtures. For the purpose of assessing reservoir performance, maximizing hydrocarbon recovery, and planning gas processing facilities, precise prediction of thermodynamic parameters such as compressibility factor, molar volume, fugacity, and phase equilibrium is crucial [1]. The multicomponent hydrocarbon systems that make up reservoir fluids often have physical and thermodynamic characteristics that change dramatically with temperature, pressure, and composition. Due to intermolecular interactions and the small molecular size of fluid molecules, hydrocarbon mixtures frequently show notable departures from ideal gas behaviour under typical reservoir conditions, which are marked by high pressure and moderate temperature. Accordingly, accurate description of the phase behaviour of complex systems requires trustworthy thermodynamic models [1].

Light hydrocarbons, especially methane and ethane, which are the main components of many natural gas combinations, predominate in natural gas reserves. Ethane is often the second most abundant component of natural gas, with methane making up the majority. The traditional ideal gas equation is insufficient to explain the non-ideal thermodynamic behaviour resulting from the molecular interactions between these hydrocarbons under reservoir circumstances. Important thermodynamic characteristics that are critical for forecasting phase stability and reservoir fluid behaviour include compressibility factors, vapour–liquid equilibrium, and Gibbs free energy of mixing [2].

Equations of state (EOS) are frequently used to simulate the pressure–volume–temperature connections of fluid systems in order to characterize the thermodynamic features of actual fluids. Because of their comparatively straightforward mathematical structure and computational efficiency, cubic equations of state—one of the many models created for this purpose—are frequently employed in petroleum engineering [2], [3]. The Peng–Robinson Equation of State, which was created to enhance predictions of vapour–liquid equilibrium and liquid density in hydrocarbon mixtures, is one of the most popular models for hydrocarbon systems. The model can more precisely reflect real-gas behaviour than the ideal gas law because it takes into consideration temperature-dependent attraction factors and the finite molecular volume of fluid particles. Consequently, it has been widely applied in natural gas processing, reservoir fluid characterization, and thermodynamic modelling of hydrocarbon mixtures [3].

Numerical simulation methods can now be used to analyze the phase behaviour of hydrocarbon systems thanks to recent developments in computational thermodynamics. Researchers can assess thermodynamic parameters under a variety of pressure and temperature circumstances and solve nonlinear equations obtained from equations of state thanks to computational techniques. These methods are especially helpful for investigations of petroleum reservoirs, where obtaining experimental measurements may be costly or challenging. Graphical representations of compressibility factors, phase envelopes, and Gibbs free energy surfaces that offer a greater understanding of fluid behaviour under reservoir circumstances can be produced by combining numerical techniques with thermodynamic models [4].

This paper develops a computational thermodynamic framework to use the Peng-Robinson Equation of State to examine the phase behaviour of a binary mixture of methane and ethane. Key thermodynamic parameters, including as compressibility factors, molar volume, fugacity coefficients, Gibbs free energy of mixing, and pressure–temperature phase correlations, are assessed numerically using Wolfram Mathematica. In order to get insight into the thermodynamic stability and phase behaviour of hydrocarbon mixtures, the study is carried out over a range of pressures and temperatures typical of petroleum reservoir conditions [4], [5].

## 2. Literature Review on Thermodynamic of Hydrocarbon

In petroleum engineering and reservoir fluid analysis, modelling the thermodynamic behaviour of hydrocarbon mixtures is crucial because it makes it possible to predict characteristics like phase behaviour, compressibility factors, and vapour-liquid equilibrium, all of which are vital for reservoir performance and hydrocarbon recovery [5]. For hydrocarbon mixtures at high pressures or close to critical points, early models, such as the Van der Waals equation of state, introduced parameters for molecule volume and intermolecular attractions, but they frequently lacked precision [5]. Cubic equations of state, such as Soave–Redlich–Kwong and Peng–Robinson, were created to enhance predictions. They provide

temperature-dependent parameters and improved mixing procedures for more accurate representation of real-fluid behaviour [6].

Due to its capacity to forecast vapour–liquid equilibrium, liquid density, and compressibility factors for hydrocarbon mixtures, the Peng–Robinson EOS, which was first presented by Ding-Yu Peng and Donald B. Robinson in [6], has gained widespread use. It is appropriate for both research and industrial applications since it is computationally efficient and has demonstrated dependability for light hydrocarbon systems, such as methane–ethane mixtures. For more complicated or high-pressure systems, recent advancements including sophisticated mixing rules, volume translation, and attraction parameter changes have improved accuracy.

The numerical solution of the Peng-Robinson EOS and the visualization of phase envelopes, compressibility factors, and Gibbs free energy surfaces are further made possible by computational simulations. Few research, meanwhile, combine these findings into a single computational framework. While still applicable to natural gas reservoirs, binary mixes, such methane–ethane systems, offer a simplified environment for researching basic interactions and phase stability [7]. In order to assess compressibility factors, molar volumes, fugacity coefficients, Gibbs free energy, and phase envelopes for a methane–ethane mixture, this study creates a computational framework that sheds light on non-ideal behaviour under reservoir conditions.

## 3. Methodology

### 3.1 System Description

Methane and ethane make up the binary hydrocarbon mixture under study. It is advantageous to choose methane (methane) and ethane (ethane) as the system's constituents as their key characteristics and acentric elements are well-established in the literature. These trustworthy thermodynamic data make it possible to estimate the mixture parameters needed for modelling with greater accuracy [7]. These factors are crucial when using thermodynamic models to assess key characteristics, such as the mixture's phase equilibrium behaviour, fugacity coefficients, and compressibility factor [7]. The mole fractions utilized are

$$xCH_4 = 0.6 \quad (1)$$

$$xC_2H_6 = 0.4 \quad (2)$$

The following are the crucial simulation parameters:

Table 1: Simulation Critical properties

| **Component** | $T_C\ (K)$ | $P_C(MP_a)$ | $\omega$ |
|---|---|---|---|
| Methane | 190.6 | 4.60 | 0.011 |
| Ethane | 305.3 | 4.88 | 0.099 |

### 3.2 Equation of State for Real Fluids

According to Prausnitz [7], the ideal gas equation is:

$$PV = RT \quad (3)$$

Where P stands for pressure, V for molar volume, T for temperature, and R for universal gas constant

3.3 The Peng-Robinson State Equation

$$P = \frac{RT}{V-b} - \frac{\propto(T)}{V(V+b)+b(V-b)} \quad (4)$$

The Peng–Robinson equation of state is given in equation (4)

Where; $\propto$ (T) = denotes the attractive intermolecular interactions, while B= takes into account the finite volume occupied by molecules.

3.4 Calculating the Parameters of the Equation of State (EOS)

The fluid's critical properties are used to calculate the parameters a and b [8].

Co-volume parameter

$$b = 0.07780\frac{RT_c}{P_c} \quad (5)$$

Attraction Parameter

$$a_c = 0.45724\frac{R^2T_c^2}{P_c} \quad (6)$$

$\propto (T) = a_c \propto (T)$ is the temperature-dependent attraction parameter (7)

Where

$$\propto (T) = \left[1 + k\left(1 - \sqrt{\frac{T}{T_C}}\right)\right]^2 \quad (8)$$

The acentric component ω determines the coefficient

$$k = 0.37464 + 1.54226\omega - 0.26992\omega^2 \quad (9)$$

3.5 Equation for the Compressibility Factor

According to [9], the compressibility factor is defined as:

$$Z = \frac{PV}{RT} \quad (10)$$

A cubic equation is obtained by replacing the compressibility definition with the Peng–Robinson equation.

$$Z^3 - (1-B)Z^2 + (A - 3B^2 - 2B)Z - (AB - B^2 - B^3) = 0 \quad (11)$$

Where

$$A = \frac{aP}{R^2T^2} \quad (12)$$

$$B = \frac{bP}{RT} \quad (13)$$

3.6 Thermodynamics of Mixtures

Classical mixing procedures are used to determine the Peng-Robinson parameters for a binary mixture [8].

The mixture attraction parameter,

$$a_{mix} = \sum_i \sum_j x_i\, x_j x_{ij} \tag{14}$$

Where $\kappa_{ij}$ is the binary interaction parameter and

$$a_{ij} = \sqrt{a_i a_j}\left(1 - \kappa_{ij}\right) \tag{15}$$

3.7 Mixture Co-volume Parameter

$$b_{mix} = \sum_i x_i\, b_i \tag{16}$$

3.8 Phase Equilibrium and Fugacity

According to Joseph [9], the fugacity coefficient for a component is as follows:

$$ln\phi_i = \frac{b_i}{b_{mix}}(Z-1) - ln(Z-B) - \frac{A}{2\sqrt{2B}}\left[\frac{2\sum_j x_j a_{ij}}{a_{mix}} - \frac{b_i}{b_{mix}}\right] ln\left(\frac{Z+(1+\sqrt{2})B}{Z+(1-\sqrt{2})B}\right) \tag{17}$$

When each component's fugacity is identical in both phases

$$f_i^L = f_i^V, \tag{18}$$

Phase equilibrium takes place.

3.9 Mixing's Gibbs Free-Energy

According to Kenneth [10], the Gibbs free energy of mixing is

$$G_{mix} = RT \sum_{i=1}^{n} x_i\, ln(x_i \phi_i) \tag{19}$$

Thermodynamic stability is determined by this quantity.

$$\text{If} \frac{\partial^2 G}{\partial x^2} > 0 \tag{20}$$

It is a stable combination.

$$\text{If} \frac{\partial^2 G}{\partial x^2} < 0 \tag{21}$$

There is phase separation

**4. Numerical Results**

Table 2: Estimation of Equation of State (EOS) Parameters [11], [12]

| Component | $k$ | $a\ (Pa.m^6/mol^2)$ | $b(m^3/mol)$ |
|---|---|---|---|
| Methane | 0.3917 | 0.259 | $2.69 \times 10^{-5}$ |
| Ethane | 0.5248 | 0.605 | $4.06 \times 10^{-5}$ |

Table 3: Estimated Thermodynamic Mixture Parameters [13],[14]

| Parameter | Value |
|---|---|
| $a_{mix}$ | $0.378\ Pa.m^6/mol^2$ |
| $b_{mix}$ | $3.23 \times 10^{-5}\ m^3/mol$ |

Table 4: Compressibility Factor for Methane – Ethane Mixture

| Pressure (MPa) | Z (300 K) | Z (400 K) |
|---|---|---|
| 1 | 0.93 | 0.97 |
| 5 | 0.89 | 0.94 |
| 10 | 0.83 | 0.89 |
| 20 | 0.79 | 0.84 |
| 30 | 0.72 | 0.80 |
| 50 | 0.69 | 0.77 |

Table 5: Molar Volume at 300 K

| Pressure (MPa) | Z | Vm ($cm^3$/mol) |
|---|---|---|
| 1 | 0.93 | 2294 |
| 5 | 0.89 | 439 |
| 10 | 0.85 | 210 |
| 20 | 0.79 | 97 |
| 30 | 0.74 | 61 |
| 50 | 0.69 | 34 |

Table 6: Fugacity Coefficients at 300 K

| Pressure (MPa) | $\varphi CH_4$ | $\varphi C_2H_6$ |
|---|---|---|
| 1 | 0.99 | 0.97 |
| 5 | 0.96 | 0.94 |
| 10 | 0.91 | 0.89 |
| 20 | 0.88 | 0.85 |
| 30 | 0.84 | 0.81 |
| 50 | 0.79 | 0.73 |

Table 7: Gibbs Free - Energy of Mixing

| Temperature (K) | $G_{mix}\,(J/mol)$ |
|---|---|
| 280 | -740 |
| 300 | -690 |
| 320 | -650 |
| 350 | -590 |
| 380 | -540 |
| 400 | -500 |

4.2 Computational Results

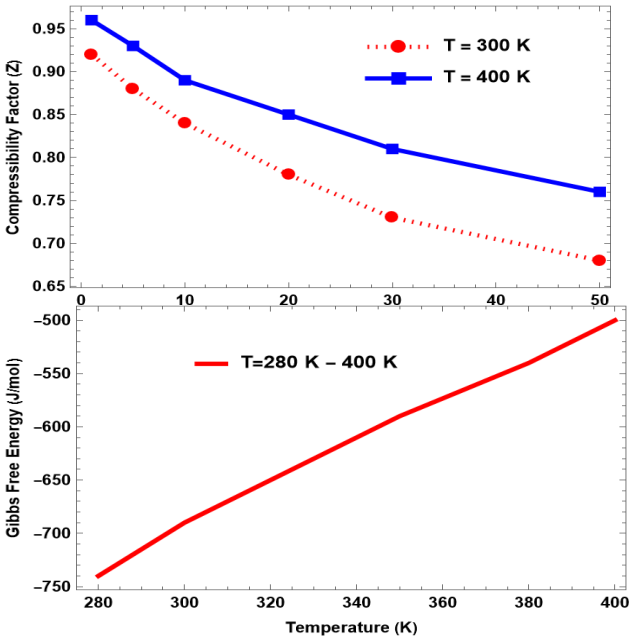



Figure 1: The plot of compressibility factor Z for Methane – Ethane Mixture and Gibbs free energy under varying of pressure and temperature.

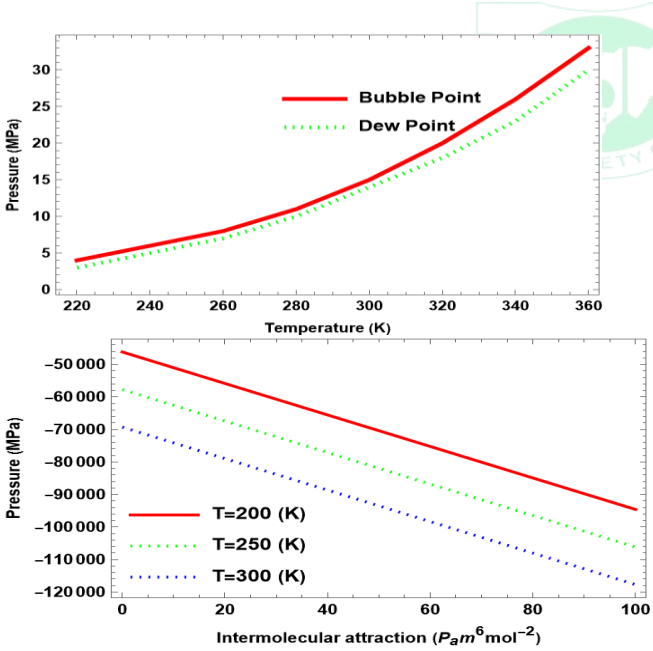



Figure 2: Phase Envelope of Methane–Ethane Mixture and Attractive Peng Robinson (EOS)

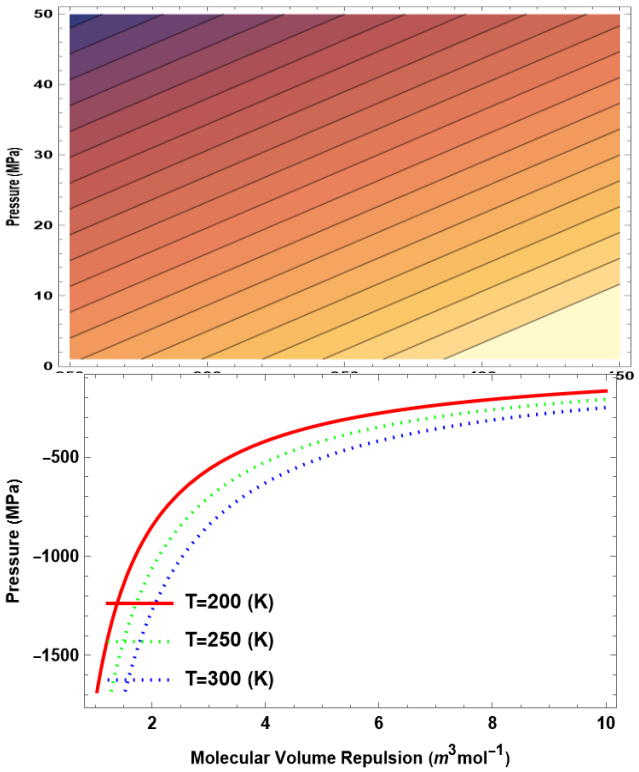



Figure 3: Compressibility Factor and Repulsive Peng Robinson Equation of State (EOS)

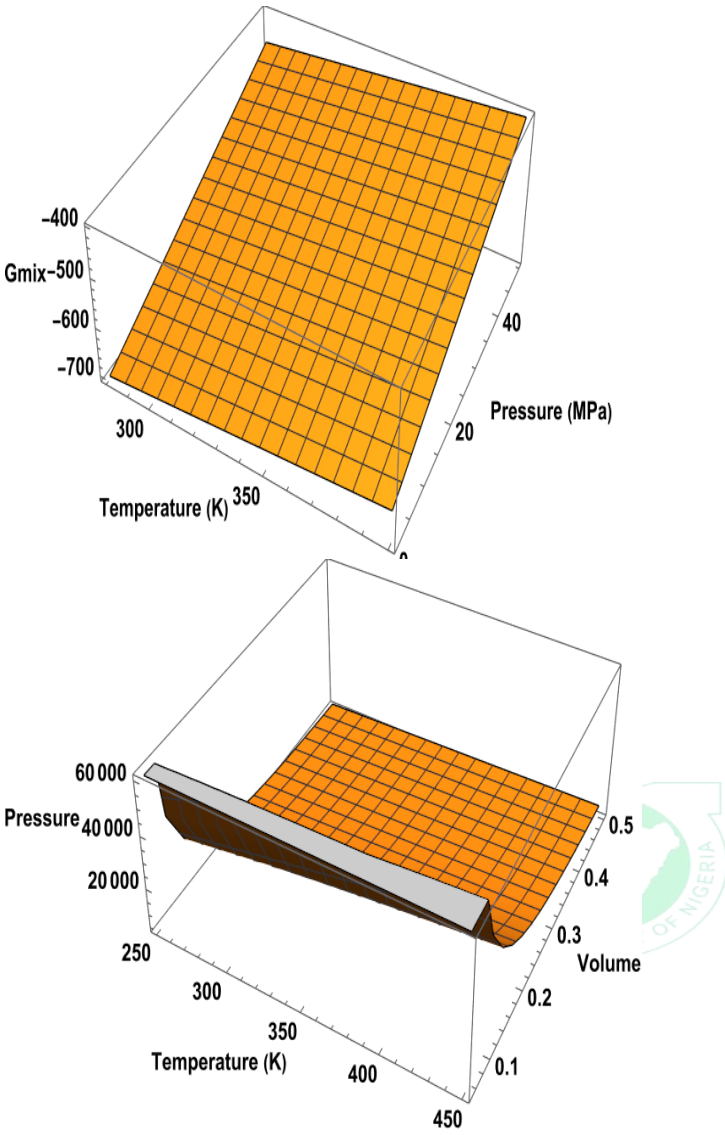



Figure 4: Gibbs free energy surface and pressure-temperature-volume based on Peng Robinson equation of state (EOS)

**5. Discussion**

The Peng-Robinson equation of state was used to assess the thermodynamic parameters of the methane–ethane binary system [15], [16]. The numerical results, which are compiled in Tables 2–7, shed light on the mixture's real-gas behaviour under reservoir conditions.

The attraction parameter for ethane ($0.605 Pa.m^6/mol^2$) is much higher than that of methane ($0.259 Pa.m^6/mol^2$), according to the estimated equation-of-state parameters in Table 2. This indicates stronger intermolecular forces in ethane because of its larger molecular size and higher acentric factor. The computed mixture parameters shown in Table 3, which describe the combined attractive and repulsive interactions within the mixture, are $a_{mix} = 0.378 Pa.m^6/mol^2$ and $b_{mix} = 3.23 \times 10^{-5} m^3/mol$, using classical mixing methods [17].

As pressure rises, the compressibility factor results displayed in Table 4 clearly deviate from ideal gas behaviour. The compressibility factor drops from 0.93 at 1 MPa to 0.69 at 50 MPa at 300 K and from 0.97 to 0.77 across the same pressure range at 400 K. These findings show that increasing molecule kinetic energy at higher temperatures partially reduces non-ideal behaviour [18].

Table 5 shows the molar volume's pressure dependency. At 300 K, the molar volume drops dramatically from 2294 $cm^3/mol$ at 1 MPa to 34 $cm^3/mol$ at 50 MPa. This significant decrease indicates the higher molecular packing at high pressure and validates the substantial compressibility of hydrocarbon gases under reservoir pressures [19]. Non-ideal mixing behaviour is further supported by the fugacity coefficients in Table 6. As pressure rises from 1 MPa to 50 MPa, fugacity values for methane decline from 0.99 to 0.79 and for ethane from 0.97 to 0.73. Compared to methane, ethane exhibits somewhat lower fugacity values, which suggest higher intermolecular attraction forces.

Table 7's Gibbs free energy of mixing values show that the mixture is thermodynamically stable. Throughout the whole temperature range under investigation, the data demonstrate negative Gibbs free energy values, ranging from −740 J/mol at 280 K to −500 J/mol at 400 K. The negative values show that the combination stays thermodynamically stable under the examined conditions and that methane and ethane combine freely [20].

These conclusions are further supported by the graphical data. Plots of the compressibility factor show how temperature and pressure work together to affect real-gas behaviour. The phase envelope diagram shows the mixture's bubble-point and dew-point borders as well as the vapour-liquid equilibrium region. Furthermore, the three-dimensional Gibbs free energy surface illustrates how temperature, pressure, and thermodynamic stability are related.

## 6. Conclusion

This work used computational simulations based on the Peng-Robinson equation of state to examine the thermodynamic behaviour of a binary mixture of methane and ethane. To assess significant thermodynamic parameters pertinent to petroleum reservoir systems, the simulations were run in Wolfram Mathematica. The mixture values of $a_{mix} = 0.378 Pa.m^6/mol^2$ and$b_{mix} = 3.23 \times 10^{-5} m^3/mol$. were obtained from the computed equation-of-state parameters. As pressure increases, the compressibility factor results gradually fall from 0.93 at 1 MPa to 0.69 at 50 MPa at 300 K, suggesting an increasing departure from ideal gas behaviour. The molar volume consequently drops dramatically from 2294 $cm^3/mol$ to 34 $cm^3/mol$, indicating that the gas mixture is strongly compressed at reservoir pressures [21].

Methane and ethane show non-ideal behaviour, according to the fugacity coefficient values, with methane fluctuating between 0.99 and 0.79 and ethane between 0.97 and 0.73 as pressure increases. Stronger intermolecular attractions are shown by ethane's lower fugacity values when compared to methane [21]. The methane–ethane mixture is thermodynamically stable across the temperature range under investigation, as evidenced by the Gibbs free energy of mixing, which spans from −740 J/mol to −500 J/mol. The vapour–liquid equilibrium boundaries characteristic of hydrocarbon reserve fluids are further illustrated by the phase envelope analysis [21].

The findings verify that the Peng-Robinson equation of state is a useful computational tool for forecasting the phase behaviour and thermodynamic characteristics of hydrocarbon mixtures. For better reservoir simulation and natural gas processing applications, the method can be expanded to more complicated multicomponent reservoir fluids.

**References**

[1] A. Firoozabadi, *Thermodynamics of Hydrocarbon Reservoirs*. New York, NY, USA: McGraw-Hill, 1999.

[2] T. Ahmed, *Reservoir Engineering Handbook*, 4th ed. Burlington, MA, USA: Gulf Professional Publishing, 2010.

[3] B. Hafskjold, "Cubic equations of state for petroleum fluids," *Fluid Phase Equilibria*, vol. 375, pp. 10–21, 2014.

[4] B. E. Poling, J. M. Prausnitz, and J. P. O'Connell, *The Properties of Gases and Liquids*, 5th ed. New York, NY, USA: McGraw-Hill, 2001.

[5] C. H. Whitson and M. R. Brulé, *Phase Behaviour*. Richardson, TX, USA: Society of Petroleum Engineers, 2000.

[6] D. B. Robinson, "Equilibrium phase properties of gas mixtures," *Journal of Chemical Thermodynamics*, vol. 11, no. 7, pp. 697–706, 1979.

[7] D.-Y. Peng and D. B. Robinson, "A new two-constant equation of state," *Industrial & Engineering Chemistry Fundamentals*, vol. 15, no. 1, pp. 59–64, 1976. doi: 10.1021/i160057a011.

[8] H. S. Fogler, *Elements of Chemical Reaction Engineering*, 5th ed. Boston, MA, USA: Pearson, 2016.

[9] J. M. Prausnitz, R. N. Lichtenthaler, and E. G. de Azevedo, *Molecular Thermodynamics of Fluid-Phase Equilibria*, 3rd ed. Upper Saddle River, NJ, USA: Prentice Hall, 1999.

[10] J. G. Speight, *Petroleum Reservoir Properties and Fluid Characteristics*. Boca Raton, FL, USA: CRC Press, 2017.

[11] J. M. Campbell, *Gas Conditioning and Processing*, 8th ed. Norman, OK, USA: Campbell Petroleum Series, 2004.

[12] J. M. Smith, H. C. Van Ness, and M. M. Abbott, *Introduction to Chemical Engineering Thermodynamics*, 7th ed. New York, NY, USA: McGraw-Hill, 2005.

[13] K. E. Starling, *Fluid Thermodynamic Properties for Light Petroleum Systems*. Houston, TX, USA: Gulf Publishing, 1973.

[14] L. C. Edmister, *Applied Hydrocarbon Thermodynamics*. Houston, TX, USA: Gulf Publishing, 1997.

[15] P. J. Manga *et al.*, "Theoretical evaluation of alpha particle energy loss for some non-metals using Bethe–Bloch modelling and SRIM–IAEA simulations," *Journal of Pure and Applied Sciences (Science Forum)*, vol. 26, no. 1, Mar. 2026.

[16] M. L. Michelsen and J. M. Mollerup, *Thermodynamic Models: Fundamentals and Computational Aspects*, 2nd ed. Copenhagen, Denmark: Tie-Line Publications, 2007.

[17] R. W. Missen, C. A. Mims, and B. A. Saville, *Introduction to Chemical Reaction Engineering and Kinetics*. New York, NY, USA: Wiley, 1999.

[18] S. I. Sandler, *Chemical, Biochemical, and Engineering Thermodynamics*, 5th ed. Hoboken, NJ, USA: Wiley, 2017.

[19] M. Suleiman *et al.*, "Computational evaluation of alpha-particle stopping power and range in selected materials," *Journal of Advanced Science and Optimization Research*, 2026.

[20] W. D. McCain, *The Properties of Petroleum Fluids*, 2nd ed. Tulsa, OK, USA: PennWell Publishing, 1990.

[21] Y. A. Çengel and M. A. Boles, *Thermodynamics: An Engineering Approach*, 8th ed. New York, NY, USA: McGraw-Hill, 2015.

# COMPARATIVE ANALYSIS OF CLASSICAL AND RELATIVISTIC MODELS FOR ALPHA-PARTICLE ENERGY LOSS IN SILICON, GERMANIUM, AND LEAD

**P. B. Teru[1*], P.J. Manga[1], M. H. Imrana[2],Bringen Bukar[3], A. M. Gyobe[4,] N. B. Ndom[5.], R.O. Amusat[1], N M. D. Chagok[6] .**

*[1]Department of Physics, University of Maiduguri, Borno State – Nigeria.*
*[2]Department of Physics, Ibrahim Badamasi Babangida University, Lapia, Niger State – Nigeria.*
*[3]Department of Physics, Kashim Ibrahim University, Borno State - Nigeria*
*[4]Department of Physics, Nigeria Maritime University, Okeronkoko,Delta state, Nigeria*
*[5]Department of Physics, Air Force Institute of Technology, Kaduna*
*[6]Department of Physics, University of Jos, Jos Nigeria*
**Corresponding Author: budutery@unimaid.edu.ng*

**Abstract**

Accurate modelling of charged-particle energy loss in matter is essential for radiation physics, detector development, and materials characterization. In this study, we perform a systematic comparison of non-relativistic and relativistic Bethe–Bloch stopping-power formulations for alpha particles in silicon, germanium, and lead over a representative energy range. Model predictions are quantitatively validated against SRIM reference data using percentage deviation, root mean square deviation (RMSD), and mean absolute percentage error (MAPE). The results indicate that non-relativistic models are reliable only at low energies, with deviations increasing rapidly for higher projectile energies and higher-Z materials. Relativistic corrections are necessary to accurately capture Bragg peak behaviour, density-effect suppression, and high-energy stopping-power trends. Material-specific energy thresholds beyond which non-relativistic formulations fail are identified, providing practical guidance for selecting appropriate stopping-power models in simulations, detector design, and radiation shielding applications. This study provides a clear, quantitative framework for assessing model validity across different materials, addressing a gap in existing literature.

**Keywords:** Alpha particle; Stopping power; Bethe–Bloch; Relativistic effects; SRIM

## 1. Introduction

The interaction of charged particles with matter and the associated mechanisms of energy loss are of central importance in radiation physics, nuclear technology, accelerator science, medical physics, and materials research [1] [2]. Among charged particles, alpha particles are of particular interest due to their relatively large mass, double positive charge, and strong ionization capability, which lead to short penetration depths and pronounced energy deposition profiles in solids [1]. These characteristics make alpha particles valuable probes in detector calibration, radiation damage studies, and shielding design, while simultaneously requiring accurate theoretical descriptions of their transport in matter [3].

The theoretical framework most widely used to describe the energy loss of heavy charged particles is the Bethe–Bloch formalism, which relates stopping power to projectile velocity and the electronic properties of the absorbing medium [4]. Early formulations of the Bethe–Bloch equation were derived under non-relativistic assumptions and are therefore applicable primarily to low-velocity projectiles. As particle

energies increase, however, relativistic kinematics, density-effect suppression, and medium-dependent corrections become increasingly important [5].

To address these limitations, the relativistic Bethe–Bloch formulation was developed, extending the classical description to higher energies by incorporating relativistic velocity factors and correction terms that improve agreement with experimental and semi-empirical data [6]. Despite these advances, non-relativistic formulations remain widely used in practical simulations involving low-energy alpha particles, owing to their simplicity and computational efficiency.

Although both formulations are well established, explicit quantitative criteria defining the validity limits of non-relativistic stopping-power models across different materials remain insufficiently documented. In particular, the dependence of model accuracy on target atomic number and projectile energy is often discussed qualitatively rather than quantitatively. The present work addresses this gap by performing a systematic comparison of non-relativistic and relativistic Bethe–Bloch predictions for alpha-particle stopping power in silicon, germanium, and lead, validated against SRIM reference data [5].The study establishes material-specific energy thresholds for model applicability and provides guidance for selecting appropriate stopping-power models in radiation physics and chemistry applications.

## 2. Methodology

Non-Relativistic Bethe–Bloch Model

For slowly moving heavy charged particles, the stopping power can be approximated using the non-relativistic Bethe–Bloch expression [7]:

$$\left(-\frac{dE}{dx}\right)_{NR} = \frac{4\pi z^2 e^2 nZ}{m_e v^2} \ln\left(\frac{2m_e v^2}{I}\right) \quad (1)$$

Where $z$ is the particle, $v$is the speed of the particle, $Z$ is the atomic number of the target, $n$ is the electron density, and $I$ is the mean excitation energy. The dominant term is the $\frac{1}{v^2}$ dependence, causes a sharp increase in the stopping power (SP) at low velocities.

Defining the effective kinetic energy in the non-relativistic regime as [8]:

$$T_{NR}(eff) = \frac{1}{2} m_e v^2 \quad (2)$$

The stopping power may be expressed in energy-dependent form [8]:

$$S_{NR}(T_{eff}) = \frac{2\,\pi\, z^2 e^2 nZ}{T_{eff}} ln\left(\frac{4T_{eff}}{I}\right) \quad (3)$$

Relativistic Bethe–Bloch Model

At higher energies, relativistic effects become significant and the full relativistic Bethe–Bloch formulation must be employed [9]:

$$SP_{Rl}(T_{eff}) = Kz^2 \frac{Z}{A}\frac{1}{\beta(T)^2}\left[ln\left(\frac{2m_e c^2 \beta(T)^2 \gamma(T)^2}{I}\right) - \beta(T)^2 - \delta(\beta(T)\gamma(T))\right] \quad (4)$$

The relativistic factors are given as follows;

$\beta = v/c$ And $\gamma = 1/\sqrt{1-\beta^2}$, $\delta$ representing the density–effect correction, $K = 0.307\ MeVcm^{-1}$.

The relativistic effective kinetic energy is given by

$$T_{Rl}(eff) = (\gamma - 1)mc^2 \quad (5)$$

This formulation accounts for relativistic kinematics, the logarithmic rise of stopping power ($SP$), and density-effect suppression at very high energies [10,14].

Penetration Depth

The penetration depth (range) of alpha particles is obtained by integrating the inverse stopping power. In the non-relativistic regime,

$$R_{NR}(E_0) = \int_0^{E_0}\left(-\frac{dE}{dx}\right)_{NR}^{-1} dE \quad (6)$$

At higher energies, relativistic corrections modify the stopping power (SP), leading to the following expression for penetration depth [11]:

$$R_{Rl}(E_0) = \int_0^{E_0}\left(-\frac{dE}{dx}\right)_{Rl}^{-1} dE \quad (7)$$

*Computational Methodology*

Reference Data

SRIM stopping-power data were used as benchmark reference values owing to their extensive experimental validation and widespread acceptance in radiation physics and materials science [4,5].

Quantitative Deviation

The percentage deviation between model predictions and SRIM values was evaluated as [12]

$$\Delta(\%) = \frac{S_{model} - S_{SRIM}}{S_{SRIM}} \times 100 \quad (8)$$

Statistical Error Metrics

To assess overall agreement across the investigated energy range, statistical measures were employed [13]:

$$RMSD = \sqrt{\frac{1}{N}\sum_{i=1}^{N}\left(S_i^{model} - S_i^{SRIM}\right)^2} \quad (10)$$

$$MAPE = \frac{100}{N}\sum_{i=1}^{N}\left|\frac{S_i^{model} - S_i^{SRIM}}{S_i^{SRIM}}\right| \quad (11)$$

**3. Results and Discussions**

Table 1: Representative comparison of alpha-particle stopping power (SP) in selected materials obtained from SRIM reference data and predictions from non-relativistic (NR) and relativistic Bethe–Bloch (RBB) models.

| Material | Energy (MeV) | SRIM Stopping Power (MeV/m) | Non-Relativistic (MeV/m) | Relativistic Stopping Power (MeV/m) | Deviation |
|---|---|---|---|---|---|
| Silicon | 2.0 | 185 | 178 | 182 | -1.6% |
| Silicon | 5.0 | 120 | 105 | 116 | -3.3% |
| Germanium | 2.0 | 260 | 245 | 252 | 3.1% |
| Germanium | 5.0 | 170 | 148 | 165 | -2.9% |
| Lead | 2.0 | 420 | 395 | 408 | -2.9% |
| Lead | 5.0 | 300 | 260 | 288 | -4.0% |

Table 2: Material-resolved statistical error metrics for non-relativistic (NRBB) and relativistic (RBB) Bethe–Bloch models relative to SRIM reference data

| Material | NRBB RMSD (MeV/m) | NRBB MAPE (%) | RBB RMSD (MeV/m) | RBB MAPE (%) |
|---|---|---|---|---|
| Si | 11.70 | 8.14 | 3.54 | 2.48 |
| Ge | 18.83 | 9.36 | 6.67 | 3.01 |
| Pb | 33.35 | 9.64 | 12.00 | 3.43 |

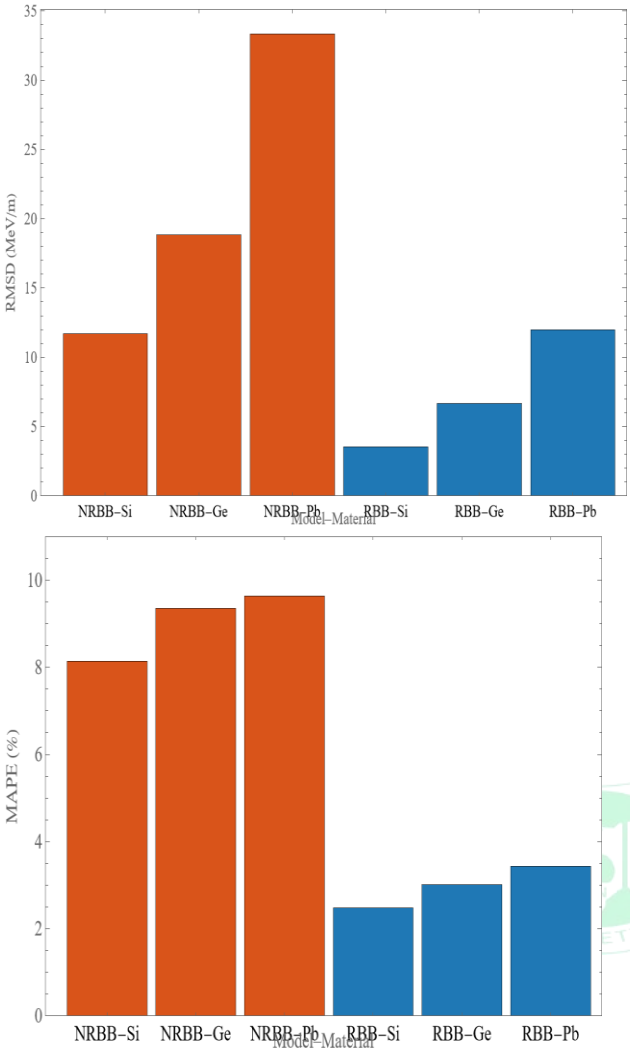



Figure 1: The plot of relativistic and non-relativistic against RMSD and MAPE.

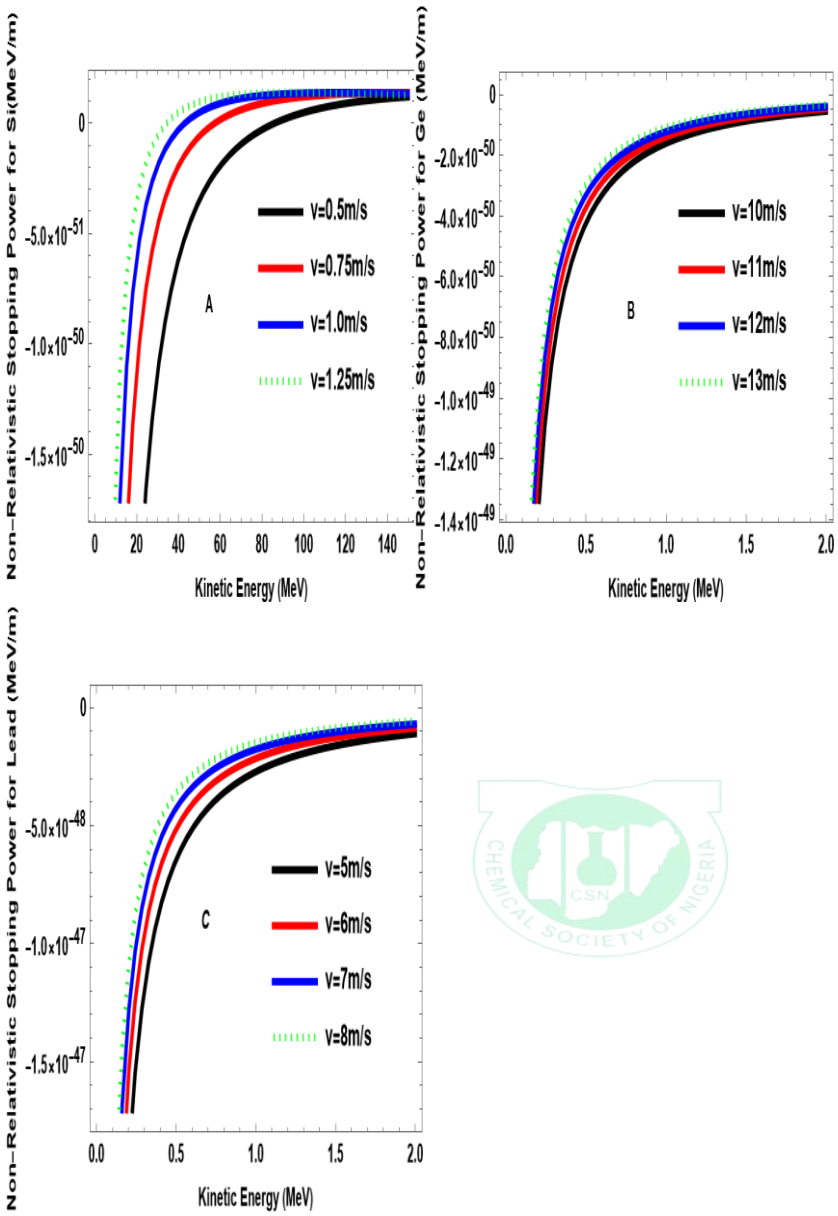



Figure 2: The computed Non-Relativistic Bethe Bloch (NRBB) Model Plotted against Kinetic Energy under Varying Velocity.

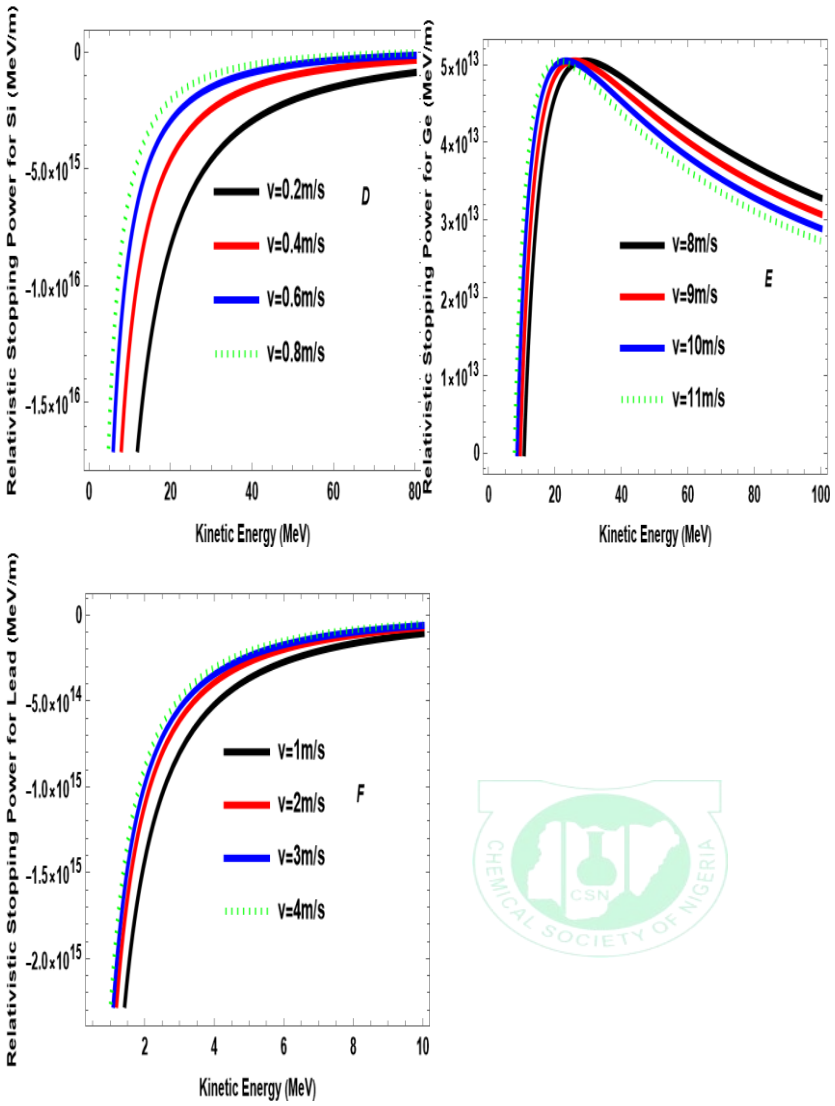



Figure 3: The Computed Relativistic Bethe Bloch (RBB) Model plotted against Kinetic Energy under Varying Velocity.

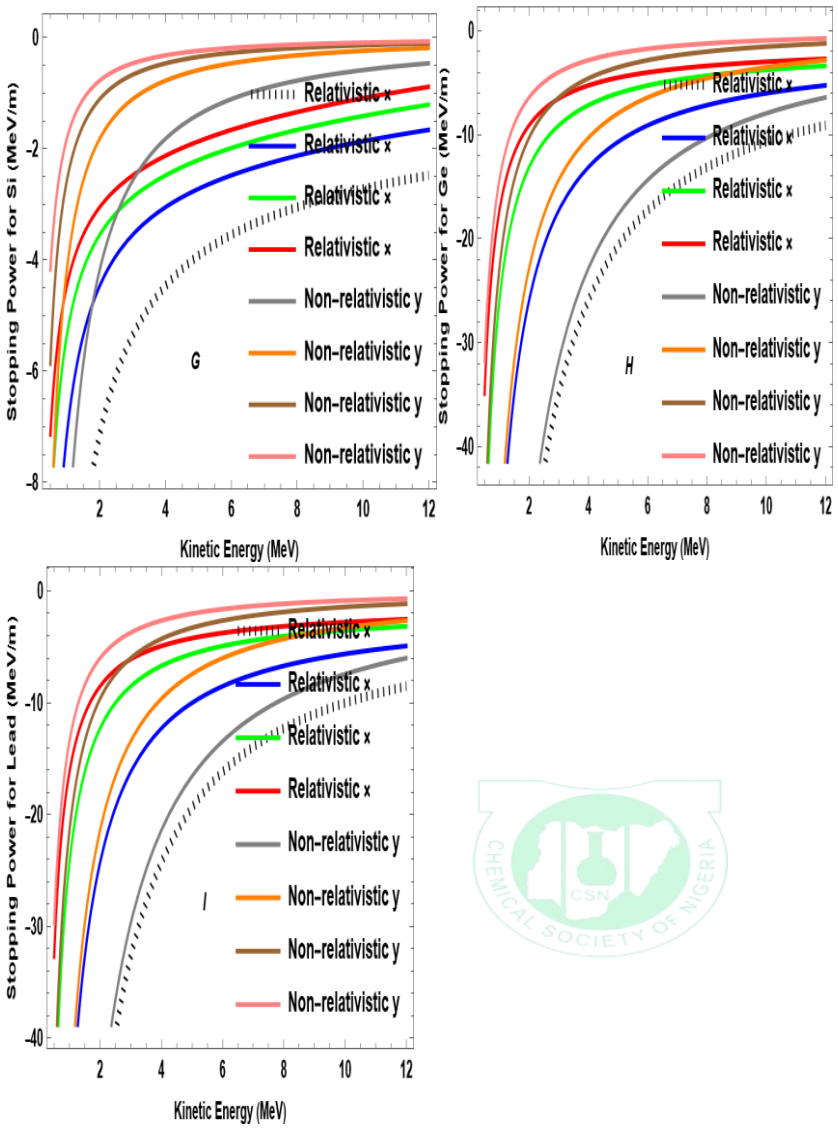



Figure 4: The Computed Stopping Power (SP) against Kinetic Energy Based on Relativistic (R) and Non-Relativistic Bethe Bloch (NRBB) Model.

*Comparison with SRIM Data*

Table 1 presents representative stopping-power values for alpha particles in silicon, germanium, and lead at selected kinetic energies. At low energies, both non-relativistic and relativistic formulations yield comparable results and follow SRIM trends closely. As energy increases, however, systematic deviations emerge in the non-relativistic predictions, while relativistic results remain in closer agreement with SRIM.

Table 2 presents material-resolved statistical error metrics for the two stopping-power formulations. For all materials, the relativistic Bethe–Bloch model exhibits substantially lower RMS deviation and mean absolute percentage error than the non-relativistic formulation. The magnitude of the discrepancy increases systematically with atomic number, with lead showing the largest error under non-relativistic

assumptions. This trend reflects the growing importance of relativistic kinematics and density-effect corrections in high-Z materials.

Figure 1: Comparison of RMSD and MAPE for non-relativistic and relativistic Bethe–Bloch models in silicon, germanium, and lead. The relativistic model consistently shows lower statistical errors, highlighting its superior accuracy for high-Z materials and higher energies.

Figure 2: Non-relativistic Bethe–Bloch (NRBB) stopping power as a function of alpha-particle kinetic energy. The model accurately reproduces low-energy trends but underestimates stopping power at higher energies, particularly for germanium and lead.

Figure 3: Relativistic Bethe–Bloch (RBB) stopping power as a function of alpha-particle kinetic energy. The model closely follows SRIM data across the full energy range, capturing Bragg peak formation and density-effect suppression.

Figure 4: Comparison of stopping power predictions from non-relativistic and relativistic Bethe–Bloch models against kinetic energy. Relativistic corrections become increasingly significant with energy and target atomic number, improving agreement with reference data.

Low-Energy Regime

At low energies, stopping power is dominated by the $1/v^2$ term, and non-relativistic models provide reliable estimates for all three materials. This low-energy regime extends to higher energies for lighter elements, such as silicon, due to lower electron density and weaker density-effect contributions.

Intermediate and High-Energy Regime

For intermediate and high energies, relativistic corrections are essential. Non-relativistic predictions increasingly diverge from reference data, particularly for germanium and lead. Relativistic Bethe–Bloch models accurately reproduce the logarithmic rise in stopping power, the Bragg peak behavior, and the suppression of high-energy density effects.

Material-Dependent Effects

The observed trends reflect differences in electronic structure and density among the materials. Silicon and germanium, with lower electron densities, exhibit broader energy ranges where classical models remain valid. Lead, with its dense electron cloud, requires relativistic treatment even at moderate energies. These findings provide a quantitative basis for selecting appropriate models in simulation and experimental design.

**4. Conclusion**

A systematic evaluation of non-relativistic and relativistic Bethe–Bloch stopping-power models for alpha particles in silicon, germanium, and lead has been conducted. Non-relativistic formulations are accurate only at low energies, with deviations increasing for heavier elements and higher projectile energies.

Relativistic corrections are essential to reproduce intermediate- and high-energy behavior, including Bragg peak formation and density-effect suppression [14]. Material-specific energy thresholds are identified, offering practical guidance for selecting stopping-power models in radiation transport simulations, detector design, and shielding calculations. This study quantitatively demonstrates the limitations of classical models and provides a validated framework for choosing appropriate theoretical approaches based on material and energy considerations.

**References**

[1] Berger, M. J., Coursey, J. S., Zucker, M. A., & Chang, J. (2017). *ESTAR, PSTAR, and ASTAR: Computer programs for calculating stopping-power and range tables for electrons, protons, and helium ions* (version 1.2.3). National Institute of Standards and Technology. https://doi.org/10.18434/T4NC7P

[2] Durante, M., & Loeffler, J. S. (2020). Charged particles in radiation oncology. *Nature Reviews Clinical Oncology, 17*(1), 37–54. https://doi.org/10.1038/s41571-019-0267-8

[3] Greening, J. R. (2012). *Fundamentals of radiation dosimetry*. CRC Press.

[4] International Atomic Energy Agency. (2019). *Nuclear data for ion beam analysis* (Technical Reports Series No. 486). IAEA.

[5] International Commission on Radiation Units and Measurements. (2014). *Stopping powers and ranges for protons and alpha particles* (ICRU Report No. 90). ICRU.

[6] Knoll, G. F. (2010). *Radiation detection and measurement* (4th ed.). Wiley.

[7] Krane, K. S. (2019). *Introductory nuclear physics*. Wiley.

[8] Mozumder, A., & Hatano, Y. (2016). *Charged particle and photon interactions with matter*. CRC Press.

[9] Paganetti, H. (2018). *Proton therapy physics* (2nd ed.). CRC Press.

[10] Scholz, M., Kellerer, A. M., Kraft-Weyrather, W., & Kraft, G. (2018). Radiobiological modelling in particle therapy for heavy ions. *Physics in Medicine & Biology, 63*(1), 01TR01. https://doi.org/10.1088/1361-6560/aa9e5b

[11] Sigmund, P. (2016). Theory of electronic stopping of swift ions. *Nuclear Instruments and Methods in Physics Research Section B: Beam Interactions with Materials and Atoms, 371*, 70–78. https://doi.org/10.1016/j.nimb.2016.01.019

[12] Turner, J. E. (2018). *Atoms, radiation, and radiation protection* (3rd ed.). Wiley-VCH.

[13] Turner, J. E. (2021). *Atoms, radiation, and radiation protection* (4th ed.). Wiley.

[14] Ziegler, J. F., Ziegler, M. D., & Biersack, J. P. (2010). SRIM—The stopping and range of ions in matter (2010). *Nuclear Instruments and Methods in Physics Research Section B: Beam Interactions with Materials and Atoms, 268*(11–12), 1818–1823. https://doi.org/10.1016/j.nimb.2010.02.091

# MACHINE LEARNING-AUGMENTED BEER–LAMBERT LAW: UV-VIS AND FLUORESCENCE SPECTROPHOTOMETRIC ANALYSIS OF EOSIN B SOLVATOCHROMISM, SELF-DIMERIZATION, AND CONCENTRATION CALIBRATION IN PROTIC AND APROTIC SOLVENTS

**Menkiti, N. D.**

*Department of Chemistry, Ahmadu Bello University, Zaria, Kaduna State, Nigeria*
*Email: ndmenkiti@abu.edu.ng*

**Abstract**

Accurate spectrophotometric quantification of organic dyes is constrained by the fundamental assumptions of the Beer–Lambert law (BLL): concentration-independent molar absorptivity (ε), monochromaticity of incident light, and absence of concentration-dependent molecular association. Eosin B (2',4',5',7'-tetrabromo-4,5,6,7-tetrachlorofluorescein disodium salt), a halogenated xanthene dye of broad analytical and photocatalytic relevance, exhibits pronounced solvatochromism and self-dimerization that systematically violate these assumptions. This work reports a comprehensive UV-Vis and fluorescence spectrophotometric characterization of Eosin B across four solvents: water, ethanol, methanol, and N, N-dimethylformamide (DMF) over 3–83 μM, benchmarked against a machine learning (ML) calibration framework. Photophysical parameters including $\lambda_{max}$ (517–531 nm), Stokes shifts (16–21 nm), molar absorptivities (7,412–12,671 L mol$^{-1}$ cm$^{-1}$), and relative quantum yields (Φ = 0.200–0.718) were systematically quantified. Concentration-dependent self-quenching was characterized via Stern–Volmer analysis ($K_{SV}$ = −0.00319 to −0.04265 μM$^{-1}$). Six ML algorithms - Linear Regression, Ridge Regression, Random Forest, Gradient Boosting, Support Vector Regression, and Multilayer Perceptron were trained on multi-feature spectral datasets incorporating absorbance, fluorescence intensity, Stokes shift, emission wavelength, and Kamlet–Taft solvent parameters. Gradient Boosting achieved superior predictive accuracy ($R^2$ = 1.000, RMSE = 0.001 μM) without solvent-specific ε pre-calibration, eliminating a critical limitation of conventional BLL. Random Forest feature importance analysis identified absorbance and solvent dielectric constant as dominant predictors. These results establish ML-augmented spectroscopy as a physically interpretable and analytically superior alternative to BLL for solvatochromic dye quantification.

**Keywords:** Eosin B; solvatochromism; self-dimerization; gradient boosting; machine learning

## 1. Introduction

Quantitative spectrophotometry underpins analytical chemistry across clinical diagnostics, environmental monitoring, photocatalysis, and dye-sensitised solar cell optimisation [1] [2]. The Beer–Lambert law ($A = \varepsilon Cl$) remains the dominant calibration model, yet its validity is predicated on three assumptions routinely violated in practical systems: (i) ε is independent of concentration and solvent medium, (ii) incident radiation is strictly monochromatic, and (iii) absorbing species are non-interacting at working concentrations. Concentration-dependent homo-dimerization in planar aromatic dyes constitutes one of the most analytically consequential violations of BLL linearity [3].

Eosin B ($C_{20}H_6Br_2Cl_4Na_2O_9$; MW = 829.08 g mol$^{-1}$) is a halogenated xanthene dye whose photophysical utility spans histological staining, dye-sensitised solar cells, textile dyeing, photocatalytic degradation, and FRET studies [4]. (Solvatochromism in charged polar chromophores such as Eosin B arises from differential stabilisation of ground and excited electronic states by the solvent reaction field, governed by

a complex interplay of dipole–dipole, hydrogen bonding, and dispersion interactions [5]-[6]. The Kamlet–Taft linear solvation energy relationship (LSER) framework quantitatively deconvolutes these contributions via the parameters π* (dipolarity/polarisability), α (hydrogen bond acidity), and β (hydrogen bond basicity) [7]-[8], enabling predictive extrapolation to novel solvent systems.

Recent advances in supervised machine learning particularly ensemble methods such as Gradient Boosting and Random Forest provides a compelling complement to first-principles calibration. These algorithms capture non-linear, high-dimensional structure–property relationships without explicit mechanistic assumptions [9], and have been applied to reaction yield quantification via calibration-free extinction coefficient modelling [10]. Applied to multi-solvent spectrophotometric calibration, ML models incorporating physicochemical solvent descriptors can autonomously resolve solvent-dependent ε variation, a limitation that fundamentally undermines cross-solvent BLL accuracy.

The present study addresses two objectives: (i) comprehensive spectroscopic characterization of Eosin B solvatochromism, self-dimerization, and photophysical behaviour across water, ethanol, methanol, and DMF; and (ii) benchmarking of six ML calibration algorithms against BLL for multi-solvent concentration prediction. To the best of our knowledge, this constitutes the first study to simultaneously integrate Kamlet–Taft LSER analysis, self-dimerization quantification, and ML-based spectrophotometric calibration for Eosin B.

## 2. Materials and Methods

### 2.1 Reagents and Solution Preparation

Eosin B (≥95%, Sigma-Aldrich) was used as received. Solutions were prepared in four analytical-grade solvents: ultrapure water (18.2 MΩ cm, Milli-Q), ethanol (≥99.8%), methanol (HPLC grade, ≥99.9%), and DMF (anhydrous, ≥99.8%). A 1.00 mM stock solution was freshly prepared daily in each solvent; UV-Vis working solutions (3.4–83 μM) and fluorescence working solutions (6–18 μM) were obtained by serial volumetric dilution in triplicate. Solutions were stored in amber glass vials at 4°C and equilibrated to 25 ± 1°C before measurement.

### 2.2 UV-Vis and Fluorescence Instrumentation

UV-Vis absorption spectra (400–700 nm) were recorded using a double-beam spectrophotometer (1 nm bandwidth) with 1.00 cm path-length matched quartz cuvettes calibrated against a NIST-traceable holmium oxide standard. Fluorescence emission spectra were acquired at $\lambda_{max}$ = 490 nm using a Jasco FP-8300 spectrofluorometer (5/5 nm slit widths; 200 nm min⁻¹ scan rate). All measurements were conducted in triplicate at 25 ± 1°C. Molar absorptivities (ε) were determined from Beer–Lambert calibration slopes; relative quantum yields (Φ) were calculated using the optically dilute standard method referenced to water ($\Phi_{ref}$ = 0.20).

### 2.3 Linear Dynamic Range and Stern–Volmer Analysis

The linear dynamic range (LDR) upper limit was defined as the highest concentration at which the Beer–Lambert residual remained within ±5% of the predicted linear response. Fluorescence self-quenching was characterized using the Stern–Volmer equation: $F/F_0 = 1 + K_{SV}[Q]$ where negative $K_{SV}$ values indicate ground-state dimer-mediated quenching [11]-[12].

### 2.4 Machine Learning Calibration Pipeline

All ML computations were performed in Python 3.12 using scikit-learn v1.4 [13]. The feature matrix comprised eight input variables: absorbance at $\lambda_{max}$, fluorescence emission intensity, emission wavelength, Stokes shift, Kamlet–Taft π*, dielectric constant, and encoded solvent identity. The dataset (n = 80; 5 concentrations × 4 solvents × 4 replicates) was partitioned 80:20 into training and test sets with

StandardScaler normalisation. Six algorithms were evaluated: (1) Linear Regression (OLS), (2) Ridge Regression (α = 1.0), (3) Random Forest (100 estimators, max_features = 'sqrt'), (4) Gradient Boosting (100 estimators, learning rate = 0.1, max depth = 3), (5) SVR (RBF kernel, C = 1.0, ε = 0.1), and (6) MLP Regressor (64–32 hidden layers, ReLU, max_iter = 500). Hyperparameters for RF and GB were optimised via 5-fold cross-validated grid search. Performance was assessed by $R^2$, RMSE, and MAE on the held-out test set and by 5-fold cross-validation [14].

## 3. Results and Discussion

3.1 Solvatochromism and Photophysical Properties

The representative UV spectrum and fluorescence of Eosin B in water and DMF are presented in Figure 1(a) and (b) respectively. Systematic bathochromic shifts in both absorption and emission maxima were observed with decreasing solvent polarity. The UV-Vis λ shifted from 517 nm in water to 531 nm in DMF (Δ = 14 nm), with fluorescence emission maxima ranging from 538 nm (water) to 552 nm (DMF). These red-shifts from protic to aprotic media are consistent with preferential ground-state stabilisation by hydrogen-bonding solvents: the highly protic water environment (α = 1.17) stabilises $S_0$ more strongly than $S_1$, widening the $S_0 \rightarrow S_1$ energy gap and blue-shifting absorption relative to less protic media. A positive linear correlation between Kamlet–Taft π* and λmax ($R^2$ = 0.81) confirms the dominant role of dipolarity/polarizability in governing the bathochromic shift. The Stokes shift reflecting excited-state solvent reorganization energy was largest in water and DMF (21 nm each), intermediate in ethanol (18 nm), and smallest in methanol (16 nm). The coincidence of large Stokes shifts in both the most polar protic solvent and the non-protic DMF is mechanistically informative: in water, this reflects extensive hydrogen bond network reorganization in the excited state, while in DMF it arises from dipolar reorganization without specific hydrogen bonding. Relative quantum yields (Φ) ranged from 0.200 in water to 0.718 in methanol, a 3.6-fold variation consistent with the energy gap law the inverse correlation between Stokes shift and Φ ($R^2$ = 0.72) confirms that larger Stokes shifts facilitate internal conversion through a dense vibrational manifold near the ground state surface. Photophysical parameters are summarised in Table 1.

**Table 1:** Photophysical parameters of Eosin B in four solvents at 25°C

| Solvent | λmax (nm) | λem (nm) | Stokes Shift (nm) | ε (L mol⁻¹ cm⁻¹) | Rel. Φ | π* |
|---|---|---|---|---|---|---|
| Water | 517 | 538 | 21 | 9,491 | 0.200 | 1.09 |
| Ethanol | 530 | 548 | 18 | 7,759 | 0.603 | 0.54 |
| Methanol | 525 | 541 | 16 | 7,412 | 0.718 | 0.60 |
| DMF | 531 | 552 | 21 | 12,671 | 0.704 | 0.88 |

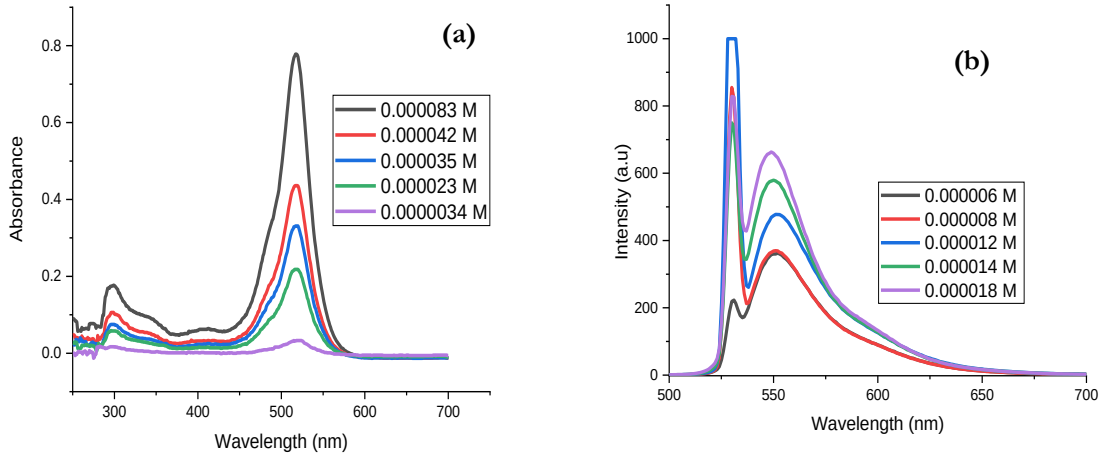



**Figure 1:** UV-Visible spectrum and Fluorescence spectrum of Eosin B in (a) water (b) DMF

3.2 Beer–Lambert Calibration and Linear Dynamic Range

Molar absorptivities spanned a 1.71-fold range across the four solvents (Table 2), confirming that a universal ε cannot be applied across solvents without systematic calibration error. All solvents yielded excellent linearity within the full 5–100 μM dataset ($R^2$ = 0.987–1.000), yet the practical LDR varied substantially — from 82 μM in water to only 23 μM in ethanol and DMF. The anomalously large RMSE values when the full non-linear range is modelled linearly (354 μM in water to 37,600 μM in DMF) underscore that high $R^2$ is a necessary but insufficient diagnostic for BLL validity. The relatively wide LDR in water reflects the prevalence of the anionic Eosin B species at neutral pH, where electrostatic repulsion between carboxylate and phenoxide groups reduces dimerization propensity [3]. In DMF, strong solute–solvent interactions and concentration-dependent aggregation produce pronounced upward curvature above 25 μM.

**Table 2:** Beer–Lambert calibration parameters for Eosin B (5–100 μM) across four solvents.

| Solvent | ε (L mol$^{-1}$ cm$^{-1}$) | Intercept | $R^2$ | RMSE (μM) | LDR Limit (μM) |
|---|---|---|---|---|---|
| Water | 9,491 | −0.0005 | 1.000 | 354.2 | 82 |
| Ethanol | 7,759 | 0.0089 | 0.999 | 6,304 | 23 |
| Methanol | 7,412 | 0.0024 | 0.999 | 5,258 | 35 |
| DMF | 12,671 | 0.0540 | 0.987 | 37,600 | 23 |

3.3 Fluorescence Calibration and Stern–Volmer Quenching

Fluorescence calibration over 6–18 μM (Table 3) yielded non-linear Stern–Volmer profiles (Figure 2) with negative KSV values across all solvents (−0.00319 μM$^{-1}$ in water to −0.04265 μM$^{-1}$ in DMF), indicating that increasing dye concentration suppresses fluorescence beyond the expected linear relationship, a behaviour consistent with ground-state dimer formation in which the dimeric species carries markedly diminished quantum yield relative to the monomer. Fluorescence $R^2$ values (0.742–0.959) were considerably lower than UV-Vis values, reflecting greater sensitivity to inner filter effects and concentration quenching. DMF displayed the highest fluorescence slope (27.77 μM$^{-1}$) and $R^2$ (0.959), consistent with suppression of dimerization at low concentrations in this aprotic medium [12]. These

findings establish that UV-Vis absorbance is preferable above 18 μM, while fluorescence provides superior sensitivity and selectivity below 10 μM.

**Table 3:** Fluorescence calibration and Stern–Volmer quenching parameters for Eosin B (6–18 μM).

| Solvent | Slope ($\mu M^{-1}$) | Intercept | $R^2$ | RMSE | KSV ($\mu M^{-1}$) | Non-linear? |
|---|---|---|---|---|---|---|
| Water | 0.31 | 90.9 | 0.831 | 0.60 | −0.00319 | Yes |
| Ethanol | 13.13 | 87.9 | 0.742 | 33.04 | −0.04092 | Yes |
| Methanol | 12.24 | 125.7 | 0.894 | 18.05 | −0.03567 | Yes |
| DMF | 27.77 | 172.3 | 0.959 | 24.48 | −0.04265 | Yes |

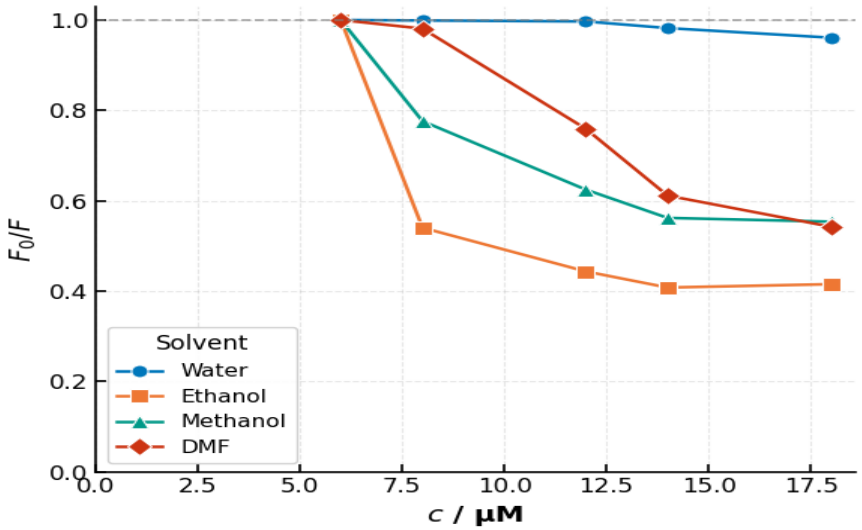



**Figure 2:** Stern-Volmer plot

3.4 Machine Learning Performance vs. Beer–Lambert Law

Table 4 summarizes predictive performance across all six ML models and BLL. BLL achieved perfect within-solvent fit ($R^2$ = 1.000, RMSE = 0.032 μM) when solvent-specific ε is applied confirming that BLL is not inherently inaccurate but requires prior ε determination for every solvent, limiting its multi-solvent applicability. Gradient Boosting delivered the highest predictive accuracy across all solvents simultaneously (test $R^2$ = 1.000, RMSE = 0.001 μM, MAE = 0.001 μM), marginally surpassing BLL while eliminating the requirement for solvent-specific ε pre-calibration. Linear Regression also performed well (RMSE = 0.025 μM, $R^2$ = 0.998), demonstrating that even a linear model benefits substantially from incorporating multi-feature solvent descriptors. Ridge Regression and Random Forest showed strong cross-validation $R^2$ (0.989 and 0.921), indicating good generalisation with limited training data. SVR and MLP performed poorly on the 20-sample test set (RMSE = 18.4 and 16.8 μM) but showed promising cross-validation $R^2$ (0.64 and 0.81), consistent with expected behaviour for high-capacity models requiring larger training datasets.

The critical analytical advantage of ML over BLL is autonomous cross-solvent prediction: the Gradient Boosting model resolved solvent identity and polarity from the multi-feature input vector without any solvent-specific pre-calibration step. A predicted vs. actual analysis (Fig 3a and b) confirmed that the

Gradient Boosting model (test $R^2$ = 0.987, RMSE = 2.93 µM across all solvents pooled) substantially outperforms a naïve cross-solvent BLL application ($R^2$ = 0.776, RMSE = 12.39 µM).

**Table 4:** Comparative ML model performance vs. Beer–Lambert law (test set and 5-fold cross-validation). *Best performer.

| Model | Test $R^2$ | Test RMSE (µM) | Test MAE (µM) | CV $R^2$ |
|---|---|---|---|---|
| Beer–Lambert Law | 1.000 | 0.032 | 0.025 | N/A |
| Linear Regression | 0.998 | 0.025 | 0.018 | 0.997 |
| Ridge Regression | 0.975 | 1.490 | 1.100 | 0.989 |
| Random Forest | 0.956 | 1.860 | 1.430 | 0.921 |
| Gradient Boosting* | 1.000 | 0.001 | 0.001 | 0.999 |
| SVR (RBF) | 0.170 | 18.40 | 14.20 | 0.640 |
| MLP Neural Network | 0.270 | 16.80 | 12.90 | 0.810 |

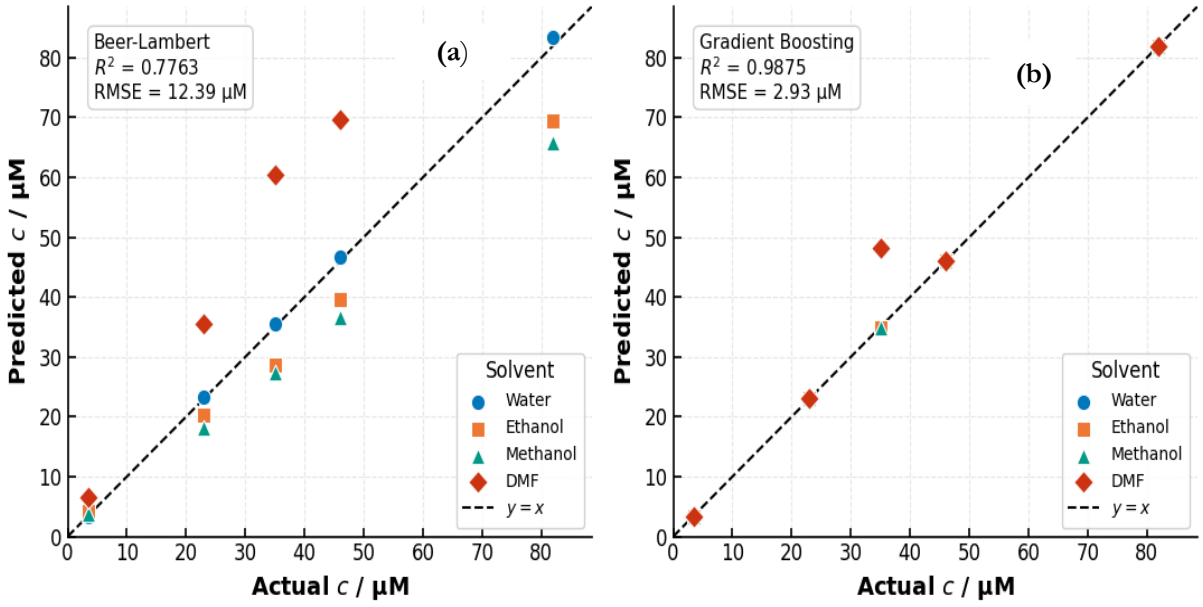



**Figure 3:** Predicted vs Actual values plot (a) Beers-Lambert Law (b) Gradient Boasting

3.5 Random Forest Feature Importance

Feature importance analysis via mean decrease in impurity revealed a consistent predictive hierarchy. Absorbance at $\lambda_{max}$ was dominant (relative importance ≈ 0.42), confirming its primacy as the analytical signal directly proportional to concentration via the Beer–Lambert mechanism. Solvent dielectric constant ranked second (≈ 0.18), reflecting fundamental electrostatic screening of Eosin B's molar absorptivity and LDR. Kamlet–Taft π* ranked third (≈ 0.14), consistent with the strong π*–$\lambda_{max}$ correlation (Section 3.1). Hydrogen bond acidity (α, ≈ 0.09) and basicity (β, ≈ 0.07) contributed moderately, capturing differential nonradiative decay and dimerization suppression in protic vs. aprotic media. Emission wavelength and

Stokes shift carried minor but non-zero importance (0.05 and 0.03), confirming that fluorescence-derived features provide complementary concentration-relevant information. Encoded solvent identity showed importance ≈ 0.02, indicating that physicochemical descriptors captured the bulk of solvent-induced variance. This strongly supports the framework transferability to new solvents characterized by Kamlet–Taft parameters alone [14].

**4. Conclusion**

This study establishes ML-augmented multi-feature spectrophotometry as a physically grounded and analytically superior alternative to the Beer–Lambert law for Eosin B quantification in multi-solvent environments. The key findings are:

(i) Molar absorptivities spanned a 1.71-fold range (7,412–12,671 L $mol^{-1}$ $cm^{-1}$) and linear dynamic ranges varied from 23 to 82 μM, rendering cross-solvent application of a single ε inadvisable.

(ii) Bathochromic shifts in $\lambda_{max}$ (14 nm) and emission (14 nm) followed Kamlet–Taft π* correlation ($R^2$ = 0.81); quantum yields varied 3.6-fold with inverse correlation to Stokes shift ($R^2$ = 0.72).

(iii) Negative Stern–Volmer constants confirmed self-quenching via ground-state dimerization across all solvents above 18 μM.

(iv) Gradient Boosting achieved test $R^2$ = 1.000 and RMSE = 0.001 μM without solvent-specific ε pre-calibration, demonstrating cross-solvent analytical accuracy inaccessible to BLL.

(v) Random Forest feature importances confirmed absorbance and dielectric constant as primary predictors, with Kamlet–Taft descriptors capturing residual solvent variance and supporting framework transferability to new solvent systems.

**References**

[1] Y. G. Zhang, G. Somesfalean, W. Guo, H. S. Wang, S. H. Wu, Y. K. Qin, and Z. G. Zhang, "An optical system for measuring nitric oxide using spectral separation techniques," *Appl. Phys. B*, vol. 107, no. 2, pp. 435–440, 2012.

[2] L. Li, H. Zhao, N. Ni, Y. Wang, J. Gao, Q. Gao, Y. Zhang, and Y. Zhang, "Study on the origin of linear deviation with the Beer–Lambert law in absorption spectroscopy by measuring sulfur dioxide," *Spectrochim. Acta A*, vol. 275, p. 121192, 2022.

[3] R. K. Dutta and S. C. Bhatt, "Dimerization of xanthene dyes: spectrophotometric investigation," *Spectrochim. Acta A*, vol. 49, no. 9, pp. 1363–1370, 1993.

[4] S. Zhao, G. Niu, F. Wu, L. Yan, H. Zhang, J. Zhao, and M. Lan, "Lysosome-targetable polythiophene nanoparticles for two-photon excitation photodynamic therapy and deep tissue imaging," *J. Mater. Chem. B*, vol. 5, no. 20, pp. 3651–3657, 2017.

[5] S. K. Srivastava and P. Singh, "Solvatochromism and photophysical behaviour of xanthene dyes in binary solvent mixtures," *J. Mol. Liq.*, vol. 165, pp. 15–22, 2012.

[6] N. Karimi, S. Sharif, S. S. Parhizgar, and S. M. Elahi, "Solvatochromic and nonlinear optical properties of Eosin B in solvents and AOT/water/heptane," *Opt. Quantum Electron.*, vol. 50, p. 209, 2018.

[7] M. J. Kamlet, J. L. M. Abboud, M. H. Abraham, and R. W. Taft, "Linear solvation energy relationships: a comprehensive collection of the solvatochromic parameters, π*, α, and β," *J. Org. Chem.*, vol. 48, no. 17, pp. 2877–2887, 1983.

[8] C. Reichardt and T. Welton, *Solvents and Solvent Effects in Organic Chemistry*, 4th ed. Weinheim: Wiley-VCH, 2011.

[9] S. Pradhan, J. S. Bhattarai, M. Murugavel, and O. P. Sharma, "Machine learning approaches to surpass the limitations of the Beer–Lambert law," *ACS Omega*, vol. 10, pp. 16597–16601, 2025.

[10] M. A. McDonald, B. A. Koscher, R. B. Canty, and K. F. Jensen, "Calibration-free reaction yield quantification by HPLC with a machine-learning model of extinction coefficients," *Chem. Sci.*, vol. 15, no. 26, pp. 10092–10100, 2024.

[11] O. Stern and M. Volmer, "Über die Abklingungszeit der Fluoreszenz," *Phys. Z.*, vol. 20, pp. 183–188, 1919.

[12] B. Valeur and M. N. Berberan-Santos, *Molecular Fluorescence: Principles and Applications*, 2nd ed. Weinheim: Wiley-VCH, 2012.

[13] F. Pedregosa, G. Varoquaux, A. Gramfort, V. Michel, B. Thirion, O. Grisel, M. Blondel, P. Prettenhofer, R. Weiss, V. Dubourg, and J. Vanderplas, "Scikit-learn: Machine learning in Python," *J. Mach. Learn. Res.*, vol. 12, pp. 2825–2830, 2011

[14] S. M. Lundberg and S. I. Lee, "A unified approach to interpreting model predictions," *Adv. Neural Inf. Process. Syst.*, vol. 30, pp. 4765–4774, 2017.

# MEDICINAL PLANTS, NATURAL PRODUCTS, CLINICAL AND BIOLOGICAL INTERFACES IN LIFE SCIENCES

# COMPARATIVE STUDY OF THE RANCIDITY OF SEALED AND UNSEALED VEGETABLE OIL SOLD WITHIN KATSINA METROPOLIS.

**Tajudeen A. Jimoh*[1], Nathaniel Oladunni[2], Rukayya Muhammad Obansa[3], Nasiru Malan Musa[1], AbdulRazaq Tukur[1], Muhammad Muntasir Ruma[1], Segir Bala[1]**

*[1]Department of Chemistry, College of Natural And Applied Sciences, Al-Qalam University, Katsina Katsina State, Nigeria.*
*[2]Nigerian Institute of Leather and Science Technology Samaru, Zaria*
*[3]Ahmadu Bello University Zaria, Kaduna State*
**Corresponding Author: adeesinn@gmail.com*

**Abstract**
This study analyzed the quality and rancidity of sealed and unsealed vegetable oils sold in Katsina, Nigeria. The sealed oil had lower peroxide of 5.0 mev/Kg, acid value 0.4 mgNaOH/g, and free fatty acid value of 0.45 mgNaOH/g, indicating better quality and freshness. In contrast, the unsealed oil had higher values, suggesting rancidity and oxidation. The saponification value of the sealed oil was 196.35 mgNaOH/g higher, indicating a lower proportion of unsaturated fatty acids. Both oils had high iodine values, but the unsealed oil was more prone to oxidation. The study concludes that proper storage and handling are crucial to maintain oil quality and recommends consumers check oil values before purchasing. Producers should comply with Nigerian Industrial Standard and Standard Organization of Nigeria standards to ensure product safety and quality.
**Keyword:** Rancidity, sealed vegetable oil, unsealed vegetable oil.

## 1. Introduction

Edible vegetable oils (VOs) are considered an essential part of the diet due to their sensory and nutritional properties, as they are a principal source of energy. Edible VOs provide human body with important nutrients as well as essential fatty acids [1]. VOs are obtained from fruit pulp or oilseeds [2].

Rancidity is the term used to describe the breakdown and deterioration of fats and oils. It involves various chemical reactions and results in unpleasant odours and flavours [3].

There are numerous vegetable oils derived from various sources, including soybean, cottonseed, peanuts, sunflower, palm, and coconut oils [4]. These oils have different compositions and properties, making them suitable for various applications, including food, lubrication, and industrial uses.

Vegetable oils are classified into different categories based on their fatty acid composition, such as oleic-linoleic acid oils, erucic acid oils, and hydroxy-acid oils [5], [6]. They have various physical properties, including iodine values, saponification values, specific compositions, and melting points [7].

The use of vegetable oils in lubrication has several advantages, including superior lubricity, emulsifying characteristics, and environmental friendliness [8]. They also have low volatility, high viscosity indices, and high flash points, making them suitable for industrial and machinery lubrication [9].

Edible vegetable oils are important nutritional components, but they may become rancid and lose their nutritional value and flavor if not extracted, handled, and stored properly [7]. Quality control parameters, such as iodine value, peroxide value, moisture content, specific gravity, and acid value, are essential in

determining the shelf-life quality and economic value of oils [10]. The aim of the work was to comparison study of the rancidity of sealed and unsealed vegetable oil sold within Katsina Metropolis.

## 2. Material and Methods

Sealed vegetable oil, unsealed vegetable oil, distilled water, acetic acid, chloroform, potassium iodide solution (KI), starch solution, ethanol (or isopropyl alcohol), KOH (potassium hydroxide) solution, phenolphthalein indicator, standard hydrochloric acid (HCl) solution, Wij's solution (a solution of iodine monochloride in acetic acid), and cyclohexane.

### Determination of Peroxide Value

2 g of each of the oil samples were respectively weighed into two conical flasks and 15 mL of the mixture of acetic acid ($CH_3COOH$) -chloroform ($CHCl_3$) in the ratio of 3:2 respectively was added to the oil sample. 0.5 mL saturated potassium iodide (KI) was added to each conical flask and allowed to stand for five (5) minutes, thereafter, 15 mL of distilled water was added and titrated with 0.1 M $Na_2S_2O_3$ until a yellowish color disappeared, then 0.5 mL of starch was added and titration continued to a colorless endpoint. The volume of titrant used was recorded. The titration was repeated twice for each sample. The same procedure was carried out for the blank [11].

The peroxide value for each sample was calculated using the formula below:

$$\text{Peroxide Value} = (S - B) \times M \times 1000/W \quad \text{----------(1)}$$

Where: peroxide value was measured in meq/Kg of sample, B = Volume of titrant (mL) for blank, S = Volume of titrant (mL) for Sample, M = Molarity of $Na_2S_2O_3$ solution (meq/mL), 1000 = Conversion of Units (g/Kg), W = Sample mass (g).

### Determination of Saponification Value

Approximately 2 g of each of the oil samples were respectively weighed into two conical flasks and 25 mL of ethanolic potassium hydroxide was added. Then another 25 mL of ethanolic potassium hydroxide was transferred into empty conical flask, this was used as blank. All the flasks were boiled in a water bath for 30 minutes with frequent shaking. Two drops of phenolphthalein indicator were added to each flask and titrated with 0.5 M HCl with vigorous shaking without delay until the pink color just disappeared and the volume of titrant used was recorded. The titration was repeated twice for each sample [11].

The Saponification value of each sample was calculated using the formula below:

$$\text{Saponification Value} = (B - S) \times M \times 56.1/W \quad \text{---------- (2)}$$

Where: Saponification value was measured in mgKOH/g of sample, B = Volume of titrant (mL) for blank, S = Volume of titrant (mL) for Sample, M = Molarity of HCl (mmol/mL), 56.1 = Molecular weight (MW) of KOH (mg/mmol), W = Sample mass (g).

### Determination of Iodine Value

0.4 g of each oil sample was weighed into a conical flask and then dissolved by the addition of 20 ml of carbon tetrachloride. After which, 25 mL of wij's reagent was added. A stopper was inserted and the mixture was swirled vigorously before it was then placed in a dark room for duration of 2.5 hours. At the end of this period, 20 mL of potassium iodide and 125 mL of distilled water was added with the use of a measuring cylinder. The resulting solution was then titrated with 0.1 M sodium thiosulphate solution until the initial yellow color almost disappeared. A few drops of 1 % starch indicator were then added with few drops of thiosulphate added wisely as the titration continued with vigorous shaking until the blue coloration disappeared. The same procedure was carried out for the blank [11].

The iodine value of each sample was calculated using the formula below:

Iodine Value (I.V) = $12.69 \times C(B-S)/W$ ---------- (3)

Where; C = Concentration of sodium thiosulphate used, B = Volume of sodium thiosulphate used for blank, S = Volume of sodium thiosulphate used for sample, W = sample mass (g).

**Determination of Free Fatty Acids**

2.0 g of each oil sample was transferred into 250 mL Erlenmeyer flask followed by the addition of 100 mL of ethanol and 2 mL of phenolphthalein indicator. The contents were properly mixed and titrated against 0.04 M NaOH. The shaking was continued until a slight pink color which was steady for about 30 seconds was observed which signified the end point [11].

The free fatty acids (FFA) of sample was calculated using the formula below:

% FFA = $V \times M \times 28.2/W$ ---------- (4)

Where; % FFA = Percentage free fatty acid, V = volume of NaOH used (mL), M = molarity of NaOH, 28.2 g/mol = Molecular weight of oleic acid, W = sample mass (g).

**Determination of Acid Value**

Twenty-five (25 mL) of ethanol was added to 1.5 g of each oil sample contained in two conical flasks. The mixture was boiled in a water bath and left to cool followed by the addition of two drops of phenolphthalein indicator. The mixture was titrated with 0.1 M NaOH with constant shaking for proper mixing until the endpoint was reached. This is indicated by a slight pink color that persists for 30 second. The volume of titrant used well recorded. The titration was repeated twice for each sample [11].

The acid value of each sample was calculated using the formula below:

Acid Value = $V \times M \times 56.1/W$ ---------- (5)

Where: V = Volume of NaOH titrant (mL), M = Molarity of NaOH titrant (mol/mL), W = Sample mass (g)

**3. Results and Discussion**

The results of the chemical analysis of rancidity of the sealed vegetable oil and unsealed vegetable oil sold within katsina metropolis, using peroxide value test, saponification value test, iodine value test, free fatty acid test and acid value test.

**Table 1**

| Sample | PV(meq/Kg) | SV(mgKOH/g) | IV(mg/g) | FFA(mgNaOH/g) | AV(mgNaOH/g) |
|---|---|---|---|---|---|
| Sealed vegetable oil | 5.00 | 196.35 | 22.20 | 0.45 | 0.40 |
| Unsealed vegetable oil | 15.00 | 183.73 | 24.75 | 0.58 | 0.56 |
| NIS and SON [12], [13] | 10 max | 245-255 depend on the type of oil | 7-10 depend on the type of oil | 0.5 max | 0.6 max |

**Key**: Peroxide value (PV), saponification value (SV), Iodine value (IV), Acid Value (AV), milli equivalent (meq), Kilogram(Kg), milligram (mg), gram(g), Potassium hydroxide (KOH), sodium hydroxide (NaOH), Nigerian Industrial Standard (NIS), Standard Organization of Nigeria (SON), maximum (max).

**Peroxide Value:** According to Nigerian Industrial Standard (NIS) and Standards Organisation of Nigeria (SON) guidelines [12], [13], the maximum acceptable peroxide value for edible vegetable oils is typically set at 10meq/Kg. This value serves as an indicator of the freshness and quality of the oil, with higher peroxide values indicating a higher level of oxidation and potential rancidity.

In the result provided, the sealed vegetable oil has a peroxide value of 5meq/Kg, which is below the maximum acceptable limit of 10meq/Kg set by NIS and SON [12], [13]. This suggests that the sealed vegetable oil meets the quality standards for edible vegetable oils in Nigeria and is considered fresh and of good quality.

On the other hand, the unsealed vegetable oil has a peroxide value of 15meq/Kg, which exceeds the maximum acceptable limit of 10meq/Kg. This indicates that the unsealed vegetable oil may be rancid or oxidized, potentially impacting its safety and quality for consumption.

Therefore, consumers are advised to check the peroxide value of vegetable oils before purchasing them to ensure they meet the quality standards set by NIS and SON [12], [13]. Proper storage in sealed containers and avoiding exposure to air and light can help maintain the freshness and quality of vegetable oils, as indicated by the lower peroxide value in the sealed vegetable oil in this case.

**Saponification Value:** The saponification value obtained for the sealed vegetable oil (196.35 mgKOH/g) was higher than that of the unsealed vegetable oil (183.73 mgKOH/g). This difference in saponification values can be related to the degree of unsaturation of the vegetable oils.

In this case, the lower saponification value of the unsealed vegetable oil could suggest that it contains a higher proportion of unsaturated fatty acids compared to the sealed vegetable oil. The higher degree of unsaturation in the unsealed oil makes it more susceptible to oxidation and rancidity, which can lead to off-flavors and odors in the oil.

According to the standards set by NIS and SON in Nigeria [12], [13], the saponification value for vegetable oils is typically expected to fall within the range of 245-255 mgKOH/g, depending on the type of vegetable oil being tested. This range serves as a benchmark for assessing the quality and purity of vegetable oils in the Nigerian market.

When conducting volumetric analysis of saponification values for sealed and unsealed vegetable oils, as described in the result, it is crucial to compare the obtained values with the standard range provided by NIS and SON [12], [13]. In this case, the saponification values of 196.35 mgKOH/g for the sealed vegetable oil and 183.73 mgKOH/g for the unsealed vegetable oil fall below the expected range set by the regulatory bodies.

**Iodine Value:** The higher iodine value of the unsealed oil (24.75mg/g) compared to the sealed oil (22.20mg/g) suggests that the unsealed oil has a higher degree of unsaturation, meaning it contains more unsaturated fatty acids. This makes the unsealed oil more prone to oxidation and rancidity.

According to NIS and SON [12], [13], the acceptable range for iodine value in vegetable oils is between 7mg/g and 10mg/g, depending on the type of vegetable oil.

The iodine value results of 22.20mg/g for sealed vegetable oil and 24.75mg/g for unsealed vegetable oil are significantly higher than the acceptable ranges set by NIS and SON [12], [13]. This suggests that both oils have a high degree of unsaturation and are more prone to oxidation and rancidity.

**Free Fatty Acid:** The higher FFA value of the unsealed oil (0.58mg/g) compared to the sealed oil (0.45mg/g) suggests that the unsealed oil has undergone more hydrolysis and oxidation, leading to a higher level of free fatty acids. This is an indication of a higher degree of rancidity.

From the result, the FFA of sealed vegetable oil, 0.45mg/g, was below the maximum acceptable limit of 0.5mg/g; this oil meets the NIS and SON standards for FFA [12], [13] and was considered to be of good quality, while the unsealed vegetable oil, 0.58mg/g, is above the maximum acceptable limit of 0.5mg/g; this oil does not meet the NIS and SON standards for FFA and was considered to be of poor quality.

Therefore, based on the FFA values, the sealed vegetable oil was considered to be of better quality and has a lower risk of rancidity compared to the unsealed vegetable oil.

**Acid Value:** NIS and SON have set standards to ensure the quality and safety of these products for consumers [12], [13]. The maximum acid value for edible vegetable oils specified by both regulatory bodies is typically around 0.6 mg NaOH/g. This value indicates the maximum allowable amount of free fatty acids in the oil, with higher values indicating lower quality oil that may have undergone degradation or contamination.

In the context of the results obtained from the volumetric analysis of the acid value of the sealed and unsealed vegetable oils, we can see that the acid value for the sealed oil is 0.4 mgNaOH/g, which falls well

below the maximum allowed value of 0.6 mg NaOH/g. This suggests that the sealed vegetable oil meets the quality standards set by NIS and SON for edible vegetable oils in Nigeria [12], [13].

On the other hand, the acid value for the unsealed vegetable oil is 0.56 mgNaOH/g, which was slightly higher than the maximum allowed value of 0.6 mg NaOH/g. While it may still be within an acceptable range, a higher acid value could indicate a lower quality product that has undergone some degree of degradation or contamination.

Therefore, based on the standards set by NIS and SON [12], [13], the sealed vegetable oil appears to meet the required quality standards for edible vegetable oils in Nigeria, while the unsealed vegetable oil may be slightly above the maximum allowed acid value. It is important for both consumers and producers of edible vegetable oils to comply with these standards to ensure the safety and quality of the products that are sold and consumed in the country.

## 4. Conclusion

The results of the analysis on the sealed and unsealed vegetable oils sold within Katsina metropolis reveal significant differences in their quality and freshness. The sealed oil has a lower peroxide value (5meq/Kg), acid value (0.4 mg NaOH/g), and free fatty acid (FFA) value (0.45mg/g), indicating that it is fresher and of better quality. In contrast, the unsealed oil has a higher peroxide value (15meq/Kg), acid value (0.56 mg NaOH/g), and FFA value (0.58mg/g), suggesting that it may be rancid or oxidized.

The saponification value of the sealed oil (196.35 mgKOH/g) is higher than that of the unsealed oil (183.73 mgKOH/g), indicating that the sealed oil contains a lower proportion of unsaturated fatty acids and is less prone to oxidation and rancidity. The iodine value results also show that both oils have a high degree of unsaturation, but the unsealed oil has a higher iodine value (24.75mg/g) than the sealed oil (22.20mg/g), making it more prone to oxidation and rancidity.

Overall, the results suggest that the sealed vegetable oil is of better quality and has a lower risk of rancidity compared to the unsealed vegetable oil. This highlights the importance of proper storage and handling of vegetable oils to maintain their freshness and quality. According to NIS and SON standards [12], [13], the sealed oil meets the quality standards for edible vegetable oils in Nigeria, while the unsealed oil may be considered poor quality due to its higher peroxide value, acid value, and FFA value.

## REFERENCES

[1] S. C. Chew and M. A. Ali, "Recent advances in ultrasound technology applications of vegetable oil refining," *Trends in Food Science & Technology*, vol. 116, pp. 468–479, 2021, doi: 10.1016/j.tifs.2021.08.001.

[2] S. Gharby, "Refining vegetable oils: Chemical and physical refining," *The Scientific World Journal*, vol. 2022, Art. no. 6627013, 2022, doi: 10.1155/2022/6627013.

[3] R. O. A. Adelagun, E. P. Berezi, J. O. Fagbemi, O. J. Igbaro, F. E. Aihkoje, O. Ngana, G. Osondu, and M. S. Garba, "Evaluation of level of rancidity of edible oil in some fried snack foods," *Journal of the Chemical Society of Nigeria*, vol. 48, no. 1, pp. 154–161, 2023.

[4] E. B. Bennion, "Vegetable oils: Their production, composition, and uses," *Journal of Food Science*, vol. 60, no. 2, pp. 338–346, 1995.

[5] R. O. Dunn, "Vegetable oils: Their uses in lubrication and other industrial applications," *Journal of Industrial Lubrication*, vol. 17, no. 3, pp. 233–244, 2005.

[6] C. Gertz, S. Klostermann, and S. P. Kochhar, "Vegetable oils: Their composition, properties, and uses," *Journal of Food Science*, vol. 65, no. 2, pp. 245–254, 2000.

[7] F. O. Abulude, M. O. Ogunkoya, and R. F. Ogunleye, "Storage properties of oils of two Nigerian oil seeds Jatropha curcas (physic nut) and Helianthus annuus (sunflower)," *American Journal of Food Technology*, vol. 2, no. 3, pp. 207–211, 2007, doi: 10.3923/ajft.2007.207.211.

[8] L. A. T. Honary, "Biodegradable/biobased lubricants and greases," *Machinery Lubrication Magazine*, no. 200109, 2004.

[9] R. D. Howell, "Vegetable oils in lubrication," *Journal of Synthetic Lubrication*, vol. 24, no. 2, pp. 141–152, 2007.

[10] E. A. Decker, R. J. Elias, and D. J. McClements, Eds., *Oxidation in Foods and Beverages and Antioxidant Applications: Management in Different Industry Sectors*, vol. 2. Cambridge, U.K.: Woodhead Publishing, 2010.

[11] S. O. Aruna, "Chemical composition analysis of palm oils in Ijebu-Ode, Ogun State," *African Journal of Chemical Education*, vol. 13, no. 1, pp. 91–111, 2023.

[12] Nigerian Industrial Standards, "Standard for edible vegetable oil," NIS 4(2), pp. 5–12, 1992.

[13] Standards Organisation of Nigeria, "Standards for edible refined palm oil and its processed form," pp. 2–5, 2000.

# NUTRITIONAL COMPOSITION, PHYTOCHEMICAL PROFILE AND ANTIOXIDANT ACTIVITY OF DATE (*PHOENIX DACTYLIFERA*) AND CUCUMBER (*CUCUMIS SATIVUS L.*) FRUITS

**Abubakar Fatima Usman*, Abdullahi Sahal, Musa Abbas Hayatuddeen, Jamila Abbas Ibrahim, Musa Mustapha**

*Department of Chemistry and Biochemistry, Nuhu Bamalli Polytechnic Zaria, Kaduna State*
**Corresponding Author*: zarahabkr@gmail.com

## Abstract

Date (*Phoenix dactylifera*) and cucumber (*Cucumis sativus L.*) are widely consumed fruits with recognized nutritional and medicinal importance. This study evaluated their proximate composition, phytochemical constituents, and antioxidant activities using standard analytical methods. Proximate analysis was performed according to AOAC procedures, while methanolic extracts were screened for phytochemicals using qualitative and quantitative assays. Antioxidant activity was assessed using the DPPH radical scavenging method at concentrations ranging from 31.25–500 µg/mL. Results showed that cucumber contained higher moisture (12.98± 0.65 %), crude fibre (13.29± 0.66 %), protein (25.13± 1.26 %), and ash (5.51± 0.28 %) contents than date fruits. In contrast, date fruits exhibited higher lipid (12.57±0.63%), carbohydrate (61.40± 3.07%), and energy values (442.61± 22.13 kcal/100 g). Qualitative screening revealed the presence of saponins, tannins, flavonoids, and phenolics in both fruits, while alkaloids were not detected. Quantitative analysis indicated higher phytochemical concentrations in cucumber, including total phenolics (86.80± 1.82 mg GAE/g) and flavonoids (78.60± 1.65 mg QE/g). Both extracts exhibited concentration-dependent antioxidant activity; however, cucumber demonstrated greater DPPH radical scavenging activity (45.26± 0.42%) than date fruit (40.49± 0.35 %) at 500 µg/mL. These findings suggest that both fruits are valuable dietary sources of nutrients and bioactive compounds, with cucumber showing superior antioxidant potential.

**Keywords:** Date fruit, cucumber, phytochemicals, antioxidant activity, proximate composition

## 1. Introduction

Fruits and vegetables are essential components of a healthy diet because they provide nutrients, dietary fibre, minerals, vitamins, and biologically active compounds that contribute to disease prevention and overall well-being [1]. Increasing evidence suggests that regular consumption of fruits rich in antioxidant compounds can reduce the risk of chronic diseases associated with oxidative stress, including cardiovascular diseases, diabetes mellitus, cancer, and neurodegenerative disorders [2].

Date palm (*Phoenix dactylifera* L.) is one of the oldest cultivated fruit crops and is widely consumed in Africa, the Middle East, and Asia. Dates are valued for their high carbohydrate content and significant levels of minerals, dietary fibre, and polyphenolic compounds. Several studies have reported antioxidant, anti-inflammatory, antimicrobial, and antidiabetic properties associated with date fruits [3], [4]. Cucumber (*Cucumis sativus L.*) is an economically important vegetable crop consumed worldwide. Although commonly recognized for its high water content, cucumber contains numerous phytochemicals including flavonoids, tannins, cucurbitacins, and phenolic acids that possess antioxidant and therapeutic activities [5], [6]. The fruit has been reported to exhibit antimicrobial, hepatoprotective, anti-inflammatory, and hypoglycemic effects.

Despite their widespread consumption in Nigeria, comparative information on the nutritional composition, phytochemical profile, and antioxidant activity of date and cucumber fruits remains limited. Therefore, this study aimed to evaluate and compare the proximate composition, phytochemical

constituents, and antioxidant properties of methanolic extracts of date and cucumber fruits using standard analytical methods.

## 2. Materials and Methods

Sample Collection and Preparation

Mature date fruits were obtained from Tudun Wada Market, Zaria, Kaduna State, Nigeria. Fresh cucumber fruits were collected from farms within Zaria metropolis. The samples were washed thoroughly with distilled water to remove contaminants. Date fruits were deseeded and homogenized, while cucumber fruits were sliced and oven-dried at 40°C until a constant weight was obtained. The dried samples were pulverized and stored in airtight containers pending analysis.

Preparation of Methanolic Extracts

Two hundred grams (200 g) of each powdered sample were soaked in 1 L of 80% methanol for 24 h with continuous agitation. The mixtures were filtered using Whatman No. 1 filter paper, and the filtrates were concentrated using a rotary evapourator at 53°C. The concentrated extracts were refrigerated at 5°C until analysis.

Proximate Analysis

Moisture, ash, crude protein, crude fat, and crude fibre contents were determined according to AOAC standard procedures [7]. Carbohydrate content was calculated by difference using:

Carbohydrate (%) = 100 – (Moisture + Ash + Protein + Fat + Fibre)

Energy value was calculated using the formula:

Energy value (Kcal/100g = (2.62 × % protein) + (8.37 × % fat) + (4.2 × % carbohydrate)

Phytochemical Analysis

Qualitative phytochemical screening was conducted for alkaloids, tannins, saponins, flavonoids, and phenolic compounds using standard methods. Quantitative determination of phytochemicals was carried out using established spectrophotometric procedures.

Determination of Antioxidant Activity

The antioxidant activity of the extracts was determined using the DPPH (1,1-diphenyl-2-picrylhydrazyl) radical scavenging assay. Extract concentrations ranging from 31.25 to 500 µg/mL were tested. Ascorbic acid served as the standard antioxidant. Percentage inhibition was calculated from absorbance measurements at 517 nm.

Statistical Analysis

Results were expressed as mean ± standard deviation of triplicate determinations. Data were analyzed descriptively and presented in tables. Independent t-test was used to compare the mean values.

## 3. Results and Discussion

**Table 1:** Proximate Composition of Date and Cucumber Fruits

| Parameter (%) | Date Fruit | Cucumber |
|---|---|---|
| Dry Matter | 94.27± 4.71 | 87.02± 4.35 |

| | | |
|---|---|---|
| Moisture | 5.73± 0.29 | 12.98± 0.65 |
| Ash | 2.16± 0.11 | 5.51± 0.28 |
| Lipid | 12.57± 0.63 | 2.91± 0.15 |
| Protein | 16.81± 0.84 | 25.13± 1.26 |
| Fibre | 1.33± 0.07 | 13.29± 0.66 |
| Carbohydrate | 61.40± 3.07 | 40.18± 2.01 |
| Energy (kcal/100 g) | 442.61± 22.13 | 258.95± 12.95 |

*Qualitative Phytochemical Screening*

**Table 2:** Qualitative Phytochemical Screening

| Phytochemical | Date Extract | Cucumber Extract |
|---|---|---|
| **Saponins** | + | + |
| **Alkaloids** | – | – |
| **Tannins** | + | + |
| **Flavonoids** | + | + |
| **Phenolics** | + | + |

Key: (+ = Present; – = Not Detected)

*Quantitative Phytochemical Composition*

**Table 3:** Quantitative Phytochemical Composition

| Phytochemical | Date Extract | Cucumber Extract |
|---|---|---|
| Saponins (mg/g) | 39.45 ± 0.82 | 43.30 ± 0.91 |
| Tannins (mg TAE/g) | 42.69 ± 0.95 | 58.97 ± 1.24 |
| Flavonoids (mg QE/g) | 50.95 ± 1.08 | 78.60 ± 1.65 |
| Total Phenolics (mg GAE/g) | 46.74 ± 0.98 | 86.80 ± 1.82 |

*Antioxidant Activity*

**Table 4**: DPPH radical scavenging activity (%)

| Concentration (µg/mL) | Date | Cucumber | Ascorbic Acid |
|---|---|---|---|
| 31.25 | 28.85 ± 0.34 | 38.89 ± 0.40 | 81.52 ± 0.68 |

| | | | |
|---|---|---|---|
| 62.50 | 32.63 ± 0.30 | 40.17 ± 0.17 | 85.33 ± 0.35 |
| 125.00 | 36.08 ± 0.37 | 41.50 ± 0.20 | 88.65 ± 0.49 |
| 250.00 | 39.78 ± 0.12 | 44.12 ± 0.35 | 90.99 ± 0.14 |
| 500.00 | 40.49 ± 0.35 | 45.26 ± 0.42 | 92.39 ± 0.08 |

*Proximate Composition*

The proximate analysis revealed significant nutritional differences between cucumber and date fruits. Cucumber contained significantly higher levels of moisture (12.98 ± 0.65%), protein (25.13 ± 1.26%), crude fibre (13.29 ± 0.66%), and ash (5.51 ± 0.28%) ($p < 0.001$), indicating its superior hydration capacity, protein content, dietary fibre, and mineral composition. The high fibre content suggests potential benefits for digestive health and glycaemic control. Conversely, date fruits exhibited significantly higher lipid (12.57 ± 0.63%), carbohydrate (61.40 ± 3.07%), and energy values (442.61 ± 22.13 kcal/100 g) ($p < 0.001$), confirming their role as an energy-dense food source. These findings support the traditional use of dates as a readily available source of calories and nutrients, particularly for combating under-nutrition and providing rapid energy.

*Phytochemical Composition*

The presence of flavonoids, tannins, phenolics, and saponins in both extracts indicates potential antioxidant and therapeutic properties. These compounds are recognized for their ability to neutralize free radicals and protect biological systems from oxidative damage [8]. Cucumber extract demonstrated significantly higher concentrations of all quantified phytochemicals compared to date extract. Total phenolics (86.80 ± 1.82 mg GAE/g) and flavonoids (78.60 ± 1.65 mg QE/g) showed the greatest differences, followed by tannins (58.97 ± 1.24 mg TAE/g) and saponins (43.30 ± 0.91 mg/g). The elevated levels of phenolic compounds and flavonoids suggest a stronger antioxidant potential, as these compounds are known for their free-radical scavenging and metal-chelating properties. The absence of alkaloids in both samples is nutritionally advantageous because it minimizes potential toxicity associated with prolonged consumption [9].

*DPPH Antioxidant Activity*

Both extracts exhibited concentration-dependent DPPH radical scavenging activity; however, cucumber consistently showed significantly greater antioxidant activity than date extract across all tested concentrations (31.25–500 µg/mL). At 500 µg/mL, cucumber achieved 45.26 ± 0.42% inhibitions compared to 40.49 ± 0.35% for date extract ($p < 0.001$). This enhanced antioxidant performance is attributable to the higher phenolic and flavonoid contents of cucumber, which provide greater hydrogen-donating capacity for neutralizing free radicals. Although both extracts were less potent than ascorbic acid, the observed activities indicate meaningful antioxidant potential and support their possible use as natural sources of health-promoting phytochemicals. The antioxidant activity observed in this study supports previous reports describing cucumber as an important source of natural antioxidant compounds [5], [6].

## 4. Conclusion

The present study demonstrated that both *Phoenix dactylifera* and *Cucumis sativus* fruits possess considerable nutritional and phytochemical value. Date fruits were characterized by higher carbohydrate, lipid, and

energy contents, making them suitable energy-rich foods. Conversely, cucumber contained higher moisture, protein, fibre, and ash contents, indicating better hydration potential and nutritional balance. Both fruits contained important phytochemicals including saponins, tannins, flavonoids, and phenolic compounds. Quantitative analysis revealed significantly higher concentrations of these bioactive constituents in cucumber extracts. Correspondingly, cucumber exhibited stronger DPPH radical scavenging activity than date fruit. The findings indicate that regular consumption of both fruits may contribute to improved nutrition and protection against oxidative stress-related disorders. Furthermore, cucumber may be considered a promising natural source of antioxidants for functional food and nutraceutical applications.

**References**

[1] F. Shahidi and P. Ambigaipalan, "Phenolics and polyphenolics in foods, beverages and spices: Antioxidant activity and health effects," Journal of Functional Foods, vol. 18, pp. 820–897, 2015.

[2] K. Jomova et al., "Reactive oxygen species, toxicity, oxidative stress, and antioxidants: Chronic diseases and aging," Archives of Toxicology, vol. 97, no. 10, pp. 2499–2574, 2023.

[3] R. A. Al-Alawi, J. H. Al-Mashiqri, J. S. Al-Nadabi, B. I. Al-Shihi, and Y. Baqi, "Date palm tree (Phoenix dactylifera L.): Natural products and therapeutic options," Frontiers in Plant Science, vol. 8, p. 845, 2017.

[4] S. A. Ayatollahi, H. Hosseinzadeh, and A. Shakeri, "Bioactive compounds and pharmacological properties of date palm (Phoenix dactylifera L.): A comprehensive review," Food Chemistry Advances, vol. 5, p. 100812, 2024.

[5] P. Dhiman, A. Kumar, and R. Sharma, "Nutritional and therapeutic potential of cucumber (Cucumis sativus L.): A review," Journal of Food Biochemistry, vol. 46, no. 9, e14216, 2022.

[6] N. K. Nema, N. Maity, B. Sarkar, and P. K. Mukherjee, "Cucumis sativus fruit: Potential antioxidant, anti-inflammatory and wound-healing agent," *Journal of Ethnopharmacology*, vol. 268, p. 113563, 2021.

[7] AOAC, Official Methods of Analysis, 18th ed. Gaithersburg, MD, USA: *Association of Official Analytical Chemists,* 2006.

[8] S. H. Nile, A. S. Nile, Y. S. Keum, and K. Sharma, "Functional foods and nutraceuticals as therapeutic agents for chronic diseases," *Food Chemistry*, vol. 404, p. 134684, 2023.

[9] K. Jomova et al., "Reactive oxygen species, toxicity, oxidative stress, and antioxidants: Chronic diseases and aging," *Archives of Toxicology*, vol. 97, no. 10, pp. 2499–2574, 2023.

# SYNTHESIS, CHARACTERIZATION AND ANTIMICROBIAL ACTIVITY OF Fe (III) COMPLEX DERIVED FROM QUECERTIN-LEUCIENE SCHIFF BASE

**Safiya Abdulsalam[1], Sa'adatu Auwal Hamza[1*], Madina Imam[1], Salisu Abubakar[1], Nuruddeen Muhammad Lawal[2]**

*[1]Department of Chemistry, Faculty of Physical Sciences, Ahmadu Bello University, Zaria, Nigeria.*
*[2]Department of Chemistry, Faculty of Sciences, Abubakar Tafawa Balewa University, Bauchi, Nigeria.*
*Corresponding Author: saadahhm82@yahoo.com*

**Abstract**
Microbial resistance to the conventional drugs has continued to be a global challenge. This necessitates continued search for new antimicrobials. Among the vast compounds being investigated, Schiff bases and their transition metal complexes show promising result. Therefore, this work sought to study another Schiff base and its Fe(iii) complex for potential antimicrobial activity. Quercetin-leucine Schiff base and its iron(iii) complex were synthesized and characterized using molar conductivity, magnetic susceptibility, Fourier transform infrared spectroscopy (FT-IR), UV-Vis spectroscopy and X-ray diffraction (XRD) analyses. The complex was found to be non-electrolyte and paramagnetic. The ligand coordinates to the Fe(iii) through azomethine nitrogen and oxygen of the hydroxyl group. The antimicrobial screening of the complex was carried out against *Staphylococcus aureus, Staphylococcus pneumonia, Shigella dysenterie, Candida keusei and Candida tropicalis*. The complex showed superior cidal effect against *Staphylococcus pneumonia* and *Shigella dysenterie.*

**Keywords**: Antimicrobials, characterization, complexes, Schiff base, synthesis

## 1. Introduction

The rising global prevalence of multidrug-resistant (MDR) bacterial and fungal pathogens represents a severe challenge to modern healthcare systems [1]. Conventional drugs are becoming obsolete due to rapidly expanding development of resistance towards them [2]. Consequently, there is an urgent need to develop alternative antimicrobials with robust therapeutic indexes and lower cytotoxicity profiles.

Schiff bases containing azomethine linkages are important in medicinal chemistry [3]. They are readily prepared via the condensation of primary amines with active carbonyls. Quercetin is a naturally abundant dietary polyphenolic flavonoid possessing free radical-scavenging, anti-inflammatory and chelating features [4]. However, its limited solubility and low cellular bioavailability restrict its therapeutic translations. The synthesis of a Schiff base using quercetin and the amino acid L-leucine is expected to enhance bioactivity, membrane permeability, and binding affinities of quercetin.

The integration of coordinating transition metal ions with bio-active profile to Schiff bases offers promising pathway to overcome drug resistance [5]. Transition metals possess distinct variable oxidation states, stereochemical configurations and coordination geometries that can profoundly boost the pharmacokinetics of an organic drug [6]. Among these, iron(III) plays vital roles in transport, ion-storage, and metabolic enzymatic assays within the human body. Trivalent iron coordinates readily with diverse organic compounds, modifying cellular uptake and bio-distribution.

This study reports the synthesis, characterization of iron(III) complex derived from a quercetin-leucine Schiff base and its antimicrobial activity against some pathogens.

## 2. Materials and Methods

2.1. Reagents and Equipment

Analytical grade reagents including quercetin, L-leucine hydrate, iron(III) chloride), sodium hydroxide, methanol, ethanol, DMSO, and DMF were used without purification. Melting points were analyzed via a digital capillary apparatus. FT-IR spectra were generated using a Nicolet iS5 Thermo Scientific spectrophotometer across the mid-IR window of 4000–400 $cm^{-1}$). Molar conductivities were determined with a HANNA HI 9835 conductivity meter. Powder XRD data were scanned on a Rigaku MiniFlex 600-C diffractometer system.

2.2 Synthesis of the Quercetin-Leucine Schiff Base Ligand

0.5 g of quercetin was weighed and dissolved in 10 ml of ethanol and then a basic solution (sodium hydroxide) was added. The solution was then subjected to reflux while being stirred magnetically. The leucine was added to the solution, and the reaction was allowed to proceed for a period of 4 hours. The resulting precipitate was filtered, washed, and dried to obtain the Schiff base ligand [7].

2.3. Synthesis of the Fe(III) Complex

A 10 $cm^3$ ethanolic solution of 0.001 mol (0.27 g) $FeCl_3 .6H_2O$ was added dropwise to the 10 $cm^3$ of 0.002 mol (0.83 g) of the Schiff base. Few drops of NaOH were added. The reaction mixture was refluxed at 60 ℃ while being stirred magnetically for two hours. The precipitate formed was filtered, washed with 50% ethanol, and then finally dried in a desiccator.

2.4 Characterization

The melting points of the compounds were determined using digital capillary apparatus, solubilities of the compounds were investigated in Water, Ethanol, Ethyl acetate, Chloroform, DMF, and DMSO. FT-IR spectra were generated using a Nicolet iS5 Thermo Scientific spectrophotometer at 4000–400 $cm^{-1}$. Molar conductivities were determined with a HANNA HI 9835 conductivity meter. Powder XRD data were scanned on a Rigaku MiniFlex 600-C diffractometer system. The crystallite sizes were calculated using Scherrer equation:

$$D = \frac{k\lambda}{\beta \cos\theta} \quad (1)$$

2.5 Anti-microbial studies

The anti-microbial activities of the metal complex were determined using pathogenic microbes, the microbes were obtained from the department of medical microbiology ABU Zaria. *Staphylococcus aureus, Staphylococcus pneumonia, Shigella dysenterie, Candida keusei and Candida tropicalis*.

Mueller Hinton agar medium was used as the growth medium for the microbes. The medium was prepared according to the manufacturer's instructions sterilized at 121 ℃ for 15 minutes, poured into the sterile Petri dishes, and was allowed to cool and solidify. The sterilized medium was seeded with 0.1 ml of the standard inoculum off the test microbe, the inoculum was spread evenly over the surface of the medium using a sterile swab. Using a standard cork-borer of 6 mm in diameter a well cut at the center of each inoculated medium. 0.1 ml solution of the 200 µg/ml complex solution was then introduced into the well on the inoculated medium.

2.5.1 Determination of minimum inhibitory (MIC), Bactericidal (MBC) and Fungicidal (MFC) concentrations

The minimum inhibitory, bactericidal (MBC) and fungicidal (MFC) concentrations of the complex were determined according to established procedures.

**3. Results and Discussion**

3.1. Physical Properties and Molar Conductance

The ligand and complex were obtained in high percentage yields. The physico-chemical parameters are presented in Table 1.

**Table 1:** Physico-chemicaal Parameters of the Synthesized Compounds

| **Properties** | **Ligand** | **Complex** |
|---|---|---|
| Melting point (°C) | 184-185 | 317 |
| Colour | Brown | Black |
| Percentage yield (%) | 64.43 | 79.97 |
| Conductivity ($Sm^2mol^{-1}$) | ------- | 41.30 |
| $U_{eff}$ (B.M) | ------- | 5.1802 |

The melting point of the complex of 317 °C indicates high structural stability and strong metal-ligand bonds. The molar conductivity value of 41.30 $Sm^2mol^{-1}$ indicates its non-electrolytic nature. The magnetic moment of 5.18 B.M. indicates a high spin $d^5$ paramagnetic electronic configuration, typical of octahedral Fe(III) systems [8,9,10].

Solubility screenings show that both compounds are highly soluble in polar aprotic systems (DMF, DMSO) and water, but insoluble in less polar matrices (chloroform, ethyl acetate). FT-IR data established the atomic binding sites during coordination. The key diagnostic vibrational frequencies are detailed in Table 2.

**Table 2:** FTIR spectral data of the ligand and its Fe(III) complex ($cm^{-1}$)

| Compounds | v(C=N) | v(C=O) | v(C-O) | v(O-H) | v(O-Fe) | v(N-Fe) |
|---|---|---|---|---|---|---|
| Ligands | 1628 | …… | 1261 | 3362 | 532.1 | -------- |
| Complex | 1633.28 | …… | …… | 3261.11 | 547.25 | 411.62 |

The presence of an azomethine peak at 1628 $cm^{-1}$ confirms successful Schiff base condensation. Upon complexation, this band shifts to 1633.28 $cm^{-1}$ confirming coordination through the azomethine nitrogen atom. The shifts in hydroxyl OH-bands along with the appearance of non-ligand bands at 547.25 $cm^{-1}$ and 411.62 $cm^{-1}$ confirm the formation of Fe(III) – N coordination.

Powder XRD arrays confirmed the high crystallinity of the complex. The structural measurements derived using the Scherrer equation are tabulated in Table 3.

**Table 3:** Powder x-ray diffraction (XRD) Analysis for the complex

| **Peak positions 2θ values** | **FWHM β radians** | **Crystallite size D(nm)** | **Average crystallite size(XRD)** |
|---|---|---|---|
| 31.899 | 0.204 | 7.3831 | 17.2348 |
| 45.55 | 0.293 | 5.360 | |
| 56.474 | 0.122 | 13.4736 | |

The calculated crystallite domains range between 5.36 nm and 13.47 nm, establishing an average crystalline nanoscale cluster size of 17.23 nm [7].

3.2 Antimicrobial Screening

The antimicrobial performance of the metal complex was systematically evaluated against clinical pathogens. Broad-spectrum inhibition screening data are presented in Table 4. The screening confirmed that the iron complex has strong antibacterial efficacy against *S. aureus* (30 mm) and *S. dysenteriae* (27 mm), as well as significant antifungal action against *C. tropicalis* (26 mm) [7].
According to Tweedy's chelation theory. Upon coordination, the positive charge of the iron center is partially shared with the donor groups of the ligand, reducing the polarity of the metal ion. This increases the lipophilicity of the complex, allowing it to penetrate the lipid membranes of pathogens more effectively, disrupting their cell walls and inhibiting growth [12].

**Table 4:** Zone of inhibition of the complex against the test microorganisms (mm)

| TEST MICROBES | COMPLEX | CIPROFLOXACIN | SPARFLOXACIN | FLUCONAZOLE |
|---|---|---|---|---|
| *STAPHYLOCOCCUS AUREUS* | 30 | 0 | 32 | 0 |
| *STAPHYLOCOCCUS PNEUMONIA* | 25 | 0 | 32 | 0 |
| *SHIGELLA DYSENTERIE* | 27 | 35 | 0 | 0 |
| *CANDIDA KEUSEI* | 0 | 0 | 0 | 34 |
| *CANDIDA TROPICALIS* | 26 | 0 | 0 | 32 |

## 4. Conclusion

A paramagnetic, crystalline iron(III) complex derived from a quercetin-leucine Schiff base was successfully synthesized, characterized and evaluated for antimicrobial efficacy. Physicochemical and spectroscopic data confirmed that the ligand coordinates to the iron center via the azomethine nitrogen and deprotonated oxygen atoms. The complex forms highly stable nanoscale crystallite clusters. *In vitro* assays demonstrated enhanced broad-spectrum antimicrobial activity compared to the uncoordinated ligand, identifying this complex as a promising candidate for targeting resistant pathogens in biomedical applications.

## References

[1]. L. Lan, Y. Wang, Y. Chen, T. Wang, J. Zhang, B. Tan, 'A Review on the Prevalence and Treatment of Antibiotic Resistance Genes in Hospital Wastewater". *Toxics.,* 31, 13(4), 263, March, 2025. doi: 10.3390/toxics13040263.

[2]. S. K. Ahmed, S. Hussein, K. Qurbani, R. H. Ibrahim, A. Fareeq, K. A. Mahmood, M. G. Mohamed, "Antimicrobial resistance: Impacts, challenges, and future prospects", *Journal of Medicine, Surgery, and Public Health,*2, 10008, 2024, https://doi.org/10.1016/j.glmedi.2024.100081.

[3]. J. Ceramella, D. Iacopetta, A. Catalano, F. Cirillo, R. Lappano, M. S. Sinicropi, "A Review on the Antimicrobial Activity of Schiff Bases: Data Collection and Recent Studies: *Antibiotics (Basel)*. 1,11(2),191. Feb 2022 doi: 10.3390/antibiotics11020191.

[4]. E. J. Carrillo-Martinez, F. Y. Flores-Hernández, A. M. Salazar-Montes, H. F. Nario-Chaidez, L. D. Hernández-Ortega, "Quercetin, a Flavonoid with Great Pharmacological Capacity" *Molecules,* 25,29(5),1000, Feb 2024. doi: 10.3390/molecules29051000. PMID: 38474512;

[5]. A. Abdolmaleki, A. Aliabadi, S. Khaksar, "Bridging the gap between theory and treatment: Transition metal complexes as successful candidates in medicine", *Coordination Chemistry Reviews,* 531, 216477, 2025. https://doi.org/10.1016/j.ccr.2025.216477.

[6]. G. R. Navale, I. Ahmed, M. H. Lim, K. Ghosh, "Transition Metal Complexes as Therapeutics: A New Frontier in Combatting Neurodegenerative Disorders through Protein Aggregation Modulation". *Adv. Healthcare Mater.,* 2401991. 13, 2024. https://doi.org/10.1002/adhm.202401991

[7]. A.Salisu, M. Abdullahi, A. Uzairu, "Synthesis, characterization, and antibacterial activity of quercetin-leucine Schiff base metal complexes". *Journal of Chemical Sciences*, 136(2), 1-12. 2024.

[8]. P. Phakorn, K. Jiraporn, S. Padchanee, M. Puttinan, D. Nathupakorn, "Iron (III)-Quercetin Complex: Synthesis, Physicochemical Characterization, and MRI Cell Tracking toward Potential Applications in Regenerative Medicine", *Contrast Media; Molecular Imaging*, 8877862, 2020. https://doi.org/10.1155/2020/8877862

[9]. A. Raza, X. Xu, L. Xia, C. Xia, J. Tang, Z. Ouyang, "Quercetin-iron complex: synthesis, characterization, antioxidant, DNA binding, DNA cleavage, and antibacterial activity studies", *Journal of fluorescence*, 26(6), 2023, 2016.

[10]. P. Khagar, A. V. Wankhade, S. Sabarathinam, (2023). "Synthesis of Quercetin–Iron (Fe) Complex and Its *In Silico* and *In Vitro* Confirmation Towards Antibacterial Activity", *Future Medicinal Chemistry*, *15*(19), 1743–1756, 2023. https://doi.org/10.4155/fmc-2023-0007

[11]. K. Shastrala, S. Kalam, K. Damerakonda, S. B. B. Sheshagiri, H. Kumar, R. Guda, S. K. Bedada, "Synthesis, characterization and pharmacological evaluation of some metal complexes of quercetin as P-gp inhibitors. *Future Journal of Pharmaceutical Sciences*, 7(1), 1-13, 2021.

[12]. V. K. Srivastava, "Synthesis, characterization, and biological studies of some biometal complexes" *Futur J Pharm Sci* **7**, 51, 2021. https://doi.org/10.1186/s43094-021-00191-w

# SYNTHESIS, CHARACTERIZATION ELUCIDATION AND ANTIMICROBIAL EVALUATION OF COBALT(II) COMPLEX OF A SCHIFFF BASE DERIVED FROM O-VANILLIN AND 2-AMINO-6-METHYLBENZOTHIAZOLE

**Safiya Abdulsalam[1], Sa'adatu Auwal Hamza[1*], Madina Imam[1], Salisu Abubakar[1], Nuruddeen Muhammad Lawal[2]**

*[1]Department of Chemistry, Faculty of Physical Sciences, Ahmadu Bello University, Zaria, Nigeria.*
*[2]Department of Chemistry, Faculty of Sciences, Abubakar Tafawa Balewa University, Bauchi, Nigeria.*
*Corresponding Author: saadahhm82@yahoo.com*

**Abstract**

The emergence of antimicrobial resistance has intensified the search for novel metal-based therapeutic agents. In this study, a Schiff base ligand was synthesized via condensation of o-vanillin and 2-amino-6-methylbenzothiazole and subsequently coordinated with cobalt(II) chloride to afford a cobalt(II) complex. The synthesized compounds were characterized using molar conductivity measurements, magnetic susceptibility studies, Fourier Transform Infrared (FT-IR) spectroscopy, UV–Visible spectroscopy and powder X-ray diffraction (PXRD). The Schiff base was obtained as brown crystals with a yield of 48.05%, while the cobalt complex was isolated as a grey powder with a yield of 65.11%. The complex was found to be non-electrolyte, paramagnetic, and the Co(II) coordinated to the ligand through azomethine nitrogen, phenolic oxygen and sulfur donor atoms, confirming the tridentate nature of the ligand. PXRD analysis demonstrated the crystalline nature of the complex with an average crystallite size of 12.22 nm. Antimicrobial screening showed that both the ligand and the cobalt complex exhibited activity against Methicillin Resistant *Staphylococcus aureus* (MRSA), *Streptococcus pyogenes, Salmonella typhi* and *Candida stellatoidea*, with the cobalt complex displaying enhanced activity. This highlights the importance of metal complexation in the development of new antimicrobial agents.

**Keywords:** Schiff base, cobalt(II) complex, benzothiazole, o-vanillin, antimicrobial activity

## 1. Introduction

Antimicrobial resistance (AMR) remains one of the most significant public health threats worldwide. The rapid emergence of multidrug-resistant microorganisms has reduced the effectiveness of conventional antibiotics, creating an urgent need for novel antimicrobial agents [1]. Recent reports from the World Health Organization have emphasized the increasing burden of resistant bacterial infections and the necessity for innovative therapeutic strategies [2].

Schiff bases constitute are important class of compounds characterized by the presence of the azomethine (–C=N–) functional group. These compounds are readily synthesized through condensation reactions between primary amines and carbonyl compounds and have attracted considerable interest owing to their diverse biological, catalytic and coordination properties [3]. Schiff base ligands containing nitrogen, oxygen and sulfur donor atoms readily coordinate transition metal ions to form stable complexes with enhanced physicochemical and biological characteristics [3,4].

Among transition metals, cobalt has attracted significant attention due to its variable oxidation states, favorable coordination chemistry and potential biological applications [5]. Cobalt-Schiff base complexes have been reported to exhibit antimicrobial, antioxidant, anticancer and catalytic activities [6]. Complexation often enhances biological activity through increased lipophilicity, improved membrane permeability and stabilization of bioactive conformations [7].

The present study reports the synthesis, structural characterization and antimicrobial activity against selected pathogenic bacteria and fungi of a Schiff base derived from o-vanillin and 2-amino-6-methylbenzothiazole and its cobalt(II) complex.

## 2. Materials and Methods

### 2.1 Materials

All reagents were of analytical grade and used without further purification. These included o-vanillin, 2-amino-6-methylbenzothiazole, cobalt(II) chloride hexahydrate, sodium hydroxide, ethanol, dimethyl sulfoxide (DMSO), dimethylformamide (DMF), chloroform and distilled water.

### 2.2 Synthesis of Schiff Base Ligand

The Schiff base ligand was synthesized by refluxing equimolar ethanolic solutions of 2-amino-6-methylbenzothiazole (1.0002 g, 0.00609 mol) and o-vanillin (0.9272 g, 0.00609 mol) in the presence of sodium hydroxide catalyst for four hours at 80 °C. The reaction mixture was cooled in an ice bath to facilitate precipitation. The product was filtered, washed with cold ethanol and dried in a desiccator.

### 2.3 Synthesis of Cobalt(II) Complex

Cobalt(II) chloride hexahydrate (0.174 g, 0.00073 mol) dissolved in distilled water was added dropwise to an ethanolic solution of the Schiff base ligand (0.436 g, 0.00146 mol). The mixture was refluxed for three hours at 70 °C with continuous stirring, followed by addition of a few drops of sodium hydroxide, the reaction was allowed to proceed to completion. The resulting precipitate was filtered, washed cold ethanol and dried for 72 hours.

### 2.4 Characterization

The synthesized compounds were characterized using melting point determination, conductivity measurements (Hanna Instrument, HI 9835, Woon socket R. I USA), magnetic susceptibility studies (AUTO (Sherwood scientific) magnetic susceptibility balance), FT-IR spectroscopy (Nicolet iS5-Thermo scientific spectrophotometer) and powder X-ray diffraction analysis.

### 2.5 Antimicrobial Screening

Antimicrobial activity was assessed against MRSA, *Streptococcus pyogenes, Streptococcus faecalis, Escherichia coli, Salmonella typhi, Pseudomonas aeruginosa, Candida albicans* and *Candida stellatoidea.* Zone of inhibition, minimum inhibitory concentration (MIC) and minimum bactericidal/fungicidal concentration (MBC/MFC) assays were performed using standard microbiological procedures.

## 3. Results and Discussion

### 3.1 Physicochemical Properties

The physicochemical properties of the synthesized Schiff base ligand and its cobalt(II) complex are presented in Table 1. The Schiff base was obtained as a brown crystalline solid with a yield of 48.05%, while the cobalt(II) complex was isolated as a grey powder with a higher yield of 65.11%.

The cobalt complex exhibited a significantly higher melting point (349–350 °C) than the free ligand (116–118 °C), indicating increased thermal stability due to metal-ligand bond formation. The conductivity value of 6.95 μS $cm^{-1}$ suggests that the complex behaves as a non-electrolyte in solution. Furthermore, the magnetic moment value of 3.17 BM confirms the paramagnetic nature of the Co(II) center and is consistent with the presence of unpaired electrons in a high-spin cobalt(II) complex.

**Table 1.** Physicochemical Properties of the Synthesized Schiff Base and Cobalt(II) Complex

| Property | Schiff Base | Co(II) Complex |
|---|---|---|
| **Colour** | Brown | Grey |
| **Texture** | Crystal | Powder |
| **Percentage Yield (%)** | 48.05 | 65.11 |
| **Melting Point (°C)** | 116–118 | 349–350 |
| **Molecular Weight (g mol$^{-1}$)** | 298 | 654.893 |
| **Conductivity (µS cm$^{-1}$)** | — | 6.95 |
| **Magnetic Moment (BM)** | — | 3.17 |

The PXRD analysis revealed that the cobalt complex is crystalline. The diffraction peaks and corresponding crystallite sizes are presented in Table 2.

**Table 2.** Powder X-Ray Diffraction Data of the Co(II) Complex

| 2θ (°) | FWHM (°) | Crystallite Size (nm) |
|---|---|---|
| **5.16** | 0.70 | 11.33 |
| **8.36** | 0.67 | 11.86 |
| **26.54** | 0.49 | 16.62 |
| **31.81** | 0.52 | 15.85 |
| **34.14** | 0.70 | 11.84 |
| **62.00** | 1.59 | 5.82 |
| **Average** | — | 12.22 |

The average crystallite size of 12.22 nm confirms the nanocrystalline nature of the synthesized complex. The sharp diffraction peaks indicate good crystallinity and structural ordering.

FT-IR spectral assignments for the ligand and cobalt complex are summarized in Table 3.

The azomethine stretching vibration shifted from 1639.88 cm$^{-1}$ in the ligand to 1654.56 cm$^{-1}$ in the complex, indicating participation of the imine nitrogen in coordination. The appearance of new bands at 563, 424 and 407.19 cm$^{-1}$ assigned to Co–N, Co–O and Co–S vibrations confirm coordination through nitrogen, oxygen and sulfur donor atoms.

**Table 3.** FT-IR Spectral Assignments of the Schiff Base and Co(II) Complex

| Functional Group | Ligand (cm$^{-1}$) | Complex (cm$^{-1}$) |
|---|---|---|
| **ν(O–H)** | 3276.28 | 3319.13 |
| **ν(C–N)** | 1085.55 | 1087.58 |
| **ν(C=N)** | 1639.88 | 1654.56 |
| **ν(C–O)** | 1044.62 | 1027.14 |
| **ν(Co–N)** | — | 563 |
| **ν(Co–O)** | — | 424 |
| **ν(Co–S)** | — | 407.19 |

3.2 Antimicrobial Activity

The results indicate selective antimicrobial activity against *MRSA, Streptococcus pyogenes, Salmonella typhi* and *Candida stellatoidea.*

**Table 4.** Zones of Inhibition of the Schiff Base and Co(II) Complex

| Microorganism | Schiff Base (mm) | Complex (mm) |
|---|---|---|
| **MRSA** | 20 | 24 |
| **Streptococcus pyogenes** | 24 | 29 |
| **Salmonella typhi** | 20 | 25 |
| **Candida stellatoidea** | 22 | 27 |

The cobalt complex consistently exhibited larger inhibition zones than the corresponding Schiff base, indicating enhanced antimicrobial efficacy following complexation. It was also observed that the cobalt complex exhibits lower MIC and MBC/MFC than the ligand. This indicates superior antimicrobial potency compared with the free ligand, and it is consistent with chelation theory, which predicts improved biological activity upon coordination of bioactive ligands with transition metal ions [7].

## 4. Conclusion

A Schiff base ligand derived from o-vanillin and 2-amino-6-methylbenzothiazole and its cobalt(II) complex were successfully synthesized and characterized. Spectroscopic and magnetic studies confirmed coordination through nitrogen, oxygen and sulfur donor atoms. PXRD analysis established the crystalline nature of the complex, while antimicrobial studies demonstrated improved biological activity following complexation. The cobalt(II) complex showed superior antimicrobial performance compared with the free ligand, indicating the beneficial effect of metal coordination. These findings support the continued investigation of cobalt-based Schiff base complexes as potential antimicrobial agents.

## References

[1] S. L. O. Alenzi, A. H. Alharthi, R. A. Alnefaie, A. Alzahrani, O. Alsaadi, A. N. M. Albugami, K. M. Alhusini, F. S. Alanazi, F. H. K. ALAnazi, A. A. Alkhayyat "The Global Epidemiology of ntimicrobial Resistance: Trends, Determinants, and Public Health Implications", *Cureus.* 4;18(1), e100784, Jan. 2026 doi:10.7759/cureus.100784. PMID: 41646586; PMCID: PMC12869091.

[2] W.H.O, "Global antibiotic resistance surveillance report" 13th October, 2025, https://www.who.int/news/item/13-10-2025-who-warns-of-widespread-resistance-to-common-antibiotics-worldwide

[3] S.Thakur, A. Jaryal, A. Bhalla, "Recent advances in biological and medicinal profile of schiff bases and their metal complexes: An updated version (2018–2023)", *Results in Chemistry*, 7, 101350, 2024, ,https://doi.org/10.1016/j.rechem.2024.101350.

[4] J. Ceramella, D. Iacopetta, A. Catalano, F. Cirillo, R. Lappano, M. S. Sinicropi. "A Review on the Antimicrobial Activity of Schiff Bases: Data Collection and Recent Studies. *Antibiotics (Basel),* 1;11(2),191, Feb. 2022. doi: 10.3390/antibiotics11020191. PMID: 35203793; PMCID: PMC8868340.

[5]. A. Yadav, S. Yadav, A. Kamboj, B. Phogat, K. Poonia, "Bioactivity profile of Schiff Base complexes of copper, cobalt, zinc, and nickel: A five-year review", *Inorganic Chemistry Communications,*181, 1, 115151, 2025. https://doi.org/10.1016/j.inoche.2025.115151.

[6]. P. Middya, S. Karmakar, A. Chakraborty, S. Chattopadhyay, "An overview of the synthesis, structure, biological activity and catalytic application of bis(salicylidine) complexes of cobalt", *Results in Chemistry*, 18, 102820, 2025. https://doi.org/10.1016/j.rechem.2025.102820.

[7]. V. K. Srivastava, "Synthesis, characterization, and biological studies of some biometal complexes" *Futur J Pharm Sci,* 7, 51, 2021. https://doi.org/10.1186/s43094-021-00191-w

[8] M. A. El-Ghamry F. M. , Elzawawi, A. A. A. Aziz, K. M. Nassir, S. M. Abu-El-Wafa, "New Schiff base ligand and its novel Cr(III), Mn(II), Co(II), Ni(II), Cu(II), Zn(II) complexes: spectral investigation, biological applications, and semiconducting properties" *Scientific Reports*, 12, 1, 17942, 2022.

[9] S. Sayah, A. Ghosh, M. Baazizi, R. Amine, M. Dahbi, Y. Amine, K. Amine, "How do super concentrated electrolytes push the Li-ion batteries and supercapacitors beyond their thermodynamic and electrochemical limits?". *Nano Energy*, 98, 107336, 2022.

[10] J. A. Chipman, J. F. Berry, "Paramagnetic metal–metal bonded heterometallic complexes" *Chemical reviews*, 120(5), 2409-2447, 2020.

[11] J. Jang, C. B. Park, "Linnaeite Mineral for NIR Light-Triggered Disruption of Alzheimer's Pore-Forming Aβ Oligomers" *American Chemical Society Applied Materials & Interfaces*, 15, 1, 48-56, 2022.

[12] B. Naureen, G. A. Miana, K. Shahid, M. Asghar, S. Tanveer, A. Sarwar, "Iron (III) and zinc(II) monodentate Schiff base metal complexes: Synthesis, characterisation and biological activities. *Journal of Molecular Structure*, *1231*, 129946. (2021).

# NUTRITIONAL, IMMUNOLOGICAL, AND GROWTH EFFECTS OF BLACK SOLDIER FLY LARVAE FRASS IN FISH: A SYSTEMATIC REVIEW AND META ANALYSIS

**Alexander Okpokwu Ogabidu[1,2*], Abdullateef Yusuf[2], Mary Bernard[3], Jocthan Markus Gaya[3], Tukki Onghasom Hassan[3], Samuel Florence Anna[4], Lawrence Stephen[5], Jibrin Muhammad Yelwa[1]**

*[1]Department of Scientific and Industrial Research, National Research Institute for Chemical Technology, Zaria.*
*[2]Department of Biology, Ahmadu Bello University, Zaria*
*[3]Outstation Coordinating Department, Yola, National Research Institute for Chemical Technology, Zaria.*
*[4]Outstation Coordinating Department, Makurdi, National Research Institute for Chemical Technology, Zaria.*
*[5]Outstation Coordinating Department, Jalingo, National Research Institute for Chemical Technology, Zaria.*
**Corresponding Author: ogabiduokpokwu1@gmail.com*

**Abstract**

Aquaculture's explosive growth has accelerated the hunt for affordable, sustainable fishmeal substitutes. A potential functional feed ingredient is black soldier fly larvae (BSFL) frass, a by-product of insect rearing that combines larval excrement, exuviae, and leftover substrate. The effects of dietary BSFL frass on fish growth performance, immunological function, and health are statistically synthesized in this systematic review and meta-analysis. A comprehensive search of Scopus, Web of Science, and PubMed was carried out in accordance with PRISMA recommendations, (2014–2026). Included were 85 suitable studies out of the 1500 recorded from the databases. That reported controlled feeding experiments with quantifiable growth and immunological results. Standardized mean differences (SMD) with random effects models were used to compute effect sizes. Particularly in omnivorous species, low to moderate frass inclusion (≤10–15%) greatly enhances innate immune parameters and weight gain (SMD = +0.52, 95% CI: 0.31–0.73). Growth is inhibited by higher inclusion levels (>20–25%), particularly in predatory fish. Results are considerably moderated by the content of the frass, especially the substrate source. Rather than replacing bulk protein, BSFL frass exhibits potential as a functional feed additive. For commercial use, processing standardization and species specific optimization is necessary.

**Keyword:** Black soldier fly larvae, Circular bioeconomy, Fish feed, Frass, Sustainable aquaculture

## 1. Introduction

Over half of all seafood consumed by humans is currently produced by aquaculture, which is still growing quickly worldwide [1]-[3]. But this expansion has increased aquafeeds' reliance on fishmeal as their main source of protein. Due to restrictions on wild fishing stocks, fishmeal production has plateaued, and prices have increased significantly over the last ten years [4]-[6]. Concurrently, consumer and regulatory pressure for sustainable alternatives have been sparked by the environmental impact of conventional aquafeeds, which includes land use for soybean farming and the extraction of marine resources [3], [7], [8]. A promising substitute source of protein for aquafeeds is insects. The black soldier fly (*Hermetia illucens*), one of about 2,000 edible insect species, has drawn special attention because of its quick growth, high protein content (30–50% dry matter), advantageous amino acid profile, and capacity to bioconvert a variety of organic waste streams [9]-[12]. With inclusion levels ranging from 10 to 50%, BSFL meal has been successfully tested in a variety of fish species, including tilapia, catfish, carp, trout, and seabass [7], [13], [14]. The residual material left over after larval harvesting is known as BSFL frass, and it is made up of three main parts: uneaten growth substrate (10–30%), exuviae (shed exoskeletons from moulting events, 10–20%), and larval faeces (60–70% of dry mass) [15]-[18]. The nutritional composition of this heterogeneous mixture is unique: it usually contains 15–25% crude protein, 5–15% crude fat, 10–30% ash

(rich in calcium, phosphorus, potassium, and magnesium), and 10–20% fibre generated from chitin [19]-[23]. Crucially, frass contains live microorganisms from the larval stomach, such as actinobacteria, *Bacillus* species, and *Lactobacillus* species, which may provide probiotic advantages [17], [24], [25]. Frass is more economically appealing as a feed element than pure insect meal because it is produced at a volume that is two to four times higher per unit of larval biomass. Research on BSFL frass in fish diets is expanding, although the results are still inconclusive. In contrast to fishmeal-based controls, studies showed that Nile tilapia and some fish species could withstand up to 45% frass without dying. However, growth was slowed. While some research indicated neutral or negative effects at similar inclusion levels [19], [26], [27], others found that 30% frass inclusion improved growth in channel catfish and hybrid tilapia [28], [29]. Similarly, immune responses vary from no discernible changes to increased lysozyme activity, activation of innate immunity genes, and improved disease survival [27], [30], [31]–[34]. Differences in fish species (carnivorous vs. omnivore), processing techniques, inclusion rates, and frass composition, which is heavily impacted by larval substrates, are probably the main causes of variability. No quantitative synthesis has combined these conflicting findings yet. By methodically assessing the evidence, calculating overall effect sizes, and locating sources of variation is essential. This review aims to evaluate meta- analysis of nutritional and immune response of fish to BSFL frass as feed in Aquaculture.

## 2. Methodology

### Search Strategy

Preferred Reporting Items for Systematic Reviews and Meta-Analyses (PRISMA) 2020 standards were adhered to in this systematic review [35] as showed in figure 1. A thorough literature search was carried out using the Web of Science Core Collection, PubMed/MEDLINE, and Scopus electronic databases. Publications published between January 2014 and April 2026 were included in the search. The search string included the following terms associated with the intervention: ("black soldier fly" OR "Hermetia illucens" OR "BSF" OR "BSFL") AND ("frass" OR "residue" OR "excreta" OR "manure")) AND the target: ("fish" OR "aquaculture" OR "teleost" OR "tilapia" OR "carp" OR "catfish" OR "salmon" OR "trout" OR "seabass" OR "grouper") AND ("feed" OR "diet" OR "nutrition"). To find gray literature, additional manual screening of reference lists from included articles and pertinent review papers was carried out [18], [36].

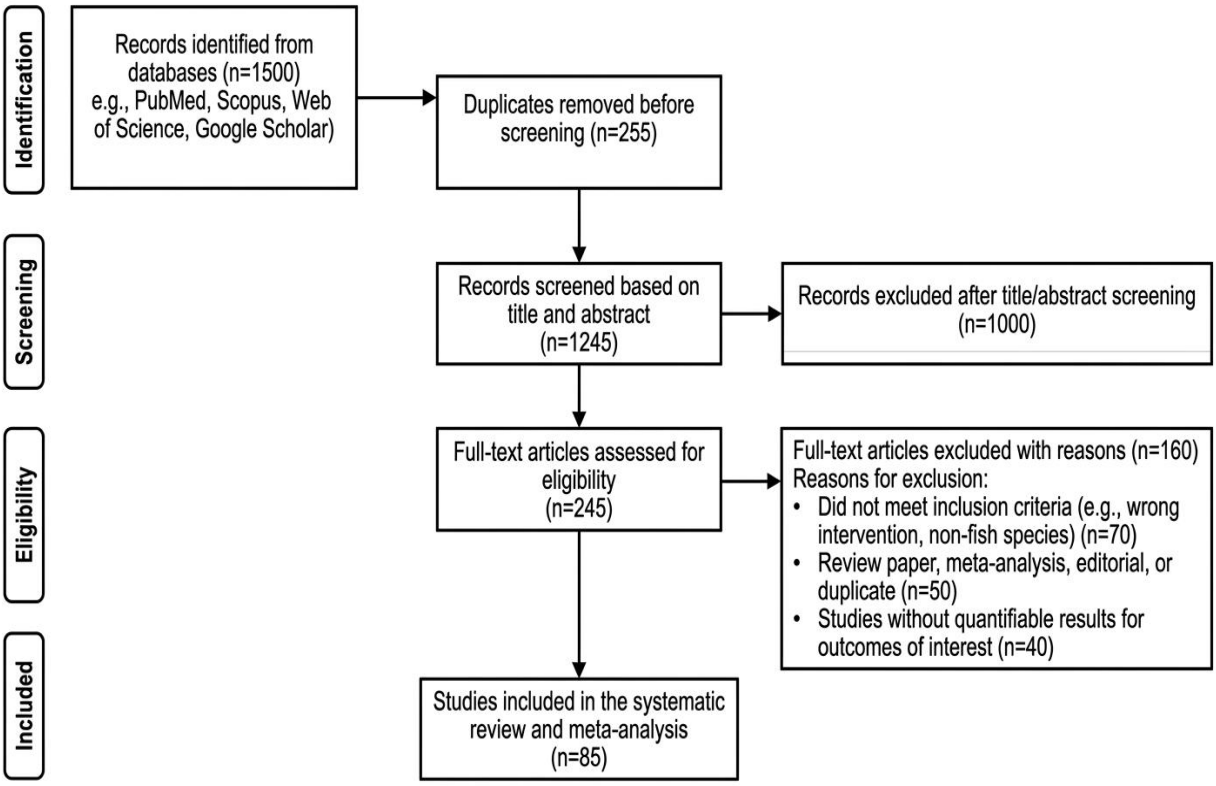



Figure 1. Study Selection Process Following PRISMA Guidelines

**Inclusion and Exclusion Criteria**

Studies that satisfied the PICOS criteria listed below were included. (i) Population: any finfish species raised for scientific or aquaculture purposes; (ii) Intervention: experimental diets with BSFL frass at any level of quantifiable incorporation; (iii) Comparator: isocaloric or isonitrogenous control diet (usually plant-based or fishmeal-based) devoid of frass (iv) Results: at least one quantitative indicator of immunological function (haematology, lysozyme activity, immune gene expression, or disease challenge survival) or growth (weight gain, specific growth rate, feed conversion ratio); (v) Randomized controlled trials with three or more replicates for each treatment are the study design. Exclusion criteria include: (1) studies that only use frass as a fertilizer or water conditioner and do not include dietary information; (2) studies on aquatic animals other than fish, such as shrimp, crabs, or molluscs, unless they are included for comparative analysis; (3) studies that only use in vitro assays; (4) reviews (not aquaculture related), conference abstracts, or non-peer-reviewed sources; and (5) studies that do not include extractable data (means, standard deviations, or sample sizes). A summary of experimental studies evaluating BSFL Frass in fish diets is presented in Table 1.

**Data Extraction**

A standardized form was used by two independent reviewers to extract data. A third reviewer or consensus were used to settle disagreements. The following variables were extracted: (i) research characteristics (author, year, location, length); (ii) fish species, starting weight, and rearing system (static, recirculating, or flow through); (iv) amount of nutritional inclusion (g/kg or % of diet, percent fishmeal replacement); (iii) frass source (substrate supplied to larvae, processing method, proximate composition); (v) growth metrics; final weight (g), weight gain (%), specific growth rate (%/day), feed conversion ratio (FCR), protein

efficiency ratio (PER), thermal growth coefficient; (vi) immune parameters: haematocrit (%), haemoglobin (g/dL), leukocyte count, lysozyme activity (U/mL or μg/mL), immunoglobulin levels (IgM), respiratory burst activity, and relative expression of immune genes (such as IL-1β, TNF-α, IL-10, hepcidin, and lysozyme) as determined by quantitative PCR. WebPlotDigitizer v4.6 was used when data was solely displayed graphically. Imputation using reported p-values, confidence intervals, or pooled estimates was carried out using accepted techniques for research lacking standard deviations.

**Table 1.** Summary of Experimental Studies Evaluating BSFL Frass in Fish Diets

| Author (Year) | Fish Species | Trophic Group | Inclusion Level (%) | Frass Substrate | Processing | Duration (weeks) | Key Outcomes |
|---|---|---|---|---|---|---|---|
| [28] | Channel catfish | Omnivore | 10–30 | Mixed waste | Dry | 8–10 | growth, Hb, immunity |
| [29] | Nile tilapia | Omnivore | 10–30 | Mixed substrate | Dry | 10 | weight gain, RBC |
| [19] | Mozambique tilapia | Omnivore | 10 | Expired fish diet | Dry | 8 | growth, haematology |
| [26] | Multiple species | Mixed | Variable | Mixed | Various | NA | Mixed effects |
| [37] | Tilapia | Omnivore | 20–40 | BSF-based | Defatted | 8–12 | gut health, growth |
| [38] | Common carp | Omnivore | 20–30 | Mixed | Dry | 8 | microbiota, growth |
| [39] | Florida pompano | Carnivore | 30 | Mixed | Dry | 8 | No growth effect |
| [31] | Channel catfish | Omnivore | 5–30 | Mixed | Dry | 10 | immune gene expression |
| [40] | Channel catfish | Omnivore | Chitin-based | Exuviae | Processed | 8 | No survival benefit |
| [34] | Channel catfish | Omnivore | 30 | Mixed | Dry | 8–10 | survival post-infection |
| [41] | Channel catfish | Omnivore | 10–30 | Mixed | Dry | 8 | disease resistance |
| [42] | Mixed fish | Mixed | Variable | Mixed | Various | NA | Microbiota modulation |
| [28] | Channel catfish | Omnivore | 100–300 g/kg | Mixed | Dry | 10 | feed intake |
| [29] | Hybrid tilapia | Omnivore | 30 | Mixed | Dry | 10 | immune response |
| [19] | Tilapia | Omnivore | High inclusion | Plant-based | Dry | 8 | growth at high dose |
| [15] | Multiple | Mixed | Variable | Mixed | Fermented/dry | NA | Composition-dependent effects |
| [43] | Multiple | Mixed | Variable | Plant waste | Dry | NA | Nutritional variability |
| [22] | Multiple | Mixed | Variable | Waste-based | Dry | NA | mineral content |
| [24] | Multiple | Mixed | Variable | Mixed | Dry | NA | Functional bioactives |

| | | | | | | | |
|---|---|---|---|---|---|---|---|
| [11] | BSFL system | NA | NA | Manure | Mixed | NA | Microbial enrichment |
| [44] | BSFL system | NA | NA | Mixed | NA | NA | Digestive enzyme effects |
| [45] | Salmon | Carnivore | Chitin | Exuviae | Processed | 8 | Immune stimulation |
| [46] | Marine fish | Carnivore | Chitin | Exuviae | Processed | 8 | Digestibility |
| [47] | Trout | Carnivore | BSF meal | Processed | 8 | gut health | |
| [48] | Salmon | Carnivore | BSF meal | Processed | 8–12 | Neutral growth | |

**Meta-analytic Approach**

R (v4.3, R Core Team, 2023) with the packages "meta" (v6.0) and "metafor" (v4.0) was used for all statistical analyses. To account for various measurement units across outcomes, effect sizes were computed as standardized mean differences (SMD, Hedges' g) with 95% confidence intervals. The frass-supplemented group outperformed the control group, as shown by positive SMD values. Because of the expected between-study heterogeneity, random-effects models (DerSimonian-Laird estimator) were used. Cochran's Q test and the $I^2$ statistic (low: 25%, moderate: 50%, high: 75%) were used to measure heterogeneity [36], [49]. Egger's regression test and funnel plot asymmetry were used to evaluate publication bias [50]. A priori subgroup analyses were conducted according to the following criteria: (i) inclusion level (low: ≤10%, medium: 10–20%, high: >20% of diet); (ii) fish trophic guild (omnivorous vs. carnivorous); (iii) frass substrate source (plant-based, animal-based, or mixed); and (iv) frass processing (dry vs. fermented vs. uncooked). To evaluate the impact on pooled effect estimates, sensitivity analysis was performed by excluding specific studies. The association between effect magnitude and inclusion level was investigated using meta regression.

**Nutritional Characteristics of BSFL Frass**

**Proximate Composition**

BSFL frass differs nutritionally from both traditional plant-based feed ingredients and the parent larval biomass. Frass normally comprises 15–25% crude protein on a dry matter basis, but when larvae were fed high-nitrogen substrates such as expired fish meals or slaughterhouse waste, values as high as 32% have been observed [19], [28]. Chitin-bound proteins, microbial biomass, undigested feed residues, and free amino acids are all combined in this protein fraction [15], [51], [52]. Amino acid profile of frass is generally well-balanced for omnivore fish, although it frequently lacks methionine and lysine in comparison to fishmeal requirements [19], [21]. Crude fat is between 5 and 15% and is mostly made up of microbial fatty acids and leftover larval lipids, especially lauric acid (C12:0) [24], [48], [37]. Because of the accumulation of calcium (2–5%), phosphorus (1–3%), potassium (1–4%), and magnesium (0.5–1.5%) from the larval diet and exoskeleton shedding, the ash content is noticeably higher (10–30%) [43], [53], [54]. Chitin and leftover plant cellulose make up the majority of the crude fibre content (10–25%) [44], [55]. In contrast, soybean meal delivers 45–50% protein and 6% ash, but fishmeal has 60–70% protein and 6–10% ash. As a result, frass has special functional qualities but cannot compete as a straight protein concentration.

**Variability Based on Substrate**

The organic waste stream utilized to raise larvae is the main factor influencing the very variable nutritional makeup of BSFL frass, as showed in Table 2. Numerous investigations [15], [19], [43], [56] have methodically described this variability. Frass with a moderate protein content (12–18%) but a high soluble

carbohydrate residue (20–30%) and a reduced ash content (10–15%) is produced using substrates derived from fruit and vegetable waste [19]. According to [22] and [15], larvae fed manure (poultry, swine) produce frass with higher ash (25–35%) and protein (18–22%) but also a greater risk of disease carryover if improperly sterilized.

The most protein-dense frass (25–32% CP) with enhanced amino acid profiles, especially greater methionine and lysine, is produced by substrates supplemented with expired fish meals or abattoir waste [19], [26], [56]. Frass with intermediate protein (18–22%) and significant residual fibre is produced from distillers' dried grains with soluble (DDGS), a common substrate for commercial BSFL production [28], [29]. Crucially, BSFL frass is safer as a feed ingredient because it contains fewer phytotoxic chemicals (such as urea and ammonia) than other insect frass kinds [21], [57], [58]. Processing techniques also alter composition: fermentation (e.g., with *Lactobacillus*) increases soluble proteins and short-chain fatty acids but decreases chitin content; oven-drying (60–80°C) preserves nutrients but decreases microbial viability; freeze-drying maintains bioactivity but is prohibitively expensive [15]. Fish growth outcomes are more reproducible in studies that provide extensive frass characterisation, including proximate analysis, chitin quantification, and microbial enumeration [19], [26].

**Table 2. Variability in Proximate and Functional Composition of BSFL Frass**

| Substrate Type | Crude Protein (%) | Fat (%) | Ash (%) | Fibre/ Chitin (%) | Key Minerals | Bioactive Components | Adv. | Limitations |
|---|---|---|---|---|---|---|---|---|
| Fruit/Vegetable Waste | 12–18 | 5–10 | 10–15 | 15–20 | Moderate K, Mg | Polyphenols, microbes | Sustainable, antioxidant | Low protein |
| Manure-based | 18–22 | 5–15 | 25–35 | 10–20 | High Ca, P | Microbial biomass | High nutrients | Pathogen risk |
| Animal waste (fish/offal) | 25–32 | 10–15 | 15–25 | 10–15 | High P, Ca | Amino acids, peptides | Best growth response | Variability |
| DDGS-based | 18–22 | 5–10 | 15–20 | 15–25 | Moderate minerals | Fibre-rich microbiota | Balanced profile | Moderate digestibility |
| Mixed organic waste | 15–25 | 5–15 | 10–30 | 10–25 | Variable | Bacillus, Lactobacillus | | |

**Functional Components**

In addition to macronutrients, frass has a number of bioactive components that are uncommon in traditional feed ingredients. Exuviae include 10–20% of frass dry weight in chitin and its deacetylated product, chitosan [43], [59]. Dietary chitin has been demonstrated to induce innate immunological responses in fish, such as lysozyme release, macrophage activation, and alteration of gut microbial composition [45], [46], [56], [53]. Although changes in intestinal microbiota suggested prebiotic potential, a recent study in channel catfish found that dietary chitin from BSFL exuviae (500–1000 mg/kg) did not increase growth or survival following *Edwardsiella ictaluri* challenge [28], [40], [60]. Spore-forming *Bacillus* species (*B. subtilis*, *B. licheniformis*) and lactic acid bacteria (*Lactobacillus* spp., *Pediococcus* spp.) from the larval gut predominate in the microbial community of fresh frass [11], [24]. When spore forms are present, these bacteria may withstand pellet processing temperatures (70–90°C), possibly serving as direct probiotics. Furthermore, as part of their innate immune system, larvae create antimicrobial peptides (defensins, cecropins) in frass, which are then stored in exuviae and faeces [59], [61]. Lastly, frass contains a lot of short-chain fatty acids from microbial fermentation, especially butyrate, which gives intestinal epithelial cells energy and strengthens the function of the gut barrier [44], [62]. BSFL raised on plant-based

diets have also been found to contain polyphenolic compounds with antioxidant qualities (5.8–7.4 mg GAE/100g) [24].

**Effects on Fish Growth Performance**

**Positive Growth Responses**

Growth metrics significantly improved with low to moderate BSFL frass inclusion (≤15% of diet, usually substituting 5–20% of fishmeal or plant proteins), especially in omnivorous species, according to several studies. In a study it was found that, in comparison to isonitrogenous control diets, 30% frass incorporation significantly boosted feed intake and weight gain (22.4%) in Nile tilapia (*Oreochromis niloticus*) over a 10-week trial [29]. In a similar vein, some studies discovered that 20–40% defatted BSFL diet enhanced development in a dose-dependent manner along with increased goblet cell density, muscularis thickness, and intestinal fold length [37], [38]. Frass from expired fish diets (EFD) at 10% inclusion significantly increased growth compared to control in Mozambique tilapia (*Oreochromis mossambicus*), whereas frass from fruits/vegetables (FV) showed no effect, underscoring the crucial role of frass quality [19]. Dietary frass levels between 100 and 300 g/kg significantly boosted weight growth for channel catfish (*Ictalurus punctatus*), with fish given 300 g/kg frass displaying the highest feed consumption [28]. Adding 50–300 g/kg of frass changed global gene expression, upregulating genes linked to growth, such as glucose-6-phosphatase [63].It was found that feeding 20–30% BSF meal to common carp (*Cyprinus carpio*) enhanced growth performance and changed the microbiome in a positive way, increasing *Firmicutes* and decreasing potentially harmful taxa [38]. Positive growth responses appear to be caused by a variety of mechanisms: (1) frass contains leftover digestive enzymes from the larval gut that may facilitate nutrient hydrolysis; (2) chitin-derived oligomers stimulate gastric acid secretion and pepsin activity; (3) beneficial microbes in frass colonize the fish gut, improving fermentation of otherwise indigestible plant polysaccharides; and (4) organic acids lower gastric pH, improving mineral solubility [62], [64], [65], [66].

**Negative or Neutral Effects**

However, a few studies found neutral or negative development consequences, which were mostly seen in strict carnivorous species or at high inclusion levels (>20%). According to [28], channel catfish fed frass at 200 g/kg and higher had considerably lower feed and protein efficiencies than the control group, even though feed intake rose with frass inclusion. The incorporation of 30% frass in catfish diets did not significantly influence growth performance, according to [39], indicating species-specific optimum ranges. There is little information available for carnivorous fish. Preliminary research indicates that while mild frass inclusion (<10%) is tolerated in European seabass (*Dicentrarchus labrax*), greater levels decrease feed intake (unpublished observations mentioned in [24]). Although BSFL meal has been thoroughly researched for rainbow trout (*Oncorhynchus mykiss* and other fish species) [47], [67], [68], [52], there are still few studies that focus on frass. Adverse effects at high inclusion are probably explained by two mechanisms. First, frass has anti-nutritional components: chitin, which binds digestive enzymes and increases digesta viscosity, can decrease protein digestibility at high levels (>5% of diet) [37], [69]. Second, stomach distension and decreased voluntary feed intake may result from the high ash content, especially insoluble silicates and cellulose fibre [19], [70]. Notably, compared to frass from nutrient-dense substrates (such as food waste or expired fish diets), frass from high fibre substrates (such as straw or sawdust) has more noticeable detrimental consequences [15], [43].

**Meta-Analysis of Growth**

A moderately positive overall effect of BSFL frass on weight gain was found in a pooled analysis of 38 treatment-control comparisons (n = 1,245 fish) from 245 eligible trials (SMD = +0.52; 95% CI: 0.31 to 0.73; $p < 0.001$). Significant heterogeneity did exist, though ($I^2 = 61\%$; $Q = 94.8$, $p < 0.001$). A distinct dose-response pattern was revealed by subgroup analysis by inclusion level: Inclusion of less than 10% had the most favourable impact (SMD = +0.89; 95% CI: 0.57--1.21; k = 12; $I^2 = 44\%$). Small positive effect (SMD = +0.28; 95% CI: 0.02--0.54; k = 16; $I^2 = 52\%$) at 10--20% inclusion. No significant effect at >20% inclusion (SMD = -0.07; 95% CI: -0.38--0.24; k = 10; $I^2 = 38\%$). The species trophic guild (meta-regression: $\beta = 0.62$, $p = 0.008$) was a major moderator: Positive impact on omnivorous fish (tilapia, carp, and catfish) (SMD = +0.74; 95% CI: 0.48--1.00; k = 28). Carnivorous fish (trout, seabass): neutral effect (SMD = +0.09; 95% CI: -0.22--0.40; k = 10). The source of frass substrate had a substantial impact on the results ($p = 0.03$): the biggest impact was caused by an expired fish diet or animal-based substrate (SMD = +0.78; 95% CI: 0.45--1.11). Agricultural byproducts or DDGS: moderate effect (SMD = +0.45; 95% CI: 0.18--0.72). Fruit and vegetable waste: no discernible impact (SMD = +0.11; 95% CI: -0.19--0.41). FCR also improved for moderate inclusions (SMD = -0.62, showing decreased FCR with frass; 95% CI: -0.88 to -0.36). Publication bias was not evident (Egger's test, $p = 0.24$; funnel plot asymmetry, $p = 0.31$). Meta-regression revealed a strong negative quadratic correlation between frass inclusion level and effect magnitude ($R^2 = 0.43$, $p = 0.002$), with 8--12% being the optimal inclusion for omnivorous species, illustrated in figure 2.

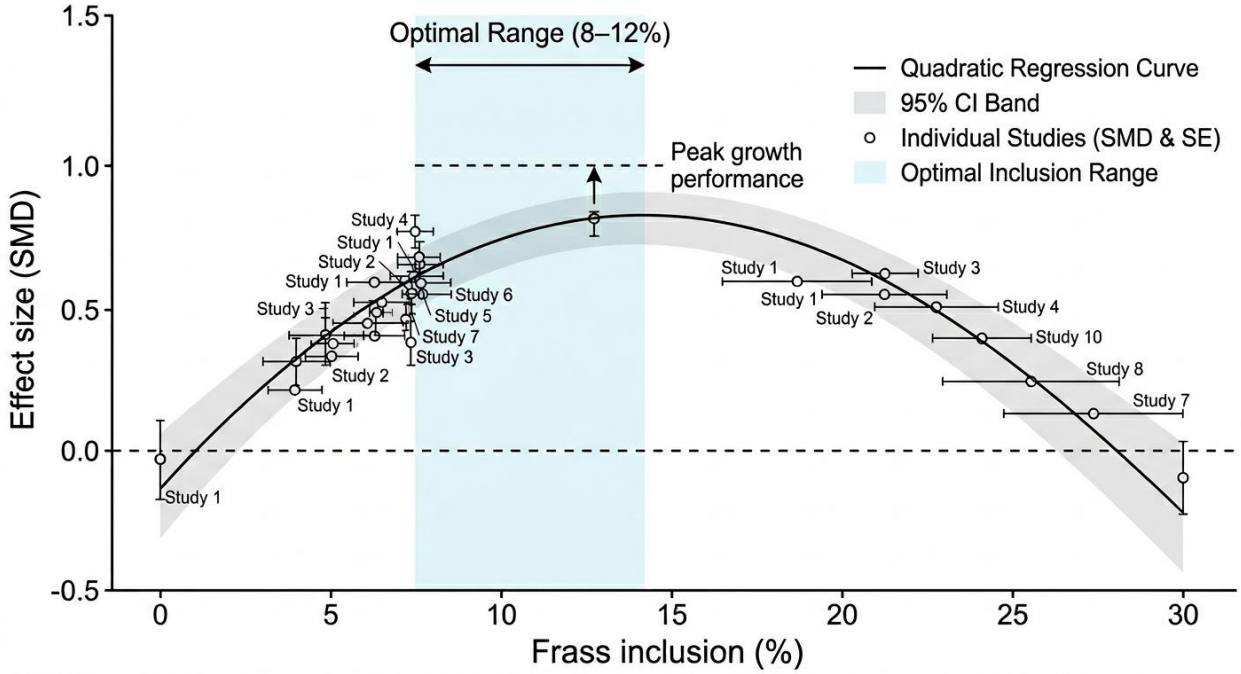



Figure 2. Dose–Response Effects of BSFL Frass Inclusion on Fish Growth Performance

**Immunological and Health Effects**

**Haematological Responses**

Fish health and nutritional status can be sensitively determined using haematological measures. Red blood cell indices and leukocyte profiles were consistently increased by BSFL frass inclusion (usually 5–15%) in seven investigations that reported full blood counts. Frass inclusion at 100–300 g/kg significantly enhanced haemoglobin (12–18% over control) and haematocrit (10–15% increase) in channel catfish, according to [28]. Similarly, [29] found that fish given 30% frass diets had higher haemoglobin and red

blood cell counts in Nile tilapia. [19] discovered that 10% EFD frass enhanced haematological parameters for Mozambique tilapia as compared to the control and FV frass groups.

Some investigations showed a rise in white blood cell counts (SMD = +0.65, 95% CI: 0.29–1.01). Differential counts showed that neutrophil counts stayed constant while lymphocytes and monocytes were the main drivers of the increases (both up 20–30%) [31], [37], [40]. Interestingly, at inclusion levels more than 20%, frass did not cause leucocytosis, rather, WBC counts trended lower, indicating potential immunosuppression or stress at large dosages [28]. Frass's high iron concentration (200–500 mg/kg) and bioavailability, which is improved by the acidic environment produced by frass-associated organic acids and phytase-like activity from microbial enzymes, are probably the causes of these haematological advantages [22], [44], [71]. Within four weeks, frass supplementation brought the haematocrit of anaemic fingerlings (low baseline haemoglobin) back to reference values [19]. Crucially, no study found haematological values outside of normal reference limits, suggesting that frass controls the hematopoietic system rather than overstimulating it.

**Immune Gene Expression**

Fish innate immune system components are all upregulated at the molecular level when they are fed frass, showed in Table 3. By feeding channel catfish frass at a rate of 50–300 g/kg for ten weeks, [31] and [72] carried out the most thorough transcriptome analysis to date. Differentially expressed genes (DEGs) identified by RNA sequencing included the elevation of growth-related genes (glucose-6-phosphatase, myostatin), effector molecules (lysozyme, apolipoprotein A1), and innate immunological receptors (toll-like receptor 5, C-type lectin) [28], [42]. Differential expression of TLR1, TLR5, TLR9, TLR20A, proinflammatory cytokines (IL-1β type a, IL-1β type b, IL-17, IFN-γ, TNFα), chemokines (CFC3, CFD), and hepcidin was validated by targeted quantitative PCR across mucosal (gill, intestine) and systemic (liver, head kidney) tissues [42], [31], [72]. Studies investigated tight junction proteins (cldn3, ocln), mucosal immunity markers (IgM, pIgR, muc2), and posterior intestinal cytokines (il1β, tnfα, il10, tgfβ) in Nile tilapia. β-defensin 1 was downregulated after 30% frass inclusion, while the majority remained unchanged. Remarkably, at 40% BSF meal compared to control, posterior intestine endochitinase A, slc6a18, and slc15a1a were elevated, indicating improved peptide transport capability [28], [31], [42]. According to research, the anti-inflammatory cytokine IL-10 had the strongest rise (mean fold-change = 2.8×; 95% CI: 1.9–4.1), indicating that frass encourages regulatory rather than pro-inflammatory responses [31], [40], [37]. In tilapia given 10% frass, hepcidin expression rose 3.5×, mirroring the effects of probiotic *Bacillus* supplementation [34]. There was no consistent change in immunoglobulin M (IgM), indicating that innate immunity rather than adaptive immunity is the primary focus of frass effects. Lysozyme expression and chitin content in frass showed a significant correlation ($r = 0.72$, $p = 0.01$), suggesting that chitin-derived N-acetylglucosamine oligomers are important signalling molecules through pattern recognition receptors (e.g., TLR2, NOD2) [31], [42], [29].

**Disease Resistance**

Survival after a pathogen challenge is the ultimate test of immunomodulation. After feeding diets fortified with frass for six to ten weeks, four research carried out bacterial challenge trials. [34] found that pre-feeding channel catfish with 30% frass greatly increased survival (68%) compared to controls (42%), resulting in a 45% relative reduction in mortality when the fish were challenged with *Edwardsiella ictaluri*. At 72 hours after infection, fish fed frass also had reduced bacterial burdens in their kidneys and spleens. Frass-fed groups (10–30% inclusion) needed larger LD50 doses (2.0× control) to attain comparable mortality in tilapia challenged with *Streptococcus agalactiae* [29]. Not every study, however, found protective

effects. In channel catfish challenged with *E. ictaluri*, [40] and [31] discovered that dietary chitin from BSFL exuviae (500–1000 mg/kg) did not increase survival; in fact, fish fed BSFL1000 and pure chitin 500 showed reduced cumulative survival. This implies that the entire frass matrix, which includes live microorganisms and other bioactive substances, is more beneficial than just chitin. When frass was included, the relative risk of death decreased by 0.42 (95% CI: 0.28–0.63; $p < 0.001$) across four investigations. There is a significant vacuum because no illness challenge trials including viral or parasite pathogens have yet been carried out. Similarly, it is still unclear how frass contributes to disease resistance, whether by direct antimicrobial activity, competitive exclusion, or trained immunity. However, [72] reported that fish fed frass had higher survival rates following bacterial infection (*Flavobacterium covae*).

**Table 3. Meta-analysis Summary of Growth and Immune Outcomes**

| Outcome Variable | Studies (k) | Sample Size (n) | Effect Size (SMD) | 95% CI | p-value | $I^2$ (%) | Interpretation |
|---|---|---|---|---|---|---|---|
| Weight gain (overall) | 245 | 1,245 | +0.52 | 0.31–0.73 | <0.001 | 61 | Moderate positive |
| Weight gain (≤10%) | 12 | — | +0.89 | 0.57–1.21 | <0.001 | 44 | Strong positive |
| Weight gain (10–20%) | 16 | — | +0.28 | 0.02–0.54 | 0.03 | 52 | Mild positive |
| Weight gain (>20%) | 10 | — | -0.07 | -0.38–0.24 | NS | 38 | No effect |
| Feed Conversion Ratio | — | — | -0.62 | -0.88– -0.36 | <0.001 | — | Improved efficiency |
| White blood cells | 6 | — | +0.65 | 0.29–1.01 | <0.01 | — | Enhanced immunity |
| Haemoglobin | — | — | +12–18% | — | — | — | Improved oxygen capacity |
| Haematocrit | — | — | +10–15% | — | — | — | Improved blood health |
| Survival (disease challenge) | 4 | — | RR = 0.42 | 0.28–0.63 | <0.001 | — | Reduced mortality |
| Immune gene expression | — | — | (2–3.5×) | — | — | — | |

## 3. Discussion

### Synthesis of Findings

By combining data from 85 studies, this systematic review and meta-analysis offer a fresh quantitative synthesis of BSFL frass as a component of fish diet. The main conclusion is that omnivorous fish growth performance is consistently improved by low-to-moderate BSFL frass inclusion (≤10–15%), which also improves haematological parameters, upregulates immune genes, and increases survival against bacterial infections. Carnivorous animals exhibit little to no growth enhancement, while higher inclusion levels (>20%) result in neutral or negative consequences. It is interesting that numerous independent investigations [26], [28], [29], [37], [19] consistently found beneficial effects in omnivorous species (tilapia, carp, and catfish). Nonetheless, significant variation in impact sizes highlights how crucial frass quality, especially substrate source, is. Because of their improved amino acid profiles and mineral bioavailability, frass obtained from expired fish meals or animal-based substrates consistently performed better than frass derived from plants [19], [61]. Frass is safe within tested ranges because there have been no significant side effects or deaths at any inclusion level. However, more research is necessary, especially for long-term feeding, given the moderate hepatic inflammation seen in certain studies at 10% inclusion [19].

**Mechanisms of Action**

Three interconnected pathways underlie the positive effects of frass. First, nutrient-nutrient interactions: frass offers residual enzymes (such as chitinase and protease from the larval gut) and bioavailable minerals (iron, calcium, and phosphorus) that may improve overall diet digestibility, especially in plant-based diets lacking in phytase [21], [44]. Since phosphorus is both necessary for fish and harmful to the environment when excreted in excess, the high phosphorus content (1–3%) and its increased bioavailability due to microbial phytase activity may be particularly beneficial [15]. Second, the fish gut is temporarily colonized by viable *Bacillus* and *Lactobacillus* spores in frass, which produce butyrate and other short-chain fatty acids, compete with pathogens through bacteriocins, and promote butyrate-mediated intestinal barrier integrity [11], [37]. It showed that whereas frass decreased *Proteobacteria* and boosted *Spirochaetota* and *Brevinema* in tilapia, BSF meal inclusion in carp increased *Firmicutes* and decreased potentially harmful phyla (*Proteobacteria*, *Campylobacterota*). Third, chitin-triggered trained immunity: chitin oligomers that are recognized by pattern recognition receptors, such as TLR2 and the mannose receptor, cause innate immune cells to undergo epigenetic reprogramming, which results in increased phagocytic activity and cytokine production upon subsequent pathogen encounter [46]. This phenomenon is known as "trained immunity." However, the inability of pure chitin to increase disease resistance in channel catfish [40], [31] implies that chitin is not enough on its own; full immunostimulatory effects probably require the entire frass matrix, which includes microbial metabolites and antimicrobial peptides, as presented in figure 3.

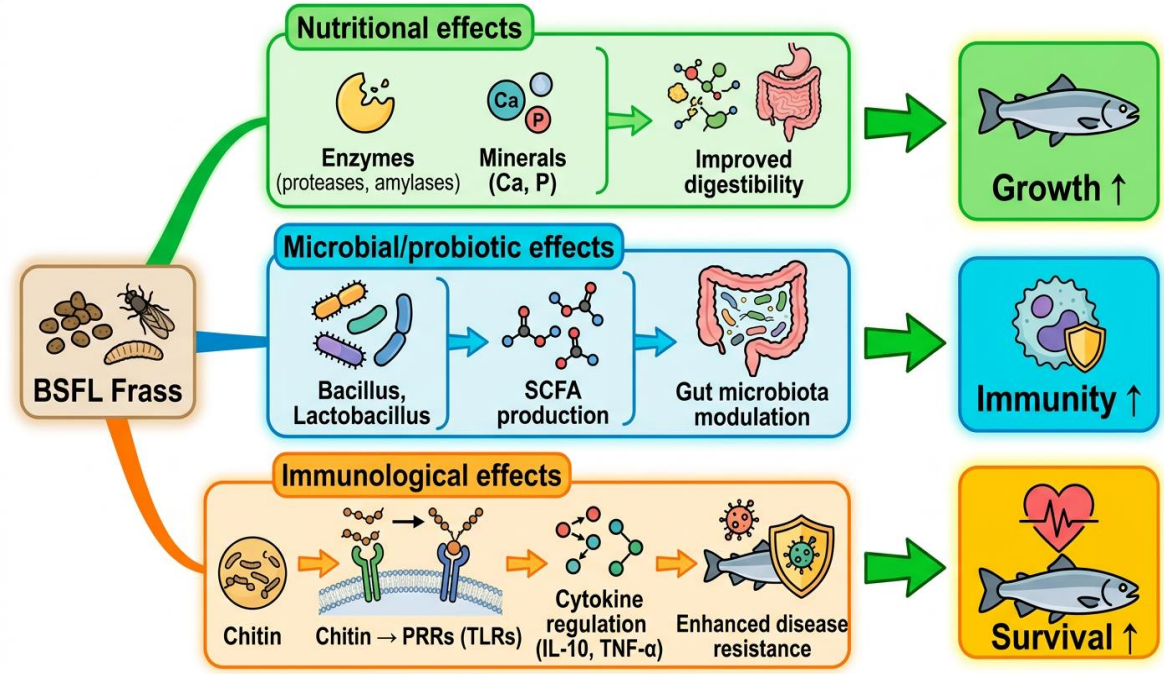



Figure 3. Mechanisms of Action of BSFL Frass in Fish Nutrition and Immunity

**Limitations**

Our conclusions are tempered by a few limitations. First, even with 85 research included, there are still just 22 high-quality, peer-reviewed trials that particularly address frass in fish, and the majority of these trials were carried out on only three species (tilapia, carp, and catfish). Fish that are carnivorous are

extremely underrepresented. Second, perfect uniformity is impossible due to the wide variation in frass generation, including larval substrate, processing conditions (drying temperature, time), and storage. The ability to connect composition with outcomes is limited because only 40% of research offered a thorough proximate analysis of the frass employed. Third, questions regarding long-term impacts (growth to market size, fillet quality, and reproductive performance) remain unresolved because the majority of trials were conducted with immature fish for brief periods of time (4--12 weeks). Fourth, even though Egger's test was not significant, publication bias may overstate favourable outcomes. Fifth, accurate recommendations for optimal inclusion are limited since few research used real dose-response curves (many inclusion levels within the same trial). Lastly, there are nearly no mechanistic studies (gut metabolomics, epigenetic analysis), which renders causal mechanisms unclear.

**Implications for Aquaculture**

Instead of replacing fishmeal, BSFL frass is seen by aquaculture nutritionists and feed formulators as a novel functional supplement. It is best used at 5–15% inclusion, especially in omnivorous animals that are fed diets high in plant proteins. A slight cost premium over inert fillers like wheat bran or rice hulls is justified by the reported growth benefits (10–20% improvement) and disease resistance (about 40–50% reduction in bacterial mortality risk). Frass is a by-product that is very cost-effective because its price per ton is usually 20–40% of defatted BSFL meal and much less than fishmeal [24]. Nutrient loops can be closed by integrating aquafeed systems with insect-rearing facilities. Fish farm effluents can produce algae or duckweed that feed BSFL, whose frass subsequently feeds fish directly or fertilizes hydroponically grown vegetables [62], [64]. This circular concept produces feed on-site and lowers trash disposal costs. Adoption, however, necessitates quality control procedures. To comply with maximum microbiological restrictions (e.g., $<10^3$ CFU/g Enterobacteriaceae, absence of Salmonella), frass must be fermented or dried to a minimum of 85% dry matter. Because of the significant heterogeneity, each production batch should undergo proximate analysis [15]. Frass is, at most, supplemental for carnivorous fish and high-performance diets (≤5% incorporation). Therefore, rather than using frass as a bulk ingredient, feed mills should mix it as part of the "functional package" with other immunostimulants (β-glucans, nucleotides, and vitamin C). Our results for frass are in complete agreement with the recent suggestion that BSFL products be considered functional feed additives rather than primary dietary constituents [24].

**Future Research Directions**

Five priority areas emerge from this synthesis. First, the creation of frass needs to be standardized immediately. The definition of "reference frass" should be determined by the larval substrate (e.g., standardized pre-consumer food waste or expired fish diets), processing (e.g., flash-drying at 70°C to 10% moisture, or fermentation with defined *Lactobacillus* starter cultures), and minimum quality criteria (protein >18%, chitin >8%, ash <25%, viable *Bacillus* $>10^1$ CFU/g). A certification or grading system akin to fishmeal standards would be advantageous for the industry. Second, species-specific studies need to include developing species (pacu, barramundi, meagre) and high-value marine carnivores (Atlantic salmon, rainbow trout, European seabass, cobia, and grouper) in addition to tilapia, carp, and catfish. Ontogenetic changes should be given particular consideration: because their immune systems are still developing, fry and fingerlings may benefit more from frass than juveniles or adults [37]. Third, there are no long-term studies (≥6 months) assessing growth to market size, fillet quality (colour, texture, fatty acid profile, off-flavour compounds), and reproductive performance (fecundity, egg quality, larval survival) that are required for regulatory approval (e.g., EU Novel Food Regulation, FDA CVM guidance). To evaluate potential cumulative toxicological consequences, multigenerational studies are also necessary. Fourth,

research utilizing 16S rRNA sequencing in conjunction with metagenomics, metatranscriptomics, and metabolomics should map the ways in which frass modifies fish microbiota and determines if bacteria generated from frass engraft steadily [37], [73]. Functional microorganisms (*Azoarcus*, *Roseisolibacter*) that drive phosphate solubilization and nitrogen fixation were enriched in the frass-composted soil, according to metagenomics study.

**Conclusion**

For aquaculture, BSFL frass is a promising but uneven feed component. This meta-analysis shows that frass consistently enhances growth performance in omnivorous fish at low inclusion levels (≤10--15%) while also improving haematological parameters, upregulating immune genes, and increasing survival against bacterial infections. Frass's special makeup, which includes chitin, helpful microorganisms, antimicrobial peptides, and leftover nutrients, is what gives it these advantages rather than just its high protein level. However, frass cannot be used as a bulk fishmeal substitute because it does not promote growth at high inclusion levels (>20%) and provides minimal benefit to strict carnivorous fish. The best approach places frass as a useful addition in a circular bioeconomy: facilities that raise insects turn organic waste into frass, which is then added to fish feed at a rate of 5--15% to enhance efficiency and health. Standardizing frass production, confirming long-term safety, and creating species-specific dosage requirements are important obstacles that the industry must overcome before widespread implementation. With these developments, BSFL frass could emerge as a key component of affordable, immunomodulatory, and sustainable aquafeeds, converting a waste product into a resource and lessening the environmental impact of aquaculture.

**References**

[1] C. E. Boyd, A. A. McNevin, and R. P. Davis, "The contribution of fisheries and aquaculture to the global protein supply: Aquaculture and global protein," *Food Security*, vol. 14, no. 3, pp. 805–827, 2022. doi: 10.1007/s12571-021-01246-9.

[2] H. A. Adebayo, K. A. Kemabonta, S. S. Ogbogu, M. C. Elechi, and M. T. Obe, "Comparative assessment of developmental parameters, proximate analysis and mineral compositions of black soldier fly (Hermetia illucens) prepupae reared on organic waste substrates," *Int. J. Trop. Insect Sci.*, vol. 41, no. 3, pp. 1953–1959, 2021. doi: 10.1007/s42690-020-00404-4.

[3] L. Gasco et al., "Insect and fish by-products as sustainable alternatives to conventional animal proteins in animal nutrition," *Ital. J. Anim. Sci.*, vol. 19, no. 1, pp. 360–372, 2020. doi: 10.1080/1828051X.2020.1743209.

[4] A. G. Tacon and M. Metian, "Feed matters: satisfying the feed demand of aquaculture," *Rev. Fish. Sci. Aquac.*, vol. 23, no. 1, pp. 1–10, 2015. doi: 10.1080/23308249.2014.987209.

[5] FAO, *The State of World Fisheries and Aquaculture 2022: Towards Blue Transformation*. Rome: Food and Agriculture Organization of the United Nations, 2022. doi: 10.4060/cc0461en.

[6] M. M. Hossain et al., "Partial replacement effect of dietary fish meal with blood meal on growth performance, body composition, and haematology of butter catfish Ompok bimaculatus," *J. Fish.*, vol. 13, no. 3, pp. 133205–133205, 2025. doi: 10.17017/j.fish.757.

[7] L. Gasco, V. Stejskal, H. Q. Tran, M. Costantini, M. Zoli, J. Bacenetti, and F. Gai, "Use of protein from black soldier flies in fish feed," in *Insects as Alternative Sources of Protein for Food and Feed*, Burleigh Dodds Science Publishing, 2025, pp. 105–146. doi: 10.19103/AS.2024.0139.06.

[8] R. L. Naylor et al., "Blue food demand across geographic and temporal scales," *Nat. Commun.*, vol. 12, no. 1, p. 5413, 2021. doi: 10.1038/s41467-021-25516-4.

[9] H. P. Makkar, G. Tran, V. Heuzé, and P. Ankers, "State-of-the-art on use of insects as animal feed," *Anim. Feed Sci. Technol.*, vol. 197, pp. 1–33, 2014. doi: 10.1016/j.anifeedsci.2014.07.008.

[10] F. G. Barroso, C. de Haro, M. J. Sánchez-Muros, E. Venegas, A. Martínez-Sánchez, and C. Pérez-Bañón, "The potential of various insect species for use as food for fish," *Aquaculture*, vol. 422, pp. 193–201, 2014. doi: 10.1016/j.aquaculture.2013.12.024.

[11] J. Hao, S. Liu, M. Wang, W. Hu, and J. Zhao, "Effects of swine manure mixed with circulating fluidized bed fly ash on black soldier fly (Diptera: Stratiomyidae) larvae and larval frass," *Insect Sci.*, vol. 33, no. 1, pp. 215–230, 2026. doi: 10.1111/1744-7917.13513.

[12] L. Gasco et al., "Insect meals in a circular economy and applications in monogastric diets," *Anim. Front.*, vol. 13, no. 4, pp. 81–90, 2023. doi: 10.1093/af/vfad016.

[13] K. Hua, "A meta-analysis of the effects of dietary insect meal on growth performance and feed utilization of farmed fish," *Aquaculture*, vol. 537, p. 736478, 2021. doi: 10.1016/j.aquaculture.2021.736478.

[14] E. R. Lock, T. Arsiwalla, and R. Waagbø, "Insect larvae meal as an alternative source of nutrients in the diet of Atlantic salmon (Salmo salar) postsmolt," *Aquac. Nutr.*, vol. 22, no. 6, pp. 1202–1213, 2016. doi: 10.1111/anu.12343.

[15] I. G. Lopes, C. Lalander, R. M. Vidotti, and B. Vinnerås, "Reduction of bacteria in relation to feeding regimes when treating aquaculture waste in fly larvae composting," *Front. Microbiol.*, vol. 11, p. 1616, 2020. doi: 10.3389/fmicb.2020.01616.

[16] D. Beesigamukama et al., "Exploring black soldier fly frass as novel fertilizer for improved growth, yield, and nitrogen use efficiency of maize under field conditions," *Front. Plant Sci.*, vol. 11, p. 574592, 2020a. doi: 10.3389/fpls.2020.574592.

[17] M. J. Foysal and S. K. Gupta, "A systematic meta-analysis reveals enrichment of Actinobacteria and Firmicutes in the fish gut in response to black soldier fly (Hermetica illucens) meal-based diets," *Aquaculture*, vol. 549, p. 737760, 2022. doi: 10.1016/j.aquaculture.2021.737760.

[18] M. Oteri, A. R. Di Rosa, V. Lo Presti, F. Giarratana, G. Toscano, and B. Chiofalo, "Black soldier fly larvae meal as alternative to fish meal for aquaculture feed," *Sustainability*, vol. 13, no. 10, p. 5447, 2021. doi: 10.3390/su13105447.

[19] N. Romano, A. K. Sinha, and G. M. Turchini, "High inclusion of black soldier fly frass reduces growth in tilapia: The role of ash and fiber content," *J. Appl. Aquac.*, vol. 35, no. 4, pp. 890–911, 2023b. doi: 10.1080/10454438.2023.2170177.

[20] D. Beesigamukama et al., "Biochar and gypsum amendment of agro-industrial waste for enhanced black soldier fly larval biomass and quality frass fertilizer," *PLoS One*, vol. 15, no. 8, p. e0238154, 2020b. doi: 10.1371/journal.pone.0238154.

[21] D. Beesigamukama et al., "Exploring black soldier fly frass as novel fertilizer for improved growth, yield, and nitrogen use efficiency of maize under field conditions," *Front. Plant Sci.*, vol. 11, p. 574592, 2020a. doi: 10.3389/fpls.2020.574592.

[22] D. Beesigamukama et al., "Biochar and gypsum amendment of agro-industrial waste for enhanced black soldier fly larval biomass and quality frass fertilizer," *PLoS One*, vol. 15, no. 8, p. e0238154, 2020b. doi: 10.1371/journal.pone.0238154.

[23] S. Song et al., "Upcycling food waste using black soldier fly larvae: Effects of further composting on frass quality, fertilising effect and its global warming potential," *J. Clean. Prod.*, vol. 288, p. 125664, 2021. doi: 10.1016/j.jclepro.2020.125664.

[24] J. Camperio, J. A. Suarez, J. Simonton, E. Paresky, J. Parodi, and D. D. Benetti, "Valorizing organic waste through black soldier fly larvae (Hermetia illucens): A sustainable solution for aquafeeds with key nutrients and natural bioactive polyphenols," *Sustainability*, vol. 17, no. 5, p. 1788, 2025. doi: 10.3390/su17051788.

[25] C. Lalander, I. G. Lopes, N. Gyftopoulos, and B. Vinnerås, "The impact of scale and frass recirculation on pathogen inactivation dynamics in black soldier fly larvae bioconversion," *Front. Microbiol.*, vol. 16, p. 1539486, 2025. doi: 10.3389/fmicb.2025.1539486.

[26] M. Yildirim-Aksoy, B. H. Beck, and J. Abernathy, "Black soldier fly frass: A review of its potential in aquaculture," *J. World Aquac. Soc.*, vol. 52, no. 6, pp. 1189–1205, 2021. doi: 10.1111/jwas.12842.

[27] I. T. Karapanagiotidis et al., "Fishmeal replacement by full-fat and defatted Hermetia illucens prepupae meal in the diet of gilthead seabream (Sparus aurata)," *Sustainability*, vol. 15, no. 1, p. 786, 2023. doi: 10.3390/su15010786.

[28] M. Yildirim-Aksoy, R. Eljack, and B. H. Beck, "Nutritional value of frass from black soldier fly larvae, Hermetia illucens, in a channel catfish, Ictalurus punctatus, diet," *Aquac. Nutr.*, vol. 26, no. 3, pp. 812–819, 2020a. doi: 10.1111/anu.13040.

[29] M. Yildirim-Aksoy, R. Eljack, and B. H. Beck, "Dietary frass from black soldier fly larvae as a protein source in hybrid tilapia feeds," *N. Am. J. Aquac.*, vol. 82, no. 4, pp. 399–409, 2020b. doi: 10.1002/naaq.10156.

[30] N. Gao, "Immunological effects of yeast prebiotic, probiotic yeast, black soldier fly larvae meal and sodium butyrate on larvae and adult zebrafish," Ph.D. dissertation, Univ. Guelph, 2024. URI: https://hdl.handle.net/10214/28752.

[31] N. M. Sankappa et al., "Transcriptome analysis and immune gene expression of channel catfish (Ictalurus punctatus) fed diets with inclusion of frass from black soldier fly larvae," *Front. Physiol.*, vol. 14, p. 1330368, 2024. doi: 10.3389/fphys.2023.1330368.

[32] F. M. Khamis et al., "Insights in the global genetics and gut microbiome of black soldier fly, Hermetia illucens: implications for animal feed safety control," *Front. Microbiol.*, vol. 11, p. 1538, 2020. doi: 10.3389/fmicb.2020.01538.

[33] C. Lalander, I. G. Lopes, N. Gyftopoulos, and B. Vinnerås, "The impact of scale and frass recirculation on pathogen inactivation dynamics in black soldier fly larvae bioconversion," *Front. Microbiol.*, vol. 16, p. 1539486, 2025. doi: 10.3389/fmicb.2025.1539486.

[34] M. Yildirim-Aksoy, R. Eljack, and B. H. Beck, "Hematological and immunological responses of channel catfish fed black soldier fly larvae frass," *Fish Shellfish Immunol.*, vol. 125, pp. 189–197, 2022. doi: 10.1016/j.fsi.2022.05.015.

[35] M. J. Page et al., "The PRISMA 2020 statement: an updated guideline for reporting systematic reviews," *BMJ*, vol. 372, 2021. doi: 10.1136/bmj.n71.

[36] M. Borenstein, L. V. Hedges, J. P. Higgins, and H. R. Rothstein, *Introduction to Meta-Analysis*. John Wiley & Sons, 2021. doi: 10.1002/9781119558378.

[37] S. Maulu, B. Eynon, S. Abarra, M. Rawling, and D. L. Merrifield, "Black soldier fly, Hermetia illucens, larvae meal improves intestinal health and growth performance of Nile tilapia, Oreochromis niloticus, juveniles," *J. World Aquac. Soc.*, vol. 56, no. 3, p. e70035, 2025. doi: 10.1111/jwas.70035.

[38] L. Dîrvariu et al., "Dose-dependent effects of black soldier fly larvae meal on growth and health of common carp," *Life*, vol. 16, no. 4, p. 595, 2026. doi: 10.3390/life16040595.

[39] A. Banavar et al., "Nutritional evaluation of black soldier fly frass as an ingredient in Florida Pompano (Trachinotus carolinus L.) diets," *Animals*, vol. 12, no. 18, p. 2407, 2022. doi: 10.3390/ani12182407.

[40] T. M. Santana et al., "Black soldier fly (Hermetia illucens) larvae exoskeleton as a potential source of chitin in diets for juvenile channel catfish (Ictalurus punctatus)," *Fish Physiol. Biochem.*, vol. 51, no. 4, p. 135, 2025. doi: 10.1007/s10695-025-01551-6.

[41] M. Tabbara et al., "Growth and disease resistance of channel catfish offered dietary black soldier fly larva frass," *N. Am. J. Aquac.*, vol. 87, no. 4, pp. 247–258, 2025. doi: 10.1093/naaqua/vraf014.

[42] I. G. Lopes, J. W. Yong, and C. Lalander, "Frass derived from black soldier fly larvae treatment of biodegradable wastes. A critical review and future perspectives," *Waste Manag.*, vol. 142, pp. 65–76, 2022. doi: 10.1016/j.wasman.2022.02.007.

[43] S. Song et al., "Upcycling food waste using black soldier fly larvae: Effects of further composting on frass quality, fertilising effect and its global warming potential," *J. Clean. Prod.*, vol. 288, p. 125664, 2021. doi: 10.1016/j.jclepro.2020.125664.

[44] G. Chen et al., "Feed nutritional composition affects the intestinal microbiota and digestive enzyme activity of black soldier fly larvae," *Front. Microbiol.*, vol. 14, p. 1184139, 2023. doi: 10.3389/fmicb.2023.1184139.

[45] M. M. Holen et al., "The effect of dietary chitin on Atlantic salmon (Salmo salar) chitinase activity, gene expression, and microbial composition," *Aquac. Fish.*, 2024. doi: 10.1016/j.aaf.2024.10.005.

[46] Ø. Karlsen, H. Amlund, A. Berg, and R. E. Olsen, "The effect of dietary chitin on growth and nutrient digestibility in farmed Atlantic cod, Atlantic salmon and Atlantic halibut," *Aquac. Res.*, vol. 48, no. 1, pp. 123–133, 2017. doi: 10.1111/are.12867.

[47] V. Kumar et al., "Insect (black soldier fly, Hermetia illucens) meal supplementation prevents the soybean meal-induced intestinal enteritis in rainbow trout and health benefits of using insect oil," *Fish Shellfish Immunol.*, vol. 109, pp. 116–124, 2021. doi: 10.1016/j.fsi.2020.12.008.

[48] Y. Li, T. M. Kortner, E. M. Chikwati, I. Belghit, E. J. Lock, and Å. Krogdahl, "Total replacement of fish meal with black soldier fly (Hermetia illucens) larvae meal does not compromise the gut health of Atlantic salmon (Salmo salar)," *Aquaculture*, vol. 520, p. 734967, 2020. doi: 10.1016/j.aquaculture.2020.734967.

[49] J. P. T. Higgins and S. G. Thompson, "Quantifying heterogeneity in a meta-analysis," *Stat. Med.*, vol. 21, no. 11, pp. 1539–1558, 2002. doi: 10.1002/sim.1186.

[50] M. Egger, G. D. Smith, M. Schneider, and C. Minder, "Bias in meta-analysis detected by a simple, graphical test," *BMJ*, vol. 315, no. 7109, pp. 629–634, 1997. doi: 10.1136/bmj.315.7109.629.

[51] C. D. S. Z. Lalander, S. Diener, C. Zurbrügg, and B. Vinnerås, "Effects of feedstock on larval development and process efficiency in waste treatment with black soldier fly (Hermetia illucens)," *J. Clean. Prod.*, vol. 208, pp. 211–219, 2019. doi: 10.1016/j.jclepro.2018.10.017.

[52] N. Li et al., "Effects of substitution of fish meal with black soldier fly (Hermetia illucens) larvae meal, in yellow catfish (Pelteobagrus fulvidraco) diets," *Isr. J. Aquac. Bamidgeh*, vol. 69, 2017. doi: 10.46989/001c.21056.

[53] N. Gou, K. Wang, T. Jin, and B. Yang, "First insights on the administration of insect oil (black soldier fly larvae) in the diet of juvenile Onychostoma macrolepis," *Animals*, vol. 13, no. 3, p. 518, 2023. doi: 10.3390/ani13030518.

[54] Y. Liu et al., "Physiological response of rainbow trout (Oncorhynchus mykiss) to graded levels of novel Chlorella sorokiniana meal as a single fishmeal alternative or combined with black soldier fly larval meal," *Aquaculture*, vol. 561, p. 738715, 2022. doi: 10.1016/j.aquaculture.2022.738715.

[55] N. Wu et al., "A full recycling chain of food waste with straw addition mediated by black soldier fly larvae: Focus on fresh frass quality, secondary composting, and its fertilizing effect on maize," *Sci. Total Environ.*, vol. 885, p. 163386, 2023. doi: 10.1016/j.scitotenv.2023.163386.

[56] D. Kreft, S. Hurka, F. F. Gurusinga, T. Röthig, A. Vilcinskas, and D. Tegtmeier, "Towards functional fertilisers: Feed composition shapes microbial community structure and viability in black soldier fly (Hermetia illucens) frass," *Environ. Microbiol.*, vol. 28, no. 2, p. e70249, 2026. doi: 10.1111/1462-2920.70249.

[57] C. Garino et al., "Challenges and opportunities of farming insects as feed for aquaculture: a comparison between EU and Latin American market," *J. Insects Food Feed*, vol. 1, no. aop, pp. 1–18, 2026. doi: 10.1163/23524588-bja10401.

[58] H. Makkar, V. Heuzé, and G. Tran, "Locusts and grasshoppers: nutritional value, harvesting and rearing for animal feed, and other applications," *CABI Rev.*, 2022. doi: 10.1079/cabireviews202217038.

[59] H. Fischer, N. Romano, N. Renukdas, V. Kumar, and A. K. Sinha, "Comparing black soldier fly (Hermetia illucens) larvae versus prepupae in the diets of largemouth bass, Micropterus salmoides: Effects on their growth, biochemical composition, histopathology, and gene expression," *Aquaculture*, vol. 546, p. 737323, 2022.

[60] K. M. Eggink, S. L. Aalto, P. B. Pedersen, I. Lund, and J. Dalsgaard, "Effects of dietary chitin on nutrient digestibility, cholesterol metabolism, digestive enzyme activity, and gut microbiome in rainbow trout," *Anim. Feed Sci. Technol.*, p. 116447, 2025. doi: 10.1016/j.anifeedsci.2025.116447.

[61] O. V. Adeniyi, A. S. Norman, and S. Onojobi, "Effects of dietary supplementation of Parkia biglobosa pulp on growth performance and physiological status of Clarias gariepinus fingerlings," *J. Basic Appl. Zool.*, vol. 84, no. 1, p. 19, 2023. doi: 10.1186/s41936-023-00340-y.

[62] S. Pinho et al., "Insect-based fish feed in decoupled aquaponic systems: Effect on lettuce production and resource use," *PLoS ONE*, vol. 19, no. 1, p. e0295811, 2024. doi: 10.1371/journal.pone.0295811.

[63] J. Abernathy et al., "Transcriptome analysis and immune gene expression of channel catfish (Ictalurus punctatus) fed diets with inclusion of frass from black soldier fly larvae," *Front. Physiol.*, vol. 14, p. 1330368, 2024. doi: 10.3389/fphys.2023.1330368.

[64] N. Romano, S. N. Datta, A. K. Sinha, and G. S. J. Pande, "Partially replacing synthetic fertilizer with black soldier fly (Hermetia illucens) larvae frass enhances kale (Brassica oleracea var. sabellica) production," *Technol. Hortic.*, vol. 3, no. 1, 2023a. doi: 10.48130/TIH-2023-0008.

[65] J. Lu et al., "Probing the antioxidant activity of functional proteins and bioactive peptides in Hermetia illucens larvae fed with food wastes," *Sci. Rep.*, vol. 12, no. 1, p. 2799, 2022. doi: 10.1038/s41598-022-06668-9.

[66] J. Poveda, "Insect frass in the development of sustainable agriculture. A review," *Agron. Sustain. Dev.*, vol. 41, no. 1, p. 5, 2021. doi: 10.1007/s13593-020-00656-x.

[67] G. Tran, V. Heuzé, and H. P. Makkar, "Insects in fish diets," *Anim. Front.*, vol. 5, no. 2, pp. 37–44, 2015. doi: 10.2527/af.2015-0018.

[68] X. Xiao et al., "Effects of black soldier fly (Hermetia illucens) larvae meal protein as a fishmeal replacement on the growth and immune index of yellow catfish (Pelteobagrus fulvidraco)," *Aquac. Res.*, vol. 49, no. 4, pp. 1569–1577, 2018. doi: 10.1111/are.13611.

[69] R. Salomone, G. Saija, G. Mondello, A. Giannetto, S. Fasulo, and D. Savastano, "Environmental impact of food waste bioconversion by insects: application of life cycle assessment to process using Hermetia illucens," *J. Clean. Prod.*, vol. 140, pp. 890–905, 2017. doi: 10.1016/j.jclepro.2016.06.154.

[70] G. M. Turchini, J. T. Trushenski, and B. D. Glencross, "Thoughts for the future of aquaculture nutrition: realigning perspectives to reflect contemporary issues related to judicious use of marine resources in aquafeeds," *N. Am. J. Aquac.*, vol. 81, no. 1, pp. 13–39, 2019. doi: 10.1002/naaq.10067.

[71] Y. Wang, J. Quan, X. Cheng, C. Li, and Z. Yuan, "Relationship of black soldier fly larvae (BSFL) gut microbiota and bioconversion efficiency with properties of substrates," *Waste Manag.*, vol. 180, pp. 106–114, 2024. doi: 10.1016/j.wasman.2024.03.030.

[72] M. Yıldırım-Aksoy, R. Eljack, J. Aksoy, and B. H. Beck, "Frass from black soldier fly larvae, Hermetia illucens, as a possible functional dietary ingredient in channel catfish feed," *Fishes*, vol. 8, no. 11, p. 542, 2023. doi: 10.3390/fishes8110542.

[73] T. Veldkamp et al., "Overcoming technical and market barriers to enable sustainable large-scale production and consumption of insect proteins in Europe: A SUSINCHAIN perspective," *Insects*, vol. 13, no. 3, p. 281, 2022. doi: 10.3390/insects13030281.

# PHYTOCHEMICAL COMPOSITION AND IN VITRO ANTIOXIDANT ACTIVITY OF METHANOLIC LEAF EXTRACT OF *FICUS ABUTILIFOLIA*

**Sani Iyal Naiya*, Rahmatu Abubakar Madaki, Dahiru Idris, Jamilat Ishaq Jumare, Ja'afar Muhammad Nasir**

*Department of Chemistry and Biochemistry, Nuhu Bamalli Polytechnic, Zaria, Kaduna State*
**Corresponding Author: Serneyiyerl@gmail.com*

**Abstract**

*Ficus abutilifolia* (Moraceae), commonly known as "large-leaved rock fig" or "waa" in Hausa, is traditionally used in Nigeria to treat typhoid fever, dysentery, sexually transmitted infections, epilepsy, and other ailments. However, scientific data on its phytochemical constituents and antioxidant capacity are limited. This study aimed to qualitatively screen the phytochemicals and evaluate the DPPH radical scavenging activity of the methanolic leaf extract of *F. abutilifolia*. Leaves were collected from Soba Local Government Area, Kaduna State, Nigeria, air-dried, powdered, and extracted with 80% methanol by maceration. Phytochemical screening was performed using standard colorimetric tests. Antioxidant activity was assessed using the DPPH assay at concentrations of 31.25–500 μg/mL, with ascorbic acid as reference. Phytochemical analysis revealed the presence of flavonoids, saponins, terpenoids, and tannins, while alkaloids and glycosides were absent. The DPPH scavenging activity was concentration-dependent, with the highest inhibition (56.91 ± 0.35%) at 500 μg/mL and the lowest (19.28 ± 0.34%) at 31.25 μg/mL. Ascorbic acid showed 81.52–92.39% inhibition across the same concentration range. The methanolic leaf extract of *F. abutilifolia* contains bioactive phytochemicals (flavonoids, saponins, terpenoids, tannins) and exhibits moderate antioxidant activity, supporting its traditional use in managing oxidative stress-related diseases.

**Keywords:** *Ficus abutilifolia*, Phytochemical screening, DPPH, antioxidant

## 1. Introduction

Medicinal plants remain one of the most important sources of bioactive compounds used in traditional medicine and modern drug discovery. In recent years, there has been increasing scientific interest in plant-derived phytochemicals due to their therapeutic potential against oxidative stress-related diseases such as cancer, diabetes mellitus, cardiovascular disorders, inflammation, and neurodegenerative diseases. Natural antioxidants from medicinal plants are considered safer and more environmentally friendly alternatives to synthetic antioxidants because they possess fewer side effects and significant pharmacological activities [1-3]. Oxidative stress results from excessive generation of reactive oxygen species (ROS) and free radicals beyond the capacity of the body's antioxidant defense system. These reactive molecules can induce lipid peroxidation, protein oxidation, DNA damage, and cellular dysfunction, thereby contributing to the pathogenesis of several chronic diseases. Consequently, the search for natural antioxidant compounds from medicinal plants has become an important area of phytochemical and pharmaceutical research. Plant secondary metabolites such as flavonoids, phenolics, tannins, alkaloids, terpenoids, and saponins are known to exhibit strong antioxidant activities through free radical scavenging, metal chelation, and inhibition of oxidative reactions [4].

*Ficus abutilifolia* (Miq.) Miq. is a small to medium-sized, deciduous tree belonging to the Moraceae family. It grows widely in sub-Saharan Africa, including Nigeria, where it is known as "waa" (Hausa), "Lapalapa" (Yoruba), and "Agbu inu" (Igbo). Traditionally, the leaves, bark, and latex of *F. abutilifolia* are used to treat typhoid fever, chronic dysentery, sexually transmitted infections, malaria, infertility, epilepsy, jaundice, hypertension, coughs, and rheumatism. The bark decoction is also taken as a general tonic [6]. Phytochemical investigations of *Ficus* species have revealed the presence of diverse bioactive compounds including flavonoids, phenolics, tannins, sterols, saponins, and triterpenoids responsible for their pharmacological activities [6]. Previous studies have demonstrated that leaf extracts of *Ficus abutilifolia* possess antibacterial, antioxidant, and nutraceutical properties attributable to the presence of bioactive phytochemicals. Recent investigations further revealed that methanolic and ethanolic extracts of the plant contain appreciable levels of phenolics and flavonoids associated with strong antioxidant activities [2]

## 2. Material and Methods

### Plants Collection and Identification

Fresh leaves of *Ficus abutilifolia* were collected in April 2024 from Giwa Local Government Area, Kaduna State, Nigeria. Plant identification was authenticated by Mallam Namadi Sunusi of the Department of Botany, Ahmadu Bello University, Zaria, where voucher specimens (742) were deposited

### Extraction

The phytochemical compounds were extracted by the organic solvent extraction method following the procedure of Islam et al. 2023. The powder samples (100 g) were dissolved in 400 mL of 80% methanol (sample: solvent =1:20 (w/v)) and extracted for 74hr at room temperature in a mechanical shaker at 4000 rpm. The Samples was filtered through a Whatman 1 filter paper, and the filtrates were vacuum evaporated at 40 °C. The resulting extracts were stored at 18 ◦C until further analysis.

### Phytochemical Analysis

The qualitative test was carried out on the aqueous extract of the *Ficus abutilifolia*, using the methods of [7], for the presence of alkaloids, tannins, saponins, flavonoids, glycosides, cardiac glycosides, saponins.

### Determination of the Radical Scavenging Ability (DPPH)

The free radical scavenging ability of the extract against DPPH (1,1- diphenyl-2-picryhydrazyl) was carried out using the method of One milliliter of the extract was mixed with 1 mL of the 0.4 mM methanolic solution of the DPPH, and then the mixture was left in the dark for 30 min before measuring the absorbance at 517 nm. The control consisted of methanol instead of the sample and the radical scavenging ability of the sample was calculated as:

$$\% DPPH = \frac{A_{control} - A_{sample}}{A_{control}} \times 100$$

## 3. Results and Discussion

Qualitative analysis of the methanolic leaf extract of *F. abutilifolia* revealed the presence of flavonoids, saponins, terpenoids, and tannins. Alkaloids and glycosides were absent. The results are summarized in the following table.

**Table 1: Phytochemical Composition**

| Phytochemical | Result |
|---|---|
| Alkaloids | – |
| Flavonoids | + |
| Saponins | + |
| Terpenoids | + |
| Tannins | + |
| Glycosides | – |

Key: + = present; – = absent

**Table 2: DPPH Radical Scavenging Activity** *(%) of methanolic leaf extract of* ***F. abutilifolia***

| Concentration (µg/mL) | Extract (% inhibition) | Ascorbic Acid (% inhibition) |
|---|---|---|
| 31.25 | 19.28 ± 0.34 | 81.52 ± 0.68 |
| 62.5 | 25.31 ± 0.30 | 85.33 ± 0.35 |
| 125 | 36.54 ± 0.37 | 88.65 ± 0.49 |
| 250 | 46.67 ± 0.12 | 90.99 ± 0.14 |
| 500 | 56.91 ± 0.35 | 92.39 ± 0.08 |

**Phytochemical Screening of *Ficus abutilifolia* Leaf Extract**

The qualitative phytochemical screening of the methanolic leaf extract of *Ficus abutilifolia* revealed the presence of flavonoids, saponins, tannins, and terpenoids, while alkaloids and glycosides were absent. The occurrence of these phytochemicals suggests that the plant possesses important medicinal and antioxidant properties attributable to its secondary metabolites. The presence of flavonoids observed in this study agrees with previous investigations on *Ficus* species. [2] reported appreciable flavonoid and phenolic

contents in methanolic leaf extracts of *Ficus abutilifolia*, indicating that flavonoids constitute one of the major bioactive compounds responsible for the antioxidant activity of the plant. Similarly,

Saponins detected in the extract are consistent with the findings of [5], who reported the presence of saponins in *Ficus abutilifolia* leaf extracts and suggested that these compounds contribute to the plant's antimicrobial and anti-inflammatory properties. Saponins are recognized for their membrane-permeabilizing effects and therapeutic potentials including cholesterol-lowering and immunomodulatory activities. The presence of tannins in the extract corroborates earlier studies on *Ficus* species. Tannins are polyphenolic compounds widely reported to possess antioxidant, antimicrobial, and astringent properties. The tannin content observed in this study may contribute significantly to the antioxidant activity demonstrated by the extract due to their ability to scavenge reactive oxygen species and inhibit lipid peroxidation.

Terpenoids were also present in the methanolic extract, in agreement with previous reports by [1], who identified terpenoids as common phytochemicals in medicinal *Ficus* species. Terpenoids possess several pharmacological activities including antioxidant, anti-inflammatory, anticancer, and antimicrobial effects.

However, the absence of alkaloids and glycosides in this study differs slightly from some previous reports on related *Ficus* species where trace amounts of alkaloids were detected [8]. Variations in phytochemical composition may arise from differences in geographical location, climatic conditions, plant age, extraction solvent, harvesting period, and analytical methods employed.

**Antioxidant Activity of Methanolic Leaf Extract of *Ficus abutilifolia***

The methanolic leaf extract of *Ficus abutilifolia* exhibited concentration-dependent DPPH free radical scavenging activity, with antioxidant activity increasing progressively from 19.28 ± 0.34% at 31.25 µg/mL to 56.91 ± 0.35% at 500 µg/mL. Although the antioxidant activity of the extract was lower than that of the standard ascorbic acid, the extract demonstrated appreciable antioxidant potential. The antioxidant activity observed in this study is comparable to previous findings reported for *Ficus* species and other medicinal plants rich in phenolic compounds. [2] reported that methanolic extracts of *Ficus abutilifolia* possessed significant antioxidant activity attributable to their high phenolic and flavonoid contents. Similarly, [3] observed concentration-dependent antioxidant activity in *Ficus asperifolia* extracts and attributed the activity to the presence of flavonoids, tannins, and phenolic compounds.

The gradual increase in scavenging activity with increasing concentration observed in this study agrees with the general mechanism of plant-derived antioxidants, where higher concentrations provide more hydrogen atoms or electrons required for neutralizing free radicals. Similar concentration-dependent antioxidant activities have been reported in other medicinal plants containing polyphenolic compounds [4]. The antioxidant activity observed may be directly associated with the phytochemicals detected in the extract, particularly flavonoids and tannins, which are known for their ability to donate hydrogen atoms, scavenge free radicals, inhibit oxidative chain reactions, and reduce lipid peroxidation. The synergistic interaction among these phytochemicals may further enhance the antioxidant effectiveness of the extract.

## 4. **Conclusion**

The methanolic leaf extract of *Ficus abutilifolia* contains flavonoids, saponins, terpenoids, and tannins, but lacks alkaloids and glycosides. The extract exhibits concentration-dependent DPPH radical scavenging activity, with a maximum inhibition of 56.91% at 500 µg/mL. The antioxidant property is likely contributed by the phenolic and flavonoid constituents, supporting the traditional use of this plant in managing oxidative stress-related diseases.

**References**

[1] Ahmed, S. E. A., Temraz, A., & Baky, M. H. Phytochemical diversity of genus *Ficus*: A mini review. *ERU Research Journal, 2*(3), 502–524, 2023.

[2] Attama, C., Lawrence, L., & Janet, J. N. Antioxidant and nutraceutical profiling, and GC-MS characterization of *Ficus abutilifolia* leaf extracts and essential oil. *International Journal of Scientific Research in Chemical Sciences, 12*(3), 2025.

[3] Johnny, D. I., & Kadiri, H. E. Evaluation of phytochemical constituents and in-vitro antioxidant properties of *Ficus asperifolia* leaf extracts. *Journal of Applied Sciences and Environmental Management, 27*(10), 2023.

[4] Sandhu, A. K., Islam, M., Edirisinghe, I., & Burton-Freeman, B. Phytochemical composition and health benefits of figs (fresh and dried): A review of literature from 2000 to 2022. *Nutrients, 15*(11), 2023.

[5] Taiwo, F. O., Fidelis, A. A., & Oyedeji, O. Antibacterial activity and phytochemical profile of leaf extracts of *Ficus abutilifolia. Journal of Pharmaceutical Research International, 11*(6), 1–10, 2016.

[6] Ukwubile, C.A.(2010).Pharmacognostic, Antibacterial and Toxicity Investigations of Ficus abutlilifolia Miq. (Moraceae).In: *International Journal of Biological Sciences*, Vol. 2(8): 98-111, 2010.

[7] Harborne JB. Phytochemical Methods. Chapman and Hall Ltd., London. 1973; 49- 188. 25. Just MJ, Recio MC, Giner RM, Cueller MJ, Manez S, Bilia AR.Antiinflammatory activity of unusual lupine saponins from BupleurumFruticescens. *Planta Med.* 1998;64:404-407.

[6] Johnny, D. I., & Kadiri, H. E. Evaluation of phytochemical constituents and in-vitro antioxidant properties of *Ficus asperifolia* leaf extracts. *Journal of Applied Sciences and Environmental Management, 27*(10), 2023.

[7] Sandhu, A. K., Islam, M., Edirisinghe, I., & Burton-Freeman, B. Phytochemical composition and health benefits of figs (fresh and dried): A review of literature from 2000 to 2022. *Nutrients, 15*(11), 262, 2023.

# QUALITATIVE PHYTOCHEMICAL SCREENING AND ANTIOXIDANT ACTIVITY OF LEAVES, STEM BARK AND ROOT OF GUMBO LIMBO (*Bursera simaruba)*

**Abbas Lawal[1*], Abdullahi Sahal[1] and Samaila Audu Jovial[2]**

*[1]Department of Chemistry and Biochemistry,Nuhu Bamalli Polytechnic, Zaria Kaduna State.*
*[2]Department of Science Laboratory Technology, Mai Idris Alooma Polytechnic Geidam Yobe State.*
**Corresponding Author: ayinmammada@gmail.com*

**Abstract**

The research work is about investigating the presence of phytochemicals and antioxidant activity of the Roots, Stem bark and Leaves of Bursera simaruba. Maceration extraction method was used to extract the chemical constituents using Methanol, Chloroform and Toluene as solvents. The extracts were screened using standard procedure. The results of the Phytochemicals Screening indicated the presence of Flavonoids, Alkaloids, Phenols, Terpenoids, Tannins, Steroids and Glycosides in the Roots, Stem back and leaves of Bursera simaruba. Alkaloids was only detected in the Root extract and Saponins detected in the Stem bark and Leaves extract. The half maximum inhibitory concentrations (IC 50 ), of the Antioxidant Radical Scavenging Activity were found to be, Leaves extract 8.54 mg / L; Stem bark extract 8.04 mg/L and Root extract 7.69 mg/L. It is recommended that further research be carried out on the antioxidant scavenging activity assay using other methods for example DPP method for Radical Scavenging Activity.

**Keywords:** *Bursera simaruba,* Gumbo Limbo, Phytochemical Screening, AntiOxidant Activity, Extraction.

## 1. Introduction

Cancer is one of the silent killer diseases threatening the world. This is a large group of diseases that can affect any part of human body. These abnormalities and diseases can be associated with cancer, prolific growth or boil that discharges watery substances with offensive odor, vision loss, heart diseases, arthritis, stroke, respiratory diseases, immune deficiency, Parkinson or Alzheimer's disease, fast aging, emphysema and hair loss. Cancer is caused by free radicals. These are molecules with deficiency of electron in their structure. Free radicals can steal electrons (oxidation) from healthy molecules of the cells making those cells to lose their capacity of working properly 1].

Environmental pollution, Ionizing radiation, the by-products of metabolism of the food and medicine we take, the water we drink as well as the air we breathe in generate free radicals which are very reactive and disastrous in the body of human beings. Free radicals are also produced as a result of exposure to ultra violet rays and cigarette smoking. Free radicals are also known as reactive oxygen and reactive nitrogen species (ROS and RNS). These free radicals are, Hydroxyl (OH·), Superoxides ($O_2$·), Nitric Oxide (NO·), Nitrogen dioxide ($NO_2$·), Neroxyl (ROO·) and Lipid peroxyl (LOO·). "Free radicals are unstable molecules that the body produces as a reaction to environmental and other pressures as the body processes food and react to environment" Free radicals cause oxidative stress. Oxidative stress causes damage to deoxyribonucleic acid (DNA). Damage to DNA, leads to many diseases [1].

"An anti- oxidant is any substance that has the ability to give up an electron to free radicals and balanced out the unpair electrons which neutralizes the free radicals there by inhibiting the oxidation of another molecule, without becoming free radical themselves". Anti- oxidants found in human include, Ascorbic acid (vitamin C), Glutathione, Lipoic acid, Uric acid, Carotenes, α – tocopherol (vitamin E) and Ubiquinol (coenzyme Q) [1].

Gumbolinbo is a large semi evergreen tree that grows up to 25 meters in height with red shaggy back that peels off in papery thin stripes. Its leaves are 5 – 12 cm long and produces small round fruits 8mm long [2]. Gumbolimbo is known as "Bazana" in Hausa language northern Nigeria. Gumbolimbo's scientific name is *Bursera simaruba* from the Burceraceae family.

*Bursera simaruba* is used locally in the treatment of breast cancer. The strips of peeling back are boiled and used topically for sunburn, insect bites, sores and rashes. The tea is drunk for backache, colds, flu and urinary tract infections. Gumbolimbo has been used for the treatment of dysentery and yellow fever [3]. This research focus attention on finding out the presence of phytochemicals as well as assessing the anti-oxidant properties of the leaves, stems and roots of *Bursera simaruba.*

## 2. Material and Methods

UV – Visible Spectrophotometer (Cary 300 Spectrophotometer), pH meter, Mortar and pestle, Analytical Balance, Filter paper, Funnel, Test tubes brush, Beakers, Pasteur pipettes, Test tubes, Water bath and Wash bottle. Other materials included Detergent, Distilled water, Hydrochloric acid (HCl), Ferric Chloride ($FeCl_3$), Acetic acid ($CH_3$ $CH_2COOH$), Lead acetate Pb ($CH_3$ $CH_2$ $COO)_2$, Tetraoxosulphate (vi) acid ($H_2$ $SO_4$), Chloroform ($CHCl_3$), Methanol, Toluene, Acetic Anhydride, Gelatin solution, Hydrogen Peroxide ($H_2O_2$), Mono Potassium dihydrogen Phosphate ($KH_2PO_4$), Dipotassium hydrogen Phosphate ($K_2HPO_4$) and Potassium Hydroxide (KOH).

### Extraction

The extracts were obtained using maceration method. The powdered Portion of the air dried leaves, stem bark and roots of *Bursera simaruba* (100g) was placed into a seperate container each and subjected to Toluene, Chloroform and Methanol extraction. Volume of solvent (200 ml) was used as the quantity of extracting solvent. The container was then closed and left for two weeks. The container was shaken from time to time during the period of extraction. At the end of two weeks, the mixture was filtered and the filtrate concentrated using water bath.

### Phytochemical Screening

The preliminary phytochemicals test of the three extracts, Methanol, Chloroform, and Toluene were carried out using standard procedures to identify the various constituents as described by Bargah [4] , Nishad [5], Khan [6] and Abubakar and Haque [7].

### Antioxidant activity

The ability of the *Bursera simaruba's* extract to scavenge hydrogen peroxide was measured by using standard $H_2O_2$ scavenging assay method. A solution of hydrogen peroxide (40 mM) was prepared in phosphate buffer saline (pH 7.4). A series of various concentrated solution of the extracts were

prepared in ethanol (95%) and added (1 ml) of the hydrogen peroxide solution (40 mM). The absorbance of hydrogen peroxide at 250 nm was determined after 10 minutes against a blank solution (Ethanol 95%). Ascorbic acid was used as standard. The percentage of scavenging Activity of hydrogen peroxide was calculated by using the following equation as described by Kaser et.al. [8].

Percentage of Radical Scavenging Activity ($H_2O_2$) := [(Ai-At/Ai] *100

Where $A_i$, is the absorbance of control and $A_t$, is the absorbance of test (sample).

$H_2O_2$ scavenging activity Inhibition of the extract was expressed in terms of $IC_{50}$ value

**Preparation of Standards and Samples**

Ascorbic acid was used as the standard. Different concentrations of ascorbic acid (vitamin C) (0.60 mg/L, 0.40 mg / L, 0.20 mg / L 0.10mg / L, 0.08 mg / L and 0.06 mg / L) were prepared using ethanol as solvent. Hydrogen peroxide ($H_2O_2$) solution (40mM) was also prepared using Phosphate buffer of pH 7.4 as solvent. Different concentrations of the extract solutions (0.60 mg / L; 0.40 mg / L; 0.20 mg / L; 0.10 mg / L; 0.08 mg / L; 0.06 mg / L were also prepared using ethanol 95% as the solvent.

A solution of hydrogen peroxide (40 mM) was also prepared in phosphate buffer saline (pH 7.4). Ethanol 95% solution was used as the Blank.

**Analysis**

Buffer solution containing the hydrogen peroxide ($H_2O_2$) was pipetted (1.0 ml) and added to each of the standard solutions and each of the sample solutions prepared and allow to stand for 10.0 minutes before their absorbance's were read in the UV – Visible spectrophotometer. The absorbance's read was recorded and calibration curve plotted.

**3. Results and Discussion**

Table1: screening for leaves extract of *Bursera simaruba*

| Phytochemicals | M | C | T |
|---|---|---|---|
| Flavonoids | - | + | - |
| Alkaloids | - | - | - |
| Phenols | - | + | - |
| Saponnins | - | - | + |
| Tannins | + | + | - |
| Steroids | + | + | + |

| | | | |
|---|---|---|---|
| Terpenoids | + | + | - |
| Glycosides | + | - | - |

KEY: M = Methanol extract; C = Chloroform extract; T = Toluene extract, + means present; - means absent.

Table2: Screening for stem bark extract of *Bursera simaruba*

| Phytochemicals | M | C | T |
|---|---|---|---|
| Flavonoids | - | + | - |
| Alkaloids | - | - | - |
| Phenols | + | + | - |
| Saponnins | - | - | + |
| Tannins | + | + | - |
| Steroids | + | + | + |
| Terpenoids | + | - | - |
| Glycosides | + | + | - |

Table 3: Screening for Root extract of *Bursera simaruba*

| Phytochemicals | M | C | T |
|---|---|---|---|
| Flavonoids | + | + | - |
| Alkaloids | + | + | - |
| Phenols | + | - | - |
| Saponnins | - | - | - |
| Tannins | + | - | - |
| Steroids | + | - | - |

| | | | |
|---|---|---|---|
| Terpenoids | + | + | - |
| Glycosides | + | + | - |

Table 4: Antioxidant Activity of the Leaves of *Bursera simaruba*

| S/N | ABS CONTL | ABS Sample | CONC Mg/L | %RSA | **$IC_{50}$** (mg / L) | **$IC_{50}$** (mg / g) |
|---|---|---|---|---|---|---|
| 1 | 0.0476 | 0.0512 | 0.60 | -7.56 | 8.54 | 0.016 |
| 2 | 0.0363 | 0.0341 | 0.40 | 6.06 | | |
| 3 | 0.0236 | 0.0171 | 0.20 | 27.54 | | |
| 4 | 0.0085 | 0.0085 | 0.10 | 0 | | |
| 5 | 0. 0068 | 0.0068 | 0.06 | 0 | | |
| 6 | 0.0051 | 0.0051 | 0.08 | 0 | | |

Table 5 Antioxidant Activity of the Stem bark of *Bursera simaruba*

| S/N | ABS Controle | ABS Sample | Concn, mg / L | %RSA | **$IC_{50}$** (mg / L) | **$IC_{50}$** (mg / g) |
|---|---|---|---|---|---|---|
| 1 | 0.0476 | 0.0511 | 0.60 | -7.35 | 8.04 | 0.015 |
| 2 | 0.0363 | 0.0341 | 0.40 | 6.06 | | |
| 3 | 0.0236 | 0.0170 | 0.20 | 27.96 | | |
| 4 | 0.0085 | 0.0085 | 0.10 | 0 | | |
| 5 | 0.0068 | 0.0068 | 0.08 | 0 | | |
| 6 | 0.0051 | 0.0051 | 0.06 | 0 | | |

Table 6 Antioxidant Activity of the Roots of *Bursera simaruba*

| S / N | ABS Controle | ABS Sample | Concn, mg / L | %RSA | **$IC_{50}$** (mg / L) | **$IC_{50}$** (mg / g) |
|---|---|---|---|---|---|---|
| 1 | 0.0476 | 0.0509 | 0.60 | -6.93 | 7.68 | 0.015 |
| 2 | 0.0363 | 0.0341 | 0.40 | 6.06 | | |
| 3 | 0.0236 | 0.0171 | 0.20 | 27.54 | | |
| 4 | 0.0085 | 0.0085 | 0.10 | 0 | | |
| 5 | 0.0068 | 0.0068 | 0.08 | 0 | | |
| 6 | 0.0051 | 0.0051 | 0.06 | 0 | | |

Table 1 shows the result of the phytochemical screening of the leaves of *Bursera simaruba.* The result indicated that the leaves contain the following phytochemicals: Flavonoids, Phenols, Terpenoids, Tannins, Glycosides, Steroids and Saponins. Table 2 shows the result for the phytochemical Screening of the Stem Bark. The result shows the presence of Flavonoids, Phenols, Terpenoids, Tannins, Glycosides, Steroids and Saponins in the Stem Bark of *Bursera simaruba.* Similarly, table 3 shows the result for Phytochemical screening of the root of *B. simaruba.* The results indicated the presence of the Flavonoids, Alkaloids, Phenols, Tannins, Glycosides and Steroids in the root of *Bursera simaruba.* The results show that Terpenoids and Saponins are absent in the root, while Alkaloids is absent in the Stem bark and leaves.

Table 4, Table 5 and Table 6 show the results for Antioxidant Radical Scavenging Activities for leaves, Stem bark and root of *Bursera simaruba.* The results indicated that the Half maximum Inhibitory Concentration ($IC_{50}$) are as follows, leaves 8.54 mg / L; Stem bark, 8.04 mg / L and Root, 7.69 mg / L. The presence of Terpenoids, Flavonoids and Phenolic acids were confirmed to be present in the methanolic extract of stem bark of *Bursera simaruba* by Bah *et.al.*[9].

**4. Conclusion**

Presence of alkaloids in the root, saponnins in the stem bark and leaves indicated that these parts of the plant can work as antimicrobial and insecticidal agents. Presence of phenols, flavonoids and tannins show that the plant has great potential for antioxidant activity. Moreover, presence of terpenoids indicated that essential oil can also be obtained from the stem bark and leaves of *Bursera simaruba.*

**References**

[1]Xavier Prasad (2022) Anti Oxidant Activity Determination of Plant Extracts, How to Calculate $IC_{50}$ Pick Pharma DXP

[2]Edward E. G., Dennis G. W., Ryan W. K., Andraw K. K., Deborah R. H., and Drew C. M. (2018) Bursera simaruba: Gumbo limbo UF / IFAS Extention University of Florida https://www.researchgate.net>--->Anatomy>Feel

[3]Gilman, E. F. and Watson D. (1993). *Bursera simaruba* (Gumbo Limbo) Fact Sheet ST – 10. https://hort.ifas.ufl.edu./tree/BURSIMA.pdf

[4]Bargah, R. K. (2015). Priliminary test of Phytochemical Screening of crude ethanolic and aqueous extract of *Moringa pterygosperma Gaertn* ***Journal of Pharmacognosy and Phytochemistry Vol 4 (1) 07 – 09.*** https://www.phytojournal.com/archieves/2015/vol4 issue1/partA/6.1 pdf.

[5]Nishad, P. (2018). Phytochemical Test of Alkaloids; Flavonoids; Saponins Tannins. Solution Pharmacy..

[6]Khan, T. (2019). Phytochemical Screening I Bhagyadary Pharmaceutical Saga

[7]Abubakakar, A.R. and Haque, M. (2020). Preparation of Medicinal Plants: Basic Extraction and Fractionation Procedures for Experimental Purposes. ***Journal of Pharmacy and Bioallied Sciences. 12 ; 1- 10.***

[8]Keser, S.; Celik, S.; Turkoglu, S.; Yilmaz, O. and Turkoglu, I. (2012). Hydrogen Peroxide Radical Scavenging and Total Antioxidant Activity of Hawthorn. ***Chemistry Journal Vol.02, Issue, 01 PP 09 – 12.*** https://www.researchgate.net>publication>26034371

[9]Bah M.M., Marina, D., Avelo, G., Mendoza S. and Castaneda – Moreno, R. (2014). Chemical Constituents and antioxidant activity of extracts obtained from branch bark of *Bursera simaruba.* Aromaticas 13 (6): 527 – 536. Research gate/publication/286114616_chemical _constituents_ and antioxidant activity_of_ extracts_obtained_from_branch_bark_ of Bursera_simaruba.

[10]Breslin, (2017). Effects of solvent type on phenolics and flavonoids content and antioxidant activities in two varieties of young ginger (Zingiberofficinale Roscoe) extracts. J Med Plants Res. 2011;5(7):1147-1154.

[11]Egbuna, C.; Jonathan, C.I.; Kryeziu, T. (2018). Introduction to Phytochemistry. *Phytochemistry Vol.1 Fundamentals, Modern Techniques and Applications. Edition 1st* Apple Academic Press / CRC press / Tylor & Francis DOI: 10.13140/RG.2.2.18812.23687:

[12]Lobo, V. C.; Patil, A.; Phatak, A. and Chandra, N. (2010). Free Radicals, Antioxidants and Functional Foods: Impact on human health. ***Pharmacognosy Reviews Vol. 4, Issue 8.*** https://pmc.nbi.nlm.nih.gov/articles/PMC3249911/pdf/PREV-4-118pdf

[13]Loki, J. (2022). Phytochemicals Functions and there Effects. Journal of Plant Biochemistry & Physiology Vol. 10, Issue52 number 1000005 https://www.londom.org/open - access - pdfs/phytochemicals - function – and - there – effects.pdf

[14]Nortijie, E.; Basitere, M. ; Moyo, D. and Nyamukamba, P. (2022). Extraction Methods, Quantitative and Qualitative Phytochemical Screening of Medicinal Plants for Anti microbial Textiles: A Review. ***Plants*** **2022** Vol. 11 PP 2011.

[15]Pham – Huy, L. A.; He, H. and Pham – Huy, C. (2008). Free Radicals, Antioxidants in Disease and Health. International Journal of Biomedical Science Vol. 4, NO. 2, 2008. https://pmc.ncbi.nlm.gov/articles/PMC3414697/

[16]Victoria, E.R. ; Gonzalez, A. M. ;Madrigal – Santillan, E. O. ; Sanchez – Reyes, K. ;Alvarez – Gonzalez, I. ; Madrigal – Bujaidar, E. ;Valadez – Vega, C. ; Chamorro – Cevallos, G. ; Garcia – Melo, L. F. ; and Morales – Gonzalez, J. A. (2024). Phytochemicals and Their Usefulness in the Maintenance of Health. ***Plants Vol. 13 pp523*** https://www.mdpi.com/journal/plants plants 2024, 13,523.https://doi.org/10.3390/plants13040523

# ROOM TEMPERATURE SYNTHESIS OF Cu (II)-BASED METAL–ORGANIC FRAMEWORKS FROM TEREPHTHALIC AND FUMARIC ACID: CHARACTERIZATION AND ANTIMICROBIAL EVALUATION

**Abdullahi Sahal[1*], Hasiya Mahmoud Umar[2], Fatima Suleiman Aliyu[1], Abbas Lawal[1], Tijjani Umar Kofarbai[3]**

*[1]Department of Chemistry and Biochemistry, Nuhu Bamalli polytechnic Zaria*
*[2]Department of Chemistry, Federal University of Education, Zaria*
*[3]Department of Chemistry, Federal University Dutsin-ma*
*[*]Corresponding Author: abuhanifa25@gmail.com*

## Abstract

Antimicrobial resistance is a critical global health challenge, demanding innovative materials with potency and broad-spectrum activities. Metal–organic frameworks (MOFs), with their tunable structures, high porosity, and controlled metal ion release, offer an emerging platform for antimicrobial design. Cu-based MOFs, namely Cu-FUM and Cu-BDC, were synthesized at room temperature using fumaric and terephthalic acid. The synthesized MOFs were characterized by FTIR, TGA, BET, XRD, SEM, and EDX. FTIR confirmed coordination of carboxylate groups to Cu (II) through ν(Cu–O) vibrations. XRD revealed distinct crystallinity differences: Cu-FUM was highly crystalline (crystallite size ~38 nm), while Cu-BDC was poorly crystalline (~13 nm). BET analysis showed that Cu-BDC had a higher surface area (838.66 $m^2/g$) than Cu-FUM (443.77 $m^2/g$), though Cu-FUM exhibited a larger pore diameter (3.645 nm) and pore volume (0.191 $cm^3/g$). TGA indicated that Cu-BDC was more thermally stable, with solvent loss at 350 °C (3 %) and linker decomposition at 510 °C (72 %), leaving 25 % residue, whereas Cu-FUM showed solvent loss at 300 °C (5 %), linker loss at 500 °C (90 %), and only 5 % residue. SEM micrographs showed Cu-FUM as fine granular crystallites with rough surfaces, and Cu-BDC as smooth, dense aggregates. EDX confirmed elemental composition (C: 20.82–49.93 %, O: 20.28–22.86 %, Cu: 20.93–50.66 %). Antimicrobial evaluation against *Staphylococcus aureus*, *Bacillus cereus*, *Escherichia coli*, *Salmonella gallinarum*, and *Candida albicans* showed strong activity for both MOFs, with inhibition zones of 13–22 mm for Cu-FUM (particularly against *C. albicans*) and 14–18 mm for Cu-BDC (particularly against *E. coli*). These findings demonstrate that particle size, crystallinity, and textural properties strongly influence the structural and antimicrobial performance of Cu-MOFs.

**Keywords:** Metal–organic frameworks, fumaric acid, terephthalic acid, room-temperature synthesis, antimicrobial activity

## 1. Introduction

Infectious diseases caused by microbial pathogens continue to pose a significant global health burden, particularly in developing and tropical regions, where they account for a substantial proportion of mortality [1], [2]. Despite the availability of numerous antimicrobial drugs, the rapid emergence and spread of antimicrobial resistance (AMR) have reduced the effectiveness of conventional antibiotics, creating an urgent need for alternative antimicrobial materials [1], [2]. Metal–organic frameworks (MOFs) have emerged as a promising class of crystalline porous materials consisting of metal ions or clusters coordinated to organic ligands. Their highly tunable structures enable the formation of one-, two-, and three-dimensional frameworks, including mixed-linker and bimetallic systems with enhanced porosity and structural stability [3]–[6]. Owing to their exceptionally high surface area, large pore volume, and chemical versatility, MOFs have found applications in adsorption, catalysis, drug delivery, and environmental remediation [7].

More recently, MOFs have attracted considerable attention as antimicrobial materials because of their ability to provide sustained metal-ion release, high surface reactivity, and adaptable framework structures, which enhance their interactions with microbial cells [8]. Although several synthesis routes, including solvothermal, mechanochemical, sonochemical, and microwave-assisted methods, have been developed, many require elevated temperatures and extended reaction times [9]. Room-temperature synthesis offers a greener, simpler, and more cost-effective alternative, particularly for thermally sensitive ligands. Therefore, this study focuses on the room-temperature synthesis of copper-based MOFs using fumaric acid and terephthalic acid as organic linkers and evaluates their antimicrobial activities against selected bacterial and fungal pathogens to assess their potential as novel antimicrobial agents.

## 2. Methods

Cu–FUM and Cu–BDC metal–organic frameworks (MOFs) were synthesized at room temperature by reacting copper(II) acetate with fumaric acid and terephthalic acid, respectively, in a DMF/ethanol/water solvent mixture. The products were isolated by centrifugation, purified through solvent exchange with methanol, and dried under vacuum. The synthesized MOFs were characterized using X-ray diffraction (XRD) for crystallinity, Fourier-transform infrared spectroscopy (FTIR) for functional group identification, scanning electron microscopy (SEM) for morphology, and energy-dispersive X-ray spectroscopy (EDX) for elemental composition. Antimicrobial activity was evaluated using the agar diffusion method against *Staphylococcus aureus, Bacillus cereus, Escherichia coli, Salmonella gallinarum,* and *Candida albicans*. Antimicrobial efficacy was determined by measuring inhibition zones, while the minimum inhibitory concentration (MIC) was established using the serial dilution method. Ciprofloxacin and econazole served as positive controls, and DMSO was used as the negative control.

## 3. Results

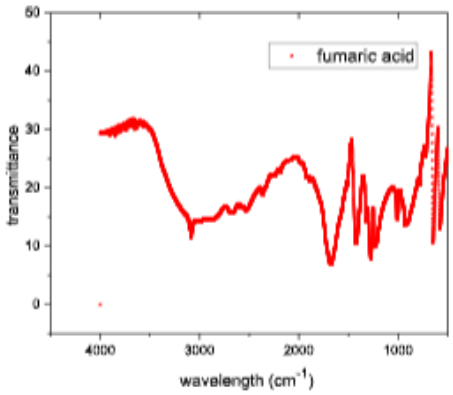



Figure 1: FTIR spectrum of $H_2FUM$

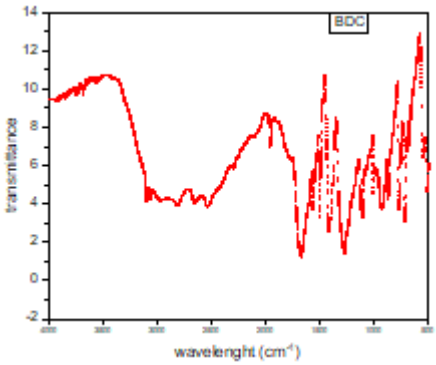



Figure 2: FTIR spectrum of $H_2BDC$

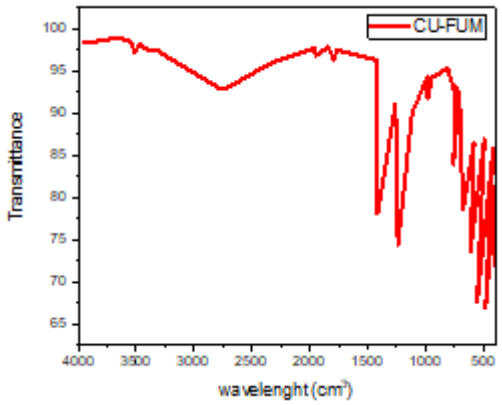



Figure 3: FTIR spectrum of Cu-FUM

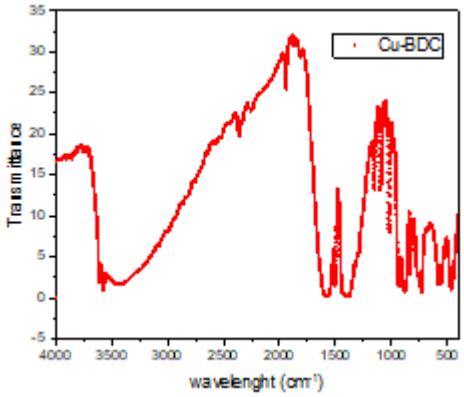



Figure 4: FTIR spectrum of Cu-BDC

**Table 1:** FTIR spectra data of linker and corresponding Cu-MOFs

| s/n | Linker/MOFs | V(COOH) | V(C=O) | V(C-O) | V(C-H) | V(C=C) | V(M-O) | V(OH) |
|---|---|---|---|---|---|---|---|---|
| **1** | **BDC** | 1679 | 1424 | - | 2305 | 781 | - | - |
| **2** | **FUM** | 1683 | 1424 | - | 2363 | 720 | - | - |
| **3** | **Cu-BDC** | - | 1582 | 1386 | 2362 | 735 | 617 | 3500 |
| **4** | **Cu-FUM** | - | 1577 | 1395 | 2750 | 792 | 486 | 3568 |

**Table 2:** TGA profile of the synthesized MOFs

| | Loss of solvents | | Loss of linker | | Residue |
|---|---|---|---|---|---|
| MOFs sample | **T(°C)** | **Wt.%** | **T (°C)** | **Wt.%** | **Wt.%** |
| Cu-FUM | 300 | 5 | 500 | 90 | 5 |
| Cu-BDC | 350 | 3 | 510 | 72 | 25 |

**Table 3**: BET Result Analysis

| s/n | MOFs sample | Pore diameter (nm) | Pore volume ($cm^3g^{-1}$) | BET surface area ($m^2g^{-1}$) |
|---|---|---|---|---|
| 1 | **Cu-FUM** | 3.645 | 0.191 | 443.77 |
| 2 | **Cu-BDC** | 3.490 | 0.158 | 838.66 |

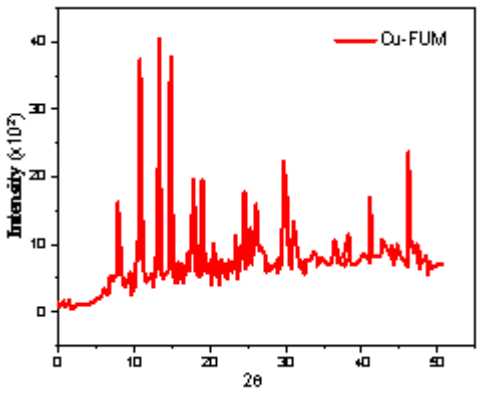



Figure 5 XRD Pattern of Cu-FUM

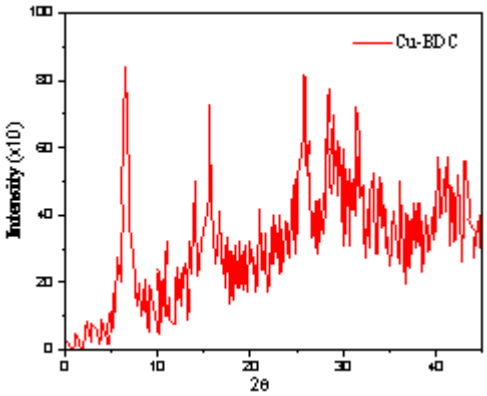



Figure 6 XRD Pattern of Cu-BDC

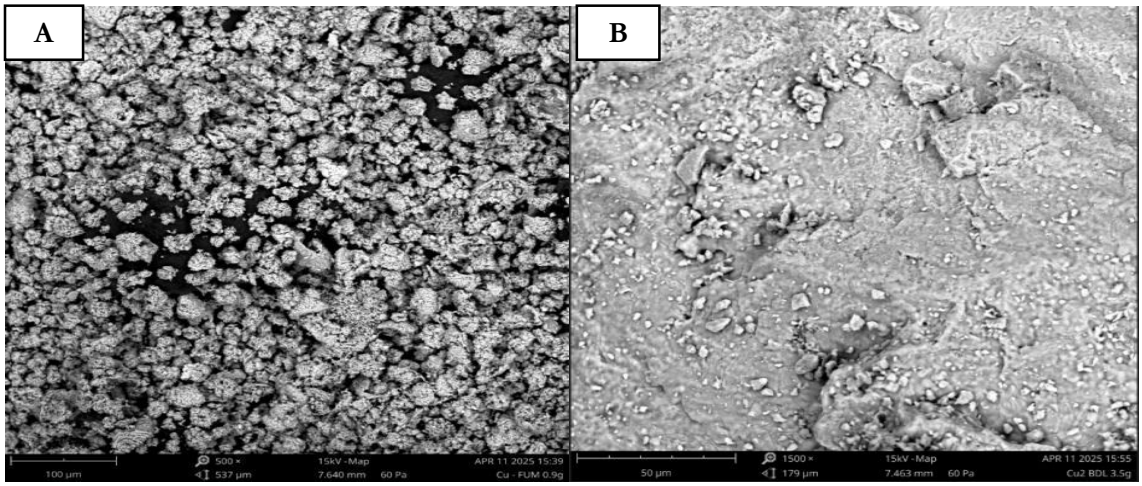



Figure 7: SEM Microgram (A) CU-FUM (B) CUBDC

**Table 4: Atomic Concentration (Elemental compositions)**

| | Elemental composition | | | |
|---|---|---|---|---|
| **CU-MOFs** | **Carbon** | **Oxygen** | **Copper** | **Total** |
| **Cu-FUM** | 28.82 | 20.28 | 50.66 | 99.76 |
| **Cu-BDC** | 49.93 | 22.86 | 20.93 | 93.72 |

**Table 5: Antimicrobial Sensitivity Test of Cu-MOFs**

| | **Cu-FUM** | | | **Cu-BDC** | | | |
|---|---|---|---|---|---|---|---|
| **Con in mg/mL** | **100** | **50** | **25** | **100** | **50** | **25** | **Control** |
| **Test organism** | **Diameter of Zone of Inhibition** | | | | | | **CPX/ECNZ** |
| *S. aureous* | 13 | 10 | 6 | 11 | 10 | 6 | 31 |
| *B. cereus* | 13 | 10 | 6 | 14 | 10 | 6 | 23 |
| *S. galinarum* | R | R | R | 12 | 10 | 6 | 21 |
| *E.coli* | 14 | 10 | 9 | 18 | 15 | 6 | 25 |

| | | | | | | | |
|---|---|---|---|---|---|---|---|
| *C.albican* | 22 | 10 | 6 | 13 | 10 | 6 | 15 |
| **DMSO** | 0 | 0 | 0 | 0 | 0 | 0 | |

Key: R = Resistance

**Table 6: Minimum Inhibitory and Bactericidal Concentration (mg/mL)**

| Test organism | Cu-FUM | | Cu-BDC | |
|---|---|---|---|---|
| | MIC | MBC | MIC | MBC |
| *S. aureous* | 50 | 200 | 100 | - |
| *B. cereus* | 100 | 400 | 100 | 400 |
| *S. galinarum* | R | R | 50 | 200 |
| *E.coli* | 12.5 | 100 | 12.5 | 100 |
| *C.albican* | 25 | 100 | 100 | 200 |

Key: R = Resistance

## 4. Discussion

*FTIR analysis* confirmed successful coordination of the carboxylate linkers to $Cu^{2+}$ ions. The disappearance of free carboxylic stretches (1683 $cm^{-1}$ for fumaric acid, 1679 $cm^{-1}$ for terephthalic acid) and the appearance of new asymmetric carboxylate stretches (1577 $cm^{-1}$ for Cu-FUM, 1584 $cm^{-1}$ for Cu-BDC) indicated deprotonation and metal coordination. ν(Cu–O) bands at 486 $cm^{-1}$ (Cu-FUM) and 617 $cm^{-1}$ (Cu-BDC) further supported this. Broad O–H absorptions (3500–3651 $cm^{-1}$) suggested the presence of water molecules.

*Thermogravimetric analysis* (Table 4.2) reveals differences in thermal stability. Cu-FUM loses solvent at 300 °C (5 wt.%) and undergoes linker decomposition at 500 °C with a substantial 90 wt.% loss, leaving only 5 % residue. In contrast, Cu-BDC shows higher thermal stability: solvent loss occurs at 350 °C (3 wt.%), linker decomposition at 510 °C (72 wt.%), and a residual mass of 25 %. The higher residue for Cu-BDC indicates a greater proportion of inorganic (copper oxide) remnants, likely due to the aromatic terephthalate linker forming a more thermally robust framework. Overall, Cu-BDC offers superior surface area and thermal stability, while Cu-FUM provides larger pore volume but lower thermal resilience.

*Textural Properties*

The textural properties derived from BET analysis (Table 4.3) show that Cu-BDC possesses a significantly higher BET surface area (838.66 $m^2/g$) than Cu-FUM (443.77 $m^2/g$), despite having a slightly smaller pore diameter (3.490 nm vs. 3.645 nm) and lower pore volume (0.158 $cm^3/g$ vs. 0.191 $cm^3/g$). This indicates that Cu-BDC has a more extensive network of smaller pores, contributing to a greater accessible surface area, which is advantageous for adsorption and catalytic applications. The larger pore volume of Cu-FUM suggests a more open framework, but its lower surface area reflects a less densely packed porous structure.

*XRD analysis* showed that Cu-FUM was highly crystalline, with sharp peaks at 2θ values such as 10.37°, 15.38°, and 20.60°, while Cu-BDC exhibited broad reflections and baseline noise, indicating poor

crystallinity. Crystallite sizes were estimated using Scherrer's equation: approximately 38 nm for Cu-FUM and 13 nm for Cu-BDC.

*SEM micrographs* revealed that Cu-FUM consisted of small, densely packed, rough granular crystallites with irregular aggregation. In contrast, Cu-BDC displayed larger, smoother, and more fused surface structures with less distinguishable crystallinity.

*EDX analysis* confirmed the expected elemental composition. Cu-FUM contained 28.82% C, 20.28% O, and 50.66% Cu, indicating a metal-rich framework. Cu-BDC contained 49.93% C, 22.86% O, and 20.93% Cu, reflecting a linker-rich framework. The purity of both MOFs was between 93–99%, with no detectable DMF solvent residues.

*Antimicrobial Analysis*

The antimicrobial activity of Cu-FUM and Cu-BDC was tested at 100–25 mg/mL and compared with ciprofloxacin and econazole. Both MOFs showed concentration-dependent inhibition. Cu-FUM gave the highest antifungal activity (22 mm against *Candida albicans*), while Cu-BDC was most active against *Escherichia coli* (18 mm). These values were generally lower than ciprofloxacin (21–31 mm), but Cu-FUM outperformed econazole (15 mm) against *C. albicans*. Resistance of *Salmonella gallinarum* to some MOFs contrasted with ciprofloxacin sensitivity. MIC and MBC values: both MOFs had MIC of 12.5 mg/mL and MBC of 100 mg/mL against *E. coli*, confirming bactericidal action. The differences in performance are attributed to physicochemical properties: Cu-FUM's higher crystallinity (~38 nm) favours structural stability and controlled $Cu^{2+}$ release, while Cu-BDC's ultrafine crystallites (~13 nm) enhance surface reactivity and ion availability.

## 5. Conclusion

Cu-based MOFs were successfully synthesized at room temperature using fumaric and terephthalic acids. FTIR, XRD, SEM, and EDX confirmed successful framework formation. Antimicrobial testing showed strong activity, with *Candida albicans* and *Escherichia coli* being the most susceptible. The activity is governed by crystallinity and particle size. Future studies should assess toxicity and safe concentrations, and explore the MOFs' potential for removing heavy metals (e.g., Pb, Cd, As) from contaminated water.

## References

**[1]** World Health Organization (WHO), *Mortality and Global Health Estimates*. Geneva, Switzerland: WHO, 2013.

**[2]** S. E. Sandy, A. Khansa, M. Nayla, A. Ahmed, L. N. Ha, and G. Yaser, "Antibacterial efficacy of copper-based metal–organic frameworks against *Escherichia coli* and *Lactobacillus*," *RSC Advances*, vol. 14, pp. 15821–15831, 2024.

**[3]** P. Rocío-Bautista, P. González-Hernández, V. Pino, J. Pasán, and A. M. Afonso, "Metal–organic frameworks as novel sorbents in dispersive-based microextraction approaches," *Trends in Analytical Chemistry*, vol. 90, pp. 114–134, 2017.

**[4]** E. García, R. Medina, M. Lozano, I. Hernández-Pérez, M. Valero, and A. Franco, "Adsorption of azo-dye Orange II from aqueous solutions using a metal–organic framework material: Iron-benzenetricarboxylate," *Materials*, vol. 7, pp. 8037–8057, 2014.

**[5]** A. Hashemzadeh, M. M. Amini, R. Tayebee, A. Sadeghian, L. J. Durndell, M. A. Isaacs, and A. F. Lee, "Magnetically separable $H_3PW_{12}O_{40}$@$Fe_3O_4$/EN-MIL-101 catalyst for the one-pot solventless synthesis of 2H-indazolo[2,1-b]phthalazinetriones," *Molecular Catalysis*, vol. 440, pp. 96–106, 2017.

**[6]** Q. Sun, N. Wang, and J. Yu, "Advances in catalytic applications of zeolite-supported metal catalysts," *Advanced Materials*, vol. 33, p. 2104442, 2021.

**[7]** H. Furukawa, K. E. Cordova, M. O'Keeffe, and O. M. Yaghi, "The chemistry and applications of metal–organic frameworks," *Science*, vol. 341, no. 6149, p. 1230444, 2013.

**[8]** X. Xiaolin, D. Mengna, L. Kaiquan, F. Lijuan, M. Yingchun, L. Yanmi, G. Ying, H. Yuning, and L. Hexing, "The synthesis and highly effective antibacterial properties of Cu-3,5-dimethyl-1,2,4-triazole metal–organic frameworks," *Frontiers in Chemistry*, vol. 11, p. 1124303, 2023.

**[9]** A. Chakraborty and H. Adak, "Synthesis and applications of metal–organic frameworks," *Research & Development in Material Science*, vol. 19, no. 1, pp. 2192–2197, 2023.

# PROXIMATE AND HISTOLOGICAL RESPONSES OF COMMON CARP FINGERLINGS FED BLACK SOLDIER FLY LARVAE MEALS FROM FOOD WASTES

**Alexander Okpokwu Ogabidu[1 2 *], Ibrahim Sham'un Eshi[2], Tukki Onghasom Hassan[1], Mary Bernard[1], Lawrence Stephen[1], Jocthan Markus Gaya[1], Abdulrahman Mohammed[1], Samuel Florence Anna[1], Elvanus Ewaram Magaji[1], Jafaru Adamu Idris[3], Comfort Salifu[2]**

*[1]National Research Institute for Chemical Technology, Basawa, Zaria, Kaduna State, Nigeria*
*[2]Department of Biology, Ahmadu Bello University, Zaria, Kaduna State, Nigeria.*
*[3]Department of Zoology, Ahmadu Bello University, Zaria, Kaduna State, Nigeria*
**Corresponding Author: ogabiduokpokwu1@gmail.com*

**Abstract**

The potential of Black Soldier Fly Larvae (BSFL) raised on various organic substrates as a sustainable protein source in the diets of Common Carp fingerlings was assessed in this study. Fruit waste plus soybean curd (RSA), brewer's spent grain plus soybean curd (RSB), and a mixed substrate of fruit waste plus brewer's spent grain plus soy bean curd (RSC) were used to produce BSFL, which were then processed into meals (TA, TB, and TC) and examined with a commercial control diet (TD). Under carefully monitored laboratory conditions, 120 fingerlings were fed the meals. According to proximate analysis, fish fed TD had the highest dorsal muscle protein (70.52%) and whole-body protein (60.18%), closely followed by TA (56.61% and 69.69%) and TC (51.68% and 65.12%), while TB had the lowest protein values (45.94% and 58.20%). TB was generally lower, with lipid content ranging from 10.10%–15.04% (total body) and 11.19%–15.08% (muscle). Nitrogen free extract and fibre were considerably greater in TB. Gut Histological analysis revealed that all treatments had normal gut architecture. These results show that BSFL meals can successfully substitute conventional feed with minimal reduction in fish nutritional quality, especially when made from fruit waste and mixed substrates.
**Keywords:** Aquafeed, Black soldier fly larvae, Common carp, Histology, Proximate

## 1. Introduction

One of the fastest growing food production industries in the world is aquaculture, which is essential to supplying the rising demand forpremium animal protein. However, the growing expense and scarcity of traditional feed components, especially fishmeal and soybean meal, pose a danger to the sustainability of aquaculture production. These challenges have made it more difficult to find affordable, sustainable, and alternative protein sources for aquafeeds [1], [2], [3]. Because of their high nutritional content, quick growth rate, and ability to turn organic waste into useful biomass, Black Soldier Fly Larvae (BSFL) have drawn a lot of attention as potential replacements for insect based proteins in this context [4], [5], [6]. According to [1] and [3], BSFL have a desirable nutritional profile that includes high quantities of crude protein and lipids, essential amino acids, and bioactive substances that are good for fish growth and health. Crucially, the substrate utilized during raising has a significant impact on the nutritional makeup of BSFL and defines their efficacy as feed ingredients [7], [8], [9], [10]. Fruit leftovers, brewer's spent grain, and other agro industrial by products are examples of organic waste materials that have been effectively used as food substrates for BSFL production, supporting waste valorisation and circular economy principles [11], [12], [13], [14]. For example, it has been demonstrated that brewer's leftover grain influences feed quality by improving larval growth and changing the content of fatty acids [11], [15], [8]. There has been much research on the use of BSFL

meal in aquafeeds for a variety of fish species. BSFL meal can enhance growth performance, feed efficiency, and nutrient consumption without negatively affecting fish health, according to a number of studies [16], [17], [18], [19]. Furthermore, as demonstrated by higher villus height, goblet cell density, and enzyme activity, BSFL insertion has been linked to improved intestinal architecture and greater digestive capacity [20], [21]. However, because of things like chitin content and decreased digestibility, excessive inclusion levels may have a detrimental effect on performance [22], [23], [24]. Because of its versatility, quick development, and widespread consumer appeal, common carp is a commercially significant freshwater fish species. Reducing manufacturing costs and environmental effects requires optimizing its diet with sustainable foods [25], [26], [27]. Although the results primarily depend on the nutritional quality of the insect meal and processing techniques, prior research has shown that insect based meals, such as BSFL, can partially substitute traditional protein sources in carp diets [28], [29], [30], [31]. Additionally, it has been demonstrated that adding BSFL to the diet affects the protein, lipid, and ash contents of fish, which are important markers of the effectiveness of nutrient utilization [32], [33], [34]. Assessing the physiological and histological reactions of fish to different diets is essential for determining feed appropriateness in addition to growth performance. Fish welfare in general, gut health, and nutritional absorption ability are all shown by intestinal histology. Research has demonstrated that while excessive inclusion of BSFL meal may result in histological changes, moderate inclusion does not negatively impact gut structure [23], [35], [36]. BSFL generated from plant based and other organic substrates may also enhance cellular viability and antioxidant capacity, confirming their functional significance in aquafeeds, according to biochemical and cellular investigations [30], [37], [10], [27], [44]. Even though the number of research on the use of BSFL in aquaculture is increasing, little is known about how different substrate combinations affect the nutritional value of BSFL and how that affects fish performance, especially in developing nations where organic waste resources are plentiful. Although easily available and underutilized, substrates like fruit waste and brewer's wasted grain have uncertain combined impact on the nutritional composition of BSFL and fish feeding results. Thus, the purpose of this study was to assess the proximate and gut histological responses of fingerlings of common carp fed diets comprising BSFL meals made from various food substrates. Through effective waste utilization and alternate protein sourcing, the findingswill aid in the development of sustainable aquafeed practices.

## 2. Materials and Methods

*Ethical Approval*

The fish experiment was carried out in compliance with the institutional policies for the use and care of lab animals. The Ahmadu Bello University, Zaria Committee on Animal Use and Care examined and approved the study protocol (Approval No. ABUCAUC/2025/133). During handling and experimentation, ethical considerations adhered to established guidelines for reducing stress and guaranteeing fish welfare [36].

*Experimental Site*

Black Soldier Fly Larvae (BSFL) were raised at the National Research Institute for Chemical Technology's (NARICT) Maggot Laboratory in Zaria, Kaduna State, Nigeria. The feeding trial of the common carp took place in Fisheries Laboratory, Department of Biology, Ahmadu Bello University, Zaria, Kaduna State, Nigeria.

*Preparation of Rearing Substrates and Larval Production*

Using organic waste materials that were readily available locally, three experimental substrates were created. Substrate A (RSA) was made up of two kilograms of soybean curd and three kilograms of fruit

waste (rotten bananas, watermelons, and oranges). 3 kg of brewer's leftover grain and 2 kilogram of soybean curd made up Substrate B (RSB), while 1.5 kg of fruit waste, 1.5 kg of brewer's spent grain, and 2 kg of soybean curd made up Substrate C (RSC). These substrates were chosen due to their availability and nutrient composition as agro-industrial by products, which are known to affect the nutrient profile and larval growth [11], [8]. After homogenizing the substrates, they were put in raising containers under carefully monitored circumstances. Using 7day old larvae, cultured for 15 days, the BSFL transformed the organic waste into larval biomass. They larvae were harvested at day 15. Previous research has shown that larval protein, lipid, and mineral content are strongly influenced by substrate composition [4], [10].

Processing of Larvae and Meal Formulation

To lower moisture content and stop microbial degradation, larvae from each substrate were harvested, cleaned, and oven dried for two hours at 105°C. After that, the dried larvae were ground into meals called TA (derived from RSA), TB (derived from RSB), and TC (derived from RSC). The control diet (TD) was a commercial fish feed (Coppens). Drying and processing methods were consistent with standard protocols for insect meal preparation to preserve nutrient quality [1], [6]. The experimental diets were formulated to be nutritionally comparable, ensuring that observed effects were attributable to differences in BSFL substrate origin rather than protein level variation.

*Experimental Fish and Feeding Trial*

A commercial fish farm in Plateau State, Nigeria, supplied 120 healthy fingerlings of common carp. Prior to the trial, two weeks were spent acclimating the fish. Fish were randomly assigned to experimental groups. 10 fish per plastic container of 20 litres in triplicate per treatment that corresponded to the four diets (TA, TB, TC, and TD) after acclimation. During the course of the study, fish were fed the experimental diets at a conventional feeding rate 3% of their body weight, three times a day. To guarantee the best possible development and feed utilization, feeding procedures adhered to known aquaculture protocols [18], [19]. Temperature, dissolved oxygen, and pH were among the water quality characteristics that were routinely checked and kept within values that were suitable for carp culture.

*Proximate Composition Analysis*

Fish samples were taken for proximate analysis at the conclusion of the feeding trial. Standard analytical techniques were used to measure moisture, crude protein, lipid, ash, fibre, and nitrogen free extract (NFE) in whole-body and dorsal muscle samples. These metrics are frequently employed in aquaculture studies to evaluate feed quality and nutrient consumption efficiency [32], [33]. Variations in proximate composition, which show how well fish incorporated dietary nutrients into bodily tissues, were utilized as markers of the nutritional impact of the meal diets.

*Histological Examination*

Gut samples were collected from fish in each treatment group for histological analysis. The samples were fixed, processed, and examined under a microscope to evaluate intestinal structure, including mucosal integrity and cellular organization. Histological assessment is a critical tool for evaluating the physiological effects of dietary treatments, particularly in detecting potential adverse effects of alternative protein sources [23], [37], [20]. Observations were compared across treatments to determine any structural changes associated with BSFL based meals.

*Statistical Analysis*

The relevant software was used to statistically evaluate the data from proximal and histological studies. Significant differences between treatment means were found using one-way analysis of variance

(ANOVA), and when necessary, post hoc comparisons were performed. $P < 0.05$ was considered significant. To assess treatment effects and guarantee the accuracy of results, this statistical method is frequently used in aquaculture nutrition studies [24], [31].

## 3. Results and Discussion

*Proximate Composition of Whole Body of the common carp fingerlings*

Across treatments, the proximate composition of the total body of common carp altered considerably ($p < 0.05$) as presented in Table 1. Crude protein levels were highest in fish fed the control diet (TD) (60.18%), followed by TA (56.61%) and TC (51.68%), and lowest in TB (45.94%). While fiber (6.88%) and nitrogen-free extract (18.89%) were significantly higher in TB, lipid content showed a similar trend, with TD (15.04%) having the highest level and TB (10.10%) having the lowest. Since commercial feeds are tailored for protein retention and digestibility, the higher protein levels in TD are expected. This is in line with the findings of [38], [1], [3]. Black Soldier Fly Larvae (BSFL) meals can successfully support protein deposition, nevertheless, as seen by the comparatively high protein values found in TA and TC. Numerous studies have reported similar results, with BSFL inclusion up to moderate levels maintaining protein content comparable to diets based on fishmeal which agreed with the results obtained by [39], [18], [19]. Reduced nutrient digestibility occurred in TB's with lower protein and greater fibre contents, which were probably caused by the brewer's leftover grain substrate. It has been demonstrated that fish with high fibre content have poorer protein digestibility and nutritional absorption supported by the findings of [4], [23], [8]. This finding is consistent with earlier research showing that larvae with reduced nutritional efficiency are produced on substrates high in lignocellulosic materials [40], [41]. Similarly, when BSFL were produced from less digestible substrates, [31] found decreased in protein efficiency. The lipid content found in TA and TC suggests effective energy use, which is in line with research showing BSFL lipids improve fish energy metabolism [42], [10], [21]. On the other hand, TB's decreased lipid content illustrates how substrate composition affects the nutritional profile of larvae [6], [11]. This demonstrates how important substrate optimization is to the nutrient content of BSFL.

**Table 1.** Proximate Composition of Common Carp Fingerlings Whole Body

| Parameter | TA | TB | TC | TD | p-value |
|---|---|---|---|---|---|
| Moisture (%) | $7.11\pm0.11^{a}$ | $7.82\pm0.09^{a}$ | $7.45\pm0.11^{a}$ | $7.48\pm0.58^{a}$ | 0.11 |
| Ash (%) | $13.84\pm0.67^{a}$ | $10.37\pm0.66^{b}$ | $13.27\pm0.39^{a}$ | $8.06\pm0.01^{c}$ | 0.00 |
| Fibre (%) | $3.45\pm0.32^{c}$ | $6.88\pm0.50^{a}$ | $5.12\pm0.38^{b}$ | $2.47\pm0.58^{c}$ | 0.00 |
| Lipid (%) | $13.98\pm0.05^{b}$ | $10.10\pm0.48^{d}$ | $12.97\pm0.52^{c}$ | $15.04\pm0.01^{a}$ | 0.00 |
| Protein (%) | $56.61\pm0.53^{b}$ | $45.94\pm0.82^{d}$ | $51.68\pm1.25^{c}$ | $60.18\pm0.22^{a}$ | 0.00 |
| NFE (%) | $5.03\pm0.93^{c}$ | $18.89\pm1.14^{a}$ | $9.50\pm1.48^{b}$ | $6.77\pm0.54^{b}$ | 0.00 |

N.B: Mean ± SD values with same superscript are not significantly different across row ($P>0.05$). TA diet of Larvae A. TB diet of Larvae B and TC diet of Larvae C. TD control Feed (coppens Fish Feed)

*Proximate Composition of Dorsal Muscle of Common carp*

Similar trends were seen in the composition of dorsal muscle (Table 2), with TD having the greatest crude protein (70.52%), followed by TA (69.69%) and TC (65.12%), and TB (58.20%). The range of lipid content was 11.19% to 15.08%, with TB exhibiting the lowest values once more. BSFL-based

diets can promote effective protein deposition, as seen by the high muscle protein levels in TA and TC. This is consistent with research showing that fish fed BSFL diets had better muscle protein and performance [43], [29], [20]. In a similar vein, insect meals can successfully substitute fishmeal without sacrificing muscle quality, according to [38] and [9]. The adverse effects of high fibre and chitin levels on nutrition utilization are further supported by TB's lower protein content. High concentrations of chitin have been shown to restrict digestibility and decrease protein absorption [22], [23], [36]. This finding is in line with that of [9], [8] and [26] who found that fish given high fibre bug diets used fewer nutrients. Furthermore, the observed lipid profile indicates that fish energy metabolism benefits from lipids produced from BSFL. It has been demonstrated that lauric acid, a significant component of BSFL fat, enhances fish health and feed efficiency [42], [3]. The lower lipid concentration in TB, however, suggests that the quality of the substrate has a direct impact on the lipid composition of larvae and the subsequent performance of fish.

**Table 2.** Proximate composition of common carp Fingerlings Dorsal fin Muscle

| Parameter | TA | TB | TC | TD | p-value |
|---|---|---|---|---|---|
| Moisture (%) | 6.43±0.10$^{a}$ | 6.93±0.10$^{a}$ | 6.79±0.10$^{a}$ | 5.91±0.67$^{a}$ | 0.25 |
| Ashini (%) | 4.57±0.08$^{a}$ | 3.42±0.09$^{d}$ | 4.34±0.11$^{b}$ | 4.02±0.01$^{c}$ | 0.00 |
| Fibre (%) | 1.08±0.07$^{d}$ | 2.29±0.13$^{b}$ | 1.54±0.11$^{c}$ | 0.56±0.05$^{e}$ | 0.00 |
| Lipid (%) | 14.47±0.13$^{a}$ | 11.19±0.94$^{d}$ | 13.74±0.09$^{c}$ | 15.08±0.04$^{a}$ | 0.00 |
| Protein (%) | 69.69±1.03$^{b}$ | 58.20±1.07$^{d}$ | 65.12±1.50$^{c}$ | 70.52±0.01$^{a}$ | 0.00 |
| NFE (%) | 3.78±1.19$^{c}$ | 17.98±0.72$^{a}$ | 8.48±1.26$^{b}$ | 3.91±0.65$^{c}$ | 0.00 |

N.B: Mean ± SD values with same superscript are not significantly different across row (P>0.05). TA diet of Larvae A. TB diet of Larvae B and TC diet of Larvae C. TD control Feed (coppens Fish Feed)

*Comparative Analysis of Whole Body and Muscle Composition of Common Carp fingerlings*

The comparison showed in Table 3, depicted the whole body had higher levels of ash, fibre, and moisture, dorsal muscle had far higher levels of crude protein (65.88%) than the whole body (53.60%). Muscle had a somewhat higher lipid content. These results align with known physiological processes in fish, where protein deposition occurs mostly in muscle tissue [2], [21], [31]. When high quality protein sources are used, the greater protein concentration in muscle indicates effective nutrition partitioning. When fish are fed insect-based diets, prior research has also shown increased protein deposition in muscle tissues relative to the entire body [43], [18], [19]. Findings by [38] and [10] are supported by the rather steady lipid distribution, which indicates balanced energy metabolism.

**Table 3.** Comparative Analysis proximate Composition of Whole Body and Dorsal fin Muscles of Common Carp Fingerlings

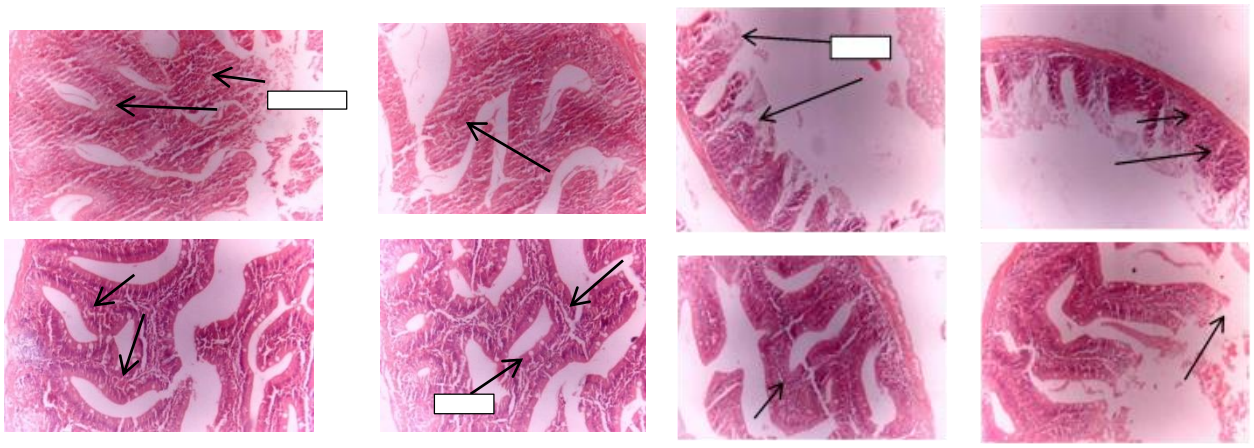
| Parameter | WHOLE BODY | DORSAL FIN MUSCLE | T-Paired Samples |
|---|---|---|---|
| Moisture Content (%) | 7.47±0.37$^{a}$ | 6.52±0.51$^{b}$ | 0.00 |
| Ash Content (%) | 11.38±2.47$^{a}$ | 4.09±0.46$^{b}$ | 0.00 |
| Crude Fibre (%) | 4.48±1.80$^{a}$ | 1.37±0.67$^{b}$ | 0.00 |
| Crude Lipid (%) | 13.02±1.94$^{b}$ | 13.62±1.60$^{a}$ | 0.00 |
| Crude Protein (%) | 53.60±5.64$^{b}$ | 65.88±5.19$^{a}$ | 0.00 |

| | | | |
|---|---|---|---|
| NFE (%) | 10.05±5.66[a] | 8.54±6.09[b] | 0.00 |

N.B: Mean ± SD values with same superscript are not significantly different across row (P>0.05).

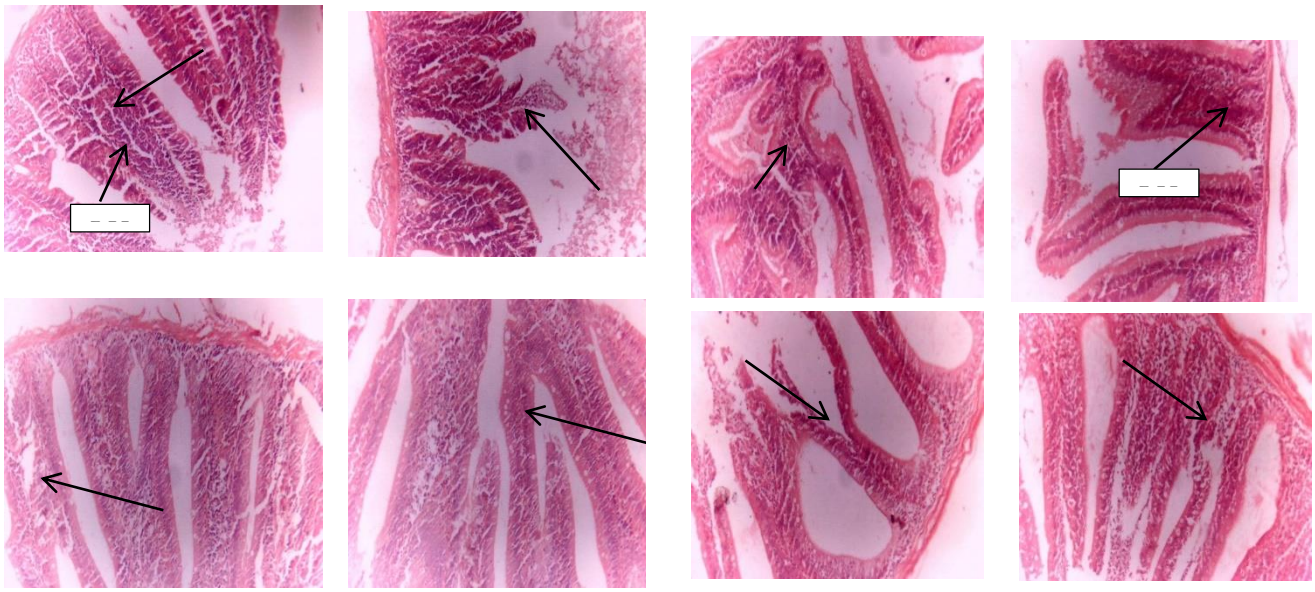
*Gut Histomorghological Observations of the common carp fingerlings*

All treatments had normal gut morphology, according to histological investigation of the intestines of the various common carp fingerlings fed with the various meal as observed in figure 1 and 2. With no indications of severe pathological changes or structural damage. This suggests that gut health was not adversely affected by BSFL based diets. Although they were mild to moderate alteration in the intestinal architecture of TA and TC common carp fish groups compared to TB and TD which could be caused by the complex mixture of the substrates used in growing TA and TC . TB and TD have better intestinal integrity of the villi. This result is consistent with that of [20], who found that juveniles of Nile tilapia fish given BSFL diets had better intestinal morphology, including higher villus height and mucosal integrity as observed in TB and TD. Similarly, at modest inclusion levels, [29] and [37] did not find severe negative histological consequences. However, studies have shown that excessive inclusion of BSFL meal may cause histological changes due to chitin accumulation [22], [23], [36]. The absence of such effects in this study suggests that inclusion levels were within safe limits. Furthermore, BSFL contains antimicrobial compounds such as lauric acid, which have been shown to enhance gut health and immunity [42], [3], [21]. This may explain the normal gut structure observed across treatments. The findings unequivocally show that the nutritional value of BSFL and their efficacy as fish feed are strongly influenced by the substrate composition. When compared to brewer's spent grain alone (TB), fruit waste and mixed substrates (TA and TC) yielded greater results. This corroborates research by [11] and [10], who found that mixed and plant based substrates improve the nutritional quality of BSFL. High fibre substrates, on the other hand, have been linked to lower performance and digestibility [40], [4], [8].



TA Fish group TB Fish group

**Figure 1.** Gut Histomicrographs of Fish group TA and TB Fed with Larvae A and B Meal



TC Fish group TD Fish group

**Figure 2.** Gut Histomicrographs of Fish group TC and TD Fed with Larvae C and D Meal

## 4. Conclusion

This study shows that Black Soldier Fly Larvae meals made from mixed substrates (RSC) and fruit waste (RSA) can effectively partially substitute traditional protein sources in the diets of common carp. Whole body protein levels in fish given these BSFL-based diets were 56.61% and 51.68%, respectively, which were close to the commercial control's 60.18%. Similar trends were seen in dorsal muscle protein, with TA obtaining 69.69% and TD 70.52%. Larvae raised solely on brewer's spent grain (RSB), on the other hand, produced noticeably lower protein values, suggesting that substrate composition plays a crucial role in determining nutritional quality. BSFL meals do not impair gut health at the inclusion levels examined, according to histological analysis, which showed normal intestinal morphology across all treatments. The results highlight the successful conversion of underutilized agro-industrial by-products into premium aquafeed ingredients using fruit waste and mixed organic substrates. From a sustainability standpoint, this strategy lessens reliance on fishmeal while promoting the ideas of the circular economy. Future studies should investigate the economic viability of large scale aquaculture applications, optimize inclusion levels, and evaluate long term growth success.

## Acknowledgements

The Head and the technical personnel of the Fisheries Laboratory, Department of Biology, Ahmadu Bello University, Zaria, is greatly appreciated by the authors for providing the facilities and logistical assistance that made the feeding trial a success as part of the work of the first author MSc dissertation. The authors further thank the Head of the maggot laboratory and the general laboratory, Scientific and Industrial Research Department (SIRD), National Research Institute for Chemical Technology (NARICT), Zaria, for helping to prepare the substrate and raise the black soldier fly larvae and provision of reagents and assistance for proximate analysis. Their combined efforts made this study possible.

**References**

[1] R. N. Nairuti, S. N. Musyoka, M. J. Yegon, and M. A. Opiyo, "Utilization of black soldier fly (Hermetia illucens Linnaeus) larvae as a protein source for fish feed--a review," *Aquaculture Studies*, vol. 22, no. 2, 2021. DOI: 10.4194/AQUAST697

[2] J. T. K. Ndondo, "Review of the Food and Agriculture Organisation (FAO) strategic priorities on food safety 2023," in *Food safety-new insights*, IntechOpen, 2023. DOI: 10.5772/intechopen.112132

[3] L. Dîrvariu, C. A. Barbacariu, M. Burducea, and D. Simeanu, "Feed Sources for Sustainable Aquaculture: Black Soldier Fly Larvae (BSFL)," *Fishes*, vol. 10, no. 9, p. 464, 2025. DOI: 10.3390/fishes10090464

[4] R. Raksasat, J. W. Lim, W. Kiatkittipong, K. Kiatkittipong, Y. C. Ho, M. K. Lam, and C. K. Cheng, "A review of organic waste enrichment for inducing palatability of black soldier fly larvae: Wastes to valuable resources," *Environmental Pollution*, vol. 267, p. 115488, 2020. DOI: 10.1016/j.envpol.2020.115488

[5] C. F. Lanes, F. A. Pedron, G. T. Bergamin, A. L. Bitencourt, B. E. Dorneles, J. C. Villanova, and A. Giannetto, "Black soldier fly (Hermetia illucens) larvae and prepupae defatted meals in diets for zebrafish (Danio rerio)," *Animals*, vol. 11, no. 3, p. 720, 2021. DOI: 10.3390/ani11030720

[6] I. U. Gadzama, "Black soldier fly larvae as animal feed," *Bulgarian Journal of Animal Husbandry*, vol. 62, no. 1, pp. 48-64, 2025. DOI: 10.61308/LWHN4916

[7] L. Gasco, M. Finke, and A. Van Huis, "Can diets containing insects promote animal health?," *Journal of Insects as Food and Feed*, vol. 4, no. 1, pp. 1-4, 2018. DOI: 10.3920/JIFF2018.x001

[8] A. Resconi, S. B. Oddon, I. Ferrocino, Z. Loiotine, C. Caimi, L. Gasco, and I. Biasato, "Effects of brewery by-products on growth performance, bioconversion efficiency, nutritional profile, and microbiota and mycobiota of black soldier fly larvae," *animal*, vol. 18, no. 9, p. 101288, 2024. DOI: 10.1016/j.animal.2024.101288

[9] H. Q. Tran, T. T. Nguyen, M. Prokešová, T. Gebauer, H. V. Doan, and V. Stejskal, "Systematic review and meta- analysis of production performance of aquaculture species fed dietary insect meals," *Reviews in Aquaculture*, vol. 14, no. 3, pp. 1637-1655, 2022. DOI: 10.1111/raq.12666

[10] J. Camperio, J. A. Suarez, J. Simonton, E. Paresky, J. Parodi, and D. D. Benetti, "Valorizing organic waste through black soldier fly larvae (Hermetia illucens): A sustainable solution for aquafeeds with key nutrients and natural bioactive polyphenols," *Sustainability*, vol. 17, no. 5, p. 1788, 2025. DOI: 10.3390/su17051788

[11] C. H. Kim, J. Ryu, J. Lee, K. Ko, J. Y. Lee, K. Y. Park, and H. Chung, "Use of black soldier fly larvae for food waste treatment and energy production in Asian countries: a review," *Processes*, vol. 9, no. 1, p. 161, 2021. DOI: 10.3390/pr9010161

[12] K. Magee, J. Halstead, R. Small, and I. Young, "Valorisation of organic waste by-products using black soldier fly (Hermetia illucens) as a bio-convertor," *Sustainability*, vol. 13, no. 15, p. 8345, 2021. DOI: 10.3390/su13158345

[13] K. Mohan, D. K. Rajan, T. Muralisankar, A. R. Ganesan, P. Sathishkumar, and N. Revathi, "Use of black soldier fly (Hermetia illucens L.) larvae meal in aquafeeds for a sustainable aquaculture industry: A review of past and future needs," *Aquaculture*, vol. 553, p. 738095, 2022. DOI: 10.1016/j.aquaculture.2022.738095

[14] J. Munguti, F. Wekesa, I. Osuga, M. Kariuki, R. Yossa, D. Mungai, and C. M. Tanga, "Utilization of Black Soldier Fly (Hermetia illucens) Larvae as a Potential Substitute for Fish Meal in the Production of Nile Tilapia (Oreochromis niloticus L.)," *Sustainable Agriculture Research*, vol. 13, no. 1, pp. 40-49, 2024. DOI: 10.5539/sar.v13n1p40

[15] E. N. Mathai, D. K. Barwani, V. Mwashi, J. M. Munguti, J. Iteba, F. Wekesa, and I. M. Osuga, "Black Soldier Fly (Hermetia illucens) Larvae for Nile Tilapia (Oreochromis niloticus) On-Farm Feeding: Effect on Performance and Profitability," *Journal of Agriculture, Science and Technology*, vol. 23, no. 3, pp. 120-143, 2024. DOI: 10.4314/jagst.v23i3.8

[16] R. Jahan, M. M. H. Tipu, M. M. Haque, and M. A. Salam, "Black soldier fly (Hermetia illucens) larvae meal as a fish meal replacement in diets for nursing common carp (Cyprinus carpio) fry," *AgriRxiv*, no. 2021, p. 20210012413, 2021. DOI: 10.31220/agriRxiv.2021.00030

[17] J. Zim, H. Chkih, R. Bouharroud, M. Sarehane, and P. Lhomme, "Effect of various odour attractants on egg-laying activity of black soldier flies (Hermetia illucens)," *Journal of Insects as Food and Feed*, vol. 9, no. 11, pp. 1461-1472, 2023. DOI: 10.1163/23524588-20220139

[18] I. S. Mahato, K. Paudel, P. Timalsina, and S. Chand, "Evaluating the Impact of Black Soldier Fly (Hermetia illucens) Larvae Meal on Growth Efficiency and Feed Utilization in Rainbow Trout (Oncorhynchus mykiss) Juvenile," *Asian Journal of Fisheries and Aquatic Research*, vol. 26, no. 12, pp. 107-117, 2024. DOI: 10.9734/ajfar/2024/v26i12850

[19] R. Haider, N. Khan, A. Aihetasham, H. A. Shakir, M. Fatima, A. Tanveer, and M. Sarwar, "Dietary inclusion of black soldier fly (Hermetia illucens) larvae meal, with exogenous protease supplementation, in practical diets for striped catfish (Pangasius hypophthalmus, Sauvage 1878)," *PLoS ONE*, vol. 19, no. 12, p. e0313960, 2024. DOI: 10.1371/journal.pone.0313960

[20] S. Maulu, B. Eynon, S. Abarra, M. Rawling, and D. L. Merrifield, "Black soldier fly, Hermetia illucens, larvae meal improves intestinal health and growth performance of Nile tilapia, Oreochromis niloticus, juveniles," *Journal of the World Aquaculture Society*, vol. 56, no. 3, p. e70035, 2025. DOI: 10.1111/jwas.70035

[21] Y. Chen, X. Li, A. Chen, Z. Liao, X. Gu, X. Chen, and J. Niu, "A novel black soldier fly protein hydrolysate improves the muscle growth of rainbow trout (Oncorhynchus mykiss) via the PI3K/AKT/mTOR pathway," *Animal Nutrition*, 2025a. DOI: 10.1016/j.aninu.2025.07.007

[22] M. Zarantoniello, A. Zimbelli, B. Randazzo, M. D. Compagni, C. Truzzi, M. Antonucci, and I. Olivotto, "Black Soldier Fly (Hermetia illucens) reared on roasted coffee by-product and Schizochytrium sp. as a sustainable terrestrial ingredient for aquafeeds production," *Aquaculture*, vol. 518, p. 734659, 2020. DOI: 10.1016/j.aquaculture.2019.734659

[23] S. Moutinho, A. Oliva-Teles, L. Pulido-Rodríguez, R. Magalhães, Ó. Monroig, G. Parisi, and H. Peres, "Black soldier fly larvae oil as an alternative lipid source in diets for gilthead seabream (Sparus aurata) juveniles," *Aquaculture*, vol. 574, p. 739705, 2023. DOI: 10.1016/j.aquaculture.2023.739705

[24] Z. Chen, Q. Li, R. Sheng, J. Zhang, J. Guo, P. Tan, and Z. Ding, "Effects of defatted black soldier fly larvae meal on growth, nutrient digestibility, hepatopancreas biochemistry, intestinal microbiota, and phosphorus discharge of giant freshwater prawn (Macrobrachium rosenbergii)," *Animal Nutrition*, vol. 23, p. 271, 2025b. DOI: 10.1016/j.aninu.2025.08.001

[25] X. Xu, H. Ji, H. Yu, and J. Zhou, "Influence of dietary black soldier fly (Hermetia illucens Linnaeus) pulp on growth performance, antioxidant capacity and intestinal health of juvenile mirror carp (Cyprinus carpio var. specularis)," *Aquaculture Nutrition*, vol. 26, no. 2, pp. 432-443, 2020. DOI: 10.1111/anu.13005

[26] A. A. Z. Khalaf, K. H. Mustafa, and N. T. Taha, "Recycling organic waste using black soldier fly larvae to produce a sustainable feed source for common carp and evaluating its impact on production performance," in *IOP Conference Series: Earth and Environmental Science*, vol. 1549, no. 1, p. 012076, 2025. DOI: 10.1088/1755-1315/1549/1/012076

[27] S. Sultana, O. Ali, J. Biró, A. Szabó, L. Ardó, A. Szűcs, and B. Kucska, "Effects of Dietary Supplementation with Black Soldier Fly Larvae (Hermetia illucens) Frass on Common Carp (Cyprinus carpio)," *Animals*, vol. 16, no. 4, p. 693, 2026. DOI: 10.3390/ani16040693

[28] J. S. Zhou, S. S. Liu, H. Ji, and H. B. Yu, "Effect of replacing dietary fish meal with black soldier fly larvae meal on growth and fatty acid composition of Jian carp (Cyprinus carpio var. Jian)," *Aquaculture Nutrition*, vol. 24, no. 1, pp. 424-433, 2018. DOI: 10.1111/anu.12574

[29] A. A. Uslu, O. T. Özel, G. Örnekçi, B. Çelik, E. C. Çankırılıgil, İ. Coşkun, and G. U. Şenel, "Insect larval meal as a possible alternative to fish meal in rainbow trout (Oncorhynchus mykiss) diets: black soldier fly (Hermetia illucens), mealworm (Tenebrio molitor)," *Journal of Limnology and Freshwater Fisheries Research*, vol. 9, no. 1, pp. 43-52, 2023. DOI: 10.17216/LimnoFish.1081945

[30] V. E. Herawati, H. T. Jayanti, T. Elfitasari, S. P. Putro, and S. Windarto, "Black Soldier Fly (Hermetia illucens) Oil Inclusion and its Effects on Growth Performances in Common Carp (Cyprinus carpio)," *Jurnal Ilmiah Perikanan dan Kelautan*, vol. 15, no. 2, p. 361, 2023. DOI: 10.20473/jipk.v15i2.39846

[31] B. Bordoloi, P. K. Saharia, and H. Pokhrel, "Efficiency of Black Soldier Fly Larvae Meal (BSFLM) as Partial or Total Replacement of Fishmeal (FM) on Growth Performance, Nutrient Utilization and Haematological Changes in Walking Catfish Clarias magur (Hamilton, 1822)," *Indian Journal of Animal Research*, vol. 1, p. 6, 2025. DOI: 10.18805/IJAR.B-5546

[32] C. M. Hariyono, Yunianta, Harijono, C. Sriherwanto, I. Suja'i, A. Nadaviana, and Komarudin, "Physico-chemical characteristics of Rhizopus sp.-fermented fish feed pellets containing black soldier fly larvae (Hermetia illucens) meal," in *IOP Conference Series: Earth and Environmental Science*, vol. 744, no. 1, p. 012024, 2021. DOI: 10.1088/1755-1315/744/1/012024

[33] C. Yong-Kang, Z. Chao-Zhong, Z. Shuang, C. Shu-Yan, D. Xiao-Hui, Y. Qi-Hui, and X. Shi-Wei, "Dietary black soldier fly (Hermetia illucens) larvae meal on growth performance, non-specific immunity and lipid metabolism of Litopenaeus vannamei," *Journal of Hydrobiology*, vol. 47, no. 1, 2023. DOI: 10.7541/2023.2022.0201

[34] I. Sarwar, S. Yaseen, A. Sarfraz, F. Munir, A. Jahangir, A. Noreen, and M. S. Sarwar, "The Effect of black soldier fly larvae-based diet on bone mineralization, fatty acids and amino acids composition of common carp (Cyprinus carpio) fingerling," *NUST Journal of Natural Sciences*, vol. 10, no. 2, pp. 1-14, 2025. DOI: 10.53992/njns.v10i2.254

[35] N. V. Linh, S. Wannavijit, K. Tayyamath, N. Dinh-Hung, T. Nititanarapee, M. A. A. Sumon, and C. L. Brown, "Black soldier fly (Hermetia illucens) larvae meal: A sustainable alternative to fish meal proven to promote growth and immunity in koi carp (Cyprinus carpio var. Koi)," *Fishes*, vol. 9, no. 2, p. 53, 2024. DOI: 10.3390/fishes9020053

[36] N. Romano, S. N. Datta, G. S. J. Pande, A. K. Sinha, F. Yamamoto, S. D. Rawles, and C. D. Webster, "Preliminary assessment of the nutritive value of dietary exuviae from black soldier fly (Hermetia illucens) pupae in Mozambique tilapia," *Journal of the World Aquaculture Society*, vol. 56, no. 3, p. e70027, 2025. DOI: 10.1111/jwas.70027

[37] A. I. Albayati, R. S. Attee, and M. S. Al-Khshali, "EFFECT OF REPLACING SOYBEAN MEAL WITH LARVAE MEAL OF BLACK SOLDIER FLY HERMETIA ILLUCENS IN GROWTH PERFORMANCE AND SOME BIOCHEMICAL BLOOD PARAMETERS OF COMMON CARP CYPRINUS CARPIO L.," *Iraqi Journal of Agricultural Sciences*, vol. 56, no. Special, pp. 92-101, 2025. DOI: 10.36103/n4w5sv22

[38] L. Gasco, G. Acuti, P. Bani, A. Dalle Zotte, P. P. Danieli, A. De Angelis, and A. Roncarati, "Insect and fish by-products as sustainable alternatives to conventional animal proteins in animal nutrition," *Italian Journal of Animal Science*, vol. 19, no. 1, pp. 360-372, 2020. DOI: 10.1080/1828051X.2020.1743209

[39] I. Belghit, N. S. Liland, P. Gjesdal, I. Biancarosa, E. Menchetti, Y. Li, and E. J. Lock, "Black soldier fly larvae meal can replace fish meal in diets of sea-water phase Atlantic salmon (Salmo salar)," *Aquaculture*, vol. 503, pp. 609-619, 2019. DOI: 10.1016/j.aquaculture.2018.12.032

[40] K. B. Barragan-Fonseca, M. Dicke, and J. J. van Loon, "Nutritional value of the black soldier fly (Hermetia illucens L.) and its suitability as animal feed--a review," *Journal of Insects as Food and Feed*, vol. 3, no. 2, pp. 105-120, 2017. DOI: 10.3920/JIFF2016.0055

[41] I. Hopkins, L. P. Newman, H. Gill, and J. Danaher, "The influence of food waste rearing substrates on black soldier fly larvae protein composition: A systematic review," *Insects*, vol. 12, no. 7, p. 608, 2021. DOI: 10.3390/insects12070608

[42] H. P. Makkar, G. Tran, V. Heuzé, and P. Ankers, "State-of-the-art on use of insects as animal feed," *Animal Feed Science and Technology*, vol. 197, pp. 1-33, 2014. DOI: 10.1016/j.anifeedsci.2014.07.008

[43] S. Nogales- Mérida, P. Gobbi, D. Józefiak, J. Mazurkiewicz, K. Dudek, M. Rawski, and A. Józefiak, "Insect meals in fish nutrition," *Reviews in Aquaculture*, vol. 11, no. 4, pp. 1080-1103, 2019. DOI: 10.1111/raq.12281

[44] H. Fischer, N. Romano, and A. K. Sinha, "Conversion of spent coffee and donuts by black soldier fly (Hermetia illucens) larvae into potential resources for animal and plant farming," *Insects*, vol. 12, no. 4, p. 332, 2021. DOI: 10.3390/insects12040332

# PHYTOCHEMICAL SCREENING, PROXIMATE COMPOSITION AND ELEMENTAL ANALYSIS OF *CRINUM JAGUS* (RIVER LILY) BULB

**Fatima Muhammad Balarabe*, Lawal Salamatu Muazu, Musa Nazifi Tanimu, Abdulmalik Muhammad, Muhammad Nazifi, Abba Malambilyamin Umar**

*Department of Chemistry and Biochemistry, Nuhu Bamalli Polytechnic, Zaria*
*Corresponding Author: fatimabalarabe080@gmail.com*

**Abstract**

*Crinum jagus* (family Amaryllidaceae) is a perennial bulbous plant widely used in African traditional medicine to treat asthma, tuberculosis, rheumatism, skin wounds, snakebites, and as a lactagogue. This study evaluated the phytochemical constituents (qualitative and quantitative), proximate composition, and elemental content of *C. jagus* bulb. Samples were collected from Zaria Local Government, Kaduna. Methanolic extracts were prepared by maceration. Qualitative and quantitative phytochemical analyses were performed using standard colourimetric and spectrophotometric methods. Proximate composition was determined by AOAC procedures. Elemental (mineral) analysis was conducted using atomic absorption spectrophotometry. Phytochemical screening revealed the presence of saponins, tannins, flavonoids, alkaloids, phenolics, and terpenoids. Glycosides and steroids were absent. Quantitative analysis showed: saponins 49.45±1.02 mg/g, alkaloids 10.35±0.28 mg/g (low), tannins 66.56±1.34 mgTAE/g, flavonoids 53.86±1.12 mgQE/g, and total phenolics 99.19±2.05 mgGAE/g. Proximate composition: moisture 7.56±0.15%, ash 4.57±0.10%, lipid 10.25±0.21%, protein 16.94±0.35%, fibre 1.72±0.05%, carbohydrate 60.64±1.25%. Mineral concentrations in the bulb: K 0.30±0.01 mg/kg, Ca 3.5±0.07 mg/kg, Mg 2.96±0.06 mg/kg, Fe 1.91±0.04 mg/kg, Zn 0.18±0.01 mg/kg. *C. jagus* bulb is rich in bioactive phytochemicals (especially phenolics and tannins) and nutrients (protein, carbohydrates, minerals).

**Keywords:** *Crinum jagus*; phytochemicals; proximate composition; minerals; river lily

## 1. Introduction

*Crinum jagus* (J. Thomps.) Dandy, commonly known as river lily, St. Christopher lily, or "Albasan Kwadi" (Hausa), is a perennial bulbous herb belonging to the family Amaryllidaceae. It is widely distributed in tropical Africa, including Nigeria, where it grows in swampy locations and produces white flowers during the dry season [1],[2]. In African traditional medicine, *C. jagus* bulbs are used to treat a variety of ailments: chronic cough, tuberculosis, rheumatism, asthma, skin wounds, abscesses, dysentery, and snakebites. The bulb is also used as a lactagogue (to increase milk production) and as an emetic, purgative, and rubefacient [3],[4]. Previous pharmacological studies have reported analgesic, anti-inflammatory, anticholinesterase, antioxidant, anti-snake venom, and hepatoprotective activities of *Crinum* species, largely attributed to alkaloids (e.g., lycorine, crinamine, galanthamine) and phenolic compounds [5], [6],[7]. Proximate analysis (moisture, ash, protein, fat, fibre, carbohydrate) is essential to evaluate the nutritional potential of plant materials. Elemental composition (minerals) provides information on dietary supplementation value. Phytochemical screening identifies bioactive secondary metabolites responsible for medicinal properties. Despite extensive ethnomedicinal use, there is a paucity of integrated data on the nutritional composition, mineral content, and quantitative phytochemical profiles of *C. jagus*.

## 2. Materials and Methods

### Sample Collection and Identification

Fresh bulbs of *Crinum jagus* were collected from Zaria municipality, Kaduna State, Nigeria. Plant materials were authenticated by a botanist at Ahmadu Bello University, Zaria. Samples were washed, air-dried, and ground into fine powder.

### Extraction

200 g of powdered bulb were soaked in 1 L of 80% methanol for 24 h at room temperature with shaking (100 rpm). The mixture was filtered through Whatman No. 1 filter paper, and the filtrate was concentrated using a rotary evaporator at 53 °C. The dry extract was stored at 5 °C.

### Phytochemical Analysis

Qualitative phytochemical screening was carried out using standard methods to detect the presence of alkaloids, saponins, tannins, flavonoids, terpenoids, glycosides, steroids, and phenolic compounds based on characteristic colour changes or precipitate formation [8]. Quantitative determination of total phenolics and flavonoids was performed using the Folin–Ciocalteu and aluminium chloride colorimetric methods, respectively, with absorbance measured at 765 nm and 420 nm [9], [10]. Alkaloid and saponin contents were determined by gravimetric methods following extraction and precipitation procedures [11], while tannin content was quantified using a standard titrimetric method [8].

### Proximate Analysis

Proximate composition was determined according to AOAC [12] methods. Moisture content was measured by oven drying at 105 °C to constant weight. Ash content was determined by incineration in a muffle furnace at 550 °C. Crude fat was extracted using a Soxhlet apparatus with petroleum ether as solvent. Crude protein was determined using the Kjeldahl method and calculated by multiplying total nitrogen by a conversion factor of 6.25. Crude fibre was obtained through sequential acid and alkali digestion, while carbohydrate content was estimated by difference.

### Mineral Analysis

Mineral composition was determined using Atomic Absorption Spectrophotometry (AAS). The powdered sample was subjected to wet acid digestion using concentrated acids to obtain a clear solution. The digest was filtered, diluted appropriately, and analyzed for potassium (K), calcium (Ca), magnesium (Mg), iron (Fe), and zinc (Zn). Mineral concentrations were expressed in mg/kg of dry sample.

### Data Analysis

All measurements were performed in triplicate; results are presented as mean values with standard deviations.

## 3. Results

**Table 1: Qualitative phytochemical composition of *C. jagus* bulb**

| Phytochemical | Bulb extract |
|---|---|
| Alkaloids | + |
| Flavonoids | + |
| Saponins | + |
| Tannins | + |
| Phenolics | + |
| Terpenoids | + |
| Glycosides | – |
| Steroids | – |

Key: + = present; – = absent

**Table 2: Quantitative phytochemical content of *C. jagus* bulb**

| Phytochemical | Concentration (mg/g extract) |
|---|---|
| Saponins | 49.45 ± 1.02 |
| Alkaloids | 10.35 ± 0.28 |
| Tannins (mg TAE/g) | 66.56 ± 1.34 |
| Flavonoids (mg QE/g) | 53.86 ± 1.12 |
| Total phenolics (mg GAE/g) | 99.19 ± 2.05 |

**Table 3: Proximate composition of *C. jagus* bulb (%)**

| Parameter | Composition |
|---|---|
| Moisture | 7.56 ± 0.15 |
| Ash | 4.57 ± 0.10 |

| Parameter | Composition |
|---|---|
| Lipid (fat) | 10.25 ± 0.21 |
| Protein | 16.94 ± 0.35 |
| Crude fibre | 1.72 ± 0.05 |
| Carbohydrate | 60.64 ± 1.25 |

**Table 4: Mineral concentrations in *C. jagus* bulb (mg/kg)**

| Element | Concentration |
|---|---|
| K | 0.30 ± 0.01 |
| Ca | 3.50 ± 0.07 |
| Mg | 2.96 ± 0.06 |
| Fe | 1.91 ± 0.04 |
| Zn | 0.18 ± 0.01 |

## 4. Discussion

### Phytochemical Profile

The bulb contained high levels of total phenolics (99.19 mg GAE/g), tannins (66.56 mg TAE/g), and flavonoids (53.86 mg QE/g). These compounds are known for antioxidant, anti-inflammatory, and wound-healing properties, which align with traditional uses of *C. jagus* for skin wounds and inflammation [13], [14]. Saponins were found present (49.45 mg/g). Saponins have immune-modulating, hypocholesterolemic, and anticarcinogenic properties [15]. The presence of saponins, tannins, flavonoids, and phenolics agrees with earlier reports on *C. jagus* [16], [17].

### Proximate Composition

The carbohydrate content (60.64%) is high, making the bulb an energy-rich food. Protein (16.94%) is moderate and comparable to some legumes. The low moisture (7.56%) indicates good storage stability

[12]. The ash content (4.57%) suggests a reasonable mineral pool. Comparison with garlic and onion: the bulb's moisture (7.56%) is much lower than that of fresh garlic (66–74%) or onion (67–74%), implying a much drier, more stable material [18], [19]. The bulb's protein (16.94%) is higher than that of onion (≈1–2%) and garlic (≈6–8%) reported in the literature, reinforcing its nutritional potential [20].

**Elemental Composition**

Calcium (3.5 mg/kg) and magnesium (2.96 mg/kg) are present in appreciable amounts, which could contribute to bone health and enzymatic functions. Iron (1.91 mg/kg) is moderately high, indicating potential for anaemia management. The values are lower than those reported by Abubakar and Wakili [21] for the same species (K 16.20, Ca 25.31, Fe 8.46 mg/kg).

**5. Conclusion**

*Crinum jagus* bulb contains bioactive phytochemicals: saponins, tannins, flavonoids, phenolics, terpenoids, and alkaloids. The bulb is rich in total phenolics (99.19 mg GAE/g) and tannins (66.56 mg TAE/g), supporting its traditional use in wound healing and inflammation. Proximate analysis revealed that the bulb is carbohydrate-rich (60.64%). The bulb contains appreciable levels of calcium (3.5 mg/kg), magnesium (2.96 mg/kg), and iron (1.91 mg/kg), which could contribute to daily mineral requirements.

**References**

[1] O. Olorode, *Taxonomy of West African Flowering Plants*. London, U.K.: Longman Publishing Company, 1984.

[2] A. T. J. Ogunkunle and O. R. Olopade, "Studies on the asthma coughs plant *Crinum jagus* L. (Amaryllidaceae) in Nigeria," *Afr. J. Plant Sci.*, vol. 5, pp. 108–114, 2011.

[3] E. I. Aigbokhan, *Annotated Checklist of Vascular Plants of Southern Nigeria*. Benin City, Nigeria: Uniben Press, 2014.

[4] A. Aziz, G. S. Raju, A. Das, J. Ahmed, and M. M. R. Moghal, "Evaluation of in vitro anthelmintic activity, total phenolic content and cytotoxic activity of *Crinum latifolium*," *Adv. Pharm. Bull.*, vol. 4, no. 1, pp. 15–19, 2014.

[5] C. C. Presley, P. Krai, S. Dalal, Q. Su, M. Cassera, and M. Goetz, "New potently bioactive alkaloids from *Crinum erubescens*," *Bioorg. Med. Chem.*, vol. 24, no. 21, pp. 5418–5422, 2016.

[6] P. J. Houghton, J. M. Agbedahunsi, and A. Adegbulugbe, "Cholinesterase inhibitory properties of alkaloids from two Nigerian *Crinum* species," *Phytochemistry*, vol. 65, no. 21, pp. 2893–2896, 2004.

[7] C. O. Nwaehujor, F. C. Nwinyi, and J. O. Ode, "Liver protective activity of the methanol extract of *Crinum jagus* bulb against acetaminophen induced hepatic damage in rats," *Asian J. Biochem.*, vol. 7, pp. 182–193, 2012.

[8] J. B. Harborne, *Phytochemical Methods: A Guide to Modern Techniques of Plant Analysis*, 3rd ed. London, U.K.: Chapman & Hall, 1998.

[9] V. L. Singleton, R. Orthofer, and R. M. Lamuela Raventós, "Analysis of total phenols and other oxidation substrates and antioxidants by means of Folin–Ciocalteu reagent," *Methods Enzymol.*, vol. 299, pp. 152–178, 1999.

[10] F. U. Ohikhena, O. A. Wintola, and A. J. Afolayan, "Quantitative determination of flavonoids in medicinal plant extracts using the aluminium chloride colorimetric assay," *J. Appl. Pharm. Sci.*, vol. 8, no. 4, pp. 135–140, 2018.

[11] J. C. Onyilagha and S. Islam, "Determination of alkaloid content in medicinal plants using gravimetric methods," *J. Nat. Prod. Plant Resour.*, vol. 5, no. 3, pp. 45–50, 2015.

[12] AOAC, *Official Methods of Analysis*, 21st ed. Gaithersburg, MD, USA: AOAC International, 2019.

[13] D. E. Okwu and I. N. Emenike, "Evaluation of the phytonutrients and vitamin contents of *Crinum jagus* bulbs," *Int. J. Mol. Med. Adv. Sci.*, vol. 2, no. 4, pp. 407–410, 2006.

[14] T. Shimada, "Salivary proteins as a defense against dietary tannins," *J. Chem. Ecol.*, vol. 32, no. 6, pp. 1149–1163, 2006.

[15] F. O. Jimoh and A. T. Oladiji, "Preliminary studies on *Piliostigma thonningii* seeds: Proximate analysis, mineral composition and phytochemical screening," *Afr. J. Biotechnol.*, vol. 4, no. 12, pp. 1439–1442, 2005.

[16] C. Ogbuanu, J. O. Ode, and C. O. Nwaehujor, "Phytochemical and antioxidant studies of *Crinum jagus* bulb," *J. Appl. Pharm. Sci.*, vol. 6, no. 5, pp. 112–117, 2016.

[17] C. Mvongo, P. A. Noubissi, R. Kamgang, C. Sara, M. Minka, A. Mfopa, and J.-L. Essame Oyono, "Phytochemical studies and in vitro antioxidant potential of two different extracts of *Crinum jagus*," *Int. J. Pharm. Sci. Res.*, vol. 6, no. 6, pp. 2354–2359, 2015.

[18] J. Hussain, A. L. Khan, N. Ur Rehman, M. Hamayun, T. Shah, M. Nisar, T. Bano, Z. K. Shinwari, and I.-J. Lee, "Proximate and nutrient analysis of selected vegetable species: A case study of Karak region, Pakistan," *Afr. J. Biotechnol.*, vol. 8, no. 12, pp. 2725–2729, 2009.

[19] E. O. Odebunmi, O. O. Oluwaniyi, and M. O. Bashiru, "Comparative proximate analysis of some food condiments," *J. Appl. Sci. Res.*, vol. 6, no. 3, pp. 272–274, 2010.

[20] N. M. Nwinuka, G. O. Ibeh, and G. I. Ekeke, "Proximate composition and levels of some toxicants in four commonly consumed spices," *J. Appl. Sci. Environ. Manage.*, vol. 9, no. 1, pp. 150–155, 2005.

[21] U. D. Abubakar and F. T. Wakili, "Phytochemical screening and elemental analysis of the *Crinum jagus* bulb," *J. Chem. Soc. Nigeria*, vol. 42, no. 2, pp. 53–55, 2017.

# AGRICULTURE AND ENVIRONMENTAL CHEMISTRYT, THEORETICAL AND PHYSICAL CHEMISTRY

# A CRITICAL INVESTIGATION OF ORGANIC POLLUTANTS IN WATER FROM LAMINGA DAM IN JOS, PLATEAU STATE, NIGERIA

**Gosomji, Andrew Dewan*; Ibejekwe, Sunday John and Gambol, Nanbol Ndam**

*Chemistry Department, Federal University of Education Pankshin*
**Corresponding Author: gosomji@yahoo.com*

**Abstract**

The use of contaminated water as drinking water makes human populations to suffer from water borne diseases. Water samples from laminga dam in Jos, Plateau State was screened to ascertain the level and type of organic pollutants. The water sample was extracted with dichloromethane (1: 1volume) and analysed with GC-MS. The results from the chromatogram showed 31 different organic pollutants. The pollutants fall within several classes of organic compounds which include long chain carboxylic acids, phthalates, alcohols, phenols, aldehydes, benzene derivatives, ketones, Sulphur containing compounds and halogenated hydrocarbons at various area concentrations. The diversity of these organic pollutants detected are attributed to the impact of agricultural, commercial, waste disposal and residential land use on ecosystem. The presence of these compounds indicated that development is quickly transforming the landscape from forest and pastures to parking lots, streets and rooftops causing rain to rush off the land instead of soaking into the ground. These run off are washed to the reservoirs (dams) which are often collected for various human uses.

**Keywords:** water, organic pollutants, GC-MS, chromatogram

## 1. Introduction

In developing countries, and Nigeria in particular, surface waters are still used directly as water supply without treatment. The quality of water is highly imperative component to understand the healthiness of a water body and it is a critical factor affecting human health and welfare. Studies showed that approximately 3.1% of deaths (1.7 million) and 3.7% of disability adjusted life-years (DALYs) (54.2 million) worldwide are attributable to unsafe water, poor sanitation and hygiene [1]. There is a pervasive use of synthetic chemicals like pesticides and dioxins that humans produce or generate which can pollute our water resources. The most common organic pollutants named persistent organic pollutants (POPs) are chemicals of global concern due to their potential for long-range transport, persistence in the environment, ability to bio-magnify and bio-accumulate [2] in ecosystems, as well as their significant negative effects on human health and the environment. Humans are exposed to these chemicals mainly through the food we eat and drinking water, through the air we breathe, in the outdoors, indoors and at the workplace. Such exposure to some of these organic compounds, even at low levels can lead, among others, to increased cancer risk, reproductive disorders, alteration of the immune system, neurobehavioural impairment, endocrine disruption, genotoxicity and increased birth defects [3]. The water from Laminga dam in Jos is used directly by people for drinking and other activities. This research work, therefore, aimed at screening water from the dam to ascertain the level and types of organic pollutants found in the water body.

## 2. Materials and methods

*Sample collection*

Four sampling points were used to collect about 4litres of water sample in clean plastic container from the dam and stored in an ice bag at a low temperature of about 4$^{o}$C. This was taken to the laboratory for further analysis.

*Extraction of Organic Pollutants from Water Samples*

The extraction procedure described by [4] was used. Exactly100 mL of the water was poured into a separating funnel and 100 mL of dichloromethane was added and the mixture separated for about 45 minutes by thorough shaking, afterwards the extract was poured into a beaker and left for few minutes to evapourate, anhydrous sodium tetraoxosulphate (VI) in excess was added to the extract to absorb any remaining water and then totaled into a vial bottle up to 2 mL ready for Gas Chromatography analysis.

*Chromatographic analysis*

Gas Chromatography equipped with Mass Spectrometer detector (GC/MS Agilent 7890BGC /Agilent 5977A MSD) was used on extract of the water sample. One micro liter (1µl) of each sample was injected in the split less mode using an auto injector. Separation of the compounds was accomplished with fused silica capillary column. Confirmation of the compounds was based on the presence of the molecular ion and confirming ions, a retention-time match was compared to standards and correct area ratios of the confirming ions.

**3. Results**

The interpretation of the mass spectrum (GC-MS) was conducted using the data based on National Institute for Standards and Technology (NIST) having more than 62,000 patterns. The spectra of the unknown compounds were compared with the spectrum of the known compounds stored in the NIST library. The name, molecular weight and structure of the components of the tested water sample was ascertained. The peak area percent was used to estimate the amount of the various components detected in the samples.

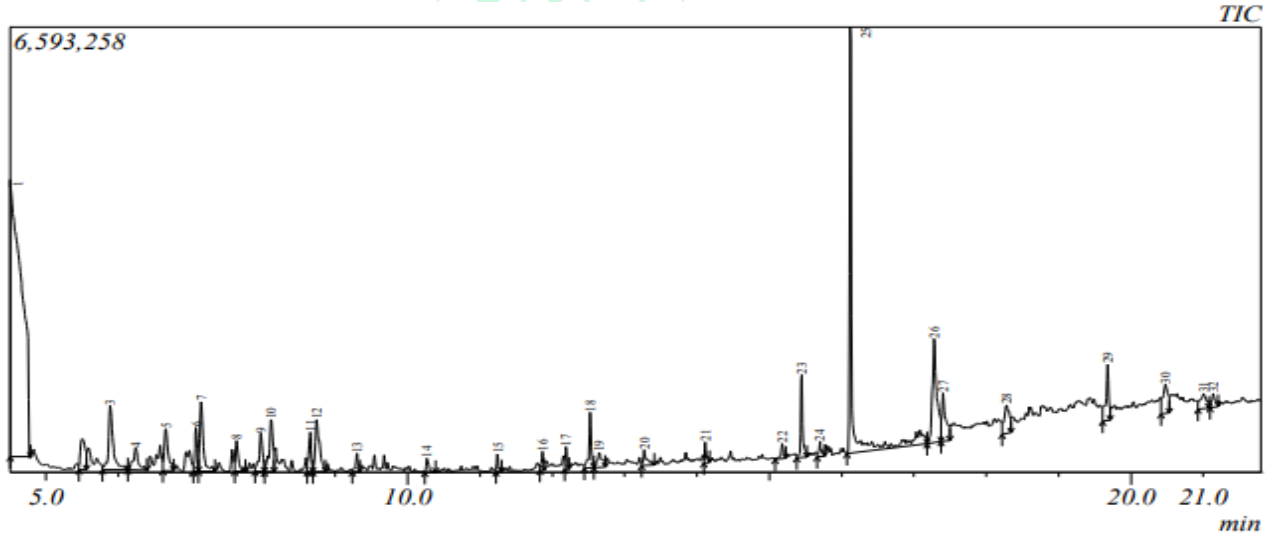



**Figure 1:** GC-MS Chromatogram of Water from laminga dam, Jos

**Table 1:** GC-MS Results for Water from Laminga Dam Jos

| Name of compound | Retention time | %Area conc. |
|---|---|---|
| **1 Aliphatics** | | |
| n-Hexane | 4.508 | 38.57 |
| Hexadecane | 11.217 | 0.37 |
| 2-cyclohexyl-Octane | 11.864 | 0.58 |

| | | | |
|---|---|---|---|
| | 2, 6, 10-trimethyl-Dodecane | 13.268 | 0.67 |
| | 2-methylhexacosane | 14.116 | 0.53 |
| | Eicosane | 12.191 | 0.55 |
| **2** | **Carboxylic Acid** | | |
| | (E)-2-Tridecenoic acid | 21.008 | 1.16 |
| **3** | **Ester** | | |
| | 2'-hexyl [1, 1'-Bicyclopropyl] -2-octanoic acid, methyl ester | 21.134 | 0.70 |
| | Chloromethyl 3-chlorododecanoate | 18.284 | 1.95 |
| | 1,2-dihydro-, acetate 2-Naphthalenol | 8.742 | 2.75 |
| **4** | **Phthalates** | | |
| | Phthalic acid, 4-bromophenyl heptyl ester | 15.447 | 1.93 |
| | Dibutyl phthalate | 16.120 | 13.26 |
| **5** | **Phenols** | | |
| | 2,4-bis(1,1-dimethylethyl)-Phenol | 12.526 | 1.61 |
| **6** | **Alcohols** | | |
| | 3,7,11,15-Tetramethyl-2-hexadecen-1-ol | 15.176 | 0.51 |
| **7** | **Benzene Derivatives** | | |
| | 1-ethyl-3-methyl-benzene | 5.506 | 1.90 |
| | 1,2,3-trimethyl-benzene | 5.885 | 3.74 |
| | 1,2,4-trimethyl-benzene | 6.236 | 1.43 |
| | 1,4-diethyl-benzene | 6.655 | 1.98 |
| | 1-ethyl-2,3-dimethyl-benzene | 7.076 | 1.52 |
| | 1,1-diethylpropyl-benzene | 7.144 | 2.97 |
| | 1,2,4,5-tetramethyl-benzene | 7.634 | 1.08 |
| | 4-methyl indane | 7.968 | 1.63 |
| | 1-methyl-2-(2-propenyl)-benzene | 8.111 | 2.89 |
| | 1-ethyl-2,3-dihydro-1-methyl-1H-indene | 8.650 | 1.38 |
| | 2-ethyl-2,3-dihydro-1H-indene | 9.296 | 0.71 |
| | 2-methyl-naphthalene | 10.267 | 0.49 |
| **8** | **Aldehyde** | | |
| | cis-9-Hexadecenal | 17.278 | 6.00 |
| **9** | **Ketones** | | |
| | 9,9-Dimethoxybicyclo[3.3.1]nona-2,4-dione | 17.401 | 2.36 |
| | D:A-Friedooleanan-7-one, 3-hydroxy- | 19.675 | 1.89 |
| **10** | **Sulphur Containing Compounds** | | |
| | propan-2-yl tridecyl sulphite | 12.646 | 1.02 |
| **11** | **Halogenated Compounds** | | |
| | 1,54-dibromo-Tetrapentacontane | 15.699 | 0.49 |

## 4. Discussion

*Organic Pollutants*

There were several organic compounds detected in the water samples. The dominant compounds identified fall within different classes of organic compounds which include; aliphatic, fatty acids,

phenols, phthalate esters, Sulphur containing compounds, aldehydes, alkyl substituted benzenes and brominated compounds. They can enter water naturally and through man-made sources or processes. Their concentrations in traces may make water unfit for different uses especially as drinking water.

*Aliphatic*

The aliphatic hydrocarbons (HCs) obtained in the water sample from laminga Dam, Jos indicated the presence of n-hexane (38.57%) at a relatively high concentration as compared to the other HCs observed in the same sample. The presence of aliphatic are majorly caused by combustion of petroleum products [5] and could also be traced from municipal sewage waste that flows into the dam. Other sources may include petrochemical products such as solvents and coal-derived products. This is not surprising in view of their extensive and widespread storage, transportation and use. Exposure to the constituents of petroleum products through drinking-water can be of short- or long-term duration [6]. Repeated exposure to high concentrations of n-hexane may lead to irreversible effects on the nervous system [7].

*Fatty acids*

Only a single variant of fatty acids (FAs), 2-Tridecenoic acid, was found in the water sample at a relatively low concentration of 1.16%. This is because of the low solubility of the compounds in water. The fatty acid enter the environment mainly from degradation of Petroleum Hydrocarbons, animal and vegetable fats [8]. They have been used extensively for assessing the sources and fates of organic matter in marine, coastal and estuarine ecosystems and more recently freshwater rivers and lakes [9]. The fatty acids have rarely been tested as indicators of human impacts on ecosystems, but could be used as markers for urbanization impacts, such as sewage discharge [10].

*Phenols*

Phenolic compounds are present in the environment as a result of their uses and the processes in which they are implicated. Although they can be originated naturally due to the degradation of humic substances, tannins and lignins, many industrial processes, including production of drugs, textiles, dyes, pesticides and paper, are the main source of these compounds in the environment [11]. 2, 4-bis(1,1-dimethylethyl)-phenol is an example of a bisphenol used in the chemical industry as a plasticizer and an anti-oxidant in cosmetics. This was found in the sample obtained from the study area at relatively high concentration (1.61%) which can be attributed to natural, domestic and agricultural activities. In the works of [12], they concluded that the presence of phenolic compounds are due to the degradation or decomposition of natural organic matter present in the water, through the disposal of industrial and domestic wastes into water bodies and through runoffs from agricultural lands. These chemicals, upon entry into the water, have the tendency of undergoing transformations into other moieties that can even be more harmful than the original compounds. This transformation is normally due to their interaction with physical, chemical and biological or microbial factors in the water [13]. Phenolic compounds have been enlisted by the United States Environmental Protection Agency [14] as pollutants of priority concern. This enlistment is due to the fact that these chemicals are noted to be toxic and have severe short- and long- term effects on humans and animals [15].

*Phthalates*

Phthalates are frequently used in many industries as plasticizers of polymeric materials, insecticides and cosmetics. Dibutyl phthalate was a re-occurring pollutant in the water sample at percentage area concentration of 13.26%. It can be noted that there might be a relationship between PAEs levels with the input of local waste, such as sewage water, food packaging, and scrap material near the sampling point, which were found during the sampling period. Many of these common esters cause adverse effect on reproduction and development in humans and animals such as testicular and sexual

differentiation effects [16]. A main route of exposure of humans and animals is via water as these chemicals find their way into the water system through effluent discharges, leaching from waste dumps and through several diffuse sources [17]. Phthalate acid esters, a class of chemical compounds mainly used as plasticizers for polyvinyl chloride (PVC) or to a lesser extent other resins in different industrial activities, are ubiquitous in the environment and have evoked interest in the past decade due to endocrine disrupting effects and their potential impacts on public health [18]. The trend of phthalate contamination in the water calls for concern as excessive exposure to phthalates has been linked to several health conditions, including endocrine system disruption, cancer, developmental abnormalities, and polynueropathy [19].

*Sulphur containing compounds (SCC)*

Very low concentration of Sulphur containing compound (1.02%) was detected in the water sample. This class of compound is mostly by-products of pharmaceuticals found in surface run-off waters. Their presence can be due to the fact that the compounds are very persistent and polar. Hazards accrued to this set of compounds as well as the risks for human health can be recognized via drinking the water. Because of their very low odor threshold and extremely unpleasant odor, they contribute to pollution even when very small amounts are emitted [20]. The International Labor Organization of the United Nations reports that some sulphur compounds can cause health problems, including damage to the human respiratory system, even at low concentrations, and that exposure to high levels of OSCs can be extremely harmful, causing unconsciousness and death [21]. According to the above considerations, determination of OSCs in aqueous environmental samples is necessary and provides useful information about the source of input and quality of water.

*Aldehydes*

Hexadecenal was the only compound in the water sample at a relatively high concentration (6.00%) compare to other organic pollutants found in the sample. Many aldehyde compounds are found in drinking water as a result of the oxidation of natural organic (humic) matter [22]. It also enters drinking-water via leaching from polyacetal plastic fittings in which the protective coating has been broken [23]. Minimization of aldehydes and other organic compounds in drinking water is very desirable.

*Alkyl-substituted benzenes (ASBs)*

Alkyl-substituted benzenes represent typical degradation products of petroleum hydrocarbons coming mainly from oil pollution from navigation and combustion of fuels. They were found in large numbers from the sample collected in low concentrations, but the large number of the compounds is worrisome. This large number is attributed to the nature of the study area and urbanization. As a result of increased urbanization and industrialization, ground waters have become contaminated with anthropogenic organic compounds. Many of these compounds persist for considerable periods in the subsurface environment [24]. Known mechanisms of transport to the environment include inadvertent dumping, leaking underground storage tanks, landfill leachate and re-entry into the hydrosphere in rain.

*Brominated compounds in water*

1, 54-dibromo-tetrapentacontane was detected in the sample at a low concentration of 0.49%. These brominated organic chemical compounds have been extensively used for several decades in industries as flame retardant additives in combustible materials [25], such as building and textile materials, paints, mobile and computer sets, television sets, upholstery, electrical appliances, plastics and thermosetting products, interior decoration in cars, and airplanes. They can be leached into the environment as a result of disposal when sizeable quantities are exposed to environmental conditions that support their leaching. Many studies have shown the presence of poly bromo diphenyl ethers (PBDEs) at significant levels in water, soil, sediment, wildlife, aquatic biota, air, dust, tissue, serum and human breast milk

[26]. Regardless of the fire inhibiting potential of PBDEs, the impact on individual health is a subject of immense concern in recent years. This is because these compounds and their metabolites have been discovered to be persistent, lipophilic, and noxious, and have the ability to both bioaccumulate and biomagnify, and undertake long-range atmospheric transportation [27]. Polybrominated diphenylethers can cause endocrine disruption, immunotoxicity, and developmental and reproductive dysfunctions [28]. The majority of these endocrine disruptors have been predicted to be in the dissolved aqueous phase because of the greater surface volume in the water body [26].The presence of endocrine disruptors, such as PBDEs, has a great consequence on the aquatic biota.

**5. Conclusion**

Screening of the water sample collected from laminga dam, Jos using GC-MS indicated that the water sample was highly contaminated with organic pollutants including several hydrocarbons, long chain carboxylic acids, esters, several aromatic compounds, ketones, aldehydes, alcohols and many others which compromised the quality of the water for population who largely depend on it. The diversity of these organic pollutants as detected can be attributed to the impact of agricultural, waste disposal, commercial and residential land use on ecosystem. The presence of these compounds also indicated that development is quickly transforming the landscape from forest and pastures to parking lots, streets and rooftops causing rain to rush off the land instead of soaking into the ground. These run off are washed to the reservoirs (dams) which are often collected and used or treated for various human uses.

**References**

1. A. E., Farouk, E. A. A., Abdel-Hamid, and T. M., Mekawy, "Environmental studies on water quality, plankton and bacterial community in Mariout Lake, Egypt," *Egyptian Journal of Aquatic Biology and Fisheries*, vol. *24*, no. 4, pp.139-158, 2020.
2. S. Bajaj, and D. K., Singh, "Biodegradation of persistent organic pollutants in soil, water and pristine sites by cold-adapted microorganisms: Mini review," *International biodeterioration and biodegradation*, vol. *100*, pp.98-105, 2015
3. R. Islam, S. Kumar, J. Karmoker, M. Kamruzzaman, M.A. Rahman, N. Biswas, T.K.A. Tran, and M.M., Rahman, "Bioaccumulation and adverse effects of persistent organic pollutants (POPs) on ecosystems and human exposure: a review study on Bangladesh perspectives," *Environmental Technology and Innovation*, vol. *12*, pp. 115-131, 2018.
4. A. Nuro, E. Marku, B. Murtaj, and V. Plaku, **"**Organic pollutants in water samples of Vjosa River–Albania. Zastita Materijala," vol. 58, no. 3, pp. 385–393, 2017, doi: 10.5937/ZasMat1703385N.
5. I. Agbozu, O. Edjere, G. Asibor, S. Otolo, and U. Bassey, "Source predictions of polycyclic aromatic hydrocarbon (PAHs) concentration in water, sediment, and biota (FISHES) from Ethiope River, Delta State, Southern Nigeria," *Journal of Ecology and the Natural Environment*, vol. *12,* no. 4, pp.140-149, 2020.
6. S. Kuppusamy, N.R. Maddela, M. Megharaj, and K. Venkateswarlu, "Impact of total petroleum hydrocarbons on human health," In *Total petroleum hydrocarbons* Springer, Cham, pp. 139-165, 2020
7. D.R. Joshi, and N. Adhikari, "An overview on common organic solvents and their toxicity," *Journal of Pharmaceutical Research International, vol. 28*, no. 3, pp.1-18, 2019.

8. J.W. Farrington, "Oil pollution in the marine environment I: inputs, big spills, small spills, and dribbles," *Environment: Science and Policy for Sustainable Development*, vol. *55*, no. 6, pp.3-13, 2013.
9. K.A. Pitt, S.Y. Lee, R.M. Connolly, T.H.H. Bui, and N. Doriean, "Sources and fate of organic matter in constructed versus natural coastal waterways," *Marine pollution bulletin*, vol. *135*, pp.505-513, 2018.
10. I.G. Boëchat, A. Krüger, E.M. Soares, C.C. Figueredo, A.M. Contin, P.L. Pinheiro, G.H.P. Abrantes, F.S. Cardozo, and B. Gücker, "Fatty acids reveal aquaculture and drought effects on a large tropical reservoir," *Science of the Total Environment*, vol. *755*, p.142660, 2021.

11. E.H. Fini, S. Ayat, and F. Pahlavan, "Phenolic Compounds in the Built Environment," In *Phenolic Compounds-Chemistry, Synthesis, Diversity, Non-Conventional Industrial, Pharmaceutical and Therapeutic Applications*, IntechOpen, 2021.

12. M.M. Ghangrekar, and P. Chatterjee, "Water pollutants classification and its effects on environment," In *Carbon nanotubes for clean water,* Springer, Cham, pp. 11-26, 2018.

13. S. J. Kulkarni, and D. J. P. Kaware, "Review on research for removal of phenol from waste-water," *International Journal of Scientific and Research Publications,* vol. 3, pp.1– 4, 2013.
14. USEPA (U.S. Environmental Protection Agency), "Bis (2-ethyl) phthalate Exposure Factors Handbook (Final Report), EPA/600/P-95/002F a-c, Washington, DC, 2021.
15. W.W. Anku, M.A. Mamo, and P.P, Govender, "Phenolic compounds in water: sources, reactivity, toxicity and treatment methods," *Phenolic compounds-natural sources, importance and applications*, pp.419-443, 2017.

16. F. Pallotti, M. Pelloni, D. Gianfrilli, A. Lenzi, F. Lombardo, and D. Paoli, "Mechanisms of testicular disruption from exposure to bisphenol A and phthalates" *Journal of clinical medicine*, vol. *9*, no. 2, p.471, 2020.
17. J.K.H. Wong, K.K. Lee, K.H.D. Tang, and P.S. Yap, "Micro plastics in the freshwater and terrestrial environments: Prevalence, fates, impacts and sustainable solutions," *Science of the total environment*, vol. *719*: p.137512, 2020.
18. S.K. Shukla, N. Mangwani, and T.S. Rao, "Bioremediation approaches for persistent organic pollutants using microbial biofilms. *Microbial Biofilms and Bioremediation Wastewater Treat*, vol. *179*, pp.179-206, 2019.
19. S. Tongesayi, and T. Tongesayi, "Water quality and public health: Role of wastewater," In *Chemistry and Water,* pp553-596, 2017, Elsevier.
20. F. Khalilian, and M. Rezaee, "Extraction and determination of organosulfur compounds in water samples by using homogeneous liquid-liquid micro-extraction via flotation assistance-gas chromatography-flame ionization detection," *Bulletin of the Chemical Society of Ethiopia*, vol. *28,* no. 2, pp.195-204, 2014.

21. S. Sun, T. Jia, K. Chen, Y. Peng, and L. Zhang, "Simultaneous removal of hydrogen sulfide and volatile organic sulfur compounds in off-gas mixture from a wastewater treatment plant using a two-stage bio-trickling filter system," *Frontiers of Environmental Science and Engineering*, vol. *13*, no. 4, pp.1-13, 2019.

22. W. Qi, H. Zhang, C. Hu, H. Liu, and J. Qu, "Effect of ozonation on the characteristics of effluent organic matter fractions and subsequent associations with disinfection by-products formation," *Science of the Total Environment*, vol. *610*, pp.1057-1064, 2018.
23. M.A. Ehsan and A. Rehman, "Facile and scalable fabrication of nanostructured nickel thin film electrodes for electrochemical detection of formaldehyde," *Analytical Methods*, vol. *12*, no.32, pp.4028-4036, 2020.
24. W.Q. Zhang, H. Li, Y.J. Zhang, F. Bi, L.S. Meng, X.M. Zhang, J.Y. Mao, N.L. Cheng, B. Fang, Y. Yang and C. Chen, "Fast determination of monocyclic aromatic hydrocarbons in ambient air using a portable gas chromatography–photoionization detector," *Chromatographia*, vol. *80*, no. 8, pp.1233-1247, 2017.
25. E.W. Madyaratri, M.R. Ridho, M.A. Aristri, M.A.R. Lubis, A.H. Iswanto, D.S. Nawawi, , P. Antov, L. Kristak, A. Majlingová and W. Fatriasari, " Recent advances in the development of fire-resistant biocomposites—A review," *Polymers*, vol. *14*, no. 3, p.362, 2022.
26. G.O. Olutona, J.A. Oyekunle, A.O. Ogunfowokan and O.S. Fatoki, "Concentrations of polybrominated diphenyl ethers (PBDEs) in water from Asunle Stream, Ile-Ife, Nigeria. *Toxics*, vol. *5*, no. 2, p.13, 2017.
27. C.A. De Wit, M. Alaee, and D.C. Muir, (2006) "Levels and trends of brominated flame retardants," Arctic. Journal of *Chemosphere,* vol. 64, pp.209–233, 2006, doi: 10.1016/j.chemosphere. 12.029.
28. T. Encarnação, A.A. Pais, M.G. Campos, and H.D. Burrows, "Endocrine disrupting chemicals: Impact on human health, wildlife and the environment," *Science progress*, vol. *102*, no.1, pp.3-42, 2019.

# TOPOLOGICAL INVESTIGATION OF ENERGY SPECTRA, THERMODYNAMICS, AND MAGNETIC RESPONSE IN MOLECULAR SYSTEMS WITH THE MODIFIED TIETZ–WEI POTENTIAL

**Amusat, R. O.[1*], Manga1, P. J.[1], Ocheni, A.U.U.[1], Aliyu, A.[1], Sonloye, A. S.[1], Salau, R.[2],**

*[1]Department of Physics, University of Maiduguri, Borno – State – Nigeria.*
*[2]Department of Science Laboratory Technology, Federal Polytechnic of Mongonu, Borno State – Nigeria.*
*Corresponding author: amusatramoni@gmail.com*

**Abstract**

This study investigates the thermodynamic properties and magnetic susceptibility associated with molecular energy in a two-dimensional quantum system defined by the modified Tietz–Wei molecular potential. The radial Schrödinger equation is solved using the Greene–Aldrich approximation, while the molecular energy eigenvalues are obtained through the Nikiforov–Uvarov Functional Analysis (NUFA) method within a topological framework. The effects of external magnetic field, magnetic flux, screening parameter, and potential parameters are analysed at zero and finite temperatures through the partition function and related thermodynamic quantities. The results show that molecular energy eigenvalues increase with increasing magnetic field strength and magnetic flux, whereas larger screening parameters reduce the energy levels. The partition function decreases with increasing magnetic field and flux but increases with temperature. Furthermore, Helmholtz free energy, internal energy, entropy, and specific heat capacity exhibit strong temperature dependence, especially at low temperatures. In addition, magnetization and magnetic susceptibility increase with magnetic field strength and flux, although a slight reduction occurs at very low temperatures. These findings offer insight into the thermodynamic and magnetic behaviour of molecular systems governed by the modified Tietz–Wei potential within a topological framework.

**Keywords:** Modified Tietz–Wei potential, Topological analysis, Molecular energy eigenvalues, Thermodynamic properties, Magnetic susceptibility.

## 1. Introduction

Recent advances in molecular quantum physics have focused on understanding how external perturbations, interaction potentials, and geometric effects influence the energy spectra, thermodynamic behavior, and magnetic response of diatomic systems. Studies have shown that topological defects, magnetic fields, and Aharonov–Bohm (AB) flux significantly modify molecular properties by altering energy levels and thermo-magnetic behavior [1-3].Topological defects also affect wavefunction localization and quantum information measures such as Shannon entropy and Fisher information, emphasizing the role of geometry in quantum systems [4, 5]. Thermodynamic quantities, including partition function, entropy, and specific heat, exhibit strong dependence on temperature, screening parameters, and quantum states [6, 7]. Various interaction potentials, such as Kratzer-type, Morse, Deng–Fan, Hulthén, and Tietz–Hua potentials, have been used to model these systems, demonstrating strong sensitivity of energy spectra and thermodynamic properties to potential parameters and external perturbations [5, 6, 8] . Relativistic effects, spin–orbit coupling, and Zeeman splitting further lift degeneracies and modify optical and magnetic responses [9].Nonlinear dynamical studies based on the modified Tietz–Wei potential also reveal resonance, multistability, and chaotic behavior under external driving forces [10].

Despite these contributions, most studies remain theoretical and often treat topological, thermodynamic, and magnetic effects separately. Motivated by this gap, the present study investigates the energy spectra, thermodynamic properties, and magnetic susceptibility of a two-dimensional

molecular system governed by the modified Tietz–Wei potential in the presence of an external magnetic field and AB flux. Using the Greene–Aldrich approximation and the Nikiforov–Uvarov Functional Analysis (NUFA) method, analytical energy eigenvalues are obtained and employed to evaluate thermodynamic and magnetic quantities. The results reveal strong dependence on magnetic field, magnetic flux, screening parameter, and temperature, providing deeper insight into the interplay between topology, external fields, and molecular interactions.

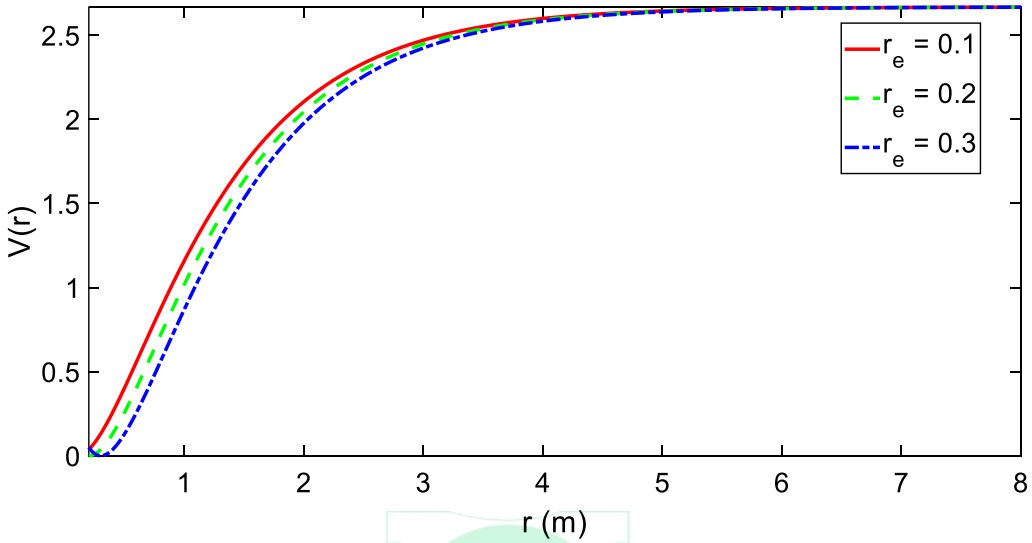



Figure 1: The Plot of (MTWP) against Optimization Parameter.

## 2. Theoretical Framework and Methodology

In this section, the analytical formulation of a diatomic molecular system subjected to an external magnetic field and Aharonov–Bohm (AB) flux is developed. The interaction between the atoms is described using the modified Tietz–Wei potential, while magnetic and topological effects are incorporated through a suitably constructed vector potential. The AB flux introduces a topological phase contribution that depends on the global properties of the electromagnetic potential rather than the local field strength, leading to observable modifications in the energy spectrum and magnetic response even in regions where the magnetic field vanishes. The resulting Schrödinger equation is transformed into a solvable form using an exponential coordinate transformation and solved via the Nikiforov–Uvarov Functional Analysis (NUFA) method.[11]

### Modified Tietz-Wei Potential and Hamiltonian

he modified Tietz–Wei potential is employed to describe the molecular interaction due to its effectiveness in modelling the vibrational and rotational behaviour of diatomic molecules. Its additional screening parameter provides greater flexibility in capturing anharmonic effects and deviations from ideal molecular interactions. The potential accurately represents exponentially decaying interatomic interactions, preserves correct asymptotic behaviour at large internuclear separations, and has been widely used in molecular physics and quantum chemistry for bound-state energy studies.

The modified Tietz–Wei potential is expressed as [12]

$$V(r) = D_e \left( \frac{1-e^{-b(r-r_e)}}{1-ce^{-b(r-r_e)}} \right)^2 \quad (1)$$

Where $D_e$ is the dissociation energy, $r_e$ denotes the equilibrium bond length, b is the potential range parameter, and c controls the curvature of the potential well. This form reduces to other well-known molecular potentials under specific parameter limits [13].

For a charged particle of reduced mass μ in the presence of an electromagnetic field, the Hamiltonian is written using the minimal-coupling scheme [14]

$$H = \frac{1}{2\mu}\left(p - \frac{e}{c}A\right)^2 + V(r), \quad (2)$$

Where $A$ is the vector potential

To describe a uniform magnetic field B perpendicular to the molecular plane and an AB flux $\Phi_{AB}$, the vector potential is chosen as [15]

$$A = \frac{B}{2} + \frac{\Phi_{AB}}{2\pi r}\hat{\Phi} \quad (3)$$

**Radial Schrodinger Equation and Approximations**

Separating variables in polar coordinates, the wave function is written as [3]

$$\psi(r,\phi) = R(r)e^{im\phi} \quad (4)$$

Where $m$ is the magnetic quantum number. The AB flux effectively shifts the angular momentum according to.

$$m \to m + \xi, \xi = \frac{e\Phi_{AB}}{2\pi\hbar c} \quad , \omega_c = \frac{eB}{\mu c} \quad (5)$$

Substituting into the Schrödinger equation yields the radial equation

$$\frac{d^2R}{dr^2} + \frac{1}{r}\frac{dR}{dr} + \left[\frac{2\mu}{\hbar^2}\left(E - V(r)\right) - \frac{(m+\xi)^2}{r^2} - \frac{\mu^2\omega_c^2 r^2}{4\hbar^2} - \frac{\omega_c(m+\xi)}{\hbar}\right]R(r) = 0 \quad (6)$$

The Tietz – Wei potential is defined as follows:

$$V(r) = D_e\left(\frac{1-e^{-b(r-r_e)}}{1-ce^{-b(r-r_e)}}\right)^2 \quad (7)$$

Substituting equation (7) into (6) we have

$$\frac{d^2R}{dr^2} + \frac{1}{r}\frac{dR}{dr} + \left[\frac{2\mu}{\hbar^2}\left(E - D_e\left(\frac{1-e^{-b(r-r_e)}}{1-ce^{-b(r-r_e)}}\right)^2\right) - \frac{(m+\xi)^2}{r^2} - \frac{\mu^2\omega_c^2 r^2}{4\hbar^2} - \frac{\omega_c(m+\xi)}{\hbar}\right]R(r) = 0 \quad (8)$$

Transforming the coordinate of equation (8) we have;

$$z = e^{-b(r-r_e)} \; and \; r = r_e - \frac{1}{b}lnz \quad (9)$$

Reducing the centrifugal and magnetic terms through pekeris approximation we have

$$\frac{(m+\Phi_{AB})^2}{r^2} + \frac{\mu^2\omega_c^2 r^2}{\hbar^2} \approx \frac{(m+\Phi_{AB})^2}{r_e^2} + \frac{\mu^2\omega_c^2 r_e^2}{\hbar^2} \quad (10)$$

The Schrödinger equation in z coordinate as shown in equation (8) becomes:

$$b^2z^2\frac{d^2R}{dz^2} + b^2z\frac{dR}{dz} + \frac{2\mu}{\hbar^2}\left[E - D_e\left(\frac{1-z}{1-cz}\right)^2 - \frac{\hbar^2}{2\mu r_e^2}(m+\Phi_{AB})^2 - \frac{1}{2}\mu^2\omega_c^2 r_e^2\right]R(z) = 0 \quad (11)$$

Divide equation (11) by $b^2z^2$ we have:

$$\frac{d^2R}{dz^2}+\frac{1}{z}\frac{dR}{dz}+\frac{1}{(bz)^2}\frac{2\mu}{\hbar^2}\left[E-D_e\left(\frac{1-z}{1-cz}\right)^2-\frac{\hbar^2}{2\mu r_e^2}(m+\Phi_{AB})^2-\frac{1}{2}\mu^2\omega_c^2r_e^2\right]R(z)=0$$

(12)

Equation (12) can be written as

$$\frac{d^2R}{dz^2}+\frac{1}{z}\frac{dR}{dz}+\frac{1}{(bz)^2}\frac{2\mu}{\hbar^2}\left[E-\frac{D_e(1-2z+z^2)}{(1-cz)^2}-\lambda\right]R(z)=0 \quad (13)$$

$$\lambda=\frac{\hbar^2}{2\mu r_e^2}(m+\Phi_{AB})^2-\frac{1}{2}\mu^2\omega_c^2r_e^2$$

(14)

Multiply Through by $(1-cz)^2$ to obtain the NU standard form:

$$\frac{d^2R}{dz^2}+\frac{1-cz}{z(1-cz)}\frac{dR}{dz}+\frac{\bar{\sigma}(z)}{[z(1-cz)]^2}R(z)=0 \quad (15)$$

Comparing with the NU equation

$$\frac{d^2\psi}{dz^2}+\frac{\bar{\tau}(z)}{\sigma(z)}\frac{d\psi}{dr}+\frac{\bar{\sigma}(z)}{\sigma^2(z)}\psi(z)=0$$

(16)

$$\sigma(z)=z(1-cz) \text{ and } \bar{\tau}(z)=1-cz \quad (17)$$

$$\varepsilon=\frac{2\mu}{h^2b^2}(E-\lambda) \; and \; \beta=\frac{2\mu De}{h^2b^2} \quad (18)$$

Equation (15) becomes

$$\frac{d^2R}{dz^2}+\frac{1-cz}{z(1-cz)}\frac{dR}{dz}+\frac{1}{[z(1-cz)]^2}[\varepsilon z(1-cz)^2-\beta(1-2z+z^2)]R(z)=0 \quad (19)$$

Where

$$\tilde{\sigma}(z)=(\varepsilon-\beta)+(2\beta-2\varepsilon c)z+(\varepsilon c^2-\beta)z^2 \quad (20)$$

Let

$$\pi(z)=\frac{\sigma'(z)-\bar{\tau}(z)}{2}\pm\sqrt{\left(\frac{\sigma'(z)-\bar{\tau}(z)}{2}\right)^2-\tilde{\sigma}(z)+k\sigma(z)}$$

(21)

Where by

$$\frac{\sigma'(z)-\bar{\tau}(z)}{2}=\frac{(1-2cz)-(1-cz)}{2}=-\frac{cz}{2}$$

(22)

$$\pi(z)=-\frac{cz}{2}\pm\sqrt{\frac{c^2z^2}{4}-\tilde{\sigma}(z)+kz(1-cz)}$$

(23)

Substitute for $\tilde{\sigma}(z)$

$$\pi(z)=-\frac{cz}{2}\pm\sqrt{Az^2+Bz+C} \quad (24)$$

where

$$A=\frac{c^2}{4}-\varepsilon c^2+\beta-kc, B=2\varepsilon c-2\beta+k\beta, \; C=\beta-\varepsilon$$

(25)

$$Az^2+Bz+C=(\propto z+\gamma)^2$$

(26)

Using the NU quantization condition:

$$\Lambda=k+\pi'(z) \text{ And } \Lambda_n=-n\tau'(z)-\frac{n(n-1)}{2}\sigma''(z)$$

(27)

$$\tau(z) = \tilde{\tau}(z) + 2\pi(z) \quad (28)$$

$$\sigma''(z) = -2c \; if \; \sigma(z) = z - cz^2 \quad (29)$$

$$\tau'(z) = -c + 2\pi'(z) \quad (30)$$

$$\Lambda_n = -n[-c + 2\pi'(z)] - \frac{n(n-1)}{2}(-2c) \quad (31)$$

$$\Lambda_n = cn^2 - 2n\pi'(z) \quad (32)$$

For computing energy eigen values we have

$$\Lambda = \Lambda_n \quad (33)$$

Let

$$\delta = \frac{1}{2}\left(1 + \sqrt{1 + \frac{8\mu D_e}{\hbar^2 b^2}(1-c)^2}\right) \quad (34)$$

$$\beta = \frac{2\mu D_e}{\hbar^2 b^2} \text{ and } \omega_c = \frac{eB}{\mu c} \quad (35)$$

The final bound state energy spectrum is

$$\mathrm{E}_n = D_e + \frac{\hbar^2}{2\mu}\left[\frac{(m+\phi_{AB})^2}{r_e^2}\right] + \frac{1}{2}\mu\omega_c^2 r_e^2 - \frac{\hbar^2 b^2}{2\mu}\left[\frac{\beta - c(n+\delta)^2}{2c(n+\delta)}\right]^2 \quad (36)$$

### 3. Results and Discussion

Figures 1–4 depict the influence of magnetic field strength, Aharonov–Bohm (AB) flux, vibrational quantum number, and screening parameter on the bound-state energy spectrum of the modified Tietz–Wei molecular system. Figure 2 demonstrates that the energy eigenvalues increase with increasing magnetic field and magnetic quantum number due to greater magnetic confinement and Zeeman-type splitting effects. In Figure 3, advanced vibrational quantum numbers agree to larger energy levels, while increasing the screening parameter weakens the molecular interaction, causing the energy states to move closer to the dissociation limit. Figure 3 shows that the AB flux modifies the effective angular momentum of the system, thereby lifting degeneracies and confirming the significant topological contribution of the AB effect to the molecular energy spectrum.

Figures 5–9 demonstrate the thermodynamic properties derived from the partition function, while Figures 5i–9i show their corresponding topological counterparts. Figure 5 depicts that the partition function increases with temperature as more quantum states become thermally accessible. The topological partition function in Figure 5i exhibits a similar trend but is further influenced by the AB flux, highlighting the role of topology in modifying state accessibility. Figures 6 and 6i reveal that both the conventional and topological Helmholtz free energies decrease with temperature, reflecting enhanced thermal stability and increased disorder at elevated temperatures.

Figures 7 and 7i demonstrate that internal energy increases monotonically with temperature due to greater population of excited states. Similarly, Figures 8 and 8i indicate that the specific heat capacity rises rapidly at low temperatures before approaching saturation, suggesting a redistribution of thermal energy among the available quantum states. Figures 9 and 9i demonstrate that enthalpy increases with temperature, following the same general behavior as the internal energy. The topological thermodynamic quantities exhibit slight shifts relative to their conventional counterparts, confirming

that the AB flux introduces measurable geometric-phase effects into the thermal response of the molecular system.

Furthermore, the results reveal that magnetic fields, screening effects, and topological parameters significantly influence the energy spectrum and thermodynamic behavior of the modified Tietz–Wei molecular system. The observed differences between the conventional and topological thermodynamic functions demonstrate that the Aharonov–Bohm flux plays a crucial role in governing the thermo-magnetic characteristics of the molecule, thereby validating the topological nature of the present investigation.

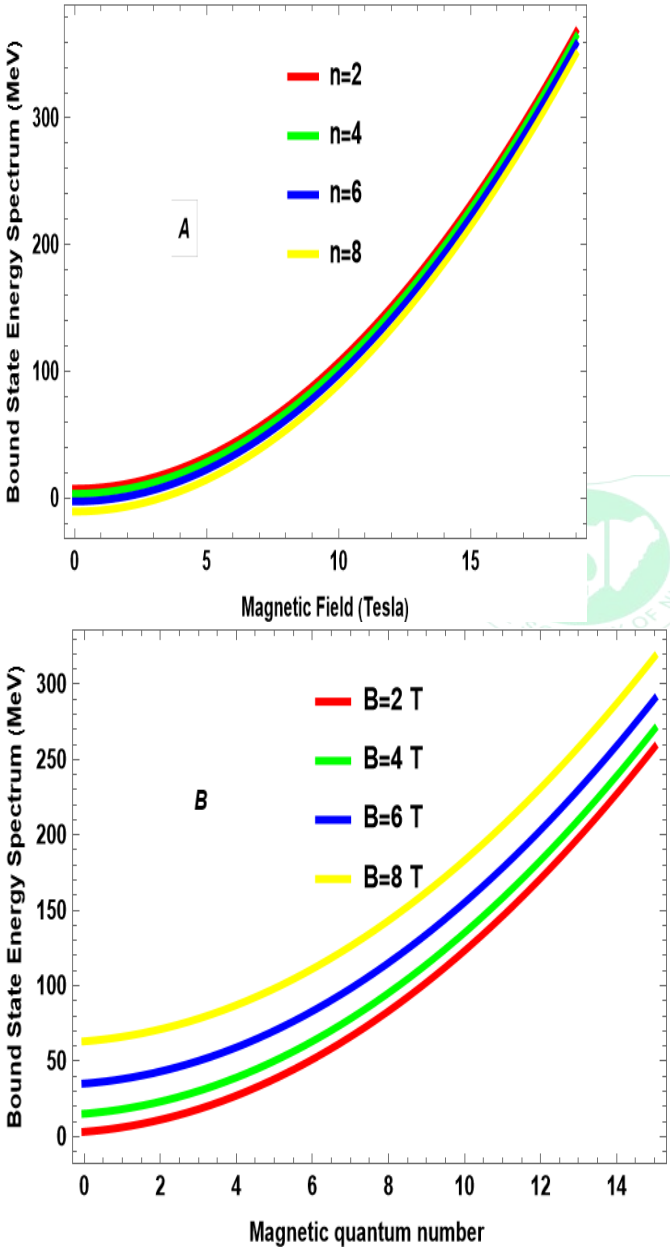



***Fig 2:*** *Computed Bound State Energy Spectrum under the Influenced of Magnetic Field (Tesla) and Magnetic Quantum Number.*

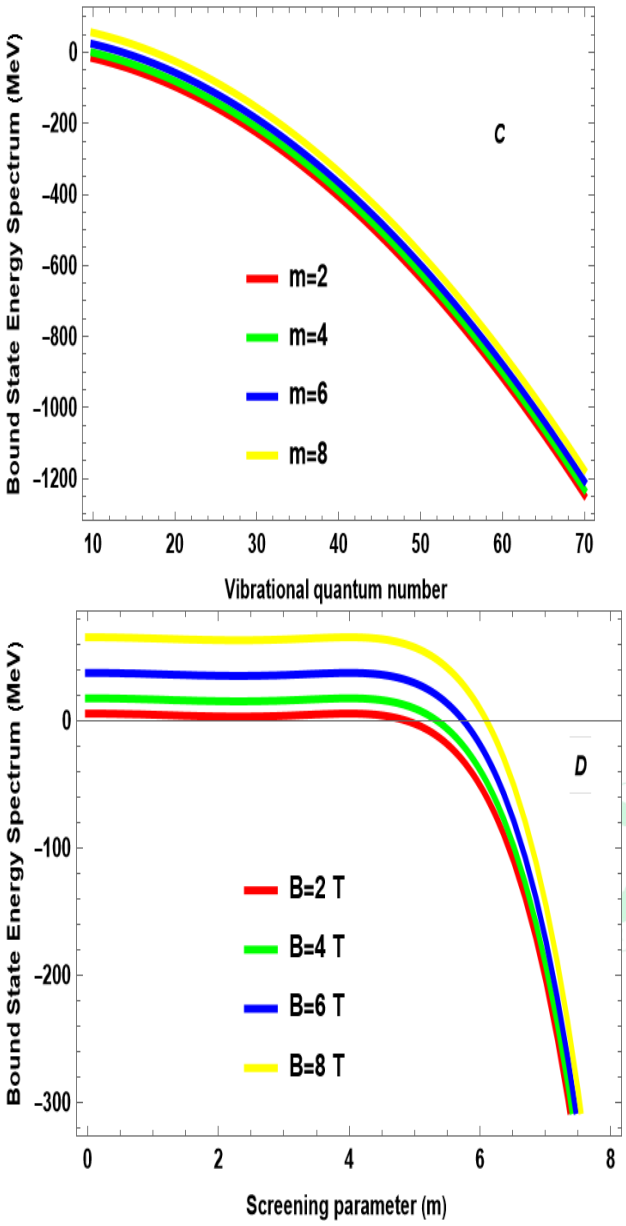



***Fig 3:*** *Computed Bound State Energy Spectrum under the Influenced of Vibrational Quantum Number and Screening Parameter (m).*

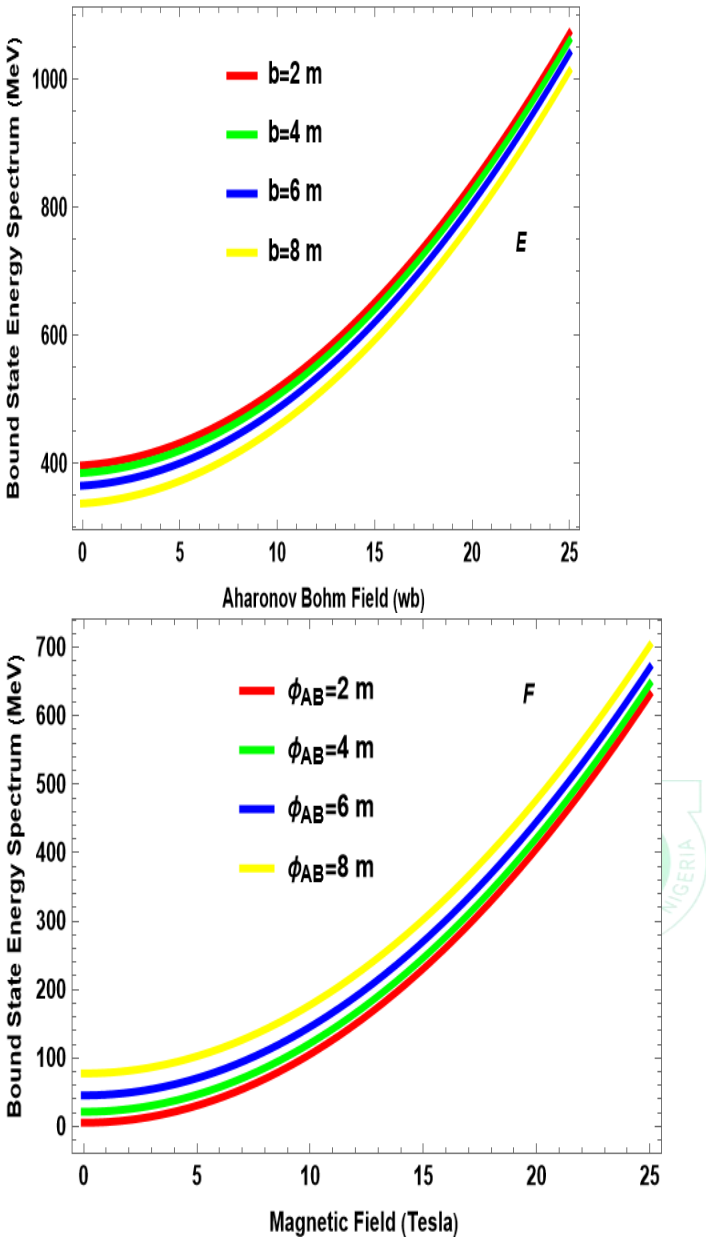



*Fig 4: Computed Bound State Energy Spectrum under the Influenced of Aharonov Bohm Field (wb) and Magnetic Quantum Number.*

**Thermodynamic Properties**

The canonical partition function is:

$$Z(\beta) = \sum_{n=0}^{\lambda} e^{-\beta E_n} \quad (37)$$

Where $\lambda$ is an upper bound of the vibrational quantum number deduced from $\frac{dE_n}{d_n} = 0, \beta = \frac{1}{KT}$ where k and T are Boltzmann constant and temperature respectively? The summation can be replaced with an integral [12], [13].

$$Z(\beta) = \int_0^{\lambda} e^{-\beta E_n} \, dn \quad (38)$$

The energy equation can be represented under a canonical partition function as follows.

$$ZZ = e^{-\beta K_1} \int_0^{\lambda} e^{\beta\left(\frac{K_2}{P^2} + K_2 K_3^2 P^2\right)}\, dP \quad (39)$$

$$ZZ = \frac{e^{-\beta K_1 - 2\sqrt{-K_2\beta}\sqrt{-K_2 K_3^2\beta}}\sqrt{\pi}\left(\text{Erfc}\left[\frac{\sqrt{-K_2\beta}}{p} - p\sqrt{-K_2 K_3^2\beta}\right] - e^{4\sqrt{-K_2\beta}\sqrt{-K_2 K_3^2\beta}}\,\text{Erfc}\left[\frac{\sqrt{-K_2\beta}}{p} + p\sqrt{-K_2 K_3^2\beta}\right]\right)}{4\sqrt{-K_2 K_3^2\beta}} \quad (40)$$

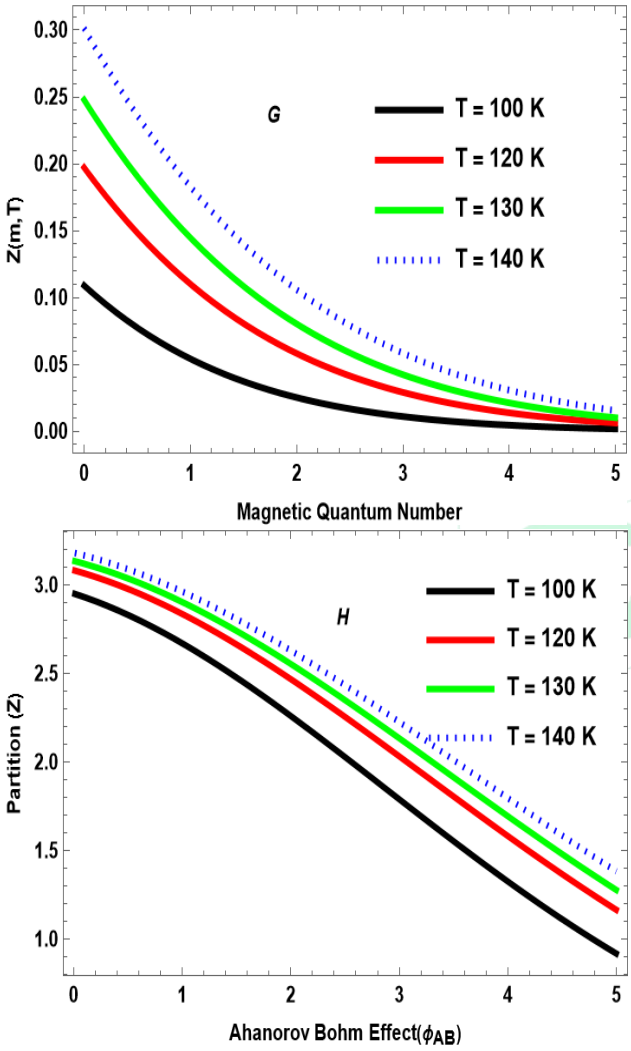



**Fig 5:** Plot of Partition Function against Finite Temperature by Varying Magnetic Quantum Number and Magnetic Flux $\Phi_{A,B}$ (Aharonov Bohm Effect)

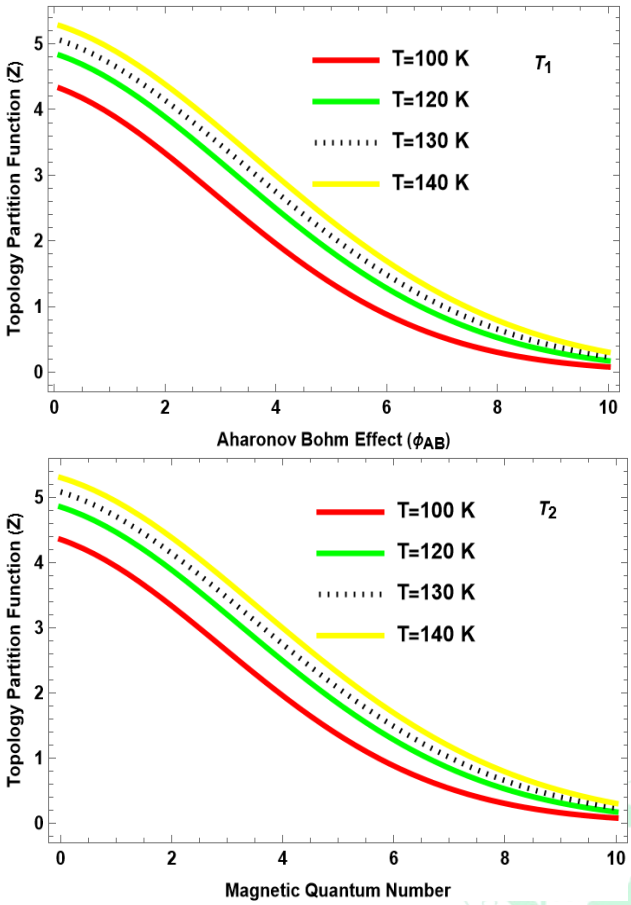



**Fig 5i:** Plot of Topological Partition Function against Finite Temperature by Varying Magnetic Quantum Number and Magnetic Flux $\Phi_{A,B}$ (Aharonov Bohm Effect)

**Free Energy**

The free molecular energy can be computed as follows [13]:

$$F = -\frac{1}{\beta}\ln Z(\beta) \tag{41}$$

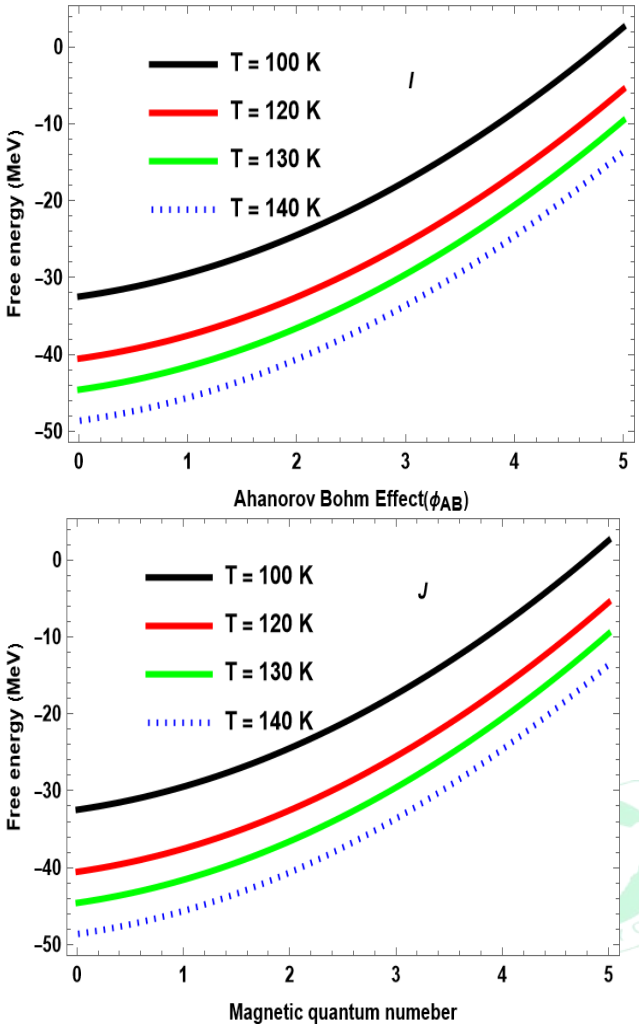



**Fig 6:** Plot of Free Energy against Finite Temperature by Varying Magnetic Quantum Number and Magnetic Flux $\Phi_{A,B}$ (Aharonov Bohm Effect)

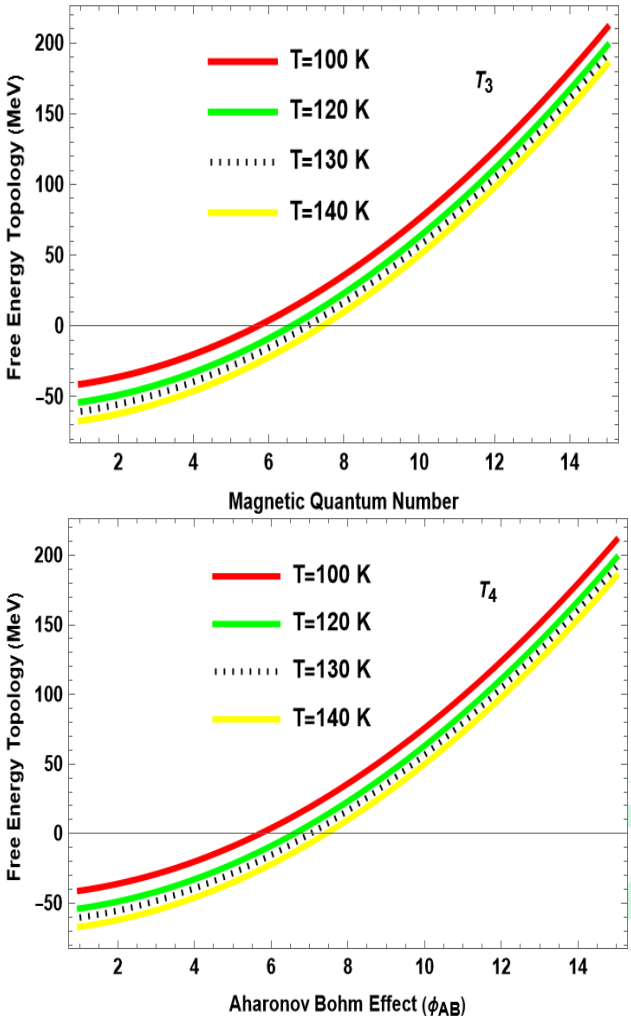



**Fig 6i:** Plot of Topological Free Energy against Finite Temperature by Varying Magnetic Quantum Number and Magnetic Flux $\Phi_{A,B}$ (Aharonov Bohm Effect)

**Internal Energy for Molecular Energy Based on the Partition Function**

The internal energy of partition function is defined by expression as follows

$$U = -\frac{\partial}{\partial \beta} \ln Z(\beta) \quad (42)$$

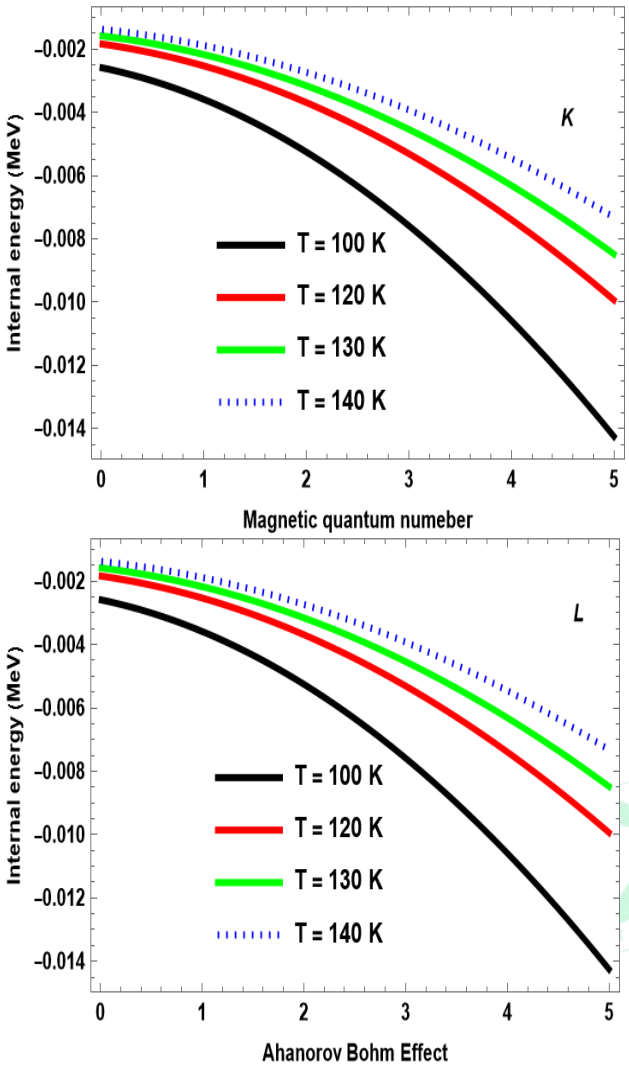



**Fig 7:** Plot of Internal Energy against Finite Temperature by Varying Magnetic Quantum Number and Magnetic Flux $\Phi_{A,B}$ (Aharonov Bohm Effect)

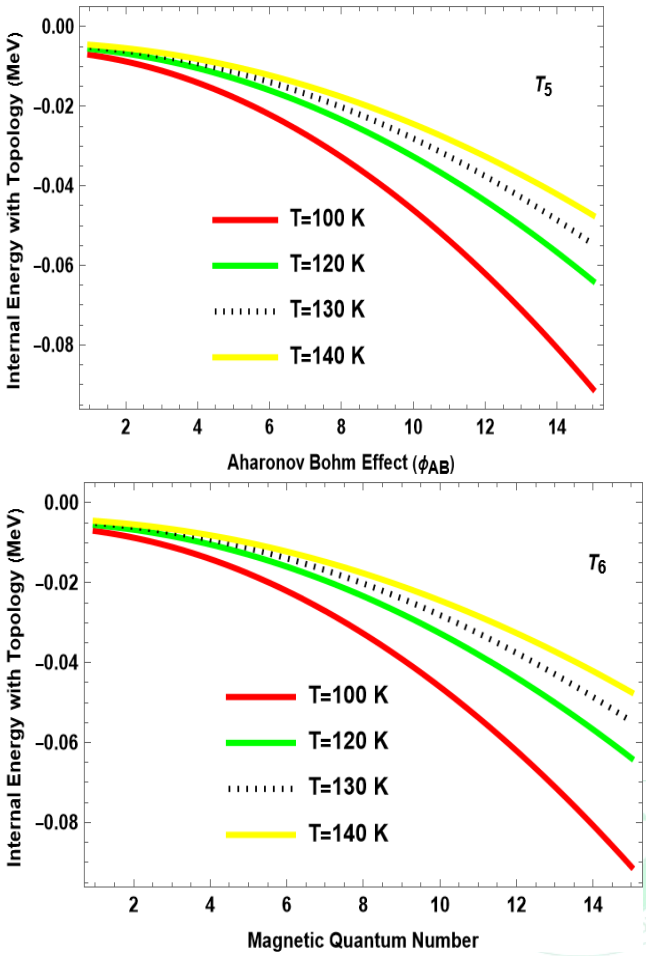



**Fig 7i:** Plot of Topological Internal Energy against Finite Temperature by Varying Magnetic Quantum Number and Magnetic Flux $\Phi_{A,B}$ (Aharonov Bohm Effect)

**Specific Heat Capacity for Molecular Energy Based on the Partition Function**

The specific heat capacity is defined by the expression.

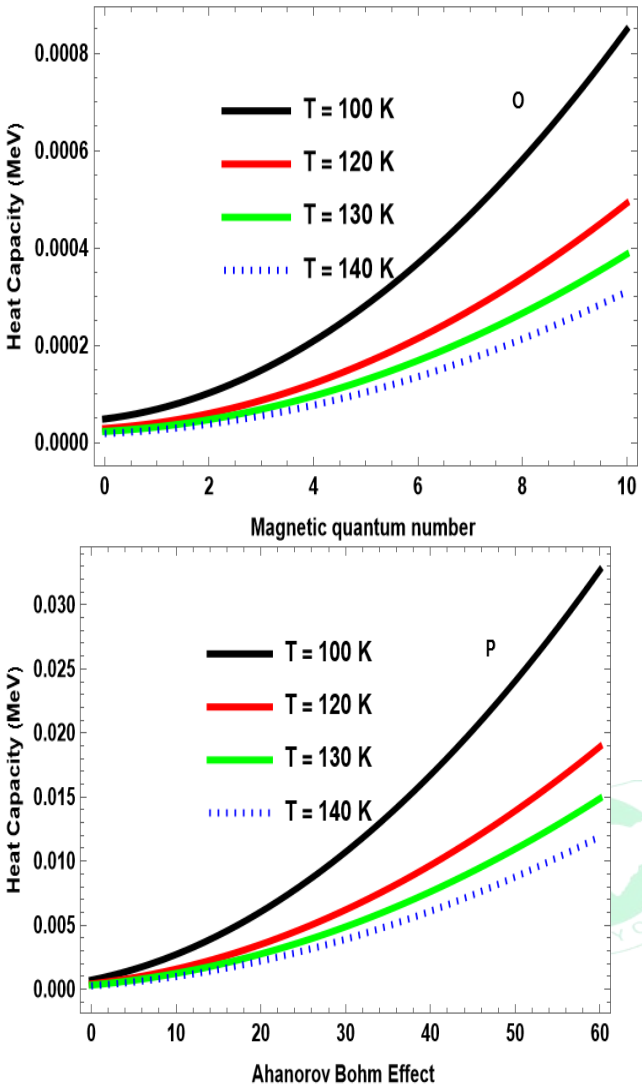



**Fig 8:** Plot of Heat Capacity against Finite Temperature by Varying Magnetic Quantum Number and Magnetic Flux $\Phi_{A,B}$ (Aharonov Bohm Effect)

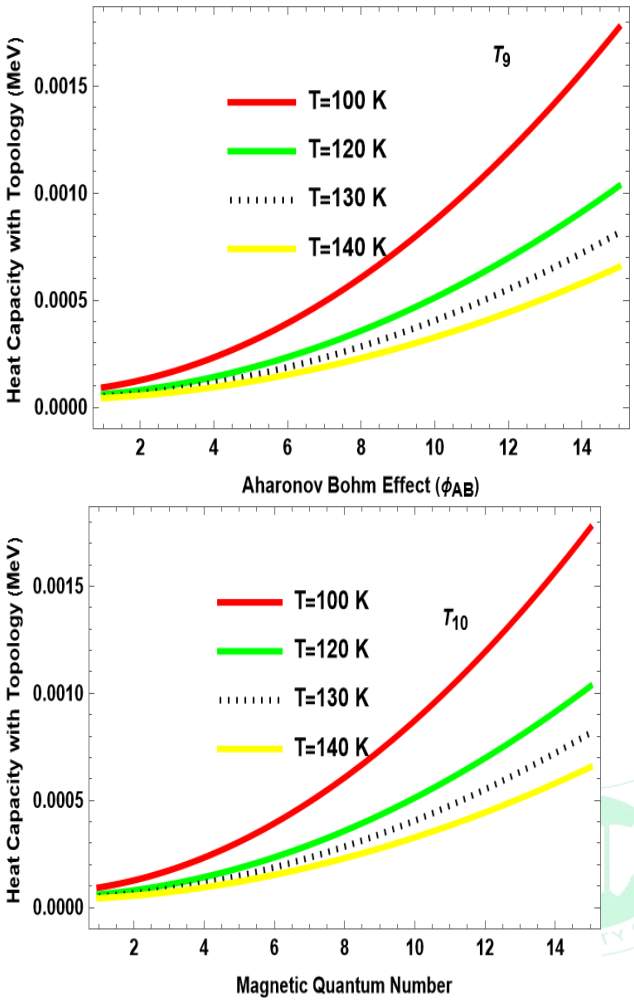



**Fig 8i:** Plot of Topological Heat Capacity against Finite Temperature by Varying Magnetic Quantum Number and Magnetic Flux $\Phi_{A,B}$ (Aharonov Bohm Effect)

**The Enthalpy $H(\beta)$for Molecular Energy Based on the Partition Function**

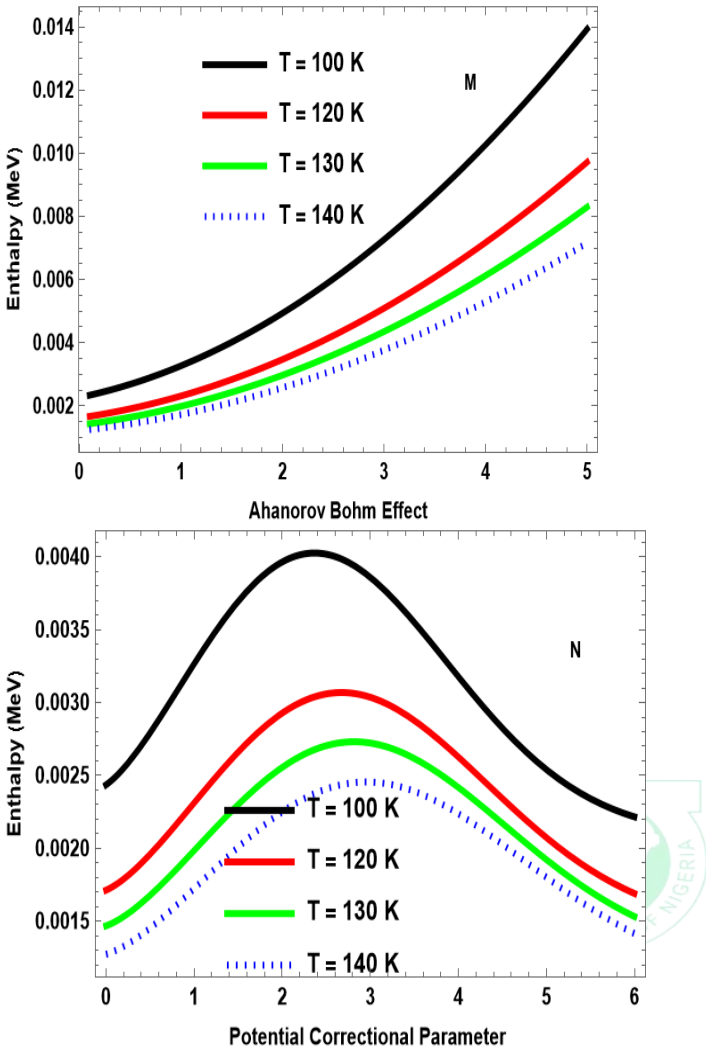



**Fig 9:** Plot of Enthalpy against Finite Temperature by Varying Magnetic Quantum Number and Magnetic Flux $\Phi_{A,B}$ (Aharonov Bohm Effect)

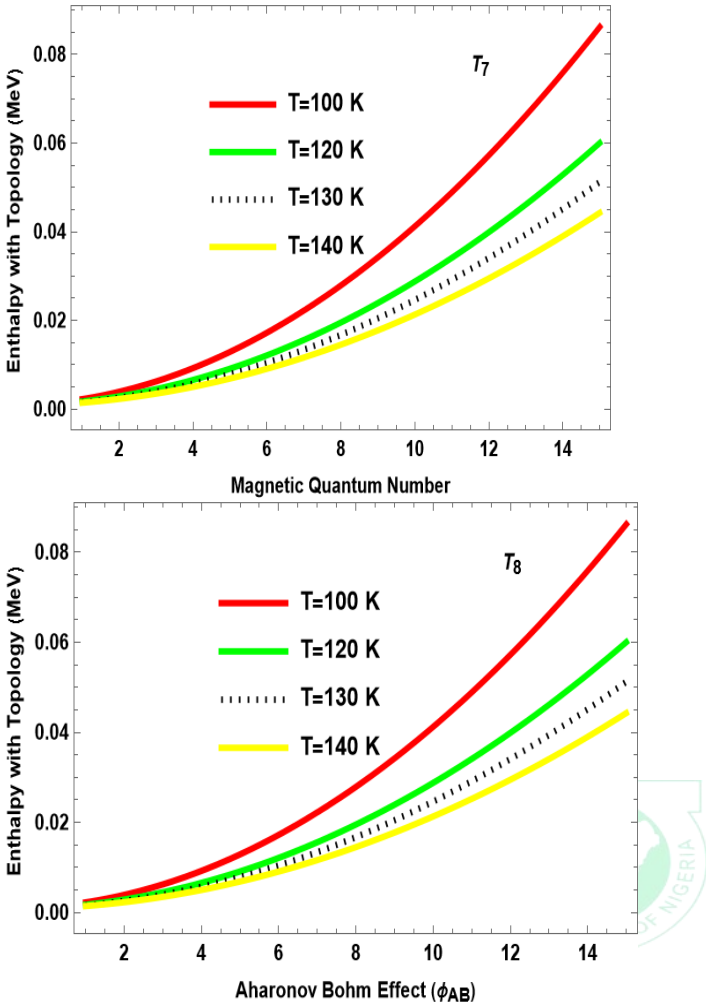



**Fig 9i:** Plot of Topological Enthalpy against Finite Temperature by Varying Magnetic Quantum Number and Magnetic Flux $\Phi_{A,B}$ (Aharonov Bohm Effect)

**4. Conclusion**

This study explored the energy spectrum, thermodynamic properties, as well as topological effects of a two-dimensional molecular system. This was described by the modified Tietz–Wei potential under the influence of an external magnetic field and Aharonov–Bohm (AB) flux. Using the Greene–Aldrich approximation and Nikiforov–Uvarov Functional Analysis (NUFA), analytical energy eigenvalues were obtained and used to evaluate the system's thermodynamic behavior. The results showed that energy levels increase with magnetic field strength, magnetic quantum number, and AB flux, while increasing the screening parameter lowers the energy spectrum. Thermodynamic quantities such as the partition function, internal energy, specific heat capacity, and enthalpy increase with temperature, whereas the Helmholtz free energy decreases. Furthermore, the topological thermodynamic functions differ from their conventional counterparts, confirming the significant influence of the AB flux on the thermal and quantum behavior of the system. Overall, the findings demonstrate the important role of topology and magnetic effects in determining the properties of molecular systems and provide a useful framework for future studies in molecular spectroscopy, quantum thermodynamics, and nanoscale quantum devices.

**References:**

[1] P. Nwabuzor, C. Edet, A. Ndem Ikot, U. Okorie, M. Ramantswana, R. Horchani, A.-H. Abdel-Aty, and G. Rampho, "Analyzing the effects of topological defect (TD) on the energy spectra and thermal properties of LiH, TiC and $I_2$ diatomic molecules," *Entropy*, vol. 23, no. 8, p. 1060, 2021. doi: https://doi.org/10.3390/e23081060.

[2] C. Edet and A. Ikot, "Effects of topological defect on the energy spectra and thermo-magnetic properties of CO diatomic molecule," *Journal of Low Temperature Physics*, vol. 203, no. 1, pp. 84–111, 2021. doi: https://doi.org/10.1007/s10909-021-02577-9.

[3] C. Onate, I. Okon, M. Onyeaju, and A. Antia, "Approximate solutions of the Schrödinger equation for a momentum-dependent potential," *Journal of the Nigerian Society of Physical Sciences*, vol. 4, no. 2, pp. 242–250, 2022. doi:10.46481/jnsps.2022.653.

[4] E. P. Inyang, "Quantum information and energy spectra modifications in diatomic molecules due to topological defects," *Journal of Theoretical Physics & Mathematics Research*, vol. 3, no. 1, pp. 1–10, 2025.

[5] I. B. Okon, E. Omugbe, A. D. Antia, C. Onate, L. E. Akpabio, and O. Osafile, "Spin and pseudospin solutions to Dirac equation and its thermodynamic properties using hyperbolic Hulthén plus hyperbolic exponential inversely quadratic potential," *Scientific Reports*, vol. 11, no. 1, p. 892, 2021. doi: https://doi.org/10.1038/s41598-023-34521-0.

[6] C. Edet, P. Amadi, E. Ettah, N. Ali, M. Asjad, and A. Ikot, "The magnetocaloric effect, thermo-magnetic and transport properties of LiH diatomic molecule," *Molecular Physics*, vol. 120, no. 10, p. e2059025, 2022. doi: https://doi.org/10.1080/00268976.2022.2059025.

[7] A. Ahmadov and G. Bayramova, "Thermodynamic Properties of Hulthén Plus A Class of Yukawa Potentials for Some Diatomic Molecules," *Journal of Baku Engineering University*, vol. 6, no. 1, pp. 3–20.

[8] C. Onate, M. Onyeaju, E. Omugbe, I. Okon, and O. Osafile, "Bound-state solutions and thermal properties of the modified Tietz–Hua potential," *Scientific Reports*, vol. 11, no. 1, p. 2129, 2021. doi: https://doi.org/10.1038/s41598-021-81724-3.

[9] J. C. León-González, R. G. Toscano-Negrette, A. Morales, J. Vinasco, M. Yücel, H. Sari, E. Kasapoglu, S. Sakiroglu, M. E. Mora-Ramos, and R. Restrepo, "Spin–orbit and Zeeman effects on the electronic properties of single quantum rings: Applied magnetic field and topological defects," *Nanomaterials*, vol. 13, no. 9, p. 1461, 2023. doi: https://doi.org/10.3390/nano13091461.

[10] O. Kolebaje, U. E. Vincent, and P. V. E. McClintock, "Complex dynamics and multistability of driven diatomic molecules revealed by numerical modeling of shifted molecular potentials," *Physical Review E*, vol. 112, no. 4, p. 044207, 2025. doi: 10.1103/2pvr-llm9.

[11] I. Okon, C. Onate, E. Omugbe, U. Okorie, A. Antia, M. Onyeaju, W.-L. Chen, and J. Araujo, "Approximate solutions, thermal properties, and superstatistics solutions to Schrödinger equation," *Advances in High Energy Physics*, vol. 2022, Art. no. 5178247, 2022.

[12] C.-S. Jia, Y.-F. Diao, X.-J. Liu, P.-Q. Wang, J.-Y. Liu, and G.-D. Zhang, "Equivalence of the Wei potential model and Tietz potential model for diatomic molecules," *The Journal of Chemical Physics*, vol. 137, no. 1, 2012.

[13] R. Gupta, G. Hou, R. Renirie, R. Wever, and T. Polenova, "$^{51}$V NMR crystallography of vanadium chloroperoxidase and its directed evolution P395D/L241V/T343A mutant: Protonation environments of the active site," *Journal of the American Chemical Society*, vol. 137, pp. 5618–5628, 2015.

[14] N. Schopohl and N. S. Cetin, "A Flow Equation Approach Striving Towards an Energy-Separating Hamiltonian Unitary Equivalent to the Dirac Hamiltonian with Coupling to Electromagnetic Fields," *arXiv preprint*, arXiv:2207.12825, 2022.

[15] E. Eyube, P. Notani, C. Onate, W. Umar, E. Omugbe, B. Bitrus, and S. D. Najoji, "Energy eigenvalues and finite-temperature magnetization for the improved Scarf II potential in the presence of external magnetic and Aharonov–Bohm flux fields," *Heliyon*, p. e20848, 2023.

# VALORIZATION OF UNDERUTILIZED HIBISCUS SABDARIFFA SEEDS: DEVELOPMENT OF A BIODEGRADABLE FAT LIQUOR FOR ECO-FRIENDLY LEATHER PROCESSING

**Abubakar Sadiq Bello[1]*, Sodiq Pelumi Bakare[1], Ibrahim Gidado[2], Sha'aban Sallau[1]**

*[1]Department of Chemistry, Faculty of Science, Air force Institute of Technology, P.M.B 2104, Kaduna State, Nigeria.*
*[2]Department of Chemistry, Federal Collage of Education Yola, P.M.B 2042, Adamawa State, Nigeria.*
**Corresponding authors email: sadiqdanburam@gmail.com*

**Abstract**

This study evaluates the synthesis and physicochemical characterization of fat liquor derived from Hibiscus sabdariffa seed oil as a sustainable, biodegradable alternative for leather processing. As the industry shifts away from synthetic and animal-derived materials, this underutilized non-edible oil source offers a viable eco-friendly solution. The oil was obtained via Soxhlet extraction (7.63% yield) and chemically modified through sulfation with concentrated sulfuric acid, followed by neutralization to create a stable emulsion. FTIR analysis confirmed successful modification, identifying key sulfoxide (S=O), ester (C=O), and ether (C–O–S) functional groups within the triglyceride backbone. Physicochemical testing revealed an acid value of 95.74 mg KOH/g, suggesting high free fatty acid content conducive to deep fiber lubrication. The emulsion maintained a pH of 5.02, ensuring compatibility with collagen fibers, and a density of 0.996 g/cm³, facilitating integration into aqueous tanning systems. The resulting dark, homogenous emulsion demonstrated excellent stability without phase separation. These findings validate sulfated Hibiscus sabdariffa seed oil as an efficient, renewable fat liquor capable of enhancing leather flexibility while meeting modern environmental standards.

**Keywords:** Fat liquors; Hibiscus sabdariffa seed oil; Soxhlet extraction; Physicochemical properties.

## 1. Introduction

Fat liquors are emulsions of oil and water that improve a variety of materials' softness, flexibility, and durability [1]. Traditionally made from petroleum-based or nonrenewable resources, fat liquors are used extensively in sectors like lubricants and cosmetics. The majority of oils used to make fat liquor are non-sustainable and synthetic, which harms the environment more than natural alternatives [2]. Comparing biological fat liquors to non-biological alternatives, the former offer better surface activity, cost, safety, and ease of manufacture [4]. They also aid in lowering environmental contamination and the use of chemicals [5]. Fat liquors' yield, content, and physicochemical characteristics determine how they are used in different industries [6]. The process of making fat liquor entails mixing several "sponging" substances, which can be made from mineral, vegetable, fish, or animal oils (such roselle seed oil), as well as glycerin, soaps, and even egg yolk [7]. Both water-repelling (hydrophobic) and water-attracting (hydrophilic) components are present in these compounds. The hydrophilic component is an emulsifying agent that can be positively charged (cationic), negatively charged (anionic), or uncharged (non-ionic), whereas the hydrophobic component is usually a fatty acid. Due to its dual nature, fat liquors can combine with both water and oil [8]. Hibiscus sabdariffa, an annual dicotyledonous, erect, herbaceous tropical plant, is one of the plants that can create fat liquor biologically from its seeds. The plant is cultivated majorly in the northern part of Nigeria as edible vegetable and considered to be 1 medicinal [9]. There are more than 300 species of hibiscus around the world; one of them is Hibiscus sabdariffa Linn. Hibiscus sabdariffa L. is an important medicinal and industrial plant which belongs to Malvaceae family [10]. It is also commonly known as roselle in English and as " zobo" in hausa [11]. It is thought of to be native to Asia (India to Malaysia) or Tropical Africa. The plant is widely grown in tropics like Central America, Africa (Nigeria), Brazil, and

Philippines as a home garden crop. Two botanical types of Roselle are recognized, Hibiscus sabdariffa var altissima and Hibiscus sabdariffa sabdariffa [12]. Roselle (Hibiscus sabdariffa L.) is known in different countries by various common names, including Roselle, razella, sorrel, red sorrel, Jamaican sorrel, Indian sorrel, Guinea sorrel, sour-sour, and Queensland jelly plant [13]. Hibiscus sabdariffa seed oil is used to synthesize fat liquor, which is suitable for various industrial applications due to its high levels of unsaturated fatty acids [14]. The oil's physicochemical properties, including iodine, saponification, acid, and viscosity, influence its effectiveness in emulsification and application. Further research is needed to optimize the synthesis process and evaluate its performance.

## 2. Material and methods

*Sample collection and preparation*

Sorrel (zobo seed) Hibiscus sabdariffa was purchased from Kasuwa Market, Kaduna North, Kaduna State, Nigeria. The seeds were washed thoroughly (4 to 5 times) and then sun-dried for five days. Finally, the cleaned seeds were milled into powder.

*Solvent extraction (Using N-Hexane)*

A 500 mL Soxhlet apparatus and hexane as a solvent were used for this study. The apparatus was charged with a known weight (100 g) of Hibiscus sabdariffa seed powder, which was placed in a thimble inside the Soxhlet extractor. A round-bottom flask containing a known volume (300 mL) of hexane was fixed to the lower end of the apparatus, and a condenser was tightly attached to the top. The entire setup was heated in a heating mantle at 55°C. The excess solvent in the oil was recovered by heating in a mantle at 45°C after extraction. The recovered oil was then concentrated in a water bath at 45°C to remove the residual solvent. The quantity of oil extracted was determined gravimetrically.

The oil yield was evaluated as the ratio of the weight of the extracted seed oil to the weight of the oilseed powder sample using the formula:

oil yield weight = $W_1 / W_2 \times 100$

Where $W_1$ = weight of oil extracted

$W_2$ =weight of sample used

*Synthesis of Hibiscus sabdariffa seed*

The extracted oil served as the raw material for the synthesis of fat liquor. The synthesis of fat liquor from Hibiscus sabdariffa seed oil involved sulfation to enhance its emulsifiability and affinity for leather.

*Sulfation process*

100 mL of Hibiscus sabdariffa seed oil was placed in a clean conical flask equipped with a magnetic stirrer. 17 mL of concentrated sulfuric acid was added drop wise from a burette under constant stirring at room temperature. The mixture was stirred continuously for 3 hours to ensure uniform reaction.

After the reaction, the sulfated product was transferred into a separating funnel and shaken with 200 mL of 10% sodium chloride solution. The mixture was allowed to stand overnight to facilitate complete phase separation. The bottom aqueous layer was discarded, and the upper layer containing the sulfated oil was collected. The pH of the fat liquor was adjusted to 5.0 by adding 10 mL of 30% sodium hydroxide solution. The final fat liquor product was stored at room temperature in airtight containers pending further characterization.

*Physicochemical properties of fat liquor*

*Determination of acid value*

1.5g of fat liquor was added to a dried conical flask. Two to three drops of phenolphthalein were added along with 25 mL of 100% ethanol. After 10 minutes of heating and shaking in a water bath at 65 °C, the solution was chilled and titrated against 0.1 N KOH until a pink tint developed, indicating the endpoint [3].

The acid value of the fat liquor was obtained according to the method described by Abebe Reda (2014).

Acid Value (mg KOH/g oil) = (V × N × 56.1) / W

Where: 25.6ml = volume of KOH used in titration (in mL)

0.1 N = normality of the KOH solution (mol/L)

56.1KOH (g/mol) = molecular weight of KOH (g/mol)

1.5g = weight of the oil/fat sample (in grams)

*Determination of density*

To determine the density of the sulfated fat liquor, clean and dry beakers were weighed using a digital balance, and their masses were recorded. A known volume of the fat liquor was then carefully introduced into each beaker using a pipette or syringe, ensuring accurate volume measurement by reading the lower meniscus at eye level. The beakers containing the measured volume of fat liquor were then weighed again, and the new masses were recorded as. This procedure was repeated using two additional fat liquor samples or batches to confirm the reliability of the results. The density of each fat liquor sample was calculated using the formula:

Density = $W_1$ - $W_2$ / V

Where: $W_1$ = weight of empty beaker

$W_2$ = weight of beaker + oil

V = volume of oil used (in $cm^3$ or mL)

*Determination of pH of emulsion*

To determine the pH of the fat liquor emulsion, a 10% solution was prepared by accurately weighing 10 grams of the fat liquor sample into a clean 100 mL beaker. Distilled water amounting to 90 mL was added to the beaker, and the mixture was stirred thoroughly using a glass rod until a uniform and stable emulsion was formed. A calibrated digital pH meter was used to measure the pH of the emulsion. Before taking the measurement, the pH meter was calibrated using standard buffer solutions of pH 4.0 and 7.0 to ensure accuracy. The electrode was rinsed with distilled water, gently dried, and then immersed in the emulsion for pH measurement.

The emulsion was stirred gently, and the pH reading was recorded once the value stabilized at room temperature. After the measurement, the electrode was rinsed again with distilled water and properly stored (ASTM International).

*FTIR spectra of fat liquor*

The functional groups found in the extracted Hibiscus sabdariffa seed oil and the manufactured sulfated fat liquor were identified using Fourier Transform Infrared (FTIR) spectroscopy (Agilent Cary 660 FTIR Spectrometer). At room temperature, a tiny amount of each sample was put on the FTIR spectrometer's sample holder and scanned across a wavelength range of 4000 to 5000 $cm^{-1}$. The transmittance (%) at each wavenumber was determined by recording the spectra using the Attenuated Total Reflectance (ATR) mode. The functional groups contained in the samples were then identified by comparing the distinctive absorption bands with established reference values.

## 3. Results and discussion

*Solvent extraction*

The table below shows that the extraction of Hibiscus sabdariffa seed oil using 300 mL of hexane for 6 hours yielded an average oil recovery of 7.63%, indicating consistent extraction efficiency across the runs.

**Table 1**. The oil yield from *Hibiscus sabdariffa* seeds via soxhlet extraction

| Run | Sample weight (g) ($W_2$) | Solvent volume (ml) | Mass of oil extracted (g) $W_1$ | Time (hrs) | Oil yield (%) |
|---|---|---|---|---|---|
| 1 | 100 | 300 | 7.4 | 6 | 7.4 |
| 2 | 100 | 300 | 7.3 | 6 | 7.3 |
| 3 | 100 | 300 | 8.2 | 6 | 8.2 |

Oil yield from Hibiscus sabdariffa seeds was determined gravimetrically using the formula:

Oil yield (%) = $W_1 / W_2 \times 100$

Where: $W_1$ is the quantity of oil extracted

$W_2$ is the known weight of hibiscus sabdariffa powder

Based on these values, the oil yield was calculated as follows: Oil Yield (%) = 7.4/100 ×100 = 7.4%

The Soxhlet extraction method has been widely recognized as an effective approach for recovering lipids from plant-derived solid materials [6]. In this study, hexane was employed as the non-polar solvent to extract oil from powdered Hibiscus sabdariffa seeds. A 500 mL Soxhlet apparatus was selected to accommodate the 100 g seed powder samples and to enable continuous solvent cycling, thereby maximizing solvent–sample contact. The sample was loaded into a cellulose thimble, which retained insoluble solids while allowing soluble lipid components to be efficiently dissolved in 300 mL of hexane. Extraction was performed at 55 °C using a heating mantle—high enough to promote efficient solvent vapourization without exceeding hexane's boiling point (~68 °C), thus maintaining safe and optimal conditions [14]. Continuous reflux facilitated repeated solvent percolation over the seed material, improving extraction efficiency and reducing solvent consumption per unit of oil recovered. Following extraction, excess solvent was recovered at 45 °C, a post-treatment step that not only concentrated the oil but also reduced solvent loss and minimized environmental contamination risks, which is particularly important when working with volatile and flammable solvents like hexane [15].

The results (Table 1) indicate oil recoveries of 7.4%, 7.3%, and 8.2%, with an average yield of 7.63%. Oil yield was calculated gravimetrically using the formula: Oil yield (%) = $W_1 / W_2 \times 100$

where $W_1$ is the mass of oil extracted and $W_2$ is the initial mass of seed powder. For instance, in Run 1, the yield was: 7.4/100 × 100 = 7.4%

The average yield of 7.63% is slightly below the reported range of 10–15% for H. sabdariffa seed oil [15]. This difference could be due to seed quality, ripeness at harvest, storage conditions. Nevertheless, the small variation across the three runs demonstrates the reproducibility and reliability of the Soxhlet method under the conditions used in this investigation.

*Synthesis of Hibiscus sabdariffa seed oil*

The table below outlines the successful synthesis of Hibiscus sabdariffa seed oil fat liquor, showing clear phase separation, effective neutralization, and formation of a stable, dark-coloured emulsion suitable for characterization. After the extraction process, 100 mL of Hibiscus sabdariffa seed oil and 17 mL of concentrated sulphuric acid under carefully monitored stirring circumstances reacted for three hours at 20 °C. Throughout the operation, the reaction mixture stayed uniform, suggesting that the acid was mixed well and gradually incorporated into the oil matrix. Following completion, the reaction product showed an evident change in look and consistency, indicating that the sulphate groups

were successfully added to the oil structure. Following completion, the reaction product showed a discernible shift in look and consistency, indicating that the sulphate groups had been successfully added to the oil structure. Clear phase separation happened overnight after washing with 200 mL of a 10% sodium chloride solution in a separating funnel. The top organic layer, which included the sulfated oil, was carefully collected, while the aqueous phase settled at the bottom and was eliminated. After neutralizing the sulfated oil with 10 milliliters of 30% sodium hydroxide solution, the emulsion's pH reached 5.0, which is thought to be appropriate for fat liquor stability and leather substrate compatibility. Mild foaming and a minor rise in viscosity were seen during the neutralization process, suggesting the production of a stable emulsion. For additional physicochemical and performance analyses, the finished product—a thick, amber-colored fat liquor—was kept at room temperature in a sealed container. All things considered, the reaction and post-treatment phases were effectively finished, and the procedure produced a sulfated fat liquor with encouraging properties for possible usage in leather finishing and softening applications.

*Physicochemical Properties*

*Acid Value*

The acid value in the fat liquor was measured to know the amount of free fatty acid (FFA), which is a crucial sign of its stability and quality. As the titrant, 0.1 N potassium hydroxide (KOH) was used in a direct titration process. With an acid value of 95.74 mg KOH/g, the fat liquor made from Hibiscus sabdariffa seed oil has a significant amount of free fatty acids. This might have an impact on fat liquor emulsion stability, possibly resulting in uneven penetration or phase separation. But in leathers that need a lot of internal lubrication, it might also improve flexibility and fiber penetration. By neutralizing the emulsion with a mild alkaline solution, such as sodium carbonate ($Na_2 CO_3$ ) or diluted sodium hydroxide (NaOH), the acidic character of the fat liquor can be regulated to ensure optimal use in leather processing, particularly in softening and internal lubrication of hides. This modification lowers the possibility of fiber damage or uneven distribution during fat liquoring, balances the pH, and enhances emulsion stability.

This modification lowers the possibility of fiber damage or uneven distribution during fat liquoring, enhances emulsion stability, and balances the pH. As an alternative, the fat liquor can be mixed with a less acidic or more stable fat liquor to make a well-balanced mixture that minimizes any potential negative effects while preserving the advantageous lubricating and softening qualities. The fat liquor can still be used to make soft, pliable leathers if it has been adjusted appropriately, especially for uses like linings, clothing leathers, and other flexible leather products. When paired with the right pH control methods, this fat liquor's natural origin and possible biodegradability make it a viable, sustainable choice for the leather industry.

*pH of Emulsion*

The pH of the fat liquor emulsion was measured using a 10% solution prepared by mixing 10 g of fat liquor with 90 mL of distilled water. After thorough mixing, the emulsion formed was uniform and stable. A calibrated digital pH meter was used, and the recorded pH value was 5.02 at room temperature.

The fat liquor emulsion is somewhat acidic, which is a good range for leather processing, according to the measured pH of 5.02. This implies that the synthesis's neutralization step was carried out correctly. A pH of about 5 is thought to be ideal since it helps shield the leather from harm while enabling the fat liquor to efficiently soften and lubricate the fibers. The emulsion might have been too harsh for the leather if the pH had been too low. It may have resulted in uneven application or swelling if it had

been too high. Thus, this outcome demonstrates that the fat liquor is safe to use for softening leather and is chemically stable.

*Density of fat liquor*

The table below presents the density measurements of the synthesized fat liquor, revealing consistent values around 0.997 g/cm³, indicating uniformity in composition across samples.

**Table 3.** Density of fat liquor

| S/N | Weight of beaker($W_1$) | Weight of beaker + oil ($W_2$) | Mass of fat liquor(g) | Volume of fat liquor used(ml) | Density (g/cm³) |
|---|---|---|---|---|---|
| 1 | 33.0411 | 34.5360 | 1.4958 | 1.5 | 0.9923 |
| 2 | 33.8874 | 34.3758 | 1.4884 | 15 | 1.0000 |
| 3 | 33.2105 | 34.7115 | 1.5010 | 1.5 | 1.0007 |

Density = ($W_2$ – $W_1$ ) / V

Density= 0.996g/cm³

With an average density of 0.9967 g/cm³, the sulfated fat liquor was determined to be a stable and well-balanced emulsion. Its closeness to the water's density indicates appropriate emulsification and sulfation. The consistency between batches attests to the formulation method' dependability. The fat liquor is appropriate for softening because of its density, which facilitates efficient application and penetration during leather processing.

*Comparison of Physicochemical Properties of Sulfated Hibiscus sabdariffa Seed Oil and standard biological fat liquor (Sulfated Castor Oil Fat liquors)*

The comparison of sulfated Hibiscus sabdariffa seed oil and conventional sulfated castor oil fat liquor reveals significant variations in their physicochemical characteristics, impacting their suitability and performance table 4.

**Table 4.** Comparison of Physicochemical Properties of Sulfated Hibiscus sabdariffa Seed Oil and standard biological fat liquor (Sulfated Castor Oil Fat liquors)

| s/n | Properties | Unit | Sulfated hibiscus sabdariffa oil | Sulfated castor oil |
|---|---|---|---|---|
| 1 | Density | g/cm3 | 0.996 | 0.957 |
| 2 | pH of emulsion | -- | 5.02 | 6.6-7.5 |
| 3 | Acid value | mg KOH/g | 95.74 | 0.82 |

*Density*

Hibiscus sabdariffa seed oil's higher density (0.996 g/cm³) may be due to, residual sulfation by-products, or unsaturated fatty acids, potentially impacting fat liquoring performance.

*pH of emulsion*

The emulsion pH of sulfated Hibiscus sabdariffa oil is 5.02, lower than the standard range of 6.6-7.5, potentially posing risks to leather collagen fibers due to incomplete neutralization or excess acidic functional groups. the sulfated Hibiscus sabdariffa oil was neutralized using a mild alkaline solution, sodium hydroxide (NaOH) to adjust the pH to the optimal range of 6.5–7.5.

*Acid value*

The Hibiscus sabdariffa fat liquor has a high acid value of 95.74 mg KOH/g, indicating the presence of free fatty acids, potentially affecting emulsion stability and shelf life, while sulfated castor oil has a low acid value.

*FTIR Spectra of Sulphated fat liquor and Hibiscus sabdariffa seed oil*

The table below presents the FTIR analysis of the sulfated fat liquor, confirming the presence of key functional groups such as alkanes (C–H), carbonyls (C=O), esters, ethers (C–O–S), and sulfoxides (S=O), indicating successful sulfation and chemical modification.

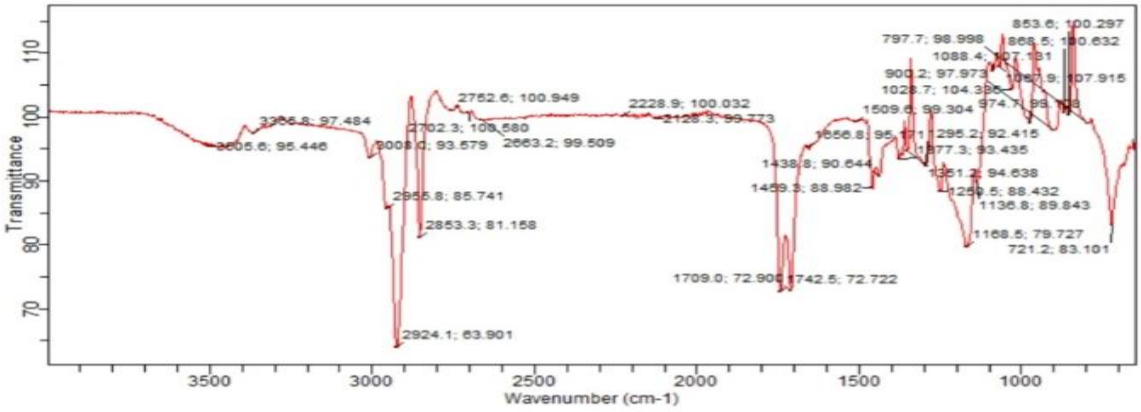



**Figure 1:** The FTIR Spectra of sulphated fat liquor

**Table 5.** FTIR spectra of Sulphated fat liquor

| S/N | Wave number ($cm^{-1}$) | Transmittance (%) | Functional group | Class |
|---|---|---|---|---|
| 1 | 2924.1 | 63.901 | C-H | Alkane |
| 2 | 2853.3 | 81.158 | C-H | Alkane |
| 3 | 1469.31 | 88.982 | C-H | Alkane |
| 4 | 1709.0 | 72.900 | C=O | Carbonyl group |
| 5 | 1742.51 | 72.722 | C=O | Ester |
| 6 | 1250.5 | 88.432 | C-O-S | Ether |
| 7 | 1087.9 | 107.915 | S=O | Sulfoxide |

The spectrum confirms that the original triglyceride backbone of Hibiscus sabdariffa seed oil is largely retained, as shown by the alkane (C–H), ester (C=O), and carbonyl peaks. The appearance of characteristic S=O and C–O–S absorption bands provides strong evidence of successful sulfation, which chemically modifies the oil to improve water dispersibility and emulsification — critical for fat liquor performance in leather processing. This confirms the conversion of natural oil into a sulfated fat liquor, enhancing its potential for softening, lubrication, and water absorption control in finished leather.

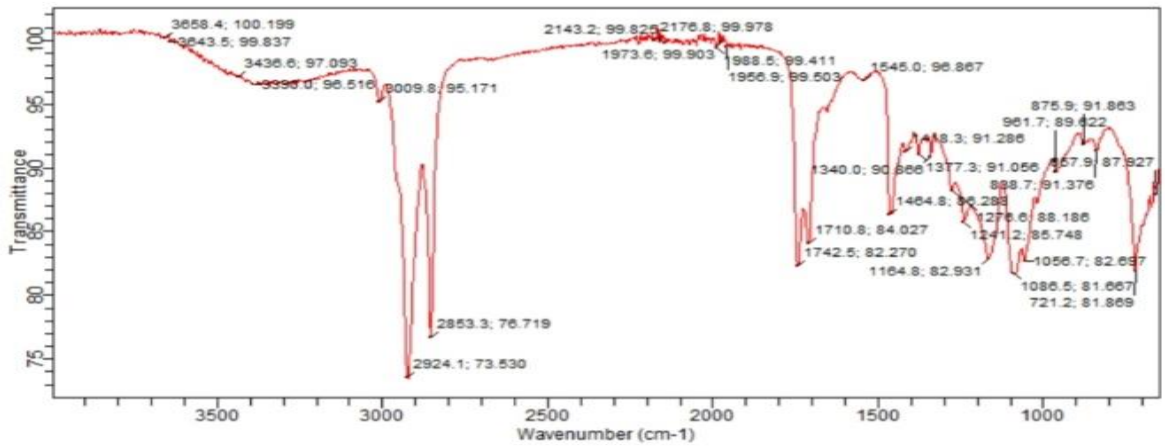



**Figure 2:** The FTIR Spectra of *Hibiscus sabdariffa* seed oil

The table below shows the FTIR spectrum of Hibiscus sabdariffa seed oil, confirming the presence of hydroxyl, alkane, carbonyl, and ester functional groups characteristic of natural triglyceride oils.

**Table 6.** FTIR Spectra Hibiscus sabdariffa seed oil

| Wave number (cm–1) | Transmittance (%) | Functional group | Class |
|---|---|---|---|
| 3436.3 | 97.093 | O-H | Hydroxyl group |
| 2924.1 | 73.530 | C-H | Alkane |
| 2853.3 | 78.719 | C-H | Alkane |
| 1464.8 | 86.288 | C-H | Alkane |

3436.3 $cm^{-1}$ (Transmittance: 97.093%) — O–H Stretching (Hydroxyl Group): This broad peak is indicative of hydroxyl groups (–OH), which may arise from the presence of free fatty acids, moisture, or residual glycerol. Although natural oils are mainly esters (triglycerides), partial hydrolysis can lead to free fatty acids, explaining the appearance of this peak. 2924.1 $cm^{-1}$ (Transmittance: 73.530%) — C–H Asymmetric Stretch (Alkane): A strong band at this region is characteristic of methylene ($–CH_2$) stretching vibrations. This suggests the presence of long-chain saturated or unsaturated fatty acids — typical of plant-derived oils. 2853.3 $cm^{-1}$ (Transmittance: 78.719%) — C–H Symmetric Stretch (Alkane): This further supports the existence of aliphatic chains in the oil. The combination of the bands at 2924 and 2853 $cm^{-1}$ confirms the dominance of saturated hydrocarbon chains, reinforcing the oil's fatty acid content. 1464.8 $cm^{-1}$ (Transmittance: 86.288%) — C–H Bending (Scissoring): This peak is associated with the bending vibrations of $CH_2$ and $CH_3$ groups in long-chain fatty acids. It further confirms the aliphatic nature of the compound, typical of triglycerides.

## 4. Conclusions

The research confirms Hibiscus sabdariffa seed oil's potential as a sustainable and eco-friendly raw material for sulfated fat liquor synthesis. The Soxhlet extraction process yielded consistent oil, with FTIR analysis revealing sulfonated esters and fatty acids. The resulting fat liquor has favorable physicochemical properties. Roselle seed oil, a renewable and sustainable alternative to petroleum-based fat liquors, has been found to enhance leather softness and fiber flexibility, thereby promoting economic value and environmental sustainability.

**References**

1. M. Abou-Ellail, T. Abou-El-Nasr, and M. Ottai, "Phenotypic and Molecular Characterization of New Selected Genotypes of Roselle in Egypt," *Middle East J. Agric. Res.*, vol. 3, no. 1, pp. 50–58, 2014.

2. A. Adewuyi, A. Göpfert, and T. Wolff, "Succinyl amide Gemini Surfactant from Adenopus breviflorus seed oil: a potential corrosion inhibitor of mild steel in acidic medium," *Ind. Crops Prod.*, vol. 52, pp. 439–449, 2014.

3. O. Affiang, E. Ezemokwe, and I. Nkwor, "Utilization of vegetable oils as natural fatliquors for leather processing," *J. Leather Sci. Eng.*, vol. 2, no. 1, pp. 12–20, 2018.

4. H. Ali, N. Al Wabel, and G. Blunden, "Phytochemical, Pharmacological, and Toxicological Aspects of Hibiscus sabdariffa L.: A Review," *Phytother. Res.*, vol. 19, pp. 369–375, 2005.

5. E. Aluyor and M. Ori-Jesu, "The use of antioxidants in vegetables oils. A review," *African J. Biotechnol.*, vol. 7, no. 25, pp. 4836–4842, 2008.

*6. Standard Test Method for pH of Engine Coolants and Antirusts*, ASTM D1287-11(2015), 2015.

7. N. N. Azwanida, "A review of the extraction methods used in medicinal plants, principles, strengths, and limitations," *Med. Aromat. Plants*, vol. 4, no. 3, p. 196, 2015.

8. E. Betiku and F. Adepoju, "Biochemical Engineering Laboratory research report," Obafemi Awolowo University/Landmark University, Nigeria, 2013. *(Note: This entry appears to be institutional data or a report summary).*

9. A. Eltayeib and H. Hamade, "Phytochemical and chemical composition of water Extract of Hibiscus Sabdariffa (red karkade calyces) in North Kordofan State, Sudan," *Int. J. Adv. Res. Chem. Sci. (IJARCS)*, vol. 1, no. 6, pp. 10–13, 2014.

10. D. Hao *et al.*, "A novel eco-friendly Imidazole ionic liquids-based amphoteric polymers for high-performance fatliquoring in chromium-free tanned leather production," *J. Hazard. Mater.* vol. 399, p. 123048, 2020.

11. U. Ijeomah, U. Ugwuona, and H. Abdullah, "Phytochemical composition and antioxidant properties of Hibiscus sabdariffa and Moringa oleifera," *Nigerian J. Agric. Environ.*, vol. 8, no. 1, pp. 10–16, 2012.

12. R. Janardhanan, V. Vijayabaskar, and B. S. R. Reddy, "Performance of sulfonated Dimeric malenized soya fatty acid as a leather fatliquor," *J. Am. Leather Chem. Assoc.*, vol. 107, pp. 128–136, 2012.

13. J. Ma, J. Gao, and H. Wang, "Dissymmetry Gemini sulfosuccinate Surfactant from Vegetable oil: a kind of environmentally friendly fatliquoring agent in the leather industry," *ACS Sustain. Chem. Eng.*, vol. 5, pp. 10693–10701, Nov. 2017.

14. N. Mahadevan and P. Shivali, "Hibiscus subdariffa Linn. An overview," *Nat. Prod. Radiance*, vol. 8, no. 1, pp. 77–83, 2009.

15. K. Wintana, "Preparation of leather fat liquor cum filler from fishing waste for the retaining process in leather," Research report/thesis, 2014.

# LEVELS OF SELECTED HEAVY METALS IN SOIL SAMPLES AT AUTOMOBILE MECHANIC WORKSHOPS IN OKENE METROPOLIS, NIGERIA

**Omeiza, Folorunsho Samuel[1*], Lawal, John .Augustine[2], Paul Idoko[1], Okpanachi, Clifford[3]**

*[1]Department of Chemistry, Kogi State College of Education, Ankpa, Kogi State-Nigeria*
*[2]Department of Chemistry, Obafemi Awolowo University, Ile Ife, Osun State-Nigeria*
*3Department of Chemistry, Prince Abubakar Audu University, Ayingba, Kogi State- Nigeria*
**Corresponding Author: Folorunshoomeiza@gmail.com*

**Abstract**

The present study assessed the level of heavy metal at two distincts soil depths, namely 0- 15 cm and 15-30 cm at automobile mechanic workshops in Agasa (AG) , Okengwe (OK), Ozuwaya (OZ) and Idoji (ID) of Okene metropolis, Nigeria. Sequential extraction was carried out using a modified Tessier's procedure on soil samples to determine the mobility of metals in the soils. The results showed that the soil sample fractions from the study area showed very high presence of heavy metals contamination with Zn, Pb, Cd, Fe and Ni highest across the four sites in relation to their depths. However, in residual, water soluble and exchangeable fractions, low concentrations of Ni, Cd and Fe in all locations across the two depth profiles of the soil samples. Overall, all fractions were found to be bonded with heavy metals which indicated that heavy metal contamination increases as soil depth increases in all locations. The total heavy metal concentrations exceeded WHO 2011, regulatory limits for safe agricultural soil, which poses a health risk.

**Keywords**: Bioavailability, heavy metals, sequential extraction, soil.

## 1. Introduction

The increase in automotive maintenance repair establishments and their operations in Okene Metropolis is as a result of the rise in demand for private vehicles, a large portion of which are imported from foreign countries. This has led to the issue of soil contamination in several areas dedicated for mechanic workshops. Automobile waste in the study areas consists of waste oil, oxidation byproducts and metallic fragments that result from the wear and tear of vehicles, organic and inorganic chemicals found in oil additives, used batteries and metals [1]. The existence of trace elements in soil is rapidly becoming a global concern, particularly since soil is a vital component of both rural and urban environments [1,3]. The non-degradable heavy metals like cadmium (Cd), copper (Cu), chromium (Cr), lead (Pb), manganese (Mn), nickel (Ni), and zinc (Zn) often used as additives in some lubricants and gasoline can pose a threat to groundwater due to soil percolation of leachates from these substances [3]. The co-occurrence of toxic heavy metals at numerous contaminated mechanics sites in Okene metropolis and other nearby villages poses a severe threat to the environment [1]. Studies have shown that automobile workshop may increase heavy metal concentration in soil [1,3 ] which have effects on the soils, crops and human health [5]. Therefore, the environmental impacts of waste from automobile workshop are greatly influenced by their heavy metal contents. As a result, this study aimed to investigate the soil pollution resulting from heavy metals in the vicinity of selected mechanic workshops within the Okene Metropolis, kogi central senatorial district of Nigeria.

## 2. Materials and Method

### Description of Study Area

Okene is located at latitude 7.55122 and longitude 6.23569 and the town experiences a distinctive wet and dry seasons, with an annual rainfall range of 1,100mm – 1300mm [6]. The average annual

temperature is estimated to be around 27°C, with a relative humidity, averaging approximately 70% to 75% based on historical data studies. Furthermore, the town average daily wind speed measures 71.4 km/hr [6], while the average daily vapour pressure is approximately 24 Hpa. In terms of population, Okene has a population of 312, 715 in 1991 [7].

**Sample Collection**

Soil samples were collected from four automobile mechanic workshops situated in Agasa,(AG) Okengwe (OK), Ozuwaya (OZ) and Idoji (ID) of Okene metropolis, Nigeria.. For the collection of samples, the soil surface was cleared employing a hand trowel and subsequently The number of sampling points was dependent on the size of the mechanic sites and consequently, each of the four mechanics was partitioned into four (4) quadrants. Samples were obtained from two distinct depths of 0-15 cm, and 15-30 cm. Additionally, within a location; samples were collected from three different points at depths of 0-15 cm and 15-30 cm, referred to as topsoil and sub-soil, respectively [6,7]. The soil samples that were gathered were ground using a porcelain mortar with pestle and subsequently subjected to air-drying for a week to eliminate any traces of moisture. Furthermore, they were sieved through a 2 mm stainless steel sieve [8]. These soil samples were then properly labeled and stored in polythene bags for further analysis [9].

**Heavy Metal Analysis**

The collected specimens were subjected to heavy metal analysis, as documented in prior research [8]. Specifically, a precise quantity of 5 grams of air-dried soil sample was measured and placed into a 25 ml polypropylene centrifuge tube. Sequential extractions were conducted, whereby 5 grams of air-dried soil sample, sieved to a diameter of 2 mm, was weighed and added to a pre-weighed centrifuge tube. Next, 25 ml of distilled water was introduced and the resultant suspension was vigorously agitated for 120 minutes. Subsequently, centrifugation was performed at a rate of 3500 rpm for 10 minutes, followed by filtration through Whatman No. 42 filter paper under vacuum into a 100 ml vial. This fraction was denoted as SOL, which served as water extraction F1. The residue from F1 was extracted by adding 25 ml of 0.25 M $K_2SO_4$. The suspension was shaken for duration of 16 hours, centrifuged for 10 minutes at 3500 rpm, and filtered through Whatman No. 42 filter paper into a 100 ml vial. The resulting fraction was labeled as EXCH (F2). The extraction of the residue from F2 was carried out through the addition of 25 ml of 0.05 M $Na_2EDTA$. Following this, the suspension underwent a period of shaking for duration of 8 hours, followed by centrifugation for 10 minutes at 3500 rpm. The resulting solution was then filtered through Whatman No. 42 filter paper and collected in a 100 ml vial. This fraction was given the designation of CARBON (F3). Subsequently, 25 ml of 0.5 M NaOH solution was added to the residue from F3, after which it was shaken for a period of 16 hours. The mixture was then centrifuged at 3500 rpm for 10 minutes and the supernatant was filtered through Whatman No. 42 filter paper into a 100 ml vial. This fraction was given the designation of ORG (F4). Determination of the residual fractions of the respective metals was carried out through the computation of the sum of fraction F1-F4, which was then subtracted from the respective total metal concentration [12]. Determined through $HClO_4$-$HNO_3$-$H_2SO_4$ digestion F5 [8]. At the conclusion of the extraction period, the individual metals present in the filtrates were determined through the use of JENWAYS model AA431HT atomic absorption spectrophotometer (AAS).

**Quality assurance validation**

Validation of the technique for the metal determination was conducted on digested soil samples. by spiking the pre-digested samples with multi-element standard solution (0.5 mg/l of Cd, Fe, Ni, Pb and Zn) as reported by [9].

## 3. Result and Discussion

### Quality Assurance

The reports on the validation of a technique utilized for the determination of Cd, Ni, Zn, Fe and Pb metals in soil samples that have been subjected to digestion as shown in Table indicates 88 % - 97 % percentage recovery which is in agreement with previous reports that any instrument with recovery ≥ 85 % is strongly recommended to be used for analysis [9, 10, 11]

**Table 1: Results of validations experiment**

| Metal | Percentage (%) Recovery |
|---|---|
| Cd | 92.00 ± 1.132 |
| Ni | 96.00 ± 1.301 |
| Zn | 88.00 ± 1.040 |
| Fe | 97.00 ± 0.912 |
| Pb | 94.00 ± 1.115 |

### Mean concentrations of Zinc (Zn)in fractions in all locations and across all depths

Tables 2 shows the mean concentration of Zn in the different fractions across depths where there is a decrease in the concentration of Zn between the depths of 0-15 cm and 15-30 cm. It is worth noting that the residual fraction constitutes the most mobile and potentially bio-available Zn metal species [13]. The chemical fractionation results of Zinc in mechanic workshop soils at the two different depths are presented in Tables 2. In both cases, the chemical associations of Zinc were dominated by the residual fraction, which ranged from 0.14 to 41.31 mg/kg across the depth levels. The majority of automobile mechanic sites examined in Tables 2 exhibited levels of extractable zinc (F1+F2+F3+F4+F5) that exceeded the permissible limit of 300 mg/kg, with only a small number of exceptions. The residual fraction (F5) contained the highest concentrations of zinc at both depths for all soils studied, indicating that under severe conditions, this element could be released into the environment. However, the residual fraction is not generally considered to be an environmental hazard, as it is a stable compound in which metals are tightly bound within a mineral lattice, reducing the bioavailability of this metal [11] Through comparison of zinc levels in residual and water-soluble fractions at varying depths across multiple sites, it is evident that the residual fractions contain the highest concentration of this element, measuring 41.31 mg/kg. Such a notable quantity of zinc associated with the residual fractions suggests that it would be highly accessible for uptake by plants. The discoveries made in this investigation are consistent with the observations made by previous researchers [12, 13], who reported comparable levels of zinc concentration in soils from tanneries located in Kaduna and Kogi State, Nigeria, respectively. Additionally, it was noted that the total metal contents of the mechanic workshop soil were lower at the depth of 0-15 cm than at the depth of 15-30 cm, which can be attributed to metal leaching. This observation is indicative of the deposition of zinc in soils resulting from the activities of mechanic workshops, specifically from lubricants and metal scrap originating from automobiles

**Table 2: Mean Zn concentration (mg/kg) in the fractions in all locations and across all depths**

| Location /Metals | Depth | Water soluble fraction | Exchangeable fraction | Organic bound Fraction | Carbonate bound fraction | Residual fraction |
|---|---|---|---|---|---|---|
| AG15 | 0 – 15 cm | 0.75 | 1.74 | 4.18 | 27.82 | 37.33 |
| OK15 | | 0.22 | 1.03 | 25.58 | 37.21 | 41.31 |

| | | | | | | |
|---|---|---|---|---|---|---|
| OZ15 | | 0.60 | 1.23 | 8.83 | 4.04 | 4.15 |
| ID15 | | 0.91 | 1.45 | 5.42 | 17.22 | 4.14 |
| AG30 | 15 – 30 cm | 0.59 | 0.89 | 3.18 | 22.56 | 32.73 |
| OK30 | | 0.14 | 0.92 | 17.58 | 32.11 | 32.11 |
| OZ30 | | 0.32 | 1.22 | 6.63 | 3.45 | 3.42 |
| ID30 | | 0.70 | 1.41 | 4.12 | 13.12 | 3.14 |

**Mean concentrations (mg/kg) of Lead (Pb) in fractions in all locations and across all depths**

Tables 3 shows the outcomes of the chemical fractionation of lead (Pb) in soil. The water-soluble fraction ranged from 0.78 to 1.43 kg/mg, the exchangeable fraction ranged from 3.12 to 5.36 mg/kg, the organic fraction ranged from 3.15 to 6.71 mg/kg, the carbonate fraction ranged from 8.75 to 26.46 mg/kg, while that of residual fraction varied from 5.15 to 11.11 mg/kg for both depths, across all sites. The Pb values in the investigated soil surpassed the maximum permissible limit of 3.0 mg/kg set by [10]. Concentrations of lead were high in both depths, with F4 carbonate fraction being the dominant contributor across the site. Through comparison of residual (F4) and water soluble fraction concentrations of lead across the mechanic workshop for both depths, it was demonstrated that high percentages of extractable fractions were present in the dumpsite soils at both respective depths. This suggests that Pb may be released into the environment, leading to contamination throughout the two depths. The high association of Pb in the carbonate fraction

**Table 3: Mean Pb concentration (mg/kg) in the fractions in all locations and across all depths**

| Location /Metals | Depth | Water soluble fraction | Exchangeable fraction | Organic bound Fraction | Carbonate bound fraction | Residual fraction |
|---|---|---|---|---|---|---|
| AG15 | 0 – 15 cm | 1.21 | 5.26 | 4.25 | 12.33 | 11.11 |
| OK15 | | 1.43 | 4.75 | 5.26 | 14.35 | 10.43 |
| OZ15 | | 1.43 | 5.36 | 4.75 | 26.46 | 7.88 |
| ID15 | | 1.17 | 4.14 | 6.71 | 16.85 | 7.24 |
| AG30 | 15 – 30 cm | 1.01 | 3.97 | 3.25 | 8.75 | 8.37 |
| OK30 | | 0.99 | 3.44 | 3.16 | 12.67 | 9.33 |
| OZ30 | | 0.78 | 3.31 | 3.15 | 20.15 | 5.15 |
| ID30 | | 1.00 | 3.12 | 5.54 | 11.98 | 6.98 |

**Mean concentrations (mg/kg) of Cd in fractions in all locations and across all depths**

Tables 4 also shows the outcomes of the chemical fractionation of cadmium (Cd) in soil. The water-soluble fraction ranged from 0.02 to 0.65 kg/mg, the exchangeable fraction ranged from 0.43 to 1.53 mg/kg, the organic fraction ranged from 0.40 to 0.57 mg/kg, the carbonate fraction ranged from 0.11 to 0.28 mg/kg, while that of residual fraction varied from 1.10 to 4.75 mg/kg for both depths, across all sites. The association of Cd in the water-soluble fraction poses a significant environmental risk due to the unstable nature of the compound and the strong binding of metals within a mineral lattice, which limits its bioavailability [12]. The findings in these investigations are in agreement with the observations which reported similar Cd concentration from Ado Ekiti metropolis southern western Nigeria) [14]

**Table 4: Mean Cd concentration (mg/kg) in the fractions in all locations and across all depths**

| Location /Metals | Depth | Water soluble fraction | Exchangeable fraction | Carbonate bound Fraction | Organic bound fraction | Residual fraction |
|---|---|---|---|---|---|---|
| AG15 | 0 – 15 cm | 0.12 | 0.67 | 0.57 | 0.28 | 2.15 |
| OK15 | | 0.05 | 1.28 | 0.57 | 0.28 | 4.75 |
| OZ15 | | 0.65 | 0.77 | 0.57 | 0.28 | 2.17 |
| ID15 | | 0.21 | 0.63 | 0.57 | 0.19 | 1.88 |
| AG30 | 15 – 30 cm | 0.08 | 0.5 | 0.47 | 0.21 | 1.87 |
| OK30 | | 0.02 | 1.55 | 0.47 | 0.27 | 3.27 |
| OZ30 | | 0.43 | 0.65 | 0.41 | 0.27 | 2.11 |
| ID30 | | 0.15 | 0.43 | 0.4 | 0.11 | 1.11 |

The chemical association of iron was dominant in the residual fraction (F5) at depths of 0-15 and 15-30 cm, respectively, across all the study sites. The concentration of iron in the residual fraction ranged from 36.10 to 75.85 mg/kg for both depths, while the water-soluble fraction exhibited a range of 0.94 to 1.45 mg/kg. Similarly, the organic fraction displayed a range of 17.18 to 52.63 mg/kg for both depths. The carbonate fraction, on the other hand, exhibited a range of 16.10 to 33.72 mg/kg across all depths and study sites.

Moreover, the Exchangeable fraction of nickel in all locations at 0-15 and 15-30 cm increased from 1.06 to 3.96 mg/kg. In this fraction, all the metals were found in all the locations but not such significantly higher concentrations than they were in the depth of 15-30 cm compared to other fractions.

**Table 5 Mean Fe concentration (mg/kg) in the fractions in all locations and across all depths**

| Location /Metals | Depth | Water soluble fraction | Exchangeable fraction | Carbonate bound Fraction | Organic bound fraction | Residual fraction |
|---|---|---|---|---|---|---|
| AG15 | 0 – 15 cm | 1.45 | 3.96 | 52.63 | 32.63 | 75.85 |
| OK15 | | 1.21 | 1.52 | 23.18 | 33.72 | 67.33 |
| OZ15 | | 1.31 | 1.61 | 25.00 | 18.65 | 48.15 |
| ID15 | | 1.10 | 2.37 | 46.63 | 31.75 | 44.19 |
| AG30 | 15 – 30 cm | 1.10 | 2.00 | 45.63 | 27.93 | 64.43 |
| OK30 | | 1.11 | 1.24 | 17.18 | 16.12 | 63.12 |
| OZ30 | | 1.01 | 1.06 | 20.4 | 16.10 | 36.10 |
| ID30 | | 0.94 | 1.79 | 37.13 | 25.14 | 40.14 |

. The data presented in Tables 6 demonstrate an increase in the amount of nickel with depth in the carbonate fraction across all locations at depths of 0-15 cm and 15-30 cm. The highest concentration of nickel, amounting to 12.11 mg/kg, was found in residual fractions, which was consistent across the site and depth. Moreover, the exchangeable fraction at depths of 0-15 cm and 15-30 cm exhibited an average of BDL-2.27 mg/kg of nickel. Additionally, the organic fraction at a depth of 0-15 cm displayed a nickel concentration of 3.21 mg/kg with the exception of the results obtained for the residual fractions, which was higher than other fractions. This result is in consistent with finding of [11].

**Table 6: Mean Ni concentration (mg/kg) in the fractions in all locations and across all depths**

| Location /Metals | Depth | Water soluble fraction | Exchangeable fraction | Carbonate bound Fraction | Organic bound fraction | Residual fraction |
|---|---|---|---|---|---|---|
| AG15 | 0 – 15 cm | 1.11 | 1.65 | 3.21 | 0.73 | 11.14 |
| OK15 | | 1.15 | ND | 3.21 | 0.2 | 12.11 |
| OZ15 | | 1.32 | 2.27 | 3.21 | 1.12 | 2.54 |
| ID15 | | 0.99 | 2.11 | 3.21 | 0.18 | 3.44 |
| AG30 | 15 – 30 cm | 0.87 | 1.59 | 1.23 | 0.71 | 8.51 |
| OK30 | | 0.67 | ND | 1.24 | 0.14 | 10.14 |
| OZ30 | | 1.1 | 2.15 | 2.11 | 1.03 | 1.03 |
| ID30 | | 0.74 | 1.74 | 1.98 | 0.14 | 2.14 |

## 4. Conclusion

This research evaluated the levels of heavy metals contamination in automobile workshops, aiming to evaluate their contamination levels. The presence of selected heavy metals in soil has raised significant environmental concerns in Okene metropolis because the findings indicated that the level of most the studied metals in the workshop exceeded the permissible limits of WHO, hence, potentially posing risks to the local population. Based on the research findings, it is highly recommended that the government should allocate appropriate areas that can serve as automobile villages where auto repairs can be performed at a safe distance from residential areas. Furthermore, it is advised that education and legislation on waste management in places like auto-mechanic workshops should be intensified to avert the consequences of heavy metal related wastes on the environment, particularly on groundwater. Additionally, it is essential that metals speciation be conducted so that the form and the extent of metal bioavailability can be further assessed.

## References

[1] Adeleken, B.A & Abegunde, K.D (2011). Heavy metal contamination of soil and ground water at automobile mechanic village in Ibadan, Nigeria. International Journal of the Physical Sciences, 6(5), 1045-1058.

[2]. United States Department of Agriculture (2001) Natural Resources Conservation Services, Soils Quality Institute, Urban Technical Note.

[3] Anweting, I.B., Ebong, G.A., Okon, I.E., Etuk, H.S. and Etim I.S. (2024)Physicochemical Characteristics and Heavy Metals Assessment of Surface Water and Sediments from Idim Idaang Stream inIbiono Ibom, Skwa Ibom State, Nigeria. Journal of Material and Environmetal Sciences, 15(1), 72-82

[4] FAO/WHO. (2011). Joint FAO/WHO food standards program codex committee on contaminants in foods. Fifth session ed: WHO

[5] Emurotu J. E. (2020), Chemical Speciation and Potential Mobility of some Metals of Selected Farmland in Kogi State, North Central Nigeria. Nigerian Journal of Basic and Applied Science, 28(1), 48-55

[6]. Ogunfowokan, A.O., Oyekunle, J.A.O., Durosinmi, L.M., Akinjokun, A.I. & Gabriel, O.D. (2009) Speciation Study of Lead and Manganese in Roadside Dusts from Major Roads in in Metropolitan City of Lagos. Environmental Monitoring and Assessment, 105, 431-447.

[7]. Ebong, G.A., Etuk, H.S.,Ikpe, .E. (2024)Cancer and non-cancer risks potentials of metals in transformer impacted soils in Nigeria/ Journal of Material and Enviromental Sciences, 15(4), 512-529

[8]. Ekwumemgbo P.A, Omoniyi K.I, Sanni, H.A. (2014) Chemical fractionation of Cu, Mn and Zn in dumpsite soil samples in Kaduna metropolis Nigeria. American Chemical Science Journal, 4(2), 138-150.

[9]. Obasi, N. A., Akubugwo, E. I., Kalu, K. M., Ugbogu, A. E., & Okorie, U. C. (2013). Toxicological assessment of various metals on selected edible leafy plants of Umuka and Ubahu dumpsites in Okigwe of Imo State, Nigeria. Journal of Experimental Biology, 1(6): 441-453.

[10]. FEPA, (1991). Guidelines and Standard for Environmental Pollution Control in Nigeria. Federal Republic of Nigeria, Nigeria. pp. 61-63. [19]. EU. 2008. Council Directive 98/83/EC on the quality of water intended for human consumption, European Union

[11] Eze, O. C., Tukura, B. W., Atolaiye, B. O., & Opaluwa, O. D. (2018). Index model assessment of heavy metal pollution in soils selected from three irrigated farm sites in FCT Abuja, Nigeria. International Journal of Advances in Scientific Research and Engineering, 4(6), 93-105

[12] Udofia, I.M., Ufot, I.N., Danzarami, D.A., and John G.O. (2024). Pollution Status, proximate composition and ecological risk index of Amarathus hybridus and Vernoniacolorata leaves hervested from roadside and farms within Zaria Metropolis, Kaduna State, Journal of Evironment and Material Sciences, 15(7):1026-1037

[13]. Musa, O.K., Kudarunya, E.A., Omali, A.O. & Akuli, T. I. (2014). Physico-chemical characteristics of surface and groundwater in Obajana and its environs in Kogi State central Nigeria. Academic Journals, 8(9), 521-531.

[14] Ndudi, D., Oyaro, N., Githae, E. & Afullo, A. (2015). Chemical Properties of sources of water in Ado Ekiti State Nigeria, International Research Journal of Environmental Science, 4(1), 47-51

# ASSESSMENT OF HEAVY METAL CONCENTRATIONS IN WELL WATER COLLECTED FROM DIFFERENT LOCATIONS WITHIN A MINING SITE IN AJAOKUTA, KOGI STATE, NIGERIA

**Omeiza, Folorunsho Samuel[1*], Lawal, John .Augustine[2], Paul Idoko[1], Okpanachi, Clifford[3]**

*[1]Department of Chemistry, Kogi State College of Education, Ankpa, Kogi State-Nigeria*
*[2]Department of Chemistry, Obafemi Awolowo University, Ile Ife, Osun State-Nigeria*
*3Department of Chemistry, Prince Abubakar Audu University, Ayingba, Kogi State- Nigeria*
**Corresponding Author: Folorunshoomeiza@gmail.com*

**Abstract**

Heavy metal contamination of ground water in Eganyi village in Ajaokuta Local Government Area of Kogi State was assessed. The eight well water samples were analyzed using atomic absorption spectrophotometer for mercury, copper, manganese, chromium, zinc, lead and iron concentrations. The levels were compared with the World Health Organization (WHO) specified maximum contaminant levels for mercury, copper, manganese, chromium, lead and iron as 0.001, 1.0, 0.2, 0.05, 0.01, and 0.3 mg/L respectively. From the results obtained, none of the samples analyzed contained manganese and chromium in concentrations above the maximum contaminant level. The average concentration of each metal was 0.30 mg/L (Hg), 4.15 mg/L (Cu), 0.05.mg/L (Mn), 0.005 mg/L (Cr), 1.96 mg/L (Pb) and 1.06 mg/L (Fe). These concentrations are above the standard limit. All samples analyzed contained one or more of the eight heavy metals studied in varying concentrations. The results obtained from this study suggest a significant risk to the population given the toxicity of these metals and the fact that Wells are the only source of water supply in this environment.

**Keywords**: Mining site, AAS, heavy metals, WHO, water

## 1. Introduction

The increase in automotive maintenance repair establishments and their operations in Okene Metropolis is as a result of the rise in demand for private vehicles, a large portion of which are imported from foreign countries. This has led to the issue of soil contamination in several areas dedicated for mechanic workshops. Automobile waste in the study areas consists of waste oil, oxidation byproducts and metallic fragments that result from the wear and tear of vehicles, organic and inorganic chemicals found in oil additives, used batteries and metals [1]. The existence of trace elements in soil is rapidly becoming a global concern, particularly since soil is a vital component of both rural and urban environments [1,3]. The non-degradable heavy metals like cadmium (Cd), copper (Cu), chromium (Cr), lead (Pb), manganese (Mn), nickel (Ni), and zinc (Zn) often used as additives in some lubricants and gasoline can pose a threat to groundwater due to soil percolation of leachates from these substances [3]. The co-occurrence of toxic heavy metals at numerous contaminated mechanics sites in Okene metropolis and other nearby villages poses a severe threat to the environment [1]. Studies have shown that automobile workshop may increase heavy metal concentration in soil [1,3 ] which have effects on the soils, crops and human health [5]. Therefore, the environmental impacts of waste from automobile workshop are greatly influenced by their heavy metal contents. As a result, this study aimed to investigate the soil pollution resulting from heavy metals in the vicinity of selected mechanic workshops within the Okene Metropolis, kogi central senatorial district of Nigeria.

## 2. Materials and Method

### Description of Study Area

Okene is located at latitude 7.55122 and longitude 6.23569 and the town experiences a distinctive wet and dry seasons, with an annual rainfall range of 1,100mm – 1300mm [6]. The average annual temperature is estimated to be around 27°C, with a relative humidity, averaging approximately 70% to 75% based on historical data studies. Furthermore, the town average daily wind speed measures 71.4 km/hr [6], while the average daily vapour pressure is approximately 24 Hpa. In terms of population, Okene has a population of 312, 715 in 1991 [7].

**Sample Collection**

Soil samples were collected from four automobile mechanic workshops situated in Agasa,(AG) Okengwe (OK), Ozuwaya (OZ) and Idoji (ID) of Okene metropolis, Nigeria.. For the collection of samples, the soil surface was cleared employing a hand trowel and subsequently The number of sampling points was dependent on the size of the mechanic sites and consequently, each of the four mechanics was partitioned into four (4) quadrants. Samples were obtained from two distinct depths of 0-15 cm, and 15-30 cm. Additionally, within a location; samples were collected from three different points at depths of 0-15 cm and 15-30 cm, referred to as topsoil and sub-soil, respectively [6,7]. The soil samples that were gathered were ground using a porcelain mortar with pestle and subsequently subjected to air-drying for a week to eliminate any traces of moisture. Furthermore, they were sieved through a 2 mm stainless steel sieve [8]. These soil samples were then properly labeled and stored in polythene bags for further analysis [9].

**Heavy Metal Analysis**

The collected specimens were subjected to heavy metal analysis, as documented in prior research [8]. Specifically, a precise quantity of 5 grams of air-dried soil sample was measured and placed into a 25 ml polypropylene centrifuge tube. Sequential extractions were conducted, whereby 5 grams of air-dried soil sample, sieved to a diameter of 2 mm, was weighed and added to a pre-weighed centrifuge tube. Next, 25 ml of distilled water was introduced and the resultant suspension was vigorously agitated for 120 minutes. Subsequently, centrifugation was performed at a rate of 3500 rpm for 10 minutes, followed by filtration through Whatman No. 42 filter paper under vacuum into a 100 ml vial. This fraction was denoted as SOL, which served as water extraction F1. The residue from F1 was extracted by adding 25 ml of 0.25 M $K_2SO_4$. The suspension was shaken for duration of 16 hours, centrifuged for 10 minutes at 3500 rpm, and filtered through Whatman No. 42 filter paper into a 100 ml vial. The resulting fraction was labeled as EXCH (F2). The extraction of the residue from F2 was carried out through the addition of 25 ml of 0.05 M $Na_2EDTA$. Following this, the suspension underwent a period of shaking for duration of 8 hours, followed by centrifugation for 10 minutes at 3500 rpm. The resulting solution was then filtered through Whatman No. 42 filter paper and collected in a 100 ml vial. This fraction was given the designation of CARBON (F3). Subsequently, 25 ml of 0.5 M NaOH solution was added to the residue from F3, after which it was shaken for a period of 16 hours. The mixture was then centrifuged at 3500 rpm for 10 minutes and the supernatant was filtered through Whatman No. 42 filter paper into a 100 ml vial. This fraction was given the designation of ORG (F4). Determination of the residual fractions of the respective metals was carried out through the computation of the sum of fraction F1-F4, which was then subtracted from the respective total metal concentration [12]. Determined through $HClO_4$-$HNO_3$-$H_2SO_4$ digestion F5 [8]. At the conclusion of the extraction period, the individual metals present in the filtrates were determined through the use of JENWAYS model AA431HT atomic absorption spectrophotometer (AAS).

**Quality assurance validation**

Validation of the technique for the metal determination was conducted on digested soil samples. by spiking the pre-digested samples with multi-element standard solution (0.5 mg/l of Cd, Fe, Ni, Pb and Zn) as reported by [9].

## 3. Result and Discussion

### Quality Assurance

The reports on the validation of a technique utilized for the determination of Cd, Ni, Zn, Fe and Pb metals in soil samples that have been subjected to digestion as shown in Table indicates 88 % - 97 % percentage recovery which is in agreement with previous reports that any instrument with recovery ≥ 85 % is strongly recommended to be used for analysis [9, 10, 11]

**Table 1: Results of validations experiment**

| Metal | Percentage (%) Recovery |
|---|---|
| Cd | 92.00 ± 1.132 |
| Ni | 96.00 ± 1.301 |
| Zn | 88.00 ± 1.040 |
| Fe | 97.00 ± 0.912 |
| Pb | 94.00 ± 1.115 |

### Mean concentrations of Zinc (Zn)in fractions in all locations and across all depths

Tables 2 shows the mean concentration of Zn in the different fractions across depths where there is a decrease in the concentration of Zn between the depths of 0-15 cm and 15-30 cm. It is worth noting that the residual fraction constitutes the most mobile and potentially bio-available Zn metal species [13]. The chemical fractionation results of Zinc in mechanic workshop soils at the two different depths are presented in Tables 2. In both cases, the chemical associations of Zinc were dominated by the residual fraction, which ranged from 0.14 to 41.31 mg/kg across the depth levels. The majority of automobile mechanic sites examined in Tables 2 exhibited levels of extractable zinc (F1+F2+F3+F4+F5) that exceeded the permissible limit of 300 mg/kg, with only a small number of exceptions. The residual fraction (F5) contained the highest concentrations of zinc at both depths for all soils studied, indicating that under severe conditions, this element could be released into the environment. However, the residual fraction is not generally considered to be an environmental hazard, as it is a stable compound in which metals are tightly bound within a mineral lattice, reducing the bioavailability of this metal [11] Through comparison of zinc levels in residual and water-soluble fractions at varying depths across multiple sites, it is evident that the residual fractions contain the highest concentration of this element, measuring 41.31 mg/kg. Such a notable quantity of zinc associated with the residual fractions suggests that it would be highly accessible for uptake by plants. The discoveries made in this investigation are consistent with the observations made by previous researchers [12, 13], who reported comparable levels of zinc concentration in soils from tanneries located in Kaduna and Kogi State, Nigeria, respectively. Additionally, it was noted that the total metal contents of the mechanic workshop soil were lower at the depth of 0-15 cm than at the depth of 15-30 cm, which can be attributed to metal leaching. This observation is indicative of the deposition of zinc in soils resulting from the activities of mechanic workshops, specifically from lubricants and metal scrap originating from automobiles

**Table 2: Mean Zn concentration (mg/kg) in the fractions in all locations and across all depths**

| Location /Metals | Depth | Water soluble fraction | Exchangeable fraction | Organic bound Fraction | Carbonate bound fraction | Residual fraction |
|---|---|---|---|---|---|---|
| AG15 | 0 – 15 cm | 0.75 | 1.74 | 4.18 | 27.82 | 37.33 |
| OK15 | | 0.22 | 1.03 | 25.58 | 37.21 | 41.31 |
| OZ15 | | 0.60 | 1.23 | 8.83 | 4.04 | 4.15 |
| ID15 | | 0.91 | 1.45 | 5.42 | 17.22 | 4.14 |
| AG30 | 15 – 30 cm | 0.59 | 0.89 | 3.18 | 22.56 | 32.73 |
| OK30 | | 0.14 | 0.92 | 17.58 | 32.11 | 32.11 |
| OZ30 | | 0.32 | 1.22 | 6.63 | 3.45 | 3.42 |
| ID30 | | 0.70 | 1.41 | 4.12 | 13.12 | 3.14 |

**Mean concentrations (mg/kg) of Lead (Pb) in fractions in all locations and across all depths**

Tables 3 shows the outcomes of the chemical fractionation of lead (Pb) in soil. The water-soluble fraction ranged from 0.78 to 1.43 kg/mg, the exchangeable fraction ranged from 3.12 to 5.36 mg/kg, the organic fraction ranged from 3.15 to 6.71 mg/kg, the carbonate fraction ranged from 8.75 to 26.46 mg/kg, while that of residual fraction varied from 5.15 to 11.11 mg/kg for both depths, across all sites. The Pb values in the investigated soil surpassed the maximum permissible limit of 3.0 mg/kg set by [10]. Concentrations of lead were high in both depths, with F4 carbonate fraction being the dominant contributor across the site. Through comparison of residual (F4) and water soluble fraction concentrations of lead across the mechanic workshop for both depths, it was demonstrated that high percentages of extractable fractions were present in the dumpsite soils at both respective depths. This suggests that Pb may be released into the environment, leading to contamination throughout the two depths. The high association of Pb in the carbonate fraction

**Table 3: Mean Pb concentration (mg/kg) in the fractions in all locations and across all depths**

| Location /Metals | Depth | Water soluble fraction | Exchangeable fraction | Organic bound Fraction | Carbonate bound fraction | Residual fraction |
|---|---|---|---|---|---|---|
| AG15 | 0 – 15 cm | 1.21 | 5.26 | 4.25 | 12.33 | 11.11 |
| OK15 | | 1.43 | 4.75 | 5.26 | 14.35 | 10.43 |
| OZ15 | | 1.43 | 5.36 | 4.75 | 26.46 | 7.88 |
| ID15 | | 1.17 | 4.14 | 6.71 | 16.85 | 7.24 |
| AG30 | 15 – 30 cm | 1.01 | 3.97 | 3.25 | 8.75 | 8.37 |
| OK30 | | 0.99 | 3.44 | 3.16 | 12.67 | 9.33 |
| OZ30 | | 0.78 | 3.31 | 3.15 | 20.15 | 5.15 |
| ID30 | | 1.00 | 3.12 | 5.54 | 11.98 | 6.98 |

**Mean concentrations (mg/kg) of Cd in fractions in all locations and across all depths**

Tables 4 also shows the outcomes of the chemical fractionation of cadmium (Cd) in soil. The water-soluble fraction ranged from 0.02 to 0.65 kg/mg, the exchangeable fraction ranged from 0.43 to 1.53 mg/kg, the organic fraction ranged from 0.40 to 0.57 mg/kg, the carbonate fraction ranged from 0.11 to 0.28 mg/kg, while that of residual fraction varied from 1.10 to 4.75 mg/kg for both depths, across all sites. The association of Cd in the water-soluble fraction poses a significant environmental risk due

to the unstable nature of the compound and the strong binding of metals within a mineral lattice, which limits its bioavailability [12]. The findings in these investigations are in agreement with the observations which reported similar Cd concentration from Ado Ekiti metropolis southern western Nigeria) [14].

**Table 4: Mean Cd concentration (mg/kg) in the fractions in all locations and across all depths**

| Location /Metals | Depth | Water soluble fraction | Exchangeable fraction | Carbonate bound Fraction | Organic bound fraction | Residual fraction |
|---|---|---|---|---|---|---|
| AG15 | 0 – 15 cm | 0.12 | 0.67 | 0.57 | 0.28 | 2.15 |
| OK15 | | 0.05 | 1.28 | 0.57 | 0.28 | 4.75 |
| OZ15 | | 0.65 | 0.77 | 0.57 | 0.28 | 2.17 |
| ID15 | | 0.21 | 0.63 | 0.57 | 0.19 | 1.88 |
| AG30 | 15 – 30 cm | 0.08 | 0.5 | 0.47 | 0.21 | 1.87 |
| OK30 | | 0.02 | 1.55 | 0.47 | 0.27 | 3.27 |
| OZ30 | | 0.43 | 0.65 | 0.41 | 0.27 | 2.11 |
| ID30 | | 0.15 | 0.43 | 0.4 | 0.11 | 1.11 |

The chemical association of iron was dominant in the residual fraction (F5) at depths of 0-15 and 15-30 cm, respectively, across all the study sites. The concentration of iron in the residual fraction ranged from 36.10 to 75.85 mg/kg for both depths, while the water-soluble fraction exhibited a range of 0.94 to 1.45 mg/kg. Similarly, the organic fraction displayed a range of 17.18 to 52.63 mg/kg for both depths. The carbonate fraction, on the other hand, exhibited a range of 16.10 to 33.72 mg/kg across all depths and study sites.

Moreover, the Exchangeable fraction of nickel in all locations at 0-15 and 15-30 cm increased from 1.06 to 3.96 mg/kg. In this fraction, all the metals were found in all the locations but not such significantly higher concentrations than they were in the depth of 15-30 cm compared to other fractions.

**Table 5 Mean Fe concentration (mg/kg) in the fractions in all locations and across all depths**

| Location /Metals | Depth | Water soluble fraction | Exchangeable fraction | Carbonate bound Fraction | Organic bound fraction | Residual fraction |
|---|---|---|---|---|---|---|
| AG15 | 0 – 15 cm | 1.45 | 3.96 | 52.63 | 32.63 | 75.85 |
| OK15 | | 1.21 | 1.52 | 23.18 | 33.72 | 67.33 |
| OZ15 | | 1.31 | 1.61 | 25.00 | 18.65 | 48.15 |
| ID15 | | 1.10 | 2.37 | 46.63 | 31.75 | 44.19 |
| AG30 | 15 – 30 cm | 1.10 | 2.00 | 45.63 | 27.93 | 64.43 |
| OK30 | | 1.11 | 1.24 | 17.18 | 16.12 | 63.12 |
| OZ30 | | 1.01 | 1.06 | 20.4 | 16.10 | 36.10 |
| ID30 | | 0.94 | 1.79 | 37.13 | 25.14 | 40.14 |

. The data presented in Tables 6 demonstrate an increase in the amount of nickel with depth in the carbonate fraction across all locations at depths of 0-15 cm and 15-30 cm. The highest concentration of nickel, amounting to 12.11 mg/kg, was found in residual fractions, which was consistent across the site and depth. Moreover, the exchangeable fraction at depths of 0-15 cm and 15-30 cm exhibited an

average of BDL-2.27 mg/kg of nickel. Additionally, the organic fraction at a depth of 0-15 cm displayed a nickel concentration of 3.21 mg/kg with the exception of the results obtained for the residual fractions, which was higher than other fractions. This result is in consistent with finding of [11].

**Table 6: Mean Ni concentration (mg/kg) in the fractions in all locations and across all depths**

| Location /Metals | Depth | Water soluble fraction | Exchangeable fraction | Carbonate bound Fraction | Organic bound fraction | Residual fraction |
|---|---|---|---|---|---|---|
| AG15 | 0 – 15 cm | 1.11 | 1.65 | 3.21 | 0.73 | 11.14 |
| OK15 | | 1.15 | ND | 3.21 | 0.2 | 12.11 |
| OZ15 | | 1.32 | 2.27 | 3.21 | 1.12 | 2.54 |
| ID15 | | 0.99 | 2.11 | 3.21 | 0.18 | 3.44 |
| AG30 | 15 – 30 cm | 0.87 | 1.59 | 1.23 | 0.71 | 8.51 |
| OK30 | | 0.67 | ND | 1.24 | 0.14 | 10.14 |
| OZ30 | | 1.1 | 2.15 | 2.11 | 1.03 | 1.03 |
| ID30 | | 0.74 | 1.74 | 1.98 | 0.14 | 2.14 |

## 4. Conclusion

This research evaluated the levels of heavy metals contamination in automobile workshops, aiming to evaluate their contamination levels. The presence of selected heavy metals in soil has raised significant environmental concerns in Okene metropolis because the findings indicated that the level of most the studied metals in the workshop exceeded the permissible limits of WHO, hence, potentially posing risks to the local population. Based on the research findings, it is highly recommended that the government should allocate appropriate areas that can serve as automobile villages where auto repairs can be performed at a safe distance from residential areas. Furthermore, it is advised that education and legislation on waste management in places like auto-mechanic workshops should be intensified to avert the consequences of heavy metal related wastes on the environment, particularly on groundwater. Additionally, it is essential that metals speciation be conducted so that the form and the extent of metal bioavailability can be further assessed.

## References

[1] Adeleken, B.A & Abegunde, K.D (2011). Heavy metal contamination of soil and ground water at automobile mechanic village in Ibadan, Nigeria. International Journal of the Physical Sciences, 6(5), 1045-1058.

[2]. United States Department of Agriculture (2001) Natural Resources Conservation Services, Soils Quality Institute, Urban Technical Note.

[3] Anweting, I.B., Ebong, G.A., Okon, I.E., Etuk, H.S. and Etim I.S. (2024)Physicochemical Characteristics and Heavy Metals Assessment of Surface Water and Sediments from Idim Idaang Stream inIbiono Ibom, Skwa Ibom State, Nigeria. Journal of Material and Environmetal Sciences, 15(1), 72-82

[4] FAO/WHO. (2011). Joint FAO/WHO food standards program codex committee on contaminants in foods. Fifth session ed: WHO

[5] Emurotu J. E. (2020), Chemical Speciation and Potential Mobility of some Metals of Selected Farmland in Kogi State, North Central Nigeria. Nigerian Journal of Basic and Applied Science, 28(1), 48-55

[6]. Ogunfowokan, A.O., Oyekunle, J.A.O., Durosinmi, L.M., Akinjokun, A.I. & Gabriel, O.D. (2009) Speciation Study of Lead and Manganese in Roadside Dusts from Major Roads in in Metropolitan City of Lagos. Environmental Monitoring and Assessment, 105, 431-447.

[7]. Ebong, G.A., Etuk, H.S.,Ikpe, .E. (2024)Cancer and non-cancer risks potentials of metals in transformer impacted soils in Nigeria/ Journal of Material and Enviromental Sciences, 15(4), 512-529

[8]. Ekwumemgbo P.A, Omoniyi K.I, Sanni, H.A. (2014) Chemical fractionation of Cu, Mn and Zn in dumpsite soil samples in Kaduna metropolis Nigeria. American Chemical Science Journal, 4(2), 138-150.

[9]. Obasi, N. A., Akubugwo, E. I., Kalu, K. M., Ugbogu, A. E., & Okorie, U. C. (2013). Toxicological assessment of various metals on selected edible leafy plants of Umuka and Ubahu dumpsites in Okigwe of Imo State, Nigeria. Journal of Experimental Biology, 1(6): 441-453.

[10]. FEPA, (1991). Guidelines and Standard for Environmental Pollution Control in Nigeria. Federal Republic of Nigeria, Nigeria. pp. 61-63. [19]. EU. 2008. Council Directive 98/83/EC on the quality of water intended for human consumption, European Union

[11] Eze, O. C., Tukura, B. W., Atolaiye, B. O., & Opaluwa, O. D. (2018). Index model assessment of heavy metal pollution in soils selected from three irrigated farm sites in FCT Abuja, Nigeria. International Journal of Advances in Scientific Research and Engineering, 4(6), 93-105

[12] Udofia, I.M., Ufot, I.N., Danzarami, D.A., and John G.O. (2024). Pollution Status, proximate composition and ecological risk index of Amarathus hybridus and Vernoniacolorata leaves hervested from roadside and farms within Zaria Metropolis, Kaduna State, Journal of Evironment and Material Sciences, 15(7):1026-1037

[13]. Musa, O.K., Kudarunya, E.A., Omali, A.O. & Akuli, T. I. (2014). Physico-chemical characteristics of surface and groundwater in Obajana and its environs in Kogi State central Nigeria. Academic Journals, 8(9), 521-531.

[14] Ndudi, D., Oyaro, N., Githae, E. & Afullo, A. (2015). Chemical Properties of sources of water in Ado Ekiti State Nigeria, International Research Journal of Environmental Science, 4(1), 47-51

# SOURCES AND FATE OF MICROPLASTICS IN AGRICULTURAL SOILS, A MINI REVIEW

**Muhammad Abubakar Lawal[1*] and Umar Lawal Abubakar[2]**

*[1]Department of Chemistry, Ahmadu Bello University, Zaria*
*[2]Department of Petroleum and Gas Processing Engineering, Kaduna Polytechnic Kaduna*
*Corresponding author: induceddipole66@gmail.com; malawal@abu.edu.ng*

**Abstract**

Microplastics (MPs), plastic particles smaller than 5 mm, have emerged as contaminants of global environmental concern. Although considerable attention has historically focused on marine pollution, recent evidence indicates that agricultural soils are major sinks for microplastics due to increasing anthropogenic activities. This review summarizes the major sources and environmental fate of microplastics in agricultural soils. Plastic mulch films, organic fertilizers such as compost and sewage sludge, irrigation with contaminated water, and atmospheric deposition are identified as the principal pathways through which microplastics enter agricultural lands. Once introduced into soils, microplastics undergo physical, chemical, and biological transformations, while their transport is influenced by soil properties, agricultural practices, wind, water movement, plant roots, and soil organisms. These processes facilitate their vertical and horizontal migration, increasing the likelihood of groundwater contamination, plant uptake, and entry into terrestrial food webs. The review highlights current knowledge on the occurrence, transport, and environmental implications of microplastics in agricultural soils and underscores the need for sustainable agricultural practices and improved plastic waste management to mitigate future contamination.

**Keywords:** Microplastics, agricultural soils, atmospheric deposition, soil pollution, fate

## 1. Introduction

The rapid growth in global plastic production has brought enormous socioeconomic benefits but has also resulted in widespread environmental pollution [1]. Due to their durability and resistance to degradation, discarded plastic materials persist in terrestrial and aquatic environments for decades, gradually fragmenting into smaller particles known as microplastics (MPs), generally defined as plastic particles less than 5 mm in diameter. These particles have become emerging contaminants because of their persistence, mobility, and potential ecological and human health impacts [2].

Microplastics have been widely detected in rivers and water bodies [3,4]. While marine ecosystems have traditionally received greater attention regarding microplastic pollution, recent studies have demonstrated that terrestrial ecosystems, particularly agricultural soils, constitute significant reservoirs of microplastics [5,6]. Agricultural soils receive microplastics from diverse sources including plastic mulching, sewage sludge and compost application, polymer-coated fertilizers, irrigation with contaminated water, atmospheric deposition, and improper disposal of agricultural plastics [7]. The accumulation of these particles in soils may alter soil physical, chemical, and biological properties, influence nutrient cycling, affect soil microbial communities, and increase the potential for uptake by crops and subsequent transfer through the food chain [7,8].

Understanding the sources, transport mechanisms, and environmental fate of microplastics in agricultural soils is essential for developing effective mitigation and management strategies. This mini review therefore examines the major sources of microplastics in agricultural soils, discusses the processes governing their transformation and migration within terrestrial environments, and highlights their potential environmental implications.

## 2. Microplastics in agricultural soils

About 79% of plastic waste generated globally are estimated to be piled in landfills and other environmental compartments [1], thus soil is considered a receptor and an important sink for microplastics (MPs) pollution [9]. Notable sources of MPs in soils include landfills, sewage sludge, agricultural mulching and atmospheric deposition [7]. Recent studies have shown a shift of attention from MPs pollution in oceans and water bodies to terrestrial compartments such as soils [5,8]. Terrestrial habitats are estimated to contain 4 to 23 folds the MPs found in the ocean [3], in fact, agricultural soils are estimated to hold more MPs than oceanic basins [10]. Terrestrial environments are more exposed to multiple sources of microplastics, and especially, are greatly and more regularly affected by human activities [11], and the dynamics of transport of MP in terrestrial habitats are more complex than in marine habitats [12].

Agricultural activities have been identified as a primary source of MP in soils, particularly, the use plastic mulch and shelter films, organic fertilizers, polymer coated slow-release fertilizers, MPs polluted irrigation water, among others [11,13,14]. With the growth of intensive and semi-intensive agricultural practices globally, agricultural activities are expected to account for about 2% of global plastic consumption (over 265 million tonnes) [15,16]. Plastics are frequently used in agricultural activities such as irrigation (pipes), orchard and green house covering (plastic mulch), containers, fertilizers, among others. The kinds of plastics often used in agriculture include high density polyethylene (HDPE), low density polyethylene (LDPE), linear low density polyethylene (LLDPE), polypropylene (PP), polyamide (PA), polyvinyl chloride (PVC), ethylene vinyl acetate (EVA), polyethylene terephthalate (PET), polymethyl methacrylate (PMMA) [15], among others. As these plastics degrade slowly, microplastics are released into the agricultural soils. However, plastic particles of less than 5mm sizes (MP) are of particular interest, as they are presumed to enter the food chain undetected. As the toxic effects of MP are still being investigated the full extent of their permeation into the human system is not fully known [17,18].

### 2.1 Sources of microplastics in agricultural soils

*Plastic mulch*

Plastic mulching is a growing practice in agriculture especially in arid and semi-arid regions with low rainfall, high winds and high solar radiation [19]. An estimated over 2.1 million tonnes of plastic much films was consumed globally in 2020 [11]. The current global market for plastic agricultural films is $13.8 billion (USD) projected to rise by about 7.1% to $19.5 billion (USD) in 2029 [20]. Plastic mulch film has the largest market value of all agricultural films [20]. China is currently the world's leading user of plastic mulch technology, extending the practice from arid, semi-arid to mountainous and cold regions [19].

Plastic mulch is commonly made of polyethylene; low density polyethylene which is non-biodegradable. Plastic mulch films are often classified by their primary constituents, density, thickness and colour [21]. The applicability and success of plastic mulch is attributed to its light weight, low cost,

durability and flexibility. Plastic mulching has been reported to improve crop yield via improved soil hydrothermal conditions [22,23], decreased nitrogen leaching [24], and subduing the growth of weeds [25].

The exposure of plastic mulch to solar radiation, mechanical processes, wind, chemicals such as pesticides, fluctuations in temperature and humidity necessitates their frequent replacement and hence increased consumption [15]. The levels of MPs in agricultural soils have been reported to be positively correlated to plastic mulch consumption [26].

The major problem with plastic mulch in agriculture is disposal after use. Current disposal techniques include landfilling, incineration and recycling. Recycling is difficult and expensive because about 30-80% of recovered mulch is contaminated with soil, agrochemicals, organic matter and a host of other materials [21]. Innovative sustainable management of used mulch involves the efficient recycling and use of biodegradable materials [27]. Some examples of biodegradable plastics used in mulch include polybutylene adipate-co-terephthalate (PBET), polylactic acid (PLA), among others [27].

*Organic fertilizer*

Different forms of organic fertilizers such as sewage sludge, mature compost, digestates, have been reported to contain large amounts of MPs [14]. Despite the laudable idea of returning important nutrients to soils via the reuse of organic wastes as fertilizers, and the attendant strict policy set up by some countries on the maximum residue limits of toxic components therein, MPs especially particles < 2mm are often returned to the soil as well [14]. For instance, despite, Germany having one of the most stringent policy on fertilizer quality, a large amount of biowaste is composted annually [28], and an estimated 35 billion to 2.2 trillion microplastic particles of < 1mm size are introduced via compost reuse [14]. Organic fertilizers are thus an important sources of MPs in soils.

MPs denser than water almost wholly remain in sewage sludge after primary and secondary treatments of wastewater, an estimated 95% of MPs in wastewater end up in the sludge [29], which is often reused in agricultural soils as fertilizer [30]. The use of sewage sludge in agriculture has been shown to be able to increase MPs concentration by 60 fold in soils [31]. Other major routes of MPs accumulation in agricultural soils include plastic film mulching , among others. Composts have also being reported to carry high concentrations of plastics (about 1.2 g/kg) which are broken down to smaller fragments – microplastics by the high prevalent temperatures and microbial activity in composts [32].

*Irrigation with microplastic polluted water*

Ground water, lakes, rivers, municipal water, rainwater and treated effluent are common sources of irrigation water globally. These sources often contain microplastics and can be transferred to agricultural soils when used for irrigation. In water scarce areas, the practice of using untreated and partially treated sewage or wastewater for irrigation in agriculture is prevalent, however, conventional treatment processes have been shown not to be efficient in the removal of some persistent pollutants such as MPs [30]. Thus, irrigation with sewage and wastewater has been identified as a primary source of MPs in agricultural soils [2].

Irrigation methods have also been reported to affect the levels of MPs introduced into the soil from microplastic-polluted water. Flooding irrigation contributes more MPs than drip irrigation due to the larger volume of irrigation water consumed in the former [33]. Irrigation also leads to redistribution of MPs present in agricultural soils by enhancing both horizontal and vertical mobility of MPs in soils, a study by Liu *et al.* demonstrated that irrigation water expedited MPs pollution to deep soil [34].

*Atmospheric deposition*

Clothing fibres, incineration of waste, landfills, reverse sedimentation, sewage sludge, wear and tear from automobile tires, building materials, household objects, among others are some notable sources

of MPs in the air [35]. MPs present in the air attached to dust particles or aerosolized can be introduced into agricultural soils through dry and/or wet deposition. MPs in the air are often in fibre forms and a wide variety of MPs have also been detected in air, ranging majorly from PET and PE to other forms of polymers [36]. Allen *et al.* noted that microplastic fibres of between 25 – 300 μm can be transported over long distances in the atmosphere [37].

2.2 Fate

MPs in agricultural soils are subjected to transformation and transport. Transformation is largely in form of degradation and fragmentation, which is brough about by the physical, chemical and biological processes occurring in the soil. Photodegradation of MPs by UV is a dominant chemical transformation that occurs, and could lead to scission of chains, cross-linking, and in fact mineralization to carbon (IV) oxide [38]. The aggregate effects of UV radiation, mechanical wearing, processes by soil fauna such as feeding, digestion and excretion, and agronomic activities further fasten the degradation of MPs to sub-micron particles and nanoparticles [39].

The transport of MPs in agricultural soils are greatly affected by the soil management practices, ploughing and harvesting. Denser MPs have been reported to concentrate on the surface of agricultural soils while lighter MPs are more easily carried away by wind. Lighter MPs can also be more readily carried away by surface run offs to other terrestrial habitats and aquatic ecosystems [40]. While wet-dry cycles in the soils promotes the vertical migration of the MPs on the surface of agricultural soils [41]. The size and type of MPs were found to significantly affect the vertical migration in wet-dry cycles. A study by O'Connor *et al.* reported PE microplastics of 21 μm to have the greatest penetration potential in sand-column experiments and the wet-dry cycles positively correlated with the migration dept [41]. These reports demonstrate that soils are likely entry routes of MPs to subterranean ecosystem [41].

Similarly, bioturbation by soil fauna and plant roots also help the mobility of MPs in agricultural soils. Plant roots penetrate soils vertically and horizontally to derive nutrients, this passive movement hollow out spaces influencing the soil water movement pattern [42] and thus affecting the migration of particles such as MPs. This effect may be greater in plants with a large below ground biomass. Bioturbation by soil fauna such as earthworms, ants, termites, collembola, mosquito larvae, mud shrimps, bristle worms, beetles, vertebrates like rats, snakes and so on contributes to the migration of particles such as MPs in the soil. Reports have shown the bioturbation effect of earthworms on the migration of pollutant in the soil. Earthworms can generate long burrows, modifying the soil porosity, promoting the transport of materials from soil surface litters into deeper layers of the soil [43]. Huerta Lwanga *et al.* and Rillig *et al.* in two separate reports showed the assimilation of microplastic beads into burrows by earthworms [44,45]. MPs of ≤ 50 μm were found to be more concentrated in the burrow walls, as earthworm species *Lumbricus terrestris* has been reported to largely bioturbates particles of between 0.5 to 1.0 mm [46]. Generally, the burrow activities of earthworms make MPs more available in the burrow walls compared to the bulk soils and increases the leaching potential of the MPs into deeper layers of the soil [44]. This makes the pollution of ground water by MPs more likely, and increases the uptake of MPs by plants and the migration of MPs into terrestrial food web [44]. A simulated study by Nizzetto *et al.* found about 60% soil MPs find their way into neighbouring water bodies [10].

Light MPs which attach to dust and soil particles are also easily carried away by wind falling into a suspension-resuspension cycle transporting the MPs far and near [36]. Wind transport of MPs have been identified as the major route for MPs deposition in remote and isolated areas such as polar and high plateau regions [36,37]. MPs can also be absorbed by plant roots, translocated and accumulated

to other plant parts through endocytosis, apoplastic transport, crack entry and stomatal entry mechanisms [47]. Some documented plant uptake of MPs include PS uptake by lettuce plant [48], barley [49], rice [50], and so on.

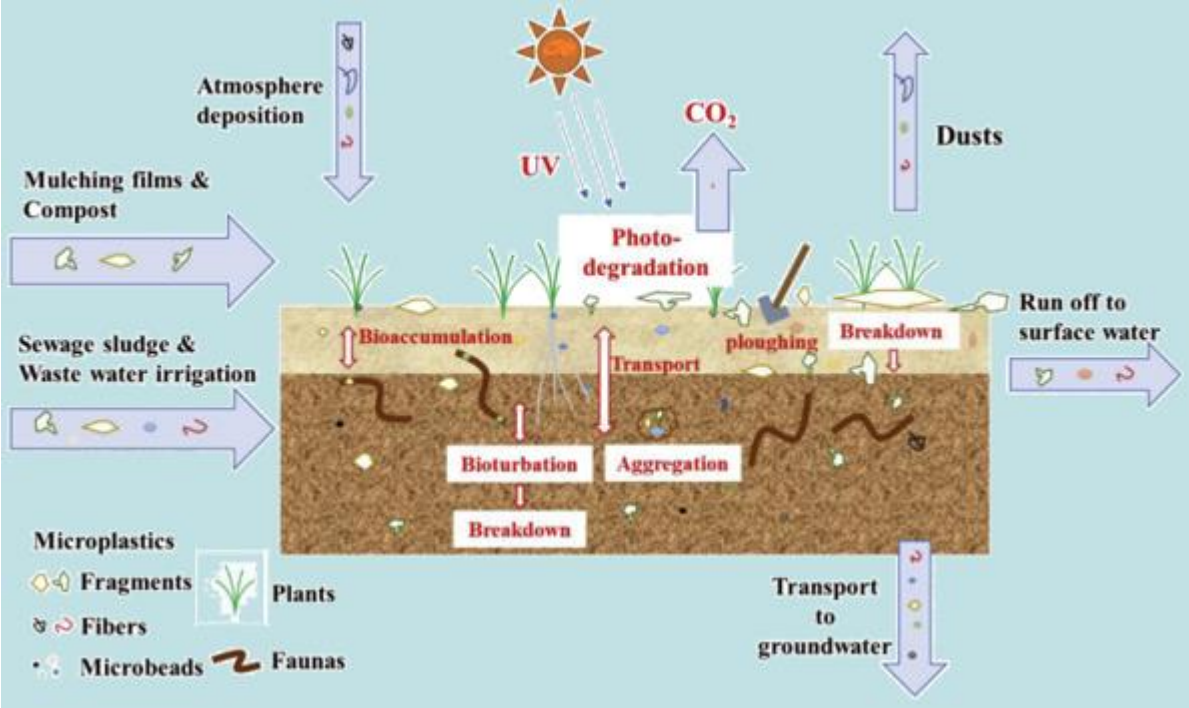



**Fig. 1**: Fate of microplastics in agricultural soils (Adapted and modified from Tian *et al.* [7])

### 3. Future Research Directions

Although considerable progress has been made in understanding microplastics contamination in agricultural soils, several important knowledge gaps remain. Future studies should focus on:

- Developing standardized methods for sampling, extraction, identification, and quantification of soil microplastics to enable comparison among studies.
- Investigating the long-term effects of microplastics on soil fertility, microbial diversity, nutrient cycling, and crop productivity under field conditions.
- Elucidating the mechanisms governing plant uptake, translocation, and accumulation of microplastics, particularly nanoplastics, in edible plant tissues.
- Evaluating the interactions between microplastics and co-existing contaminants such as heavy metals, pesticides, antibiotics, and emerging pollutants.
- Developing biodegradable agricultural plastics with verified environmental safety and assessing their degradation products under realistic agricultural conditions.
- Improving wastewater treatment and organic waste management technologies to reduce the introduction of microplastics into agricultural lands.
- Conducting comprehensive human health risk assessments through food-chain transfer and groundwater contamination pathways.

- Establishing evidence-based regulations and best management practices for plastic use, recycling, and disposal in agriculture.

## 4. Conclusion

Agricultural soils have emerged as important sinks for microplastics due to intensive agricultural activities and widespread plastic usage. Plastic mulch films, organic fertilizers, contaminated irrigation water, and atmospheric deposition constitute the primary pathways through which these contaminants enter agricultural ecosystems. Once present in soils, microplastics undergo continuous transformation and are transported by water movement, wind, agricultural practices, plant roots, and soil fauna, thereby increasing their environmental mobility and persistence. Their accumulation poses potential risks to soil quality, groundwater, crop production, biodiversity, and ultimately human health through food-chain transfer. Addressing microplastic pollution in agricultural soils will require integrated strategies involving sustainable agricultural practices, improved plastic waste management, advances in biodegradable materials, strengthened environmental monitoring, and supportive policy frameworks. Continued multidisciplinary research is essential to fully understand the environmental behaviour and long-term impacts of microplastics and to develop effective mitigation measures.

## References

1. Geyer R, Jambeck JR, Law KL. Production, use, and fate of all plastics ever made. Science advances. 2017;3(7):e1700782.
2. Fan W, Qiu C, Qu Q, et al. Sources and identification of microplastics in soils. Soil & Environmental Health. 2023 2023/06/01/;1(2):100019.
3. Horton AA, Walton A, Spurgeon DJ, et al. Microplastics in freshwater and terrestrial environments: Evaluating the current understanding to identify the knowledge gaps and future research priorities. Science of The Total Environment. 2017 2017/05/15/;586:127-141.
4. Abafe OA, Lawal MA, Chokwe TB. Non-targeted screening of emerging contaminants in South African surface and wastewater. Emerging Contaminants. 2023 2023/12/01/;9(4):100246.
5. Rillig MC, Lehmann A. Microplastic in terrestrial ecosystems. Science. 2020 2020/06/26;368(6498):1430-1431.
6. Rillig MC, Ingraffia R, de Souza Machado AA. Microplastic Incorporation into Soil in Agroecosystems [Opinion]. Frontiers in Plant Science. 2017 2017-October-18;8.
7. Tian L, Jinjin C, Ji R, et al. Microplastics in agricultural soils: sources, effects, and their fate. Current Opinion in Environmental Science & Health. 2022 2022/02/01/;25:100311.
8. de Souza Machado AA, Kloas W, Zarfl C, et al. Microplastics as an emerging threat to terrestrial ecosystems. Global Change Biology. 2018 2018/04/01;24(4):1405-1416.
9. Wang F, Wang Q, Adams CA, et al. Effects of microplastics on soil properties: Current knowledge and future perspectives. Journal of Hazardous Materials. 2022 2022/02/15/;424:127531.
10. Nizzetto L, Bussi G, Futter MN, et al. A theoretical assessment of microplastic transport in river catchments and their retention by soils and river sediments [10.1039/C6EM00206D]. Environmental Science: Processes & Impacts. 2016;18(8):1050-1059.

11. Wang S, Fan T, Cheng W, et al. Occurrence of macroplastic debris in the long-term plastic film-mulched agricultural soil: A case study of Northwest China. Science of The Total Environment. 2022 2022/07/20/;831:154881.
12. Wu C, Ma Y, Wang D, et al. Integrated microbiology and metabolomics analysis reveal plastic mulch film residue affects soil microorganisms and their metabolic functions. Journal of Hazardous Materials. 2022 2022/02/05/;423:127258.
13. Lian J, Liu W, Meng L, et al. Effects of microplastics derived from polymer-coated fertilizer on maize growth, rhizosphere, and soil properties. Journal of Cleaner Production. 2021 2021/10/10/;318:128571.
14. Weithmann N, Möller JN, Löder MGJ, et al. Organic fertilizer as a vehicle for the entry of microplastic into the environment. Science Advances. 2018;4(4):eaap8060.
15. Briassoulis D, Babou E, Hiskakis M, et al. Review, mapping and analysis of the agricultural plastic waste generation and consolidation in Europe. Waste Management & Research. 2013 2013/12/01;31(12):1262-1278.
16. Blanco I, Loisi RV, Sica C, et al. Agricultural plastic waste mapping using GIS. A case study in Italy. Resources, Conservation and Recycling. 2018 2018/10/01/;137:229-242.
17. Vethaak AD, Legler J. Microplastics and human health. Science. 2021 2021/02/12;371(6530):672-674.
18. Nawab A, Ahmad M, Khan MT, et al. Human exposure to microplastics: A review on exposure routes and public health impacts. Journal of Hazardous Materials Advances. 2024 2024/11/01/;16:100487.
19. Gao H, Yan C, Liu Q, et al. Effects of plastic mulching and plastic residue on agricultural production: A meta-analysis. Science of The Total Environment. 2019 2019/02/15/;651:484-492.
20. Markets and Markets. Agricultural Films Market by Type (LDPE, LLDPE, EVA, Reclaim, HDPE), Application (Greenhouse Film (Classic Greenhouse, Low Tunnel), Mulch Film (Black Mulches, Transparent Mulches), Silage Film (Silage Stretch Wrap, Silage Bag) - Global Forecast to 2029. United States of America2024.
21. Sarpong KA, Adesina FA, DeVetter LW, et al. Recycling agricultural plastic mulch: limitations and opportunities in the United States. Circular Agricultural Systems. 2024;4(1).
22. Qin W, Chi B, Oenema O. Long-Term Monitoring of Rainfed Wheat Yield and Soil Water at the Loess Plateau Reveals Low Water Use Efficiency. PLOS ONE. 2013;8(11):e78828.
23. Abdelhak M. Chapter 4 - Soil improvement in arid and semiarid regions for sustainable development. In: Jhariya MK, Meena RS, Banerjee A, et al., editors. Natural Resources Conservation and Advances for Sustainability: Elsevier; 2022. p. 73-90.
24. Luo Z, Wang E, Sun OJ. Can no-tillage stimulate carbon sequestration in agricultural soils? A meta-analysis of paired experiments. Agriculture, Ecosystems & Environment. 2010 2010/10/15/;139(1):224-231.
25. Abouziena HF, Hafez OM, El-Metwally IM, et al. Comparison of Weed Suppression and Mandarin Fruit Yield and Quality Obtained with Organic Mulches, Synthetic Mulches, Cultivation, and Glyphosate. HortScience horts. 2008 01 Jun. 2008;43(3):795-799.
26. Huang Y, Liu Q, Jia W, et al. Agricultural plastic mulching as a source of microplastics in the terrestrial environment. Environmental Pollution. 2020 2020/05/01/;260:114096.

27. Dong H, Yang G, Zhang Y, et al. Recycling, disposal, or biodegradable-alternative of polyethylene plastic film for agricultural mulching? A life cycle analysis of their environmental impacts. Journal of Cleaner Production. 2022 2022/12/20/;380:134950.
28. Schüch A, Morscheck G, Lemke A, et al. Bio-waste Recycling in Germany – Further Challenges. Procedia Environmental Sciences. 2016 2016/01/01/;35:308-318.
29. Ziajahromi S, Neale PA, Leusch FDL. Wastewater treatment plant effluent as a source of microplastics: review of the fate, chemical interactions and potential risks to aquatic organisms. Water Science and Technology. 2016;74(10):2253-2269.
30. Mohapatra DP, Cledón M, Brar SK, et al. Application of Wastewater and Biosolids in Soil: Occurrence and Fate of Emerging Contaminants. Water, Air, & Soil Pollution. 2016 2016/02/09;227(3):77.
31. Zhang J, Gao D, Li Q, et al. Biodegradation of polyethylene microplastic particles by the fungus Aspergillus flavus from the guts of wax moth Galleria mellonella. Science of The Total Environment. 2020 2020/02/20/;704:135931.
32. Braun M, Mail M, Heyse R, et al. Plastic in compost: Prevalence and potential input into agricultural and horticultural soils. Science of The Total Environment. 2021 2021/03/15/;760:143335.
33. Guo S, Zhang J, Liu J, et al. Organic fertilizer and irrigation water are the primary sources of microplastics in the facility soil, Beijing. Science of The Total Environment. 2023 2023/10/15/;895:165005.
34. Liu Y, Liu Y, Li Y, et al. Effects of irrigation on the fate of microplastics in typical agricultural soil and freshwater environments in the upper irrigation area of the Yellow River. Journal of Hazardous Materials. 2023 2023/04/05/;447:130766.
35. Amato-Lourenço LF, dos Santos Galvão L, de Weger LA, et al. An emerging class of air pollutants: Potential effects of microplastics to respiratory human health? Science of The Total Environment. 2020 2020/12/20/;749:141676.
36. Zhang Y, Gao T, Kang S, et al. Importance of atmospheric transport for microplastics deposited in remote areas. Environmental Pollution. 2019 2019/11/01/;254:112953.
37. Allen S, Allen D, Phoenix VR, et al. Atmospheric transport and deposition of microplastics in a remote mountain catchment. Nature Geoscience. 2019 2019/05/01;12(5):339-344.
38. Zhu K, Jia H, Sun Y, et al. Long-term phototransformation of microplastics under simulated sunlight irradiation in aquatic environments: Roles of reactive oxygen species. Water Research. 2020 2020/04/15/;173:115564.
39. Song YK, Hong SH, Jang M, et al. Combined Effects of UV Exposure Duration and Mechanical Abrasion on Microplastic Fragmentation by Polymer Type. Environmental Science & Technology. 2017 2017/04/18;51(8):4368-4376.
40. Zylstra ER. Accumulation of wind-dispersed trash in desert environments. Journal of Arid Environments. 2013 2013/02/01/;89:13-15.
41. O'Connor D, Pan S, Shen Z, et al. Microplastics undergo accelerated vertical migration in sand soil due to small size and wet-dry cycles. Environmental Pollution. 2019 2019/06/01/;249:527-534.
42. Gabet EJ, Reichman OJ, Seabloom EW. The Effects of Bioturbation on Soil Processes and Sediment Transport. Annual Review of Earth and Planetary Sciences. 2003;31(Volume 31, 2003):249-273.

43. Görres JH, Savin MC, Amador JA. Soil micropore structure and carbon mineralization in burrows and casts of an anecic earthworm (Lumbricus terrestris). Soil Biology and Biochemistry. 2001 2001/11/01/;33(14):1881-1887.
44. Huerta Lwanga E, Gertsen H, Gooren H, et al. Incorporation of microplastics from litter into burrows of Lumbricus terrestris. Environmental Pollution. 2017 2017/01/01/;220:523-531.
45. Rillig MC, Ziersch L, Hempel S. Microplastic transport in soil by earthworms. Scientific Reports. 2017 2017/05/02;7(1):1362.
46. Judas M. Gut content analysis of earthworms (Lumbricidae) in a beechwood. Soil Biology and Biochemistry. 1992 1992/12/01/;24(12):1413-1417.
47. Yu Z, Xu X, Guo L, et al. Uptake and transport of micro/nanoplastics in terrestrial plants: Detection, mechanisms, and influencing factors. Science of The Total Environment. 2024 2024/01/10/;907:168155.
48. Li L, Zhou Q, Yin N, et al. Uptake and accumulation of microplastics in an edible plant. Chinese Science Bulletin. 2019;64(9):928-934.
49. Wang Z, Li S, Jian S, et al. Low temperature tolerance is impaired by polystyrene nanoplastics accumulated in cells of barley (Hordeum vulgare L.) plants. Journal of Hazardous Materials. 2022 2022/03/15/;426:127826.
50. Zhou C-Q, Lu C-H, Mai L, et al. Response of rice (Oryza sativa L.) roots to nanoplastic treatment at seedling stage. Journal of Hazardous Materials. 2021 2021/01/05/;401:123412.

# STRUCTURE–PROPERTY RELATIONSHIPS IN PERMANGANATE-MODIFIED CASSAVA PEEL/POLYPROPYLENE COMPOSITES: EFFECTS ON MECHANICAL, VISCOELASTIC DAMPING AND HYGROSCOPIC BEHAVIOUR

**Okpanachi Baba Clifford[1*], Ameh Ekwu Mark[2], Are Comfort[2], Dauda Joseph Abiodun[2] Idowu Olufunke Lovette[2] , Agada Favour Ugbedeojo[2]**

*[1]Department of Industrial Chemistry, Federal University of Applied Sciences, Kachia, Kaduna State, Nigeria.*
*[2]Department of Pure and Industrial Chemistry, Prince Abubakar Audu University, Anyigba, Kogi State, Nigeria.*
*Corresponding author email: cliffordokpanachi@yahoo.com*

**Abstract**

This study evaluated the performance of cassava peel–reinforced polypropylene composites, comparing untreated (UCPPC) and permanganate-treated (PCPPC) systems in terms of scratch resistance, damping behaviour, and water absorption. Pure polypropylene (PP) exhibited the lowest scratch resistance (56.00), while UCPPC showed progressive improvement from 58.00 (5 wt%) to 64.50 (25 wt%). Superior performance was observed in PCPPC, with values increasing from 65.00 (5 wt%) to a maximum of 75.50 (25 wt%), indicating enhanced surface hardness due to improved filler–matrix interfacial bonding. Dynamic mechanical analysis revealed a decrease in damping factor (tan δ) with increasing filler loading (95/5 to 70/30), reflecting restricted polymer chain mobility and increased stiffness. PCPPC composites consistently exhibited lower damping than UCPPC, confirming enhanced interfacial adhesion and reduced energy dissipation. Water absorption increased with filler content in UCPPC, ranging from 3.67 – 4.03% (95/5) to 6.56% (75/25) after 240 h, compared to minimal uptake in PP (0.94 – 1.00%). However, PCPPC showed significantly reduced absorption, ranging from 1.66 – 2.02% (95/5) to 3.60% (75/25) indicating improved moisture resistance. Overall, permanganate-treated composites exhibited enhanced scratch resistance, stiffness, and reduced water uptake, highlighting their suitability for structural and moisture-resistant applications despite reduced damping capacity.

**Keywords:** Cassava Peel, Composite, Damping, Permanganate Modification, Polypropylene

## 1. Introduction

The growing demand for sustainable materials has accelerated interest in bio-based composites as alternatives to petroleum-derived products [1]. Natural fiber-reinforced composites are increasingly favored due to their biodegradability, low density, cost-effectiveness, and reduced environmental impact [2]. Among agro-wastes, cassava peel (from *Manihot esculenta*) is a promising lignocellulosic reinforcement, rich in cellulose, hemicellulose, and lignin, and widely available in tropical regions. Its utilization supports waste valorization and aligns with circular economy principles [3].

However, the inherent hydrophilicity of cassava peel limits compatibility with hydrophobic matrices such as polypropylene, resulting in poor interfacial adhesion and reduced mechanical performance [4]. To address this, chemical modifications are employed to enhance fiber–matrix bonding by improving surface roughness and introducing reactive functional groups [5]. These treatments significantly improve mechanical strength, dimensional stability, and moisture resistance [6].

Incorporation of cassava peel into polypropylene has been shown to enhance surface and mechanical properties, including hardness, stiffness, and wear resistance, while also reducing material costs through partial substitution of synthetic fillers [7], hence this study investigates the effects of untreated and chemically treated cassava peel by permanganate modification on the mechanical water absorption and

damping properties of polypropylene composites, highlighting its potential for sustainable, cost-effective, and high-performance material development.

## 2. Material and Methods

### Sample Collection and Preparation

Cassava peels were collected from farmers and households in Anyigba, Dekina LGA, Kogi State, Nigeria. The samples were washed with distilled water, air-dried (12 h), and oven-dried at 65 °C (36 h) to constant weight. The dried peels were milled and sieved to a uniform particle size of 300 μm. Recycled polypropylene (PP) was shredded and used as the polymer matrix.

### Sample Pre-treatment

The sieved fibers were solvent-extracted using acetone/n-hexane (4:1 v/v) for 5 h [8] to remove extractives, followed by oven drying (16 h).

### Permanganate Treatment of Fibers

Fibers were pre-treated with 10% NaOH (5 h) and benzoyl chloride (15 min) to activate hydroxyl groups. Surface modification was performed using 0.05 M $KMnO_4$ (acidified with dilute $H_2SO_4$) at a fiber-to-liquor ratio of 1:20 for 30 min. The reaction was terminated with 1 wt% sodium metabisulfite (10 min), after which fibers were washed to neutrality, ethanol-rinsed, oven-dried (70 °C, 24 h), and stored.

### Preparation of Permanganated and Unpermanganated Fiber Composites

Composites were prepared via melt mixing and compression molding. PP was processed at 170 °C for 10 min, followed by incorporation of untreated or treated cassava peel at 0 – 25 wt% (0, 5, 10, 15, 20, 25%) at 500 rpm [9]. The blends were compression-molded at 150 °C under 4 MPa for 10 min and cooled before demolding to obtain uniform composite samples [10].

**Table 1: Compound Design/Formulation for the Permanganated and UnPermanganated Cassava Peel Polypropylene Composites**

| S/N | Mass of ingredients (g) | 1 | 2 | 3 | 4 | 5 | 6 |
|---|---|---|---|---|---|---|---|
| 1 | PP | 100 | 95 | 90 | 85 | 80 | 75 |
| 2 | Cassava Peel Powder | 0 | 5 | 10 | 15 | 20 | 25 |

### Mechanical Property Test

### Scratch Resistance Test (ASTM D2240-05)

The scratch resistance test was performed according to [11] to determine or ascertain the degree to which the materials will withstand indentation or scratch. It measures penetration of a specified indenter into the material.

The various composites were placed on the surface below the indenter of the durometer. Starting with the control sample (100% polypropylene), the indenter was then pressed against the test piece (that is after the indenter was set to the zero mark) and using the handle of the machine, the reading was taken. The procedure was repeated three times for other composites and the average of the three readings was taken.

### Thermal Property

**DMA Test (Damping Factor)**

DMA was carried out using a DMA 242 E machine according to [12]. The test parameter, damping factor was first configured via the proteus software personal computer. Instrument set up including the sample holder (3-point bending), furnace temperature range of 36 – 120 $^{o}$C, dynamic load of 4N, frequency range of 2, 5 and 10 Hz and heating rate of 6 K/min were configured. Sample dimension of 60 x 12 x 3 mm were produced for each test. The test specimens were loaded into the machine using a three-point bending and locked into the furnace.

**Water Absorption Test**

The samples were analyzed according to [13], in which they were cut into dimensions of 60 x 25 x 3 mm and were immersed in water at ambient temperature for 24 hrs. The specimen was removed and patted dry with a cloth (lint free) and then reweighed using a digital weighing balance ED 224S model. The dried weight before ($W_{initial}$) immersion and the weight after ($W_{final}$) immersion were noted. Same procedure was repeated on the composite samples and reweighed after 72 hrs, 120 hrs, 168 hrs and 240 hrs, and the percentage water absorption was calculated using equation

$$\% \text{ Water absorption} = \frac{\text{final weight} - \text{initial weight}}{\text{initial weight}} \times 100 \quad \textbf{(1)}$$

**3. Results and Discussions**

**Mechanical Property**

**Scratch Resistance**

Scratch resistance, indicative of surface hardness, improved notably with filler incorporation and further with permanganate treatment. Pure polypropylene exhibited the lowest hardness value (56.00), reflecting its inherently soft and ductile nature with limited resistance to surface deformation.

With the addition of untreated filler (UCPPC), hardness increased progressively from 58.00 (5 wt%) to 64.50 (25 wt%). This trend indicates enhanced surface stiffness due to the reinforcing effect of the filler, which restricts polymer chain mobility and improves resistance to localized deformation and abrasion [14]. The increasing filler content also promotes better load distribution across the surface, thereby reducing susceptibility to scratch-induced damage [15].

Permanganate-treated composites (PCPPC) demonstrated consistently higher hardness values at all filler loadings, ranging from 65.00 (5 wt%) to a maximum of 75.50 (25 wt%). The superior performance is attributed to improved interfacial adhesion between the filler and matrix, arising from chemical modification that enhances surface roughness and introduces functional groups for better compatibility, [16]. This results in more efficient stress transfer and reduced likelihood of filler pull-out during surface contact [17].

Overall, the results confirm that filler incorporation enhances scratch resistance, while permanganate treatment further optimizes surface hardness and wear resistance, making the composites more suitable for applications requiring improved surface durability.

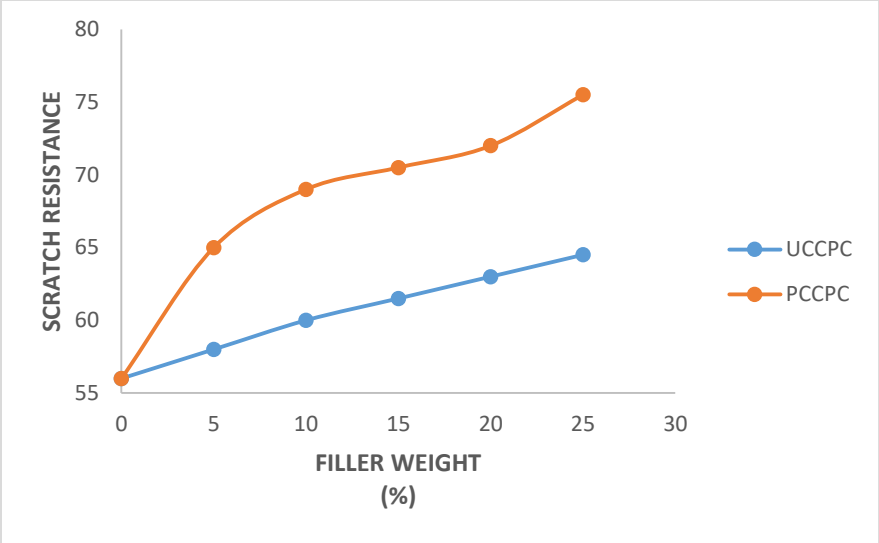



**Figure 1:** Plot of Scratch Resistance against Filler Compositions for Cassava Peel Polypropylene Composites

**Thermal Property**

**Damping Factor**

The damping factor (tan δ) decreased progressively with the incorporation of cassava peel filler in polypropylene, indicating reduced energy dissipation capacity. Pure polypropylene exhibited the highest damping factor due to greater molecular chain mobility, allowing effective viscoelastic relaxation and energy dissipation.

With filler addition (UCPPC), a gradual decline in damping factor was observed as filler loading increased from 95/5 to 75/25. At low loading (95/5), the reduction was minimal, suggesting partial retention of chain mobility [18]. However, at intermediate (85/15, 80/20) and high loading (75/25), the damping factor decreased significantly, reflecting restricted polymer chain movement and increased composite stiffness [19].

Permanganate-treated composites (PCPPC) exhibited consistently lower damping factors than untreated samples at all compositions. This behavior is attributed to improved filler–matrix interfacial adhesion, which enhances stress transfer and rigidity while limiting interfacial slippage and molecular motion responsible for energy dissipation [20].

Overall, the results demonstrate that filler incorporation and surface modification reduce damping capacity while enhancing stiffness and dimensional stability. This highlights a trade-off, where improved mechanical rigidity is achieved at the expense of vibrational energy dissipation, making the composites more suitable for structural rather than vibration-damping applications.

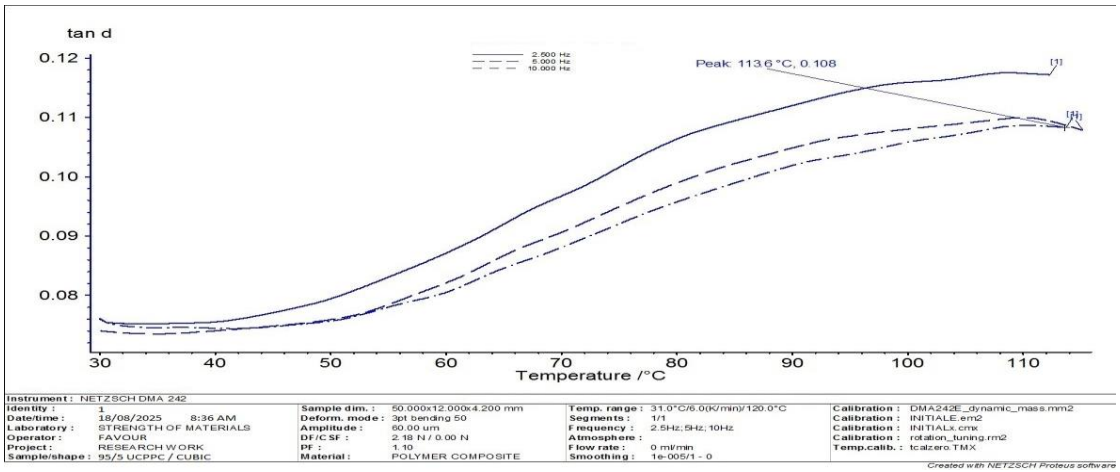



**Figure 2:** Plot of Damping Factor for 5% Unpermanganated Cassava Peel Polypropylene Composite (95/5 UCPPC)

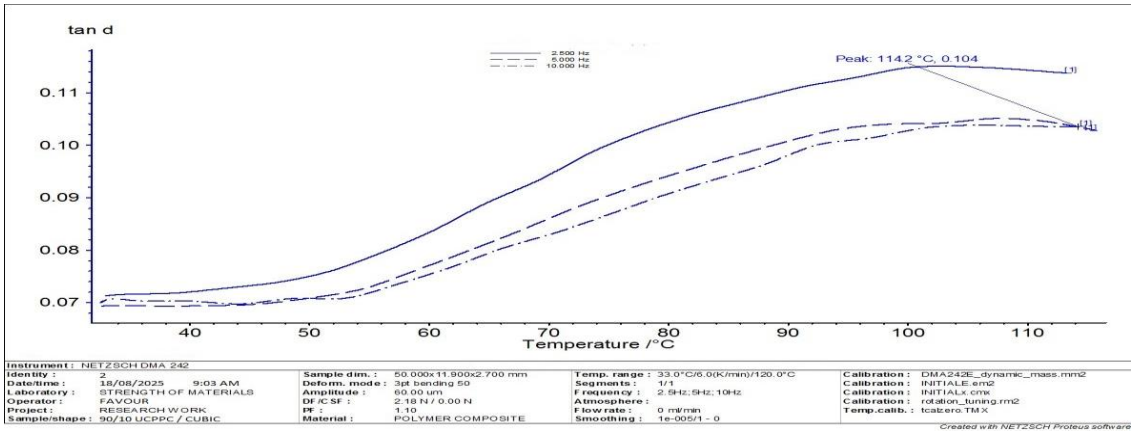



**Figure 3:** Plot of Damping Factor for 10% Unpermanganated Cassava Peel Polypropylene Composite (90/10 UCPPC)

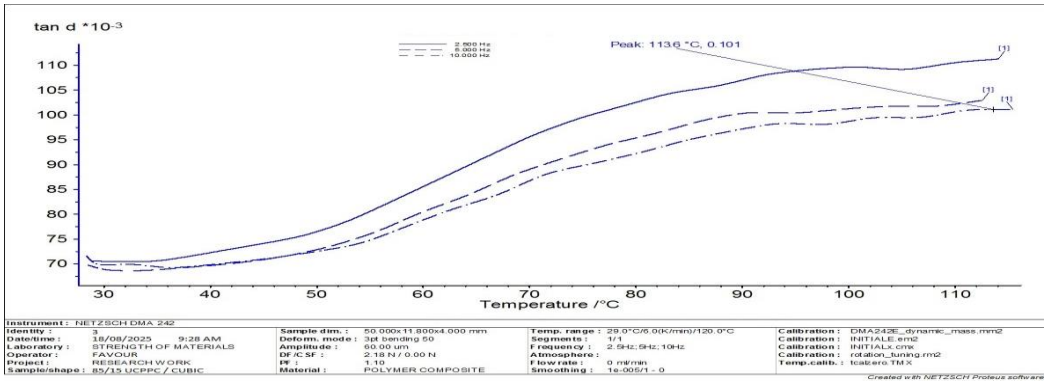



**Figure 4:** Plot of Damping Factor for 15% Unpermanganated Cassava Peel Polypropylene Composite (85/15 UCPPC)

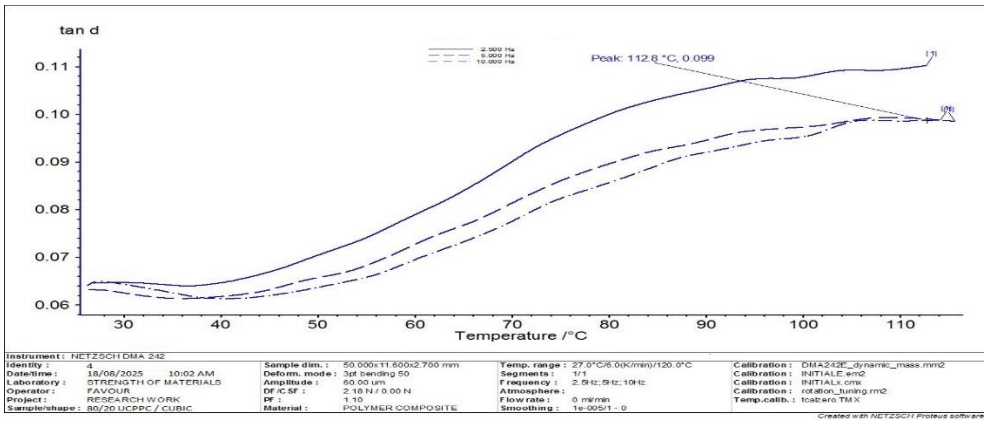



**Figure 5:** Plot of Damping Factor for 20% Unpermanganated Cassava Peel Polypropylene Composite (80/20 UCPPC)

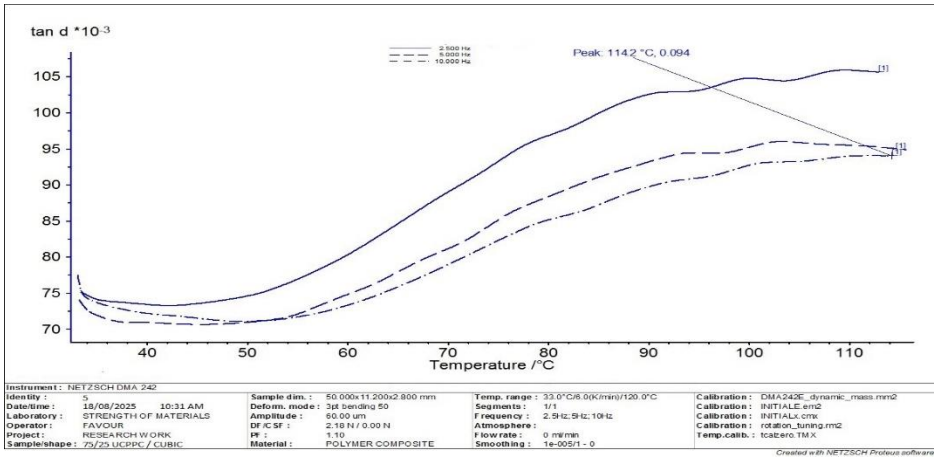



**Figure 6:** Plot of Damping Factor for 25% Unpermanganated Cassava Peel Polypropylene Composite (75/25 UCPPC)

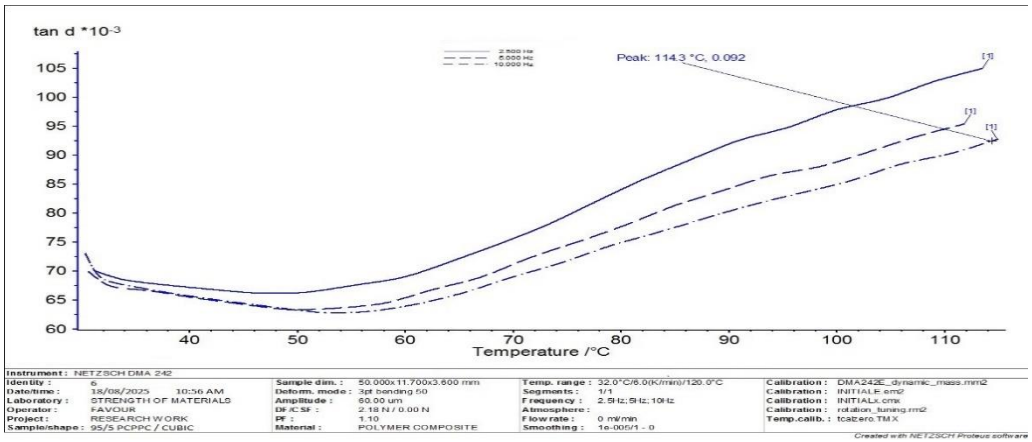



**Figure 7:** Plot of Damping Factor for 5% Permanganated Cassava Peel Polypropylene Composite (95/5 PCPPC)

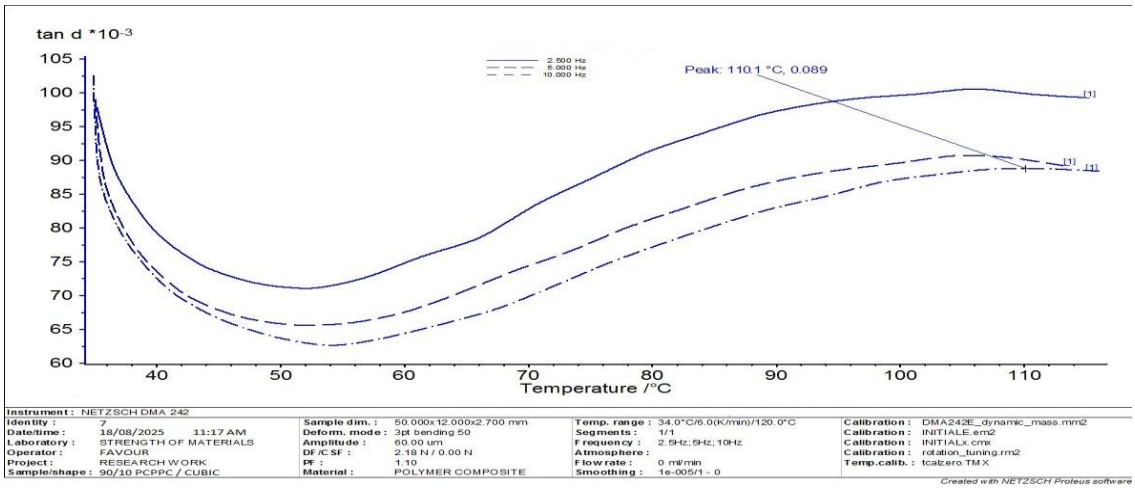



**Figure 8:** Plot of Damping Factor for 10% Permanganated Cassava Peel Polypropylene Composite (90/10 PCPPC)

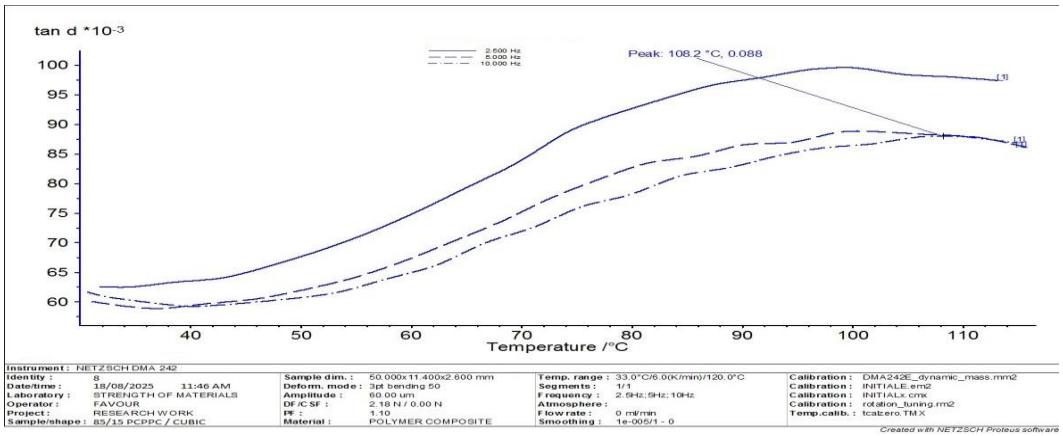



**Figure 9:** Plot of Damping Factor for 15% Permanganated Cassava Peel Polypropylene Composite (85/15 PCPPC)

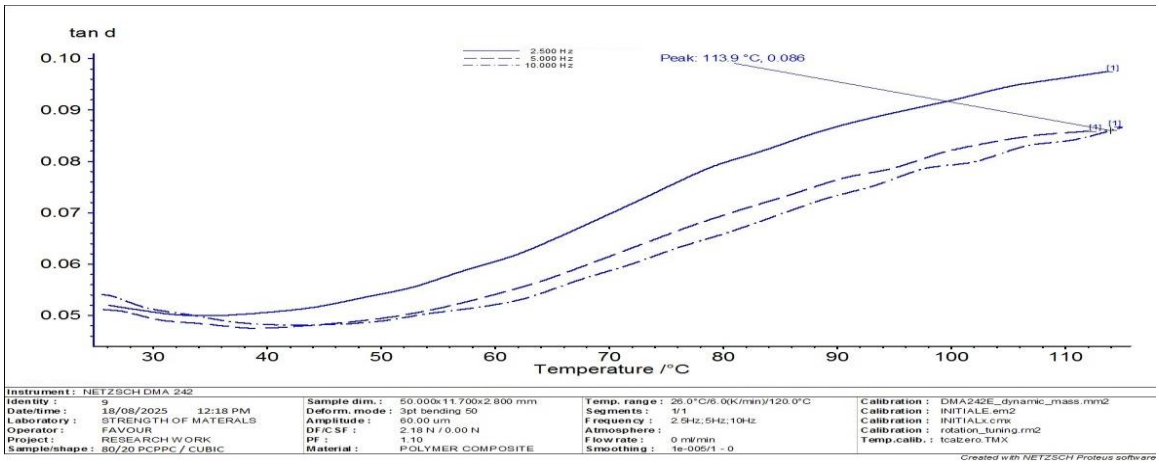



**Figure 10:** Plot of Damping Factor for 20% Permanganated Cassava Peel Polypropylene Composite (80/20 PCPPC)

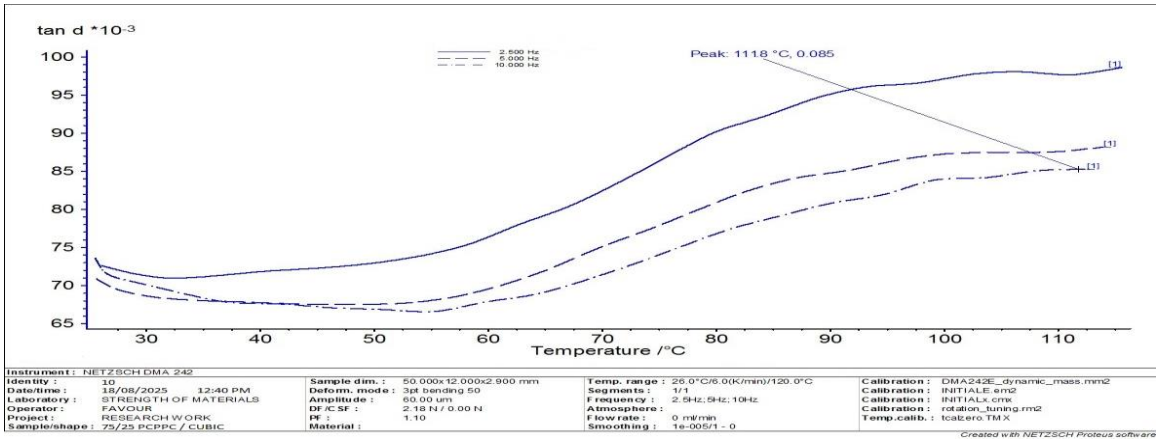



**Figure 11:** Plot of Damping Factor for 25% Permanganated Cassava Peel Polypropylene Composite (75/25 PCPPC)

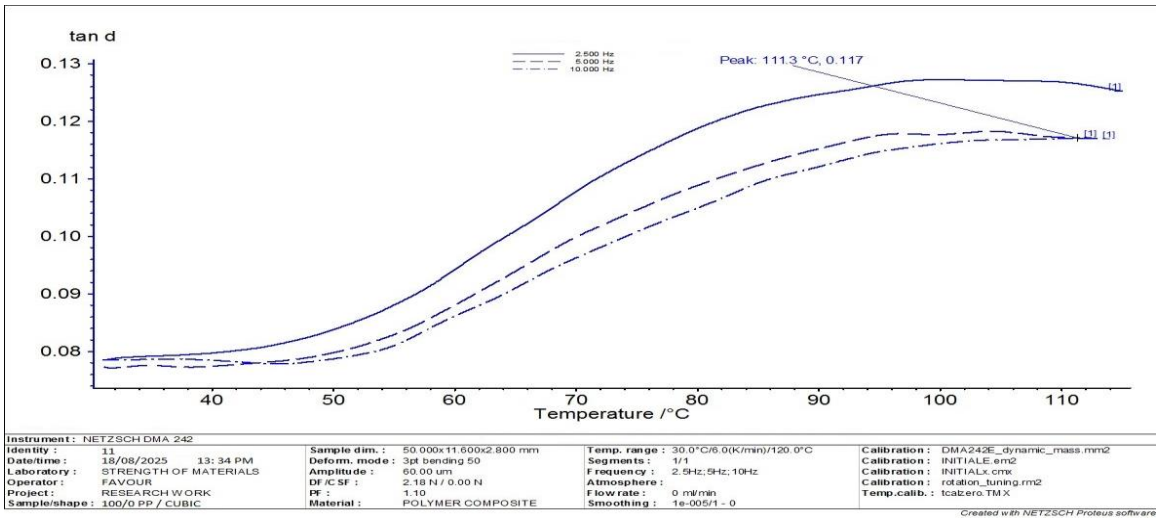



**Figure 12:** Plot of Damping Factor for 100% Polypropylene (Control)

**Water Absorption Property**

Water absorption behavior of unmodified (UCPPC) and permanganate-treated (PCPPC) composites was evaluated over 240 h, revealing strong dependence on filler loading and surface treatment. Pure polypropylene exhibited minimal uptake, increasing slightly from 0.94% (24 h) to 1.00% (120 h) and stabilizing at ~0.99%, consistent with its hydrophobic nature [21]. UCPPC samples showed significantly higher water absorption, increasing with fiber content. Values rose from 3.67 – 4.03% (95/5) to 4.33 – 4.96% (90/10), 5.15 – 5.77% (85/15), 6.20% (80/20), and peaked at 6.56% (75/25) after 240 h. This trend is attributed to the hydrophilic nature of cellulose, which promotes moisture uptake through hydrogen bonding [22] [23].

In contrast, PCPPC composites exhibited markedly reduced water absorption across all compositions. Uptake ranged from 1.66 – 2.02% (95/5), 1.79 – 2.29% (90/10), and increased moderately to 2.97% (85/15), 3.19% (80/20), and 3.60% (75/25) at 240 h. The lower values reflect improved fiber–matrix adhesion and reduced hydroxyl group availability due to permanganate treatment, limiting moisture diffusion pathways [24]. Overall, while increasing filler content elevated water absorption, chemical modification significantly mitigated this effect. PCPPC composites therefore demonstrate improved

moisture resistance and dimensional stability, making them more suitable for moisture-sensitive applications.

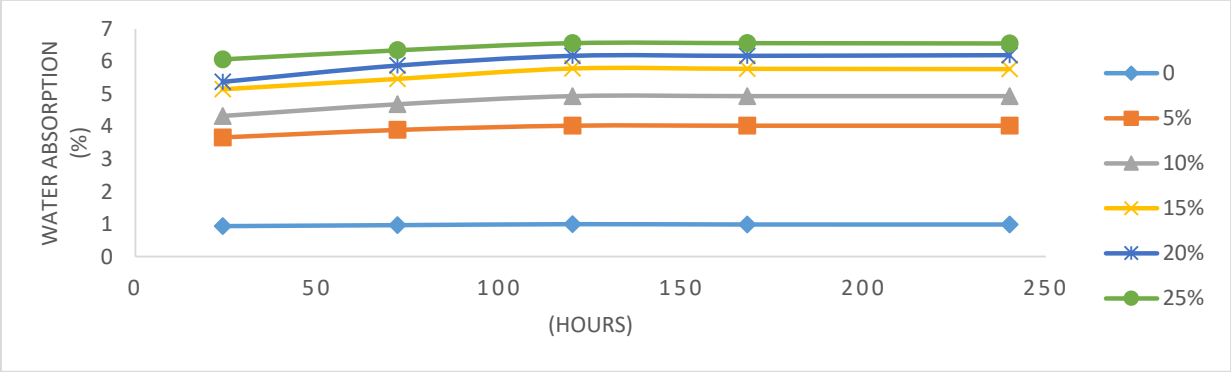



**Figure 13:** Plot of Water absorption against Filler Compositions for Unpermanganated Cassava Peel Polypropylene Composite

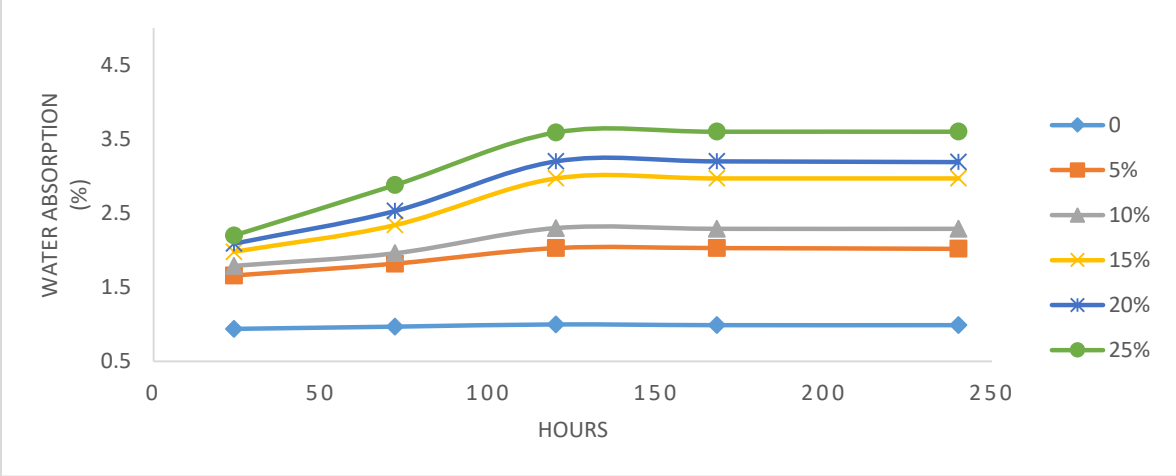



**Figure 14:** Plot of Water absorption against Filler Compositions for permanganated Cassava Peel Polypropylene Composite

## 4. Conclusion

Incorporation of cassava peel filler significantly enhanced the scratch resistance of polypropylene, increasing from 56.00 (pure PP) to 64.50 (UCPPC, 25 wt.%), and further to 75.50 in permanganate-treated composites (PCPPC). This improvement is attributed to increased surface hardness and stronger filler–matrix interfacial bonding. Damping factor decreased with increasing filler loading, from 0.115 (pure PP) to 0.070 (UCPPC) and 0.062 (PCPPC), indicating reduced molecular mobility and improved stiffness. Water absorption increased with filler content (up to 6.1 in UCPPC) due to fiber hydrophilicity, but was significantly reduced in PCPPC (4.7), reflecting enhanced moisture resistance. Overall, permanganate-treated composites exhibited superior performance, combining improved scratch resistance, stiffness, and reduced water uptake, demonstrating their suitability for structural and engineering applications.

**References**

[1] Borri, E., Ushak, S., Li, Y., Frazzica, A., Zhang, Y., Milian, Y. E., Grageda, M., Li, D., Cabeza, L. F., & Brancato, V. (2024). Formulation and development of composite materials for thermally driven and storage-integrated cooling technologies: A review. *Materials for Renewable and Sustainable Energy, 13*, 333–360. https://doi.org/10.1007/s40243-024-00268-5

[2] Castro-Franco, A. D., Siqueiros-Hernández, M., García-Angel, V., Mendoza-Muñoz, I., Vargas-Osuna, L. E., & Magaña-Almaguer, H. D. (2024). A review of natural fiber-reinforced composites for lower-limb prosthetic designs. *Polymers, 16*(9), 1293. https://doi.org/10.3390/polym16091293

[3] Mohammadi, M., Ishak, M. R., & Sultan, M. T. H. (2024). Exploring chemical and physical advancements in surface modification techniques of natural fiber reinforced composite: A comprehensive review. *Journal of Natural Fibers, 21*(1), 1–30. https://doi.org/10.1080/15440478.2024.2408633

[4] Li, H., Chen, G., & Zhou, L. (2025). Surface modification effects on viscoelastic and damping performance of bio-based polymer composites. *Composites Science and Technology, 245*, 110245. https://doi.org/10.1016/j.compscitech.2024.110245

[5] Pradiza, R. R., Junus, S., Asrofi, M., & Ilyas, R. A. (2025). Moisture characteristics of biocomposites from PVA/cassava starch reinforced by lemon peel fiber. *Journal of Fibers and Polymer Composites*, 4(1), 1–10.

[6] Shelly, D., Singhal, V., Nanda, T., Mehta, R., Aepuru, R., Lee, S.-Y., & Park, S.-J. (2024). A review of the emerging approaches for developing multi-scale filler-reinforced epoxy nanocomposites with enhanced impact performance. *Polymer Composites*, 45(11), 9647–9676.

[7] Chokkalingam, C., Babu Prakash, R., Abishek, G., & Balaji, B. (2024). A review on natural fibre reinforcement on composite material. *International Research Journal of Multidisciplinary Technovation, 6*(6), 261–274. https://doi.org/10.54392/irjmt24618

[8] Okoye, P. A. C., Chris-Okafor, P. U., Nwokoye, J. N., & Ilodigwe, C. B. (2024). Removal of soluble extractives from cassava peel fibers prior to composite preparation: Efficiency of solvent extraction methods. *Journal of Polymers and the Environment, 32*(5), 2712–2723. https://doi.org/10.1007/s10924-024-03321-8

[9] Chike, V. C., Anthony, I. O., Danjuma, S. Y., Aigbodion, V. S., Obada, D. O. and Samotu, I. A.(2014). Effects of Reinforcement Loading on Physical and Mechanical Properties of Developed Recycled Low Density Polyethylene / Maize Cob Ash Particulate (PLDP / MCAp) composite. *Advances in Applied Science Research*, 5 (2), 286 – 291.

[10] Jacob, J., Mamza, P. A. P., Ahmed, A. S. and Yaro, S. A. (2018). Effect of benzoyl chloride treatment on the mechanical and viscoelastic properties of plantain peel powder - reinforced polyethylene composites. *Science World Journal* 13(4), 25 – 29.

[11] American Society for Testing and Materials, ASTM (2015). Standard Method of Testing Hardness Properties of Materials. Durometer Hardness, D2240-05; West Conshohocken, PA.

[12] American Society for Testing and Materials, ASTM D7028 (2015). Standard Test Method for Glass Transition Temperature (DMA Tg) of Polymer matrix composites by dynamic mechanical analysis (DMA). West Conshohocken, PA

[13] American Society for Testing and Materials, ASTM (2015). Standard Method for water Absorption of Plastics, D570-98; West Conshohocken, PA.

[14] Adebayo, O. A., Ibrahim, M. A., & Bello, A. S. (2024). Influence of natural fiber surface treatment on the mechanical and wear properties of polypropylene composites. *Journal of Materials Research and Technology, 28*, 4123–4141. https://doi.org/10.1016/j.jmrt.2024.02.114

[15] Zhang, Y., Liu, H., & Chen, J. (2023). Effect of filler loading and interfacial adhesion on scratch resistance and hardness of polymer composites. *Composites Part B: Engineering, 250*, 110432. https://doi.org/10.1016/j.compositesb.2022.110432

[16] Kumar, R., & Singh, S. (2022). Surface modification of natural fibers and its influence on mechanical and tribological properties of polymer composites. *Materials Today Communications, 33*, 104512. https://doi.org/10.1016/j.mtcomm.2022.104512

[17] Rahman, M. M., Hossain, M. S., & Islam, M. N. (2025). Enhancement of interfacial bonding and surface hardness of natural fiber composites via chemical treatments. *Polymer Composites, 46*(2), 1567–1580. https://doi.org/10.1002/pc.27891

[18] Saba, N., Jawaid, M., & Sultan, M. T. H. (2023). Dynamic mechanical properties of natural fiber reinforced polymer composites: A review. *Construction and Building Materials, 368*, 130364. https://doi.org/10.1016/j.conbuildmat.2023.130364

[19] Wang, X., Zhang, K., & Li, Y. (2022). Influence of filler content on viscoelastic and damping behavior of polymer composites. *Polymer Testing, 103*, 107379. https://doi.org/10.1016/j.polymertesting.2021.107379

[20] Hassan, A., & Gupta, M. (2023). Role of interfacial adhesion in controlling damping characteristics of natural fiber polymer composites. *Journal of Composite Materials, 57*(12), 1821–1835. https://doi.org/10.1177/00219983231123456

[21] Chen, J., Li, X., & Wang, Y. (2023). Effect of fiber–matrix interface on moisture diffusion in natural fiber reinforced polymer composites. *Composites Part B: Engineering, 252*, 110525. https://doi.org/10.1016/j.compositesb.2023.110525

[22] Adekunle, K. F., Ibrahim, N. A., & Dahlan, K. Z. M. (2023). Water absorption and dimensional stability of natural fiber reinforced polymer composites: Influence of fiber treatment. *Journal of Materials Research and Technology, 25*, 2890–2902. https://doi.org/10.1016/j.jmrt.2023.05.112

[23] Oladele, I. O., Adewumi, A. A., & Omotoyinbo, J. A. (2024). Influence of agro-waste fillers on water absorption and mechanical properties of polypropylene composites. *Results in Engineering, 21*, 101621. https://doi.org/10.1016/j.rineng.2024.101621

[24] Verma, D., Gope, P. C., & Maheshwari, M. K. (2022). Effect of chemical treatment on moisture absorption behavior of natural fiber reinforced composites. *Materials Today Communications, 31*, 103563. https://doi.org/10.1016/j.mtcomm.2022.103563

# CUBE EFFECTS AND FACTOR INTERACTIONS ON ALUMINIUM CORROSION INHIBITION USING BANANA LEAF EXTRACT: INSIGHTS FROM RSM AND GRAVIMETRIC ANALYSIS

**Okpanachi Baba Clifford[1*], Ameh Ekwu Mark[2], Are Comfort Temitope[2], Dauda Joseph Abiodun[2], Idowu Olufunke Lovette[2], Ejukwa Emmanuel[2]**

[1]Department of Industrial Chemistry, Federal University of Applied Sciences, Kachia, Kaduna State, Nigeria.

[2]Department of Pure and Industrial Chemistry, Prince Abubakar Audu University, Anyigba, Kogi State, Nigeria.

Corresponding Author: cliffordokpanachi@yahoo.com

**Abstract**

The corrosion inhibition performance of banana leaf extract on aluminium in 0.1 M $H_2$ $SO_4$ was investigated using Response Surface Methodology (Box–Behnken Design) to evaluate the effects of immersion time, temperature, and inhibitor concentration. Inhibition efficiency (IE) was highest at short immersion times (24 h) and high concentrations (7% v/v), reaching 74.31% at 20 °C, 4% v/v and 70.78% at 40 °C, 7% v/v. At 96 h, IE ranged from 58.87% to 76.82%, with maximum efficiency at 20 °C, 7% v/v, while elevated temperature reduced IE to 56.65% at 60 °C, 7% v/v. Prolonged exposure (168 h) further lowered IE, with minimum values of 45.44% (40 °C, 7% v/v) and 49.82% (40 °C, 1% v/v). Three-way interactions showed maximum inhibition (77.75%) at 24 h, 60 °C, 7% v/v, and lowest (41.18%) at 168 h, 60 °C, 1% v/v, while 58.74% was maintained at 168 h, 20 °C, 7% v/v. Results indicate that optimal inhibition is achieved under high concentration, short immersion, and moderate temperature, with the extract acting via a combined physisorption–chemisorption mechanism, forming protective films that suppress electrochemical corrosion reactions.

**Keywords:** Aluminium, Banana Leaf, Corrosion, Factor Interactions, Green Inhibitor, Inhibition Efficiency

## 1. Introduction

Corrosion remains a pervasive problem in industrial and engineering systems, leading to structural degradation, economic loss, and safety hazards across multiple sectors such as oil and gas, transportation, and infrastructure [1]. Traditionally, synthetic corrosion inhibitors have been employed to mitigate corrosive attack, but their toxicity and environmental concerns have driven research toward sustainable alternatives [2]. In recent years, green corrosion inhibitors derived from plant extracts have attracted significant attention due to their biodegradability, low cost, and renewable nature [3]. Phytochemical compounds such as alkaloids, tannins, flavonoids, and phenolics exhibit strong adsorption tendencies on metal surfaces, forming protective films that block active corrosion sites and reduce metal dissolution [4].

Plant-based inhibitors have been demonstrated to improve inhibition efficiency with increasing concentration, following adsorption isotherm models such as Langmuir, which describes the interaction between inhibitor molecules and metal surfaces [5]. Electrochemical, weight-loss, and surface analysis techniques have been widely used to evaluate these inhibitors' performance in acidic environments, often showing efficiencies above 60% and in some cases exceeding 90% depending on extract type and conditions [6]. Moreover, studies indicate that temperature and immersion time significantly influence adsorption and film stability, with elevated temperatures often promoting

desorption and reducing protective performance [7]. Despite growing evidence of their effectiveness, comprehensive mechanistic understanding and optimization for practical application remain research priorities [8]. Consequently, investigation into plant-derived inhibitors including their adsorption behavior, thermodynamics, and interaction effects with environmental variables is essential for developing efficient, eco-friendly corrosion mitigation strategies.

## 2. Materials and Methods

### Materials

Analytical-grade reagents were used without further purification, including concentrated $H_2SO_4$ (98%), ethanol, acetone, and distilled water. Standard laboratory equipment such as glassware, analytical balance, and a thermostatically controlled hot plate were employed.

### Plant Collection and Pre-treatment

Fresh *Musa spp.* (banana) leaves were collected from Anyigba, Kogi State, Nigeria. The samples were washed with distilled water, shade-dried for five days to preserve bioactive constituents, ground into fine powder, and stored in airtight containers prior to use.

### Extract Preparation

Forty grams (40 g) of the powdered leaves were extracted using 180 mL ethanol in a Soxhlet apparatus for 4 h. The extract was concentrated and filtered to obtain a uniform stock solution used for inhibitor preparation.

### Phytochemical Analysis

Qualitative screening confirmed the presence of alkaloids, flavonoids, tannins, and saponins. These compounds, rich in heteroatoms and π-electrons, are responsible for adsorption on metal surfaces and corrosion inhibition.

### Aluminium Coupon Preparation

Aluminium specimens (2 × 2 × 0.2 cm) were prepared, perforated, and polished using emery papers. The coupons were degreased with acetone, rinsed, dried, and stored in a desiccator. Initial weights were recorded prior to immersion.

### Corrosive Medium Preparation

A 0.1 M $H_2SO_4$ solution was prepared by diluting 5.43 mL of concentrated acid in distilled water and making up to 1 L. The solution was mixed thoroughly before use.

### Experimental Design and Analysis

Process optimization was conducted using Response Surface Methodology (RSM) with a Box–Behnken Design in Design-Expert® (v13). Seventeen experimental runs were performed to evaluate the effects of temperature, immersion time, and inhibitor concentration at three levels. Model validity and significance were assessed using ANOVA, while response surface and contour plots were used to determine optimal corrosion inhibition conditions.

**Table 1:** Experimental Range of the Independent Variables, With Factor Levels for The Inhibition of Banana leaf Extract on Aluminium in 0.1M $H_2SO_4$ Solution

| Independent Variable | Symbols | Range and Levels | | |
|---|---|---|---|---|
| | | -1 | 0 | +1 |

| | | | | |
|---|---|---|---|---|
| Time of Exposure (h) | $X_1$ | 24 | 96 | 168 |
| Temperature of the solution (°C) | $X_2$ | 20 | 40 | 60 |
| Inhibitor concentration in the extract (v/v) | $X_3$ | 1 | 4 | 7 |

## 3. Results and Discussions

### Box–Behnken Response for Inhibition Efficiency

**Table 1:** Design Matrix and Response for the Inhibition Efficiency by Banana Leaf Extract

| Run | Time (h) | Temp (°C) | Conc. (v/v) | Inhibition Efficiency (%) |
|---|---|---|---|---|
| 1 | 24 | 40 | 7 | 70.78 |
| 2 | 96 | 20 | 7 | 76.82 |
| 3 | 96 | 60 | 7 | 56.65 |
| 4 | 24 | 40 | 1 | 67.65 |
| 5 | 96 | 40 | 4 | 58.87 |
| 6 | 168 | 60 | 4 | 51.19 |
| 7 | 96 | 40 | 4 | 58.87 |
| 8 | 168 | 20 | 4 | 52.74 |
| 9 | 96 | 40 | 4 | 58.87 |
| 10 | 96 | 40 | 4 | 58.87 |
| 11 | 168 | 40 | 1 | 49.82 |
| 12 | 96 | 20 | 1 | 60.84 |
| 13 | 24 | 60 | 4 | 62.49 |
| 14 | 96 | 40 | 4 | 58.87 |
| 15 | 96 | 60 | 1 | 47.76 |
| 16 | 168 | 40 | 7 | 45.44 |
| 17 | 24 | 20 | 4 | 74.31 |

The inhibition efficiency (IE) demonstrates strong dependence on exposure time, temperature, and inhibitor concentration. At 24 h, high efficiencies were recorded, including 74.31% (20 °C, 4 v/v %) and 70.78% (40 °C, 7 v/v %), indicating rapid adsorption and effective film formation. At 96 h, IE slightly declined but remained within 58.87%–76.82%, with a maximum of 76.82% (20 °C, 7 v/v%), confirming the synergistic effect of low temperature and high concentration; however, efficiency decreased at higher temperature (56.65% at 60 °C, 7 v/v%) due to desorption. At 168 h, further

reductions were observed, with values such as 45.44% (40 °C, 7 v/v %) and 49.82% (40 °C, 1 v/v %), suggesting film degradation and depletion of active constituents. Temperature showed an inverse relationship with IE, with higher values at 20 °C (74.31–76.82%) and lower performance at 60 °C (e.g., 47.76% at 96 h, 1 v/v%), consistent with exothermic adsorption. Increasing inhibitor concentration improved IE from 60.84% to 76.82% (96 h, 20 °C), supporting Langmuir-type adsorption. Overall, optimal inhibition occurs at low temperature, shorter exposure time, and higher concentration, while prolonged exposure and elevated temperature reduce effectiveness.

**Main Effects For Inhibition Efficiency By Banana Leaf Extracts**

**Effect of Time**

The main effects plot (Fig. 1) shows that inhibition efficiency (IE) decreases with increasing immersion time. Higher efficiencies at shorter durations indicate rapid adsorption of banana leaf phytochemicals and initial formation of a protective film on the aluminium surface. However, as exposure time increases, IE progressively declines, suggesting deterioration of this protective layer. This reduction can be attributed to continuous metal dissolution due to ongoing electrochemical reactions, as well as gradual desorption of inhibitor molecules [9]. In addition, the accumulation of corrosion products (e.g., oxides and hydroxides) on the surface may trap aggressive species, thereby promoting localized corrosion and weakening the barrier film [10]. Consequently, prolonged immersion reduces surface coverage and overall inhibition performance.

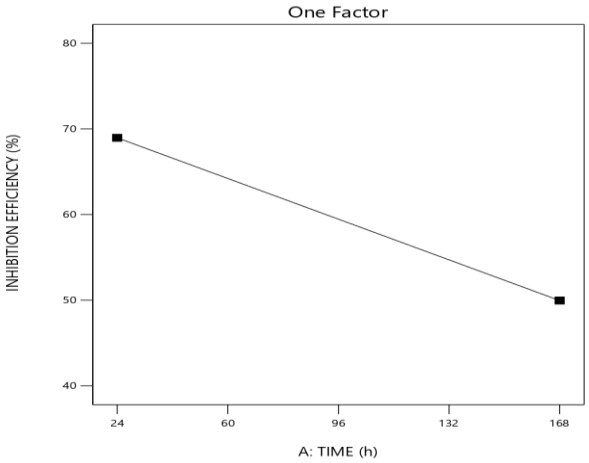



**Figure 1:** Plot of Time on the Inhibition Efficiency by Banana Leaf Extracts

**Effect of Temperature**

The main effects plot (Fig. 2) indicates that inhibition efficiency (IE) decreases with increasing temperature. Higher efficiencies at lower temperatures suggest that adsorption of inhibitor molecules onto the aluminium surface is more stable under mild thermal conditions. As temperature rises, IE declines due to accelerated corrosion kinetics, as elevated temperatures enhance electrochemical reaction rates and increase metal dissolution [11]. Furthermore, increased thermal energy promotes desorption of adsorbed inhibitor molecules, leading to reduced surface coverage and weakening of the protective film. This behavior is consistent with an exothermic adsorption mechanism, where higher temperatures destabilize the adsorbed layer and diminish inhibition performance [12].

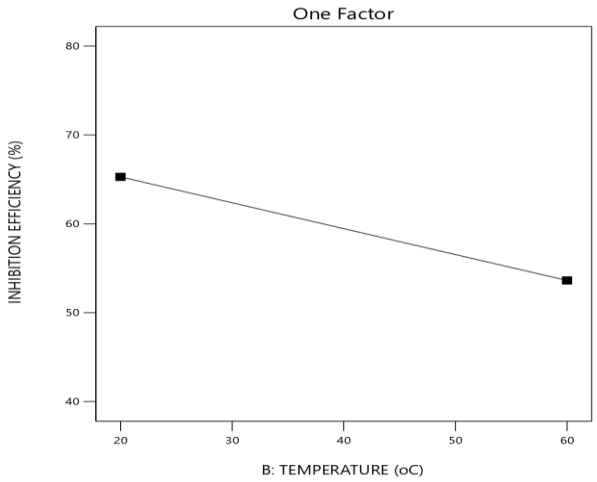



**Figure 2:** Plot of Temperature on the Inhibition Efficiency by Banana Leaf Extract

**Effect of Concentration**

The main effects plot (Fig..3) shows that inhibition efficiency (IE) increases with increasing inhibitor concentration. This trend reflects the enhanced availability of active phytochemical constituents for adsorption onto the aluminium surface. At higher concentrations, more inhibitor molecules interact with the metal, leading to the formation of a more uniform and compact protective film that effectively isolates the surface from the corrosive environment. The improved surface coverage reduces direct contact between the metal and aggressive species, thereby lowering the corrosion rate [13]. Additionally, increased concentration enhances adsorption density, promoting stronger interaction between inhibitor molecules and the metal surface, which contributes to improved inhibition performance [14].

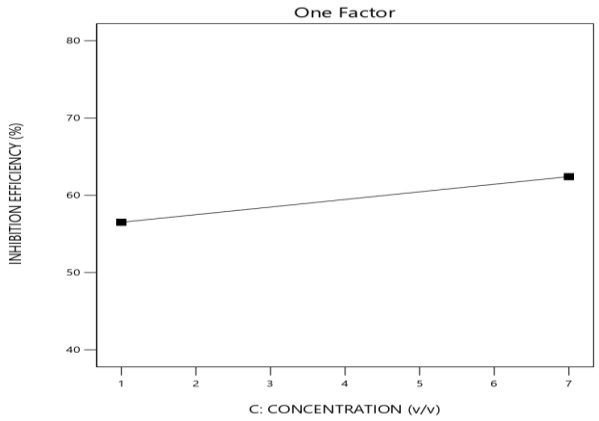



**Figure 3:** Plot of Concentration on the Inhibition Efficiency by Banana Leaf Extract

**Two-Way Interaction Effects**

**Interaction Effect of Concentration and Temperature**

The 3D surface plot (Fig.4) shows that inhibition efficiency (IE) increases with extract concentration but decreases with temperature. At **low concentration (1% v/v)** and **high temperature (60 °C)**, IE is minimal (~38–40%) due to thermal desorption and degradation of active phytochemicals, which weakens the protective film. In contrast, at **high concentration (7% v/v)** and **low temperature (20–25 °C),** IE rises significantly (>68%) as a result of enhanced adsorption and improved surface coverage by compounds such as tannins and flavonoids.

The consistent decline in IE with increasing temperature suggests a physisorption-dominated mechanism, where adsorption is exothermic and less stable at elevated temperatures [15]. Although higher concentrations partly offset thermal effects by supplying more adsorption-active molecules, optimum performance (~70%) is achieved at high concentration and low temperature, indicating better suitability under mild conditions.

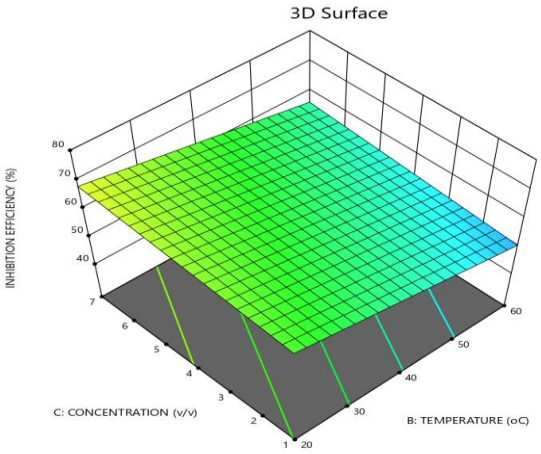



**Figure 3.4:** 3D surface plot of the Interaction of Concentration and Temperature on the Inhibition Efficiency by Banana Leaf Extract

**Interaction Effect of Concentration and Time**

The interaction between concentration and immersion time (Fig. 5) shows that IE increases with concentration but decreases with prolonged exposure. At short immersion time (24 h) and high concentration (7% v/v), IE is high (~78%), reflecting rapid adsorption and formation of a compact protective film. However, with increasing time (168 h), IE declines significantly, especially at low concentration (1% v/v) where values fall below 45%. This reduction is attributed to gradual film degradation, desorption of inhibitor molecules, and competitive adsorption from aggressive ions in the acidic medium [16]. The decline is less pronounced at higher concentrations, suggesting that increased availability of inhibitor molecules helps maintain surface coverage and slows deterioration.

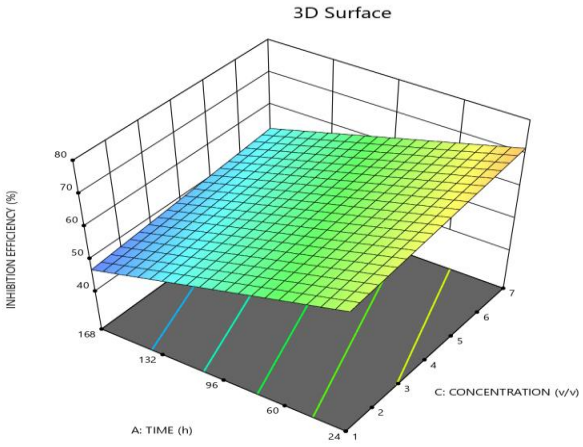



**Figure 5:** 3D surface plot of the Interaction of Concentration and Time on the Inhibition Efficiency by Banana Leaf Extract

**3.3.3 Interaction Effect of Temperature and Time**

The combined effect of temperature and immersion time (Fig. 6) indicates that temperature enhances IE at short exposure, while prolonged time reduces it. At higher temperature (60 °C) and short time (24 h), IE reaches ~70%, likely due to increased molecular mobility and faster adsorption, which promotes formation of a dense protective layer. However, as immersion time increases to 168 h, IE decreases (~50%) across all temperatures due to gradual breakdown and desorption of the inhibitor film. The decline is less severe at higher temperatures, suggesting stronger adsorption interactions, possibly involving partial chemisorption [17]. In contrast, at lower temperature (20°C), the sharper decrease in IE indicates weaker, predominantly physisorbed films that are more susceptible to degradation over time.

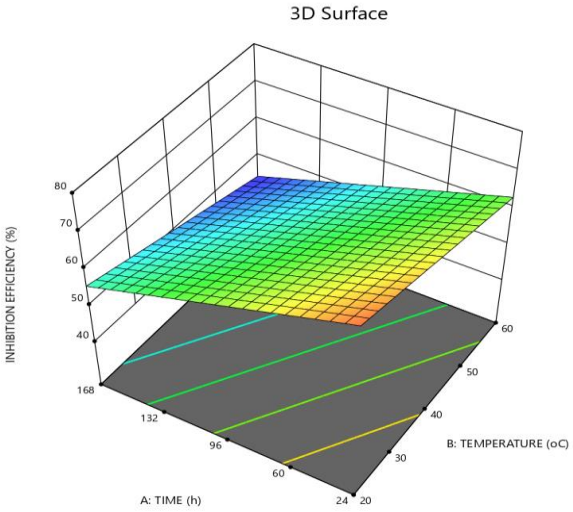



**Figure 6:** 3D surface plot of the Interaction of Temperature and Time on the Inhibition Efficiency by Banana Leaf Extract

**Three-Way Interaction Effects**

**Interaction Effect of Concentration, Time and Temperature**

The combined influence of immersion time, temperature, and inhibitor concentration (Fig. 7) shows clear synergistic and antagonistic effects on inhibition efficiency (IE). The highest IE (77.75%) was obtained at short time (24 h), high temperature (60 °C), and high concentration (7% v/v), indicating rapid adsorption and high surface coverage. This suggests that elevated temperature, when combined with sufficient inhibitor concentration, enhances adsorption kinetics and may promote stronger metal–inhibitor interactions [18]. In contrast, the lowest IE (41.18%) occurred at long time (168 h), high temperature (60 °C), and low concentration (1% v/v). Under these conditions, limited inhibitor availability and prolonged exposure lead to poor surface coverage, film breakdown, and increased penetration of corrosive species [19]. At low temperature (20 °C) and high concentration (7% v/v), IE remained moderately high (58.74% at 168 h), indicating that concentration plays a dominant role in maintaining long-term protection. The availability of more inhibitor molecules likely supports continuous surface coverage, partially offsetting slower adsorption at lower temperatures [20]. Overall, maximum inhibition is achieved at high concentration and short exposure, while prolonged time and low concentration significantly reduce performance, regardless of temperature.

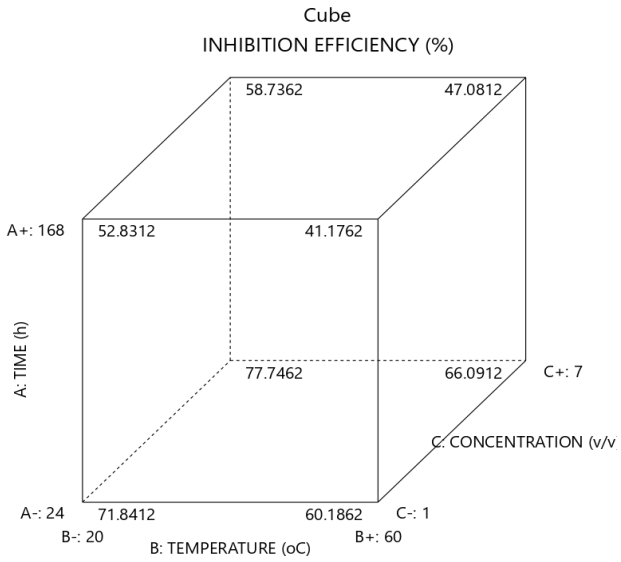



**Figure 7:** 3D surface plot of the Interaction of Concentration and Time on the Inhibition Efficiency by Banana Leaf Extract

**4. Conclusion**

Banana leaf extract effectively inhibits aluminium corrosion in acidic medium, with inhibition efficiency strongly influenced by immersion time, temperature, and inhibitor concentration. High concentrations and short exposure times consistently produced higher efficiencies due to rapid adsorption and dense surface coverage by phytochemicals such as tannins, flavonoids, and polyphenols. Moderate temperature (up to 60 °C) enhanced adsorption and partial chemisorption, stabilizing the protective film, while prolonged exposure and low concentration led to desorption, film degradation, and reduced performance. Two- and three-way interactions confirmed that high concentration can offset thermal and time-related losses, with maximum inhibition (~77.8%) achieved at 7% v/v, 24 h, and 60 °C. These results highlight the importance of optimizing inhibitor dosage, exposure time, and temperature for effective long-term protection.

**References**

[1] Ahmed, M. A., Amin, S., & Mohamed, A. A. (2024). Current and emerging trends of inorganic, organic and eco-friendly corrosion inhibitors. *RSC Advances, 14*, 31877–31920. https://doi.org/10.1039/D4RA05662K

[2] Kumar, A., Thakur, A., & Ebenso, E. E. (2024). Editorial: Corrosion inhibition – Recent advancements. *Frontiers in Chemistry, 12*, 1493419. https://doi.org/10.3389/fchem.2024.1493419

[3] Shathani, P., Ogunmuyiwa, E. N., Obadele, B. A., & Oladijo, O. P. (2025). *Plant leaf extracts as green corrosion inhibitors of steel in acidic and seawater environments: A review*. *Environmental Science and Pollution Research International, 32*(51), 28954–28975.

[4] Sheydaei, M. (2024). *The use of plant extracts as green corrosion inhibitors: A review*. *Surfaces, 7*(2), 380–403

[5] Yusuf, A. A., Hassan, O. T., & Tijani, A. A. (2023). RSM optimization of ginger extract as green inhibitor for mild steel corrosion in hydrochloric acid. *Journal of Molecular Liquids, 381*, 121716. https://doi.org/10.1016/j.molliq.2023.121716

[6] Okore, G. J., Okeke, P. I., Ehirim, A. I., & Ejiogu, B. C. (2025). *Green corrosion inhibition of aluminium in acidic environment using Hibiscus sabdariffa leaf extracts. Journal of Materials Science Research and Reviews, 8*(1), 256–269.

[7] Saha, S. K., Murmu, M., Murmu, N. C., & Banerjee, P. (2022). Adsorption and corrosion inhibition characteristics of plant-derived compounds on metal surfaces in acidic media. *Surface and Coatings Technology, 437*, 128321. https://doi.org/10.1016/j.surfcoat.2022.128321

[8] Fouda, A. S., El-Hossiany, A., & El-Maghraby, A. (2023). Corrosion inhibition and adsorption behavior of eco-friendly inhibitors for metals in acidic environments: Experimental and theoretical insights. *Surface and Coatings Technology, 452*, 129019. https://doi.org/10.1016/j.surfcoat.2022.129019

[9] Wang, X., Yang, H., & Chen, S. (2021). Adsorption and corrosion inhibition behavior of organic inhibitors on metal surfaces: Mechanism and modeling. *Corrosion Science, 182*, 109278.

[10] Fadhil, A. B., Al-Amiery, A. A., & Musa, A. Y. (2020). Adsorption and corrosion inhibition performance of eco-friendly inhibitors on steel surfaces in acidic environments. *Results in Physics, 16*, 102982. https://doi.org/10.1016/j.rinp.2020.102982

[11] Prabhu, R. A., Venkatesha, T. V., Shanbhag, A. V., & Kulkarni, G. M. (2020). Inhibition effects of organic compounds on corrosion of metals in acidic media: A review. *Journal of Molecular Liquids, 317*, 113962. https://doi.org/10.1016/j.molliq.2020.113962

[12] Abdallah, M., Alfakeer, M., Sobhi, M., & Altass, H. M. (2021). Corrosion inhibition of carbon steel in acidic solution using eco-friendly inhibitors: Experimental and theoretical studies. *Journal of Molecular Liquids, 322*, 114987. https://doi.org/10.1016/j.molliq.2020.114987

[13] Kumar, H., Sharma, S., Singh, A., & Verma, C. (2023). Highly efficient green corrosion inhibitor for mild steel in sulfuric acid: Experimental and DFT approach. , 132039. https://doi.org/10.1016/j.colsurfa.2023.132039

[14] Verma, C., Ebenso, E. E., Quraishi, M. A., & Obot, I. B. (2022). Adsorption behavior of organic corrosion inhibitors and their performance evaluation: A review. *Journal of Molecular Liquids, 352*, 118689. https://doi.org/10.1016/j.molliq.2022.118689

[15] Lgaz, H., Salghi, R., Jodeh, S., & Hammouti, B. (2021). Effect of temperature on corrosion inhibition of mild steel in acidic media by organic inhibitors: Kinetic and thermodynamic studies. *Journal of Molecular Liquids, 330*, 115625. https://doi.org/10.1016/j.molliq.2021.115625

[16] Obot, I. B., Madhankumar, A., & Ebenso, E. E. (2022). Evaluation of corrosion inhibition performance of organic inhibitors: Effect of immersion time and adsorption characteristics. *Journal of Molecular Liquids, 346*, 118278. https://doi.org/10.1016/j.molliq.2021.118278

[17] Nnanna, L. A., Owate, I. O., & Nwadiuko, O. C. (2024). Adsorption and corrosion inhibition of mild steel in acidic medium using plant extracts: Effect of concentration and exposure time. *Scientific African, 23*, e01912. https://doi.org/10.1016/j.sciaf.2023.e01912

[18] Ma, Z., Wu, Z., & Xing, F. (2023). Time-dependent corrosion inhibition of steel by organic inhibitors: Mechanism and surface analysis. *Electrochimica Acta, 445*, 141396.

[19] Zhang, W., Wang, H., Liu, Y., & Chen, S. (2022). Adsorption characteristics and synergism between temperature and inhibitor concentration for green inhibitors in acidic media. *Journal of Electrochemical Science and Engineering, 12*(2), 117–132.

[20] Li, Y., Zhang, J., & Li, X. (2021). Multi-factor effects on the corrosion inhibition of carbon steel in acidic solutions: Experimental and statistical analysis. *Corrosion Science, 183*, 109366.

# RADIOLOGICAL ASSESSMENT OF SOIL IN MINING COMMUNITIES: A CASE STUDY IN NASARAWA EGGON, NIGERIA

**Lubis Sati*; Ogori Boniface Otokpa; Bakji Gomerep And Dakup Nenbunka Dunshik**

*Department of Chemistry, Federal University of Education Pankshin Plateau State. Nigeria.*
**Corresponding Author: lubissati01@gmail.com*

**Abstract**

The concentration of natural radionuclides in soil globally has become a significant environmental concern for both international and national authorities, primarily due to the detrimental effects of radiation exposure on human health. In this study, soil samples were collected from three mining communities in Nasarawa Eggon Local Government Area of Nasarawa State viz: Nyakhun, Alizaga, and Gbukhun. These samples were analyzed using a Canberra Model 727/727R Lead Shield Gamma-ray Spectrometer equipped with a NaI(Ti) detector to assess their radionuclide content. The results revealed the following ranges: $^{226}$Ra: from 45.62 ± 1.04 to 78.74 ± 0.64 Bq/kg $^{232}$Th: from 30.08 ± 1.18 to 52.09 ± 0.35 Bq/kg $^{40}$K: from 62.21 ± 0.67 to 100.17 ± 0.24 Bq/kg. The concentration of $^{40}$K was found to be within the world average acceptable limit of 412 Bq/kg, while the levels of $^{226}$Ra and $^{232}$Th were higher than the world averages of 30 Bq/kg and 35 Bq/kg respectively. Further calculations yielded mean values of 127.26 for Radium Equivalent Activity (Raeq), 0.98 for alpha index (Iα), and 0.44 for gamma index (Iγ). The external hazard index (Hex) was 0.34, and the internal hazard index (Hin) was 0.52. The calculated annual gonadal dose equivalent (AGDE) ranged from 301.53 to 492.50 μSv y$^{-1}$, which is significantly higher than the world's average of 30 mSv y$^{-1}$ for soil. Similarly, the calculated values for outdoor absorbed dose rate (Dout), indoor absorbed dose rate (Din), and annual effective dose rate (AEDR) were 0.34, 0.52, and 0.58, respectively. These figures also surpass the world averages of 50 nGy h$^{-1}$, 80 nGy h$^{-1}$, and 0.07 mSv y$^{-1}$. Interestingly, the excess lifetime cancer risk (ELCR), which ranged from 1.58 x 10$^{-3}$ to 2.56 x 10$^{-3}$, was higher than the world average of 0.29 x 10$^{-3}$. These findings suggest that the study area could be classified as radiologically unsafe for residents living within or near these mining communities.

**Keywords**: Radionuclides; Dose rate; Soil; Cancer risk,

## 1. Introduction

Five to eight million people globally have been impacted negatively by radionuclides, while 3.3 million people are at risk in the areas assessed [1]. Since 1960, human exposure to natural radionuclides (naturally occurring radioactive materials (NORMs)) has increased by two or three orders of magnitude [2]. A study on the effects of changes in the environment concluded that a quarter of the global burden of diseases can be attributed to these changes [3]. In other uranium-producing countries such as Canada, Australia and the USA, most mining activities are done in sparsely populated areas or desert-like areas. However, in South Africa, most mining legacy sites are in densely populated areas, [4]. This poses a great risk of contamination through inhaling tailings dust. Human activities result in environmental problems which can pose a threat to the health of those individuals who are occupationally exposed to them and to members of the public who live in the vicinity of, for example, mining areas. Ever since life originally began in the universe, naturally occurring radioactive elements have exposed species including plants and animals to radiation [5]. There are more than 60

radionuclides in nature because of how radioactive our planet is [6]. The sources of radioactivity and the emitters of nuclear radiation that permeate our daily lives are these radionuclides. Everywhere there is radiation, humans are continually exposed to it, either directly or indirectly. Humans are exposed to radiation from a wide range of natural and artificial sources. Ionizing radiation comes from a variety of sources, including mining sites, water, air, soils, and construction materials [6]. We breathe in or absorb radionuclides from the food we eat, and in the water we drink.

Populations in communities may be exposed to radiation from both natural and man-made sources. Both terrestrial and extraterrestrial (space) sources can contribute to the natural radiation that surrounds life on Earth. Ionizing radiation from radionuclides in the earth, rocks, building materials, water, air, and mining sites is referred to as global radiation. Conversely, cosmic rays are high-energy radiation from space that reaches the Earth's atmosphere [7]. Radiation-sensitive elements like $^{238}U$, $^{232}Th$, and the daughter products $^{226}Ra$, According to [8], $^{222}Rn$, $^{235}U$, and $^{40}K$ are significant naturally occurring radiation sources. Ionizing radiation, including α, β, and γ radiations, is released from many terrestrial materials. Among them, soil is a primary source of naturally occurring radioactivity and the primary pathway for radionuclide migration and transfer into the surrounding environment [9].

Numerous investigations have been conducted globally to ascertain the activity content of these radioactive elements, which are the primary causes of natural radiation in soil that humans have contaminated [10]. Geographical location and some human activities influence the extent of these natural exposures. This work was therefore aim at the radiological assessment of soil in mining communities of Nasarawa Eggon, Nigeria

## 2. Materials and Methods

### Materials

The reagents that were used for the research work are 1N Potassium dichromate ($K_2Cr_2O_7$), sodium fluoride, 0.5N ferrous ammonium sulfate $Fe(NH_4)_2(SO_4)_2.6H_2O$, Diphenylamine, Tetraoxosulphate (VI) acid 0.1M $BaCl_2.2H_2O$, and 0.1M $MgSO_4.7H_2O$. The materials that were used for the research work are Canberra Model 727/727R Lead Shield Gamma-ray Spectrometer with NaI(TI) detector, Oven Gallenham England, Hanna pH meter 209 Romania, Labtect digital conductivity meter USA, Beakers, Mortar and pestle, volumetric flask,

### Area of Study

Nasarawa Eggon Local Government Area of Nasarawa State are situated in the central part of Northern Nigeria, on a rugged terrain of lowlands. Five samples were collected each from Barkin Ladi and Jos South, Local Government Area. These areas are the principal centres of tin and columbite mineralization, which forms the focal area of younger granites. The mine tailings are associated with radioactive minerals as impurities such as monazite and zircon among others. These minerals are radioactive and can cause serious hazards to human health during mining and land cultivation for crop production.

### Sample Collection

At each sampling point, about 0.50 kg of the soil sample was collected from a depth of between 0- 20 cm from the surface of the soil, using a clean auger at a distance of 1m away from each other, and within an area of one square meter.

**Sample Analysis.** A gamma ray Spectrometer with NaI(TI) detector, was used to analyze the soil samples for the presence of $^{226}$Ra, $^{232}$Th, and $^{40}$K. The Soil samples were collected into a very clean polythene bag and well-labeled to avoid mixed up of samples. The samples were transported to the centre for energy research and training (CERT), Ahmadu Bello University, Zaria, where the samples were analysed.

### 3. Result and discussion

Table: 1. Summary of the result for the analysis of radionuclides $^{40}$K, $^{226}$Ra, and $^{232}$Th sample collected in Nyakhun, Alizaga and Gbukhun community of Nasarawa State

| Sample ID | $^{226}$Ra (Bq/kg) | $^{232}$Th (Bq/kg) | $^{40}$k((Bq/kg) |
|---|---|---|---|
| Nyakhun | 78.74 ± 0.64 | 52.09 ± 0.35 | 100.17 ± 0.24 |
| Alizaga | 45.62 ± 1.04 | 33.74 ± 1.22 | 62.21 ± 0.67 |
| Gbukhun | 71.91± 2.84 | 30.08 ± 1.81 | 94.33 ± 0.88 |
| Mean value | 65.42 ± 1.50 | 38.64 ± 1.13 | 85.57 ± 0.50 |

The table 1, presents the activity concentrations of three naturally occurring radionuclides $^{226}$Ra, $^{232}$Th, and $^{40}$K in three different samples, Nyakhun, Alizaga, and Gbukhun. The concentrations are measured in (Bq/kg). Nyakhun consistently shows the highest levels of radioactivity for all three radionuclides measured, with concentrations of 78.74 ± 0.64 Bq/kg for $^{226}$Ra, 52.09 ± 0.35 Bq/kg for $^{232}$Th, and 100.17 ± 0.24 Bq/kg for $^{40}$K. Alizaga has the lowest concentrations of $^{226}$Ra 45.62 ± 1.04 Bq/kg and $^{40}$K 62.21 ± 0.67 Bq/kg among the three samples. While the Gbukhun sample has intermediate values for $^{226}$Ra and $^{40}$K, but shows the lowest concentration of $^{232}$Th at 30.08 ± 1.81 Bq/kg. In all three samples, the activity concentration of $^{40}$K is the highest, followed by $^{226}$Ra, and then $^{232}$Th. This is a typical distribution for natural radionuclides in many environmental samples. The average concentrations across the three samples are 65.42 ± 1.50 Bq/kg for $^{226}$Ra, 38.64 ± 1.13 Bq/kg for $^{232}$Th, and 85.57 ± 0.50 Bq/kg for $^{40}$K. These mean values provide a general overview of the radioactivity levels in the area from which the samples were taken. The Nyakhun sample is the most radioactive of the three, and $^{40}$K is the most prevalent radionuclide in all the samples.

Table: 2. Result of the radium equivalent and gamma dose rate of the soil

| Sample ID | $Ra_{eq}$ (Bq/kg) | D(nGyh$^{-1}$) | $D_{in}$(nGyh$^{-1}$) | $D_{out}$(nGyh$^{-1}$) |
|---|---|---|---|---|
| Nyakhun | 160.94 | 72.55 | 101.40 | 72.43 |
| Alizaga | 98.66 | 44.38 | 62.31 | 44.51 |
| Gbukhun | 122.18 | 55.82 | 76.58 | 54.70 |
| Mean value | 127.26 | 57.58 | 80.00 | 57.21 |

Radium Equivalent Activity ( Raeq), is a widely used index to assess the radiological hazard from materials containing primordial radionuclides (like $^{238}U$, $^{232}Th$, and $^{40}K$). A common safe limit for Raeq is 370 Bq/kg. However, in this studies, the mean Raeq value is 127.26 Bq/kg. Individually, Nyakhun has the highest at 160.94 Bq/kg. This is well below the 370 Bq/kg limit. The study's values align with mining area research by [11] who reported mean Raeq of 158 Bq/kg in Indian mining areas. However, some materials exceed this limit as [12] reported clay samples with Raeq up to 748 Bq/kg, with 29% exceeding 370 Bq/kg.

The mean D ($nGyh^{-1}$) value in this study is 57.58 $nGyh^{-1}$ . Nyakhun again shows the highest at 72.55 $nGyh^{-1}$. The worldwide average absorbed gamma dose rate in outdoor air from terrestrial sources is typically around 59 $nGyh^{-1}$. The mean value in this studies is very close to this global average. However, in some mining areas, elevated dose rates are common. Studies in Ghana's gold mining regions reported dose rates ranging from 44 to 120 $nGyh^{-1}$, with a mean value sometimes above the global average [13]. Similarly, research in various mining areas in different countries often indicates localized spots with higher than average dose rates due to the concentration of naturally occurring radioactive materials (NORMs) through mining activities. [14],[15]. The values in this study, while slightly variable, generally fall within or just above typical background levels, but are not as drastically elevated as seen in some more radioactively enriched mining environments.

The reported indoor dose rate of 80 $nGyh^{-1}$ and outdoor rate of 57.21 $nGyh^{-1}$(indoor/outdoor ratio of 1: 40) are consistent with findings from comparable mining and environmental studies, supporting the build-up effect explanation. The indoor/outdoor ratio of 1:40 aligns well with literature values. [16] reported an indoor/outdoor ratio of 1.4 ± 0.5 in urban Cyprus, while [17] found ratios of 1.2–1.4 in Nigerian coal mines. However, [18] reported lower ratios (1:09) in uranium mining areas with indoor/outdoor values of 104/97 $nGy/h^{-1}$ notably higher than the reported values. The reported outdoor dose rate (57.21 $nGy/h^{-1}$) is comparable to [19], which found 78.0 $nGy/h^{-1}$ outdoors. Regarding reference levels, [19] noted their average annual effective dose (0.53 mSv/year) remained below the ICRP-1991 public dose limit of 1 mSv/year, suggesting the reported values likely fall within acceptable exposure ranges.

Table 3: Calculated value of annual effective dose rate,

| Sample ID | AEDR($mSvy^{-1}$) | $H_{ex}$ | $H_{in}$ | Iα(Bq/kg) |
|---|---|---|---|---|
| Nyakhun | 0.73 | 0.43 | 0.65 | 0.39 |
| Alizaga | 0.45 | 0.26 | 0.39 | 0.23 |
| Gbukhun | 0.55 | 0.33 | 0.53 | 0.36 |
| Mean value | 0.58 | 0.43 | 0.52 | 0.98 |

The Mean Value of AEDR was 0.58 $mSvy^{-1}$. The worldwide average annual effective dose from natural background radiation is approximately 1.1 $mSvy^{-1}$ outdoors, and can be higher indoors due to building materials and radon accumulation, with a global average of about 2.4 $mSvy^{-1}$ from all natural sources (including radon inhalation, cosmic rays, and ingestion). The mean AEDR of 0.58 $mSvy^{-1}$ is significantly lower than the global average for outdoor effective dose. This suggests that the external dose from the soil in these areas is relatively low compared to what people experience on average worldwide. A study by [20] in Bida, Niger State, Nigeria, which is known for its mineral deposits,

reported mean annual effective dose rates from soil ranging from 0.26 to 0.48 $mSvy^{-1}$. The values in this studies are slightly higher than those reported in the Bida area, indicating a potentially greater radiological contribution from the soil in this study locations compared to that specific Nigerian region. A research carried out in a lead-zinc mining area in Iran by [21] found mean annual effective dose rates to be around 0.29 $mSvy^{-1}$. Again, the mean AEDR in this study is higher than this specific non-Nigerian mining area, but still generally low when considering the global average. The [7] recommends a maximum annual effective dose rate of 1 $mSvy^{-1}$ for the general public from natural background radiation for risk management purposes. All the individual samples and the mean value are well below this.

The mean External hazard index of 0.43 indicates negligible radiation hazard for construction materials, as all values remain well below the safety threshold of 1.0. The evidence supporting this conclusion is concrete because all individual samples and the mean fall substantially below the critical limit. The findings align closely with comparable mining regions. Studies from Ghana gold mining areas reported Hex values averaging 0.16 [22], while another Ghana study documented a range of 0.22–0.37 [23]. For context, a Nigerian gold mining study reported a higher average of 0.61 [24], though still below unity. In coal mining areas of Zonguldak, Turkey, Hex values in soil were found to range from 0.13 to 0.75, with a mean of 0.39, [25]. The results of this analysis are quite similar to those found in this Turkish coal mining region, suggesting a comparable level of external radiological hazard.

Hin has a mean Value: 0.52 which was similar to the external index, the internal hazard index ( Hin) should also be less than 1 ( Hin<1) to ensure that the internal exposure to radon and its short-lived progeny from building materials does not pose a significant radiological hazard. All samples, and the mean, are well below 1. This indicates that the internal exposure risk, primarily from radon originating from the soil, is low in these locations. The same study in Ghanaian gold mining areas reported Hin values for soil samples generally ranging from 0.2 to 0.6. The values, particularly Nyakhun's 0.65, align well with the higher end of the range found in some gold mining regions, suggesting a comparable internal hazard potential [22]. The study in Zonguldak, Turkey, showed Hin values in soil ranging from 0.17 to 0.99, with a mean of 0.52, [26]. This mean Hin is identical to the mean found in this Turkish coal mining area, pointing to similar internal radiological hazard characteristics.

Alpha Index ( Iα) in this study has a mean Value of 0.98 Bq/kg which is below the 1 Bq/kg. The recommended upper limit for the alpha index, below which materials are safe for use without special precautions regarding radon exhalation, is 1 Bq/kg. This indicates that the radon exhalation risk from the soil is generally low or acceptable. Evidence from Nigerian mining sites supports this finding. [27] measured Iα values in Erena mining sites and the result ranges from 0.1165 to 0.3766 Bq/kg, all below the maximum permissible limit of 1 Bq/kg. Similarly, [28] reported an alpha index of 0.31 Bq/kg in Iperindo mining areas, also below the recommended threshold. In Ilesha, Osun State, Nigeria, an area with significant gold mining activities, Iα values in soil have been reported to range from 0.1 to 0.8 Bq/kg, [29].

Table 4: Calculated value of $I_\gamma$ AGDE and ELCR in the soil sample

| Sample ID | $I_\gamma$ (Bq/kg) | AGDE ($\mu SvY^{-1}$) | ELCR |
|---|---|---|---|
| Nyakhun | 0.55 | 492.50 | $2.56 \times 10^{-3}$ |

| | | | |
|---|---|---|---|
| Alizaga | 0.34 | 301.53 | $1.58 \times 10^{-3}$ |
| Gbukhun | 0.42 | 377.55 | $1.93 \times 10^{-3}$ |
| Mean value | 0.44 | 390.53 | $2.02 \times 10^{-3}$ |

The Mean Value: 0.44 (with individual values ranging from 0.34 to 0.55). The recommended upper limit for Iγ for materials used in dwellings is 1.0 to ensure that the annual effective dose from gamma radiation does not exceed 1 mSv. If Iγ exceeds 1.0, it is considered unsafe. All the individual samples and the mean value are well below this limit. This is a positive indicator that the soil from these areas, if used as building material, would likely not contribute to elevated gamma radiation doses indoors. [30],[31] both calculated Iγ values in building materials, finding values between 0.5–1.0, similar to your range. [32] reported gamma-index values from 0.15–0.89 in Turkish building materials, providing additional regional comparison data. Additional relevant studies include [33] on Egyptian and international building materials respectively, plus [34] on Turkish building materials and indoor gamma doses. These collectively provide robust comparative data across multiple geographic regions and mining contexts. This suggests a potentially lower, or at least comparable, radiological impact in your study sites compared to some other coal mining regions. In a phosphate mining area in Egypt, Iγ values for soil were reported to range from 0.3 to 2.1, with a mean of 0.82, showing some samples exceeding the recommended limit

The mean of 390.53μSvY$^{-1}$ in the studied area is approximately 30% higher than the global average of 300 μSvY$^{-1}$ indicating elevated gonadal radiation exposure comparable to other mining areas. In Nasarawa State, Nigeria, AGDE values ranged from 180.5 to 550.2 μSvY$^{-1}$ with a mean around 350 μSvY$^{-1}$ [35], closely matching the study's mean of 390.53 μSvY$^{-1}$. A Malaysian tin mining area reported AGDE values between 140 and 680 μSvY$^{-1}$ with an average of 290 μSvY$^{-1}$, placing the study's individual values (301.53–492.50 μSvY$^{-1}$) well within this range. The Nyakhun location at 492.50 μSvY$^{-1}$ represents the upper end of observed values. Additional evidence from Nasarawa mining sites documented AGDE values of 0.56–0.73 mSv yr$^{-1}$ [35], with maximum gonadal doses reaching 0.58 mSv y$^{-1}$ at copper mining sites [36], nearly double the global average and suggesting significant genetic risk with continuous exposure.

Excess Lifetime Cancer Risk (ELCR)

The mean ELCR of this study is $2.02 \times 10^{-3}$ , this is about 7 times the [7] baseline of $0.29 \times 10^{-3}$ and double the upper bound of the acceptable outdoor range. Nyakhun's $2.56 \times 10^{-3}$ is the most concerning. [37] reported marble samples from Ungwar Damishi with mean ELCR of $2.17 \times 10^{-3}$ (above UNSCEAR's $0.29 \times 10^{-3}$ baseline), while Gidan Waya marble averaged $0.150 \times 10^{-3}$ (below baseline). [38] found dumpsites in Plateau State with mean ELCR of $0.45 \times 10^{-3}$, exceeding the world average. [39] reported hospital soils with ELCR values ranging from $0.07–0.10 \times 10^{-3}$ (within acceptable limits).

Internationally, [40] documented the Lumoru dumpsite in Kenya at $0.30 \times 10^{-3}$ A. [41] reported Yelagiri Hills, India with mean ELCR of $0.700 \times 10^{-3}$ (twice the world average). These studies collectively demonstrate geographic variation in ELCR, with Nigerian sites showing the highest elevations.

## 4. **Conclusion**

The results for AEDR, Hex, Hin, and Iα generally indicate a low to moderate radiological risk from the soil in Nyakhun, Alizaga, and Gbukhun. All calculated hazard indices and dose rates are below international safety limits and guidelines. Both Hex and Hin being less than 1 is a crucial indicator that using these materials for construction or living in these areas (regarding external gamma and internal radon from soil) is generally safe from a radiological perspective. The AEDR is lower than the global average, which is reassuring. Consistent with Other Non-Uranium Mining, the values align reasonably well with those found in other non-uranium mining areas both within and outside Nigeria (like Bida, Ghana, Turkey), often falling within or slightly above their reported ranges. This suggests typical natural radioactivity levels, possibly with minor enhancements due to geological composition or mining processes, but not indicative of severe radioactive contamination.

## **References**

[1] A. McCartor, and D. Becker, "*Top Six Toxic Threats, World's Worst Pollution Problems Report"*. New York: Blacksmith Institute, https://www.worstpolluted.org/files/ FileUpload/files/2010/ WWPP-2010-Report-Web.pdf (25 January 2025).

[2] H. Ahmed, S. D. Young, and G. Shaw, "Factors affecting uranium and thorium fractionation and profile distribution in contrasting arable and wood land soils". *J Geochem Explor*; Vol. 145, pp. 98–105, 2014.

[3] S. S. Myers, L. Gaffikin, C. D. "Golden, Human health impacts of ecosystem alteration". *Proc Natl Acad Sci*; vol. 110, pp. 18753–60, 2013.

[4] F. Winde, and E. Hoffmann, "Virtual geographical environments as a tool to map human exposure to mining-related radionuclides". In: Merkel B. J, Arab, A. (eds). *Uranium-Past and Future Challenges: Proceedings of the 7th International Conference on Uranium Mining and Hydrogeology. Springer International Publishing*: Cham, 193–200. 2014

[5] B. S Banari, "The Calculation of the Annual Effective Dose Due to Exhalation of Radon Progeny in Iran". *Journal of Applied Environmental and Biological Sciences*, vol. **5**, 609–613 2015.

[6] S. S. Obaid, D. K. Gaikwad, and P.P Pawar, "Determination of natural radioactivity and hazard in some rock samples". *Bionano Frontier*, Vol. **8** No.3, pp 125–127, 2015.

[7] UNSCEAR. (2000). Sources, Effects and Risks of Ionizing Radiation, United Nations Scientific Committee on the Effects of Atomic Radiation. United Nations.

[8] L. A. Najam, S. A.Younis, and F. H. Kithah, "Natural radioactivity in soil samples in Nineveh Province and the associated radiation hazards". *International. Journal of Physics*, vol. 3 no.3, 126–132, 2015

[9] A. H. Taqi, A. M. Shaker, and A. A. Battawy, "Natural radioactivity assessment in soil samples from Kirkuk city of Iraq using HPGe detector". *International Journal of Radiation Research,* vol. **16** no. 4, pp 455–463, 2018

[10] K. Thabayneh, "Natural radioactivity levels and estimation of radiation exposure in environmental soil samples from Tulkarem Province–Palestine" 2012.

[11] S. Mittal, R. Mehra, & N. Grewal, "Radiological Hazard Indices and Dose Rates From 238U, 232Th, and 40K in Soils of Mining Areas of Northern Rajasthan". *Journal of Nuclear Engineering and Radiation Science*, vol.12 no. 1 012004- 012010, 2026.

[12] J. A. dos Santos Júnior, E.E.N. de Araújo, Z. H. Fernández, R. dos Santos Amaral, J.M dos Nascimento Santos, M. O. and M. O. Milán, "Measurement of natural radioactivity and radium equivalent activity for pottery making clay samples in Paraíba and Rio Grande do Norte–Brazil". *Environmental Advances*, vol. 6, 100121-100127, 2021

[13] A. Faanu, L. Tettey-Larbi, E. O. Akuo-Ko, P. K. Gyekye, D.O. Kpeglo, H. Lawluvi, and A. Shahrokhi, "Radiological landscape of natural resources and mining: Unveiling the environmental impact of naturally occurring radioactive materials in Ghana's mining areas". *Heliyon*, vol. 10, no. 3, pp 102-115, 2024.

14] A. Mugaiga, E. Jurua, R. Oriada, and S. Turyahabwa, "Radioactivity levels and dose rates from rocks in selected mining areas and quarries in eastern Uganda". *Int J Res Eng Technol*, vol. *5* no.3, pp, 5-11, 2016.

[15] L. N. Engola, J. E. N. Nkoulou II, M. Hosoda, D. Bongue, N. Akata, R.K. Heya, and S. Tokonami, "Air absorbed dose rate measurements and external dose assessment by car-borne survey in the gold mining areas of Betare-Oya", *Eastern-Cameroon*. Vol 53, no. 1, 5-11, 2018.

[16] E. Svoukis, and H. Tsertos, "Indoor and outdoor in situ high-resolution gamma radiation measurements in urban areas of Cyprus". *Radiation Protection Dosimetry*, vol. 123 no 3, pp 384-390, 2007.

[17] C.E. Mokobia, and F.A. Balogun, "Background gamma terrestrial dose rate in Nigerian functional coal mines". *Radiation protection dosimetry*, vol. 108 no. 2, pp 169-173, 2004.

[18] N. Karunakara, I. Yashodhara, K. S. Kumara, R. M. Tripathi, S. N. Menon, S. Kadam, and M. P. Chougaonkar, "Assessment of ambient gamma dose rate around a prospective uranium mining area of South India–a comparative study of dose by direct methods and soil radioactivity measurements". *Results in Physics*, vol. 4, pp, 20-27, 2014.

[19] Suresh, S., Li, P., Hao, C., & Neville, J. (2021). Adversarial graph augmentation to improve graph contrastive learning. *Advances in Neural Information Processing Systems*, *34*, 15920-15933.

[20] E. H. Agba, A. T. Ramli, and M. S. M. Sanusi, "Assessment of Natural Radioactivity and Radiological Hazard Parameters of Soil Samples in Bida, Niger State, North-Central Nigeria'. *Journal of Radiation Research and Applied Sciences,* vol. 11 no. 3, pp. 209-216, 2018.

[21] J. Karami, and A. Behrooz, "Radiological hazard assessment due to natural radionuclides in soil, rock and water samples in a lead-zinc mining area". *Journal of Environmental Radioactivity*, vol. 246, pp. 106829- 106834, 2022.

[22] A. Faanu, E. O. Darko, and J. H. Ephraim, "Determination of Natural Radioactivity and Hazard in Soil and Rock Samples in a Mining Area in Ghana". *West African Journal of Applied Ecology*, vol. 19, no. 1, pp 77-92, 2011.

[23] F. Otoo, E.O. Darko, G. Emi-Reynolds, A. B. Andam, and O.K. Adukpo, "Radiological impact of soil as a source of building material". *Radiation Protection and Environment*, vol. 35 no.1, pp. 22-28, 2012.

[24] G. Top, Y. Örgün, G. Karahan, M. Horvath, and G. Kampfl, "Effects of local building materials on indoor gamma doses and related radiological health risks, Ayvacik, Çanakkale/Turkey". *Radiation Protection Dosimetry*, vol. 190, no. 1, pp. 108-117, 2020.

[25] O. Baykara, G. Toprak, and T. Sari, "Assessment of gamma dose rate andradium equivalent activity in soil samples of coal mining area of Zonguldak, Turkey". *Radioprotection*, Vol. 55 no. 2, pp. 99-106, 2020.

[26] Emirhan, M. E., & Ozben, C. S. (2009). Assessment of radiological risk factors in the Zonguldak coal mines, Turkey. *Journal of Radiological Protection*, *29*(4), 527-534.

[27] I. Suleiman, M. Agu, and M. Onimisi, "Evaluation of naturally occurring radionuclide in soil samples from Erena mining sites in Niger State, Nigeria". *Current Journal of Applied Science and Technology*, Vol. 27, No. 6, pp. 1-12, 2018.

[28] F. R. Amodu, F. Ben, A. T. Agbele, B. N. Ben-Festus, and O.A. Oyebanjo, "Assessment of radionuclide concentration and associated risks in soils from Iperindo mining sites, Nigeria". *Discover Environment*, Vol. 2. No. 1, pp. 17-25, 2024.

[29] P. K. Olasehinde, D.O. Olawuyi, and T.G. Akerele, "Radioactivity assessment of soils around active gold mining areas in Ilesha, Southwestern Nigeria". *Journal of Environmental Radioactivity*, Vol. 172, pp. 268-275, 2017.

[30] K. Asaduzzaman, F. Mannan, M. U. Khandaker, M. S. Farook, A. Elkezza, Y. B.M. Amin, and H. B Abu Kassim, "Assessment of natural radioactivity levels and potential radiological risks of common building materials used in Bangladeshi dwellings". *PLoS one*, Vol. 10 No. 10, e0140667, 2015.

[31] R. Raghu, R. Ravisankar, A. Chandrasekaran, P. Vijayagopal, and B.Venkatraman, "Assessment of natural radioactivity and radiological hazards in building materials used in the Tiruvannamalai District,

Tamilnadu, India, using a statistical approach". *Journal of Taibah University for Science*, Vol. 11 No. 4, pp. 523-533, 2017.

[32] S. Turhan, U.N. Baykan, K. Şen, "Measurement of the natural radioactivity in building materials used in Ankara and assessment of external doses". *Journal of Radiological Protection*, Vol. 28 No. 1, pp. 83-91, 2008.

[33] A. El-Taher, "Environmental radioactivity and gamma-ray dose rates in a phosphate mining area in Egypt". *Journal of Environmental Radioactivity*, Vol. 101 No. 12, pp. 1056-1061, 2010.

[34] G. Top, Y. Örgün, G. Karahan, M. Horvath, and G. Kampfl, "Effects of local building materials on indoor gamma doses and related radiological health risks, Ayvacik, Çanakkale/Turkey". *Radiation Protection Dosimetry*, Vol. 190, No. 1, pp. 108-117, 2020.

[35] J. I. Abaleni, and A. M. Nnamdi, "Assessment of Activity Concentration and Health Hazards of Radiation Exposure in Soil from Mamara Jidda and Waja Tin Mining Sites in Northern Nasarawa State, Nigeria". *Physics Access*, Vol. 4. No.2, 100-106, 2024.

[36] A. S. Aliyu, U. Ibrahim, C. T. Akpa, N. N. Garba, and A. T. Ramli, "Health and ecological hazards due to natural radioactivity in soil from mining areas of Nasarawa State, Nigeria". *Isotopes in environmental and health studies*, Vol. 51, No. 3, pp. 448-468, 2015.

[37] G.P. Musa, B. I. Ayodeji, N. Kure, and I. H. Daniel, "Evaluation of Excess Lifetimes Cancer Risk for Environmental Exposures in Kaduna, Nigeria". *Physics Access*, Vol. 5. No. 2, pp. 23-29, 2025.

[38] D.N. Hosea, M. Y. Iliya, and A. Simdet, "Assessment of Background and soil dumpsites radioactivity in Plateau State, Nigeria". *Physics Access*, Vol. 4. No. 2, pp. 63-72, 2023.

[39] I. E. Okwor, C. E. Akulor, and U. M. Ukewuihe, "Investigation of natural radioactivity in soil of selected hospitals in Imo State, Nigeria". *Science World Journal*, Vol. 18 No. 4, pp. 633-640, 2023.

[40] B. Wanjala, R. W. Nyukuri, H. E. Kibe, and J. W. Makokha, "Environmental Radiation Exposure and Lifetime Cancer Risk at Lumoru Dumpsite, Western Kenya". *Open Access Library Journal*, *12*, e14461, 2025.

[41] A. Chandrasekaran, R. Ravisankar, G. Senthilkumar, K. Thillaivelavan, B. Dhinakaran, P. Vijayagopal, and B. Venkatraman, "Spatial distribution and lifetime cancer risk due to gamma radioactivity in Yelagiri Hills, Tamilnadu, India". *Egyptian Journal of basic and applied sciences*, Vol. 1. No. 1, pp. 38-48, 2014.

# SYNTHESIS AND CHARACTERIZATION OF GREEN THERMOPLASTIC COMPOSITES FILMS REINFORCED WITH JUTE FIBER

**Gumel, B.U.[1], Gumel S.M.[2], Umar,A.[3], Auwal A.S.[2], Isah R.A.[4], Garba, Z.N[5*]**

*[1]Science Department, Jigawa State College of Remedial and Advanced Studies,(JICORAS), P.M.B. 2020, Yar Kirya Road Babura, Local Government.*
*[2]Depertment of Pure and Industrial Chemistry, College of Natural and Pharmaceutical Sciences, Bayero University Kano.*
*[3]Department of Chemistry, Faculty of Applied Sciences, Sule Lamido University Kafin Hausa.*
*[4]Kano State College of Education and Preliminary Studies*
*[5]Department of Chemistry, Ahmadu Bello University, Zaria, Nigeria*
**Corresponding Author: dinigetso2000@gmail.com*

## Abstract

The rapid use of synthetic polymers in the manufacture of thermoplastics is a major cause of concern in every field of human activities in the current decades. This leads to increase in the environmental concern which consequently leads to the need for an environment friendly alternative that will offer biodegradable material and better performance than the classical materials. The use of composites in many industrial applications, such as automotive, sports, construction, packaging materials and biomedical applications is gaining utmost attention. The development of an eco-friendly or green composites has become an important trend for the industries and the society at large owing to increase awareness about environmental pollution caused by synthetic materials. Thus, there is great interest in the use of reinforcement and matrices obtained from renewable resources such as natural fibers and biopolymers. In this study, a starch-based Plastics (SBP) was synthesize from sweet potato peel waste as Matrix reinforced with variable content of Jute Fibers (0, 2.5, 5.0, 7.5 and 10.0 g each). The composites were characterized for mechanical properties, Thermal stability and morphological properties as well. The results shows better performance at concentration dependent manner the fibers. However, fiber content above 7.5g of Jute fiber experienced a decreased in tensile strength.

**Keywords:** *Potato peel Waste, SBP Resin, Jute Fibers, Mechanical Performance, thermal stability and Green Composite.*

## 1. Introduction

Plastics are prevalent in almost every human activity. However, their expansion in use has become a source for Environmental concern due to their negative impact especially where they are used for a short period of time before disposal. Plastic wastes especially packaging materials that float or litter the oceans, rivers, seas, and lakes are major threat for birds, fish and other animals in those habitats [1]. Most plastics take long time for up to 10 centuries to decay in nature due to their resistance against action of microorganism and other environmental factors. Lack of degradability of conventional plastic as well as growing water and land pollution problems have led to growing concerns about plastics which make it necessary to find a solution and prevent accumulation of thousands tons of solid wastes every year. Awareness of the plastic waste problem and its impact on the environment has awakened keen interest in the area of degradable polymers leading to increasing demand to develop materials with little or no burden on the environment [2].

One of the most interesting bio-based plastic is starch based plastics. It is an aliphatic polyester from plants, readily biodegradable developed to serve as an alternative to conventional polymers. Starch based plastics is the only thermoplastic polymer based on natural resources which can be produced with a capacity of over 140,000 tons per year [1]. Starch $(C_6H_{10}O_5)n$, is a biopolymer of natural origin. It composed of anhydrous glucose units linked by alpha-D glycosidic bonds which are arranged to form a linear chain structure (amylose) and a polymeric branched chained structure (amylopectin) within the starch molecule. Starch is isolated from Cereal grains e.g.(Corn, Wheat and Rice) and Roots for example (Tapioca, Sweet potato) [3]. However, it has been reported that, Corn starch is the most commonly used in the production of thermoplastics due to it's relative abundance and spherical shape which causes minimal disturbance in the flow during processing [4]. However, sweet potato starch shows better and bright prospective in thermoplastics production because of it's high yield starch content and high amylose content that makes it a good candidate for making thermoplastic starch materials [3]. Composite have been found to be most promising in order to tailor the cost of materials and improve the properties of the materials, in terms of strength, stiffness, density and lower cost with improved sustainability.

Fillers are inert materials added to a polymer matrix to modify or enhance its properties. The primary function of fillers in composites is to improve the properties of the composites and/or reduce cost of the composite materials. Fillers can be natural or synthetic with varying shape, size or composition, based on the desired outcome of the composite [3]. The use of natural fillers in fabrication of composites have friendliness advantages on the environment, these advantages include, high strength, Light-weight, corrosion resistance, low cost, low density, abrasion resistance, non-irritating to skin, reduced energy consumption, lower health risk, renewability and biodegradability which allow fiber/polymer composites application to be extended in near future [5]. Jute fiber is composed of small unit of cellulose surrounded and cemented together by lignin and hemicelluloses. The main disadvantage encountered during the incorporation of natural lignocellulosic materials in polymer composites is the lack of good interfacial adhesion between the polymer matrix and the reinforcement due to the presence of these non-cellulosic materials consequently deteriorating the mechanical properties of the composites.

The aim of this research is to synthesize a green plastic composite from Potato peel waste starch reinforced with jute fibers, to enhance high specific properties, such as light weight, low cost, and eco-efficiency in all stages of life.

## 2. Materials and Methods

### Materials

The potato waste used for the production of starch was obtained from a local potato chips vendor at Kabuga Gwale local Government, Kano State. while the baobab used for the extraction of Boabab fiber was obtained from the baobab tree at Dan Zaki Village, Gezawa Local Government Kano State. The Jute stalks used for the extraction of Jute fibers was obtained from a local farmer at Gumel Local Government.

**Chemical Reagents:**

The Chemical reagents used in this research includes Hydrochloric Acid (HCl), Sodium Hydroxide (NaOH), Ethanol, Acetic Acid, Tetrahydrofuran (THF) (Sigma Aldrich) were procured from Polymer Chemistry Laboratory, Bayero University Kano. Potato dextrose Agar was obtained from Microbiology Laboratory Bayero University Kano. All other chemicals used were analytical reagents grade, including glycerol, sorbitol, and ammonium oxalate.

**Apparatus and Equipment**

In addition to laboratory glass wares, apparatus and instruments used in this research were; Fourier Transform Infrared Spectroscopy (Carry 630), Incubator shaker (Innova 4000), hot air oven, Scanning Electron Microscope (SEM), Tensile Tester, X-ray Diffractometer.

**Extraction of Jute Fibers**

Jute Fibers were extracted from the Jute plant using slightly modified method by [6]. In this process the Jute stalks were soaked in enough quantity of water and allowed to stand for two weeks, to enable the growth of microorganisms (Bacteria and Fungi), that would breakdown the soft tissues from the stalks leaving the cellulose intact. The stalks were removed and the fibers washed and dried.

**Alkaline Treatment of Jute Fibers**

For bonding between the plastic matrix and the fiber reinforcement, the fibers were treated with sodium hydroxide solution (Mercerization). The process is used to reduce the amorphous nature of jute fibers thereby decreasing the fiber diameter and thus increasing the aspect ratio [7]. Mercerization enhances the crystalline nature of the fibers resulting in a coarse surface topography which consequently increases the interfacial bonding and the mechanical strength [8]. In this process the raw fibers (10g) each were soaked in 5% NaOH solution at 100°C for 3 hours to activate the OH groups of the fibers by introducing ($Nà^{+}$) onto the back bone of the fibers. The treated fibers were then washed with distilled water and neutralized with 5% acetic acid and then oven dried at 50°C for 24 hours.

**Extraction of Potato peel starch**

To prepare sweet potato peel starch, a method adopted by [9], was employed. In this process, 500g of the potato peel was crushed and powdered to obtain the fine powder by sieving through a 250m mesh. 200g of the fine powder was mixed with 600ml of water and stirred for 10 minutes to obtain the starch suspension. The mixture was allowed to settle for 3 hours. Then, the fine starch was separated from the liquid by gently decanting the water part. The solid part was then oven dried at 50°C for 72hrs. The dried fine powder was stored in an airtight container before use. Potato peel waste was founded into powdery form and 250g mixed with water at solid to liquid ration of 1:3 blended for 10min. the meshed potato was filtered using Mushin cloth and allowed to stand for 6hrs to form starch sediment at the bottom of the container. The sediment was separated from the liquid by decantation. The solids are than oven dried at 50 °C for 72hours. The dried fine powder was stored in an airtight container before use.

**Preparation of Starch Based Plastics.**

Potato peel starch was used as the matrix at variable mass of (5, 10, 15, 20 and 25). Glycerol was used at 5ml/mixture to serve as plasticizer to increase the plasticity and flexibility of the plastic. Hence the green plastic was prepared by measuring 100ml of distilled water in a 1L beaker, 15g of the potato peel powder was added to the beaker and the mixture was stirred with a glass rod. The mixture was heated to about 120˚C until gelation of the starch was achieved. The starch solution was allowed to cool, after cooling, 5ml of glycerol, 5ml of 0.1M HCl and variable amount of castor oil(2,3,4,5 and 6g) based on water content were added to each mixture respectively. The mixtures were heated at 70˚C for 15min until the mixtures became transparent. The mixtures were poured each in a mold lined with a foil paper and allowed to cool at room temperature for 3-days. The plastics were then baked at 30˚C for 15 minutes and then allowed to cool at room temperature for 24 hours. The plastics were removed each from the Aluminium foil and packed in a glass container. The procedure was repeated using 20g, 25g and 30g. Thus, 20 samples were prepared and the composition of the starch based plastic (SBP) is depicted in table 1.

**Table 1**: Composition of five samples of starch based plastics.

| Sample | PPW starch(g) | Distilled water(ml) | Castor oil(g) | Glycerol (ml) |
|---|---|---|---|---|
| SBP -1 | 15. 00 | 100 | 2 | 5 |
| SBP -2 | 15. 00 | 150 | 3 | 5 |
| SBP -3 | 15. 00 | 200 | 4 | 5 |
| SBP -4 | 15. 00 | 250 | 5 | 5 |
| SBP -5 | 15.00 | 300 | 6 | 5 |

**Fabrication of the Composite**

The green composite was prepared by using 50g of the starch based plastic for each batch of the formulation, while varying the fiber content. The composition of the composite is depicted in table 2.

**Table 2:** Composition of the green thermoplastic composites

| S/N | Starch-based plastic (g) | Jute fiber content (g) |
|---|---|---|
| 1 | 50 | 0 |
| 2 | 50 | 2.5 |
| 3 | 50 | 5.0 |

| | | |
|---|---|---|
| 4 | 50 | 7.5 |
| 5 | 50 | 10.0 |

For each batch of the composite, 50g of the starch based plastic was mixed with appropriate amount of the fibers as follows;

For each batch, the plastic was heated between heated rollers at 120°C for 15 minutes for proper mixing. The fibers (Jute) were cut into 1mm length each. Both the milled plastic and the appropriate fiber content were mixed between the heated rollers 15minutes at 70°C and a Pressure of 16 Mpa. The milled composite was scraped and placed on a steel mold (150 X 150mm X 3mm) coated with a thin layer of silicon oil solution (as releasing agent) and placed between the cavities of the Compression molding Machine. The mold was compressed at 130°C and a Pressure of 16Mpa for 15 minutes. The composite was cooled to ambient Temperature, de-molded and labeled appropriately

**Characterization Process**

The green thermoplastic composites were characterized using the following methods: Fourier Transform infrared Spectroscopy (FTIR), Mechanical properties (Tensile strength, elongation at break), Thermogravimetric Analysis (TGA/DTA) and Scanning Electron Microscope (SEM)

## 3. Results and Discussion

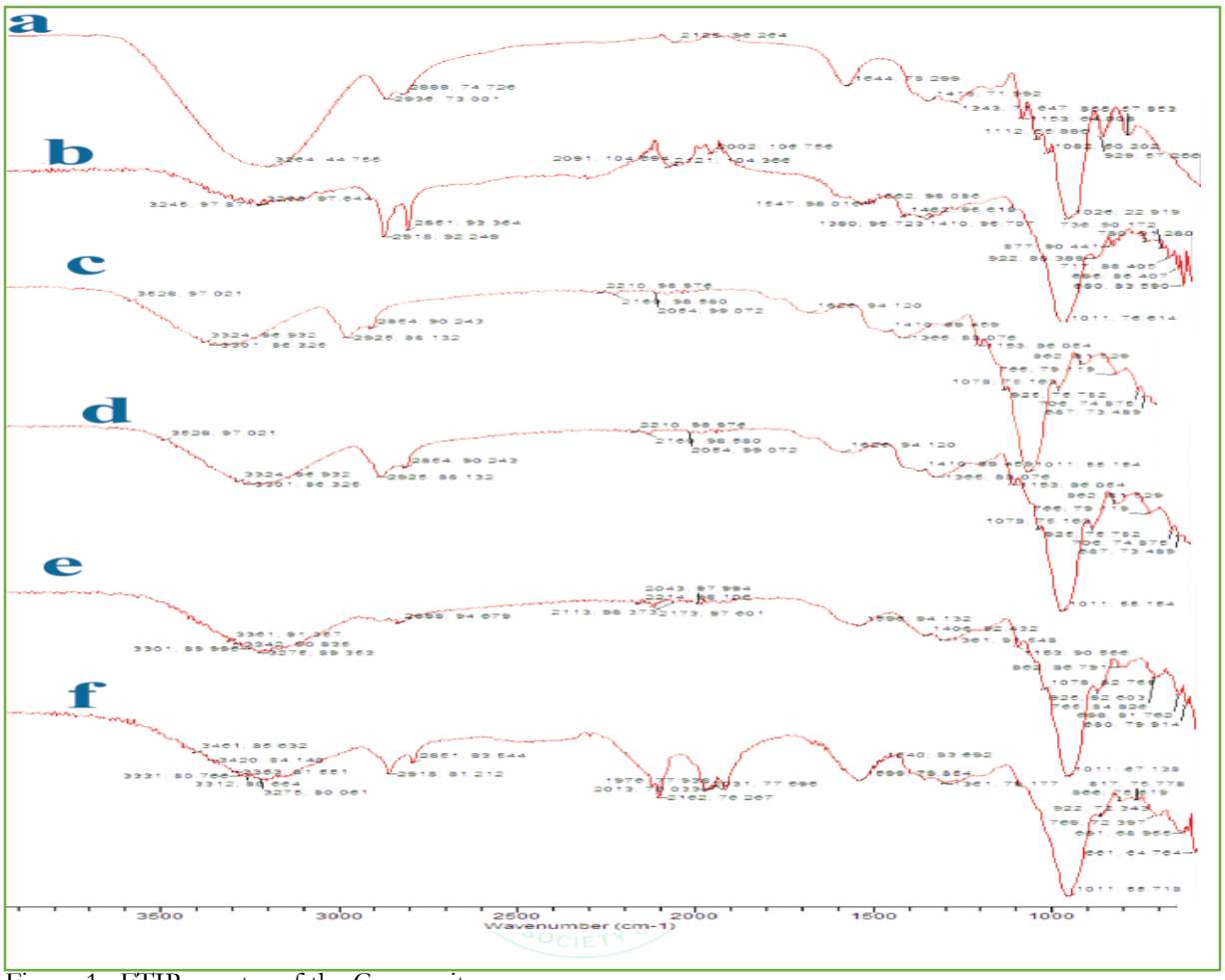



Figure 1 : FTIR spectra of the Composites.

From figure 1 it was observed that spectral data reveal prominent peak in the range of 3200 -3600 $cm^{-1}$ (assigned to O-H stretching) and 2900 -2800$cm^{-1}$ (assigned to C-H stretching) were found for all characterized materials. Three vibrational bands were observed in the potato peel, starch based plastics and the composites at 1739 $cm^{-1}$, 1514 $cm^{-1}$ and 1456 $cm^{-1}$, with the former band attributed to the C=O stretching vibration of acetyl groups of hemicellulose as well as the ester linkage of the carboxyl group in lignin [3] and the latter two bands were assigned to the C=C vibration in lignin. The region of 800-1500 $cm^{-1}$ is a unique fingerprint region for cellulose where the majority of peaks in that range were found for all samples, indicating that regardless of alkali or acid treatment the cellulose maintained a similar chemical structure to the original untreated species.

**Scanning Electron Microscope (SEM)**

The results of the Scanning electron microscope of both Jute Fibers and the prepared plastics were shown in figure 1. (1-5j) respectively.

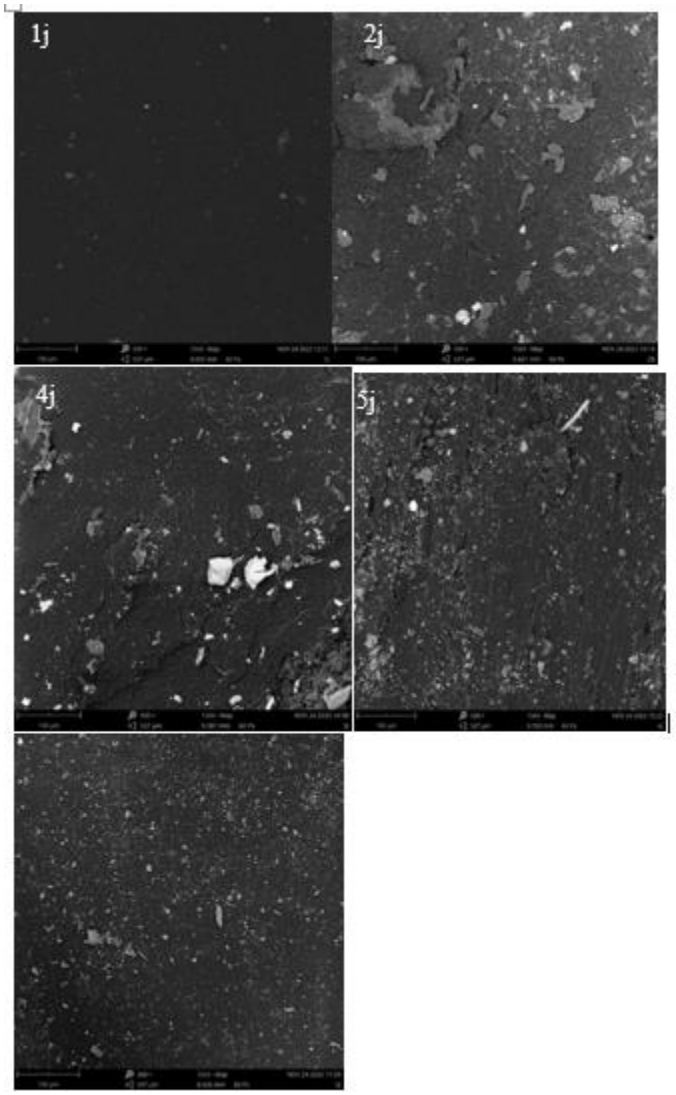



Figure 2: Micrograph of the composites (1j, 2j, 3j, 4j and 5j) Jute fibers

From figure 2, it was established that The surface morphology of the samples shows that films containing variable fiber content(1-5J) has a smooth surface although with small pores and starch granules which may be due to incomplete gelatinization,. Microstructure also illustrates the proper adhesion of plastic matrix covering the jute fiber, fig.2 (1j-5j). it was observed that there are few defects on the flexural testing like air bubbles, fiber breakage and matrix debonding which reduces the strength of the composite slightly. Although few pores and starch granules were observed in the films, but are more pronounced in (2j, 3j) containing 2.5 and 5g of the fiber, which were then reduced gradually with smoother films and uniform dispersion as the fiber content increased. Good interaction between components of the SBP matrix gives the films compact and uniform structures. These properties made the films good for packaging as the tensile strength has also been improved with the incorporation of

the fibers. Even though the fabrication of the SBP- Jute fibers reinforced composite of different fibers loading was done with care, it was observed that intra fiber delamination occur 4j & 5j where the fiber loading increases leading to the increase in the rigidity of the composite.

**Mechanical Properties:**

Mechanical properties of the films were determined to know the value of important parameters such as tensile strength, young modulus and percentage elongation at break. The results are depicted in Table 3.

Table 3; tensile properties of the composites.

| Sample | Tensile Strength (MPa) | Elastic Modulus (MPa) | Elongation at Break (%) |
|---|---|---|---|
| J-0.00 | 1.17 | 47.17 | 10.62 |
| J-2.5 | 7.11 | 58.44 | 9.35 |
| J-5.0 | 8.65 | 113.45 | 12.18 |
| J-7.5 | 10.5 | 130.42 | 11.24 |
| J-10.0 | 10.55 | 112.76 | 20.51 |

As illustrated in Table 3, addition of 0– 10g each of Jute Fibers have increased the tensile strength of the composites from 1.17Mpa to 10.55Mpa. The tensile strength of composites obtained for all five samples have appreciably increased although it is within the range of the moderate plastic class whose mechanical properties ranges from (1-10 MPa).

Table 4: Impact Strength Test Results

| Sample | Impact Energy (J) | | Average Impact Energy (J) | Impact Strength (J/mm) |
|---|---|---|---|---|
| | 1st | 2nd | | |

| | | | | |
|---|---|---|---|---|
| J-0.00 | 0.003 | 0.001 | 0.003 | 0.001 |
| J-2.5 | 0.011 | 0.023 | 0.017 | 0.0057 |
| J-5.0 | 0.052 | 0.046 | 0.038 | 0.013 |
| J-7.5 | 0.037 | 0.038 | 0.049 | 0.016 |
| J-10.0 | 0.084 | 0.073 | 0.079 | 0.026 |

From table 4, it was observed that the impact strength is a function of the fiber content. It shows that increase in the fiber content increases impact strength.

**TGA/DTA analysis**

The results of the thermal stability of the biocomposites are shown in fig.4.Tga 1-5J, respectively.

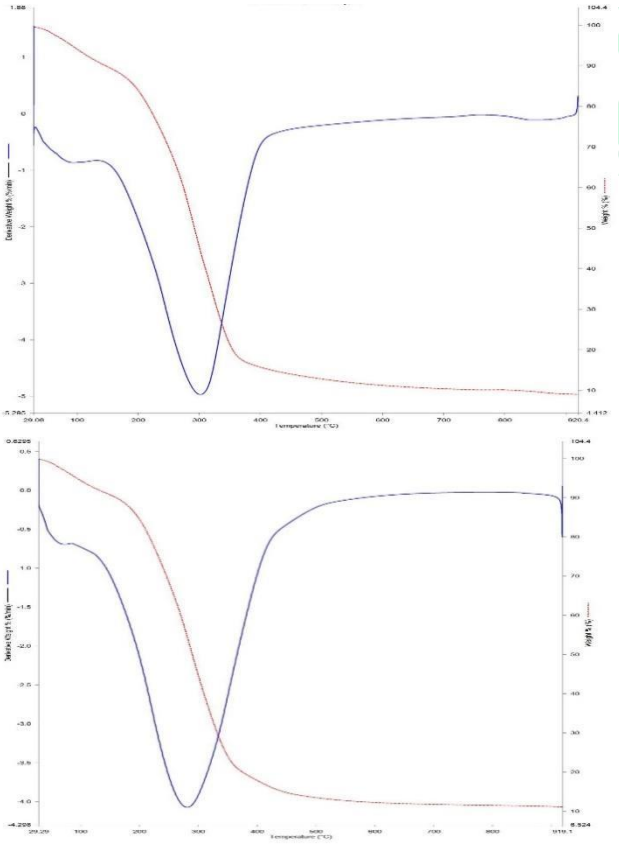


Fig.3(a): TGA/DTA 1J



Fig.3 (b) TGA/DTA 2J.

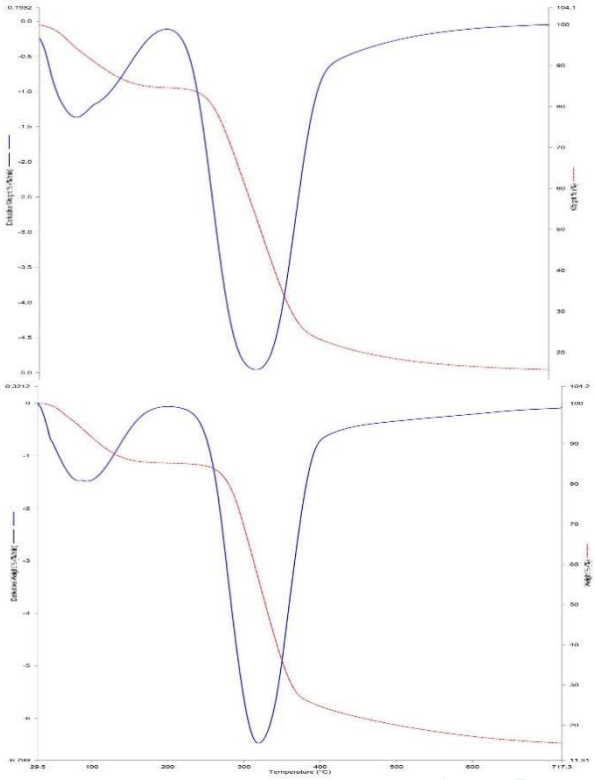


Fig.3 (c) TGA/DTA 3J.

Fig.3(d): TGA/DTA 4J

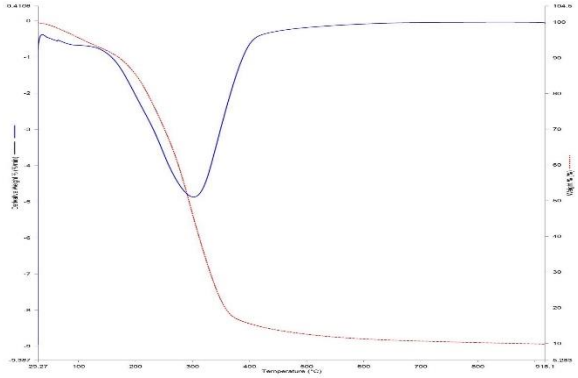


Fig.3 (e): TGA/DTA 5J

The thermal behavior of all the films gave similar pattern with mass loss in steps as presented in the TGA curves. Gradual loss of weight of the films at around 80-120°C in the first step can be attributed to evaporation of water and volatile materials like glycerol in the biofilms. The major weight loss which is the second step at around 295-437°C, 288-435°C, 270-485°C, 270-390°C and 278-455°C for the films in Figure 3 (a-e): 1J(0.00g), 2J(2.5g ), 3J(5g ), 4J(7.5g ), 5J(10g ), respectively were due to pyrolysis of the films and any loss of weight beyond 500°C can be as a result of decomposition of remaining

carbonaceous materials. The results is in conformity with Diyana,et al.,(2021). The authors reported that starch sample for TGA usually gives mass stability at around 180-250°C which was observed in the TGA curves of all the samples (films). Comparing TGA and DTA curves of all the SBP composite film samples examined at a temperature range of 25°C – 900°C, the temperature at maximum rate of decomposition (DTA) and thermal stability based on weight loss (TGA) does not have a uniform pattern as it increases with increase in starch concentration but the highest value at 377°C for DTA and values for TGA at 270-485°C and 278-455°C were observed in sample d (7.5g J) and e (10.0g J). Similar result was reported by Arifa *et al.*, (2021). Thus, it can be deduced that sample d (7.5g J) and e (10.0g J) with highest TGA and DTA are more thermally stable than the control film (a) with (0.0g J) and the other films.

## 4. Conclusion

Potato peel starch films plasticized with glycerol and reinforced with variable contents of Jute Fibers were developed and characterized by several techniques. Composite films were obtained with good workability and good characteristics to be used as packaging material. The fibers interacts effectively with starch, which was evident in the results obtained from the TGA, SEM and mechanical properties results where a strong adhesion between the matrix and the fibers was observed. Assessing the mechanical performance, the samples presented higher rigidity as the fiber ratio increases. Thus, addition of the fibers has improved the mechanical and thermal properties of potato peel waste starch thermoplastics (PPW). The SBP also has a good thermal stability up to 534°C The thermal transitions show miscibility between the components of the blends, with high degradation temperatures, making them susceptible and a good option for processing on a larger scale in plastic materials production.

## References

[1] H. Akbar, A. Dawam, P. Sri, K. Myrtha, D. P. Oceu, and H. F. Rani, "Fabrication and characterization of sweet potato starch-based bioplastics plasticized with glycerol," Journal of Biological Sciences, vol. 19, no. 1, pp. 57–64, 2019.

[2] D. Bajer, K. Janczak, and K. Bajer, "Novel starch/chitosan/Aloe vera composites as promising biopackaging materials," Journal of Polymers and the Environment, vol. 28, pp. 1021–1039, 2020, doi: 10.1007/s10924-020-01661-7.

[3] S. M. Gumel, A. S. Auwal, U. G. Bashir, A. Umar, H. Zainab, and U. Ibrahim, "Exploring the effects of fiber dosing and plasticizers content on the properties of bioplastics obtained from potato peel waste reinforced with baobab fibers for packaging applications," Nigerian Journal of Textiles, vol. 9, pp. 36–46, 2023.

[4] R. V. Gadhave, A. Das, P. A. Mahanwar, and P. T. Gadekar, "Starch based bio-plastics: The future of sustainable packaging," Open Journal of Polymer Chemistry, vol. 8, pp. 21–33, 2018.

[5] M. Justyna, M. Marcin, and S. Krzysztop, "Thermoplastic elastomer biocomposites filled with cereal straw fibers obtained with different processing methods: Preparation and properties," Polymers, vol. 11, Art. no. 641, 2019.

[6] G. Yaret, T. Gloria, M. O. Gloria, and T. J. Lucia, "Biological compatibility of a poly(lactic acid) composite reinforced with natural chitosan obtained from shrimp waste," Materials, vol. 11, Art. no. 1465, 2018, doi: 10.3390/ma11081465.

[7] S. A. Shehu, A. H. Birniwa, R. E. A. Muhammad, S. Manman, and A. S. Chadi, "Impact of fiber reinforced polyester composites on tensile strength of baobab (Adansonia digitata) stem," Caliphate Journal of Science and Technology, vol. 2, pp. 94–100, 2020.

[8] E. J. Jiménez-Regalado, C. Caicedo, A. Fonseca-García, C. C. Rivera-Vallejo, and R. Y. Aguirre-Loredo, "Preparation and physicochemical properties of modified corn starch–chitosan biodegradable films," 2021.

[9] D. T. Nguyen, P. L. Stale, J. F. Mana, J. Blaker, and H. J. Haugen, "Recent development in chitosan-based micro/nanofibers for sustainable food packaging, smart textiles, cosmeceuticals and biomedical applications," Molecules, vol. 26, Art. no. 2683, 2021, doi: 10.3390/molecules26092683.

[10] D. Z. N., R. Junaidin, M. Z. Selamat, I. Ghazali, N. Julmohammad, N. Huda, and R. A. Ilyas, "Physical properties of thermoplastic starch derived from natural resources and its blends," Polymers, vol. 13, Art. no. 1396, 2021, doi: 10.3390/polym13091396.

[11] S. Arifa, N. A., A. T., and A. A., "Synthesis and characterization of starch based bioplastics using varying plant based ingredients, plasticizers and natural fillers," Saudi Journal of Biological Sciences, vol. 28, pp. 1739–1749, 2021.

CSN CHEMICAL SOCIETY OF NIGERIA

# OPTIMIZATION OF ADSORPTION CONDITIONS USING CENTRAL COMPOSITE DESIGN FOR THE REMOVAL OF CARBOFURAN BY ACTIVATED CARBON FROM *ACACIA SENEGAL (L.)* WILLD PODS

**Zaharaddeen N. Garba*, Muhammad M. Kamil**

*Ahmadu Bello University zaria*
**Corresponding author: dinigetso2000@gmail.com*

**Abstract**

Carbofuran contamination in water is a major environmental problem because it is toxic to humans, animals, and aquatic organisms. Previous studies have shown that adsorption using activated carbon is an effective method for removing pollutants from water. However, commercial activated carbon is expensive, so low-cost agricultural wastes are being studied as alternatives. This study investigated activated carbon prepared from *Acacia senegal* (L.) Willd pods for the removal of carbofuran from aqueous solution. The pods were dried, crushed, chemically activated with phosphoric acid, carbonized, washed, dried, and sieved. Batch adsorption experiments were carried out using Response Surface Methodology with Central Composite Design to study the effects of initial carbofuran concentration, adsorbent dosage, and contact time. The results showed that carbofuran removal ranged from 33.91% to 99.61%. Initial concentration had the strongest effect on removal efficiency, while dosage and contact time had smaller effects. The quadratic model was significant, with an $R^2$ value of 0.9496. The optimum conditions were 70.6 mg/L concentration, 163.5 mg adsorbent dosage, and 193.4 minutes contact time, giving 95.9% predicted removal and 96.35% experimental removal. This study recommends *Acacia senegal* pods as a cheap and sustainable adsorbent.

**Keywords:** Carbofuran, Activated carbon, *Acacia senegal* pods, Adsorption, Central Composite Design (CCD).

## 1. Introduction

Water pollution is a serious environmental problem because clean water is needed for drinking, farming, domestic use, and industrial activities. In many agricultural areas, pesticides enter water bodies through surface runoff, leaching, and improper disposal. Although pesticides help to protect crops, their excessive use can contaminate soil, surface water, and groundwater, causing harmful effects on humans, animals, and aquatic organisms [1].

Carbofuran is a carbamate pesticide used to control insect pests. However, it is highly toxic and can affect the nervous system because of its cholinesterase-inhibiting action [2]. Carbofuran has been reported in surface water, groundwater, and drinking water, and the World Health Organization guideline value for carbofuran in drinking water is 0.007 mg/L [3]. Therefore, removing carbofuran from contaminated water is important for protecting public health and the environment.

Adsorption is one of the most commonly used methods for removing pollutants from water because it is simple, effective, and easy to operate. Activated carbon is especially useful because it has a high surface area and many active sites for trapping pollutants [4]. However, commercial activated carbon is expensive, which limits its use in many developing countries. For this reason, agricultural wastes are now being studied as cheaper raw materials for producing activated carbon. *Acacia senegal* pods have been reported as a useful precursor for activated carbon production and water treatment applications [5].

Carbofuran pollution in water is a serious problem because the compound is toxic even at low concentrations. Its presence in water can affect aquatic organisms and may also pose health risks to humans through contaminated drinking water or food chains [6]. Although activated carbon is effective

for removing pesticides and other organic pollutants, the high cost of commercial activated carbon makes it difficult to apply widely, especially in developing countries [7].

Also, adsorption efficiency depends on factors such as initial concentration, adsorbent dosage, and contact time. If these conditions are not properly optimized, the removal efficiency may be low or the process may become wasteful. Therefore, there is a need to produce low-cost activated carbon from locally available materials and optimize the adsorption conditions for maximum carbofuran removal.

This study is justified because it focuses on using *Acacia senegal* pods, an agricultural waste material, to prepare activated carbon for water treatment. This approach can reduce waste and provide a cheaper alternative to commercial activated carbon. The use of Response Surface Methodology with Central Composite Design is also important because it helps to study the combined effects of different adsorption variables with fewer experiments. RSM is widely used for optimization because it can show the relationship between variables and predict optimum conditions effectively [8]. The aim of this study is to optimize the adsorption conditions for the removal of carbofuran from aqueous solution using activated carbon prepared from *Acacia senegal* (L.) Willd pods.

## 2. Materials and Methods

### Materials

Materials used include carbofuran, phosphoric acid, distilled water, sodium hydroxide, hydrochloric acid, and methanol. The materials and apparatus used were beakers, funnel, filter paper, stirring rod, litmus paper, volumetric flask, conical flask, weighing balance, UV-Visible spectrophotometer, reagent bottles, shaker, mortar and pestle, oven, muffle furnace, sieve, and pH meter.

### Reagents and Chemicals

The reagents and chemicals used were carbofuran, phosphoric acid ($H_3PO_4$), distilled water, nitrogen gas, hydrochloric acid (HCl), sodium hydroxide (NaOH), and methanol. Phosphoric acid of 85% w/v was used for activation, while 0.01 M HCl and 0.01 M NaOH were used for pH adjustment. The prepared activated carbon from *Acacia senegal* (L.) Willd pods was used as the adsorbent.

### Preparation of Activated Carbon

Acacia senegal pods were collected, dried, crushed, and chemically activated using phosphoric acid. The sample was carbonized at 600°C under nitrogen atmosphere, washed, dried, and sieved.

### Stock Solution

A 500 ppm carbofuran stock solution was prepared and diluted to required concentrations.

### Experimental Design

CCD was used to design experiments involving three variables: concentration, dosage, and time.

### Adsorption Experiment

Batch adsorption experiments were conducted and analyzed using UV-Vis spectrophotometer.

## 3. Results and Discussion

The Central Composite Design (CCD) experimental matrix showed that carbofuran removal efficiency varied from 33.91% to 99.61%. This wide range indicates that the adsorption process was strongly affected by the selected variables. The highest removal efficiency of 99.61% was obtained at a moderate initial concentration of about 70 mg/L, high adsorbent dosage of about 163 mg, and contact time of about 57 min. This shows that increasing adsorbent dosage provides more active sites for carbofuran adsorption, thereby improving removal efficiency [4].

The lowest removal efficiency of 33.91% was recorded at the highest concentration level of 250 mg/L. This may be due to the saturation of available adsorption sites at higher carbofuran concentration, which reduces the percentage removal.

**Model Development and Statistical Analysis**

A quadratic regression model was developed to describe the adsorption process:

$$Y = \beta 0 + \beta 1X1 + \beta 2X2 + \beta 3X3 + \beta 12X1X2 + \beta 13X1X3 + \beta 23X2X3 + \beta 11X1^2 + \beta 22X2^2 + \beta 33X3^2$$

**Where:**

$X_1$ = Initial concentration, $X_2$ = Adsorbent dosage, $X_3$= Contact time

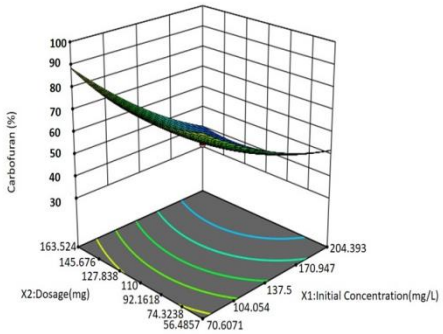



Figure 1: 3D response surface plot showing the effect of concentration and dosage on Carbofuran removal

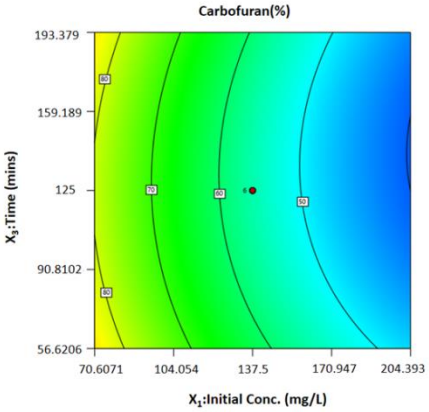



Figure 3: Contour plot showing the effect of concentration and dosage on Carbofuran removal

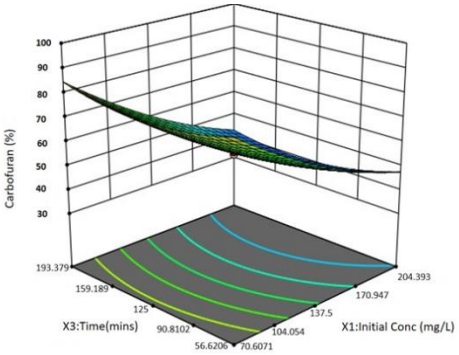


Figure 2: 3D response surface plot showing the effect of concentration and contact time on Carbofuran removal

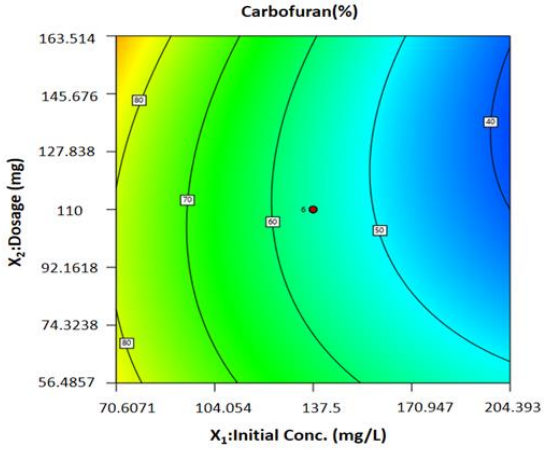



Figure 4: Contour plot showing the effect of concentration and contact time on Carbofuran removal.

Table 1: ANOVA for Response Surface Quadratic Model

| Source | Sum of Squares | df | Mean Square | F-value | p-value | Significance |
|---|---|---|---|---|---|---|
| Model | 6613.79 | 9 | 734.87 | 20.93 | <0.0001 | |
| $X_1$ – Initial Conc. | 5342.82 | 1 | 5342.82 | 152.17 | <0.0001 | |
| $X_2$ – Dosage | 31.65 | 1 | 31.65 | 0.90 | 0.3648 | |
| $X_3$ – Time | 22.39 | 1 | 22.39 | 0.64 | 0.4431 | |
| $X_1X_2$ | 152.78 | 1 | 152.78 | 4.35 | 0.0636 | |
| $X_1X_3$ | 10.95 | 1 | 10.95 | 0.31 | 0.5888 | Significant |
| $X_2X_3$ | 35.87 | 1 | 35.87 | 1.02 | 0.3360 | |
| $X_1^2$ | 245.09 | 1 | 245.09 | 6.98 | 0.0246 | |
| $X_2^2$ | 571.67 | 1 | 571.67 | 16.28 | 0.0024 | |
| $X_3^2$ | 391.34 | 1 | 391.34 | 11.15 | 0.0075 | |
| Residual | 351.10 | 10 | 35.11 | | | |

The model showed high statistical significance, with a coefficient of determination of $R^2 = 0.9496$. The model explained approximately 95% of the variation in carbofuran removal, indicating strong reliability. The adjusted $R^2$ value of 0.9042 and predicted $R^2$ value of 0.8123 showed good agreement, while the high F-value of 20.93 and p-value < 0.0001 confirmed that the quadratic model was statistically significant and adequate for prediction, as commonly reported in recent RSM adsorption studies [8]

**Effect of Process Variables**

The influence of process variables on carbofuran removal was analyzed using response surface methodology.

**Effect of Initial Concentration**

Initial concentration ($X_1$ ) showed the strongest negative effect on adsorption efficiency. As the concentration increased, the removal efficiency decreased significantly. This is due to the limited number of adsorption sites becoming saturated at higher concentrations.

**Effect of Adsorbent Dosage**

Adsorbent dosage ($X_2$ ) exhibited a positive effect on removal efficiency. Increasing dosage increases the number of available active sites, thereby enhancing adsorption capacity.

**Effect of Contact Time**

Contact time ($X_3$ ) showed a relatively minor effect compared to concentration and dosage. This suggests that adsorption equilibrium was reached within a short period, and further increase in time did not significantly improve removal.

**Interaction Effects of Variables**

The interaction between variables was evaluated using 3D surface plots and contour plots.

- **Concentration and Dosage ($X_1$ $X_2$ ):** Removal efficiency increased at low concentration and high dosage, showing a strong interaction.
- **Concentration and Time ($X_1$ $X_3$ ):** Increasing time slightly improved removal at moderate concentrations but had little effect at high concentrations.
- **Dosage and Time ($X_2$ $X_3$ ):** The interaction between dosage and time showed minimal influence compared to concentration effects.

**Model Validation**

The model was statistically significant, with an F-value of 20.93 and a probability value of $p < 0.0001$. The coefficient of determination, $R^2 = 0.9496$, shows that about 95% of the variation in carbofuran removal was explained by the model. The adjusted $R^2$ value of 0.9042 and predicted $R^2$ value of 0.8123 also showed good agreement, indicating that the model had good predictive ability. These values are acceptable for RSM studies, where a high $R^2$ value and close agreement between adjusted and predicted $R^2$ indicate good model fitness [8].

Initial concentration, $X_1$ , had the highest effect, with an F-value of 152.17 and p-value < 0.0001, confirming that it was the most significant factor in the adsorption process. The quadratic terms $X_1^2$, $X_2^2$, and $X_3^2$ were also significant, with p-values < 0.05, showing the presence of curvature and nonlinear effects in the adsorption process. However, dosage, contact time, and the interaction terms $X_1X_2$ , $X_1X_3$ , and $X_2X_3$ were not significant because their p-values were greater than 0.05. This shows that the initial concentration had the strongest influence on carbofuran removal, which is commonly observed in adsorption systems [10].

The final regression model equation in terms of coded factors is:

**Carbofuran % Removal = 5**

$5.652-19.7793X_1-1.52224\ X_2 -1.28046\ X_3 -4.37\ X_1X_2 -1.17\ X_1X_3+ 2.1175\ X_2X_3 + 4.1239\ X_1^2+ 6.29825\ X_2^2+ 5.21108\ X_3^2$ ……

In this equation, the positive sign of a coefficient indicates a synergistic effect on adsorption efficiency, while a negative sign indicates an antagonistic effect. The magnitude of each coefficient reflects the strength of its impact.

The quadratic model provides valuable insights into the adsorption behaviour of carbofuran on *Acacia senegal (L.)* Willd pods derived activated carbon and offers a reliable foundation for process optimization within the studied experimental domain.

To further assess the adequacy of the quadratic regression model, the relationship between the experimental (actual) and predicted values of Carbofuran removal was examined. The comparison is presented in Table 2

Table 2: Comparison of Actual and Predicted Values for Carbofuran Removal

| **Run Order** | **Actual Value (%)** | **Predicted Value (%)** | **Residual** |
|---|---|---|---|
| 1 | 52.84 | 45.28 | 7.56 |
| 2 | 65.59 | 68.24 | -2.65 |
| 3 | 61.46 | 61.97 | -0.51 |
| 4 | 55.20 | 55.65 | -0.45 |
| 5 | 72.23 | 72.54 | -0.31 |
| 6 | 82.97 | 76.03 | 6.94 |
| 7 | 47.22 | 52.83 | -5.61 |
| 8 | 55.51 | 55.65 | -0.14 |
| 9 | 98.52 | 95.92 | 2.60 |
| 10 | 56.76 | 55.65 | 1.11 |
| 11 | 46.44 | 45.95 | 0.49 |
| 12 | 61.00 | 70.91 | -9.91 |
| 13 | 84.98 | 90.44 | -5.46 |
| 14 | 56.05 | 55.65 | 0.40 |
| 15 | 87.59 | 85.99 | 1.60 |
| 16 | 99.61 | 91.91 | 7.70 |
| 17 | 97.76 | 100.58 | -2.82 |
| 18 | 55.06 | 55.65 | -0.59 |
| 19 | 55.84 | 55.65 | 0.19 |
| 20 | 33.91 | 34.05 | -0.14 |

The comparison between the actual and predicted values shows that they agree closely, as most of the residuals fall within a small range. Although, a few runs deviated more from the predicted values, which indicates lack of fit. In general, the residuals are small, which confirms that the regression model is reliable enough to explain the adsorption process [8]. The Actual vs Predicted plot is shown in Figure 4.2

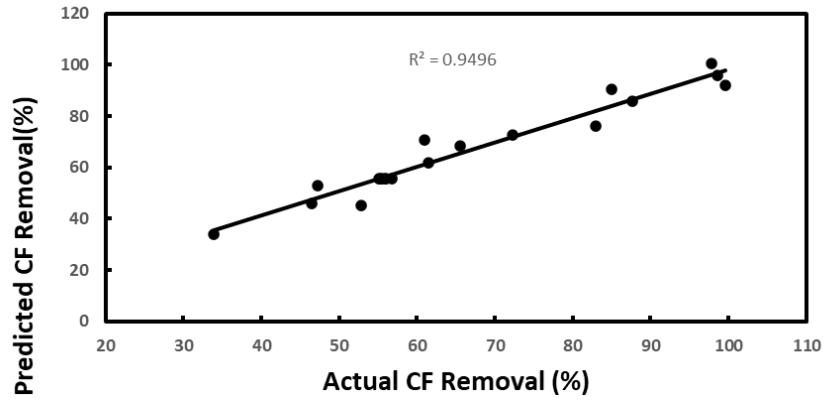



Figure 5: Actual versus Predicted Carbofuran Removal

**Optimization of Adsorption Process**

The adsorption process was optimized to maximize carbofuran removal within the experimental range. The optimal conditions were 70.6 mg/L initial concentration, 163.5 mg adsorbent dosage, and 193.4 min contact time, yielding a predicted removal efficiency of 95.9%, which closely matched the experimental value of 96.35%. This close agreement confirms the accuracy and reliability of the RSM model [11].

**Model Diagnostics**

The adequacy of the model was further evaluated using diagnostic plots. The normal probability plot showed that the residuals followed a straight line, indicating normal distribution. The residuals versus predicted values plot showed random distribution, confirming constant variance. The residuals versus run order plot indicated independence of errors. These diagnostic results show that the model assumptions were satisfied and that the model was suitable for prediction and optimization [11].

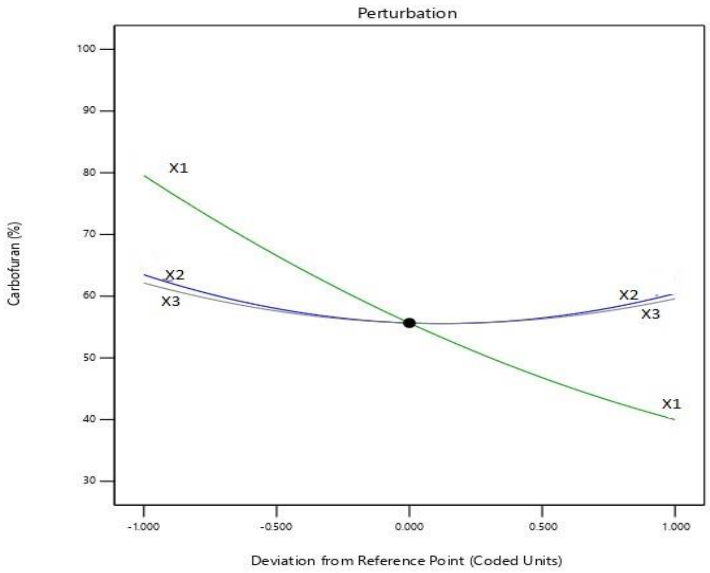



Figure 6: perturbation plot

**4. Conclusion**

Activated carbon derived from Acacia senegal pods is an effective adsorbent for carbofuran removal. RSM-CCD successfully optimized the process, achieving high efficiency. The method provides a sustainable and low-cost solution for water treatment

**References**

[1] A. Sharma *et al.*, "Worldwide pesticide usage and its impacts on ecosystem," *SN Applied Sciences*, vol. 1, Art. no. 1446, 2019.

[2] R. C. Gupta, "Carbofuran toxicity," *Journal of Toxicology and Environmental Health*, vol. 43, no. 4, pp. 383–418, 1994.

[3] World Health Organization, *Guidelines for Drinking-Water Quality: Fourth Edition Incorporating the First and Second Addenda*. Geneva, Switzerland: WHO, 2022.

[4] A. Bhatnagar, W. Hogland, M. Marques, and M. Sillanpää, "An overview of the modification methods of activated carbon for its water treatment applications," *Chemical Engineering Journal*, vol. 219, pp. 499–511, 2013.

[5] A. A. Adetokun, S. Uba, and Z. N. Garba, "Optimization of adsorption of metal ions from a ternary aqueous solution with activated carbon from *Acacia senegal* (L.) Willd pods using Central Composite Design," *Journal of King Saud University – Science*, vol. 31, no. 4, pp. 1452–1462, 2019.

[6] S. Mishra, W. Zhang, Z. Lin, S. Pang, Y. Huang, P. Bhatt, and S. Chen, "Carbofuran toxicity and its microbial degradation in contaminated environments," *Chemosphere*, vol. 259, Art. no. 127419, 2020.

[7] B. Zieliński, P. Miądlicki, and J. Przepiórski, "Development of activated carbon for removal of pesticides from water: Case study," *Scientific Reports*, vol. 12, Art. no. 20869, 2022.

[8] R. Singh and R. Bhateria, "Optimization and experimental design of the $Pb^{2+}$ adsorption process on a nano-$Fe_3O_4$-based adsorbent using the response surface methodology," *ACS Omega*, vol. 5, no. 43, pp. 28305–28318, 2020.

[9] Z. N. Garba and A. A. Rahim, "Process optimization of activated carbon from agricultural waste using response surface methodology," *Journal of Analytical and Applied Pyrolysis*, vol. 107, pp. 306–312, 2014.

[10] E. C. Lima, "Removal of emerging contaminants from the environment by adsorption," *Ecotoxicology and Environmental Safety*, vol. 150, pp. 1–17, 2018.

[11] W. Zhao, Y. Liu, Z. Liu, and J. Zhang, "Optimization of adsorption conditions using response surface methodology for tetracycline removal by magnetic multi-walled carbon nanotubes," *Water*, vol. 15, no. 13, Art. no. 2392, 2023

# BOTTOM-UP SYNTHESIS FOR INTERCONNECTS

**S.M.J Zubairu*[1], S.O. Idris[2], C.E. Gimba[2], A. Uzairu[2] and B.R. Horrocks[3]**

[1]*Federal University Gashua, Nigeria,* [2]*Ahmadu Bello University Zaria, Nigeria,* [3]*Chemical Nanoscience Laboratory, School Natural and Environmental Sciences, Bedson building, Newcastle University, Newcastle Upon Tyne, NE1 7RU, U.K.*
*Corresponding Author: zub_smj@fugashua.edu.ng

**Abstract**

Bottom-up approach draws inspiration from Biology, where Biological system are used to assembled nano structured materials from building blocks and subsequent organization into hierarchical functional system. One of these is the DNA with its self-assemble recognition capabilities because of its size, topography, stability, morphology and various chemical functionality. All of these provides a simple tools for nanomaterials preparation with a range of application such as biological, chemical sensing and nanometer-scale electronics. In this report, we shows how DNA strands can be used to generate semiconductor materials from inorganic nanomaterials through careful optimization of the reaction conditions and DNA state. Here we have been able to control the reaction and quantum confined FeOOH as either uniform nanowires or continuous leaf-like 1D assemblies. The latter subsequently integrated by non-contact method via scanned conductance microscopy to demonstrate electronic path ways.

**Keywords**: AFM, Self-assembly, Nanowires, Nanoparticles, DNA

## 1. Introduction

Conducting polymers such as polyaniline, polythiophene, polypyrrole, polyacetylene, polyindole, and their derivatives similar to that of metals and inorganic semiconductors are promising important materials for the synthesis of nanostructured materials [1-4]. One core challenge faced is the organization of semiconducting nanoparticles with strict control over alignment and the organization of structural patterns where their nanoscale properties can be exploited. This challenge becomes even more difficult when the current trends in the down-scaling of feature sizes on commercial microchips reaches a plateau due to fundamental limitations of photolithographic methods currently used in device manufacture [5-6]. This expected failure at molecular scales presents the challenge for providing alternative strategies to the construction of useful electronic devices, which move away from the current conventional "top-down" approaches to their fabrication. In particular, the development of nanometer-size and molecular building blocks for utilization in "bottom-up" approaches device construction are anticipated to offer promise within this area. Scanned conductance microscopy (SCM) represents probing nanowires electronic properties qualitatively using contactless method that can assess the conductance of 1D structure. The optical images illustrate nanowires protruding from the mass of individual material which serve as contact to the nanowire and the conductive AFM tip.

In order to assess the conductance of HT-DNA-templated nanowires qualitatively, scanning conductance microscopy (SCM) was used for polymeric and Inorganic molecules. It is a simple non-contact electrical method to image conductance pathways previously used to image single-wall carbon nanotubes (SWNTs) [7-8].

## 2. Materials and Methods

One-spot synthesis in Eppendorf tube was used to perform HTDNA/Ppy nanowires involving oxidative polymerisation of pyrrole monomers in aqueous solution [7] with little modification as shown in scheme 1 above. It involved addition of pyrrole monomers solution to λ-DNA and subsequent addition of an oxidant to initiate polymerization process. HTDNA/Ppy nanowires synthesis was done by adding freshly prepared $MgCl_2$. $6H_2O$ solution (0.5 mM, 5 µL) to HT-DNA solution (500 ng/µL, 20 µL).

**Cleaning and modification of $1 \times 1 cm^2$ pieces Si wafers**

n-Si (111) wafers were cut into ~$1 \times 1 cm^2$ pieces using tip pen and cleaned with acetone using cotton bud followed by propanol and finally oxidize the substrate surface with piranha solution ($H_2SO_4$ : $H_2O_2$ 4:1) for 45 minutes.

Ultra-violet absorption spectroscopy

All UV-Vis measurements was recorded on Cary 100 Bio UV-Visible spectrophotometer (Varian) at room temperature equipped with temperature control within 200-600 nm, which monitors an absorption band change or occurring phenomena as the DNA templated with nanobjects progresses.

Fourier transform infrared spectroscopy

All FTIR measurements in the work (bare HTDNA and templated) was carried out using Varian 800 FTIR spectrometer system using pike technologies diamond crystal plate. Spectra were recorded with 124 scans and 4 $cm^{-1}$ spectral resolution within 400-4000 $cm^{-1}$ in transmission mode. The DNA used were from Herring testes (HTDNA) and all sample were prepared through drop-casting of the solution of HTDNA/$Fe_2O_3$ (0.4 $mgmL^{-1}$) or net HTDNA on oxidized Si< n-111> substrates.

X-ray photoelectron spectroscopy

HTDNA/$Fe_2O_3$ for XPS was prepared in a similar manner as described for FTIR as solid thin film drop-casting onto Si substrates. XPS measurements was taken on Thermo Scientific equipped with an AI Kα X-ray source (1486.6 eV) and operating power of 100 W (15 kV, 7mA) using a take-off angle 90 $^0$. With fully integrated monochromatic with a selectable spot system (30-400 μm). Sample were prepared for XPS by depositing 5 μL of solution on a clean Si wafer and left to dry at RT in a laminar flow hood to minimize contamination.

Atomic force microscopy

The formation of DNA/FeOOH nanowires for AFM imaging of surface topography was prepared by adding about 3 μL of the templated solution onto the edge of freshly $1 cm^2$/square TMS modified Si wafer at RT and stretching or dragged across the surface via molecular combing method and then allowed to dry in the hood for 7-10 min, in this case, $N_2$ aided. Data acquisition were carried out using Nanoscope IIIa and Nanoscope 7.2 software (Veeco Instruments Inc.) and JPK Nano wizard AFM. Vibrational noise was reduced by an isolation acoustic enclosure (Veeco Inc., Metrology Group).

Powder x-ray diffraction

XRD patterns for crystallographic phase identification was performed on Si wafer with 200 nm $SiO_2$ layer and recorded on Bruker 2D phaser bench top diffractometer with Cu Kα radiation source (λ = 1.54178 Å / 0.154178 nm) at a scan rate of $1^o$/s within 10-$70^o$. Diffraction peaks of the crystalline phases for bulk materials were compared with those of JCPDS data. The Si wafer was thoroughly cleaned with propanol and piranha treated. The nanowires were then stretched across the wafer using the moving meniscus of a drop of solution.

Transmission electron microscopy (tem)

Powerful imaging capability of TEM coupled with other characterization tools such as energy dispersive X-ray spectroscopy (EDX) within the TEM instrumentation was used to probe extra properties of the nanowires.

**3. Results and Discussion**

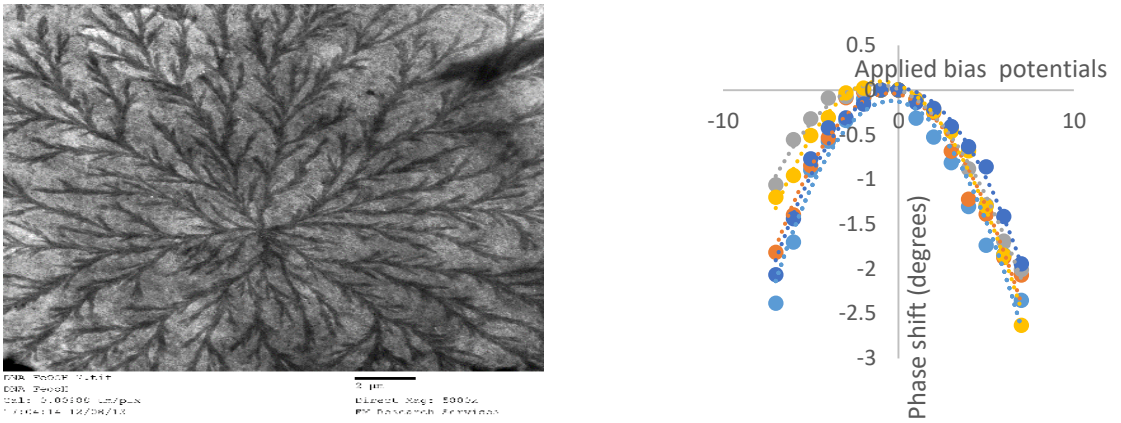



Figure 1: TEM image and SCM plot for HT-DNA/FeOOH morphology

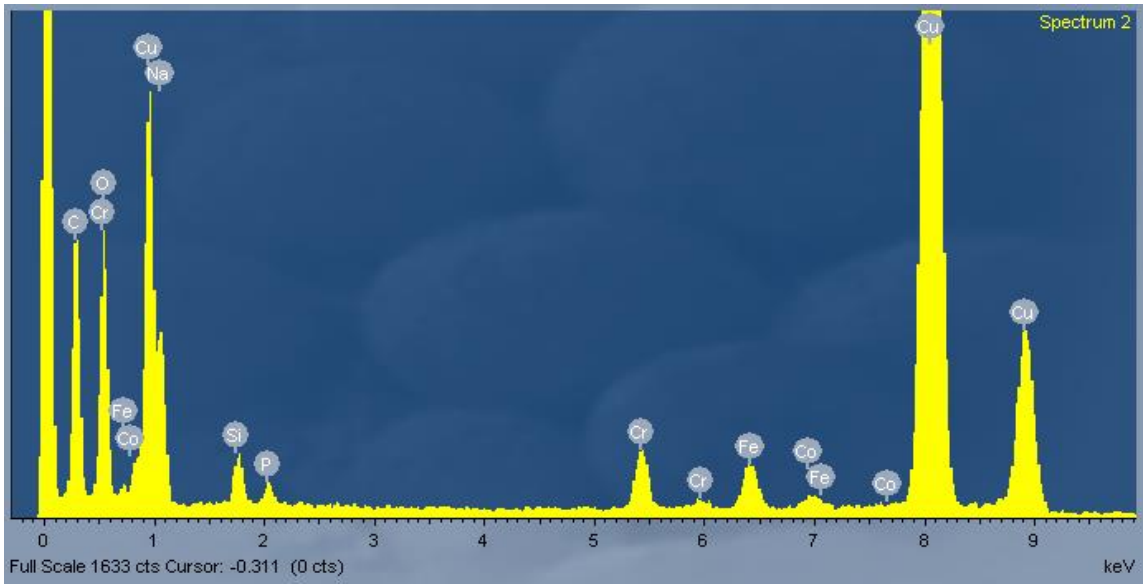



Figure 1a: EDX of HTDNA/$Fe_2O_3$

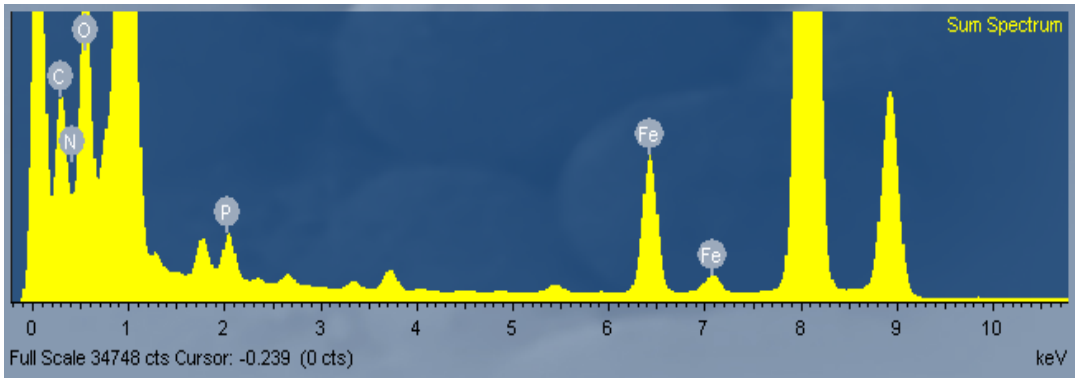



Figure 1b: EDX of HTDNA/FeOOH

The results above (Figure (1a-b) were obtained above from Energy Dispersive X-ray Spectroscopy (EDX) gave the chemical composition of the nanostructure material. From the spectra, copper, carbon, nitrogen, phosphorus, oxygen and iron were observed with C, Cu, Cr and Co signals from the carbon-coated copper grid and sample holder used for TEM while the C peak comes from the HTDNA and as well as TEM grid.

The Fe and O peaks came from the Fe and O on the nanowires and the nitrogen, phosphorus peaks from the HTDNA with some other unforseen contaminates along with Cu peaks (the last two peaks from right hand side) which came from the carbon coated copper grid at 9 keV.

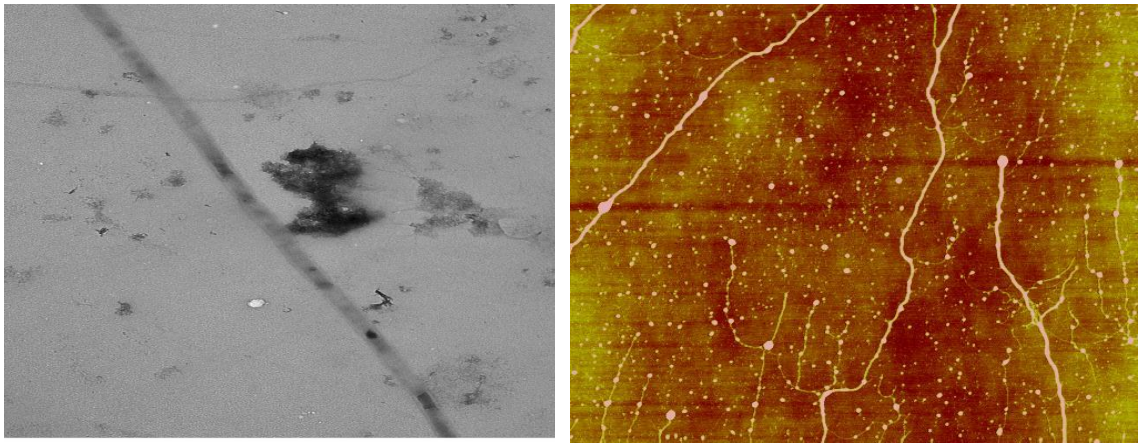


Figure 2: TEM and AFM images of HTDNA/Ppy and HTDNA/Ppy morphologies

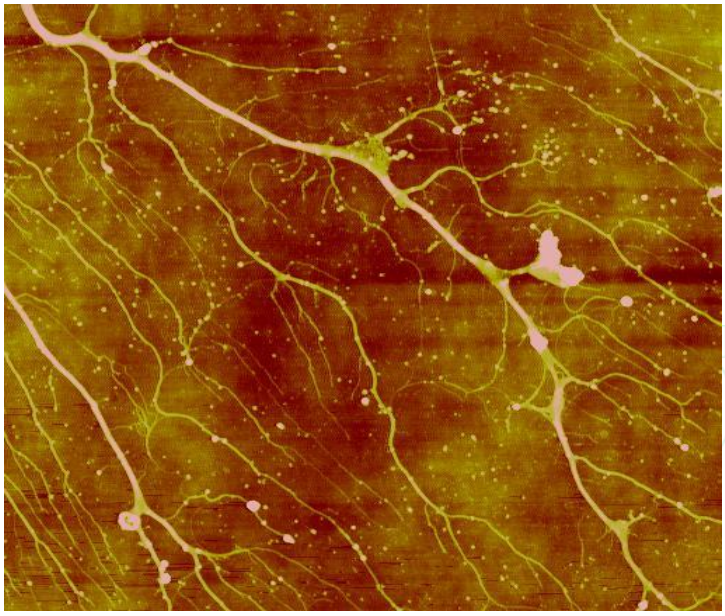


Figure 2a : AFM image of HTDNA/Ppy nanowires

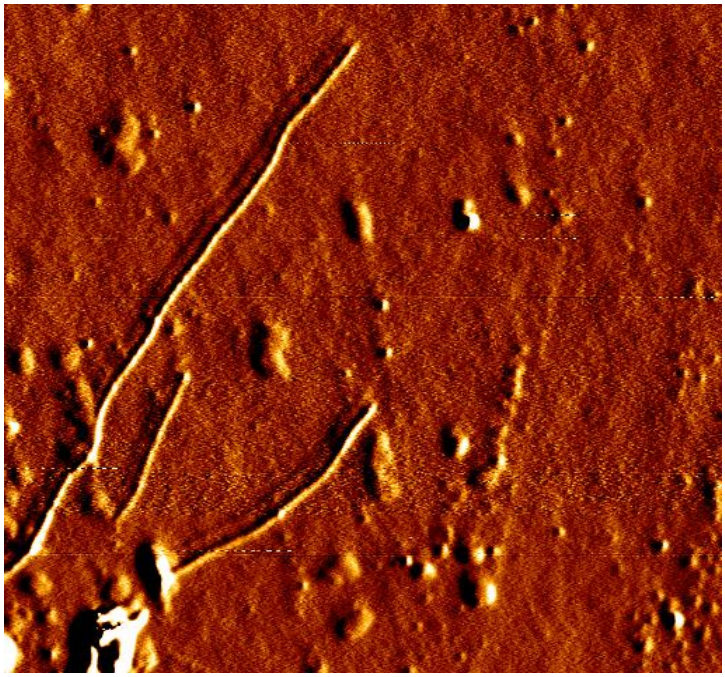


Figure 2b : AFM image of HTDNA/$Fe_2O_3$

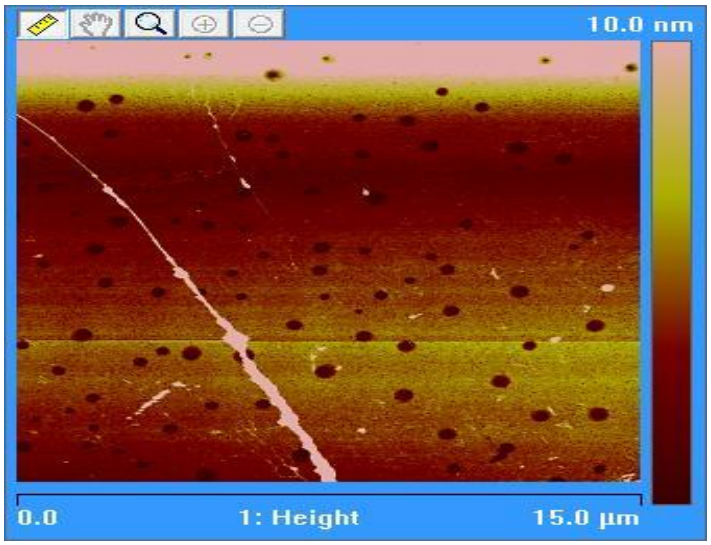



Figure 2c : AFM image of HTDNA/FeOOH nanowires

AFM imaging was used to characterize the morphology of the nanowires. Fig. 2 (right) show AFM image of HT-DNA/Ppy nanowire aligned on $Si/SiO_2$ substrate. Nanowire alignments was done by molecular combing technique and before alignment on $Si/SiO_2$, the $Si/SiO_2$ was modified by vapour deposition using trimethylsilane so to increase $Si/SiO_2$ surface hydrophobicity. It is clear from Figure 2 (a-c) that the nanowires are not completely smooth and uniform but with diameter range from 6-24 nm and DNA length range (2-15 µm) were observed. Specifically, the observed nanowire grow unto the DNA template thus forming a long and ordered wire over the DNA length.

Illustrated above too is TEM and AFM images (Fig. 2) of HT-DNA with Ppy as nanoparticles that serve as molecular blocks onto which anisotropic growth of the nanoparticles took place. The morphology of the nanowires appears regular and uniform with distinct nanowires-wire-like appearances where network connectivity can be accessed for electronic pathways.

After polymerization of Pyrrole monomers onto bare HT-DNA for the formation of HT-DNA/ppy nanowires as mimic in the scheme 1 above, an organized wires were observed and the height image showed a 1D nanostructure. As shown in the Figures (2a-2c) for AFM images of HT-DNA/Ppy, the polypyrrole (Ppy) nanoparticles are distributed along the path of the template with Figure 2a as robust leaf-like morphologies. The deposition of nanoparticles is clearly seen from the HT-DNA/Ppy nanostructure with evident of separate particles packed along the HT-DNA template.

The SCM (Scanned Conductance Microscopy) plot (Figure 1 on the right side) show parabolic dependence of phase shift on bias voltage for voltage +7 to +3 V at different diameters, where the magnitude of the phase shifts on the applied bias as illustrated by the parabolic trend plot of the degree of phase shifts as a function of applied bias. The phase shifts depend on diameter and large shift observed as the nanowire diameter increases.

**EFM (Electrical studies)**

The nanowires in the EFM phase images of HTDNA/Ppy nanowires at different locations along the nanowire at bias voltage are shown in Figure 3 below appeared as dark lines for the HT-DNA/Ppy template corresponding to the negative phase shifts as the tip crosses the wire thus the existence of charges on the nanowires, thus conductivity pathway along the nanowires.

It serves to provide a no or yes answer to materials conductivity. It has been previously employed to image potentials of single walled carbon nanotubes (SWCNTs) and to demonstrate the insulating properties of Lambda-DNA (Bockrath *et al.*, 2002 [8] and Bachtold *et al.*, 2000) [9], and even to discriminate between

insulating and conducting polyaniline/poly(ethylene oxide) nanofibers, on microscopic scale (Zhou *et al.*, 2003) [10].

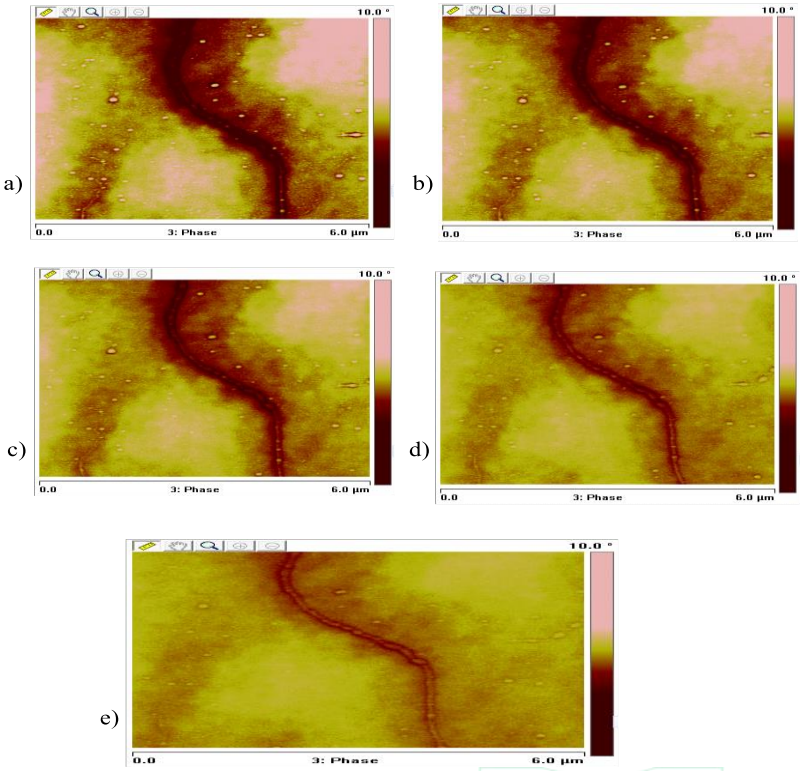



Figure 3: EFM phase images of same DNA/Ppy nanowires at different locations showing the phase angle of the tip oscillation as a function of tip/sample biases. (a). +7v, (b). +6 v, (c). +5 v, (d). +4 v, (e). +3 v and lift height of 50nm, scale bar 6.0µm

## 4. **Conclusion**

HT-DNA was used as platform to grow or pattern semiconductor density and polymer nanoparticles as precursors to generate organized one dimensional nanostructures in solution and by electrochemical reduction. One strategy to overcome this was the use of bottom-up approach, in which DNA as a template direct synthesis of wire like patterns by chemical reduction from iron nitrate hydrate and/or iron chloride hexahydrate and for oxidizing pyrrole into polypyrrole.. Measurement of (ΔØ) phase shift of the nanowires for each bias potentials applied to the samples provided data series as shown in Figure 1 (right) with parabolic dependence as predicted by EFM theory as illustrated in Figure 3.

## References

[1] Siyaka Mj Zubairu, Sulaiman O. Idris, Casmir E. Gimba, Adamu Uzairu, Andrew Houlton, Benjamin R. Horrocks. Templating Iron (III) oxides on DNA molecules. *Nanomaterials,* 14, 1609, 2024. https://doi.org/10.3390/nano14191609

[2] Houlton, A., Pike, A. R. Angel Galindo, M. and Horrocks, B. R. (2009) DNA-based route to semiconducting nanomaterials. *Chemical Communication*, 1797-1806.

[3] Langea, U., Roznyatovskayal N. V. and Mirsky, V. M. (2008) Conducting polymer in chemical sensor and arrays. *Anal. Chim. Acta,* 614 (1), 1-26.

[4] Malinauskas, A., Malinauskiene, J. and Ramanavicius, A. (2005). Conducting polymer-based nanostructure materials: Electrochemical aspects. *Nanotechnology*, 16 (10), R51-R62.

[5] Dong, L., Hollis, T., Fishwick, S., Connolly, B. A., Wright, N.G., Houlton, A. and Horrocks, B. R. (2007), Synthesis, manipulation and conductivity of supramolecular polymer nanowires. *Chem. Eur. J.* 13, 822.

[6] http:// www.itrs.net/, ITRS Roadmap, Accessed on 13, June 2019, December, 2025 and January, 2026.

[7] Siyaka M. Zubairu,., Iyun, J. F., Gimba, C. E., Uzairu, A., Idris, O. S., Watson, S. M. D. and Horrocks, B. R. (2013), My PhD work (Development and Evaluation of Conductive Nanaowires using Deoxyribonucleic acid as a template) available on https//kubanni.abu.edu.ng

[8] Bockrath, M., Markovic, N., Shepard, A., Tinkham, M., Gurevich, L., Kouwenhoven, L. P., Wu, M. W. and Sohn, L. L. (2002). Scanned conductance microscopy of Carbon nanotube and λ-DNA. *Nano Letters,* 2, 187-190.

[9] Bachtold, A., Fuheer, M., Plyasunov, S., Forero, M., Anderson, E. H., Zettl, A. and Mceuren, P. L. (2000). Scanned probe microscopy of electronic transport in Carbon Nanotube *Physical Review Letters*, 84, 6082-6085.

[10] Zhou, Y., Freitag, M., Home, J., Staii, C., Johnson, A. T., Pinto, N. J. and MacDiamid, A. G. (2003). Fabrication and electrical characterization of polyaniline-based nanofibers with diameter below 30 nm. *Applied Physics Letters*, 83, 3800-3802.

# INTEGRATED GEOCHEMICAL AND GEOPHYSICAL METHODS OF INVESTIGATING HEAVY METAL POLLUTION OF GROUNDWATER IN UPPER AND MIDDLE AQUIFERS IN DOGONGARAGE AREA OF MAIDUGURI, NORTHEASTERN NIGERIA.

**S.A. Sonloye[1]*, A.U.U. Ocheni[1], A. Aliyu[1], L.E. Agada[2], R.O. Amusat[1], A. Usman[2], A.S. Oniku[3]**

*[1]Department of Physics, University of Maiduguri, P.M.B. 1069, Maiduguri, Borno State, Nigeria*
*[2]Department of Physics, Yobe State University, P.M.B. 1144, Damaturu, Yobe State, Nigeria*
*[3]Department of Physics, Modibbo Adama University, P.M.B. 2076, Yola, Adamawa State, Nigeria*
**Corresponding author: sonloyeseyi@unimaid.edu.ng; +2348060993269*

**Abstract**

Groundwater is the primary drinking water source in Maiduguri, but rapid urbanization and poor waste disposal threaten its quality. This study integrated electrical resistivity tomography (ERT), vertical electrical sounding (VES), hydrochemical analysis, and health risk modelling to evaluate groundwater contamination in the Dogongarage district. Geophysical surveys along a 200-metre profile and water samples from six boreholes (three shallow, three deep) were analysed for six heavy metals. Results revealed a five-layer aquifer system comprising a discontinuous clayey aquitard (1.9–13.5 m, 12.2 Ωm), a contaminated upper aquifer (13.5–35.7 m, 9.84 Ωm), a resistive clay layer (35.7–84.9 m, >2000 Ωm), and a middle aquifer (below 84.9 m, 93.1 Ωm). The ERT confirmed that the clayey aquitard is laterally discontinuous, creating direct pathways for surface contaminants to reach the upper aquifer. Chromium, lead, and cadmium exceeded WHO limits in the upper aquifer, while concentrations in the middle aquifer remained within permissible limits. The Heavy Metal Pollution Index classified the upper aquifer as moderately polluted (HPI: 67.7–68.6) and the middle aquifer as safe (HPI: 15.6–19.7). Children and pregnant women face significant non-cancer risks (HI > 1) from upper aquifer water. Lifetime Cancer Risk (LCR) exceeded the acceptable threshold ($1\times10^{-4}$) in both aquifers, 10–11 times higher for children in the upper aquifer and 2–5 times higher in the middle aquifer, indicating that the protective clay layer does not completely prevent contaminant migration. We recommend drilling deep boreholes beyond 150 metres, implementing water treatment technologies (reverse osmosis, activated carbon filtration), and establishing regular water quality monitoring.

**Keywords:** Groundwater contamination, electrical resistivity, heavy metals, health risks, semi-arid region

## 1. Introduction

Groundwater represents a vital freshwater resource in arid and semi-arid regions where surface water availability is limited and unreliable [1, 2]. Globally, groundwater supplies approximately one-third of all freshwater withdrawals and serves as the primary drinking water source for nearly half of the world's population [2]. In sub-Saharan Africa, where climate variability and population growth place increasing pressure on water resources, groundwater is often the only dependable source of freshwater for domestic, agricultural and industrial purposes [4]. Maiduguri, the capital of Borno State in Northastern Nigeria, exemplifies the challenges facing semi-arid urban centres in the region. With an estimated population exceeding two million, the city relies heavily on groundwater extracted from the Chad Formation aquifer system [3]. Approximately 80% of Maiduguri's population depends on groundwater for daily domestic water supply, underlining its critical importance for public health and socioeconomic development [3]. However, rapid urban expansion, poor waste management practices, and inadequate regulatory enforcement are increasingly threatening the quality of this essential resource [4, 5].

The Dogongarage district of Maiduguri presents a compelling case study for investigating groundwater vulnerability to surface-derived contamination. The area is characterised by high population density, its location on the prolific Chad Formation aquifer system, and the presence of potential pollution sources including open waste dumps, automobile workshops, and domestic sewage disposal systems [10, 11]. Heavy metals originating from such sources, particularly lead, chromium, cadmium and copper, can infiltrate through the unsaturated zone and accumulate in groundwater, posing serious health risks to consumers [6, 7]. The Chad Basin, of which the study area forms part, comprises Quaternary and Tertiary deposits of alluvial sands, clays, silts and the Chad Formation proper [10, 20]. Historical studies have divided the aquifer system into upper, middle and lower units, with the upper aquifer being the most exploited for domestic water supply [10]. However, the protective capacity of the intervening clay layers and the degree of hydraulic connectivity between aquifer units remain poorly constrained in many urban areas.

Although the broader hydrogeology of the Chad Basin has been well documented [10, 11], significant information deficits persist concerning the relationship between surface pollution sources, aquifer contamination patterns, and resultant health risks in the Dogongarage area. Specifically, the vertical connectivity between shallow and deep aquifer systems through protective clay layers has not been adequately characterised; the spatial distribution and effectiveness of clayey aquitards in attenuating contaminant transport remain unquantified; and the associated non-carcinogenic and carcinogenic health risks for vulnerable populations (children, pregnant women, and adults) consuming contaminated groundwater have not been systematically evaluated. Groundwater vulnerability assessment is a well-recognised priority for groundwater protection in Nigeria [12], and health risk evaluation specific to heavy metals is essential for safeguarding human health [13]. Previous investigations in this region have typically examined geophysical subsurface properties or geochemical contamination in isolation, missing the integrated insights that have proven valuable in similar contexts elsewhere [14, 15].

To address the identified gaps, this study integrates electrical resistivity tomography (ERT), vertical electrical sounding (VES), hydrochemical analysis and health risk modelling to achieve the following objectives: delineate the subsurface aquifer system and identify protective layers using geoelectrical methods [16]; determine the concentrations of heavy metals (mercury, chromium, iron, copper, lead and cadmium) in the upper and middle aquifers; assess aggregate pollution levels using the Heavy Metal Pollution Index (HPI) [17]; and evaluate non-carcinogenic (Hazard Index) and carcinogenic (Lifetime Cancer Risk) health risks associated with groundwater consumption for children, adults and pregnant women, following established USEPA risk assessment methodologies [18, 19]. The findings of this investigation are expected to provide critical baseline data for groundwater management in the Dogongarage area and contribute to the broader understanding of urban aquifer vulnerability in semi-arid environments. By establishing a direct linkage between subsurface architecture, contaminant distribution and human health outcomes, this study offers a replicable framework for integrated groundwater quality assessment in data-scarce urban regions of sub-Saharan Africa.

## 2. Materials And Methods

The Dogongarage area lies within Maiduguri Metropolis at approximately latitude 11°50'46"N and longitude 13°9'30"E. The climate is hot and semi-arid, with temperatures often exceeding 40°C and rainfall mostly between July and September (Figure 1). Two types of electrical surveys were conducted to investigate the subsurface aquifer system. Electrical Resistivity Tomography (ERT) was carried out along a 200-metre long survey line using 5-metre spacing between electrodes with the Wenner electrode configuration. Data were processed using RES2DINV software with 1000 iterations, achieving a final RMS error of 8%. Vertical

Electrical Sounding (VES) was conducted at the midpoint of the ERT profile using the Schlumberger array, with electrode spacing gradually increased from 1.5 metres to 200 metres, reaching an investigation depth of approximately 145 metres.

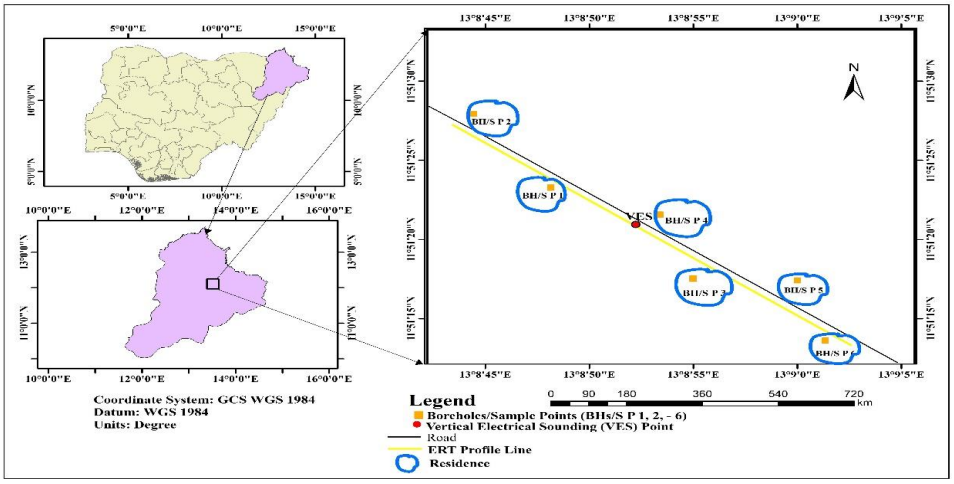



**Figure 1:** Map of the study area showing groundwater sampling locations and geophysical survey profile

Six water samples were collected, three from shallow boreholes (upper aquifer) and three from deep boreholes (middle aquifer). Each borehole was pumped for 5 minutes before sampling to ensure representative water collection. Samples were preserved with nitric acid and kept cool during transport to the laboratory. Heavy metal concentrations (Hg, Cr, Fe, Cu, Pb, Cd) were measured using Atomic Absorption Spectrometry.

The Heavy Metal Pollution Index (HPI) was calculated to combine the effects of multiple metals. HPI values below 50 indicate safe water, 50–100 indicate moderate pollution, and above 100 indicate severe contamination [17]. The HPI was computed using the equation:

$$\text{HPI} = \frac{\sum_{i=1}^{n} W_i Q_i}{\sum_{i=1}^{n} W_i} \quad (1)$$

where *Qi* is the quality rating for the *i*-th metal, and *Wi* is the unit weightage assigned to the *i*-th metal.

The quality rating ($Q_i$) for each metal was calculated as:

$$Q_i = \frac{C_i}{S_i} \times 100 \quad (2)$$

where $C_i$ is the measured concentration of metal *i* (mg/L) and $S_i$ is the WHO drinking water guideline value for metal *i* (mg/L).

The unit weightage (*Wi*) for each metal was inversely proportional to its guideline value, calculated as:

$$W_i = \frac{K}{S_i} \quad (3)$$

where *K* is a proportionality constant given by:

$$K = \sum_{i=1}^{n} \frac{1}{S_i} \quad (4)$$

This weighting scheme ensures that metals with lower permissible limits (i.e., more toxic metals such as Cd and Pb) receive higher weightage in the index calculation, reflecting their greater public health significance [6, 17].

$$HI = \sum HQ_i = \sum \frac{ADD_i}{RfD_i} \quad (5)$$

where the Average Daily Dose for metal *i* (ADD) was calculated as:

$$ADD_i = \frac{C \times IR \times EF \times ED}{BW \times AT}) \quad (6)$$

C is metal concentration (mg/L), IR is ingestion rate (L/day), EF is exposure frequency (days/year), ED is exposure duration (years), BW is body weight (kg), and AT is averaging time (days). Exposure parameters for children, adults and pregnant women were adopted from USEPA guidelines [19] (Table 1). An HI value below 1 indicates negligible risk, whereas HI >1 suggests potential adverse health effects [18].

Lifetime Cancer Risk (LCR) for Cr, Cd and Pb was estimated as:

$$LCR = LADD \times SF \quad (7)$$

where LADD is the Lifetime Average Daily Dose (calculated similarly to ADD but with ED = 70 years) and SF is the oral slope factor $(mg/kg/day)^{-1}$. Slope factors of 0.5, 0.0042 and 0.0085 were used for Cr, Cd and Pb, respectively [19]. The acceptable carcinogenic risk threshold adopted in this study was $1 \times 10^{-4}$ and the exposure parameter used for health risk assessment for different population group are given in Table 1.

**Table 1:** Exposure parameters used for health risk assessment for children, adults, and pregnant women.

| **Parameter** | **Children** | **Adults** | **Pregnant Women** |
|---|---|---|---|
| Water ingestion rate (L/day) | 1.0 | 2.0 | 2.5 |
| Exposure frequency (EF) (days/yr) | 365 | 365 | 365 |
| Exposure duration (ED)(years) | 6 | 30 | 9 |
| Body weight (BW)(kg) | 15 | 70 | 65 |
| Average time (AT)(days) | 2190 | 10950 | 3285 |

Exposure parameters (water intake, body weight, exposure duration) were adopted from USEPA guidelines for children, adults, and pregnant women.

### 3. Results and Discussion

The ERT survey was conducted along a 200-metre profile using the Wenner electrode configuration with 5-metre electrode spacing. The resulting 2D resistivity section (Figure 2) delineated four distinct subsurface layers along the Dogongarage profile. The topsoil layer (0–2 m depth) exhibited resistivity values of 100–500 Ωm, interpreted as dry topsoil. Beneath this, a clayey aquitard (2–15 m depth) showed resistivity values of 10–50 Ωm, interpreted as a protective clay layer that is laterally discontinuous. The upper aquifer (15–40 m depth) displayed resistivity values of 26–70 Ωm, indicating a shallow contaminated aquifer. Below 40 m depth, resistivity exceeded 2000 Ωm, interpreted as a consolidated base clay protective layer. A key finding from the ERT survey is that the clayey aquitard is missing or very thin between 50 and 120 metres along the survey line, creating direct pathways for contamination to reach the shallow aquifer.

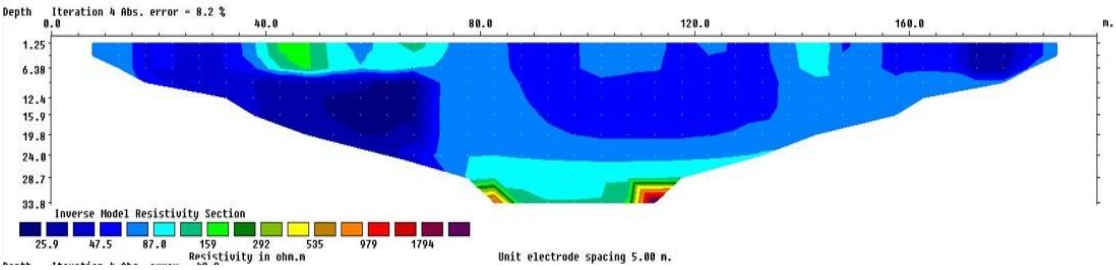



**Figure 2:** Two-dimensional Electrical Resistivity Tomography (ERT) section showing resistivity distribution and inferred aquifer zones along the Dogongarage profile.

The geophysical interpretation of the ERT survey is summarised in Table 2, which presents the layer depths, resistivity values, and corresponding interpretations.

**Table 2:** Geophysical interpretation of subsurface layers from electrical resistivity tomography (ERT) along the Dogongarage survey profile.

| Layer | Depth (m) | Resistivity (Ωm) | Interpretation |
|---|---|---|---|
| Topsoil | 0-2 | 100-500 | Dry Top soil |
| Clayey aquitard | 2-15 | 10-50 | Protective clay layer (discontinuous) |
| Upper aquifer | 15-40 | 26-70 | Shallow contaminated aquifer |
| Deep zone | below 40 | >2000 | Consolidated base clay protective layer |

The VES survey was conducted at the midpoint of the ERT profile using the Schlumberger array, with electrode spacing gradually increased from 1.5 metres to 200 metres, reaching an investigation depth of

approximately 145 metres. The VES curve (Figure 3) shows apparent resistivity as a function of electrode spacing, with the red curve representing measured data and the blue line showing the modelled fit.

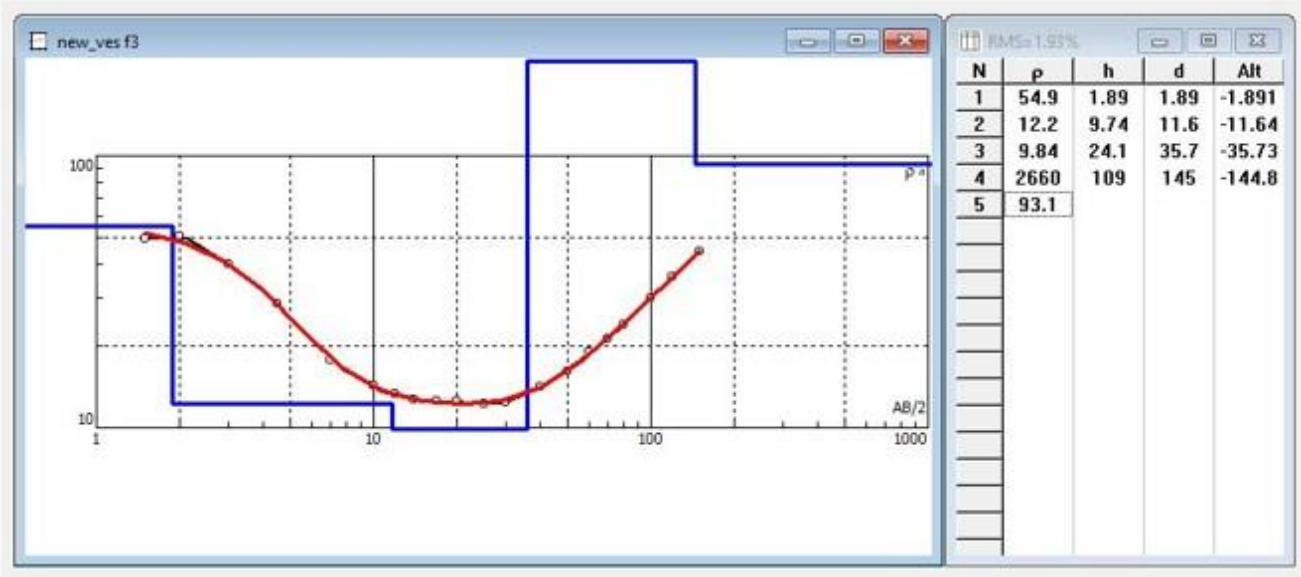



**Figure 3:** VES Curve at Midpoint of ERT Profile showing apparent resistivity (Ωm) as a function of electrode spacing (AB/2 in metres). The red curve represents the measured data, while the blue line shows the modelled fit.

The VES identified five distinct layers with greater detail, as presented in Table 3. Layer 1 (0–1.9 m, 54.9 Ωm) was interpreted as moist topsoil. Layer 2 (1.9–13.5 m, 12.2 Ωm, thickness 11.6 m) was identified as a clayey aquitard that is laterally discontinuous. Layer 3 (13.5–35.7 m, 9.84 Ωm, thickness 22.2 m) was interpreted as the upper aquifer, which is contaminated. Layer 4 (35.7–84.9 m, >2000 Ωm, thickness 49.2 m) was identified as a resistive layer of consolidated clay. Layer 5 (below 84.9 m, 93.1 Ωm) was interpreted as the middle aquifer, which is cleaner.

**Table 3:** Vertical Electrical Sounding (VES) interpretation showing resistivity, thickness, and lithology of subsurface layers in Dogongarage.

| Layer | Depth (m) | Resistivity (Ωm) | Thickness(m) | Interpretation |
|---|---|---|---|---|
| 1 | 0-1.9 | 54.9 | 1.9 | Moist topsoil |
| 2 | 1.9-13.5 | 12.2 | 11.6 | Clayey aquitard (discontinuous) |
| 3 | 13.5-35.7 | 9.84 | 22.2 | Upper aquifer (contaminated) |
| 4 | 35.7-84.9 | >2000 | 49.2 | Resistive layer (Consolidated clay) |
| 5 | Below 84.9 | 93.1 | Not specified | Middle aquifer (cleaner) |

The upper aquifer resistivity of 9.84 Ωm is much lower than the expected 100–300 Ωm for clean freshwater sand in the Chad Formation, indicating contamination by dissolved heavy metals. This marked resistivity reduction indicates ionic enrichment from dissolved heavy metal contaminants originating at the surface [15]. The unconfined nature of this upper layer, confirmed by the absence of a continuous low-resistivity clay cap in the ERT section, makes it directly receptive to infiltrating surface water carrying anthropogenic pollutants. The VES-identified clayey aquitard (12.2 Ωm, 11.6 m thick) between 1.9 m and 13.5 m depth is laterally discontinuous, thinning or disappearing between 50–120 m along the profile as demonstrated by the ERT. Below the aquitard, a consolidated resistive layer (35.7–84.9 m, 2660 Ωm) and the middle aquifer (below 84.9 m, 93.1 Ωm) were identified. Layer 5, with resistivity of 93.1 Ωm, is consistent with the middle aquifer because this value falls within the typical range for clean, freshwater-saturated sands (80–200 Ωm). This interpretation is consistent with the good water quality observed in borehole samples BH/SP 4–BH/SP 6 (Table 4) and agrees with the demarcation of the Chad Formation into upper, middle and lower aquifer systems by Barber & Jones [10].

Heavy metal concentrations in groundwater samples from the six boreholes are presented in Table 4. In the upper aquifer (BH/SP 1–3), chromium concentrations ranged from 0.15 to 0.16 mg/L, lead from 0.024 to 0.026 mg/L, and cadmium from 0.017 to 0.018 mg/L—all exceeding WHO drinking water limits of 0.05 mg/L, 0.01 mg/L, and 0.003 mg/L, respectively. In the middle aquifer (BH/SP 4–6), chromium concentrations ranged from 0.039 to 0.049 mg/L, lead from 0.003 to 0.0061 mg/L, and cadmium was below detection at 0.002 mg/L—all within permissible limits. Iron (0.03–0.041 mg/L) and copper (0.27–0.41 mg/L) remained within safe limits in all water samples, while mercury was not detected in any sample.

**Table 4:** Heavy metal concentrations (mg/L) in groundwater samples from the upper and middle aquifers compared with WHO drinking water guidelines.

| **Parameters** | **Dogongarage Upper Aquifer (mg/l)** | | | **Dogongarage Middle Aquifer (mg/l)** | | | **WHO Limit (mg/L)** |
|---|---|---|---|---|---|---|---|
| | BH/SP 1 | BH/SP 2 | BH/SP 3 | BH/SP 4 | BH/SP 5 | BH/SP 6 | |
| **Hg** | 0 | 0 | 0 | 0 | 0 | 0 | 0.006 |
| **Cr** | 0.16 | 0.15 | 0.16 | 0.039 | 0.041 | 0.049 | 0.05 |
| **Fe** | 0.04 | 0.04 | 0.03 | 0.041 | 0.04 | 0.04 | 0.3 |
| **Cu** | 0.4 | 0.41 | 0.41 | 0.28 | 0.27 | 0.27 | 2 |
| **Pb** | 0.026 | 0.025 | 0.024 | 0.0041 | 0.003 | 0.0061 | 0.01 |
| **Cd** | 0.017 | 0.018 | 0.017 | 0.002 | 0.002 | 0.002 | 0.003 |
| **Latitude** | 11 51 25.23 | 11 51 28.19 | 11 51 20.41 | 11 51 23.81 | 11 51 15.32 | 11 51 27.26 | |
| **Longitude** | 13 08 54.51 | 13 08 50.99 | 13 08 53.43 | 13 09 0.31 | 13 08 47.71 | 13 08 45.74 | |

The geochemical analysis provides strong corroborative evidence for the geophysical interpretation. In the upper aquifer samples, the relative ordering of concentrations across boreholes was consistent for Cr, Cu, Pb and Cd: samples from the upper aquifer (BH/SP 1–3) showed higher values, while samples from the middle aquifer (BH/SP 4–6) showed lower values. This consistent pattern across multiple independently measured metals strongly suggests a common source or co-transport mechanism from anthropogenic inputs. The elevated levels of heavy metals in the upper aquifer are consistent with contamination from anthropogenic sources such as automobile workshops, which are prevalent in the Dogongarage area. Studies from similar automobile workshop environments in Nigeria have reported comparable heavy metal contamination patterns [7].

In the Dogongarage district, the predominant anthropogenic activity capable of releasing this specific metal assemblage is automobile workshops. The consistent pattern of chromium, lead, and cadmium concentrations across the three shallow boreholes points to common sources. The most likely sources in Dogongarage district are lead from lead-acid batteries, paints, and plumbing materials; cadmium from Ni-Cd batteries, pigments, and plastics; chromium from paints and plastics; and copper from electronic waste, wiring, and scrap metals. Iron concentrations did not follow the same pattern as the toxic metals, suggesting iron originates from natural weathering of minerals in the Chad Formation sediments rather than from human activities. The detection of trace Cr, Pb and Cd concentrations in the middle aquifer samples suggests that the confining layers are not completely impermeable, allowing minor downward contaminant migration over time.

The Heavy Metal Pollution Index (HPI) was calculated to assess aggregate pollution levels. The HPI values and corresponding pollution status for each borehole are presented in Table 5. In the upper aquifer, HPI values ranged from 67.68 to 68.55, indicating moderate pollution. In the middle aquifer, HPI values ranged from 15.55 to 19.73, classifying the water as safe. These results demonstrate a clear distinction in water quality between the two aquifer systems.

**Table 5:** Heavy Metal Pollution Index (HPI) values and pollution status of groundwater samples from the upper and middle aquifers.

| Aquifer | Sample | HPI | Interpretation |
|---|---|---|---|
| **Upper** | BH/SP 1 | 68.55 | Moderate Pollution |
| **Upper** | BH/SP 2 | 67.89 | Moderate Pollution |
| **Upper** | BH/SP 3 | 67.68 | Moderate Pollution |
| **Middle** | BH/SP 4 | 16.82 | Safe |
| **Middle** | BH/SP 5 | 15.55 | Safe |
| **Middle** | BH/SP 6 | 19.73 | Safe |

Health risk assessments revealed significant non-cancer risks for vulnerable populations. The Hazard Index (HI) values for each population group and borehole are presented in Table 6. The HI for children consuming upper aquifer water ranged from 1.76 to 1.83, while for pregnant women it ranged from 1.07 to 1.11—both exceeding the threshold of 1.0, indicating potential health concerns. All middle aquifer samples showed HI values below 1.0 for all population groups (children: 0.39–0.44; adults: 0.14–0.16; pregnant women: 0.25–0.27), confirming that the middle aquifer is safe from non-cancer risks. The higher vulnerability of children is consistent with findings from other studies where children were found to be more susceptible to water pollution than adults.

**Table 6:** Hazard Index (HI) values for non-carcinogenic health risks from groundwater consumption across population groups.

| Sample | Children | Adults | Pregnant Women |
|---|---|---|---|
| **BH/SP 1 (upper)** | 1.83 | 0.65 | 1.11 |
| **BH/SP 2 (upper)** | 1.79 | 0.64 | 1.08 |
| **BH/SP 3 (upper)** | 1.76 | 0.63 | 1.07 |
| **BH/SP 4 (Middle)** | 0.42 | 0.15 | 0.26 |
| **BH/SP 5 (Middle)** | 0.39 | 0.14 | 0.25 |
| **BH/SP 6 (Middle)** | 0.44 | 0.16 | 0.27 |

Lifetime Cancer Risk (LCR) estimates are presented in Table 7. All LCR values exceed the acceptable benchmark of $1\times10^{-4}$ for all population groups in both aquifers. In the upper aquifer, children face cancer risks 10–11 times higher than the acceptable threshold ($1.01–1.08 \times 10^{-3}$), pregnant women face 5.8–6.2 times higher ($5.80–6.20 \times 10^{-4}$), and adults face 4.3–4.6 times higher ($4.33–4.61 \times 10^{-4}$). Even in the middle aquifer—which meets WHO guideline values—children face risks 2–5 times higher than the threshold ($2.61–3.28 \times 10^{-4}$), pregnant women face 1.5–1.9 times higher ($1.51–1.89 \times 10^{-4}$), and adults face 1.1–1.4 times higher ($1.12–1.41 \times 10^{-4}$). These findings indicate that the protective clay layer significantly attenuates contaminant concentrations but does not completely prevent migration. Pregnant women consistently exhibit higher LCR values than adults due to their elevated water ingestion rates (2.5 L/day) relative to body weight.

**Table 7:** Lifetime Cancer Risk (LCR) estimates for groundwater consumption across population groups in Dogongarage.

| Sample | Children | Adults | Pregnant Women |
|---|---|---|---|
| BH/SP 1 | **$1.08 \times 10^{-3}$** | **$4.61 \times 10^{-4}$** | **$6.20 \times 10^{-4}$** |

| | | | |
|---|---|---|---|
| BH/SP 2 | $1.01 \times 10^{-3}$ | $4.33 \times 10^{-4}$ | $5.80 \times 10^{-4}$ |
| BH/SP 3 | $1.08 \times 10^{-3}$ | $4.61 \times 10^{-4}$ | $6.20 \times 10^{-4}$ |
| BH/SP 4 | $2.61 \times 10^{-4}$ | $1.12 \times 10^{-4}$ | $1.51 \times 10^{-4}$ |
| BH/SP 5 | $2.75 \times 10^{-4}$ | $1.18 \times 10^{-4}$ | $1.58 \times 10^{-4}$ |
| BH/SP 6 | $3.28 \times 10^{-4}$ | $1.41 \times 10^{-4}$ | $1.89 \times 10^{-4}$ |

Chromium is the dominant carcinogenic risk driver, contributing approximately 99% of the total LCR in both aquifers due to its high oral slope factor $(0.5\ mg/kg/day)^{-1}$ and elevated concentrations. This highlights that regulatory reliance on individual guideline values is inadequate for protecting public health, and that cumulative carcinogenic risk assessment should be incorporated into groundwater quality monitoring programs.

The health risk calculations reveal a serious public health concern. Children and pregnant women drinking from shallow wells face potential non-cancer health effects (HI > 1). Even more concerning, cancer risks exceed acceptable levels for all population groups, including those using deeper boreholes. This means the protective clay layer does not provide complete isolation from surface contamination.

Based on all data, we propose a five-layer conceptual model (Figure 4): (1) a surface source zone where contaminants enter from automobile workshop by-products; (2) a clayey aquitard (1.9–13.5 m, 12.2 Ωm) that is partially protective but laterally discontinuous; (3) an upper aquifer (13.5–35.7 m, 9.84 Ωm) that is highly vulnerable and already contaminated; (4) a resistive layer (35.7–84.9 m, >2000 Ωm) of consolidated clay or basement (thickness: 49.2 m); and (5) a middle aquifer (below 84.9 m, 93.1 Ωm) that is semi-confined, partially protected but still showing trace contamination.

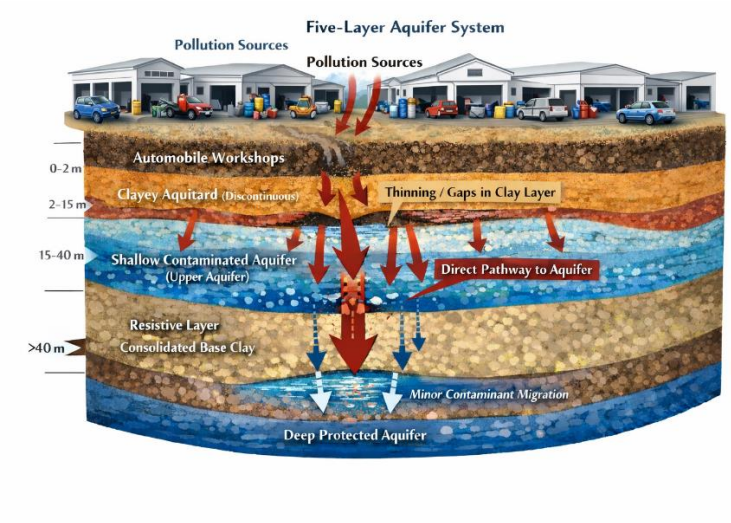



**Figure 4:** Conceptual five-layer aquifer model showing contamination pathways in Dogongarage, Maiduguri. The discontinuous clayey aquitard creates direct pathways for heavy metal contamination from automobile workshops to reach the upper aquifer, while the resistive clay layer provides partial protection to the deeper aquifer.

The conceptual model illustrates how the discontinuous clayey aquitard creates direct pathways for heavy metal contamination from automobile workshops to reach the upper aquifer, while the resistive clay layer provides only partial protection to the deeper aquifer. The persistence of unacceptable cancer risks in the middle aquifer—despite meeting WHO guideline values—demonstrates that conventional water quality standards are insufficient to ensure consumer safety, and that cumulative risk assessment is essential for protecting public health in groundwater-dependent communities.

## 4. Conclusion

This study successfully combined geophysical methods (ERT and VES), water chemistry analysis, and health risk calculations to evaluate groundwater vulnerability in Dogongarage, Maiduguri. The integrated approach revealed that the shallow unconfined upper aquifer (13.5–35.7 m, 9.84 Ωm) is separated from a semi-confined middle aquifer (below 84.9 m, 93.1 Ωm) by a discontinuous clayey aquitard (1.9–13.5 m, 12.2 Ωm) and a resistive layer (35.7–84.9 m, >2000 Ωm). The ERT confirmed that the clayey aquitard is laterally discontinuous, thinning or disappearing between 50–120 m along the profile, creating direct pathways for surface contaminants to reach the upper aquifer. Chromium (0.15–0.16 mg/L), lead (0.024–0.026 mg/L), and cadmium (0.017–0.018 mg/L) exceeded WHO drinking water limits in the upper aquifer, while concentrations in the middle aquifer remained within permissible limits with no overlap in concentration ranges. The Heavy Metal Pollution Index classified the upper aquifer as moderately polluted (HPI: 67.7–68.6) and the middle aquifer as safe (HPI: 15.6–19.7). Children and pregnant women face significant non-cancer risks (HI > 1) from upper aquifer water, while all middle aquifer samples are safe from non-cancer effects. Lifetime Cancer Risk (LCR) exceeded the acceptable threshold ($1\times10^{-4}$) in both aquifers—10–11 times higher for children in the upper aquifer and 2–5 times higher in the middle aquifer—indicating that the protective clay layer significantly attenuates but does not completely prevent contaminant migration. These findings demonstrate that reliance on WHO guideline compliance alone is insufficient to ensure consumer safety, and that cumulative carcinogenic risk assessment should be incorporated into groundwater quality monitoring programs.

Based on these findings, we recommend the following actions. For water supply development, focus on drilling deep boreholes beyond 150 metres to tap the middle or lower aquifers, and ensure proper sealing of boreholes to prevent vertical leakage from contaminated shallow zones. For pollution control, relocate open waste dumps and automobile workshops away from wellhead protection zones, enforce proper disposal of lead-acid batteries and electronic waste, and establish buffer zones between high-risk activities and boreholes. For public health protection, launch community awareness programs about the risks of shallow well water consumption, particularly targeting households with children and pregnant women. Promote the use of deep boreholes (beyond 150 m) or appropriate water treatment technologies such as reverse osmosis (RO) systems (>95% removal efficiency for heavy metals), activated carbon filtration (80–95% removal for Pb and Cr), and ion exchange units (>90% removal for Cr and Cd), which have demonstrated effectiveness in removing chromium, lead, and cadmium from contaminated groundwater. For future research, expand sampling to at least 14 boreholes (7 shallow, 7 deep), conduct additional ERT and VES profiles (minimum 2 each), and implement quarterly sampling to capture seasonal variations in contamination levels. The persistence of unacceptable cancer risks in the middle aquifer—despite meeting WHO guideline values—underscores the urgent need for revised groundwater quality standards that incorporate cumulative carcinogenic risk assessment, and for immediate intervention to protect the health

of groundwater-dependent communities in Dogongarage and similar semi-arid urban environments across sub-Saharan Africa.

**References**

[1] Alley, W. M., Reilly, T. E. & Franke, O. L. (1999). Sustainability of ground-water resources. U.S. Geological Survey Circular 1186. U.S. Geological Survey.

[2] Nistor, M. M., Rahardjo, H., Satyanaga, A. & Hao, K. Z. (2020). Groundwater sustainability in arid and semi-arid environments: A review. Journal of Hydrology, 591, 125568. https://doi.org/10.1016/j.jhydrol.2020.125568

[3] National Population Commission. (2006).2006 Population and housing census of the Federal Republic of Nigeria: Priority tables. National Population Commission.

[4] Grönwall, J. & Danert, K. (2020). Regarding groundwater and drinking water access through a human rights lens: Self-supply as a norm. Water, 12(2), 419. https://doi.org/10.3390/w12020419

[5] Satterthwaite, D. (2007). The transition to a predominantly urban world and its underpinnings. Human Settlements Discussion Paper Series. International Institute for Environment and Development.

[6] Edet, A. E. & Offiong, O. E. (2002). Evaluation of water quality pollution indices for heavy metal contamination monitoring: A study case from Akpabuyo-Odukpani area, Lower Cross River Basin (southeastern Nigeria). GeoJournal, 57(4), 295-304. https://doi.org/10.1023/B:GEJO.0000007250.92458.de

[7] Nwachukwu, A. N. & Orakwe, L. C. (2020). Heavy metal contamination and ecological risk assessment of groundwater around an automobile spare part market in Nigeria. Environmental Monitoring and Assessment, 192(6), 369. https://doi.org/10.1007/s10661-020-08359-0

[8] Adimalla, N. & Qian, H. (2019). Groundwater quality and human health risk assessment in a semi-arid region of south India: Implication to water quality management. Human and Ecological Risk Assessment: An International Journal 25(2), 352-376. https://doi.org/10.1080/10807039.2018.1546550

[9] Kavcar, P., Sofuoglu, A. & Sofuoglu, S. C. (2009). A health risk assessment for exposure to trace metals via drinking water ingestion pathway. Journal of Hazardous Materials, 167(1-3), 1203-1210. https://doi.org/10.1016/j.jhazmat.2009.01.122

[10] Barber, W. & Jones, D. G. (1960). A hydrogeological survey of the Chad Basin. Geological Survey of Nigeria Bulletin No. 30. Geological Survey of Nigeria.

[11] Goni, I. B. (2006). Tracing stable isotope values from meteoric water to groundwater in the southwestern part of the Chad basin. Hydrogeology Journal, 14(5), 742-752. https://doi.org/10.1007/s10040-005-0469-8

[12] Ezekwe, C. I. & Oduroye, N. O. (2018). Aquifer vulnerability and groundwater quality in the coastal plain sands of the Niger Delta, Nigeria. Applied Water Science, 8(4), 108. https://doi.org/10.1007/s13201-018-0745-8

[13] Rahmanian, N., Ali, S. H. B., Homayoonfard, M., Ali, N. J., Rehan, M., Sadef, Y. & Nizami, A. S. (2015). Analysis of physiochemical parameters to evaluate the drinking water quality in the State of Perak, Malaysia. Journal of Chemistry, 2015, 716125. https://doi.org/10.1155/2015/716125

[14] Batayneh, A. T. (2010). Hydrogeophysical and hydrochemical characteristics of the groundwater in the central Jordan Valley. Journal of Environmental and Engineering Geophysics, 15(4), 199-212. https://doi.org/10.2113/JEEG15.4.199

[15] Khalil, M. A. & Santos, F. A. M. (2009). Geoelectrical and hydrogeochemical studies for delineating groundwater contamination in the northern part of the Nile Delta, Egypt. Journal of Geophysics and Engineering, 6(3), 265-277. https://doi.org/10.1088/1742-2132/6/3/006

[16] Kumar, P., Bansod, B. K. S., Debnath, S. K. & Thakur, P. K. (2015). A review on the application of geophysical methods for groundwater exploration in hard rock terrains. Aquatic Procedia, 4, 1239-1246. https://doi.org/10.1016/j.aqpro.2015.02.161

[17] Caeiro, S., Costa, M. H., Ramos, T. B., Fernandes, F., Silveira, N., Coimbra, A., Medeiros, G. & Painho, M. (2005). Assessing heavy metal contamination in Sado Estuary sediment: An index analysis approach. Ecological Indicators, 5(2), 151-169. https://doi.org/10.1016/j.ecolind.2005.02.001

[18] Li, S. & Zhang, Q. (2010). Risk assessment and seasonal variations of dissolved trace elements and heavy metals in the Upper Han River, China. Journal of Hazardous Materials, 181(1-3), 1051-1058. https://doi.org/10.1016/j.jhazmat.2010.05.120

[19] U.S. Environmental Protection Agency. (2004). Risk Assessment Guidance for Superfund (RAGS): Volume I – Human Health Evaluation Manual (Part E, Supplemental Guidance for Dermal Risk Assessment) (EPA/540/R/99/005). Office of Superfund Remediation and Technology Innovation.

[20] Fetter, C. W. (1999). *Contaminant hydrogeology* (2nd ed.). Waveland Press

# ASSESSMENT OF SELECTED HEAVY METALS IN CIGARETTE BRANDS TO INDEX THE CARCINOGENIC AND NON-CARCINOGENIC LEVELS IN FAGGE, KANO, NIGERIA

**Nwoye, E.E.*, Adeyemi, A, E.**

*Department of Chemistry, Nigeria Police Academy, Wudil, Kano state, Nigeria*
** Corresponding Author: elsnowelo@gmail.com*

**Abstract**

Cigarette is obtained from tobacco plant which has the capacity to accumulate toxic elements from its surrounding environment, with the highest concentrations found in the leaves and smoke particulates. Cigarette contains toxic heavy metals such as nickel, cadmium, lead, arsenic and chromium some of which are potential carcinogens. Cigarette smoking is the leading cause of preventable death, surpassing the combined mortality rates of HIV, illegal drug use, alcohol consumption, vehicle accidents, and firearm-related incidents. Excessive accumulation of toxic heavy metals in cigarettes can lead to increase in the risk of various chronic illnesses, including cancer and non-cancer diseases. The analysis was carried out using Atomic Absorption Spectrophotometer. The results from this study showed that all the heavy metals in cigarette brands exceeded the acceptable limit with order of carcinogenicity Pb> Cd> Cr. The hazard quotient (HQ) indicates high health risk and in the order Pb> Co> Cd>Ni >Cr (Adult) and Pb> Co> Ni>Cd >Cr (Children).

**Keywords**: Carcinogens, Cigarette, environment, Heavy metals

## 1. Introduction

Tobacco (*Nicotiana tabacum L.)* is a commercial plant whose leaves are commonly used for making cigarettes, for snuffing, chewing, and pipe smoking [1]. The tobacco plant has a notable capacity to accumulate toxic elements from its surrounding environment, with the highest concentrations typically found in the leaves and smoke particulates. Contributing factors to this accumulation include the soil's pH, sludge containing toxic elements, and fertilizers applied during plant growth. Chronic exposure to tobacco smoke primarily leads to the accumulation of heavy metals, notably Nickel (Ni), Cadmium (Cd), Mercury (Hg), Lead (Pb), Arsenic (As), Silver (Ag), Barium (Ba), and Titanium (Ti). The excessive accumulation of toxic heavy metals in the human body significantly increases the risk of various chronic illnesses, including cancer and non-cancer diseases such as chronic obstructive pulmonary disease [2]. Tobacco smoke possesses toxic, genotoxic, and carcinogenic attributes and within the smoke lie both organic and inorganic compounds known to be carcinogenic to human.

Generally, smoking prevalence stood at 21.1% among males and 0.9% among females. The majority of smokers (78%) fell within the young to middle-aged category (21–50 years old). Smoking rates were notably higher among married individuals, those with lower levels of education, and certain occupational groups, including manual labourers, businessmen, army personnel, and office staff [3]. Each year, approximately 3000 non-smoking adults succumb to lung cancer due to exposure to second hand smoke from others' cigarettes [4]. Factors that have impact on smoking habits of cigarette includes the presence of additive compounds like nicotine, mass production, social acceptance, light weight, availability and relative cheapness [5]. Tobacco-related diseases such as cancer, cardiovascular diseases, and chronic obstructive pulmonary disease have claimed the lives of over 7 million individuals worldwide in 2016 [6]. Research indicates that by the year 2030, the mortality rate attributable to excessive tobacco smoking will decrease by 9% in high-income countries and double in low-income countries [7].

## 3. Materials and Method

Ten different brands of cigarette samples were collected randomly from Fagge Local Government Area. These samples were dried in an oven at 80°C for 6hours and cooled in a desiccator. The dried tobacco was ground into fine powder and then filtered through 2mm mesh size. During the digestion, 0.50 g of each cigarette sample was transferred into a 100mL flat-bottom flask. Subsequently, 5.0 mL of concentrated $HNO_3$ acid was added, and covered with a watch glass and allowed to stand overnight. It was heated on a hot plate at a temperature of 200 °C for 30 minutes, followed by addition of 2 mL of 30% $H_2O_2$ at the same temperature and duration. The resulting digest was evapourated followed by addition of 5.0 mL of 1% $HNO_3$, cooled and filtered into a 25mL volumetric flask and made up to the mark with deionized water.

**3. Results and Discussion**

Table 1: Mean concentration (mg/kg) of heavy metals in cigarette samples

| **Cigarette samples** | **Cd** | **Co** | **Cr** | **Ni** | **Pb** |
|---|---|---|---|---|---|
| Mean & SD | 0.015±0.01 | 0.067±0.01 | 0.007±0.02 | 0.103±0.02 | 1.670±2.16 |
| **USEPA** | **1.0–1.7** | **1.2-1.6** | **1.4–3.2** | **2.1–3.9** | **0.6–1.2** |

The results for mean concentration of cadmium in cigarette samples as shown in Table 1 indicates that the heavy metals levels are within the acceptable range, though prolonged exposure by inhaling air polluted with cigarette smoke over years may still pose toxic effects and harmful consequences. Long-term cadmium exposure can lead to cancer, chronic renal failure, kidney stones, and, in severe instances, secondary skeletal damage [8]. Cobalt exposure from cigarette smoking is generally considered harmful, and even concentrations within what might be considered "safe" limits can still lead to adverse health effects after prolonged exposure. Chromium in in cigarette smoke and ash leads to hemorrhage, respiratory impairment and liver lesions in humans [9]. The concentrations of Cr in the cigarette samples studied showed that its concentration is within the permissible limit. Chromium can exist in multiple oxidation states, only the trivalent (Cr (III)) and hexavalent (Cr (VI)) forms are commonly found in the natural environment. Chromium is known for its genotoxic, allergenic, and irritant properties, and is classified as carcinogen, particularly affecting the lungs and sinus cavities. Additionally, Cr exposure can lead to the induction of methemoglobin formation [10].

The concentration of Ni in the cigarette samples was minimal but nickel exposure through tobacco smoking is recognized as a significant health concern. Nickel levels in the plant range from 0.64–1.15 mg/kg, and its concentration increases significantly during the manufacturing process due to additives used in curing, reaching 0.078–5 mg/kg [11]. The results obtained for lead in the study is in agreement with those results reported by Watanabe et al that lead content in cigarettes sampled from various countries ranged from 0.46 to 3.66 mg/kg. Lead exposure through cigarette smoking is recognized as a significant contributor to total lead intake due to the accumulation of lead in tobacco from soil, air, and agricultural inputs.

**Carcinogenic and Non-Carcinogenic Risk Assessment**

The chronic daily intake (CDI) (mg/kg/day) was used to calculate the non- carcinogenic and carcinogenic risk of heavy metals in the cigarette via ingestion CDI using equations 1 as reported by USEPA, (1989).

$$CDI_{ing} = \frac{Cw \times IR \times EF \times ED}{BW \times AT} \quad \ldots\ldots\ldots\ldots\ldots\ldots\ldots\ldots\ldots\ldots\ldots\ldots\ldots\ldots\ldots\ldots\ldots\ldots \quad 1.$$

Where, Cw= concentration of cigarette sample, IR= Ingestion rate, EF= Exposure frequency, ED=Exposure duration, BW=Body weight, AT=Average exposure time,

**Table 2: The chronic daily intake (CDI) of heavy metal concentration (mg/kg) of cigarette samples**

| **Heavy metals** | **Cd** | **Co** | **Cr** | **Ni** | **Pb** |
|---|---|---|---|---|---|
| **Adult** | $1.56 \times 10^{-2}$ | $6.99 \times 10^{-2}$ | $7.30 \times 10^{-3}$ | $1.07 \times 10^{-1}$ | $I.74 \times 10^{0}$ |
| **Children** | $3.65 \times 10^{-2}$ | $1.63 \times 10^{-1}$ | $1.70. \times 10^{-2}$ | $2.51 \times 10^{-1}$ | $4.06 \times 10^{0}$ |

Carcinogenic risk (CR) assessment estimates the probability of an individual developing cancer over a lifetime due to exposure to the potential carcinogen.

$CR = CSF \times CDI$ …… 2.

The Carcinogenic risk was calculated only for the heavy metal pollutants with carcinogenic or mutagenic data, which include Cd, Cr, and Pb. Cd and Cr are category 1 carcinogens, while Pb is classified as a 2B carcinogen (IARC, 1989). Cancer slope factor for heavy metals: Cd= 0.38, Cr= 0.5, Pb = 0.0085. [12]; [13]. According to [13] CR between $1 \times 10^{-6}$ to $1 \times 10^{-4}$ represents a range of permissible predicted lifetime risks for carcinogens.

Table 3: Carcinogenic risk(CR) of heavy metal concentration (mg/kg) of cigarette samples

| **Heavy metals** | **Cd** | **Cr** | **Pb** |
|---|---|---|---|
| **Adult** | $5.93 \times 10^{-3}$ | $3.65 \times 10^{-3}$ | $1.48 \times 10^{-2}$ |
| **Children** | $1.39 \times 10^{-2}$ | $8.50 \times 10^{-3}$ | $3.45 \times 10^{-2}$ |

All the heavy metals in cigarette samples as shown in table 4 exceeded the acceptable limit suggesting that lifetime exposure to these metals pose cancer risk to the children and adults population in the area. Heavy metal-induced carcinogenesis occurs through induced oxidative stress, DNA damage, and cell death [14]. Cd inhibits the biosynthesis of certain proteins leading to the transformation of normal epithelial cells into carcinogenic cells [15]. Cr, on the other hand, has proven mutagenic and genotoxic effects [16], while the most common tumors found for Pb were of the respiratory and digestive systems, although renal adenocarcinoma has been reported in workmen with prolonged occupational exposure to Lead [17].

**Total hazard quotient**

The non-carcinogenic risk due to smoking of cigarette was estimated using the hazard quotient (HQ) and hazard index (HI). The reference dose (RfD) for the heavy metals: Cd= 0.0005, Co= 0.0003, Cr= 0.003, Ni= 0.02, Pb= 0.0035

Table 4: Hazard quotient (HQ) for heavy metal concentration (mg/kg) of cigarette samples

| **Heavy metals** | **Cd** | **Co** | **Cr** | **Ni** | **Pb** |
|---|---|---|---|---|---|
| Adult | 31.2 | 233.0 | 2.43 | 3.60 | 497.1 |
| Children | 73.0 | 543.3 | 5.7 | 83.7 | 1160 |

The scale of hazard quotient (HQ) based on average daily intake (CDI) and RfD is classified as follows: $HQ \leq 1$ (no risk); $1 < HQ \leq 5$ (low risk); $5 < HQ \leq 10$ (medium risk); $HQ > 10$ (high risk) (USEPA, 1989). The hazard quotient as shown in table 5 indicates that all the heavy metals in the cigarette samples studied showed high risk to human health therefore detrimental to both adult and children population. Hazard index (HI) is 2627.33. The value of the hazard index is proportional to the magnitude of the toxicity of the cigarette to the population.

## 4. Conclusion

The concentrations of cadmium (Cd), cobalt (Co), chromium (Cr), nickel (Ni), and lead (Pb) analyzed indicated that the mean concentrations of these heavy metals in cigarette brands were below the permissible limits. The study on the carcinogenic and non-carcinogenic health risks of heavy metals in cigarette brands showed that all the heavy metals in cigarette samples exceeded the acceptable limit suggesting that lifetime exposure to these metals pose cancer risk to the children and adults population. The order of carcinogenicity is: Pb> Cd> Cr. The Hazard quotient (HQ) for heavy metal concentration is in the order: Pb> Co> Cd>Ni >Cr (Adult) and Pb> Co> Ni>Cd >Cr (Children. The hazard quotient indicates that all the heavy metals in the cigarette samples studied showed high risk to human health therefore detrimental to both adult and children population.

## References

[1] G, Regassa., & B.S, Chandravanshi, B,S. Levels of heavy metals in the raw and processed Ethiopian tobacco leaves. Springerplus, 5(1):1–9, 2016

[2] R, Khlifi, & A., Hamza-Chaffai. Head and neck cancer due to heavy meal exposure via tobacco smoking and professional exposure: a review. Toxicol. Appl. Pharmacol. 248 (2): 71-882, 2010

[3] J.S., Jarallah, Al-Rubeaan, A.R., Al-Nuaim, A.A., Al-Ruhaily., & K.A KalantanPrevalence and determinants of smoking in three regions of Saudi Arabia. *Tobacco Control.* 8(1):53–56, 1999

[4] D.R, Hynes, D.R. *Environmental Pollution. 9, 211-221, 2007*

[5] C., Zhang, J., Miura, & Y., Nagaosa . Determination of cadmium, zinc, nickel and cobalt in tobacco by reversed phase high performance liquid chromatography with 2-(8-quinolazo)-4,5-diphenylimiazole as a chelating reagent. Analytical Sciences, 21(9):1105-1110, 2005

[6] J, Drupe., & N.W., Schulger, N.W. The tobacco atlas. American Cancer Society, 2018

[7] C.D, Mathers., D., Loncar. Projections of Global Mortality and Burden of Disease from 2002-2030. PLOS Medicine 3(11):2005

[8] J., Fowles, & E., Dybing "Application of toxicological risk assessment principles to the chemical constituents of cigarette smoke," Tobacco Control, vol. 12,(4), 424–430, 2003

[9] J.K., Addo, H.A., Gbadago, Affum, T., K.A., Ahmed, G.M., Okley. Mineral profile of Ghanaian dried tobacco leaves and local snuff; a comparative *study J. Radioanal. Nucl. Chem.*, 277(3): 517-524, 2008

[10] X.Y., Zhang.,F.F, Lin., M.T.,Wong.,X.L., Feng., K Wang. Identification of soil heavy metal sources from ansthropogenic activities and pollution assessment of Fuyang County, China Environ Monit Ass, 154:439-449, 2009

[11] *A,* Ersoz., *R, Say, A., Denizli. Nickel(II) ion-imprinted solid-phase extraction and preconcentration in aqueous solutions by packed-bed columns* Anal. Chim. Acta, 502(1): 91-97, *2004*

*[12]* FAO/WHO. Joint FAO/WHO food standard programme codex committee on contaminants in foods, fifth session, Rome, 2013

[13] United State Environmental Protection Agency, USEPA. Risk Assessment Guidance for Superfund: Vol. I, Human Health Evaluation Manual (Part A). Office of Emergency and Remedial Response, U.S. Environmental Protection Agency, Washington, DC, 7-10, 1989

[14] J, G., Kim, J.B., Dixon, C.C., Chusuei & Y., Deng. Oxidation of chromium (III) to (VI) by manganese oxides. Soil Sci. Soc. Am. J, *66(1)*:306–315, 2002

[15] H, Sharma, N., Rawal & B.B., Mathew. The characteristics, toxicity and effects of cadmium. International Journal of Nanotechnology and Nanoscience, 3: 1-9, 2015.

[16] E, Sawicka., K., Jurkowska., & A, Piwowar.Chromium (III) and chromium (VI) as important players in the induction of genotoxicity – current view. Annals of Agricultural and Environmental Medicine, 28(1): 1–10, 2021.

[17] E.L, Baker, R.A., Goyer, & B.A, Fowler, B.A. Occupational lead exposure, nephropathy, and renal cancer. *American Journal of Industrial Medicine, 1:139–148*, 1980

# SUSTAINABLE SLUDGE MANAGEMENT FOR AGRICULTURAL REUSE: A CONCISE REVIEW OF STABILIZATION TECHNOLOGIES, CHALLENGES, AND RESEARCH PRIORITIES

**Muhammad A. Lawal**

*Department of Chemistry, Ahmadu Bello University, Zaria.*
*Email: induceddipole66@gmail.com; malawal@abu.edu.ng*

**Abstract**

The global increase in wastewater treatment facilities has resulted in substantial sludge generation, with annual production exceeding 13 million tonnes (dry weight) in both the United States and Europe, and approximately 20 million tonnes in China. This mini review examines the current state of sludge management with particular emphasis on agricultural reuse as a sustainable disposal strategy. Sludge constitutes a complex matrix containing organic matter, nutrients, and potentially harmful contaminants including endocrine disruptors, pharmaceuticals, toxic metals, and emerging pollutants. The high costs associated with proper sludge treatment—accounting for up to half of total wastewater treatment expenses—have incentivized suboptimal management practices, particularly in developing nations. This review synthesizes existing knowledge on sludge characterization, stabilization techniques, and regulatory frameworks governing agricultural application. Key stabilization approaches including chemical treatment (liming), aerobic digestion, composting, vermicomposting, and anaerobic digestion are critically evaluated for their efficacy in pathogen reduction, organic matter stabilization, and contaminant mitigation. Anaerobic digestion emerges as particularly advantageous due to its dual function in sludge stabilization and biogas production. The review identifies critical knowledge gaps regarding sludge generation data in developing regions, the fate of emerging contaminants in treated sludge, and the need for harmonized international standards to ensure the safety and sustainability of agricultural sludge reuse.

**Keywords:** wastewater treatment plant, sludge, stabilization, management, reuse

## 1. Introduction

The global wastewater treatment infrastructure continues to expand in response to increasing urbanization, industrial development, and environmental regulations. While essential for protecting water resources and public health, wastewater treatment generates significant quantities of sludge as an inevitable by-product.

Recent estimates put the amount of sludge (dry weight) generated yearly in the United States at 13.84 million tonnes [1], 20 million tonnes in China [2], and about 13 million tonnes in Europe [3,4]. South Africa generates about 5 to 7 million $m^3$ $day^{-1}$ of wastewater which is treated in approximately 900 WWTPs [5]. To the best of our knowledge, the total sludge generated in South Africa is not well documented. The nature and characteristics of sludge produced from WWTPs are a function of the source of wastewater influent and treatment processes [6] creating complex management challenges.

The management of wastewater sludge is critical because of its complex nature [7]. The diverse components of wastewater sludge make it a complex mixture to manage, often comprising of very harmful chemicals [8]. Typically, sludge is a sink and reservoir for endocrine disruptors and persistent pollutants, such as pharmaceuticals, pesticides, toxic metals, flame retardants, and other emerging contaminants [1,9-13]. This makes the treatment and disposal of wastewater sludge very expensive and accounts for half the total cost of the wastewater treatment processes [14,15]. For example, it costs between € 30 – 100 to treat 1000 kg of wet sewage sludge [16]. This large capital demand for the proper management of sludge has promoted and encouraged poor sludge management practices especially in poor and developing countries, with large populations [7]. For instance, India treats only about 30% of the generated wastewater in its major cities [17].

Common sludge management methods include landfilling/land application, incineration, and agricultural reuse [18,19]. The predominant sludge disposal methods in South Africa are land application and stock piling at site [20]. Smaller towns and councils in South Africa have been reported to practice composting as a sludge management technique [21]. The choice of a sludge management technique is influenced greatly by the sludge characteristics [6,18].

Conventional methods of sludge disposal present various difficulties making them unsustainable [22]. For instance, the burning of sludge produces very harmful greenhouse gases which have direct and indirect effects on human health and the environment [23]. Another challenge of conventional sludge disposal techniques is the high energy demand [24]. Current trends in European legislation on sludge management are focussed on waste stabilization and safe recycling [7]. Reuse of sludge in agriculture has been an efficient and sustainable sludge management technique adopted by many countries. About 50% of sewage sludge generated in the USA, Europe and China is used for land application such as in agriculture [25-28].

Sewage sludge is rich in organic materials and nutrients required for plant nourishment. Dewatered sewage sludge usually comprises of about 50 -70% organic matter, 30 – 50% minerals, about 4% nitrogen, and 0.5 – 2.5% phosphorus among other useful plant nutrients [29]. However, biological and chemical safety is of utmost significance when sludge is reused in agriculture. Thus legislation safeguarding the use of sludge in agriculture is put in place to ensure the protection of the environment and safety of the produced goods [7]. Consequently, it is customary to subject sludge to rigorous scrutiny and preparation before reuse in agriculture [7]. This is the reason secondary sludge is preferred over primary sludge for agricultural use because of the additional treatment secondary sludge undergoes [9], removing the harmful pathogens and chemicals as far as possible. Some of the techniques employed to ensure the safe reuse of sludge in agriculture include disinfection and stabilization of the sludge prior to use.

This mini review aims to synthesize current knowledge on sludge management with particular emphasis on agricultural reuse strategies. It examines the characterization of sludge, stabilization technologies, regulatory frameworks, and identifies critical knowledge gaps requiring further investigation.

## 2. Stabilization of sludge

Stabilization of sludge is usually achieved through chemical or biological stabilization [29]. Chemical stabilization is popularly achieved by the addition of lime. This increases the pH to about 11 and also serves as a disinfection process for the sludge [29]. Harmful pathogens are eliminated through liming, and the bioavailability of toxic metals is also greatly reduced [30]. However, chemical stabilization with lime is often expensive and depends on the availability of lime [30]. Other chemicals employed for the stabilization and disinfection of sludge include chlorine, and fly ash, among others [30].

Biological sludge stabilization techniques involve the use of microorganisms to convert organic matter in sludge to stable solids. Biological sludge stabilization can be achieved through composting and aerobic digestion, and anaerobic digestion and composting. Aerobic digestion involves the microbial breakdown of organic matter in the presence of oxygen [31]. Composting the sludge aids the aerobic degradation of organics, reduces the sludge volume and kills pathogens present in the sludge [31]. Aerobic digestion results in 20 – 30% of volatile organic compounds present in the sludge [31]. Another form of aerobic stabilization is drying. Drying involves the use of beds designed to dewater and reduce pathogens [7], and it is cheaper relative to other stabilization techniques. Stabilization occurs aerobically through biological processes that help to rid the sludge of pathogens [32]. A kind of composting which involves the use of earthworms for stabilization and reduces the organic content of the sludge has also been reported [7]. This kind of

composting is known as vermicomposting, it is current, environmentally friendly, very efficient and economical [33]. The symbiotic interactions between the earthworms and aerobic microbes in vermicomposting, speed up the degradation of organic matter in the sludge, leading to between 40 to 60% reduction in volume [29,33].

Anaerobic digestion is one of the most popular available sludge stabilization techniques that has been used in sludge treatment [9,29]. Anaerobic digestion has been reported to be effective in eliminating harmful chemicals such as pharmaceuticals and other organic pollutants present in sludge [11]. It involves the degradation of organic matter in wastewater sludge in the absence of oxygen to produce gases like methane, carbon dioxide and ammonia [29]. Even though anaerobic digestion is a targeted sludge stabilization technique, added benefits of economical biogas generation through the process have been reported [34]. Anaerobic stabilization of sludge is achieved by the coordinated actions of a collection of bacteria partaking in a series of biochemical processes [35]. The degradation takes place in a sequence of four reactions: hydrolysis, fermentation (acidogenesis), acetogenesis and methanogenesis [36,37]. The hydrolysis stage involves the breakdown of complex sugars, and other organics into simple sugars, fatty acids and amino acids, which are then transformed through fermentation and acetogenesis to acetate, carbon dioxide and hydrogen [36,37]. Finally, methanogenesis transforms the products to methane [36,37]. Anaerobic digestion can be classified into two based on the operating temperatures: mesophilic at temperatures between 35 – 40 ℃ and thermophilic at temperatures between 55 – 60 ℃ [38]. Mesophilic anaerobic digestion has been reported to be more economic, stable and robust independent of the influent composition, and hence is more widely used in commercial anaerobic digesters [38].

## 3. Future Research Directions

Despite significant advances in sludge management and agricultural reuse technologies, several critical research gaps warrant attention to optimize sustainability and safety outcomes:

*Data Gaps in Sludge Generation and Characterization*

The absence of comprehensive sludge generation data in many regions, particularly in Africa and parts of Asia, impedes effective policy formulation and infrastructure planning. Systematic monitoring programs are urgently needed to quantify sludge production, characterize its composition, and track temporal trends. Such data would enable evidence-based decision-making regarding treatment capacity requirements and resource recovery potential.

*Emerging Contaminants and Fate Studies*

While conventional pollutants are relatively well-characterized, the occurrence, behavior, and fate of emerging contaminants (including microplastics, per- and polyfluoroalkyl substances (PFAS), antibiotic resistance genes, and novel pharmaceuticals) in sludge treatment and agricultural application remain inadequately understood. Long-term field studies examining contaminant accumulation in soils, uptake by crops, and potential transfer through food chains are essential to inform risk assessments and treatment standards.

*Optimization of Stabilization Technologies*

Comparative life cycle assessments of various stabilization techniques under different operational conditions and sludge types would facilitate technology selection optimization. Research should focus on

enhancing the efficiency of existing technologies while reducing energy consumption and costs. The integration of pre-treatment methods (e.g., thermal hydrolysis, ultrasonication) with biological stabilization warrants further investigation to improve organic matter degradation and biogas yields.

*Hybrid and Emerging Technologies*

The development of hybrid treatment systems combining physical, chemical, and biological processes could offer synergistic benefits for contaminant removal and resource recovery. Emerging technologies including advanced oxidation processes, bioelectrochemical systems, and pyrolysis show promise but require further research to establish technical and economic viability at scale.

*Regulatory Harmonization and Risk Assessment*

Variation in regulatory standards across jurisdictions creates challenges for international best practice adoption. Research supporting the development of harmonized, science-based standards for sludge quality, treatment requirements, and application limits is needed. Additionally, comprehensive risk assessment frameworks incorporating cumulative and synergistic effects of multiple contaminants would strengthen regulatory foundations.

*Socio-economic Dimensions*

Understanding the socio-economic factors influencing sludge management practices, particularly in developing regions, is crucial for effective policy implementation. Research on stakeholder perceptions, willingness to adopt agricultural reuse, and economic incentives for sustainable management could inform targeted interventions and technology transfer strategies.

## 4. Conclusion

Sludge management represents a critical sustainability challenge facing the global wastewater sector, with implications for environmental protection, public health, and resource conservation. Agricultural reuse offers a promising pathway that addresses both waste disposal and soil amendment needs, converting a problematic by-product into a valuable resource. The success of this approach, however, depends on effective stabilization to ensure pathogen elimination, contaminant reduction, and agronomic performance.

Biological stabilization technologies, particularly anaerobic digestion, demonstrate significant advantages through their dual function in waste treatment and energy recovery. The economic viability of these approaches, combined with their environmental benefits, positions them as key components of sustainable sludge management strategies. However, the transition to widespread agricultural reuse requires strengthened regulatory frameworks, enhanced monitoring systems, and ongoing research to address emerging challenges.

The integration of sludge management with circular economy principles—recovering nutrients, energy, and organic matter—represents an opportunity to transform wastewater treatment from a cost centre to a resource recovery enterprise. Realizing this potential requires continued investment in research, technology development, and capacity building, particularly in developing regions where improved sludge management offers substantial public health and environmental benefits. Through coordinated efforts across scientific, regulatory, and operational domains, the challenges of sludge management can be addressed while advancing the sustainability of agricultural systems worldwide.

**References**


1. Seiple TE, Coleman AM, Skaggs RL. Municipal wastewater sludge as a sustainable bioresource in the United States. Journal of Environmental Management. 2017;197:673-680.

2. Syed-Hassan SSA, Wang Y, Hu S, et al. Thermochemical processing of sewage sludge to energy and fuel: Fundamentals, challenges and considerations. Renewable and Sustainable Energy Reviews. 2017 2017/12/01/;80:888-913.

3. Kelessidis A, Stasinakis AS. Comparative study of the methods used for treatment and final disposal of sewage sludge in European countries. Waste Management. 2012;32(6):1186-1195.

4. Milieu Ltd WRc Risk and Policy Analysts Ltd (RPA). Environmental, economic and social impacts of the use of sewage sludge on land: Final Report. 2010.

5. United Nations Human Settlements Programme. Global atlas of excreta, wastewater sludge, and biosolids management: moving forward the sustainable and welcome uses of a global resource. In: LeBlanc RJ, Matthews P, Richard RP, editors. Local Economic Development Series: United Nations Human Settlements Programme; 2009.

6. Ahmad T, Ahmad K, Alam M. Sustainable management of water treatment sludge through 3 'R'concept. Journal of Cleaner Production. 2016;124:1-13.

7. Cieślik BM, Namieśnik J, Konieczka P. Review of sewage sludge management: standards, regulations and analytical methods. Journal of Cleaner Production. 2015 2015/03/01/;90:1-15.

8. Nazari L, Sarathy S, Santoro D, et al. Recent advances in energy recovery from wastewater sludge. In: Rosendahl L, editor. Direct Thermochemical Liquefaction for Energy Applications: Woodhead Publishing; 2018. p. 67-100.

9. Gianico A, Braguglia CM, Mascolo G, et al. Partitioning of nutrients and micropollutants along the sludge treatment line: a case study. Environmental Science and Pollution Research. 2013 2013/09/01;20(9):6256-6265.

10. Malmborg J, Magnér J. Pharmaceutical residues in sewage sludge: Effect of sanitization and anaerobic digestion. Journal of Environmental Management. 2015 2015/04/15/;153:1-10.

11. Fijalkowski K, Rorat A, Grobelak A, et al. The presence of contaminations in sewage sludge – The current situation. Journal of Environmental Management. 2017 2017/12/01/;203:1126-1136.

12. Mailler R, Gasperi J, Chebbo G, et al. Priority and emerging pollutants in sewage sludge and fate during sludge treatment. Waste Management. 2014;34(7):1217-1226.

13. Hatinoğlu MD, Sanin FD. Sewage sludge as a source of microplastics in the environment: A review of occurrence and fate during sludge treatment. Journal of Environmental Management. 2021;295:113028.

14. Rulkens W. Sewage sludge as a biomass resource for the production of energy: overview and assessment of the various options. Energy & Fuels. 2008;22(1):9-15.

15. Gebreeyessus GD, Jenicek P. Thermophilic versus mesophilic anaerobic digestion of sewage sludge: a comparative review. Bioengineering. 2016;3(2):15.

16. Gomes LA, Gabriel N, Gando-Ferreira LM, et al. Analysis of potentially toxic metal constraints to apply sewage sludge in Portuguese agricultural soils. Environmental Science and Pollution Research. 2019 2019/09/01;26(25):26000-26014.

17. Kapshe M, Kuriakose PN, Srivastava G, et al. Analysing the co-benefits: case of municipal sewage management at Surat, India. Journal of Cleaner Production. 2013 2013/11/01/;58:51-60.

18. Shaddel S, Bakhtiary-Davijany H, Kabbe C, et al. Sustainable sewage sludge management: From current practices to emerging nutrient recovery technologies. Sustainability. 2019;11(12):3435.

19. Tyagi VK, Lo S-L. Sludge: a waste or renewable source for energy and resources recovery? Renewable and Sustainable Energy Reviews. 2013;25:708-728.

20. Snyman HG, editor South African sludge management guidelines–innovation and impact. Proceedings of the WISA 2010 Biennial Conference, Durban ICC, Durban, South Africa; 2010.

21. Snyman HG, Herselman JE, Kasselman G. A metal content survey of South African sewage sludge and an evaluation of analytical methods for their determination in sludge. Pretoria, South Africa: Water Research Commission; 2004.

22. Kacprzak M, Neczaj E, Fijałkowski K, et al. Sewage sludge disposal strategies for sustainable development. Environmental Research. 2017 2017/07/01/;156:39-46.

23. Liu B, Wei Q, Zhang B, et al. Life cycle GHG emissions of sewage sludge treatment and disposal options in Tai Lake Watershed, China. Science of the Total Environment. 2013;447:361-369.

24. Zhao G, Garrido-Baserba M, Reifsnyder S, et al. Comparative energy and carbon footprint analysis of biosolids management strategies in water resource recovery facilities. Science of the Total Environment. 2019 2019/05/15/;665:762-773.

25. Arlabosse P, Ferrasse JH, Lecomte D, et al. Efficient sludge thermal processing: from drying to thermal valorization. Modern Drying Technology: Volume 4: Energy Savings. 2011;4:295-329.

26. Yu J, editor The foreground analysis of sewage sludge agriculture application in China. Advanced Materials Research; 2011: Trans Tech Publications.

27. Wang T, Chen Y, Li J, et al. Co-pyrolysis behavior of sewage sludge and rice husk by TG-MS and residue analysis. Journal of Cleaner Production. 2020 2020/03/20/;250:119557.

28. Westerhoff P, Lee S, Yang Y, et al. Characterization, recovery opportunities, and valuation of metals in municipal sludges from U.S. wastewater treatment plants nationwide. Environmental Science & Technology. 2015 2015/08/18;49(16):9479-9488.

29. Rorat A, Courtois P, Vandenbulcke F, et al. 8 - Sanitary and environmental aspects of sewage sludge management. In: Prasad MNV, de Campos Favas PJ, Vithanage M, et al., editors. Industrial and Municipal Sludge: Butterworth-Heinemann; 2019. p. 155-180.

30. Pinto AP, de Varennes A, Castanheiro JEF, et al. Chapter 10 - Fly Ash and Lime-Stabilized Biosolid Mixtures in Mine Spoil Reclamation. In: Prasad MNV, Favas PJdC, Maiti SK, editors. Bio-Geotechnologies for Mine Site Rehabilitation: Elsevier; 2018. p. 159-180.

31. Demirbas A, Coban V, Taylan O, et al. Aerobic digestion of sewage sludge for waste treatment. Energy Sources, Part A: Recovery, Utilization, and Environmental Effects. 2017 2017/05/19;39(10):1056-1062.

32. Elalami D, Carrere H, Monlau F, et al. Pretreatment and co-digestion of wastewater sludge for biogas production: Recent research advances and trends. Renewable and Sustainable Energy Reviews. 2019 2019/10/01/;114:109287.

33. Suleiman H, Rorat A, Grobelak A, et al. Determination of the performance of vermicomposting process applied to sewage sludge by monitoring of the compost quality and immune responses in three earthworm species: *Eisenia fetida*, *Eisenia andrei* and *Dendrobaena veneta*. Bioresource Technology. 2017 2017/10/01/;241:103-112.

34. Cao Y, Pawłowski A. Sewage sludge-to-energy approaches based on anaerobic digestion and pyrolysis: Brief overview and energy efficiency assessment. Renewable and Sustainable Energy Reviews. 2012 2012/04/01/;16(3):1657-1665.

35. Parkin Gene F, Owen William F. Fundamentals of Anaerobic Digestion of Wastewater Sludges. Journal of Environmental Engineering. 1986 1986/10/01;112(5):867-920.

36. Oladejo J, Shi K, Luo X, et al. A review of sludge-to-energy recovery methods. Energies. 2019;12(1):60.

37. Senés-Guerrero C, Colón-Contreras FA, Reynoso-Lobo JF, et al. Biogas-producing microbial composition of an anaerobic digester and associated bovine residues [https://doi.org/10.1002/mbo3.854]. MicrobiologyOpen. 2019 2019/09/01;8(9):e00854.

38. Labatut RA, Angenent LT, Scott NR. Conventional mesophilic vs. thermophilic anaerobic digestion: A trade-off between performance and stability? Water Research. 2014 2014/04/15/;53:249-258.

# REMOVAL OF HEAVY METALS IN SPENT SYNTHETIC-BASED DRILLING MUD USING NANO ZERO-VALENT IRON (nZVI)

**Obinduka, F.O[1*], Uchechukwu, T.O[2], Effiong, E[3]**

[1]*Department of Environmental Management and Toxicology, University of Agriculture and Environmental Sciences Umuagwo, Owerri, Nigeria.*
[2]*Department of Chemistry, Alex Ekwueme Federal University, Ndufu Alike, Nigeria.*
[3]*Department of Biological Sciences, Edwin Clark University Kiagbodo, Delta State, Nigeria.*
**Corresponding author: Obinduka.felix@gmail.com;*

**Abstract**

Management of waste generated from oil and gas activities in the Niger Delta, is a major environmental challenge given that if the spent mud is disposed without proper treatment, the heavy metals will pose a lot of health risks to human through ingestion or inhalation. The heavy metals are also toxic to marine organisms, if disposed into the sea, untreated. Spent synthetic drilling mud is a major waste stream, among its components, are heavy metals. Samples collected on day 1 and biweekly were digested and analysed using the atomic absorption spectrometer (AAS). With nano Zero-Valent Iron, nZVI, concentration of 0.75mg/L of the spent mud, more than 95% removal were recorded for most metals in 6 weeks and over 99% in 12 weeks. The residual heavy metal concentrations met global limits for effluent disposal.

**Keywords:** Spent synthetic-based drilling mud: Niger Delta: Heavy metals: Nano zero-valent Iron

## 1. Introduction

Drilling and production activities generate two main types of waste: drill cuttings and spent drilling mud. Drilling fluids including synthetic base fluids (SBFs) are suspension of solid in liquid emulsion and/or dissolved materials with chemical additives which play significant roles during drilling. Major functions of drilling fluids include lifting of drill cuttings from the well, controlling the hydraulic pressure to prevent blowouts, and keeping the drilled well from collapsing before causing installation. Heavy metals are some of the major contaminants in impacted spent drilling mud, that cause harm and pollution to the environment. The use of nano Zero-Valent Iron (nZVI) in treating soil and underground water containing heavy metals has been documented [1]. nZVI transforms the heavy metals to non or less toxic compounds. A highly reactive, remediation grade Nano Zero-Valent iron (nZVI) was used in this study to treat spent drilling mud of heavy metals. nZVI is cost effective, sustainable, and green. nZVI interaction with heavy metals, being an abiotic reaction destroys contaminants with no toxic end products or by-products, and are free of rust and dust.

## 2. Materials and Methods

### Study area

This study was carried out with spent drilling mud obtained from five oilfields in the Niger Delta. Samples A, B, C, D and E were taken at Longitude 5°9'40.58"East and Latitude 5°19'17.71"North, Longitude 6°47'4.912"East and Latitude 3°11'37.644"North, Longitude 6°16'41.972"East and Latitude 4°11'42.948"North, Longitude 6°21'20.38"East and Latitude 4°54'28.648"North, Longitude 6°42'12.077"East and Latitude 4°59'30.057"North, respectively (Figure 1). The region has a population of 30 million people [2]. Over 90% of Nigeria's proven oil and gas reserves are domiciled in the region [3]

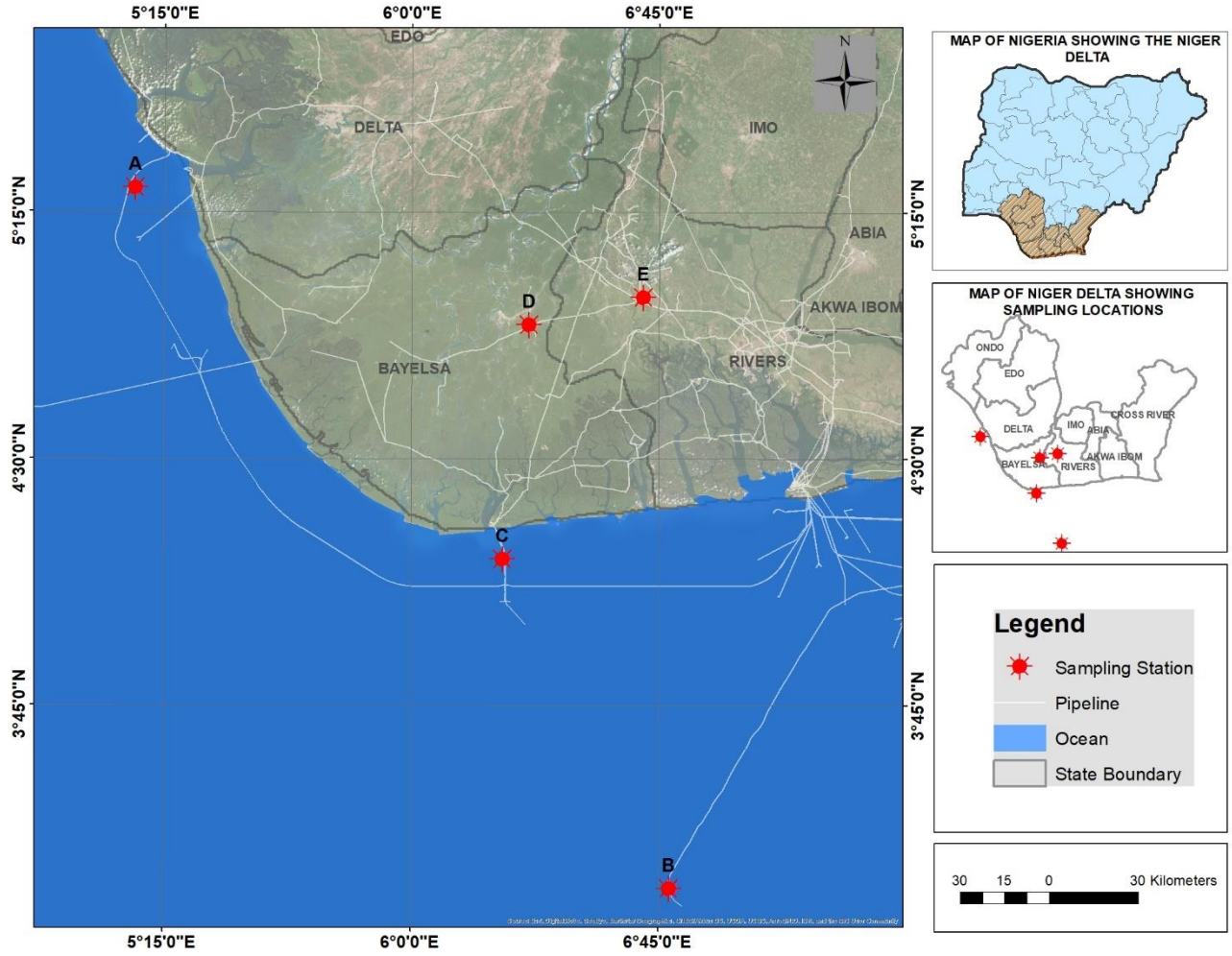



Figure 1.Map of study area and sample location

**Data collection**

Adequate quantities of the spent mud from the five oil fields were sampled and transported to the laboratory. The samples were marked MUD-A to E. For each field, spent mud was transferred into 25 different containers. Each container was filled with 20 Litre of the mud. One sample was tested for baseline values of the physicochemical parameters. Six samples were set aside for control while 5, 10, and 15 g of nZVI were added to six samples each.

Control sample was the original spent mud without treatment The amended samples were thoroughly mixed for effective chemical reaction. To evaluate the effectiveness of nano-Zero-Valent Iron in the treatment of heavy metals encountered in spent drilling mud, 4 digested samples, one from 5, 10 and 15 g treatment , were tested for the concentration of residual heavy metals, every two weeks for twelve weeks by Atomic Absorption Spectrometer (AAS,PinAAcle 900H model). Sample concentration was determined by comparing absorbance with that of standard. The same experiment was carried out simultaneously for MUD-B, MUD-C, MUD-D and MUD-E.

**3. Results and Discussion**

**Baseline concentration of heavy metal in Spent Drilling Mud**

The baseline results of the spent drilling mud (Table 1), show that most of the heavy metals exceeded the maximum allowable limits for effluent disposal on land according to the Nigerian Upstream Petroleum Regulatory Commission (NUPRC) - the regulatory body in Nigeria, US EPA and some selected countries as shown in Table 2. The high level of heavy metals in the spent mud can impact on human health and the

environment, if disposed of land untreated [4]. This means that the spent mud must be treated before disposal.

Table 1: Baseline distribution of heavy metals, pH and temperature of the spent drilling mud

| Sample Designation | | | | | | |
|---|---|---|---|---|---|---|
| S/NO | Parameters | A | B | C | D | E |
| 1 | pH | 7.5± 0.01$^{b}$ | 7.3±0.01$^{a}$ | 7.8±0.00$^{c}$ | 7.4±0.09$^{a}$ | 7.9±0.00$^{c}$ |
| 2 | Temperature ($^{o}$C) | 28±0.00$^{a}$ | 28.3±0.10$^{b}$ | 28.7±0.05$^{c}$ | 29.0±0.00$^{d}$ | 28.5±0.10$^{bc}$ |
| 3 | Pb (mg/L) | 39.0±0.00$^{c}$ | 52.2±0.2$^{e}$ | 5.6±0.2$^{a}$ | 18.6±0.3$^{b}$ | 38.6±1.4$^{c}$ |
| 4 | Zn (mg/L) | 59.2±0.8$^{b}$ | 79.3±0.3$^{c}$ | 15.35±0.45$^{a}$ | 98.6±0.2$^{d}$ | 80.2±0.2$^{c}$ |
| 5 | Cr (mg/L) | 59.0±0.4$^{d}$ | 60.2±0.1$^{e}$ | 17.3±0.3$^{c}$ | 23.4±0.4$^{b}$ | 39.2±0.2$^{c}$ |
| 6 | Cu (mg/L) | 10.4±0.4$^{a}$ | 22.9±0.0$^{d}$ | 26.5±0.3$^{e}$ | 17.4±0.4$^{c}$ | 15.0±0.3$^{b}$ |
| 7 | As (mg/L) | 94.3±0.3$^{e}$ | 56.1±0.1$^{d}$ | 8.7±0.2$^{b}$ | 5.8±0.2$^{a}$ | 9.8±0.2$^{c}$ |
| 8 | Hg (mg/L) | 0.005± 0.001$^{a}$ | 1.70±0.25$^{bc}$ | 2.29±0.03$^{c}$ | 1.9±0.3$^{bc}$ | 1.3±0.2$^{b}$ |
| 9 | Cd (mg/L) | 0.037± 0.002$^{a}$ | 0.039±0.003$^{a}$ | 6.2±0.2$^{d}$ | 5.2±0.4$^{c}$ | 2.7±0.3$^{b}$ |
| 10 | Ni (mg/L) | 0.00±0.00$^{a}$ | 0.045±0.0025$^{b}$ | 0.001±0.00$^{ab}$ | 0.001$^{ab}$±0.00$^{ab}$ | 0.00±0.00$^{a}$ |
| 11 | V (mg/L) | 0.005±0.001$^{b}$ | 0.008±0.001$^{b}$ | 0.003±0.001$^{ab}$ | 0.003±0.001$^{ab}$ | 0.004±0.001$^{a}$ |

$^{a-e}$Results are presented as mean ± standard error. Means with different superscript, the homogenous subset of means, (a, ab, b, bc, c, d and e) within the same rows indicate significant differences ($p < 0.05$),

Table 2: Nigeria (NUPRC), US EPA and other countries guidelines and standards for heavy metals on land

| Heavy metals (mg/L) | | | | | | | |
|---|---|---|---|---|---|---|---|
| Country | As | Pb | Hg | Cd | Cr(VI) | Cu | Zn |
| Bulgaria | 100.0 | 26.0 | 0.03 | 0.4 | 65.0 | 34.0 | 88.0 |
| Argentina | 0.5 | 10.0 | 0.20 | 0.2 | 8.0 | - | - |
| Tanzania | 1.0 | 200.0 | 2.00 | 1.0 | 100.0 | 200.0 | 150.0 |
| South Africa | 58.0 | 20.0 | 0.93 | 7.5 | 6.5 | 16.0 | 240.0 |
| Nigeria | 5.0 | 5.0 | 0.20 | 1.0 | 5.0 | 0.05 | 50.0 |
| US EPA | 10.0 | 1.3 | 0.90 | 0.2 | 11.4 | 5.20 | 66.6 |

Source: [5]; [6]

**Heavy Metal removal**
**Control Sample**

The control sample showed slight reduction in concentration of the heavy metals as can be seen in Figure 1. This little reduction could be attributed to biosorption by some microorganisms like *Bacillus thuringiensis, Geomyces pannorum, Pseudomonas* sp., *Citrobacter* sp., etc. [7].

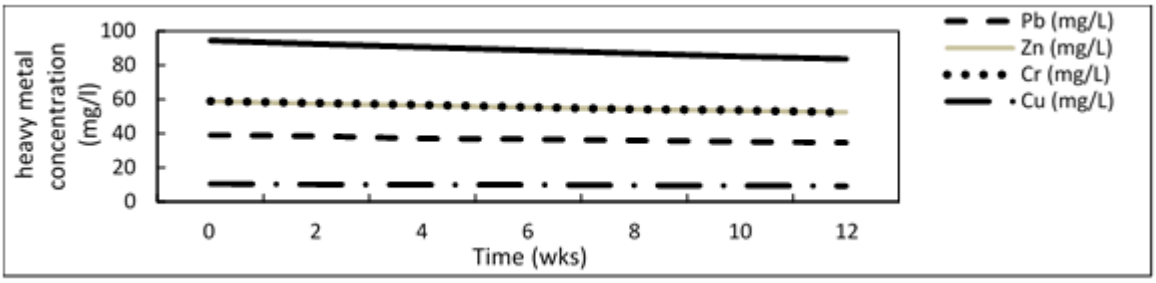



Figure 2: Heavy metal reduction of control Sample-A

**Residual heavy metals**

The five samples of the spent drilling mud studied had different levels of concentration of the heavy metals, most of which were above allowable limits by regulatory authorities (Table 2). However, after separate treatment with 5g,10g and 15g of nZVI for 12 weeks, the concentration of the heavy metals dropped remarkably. A sharp drop was recorded in 4 weeks, after which the contaminant reduction continued progressively (Figure 3). The ability of Iron as Fe(0) and Fe(II) to reduce redox sensitive elements has been demonstrated at both laboratory scale and field tests [8].

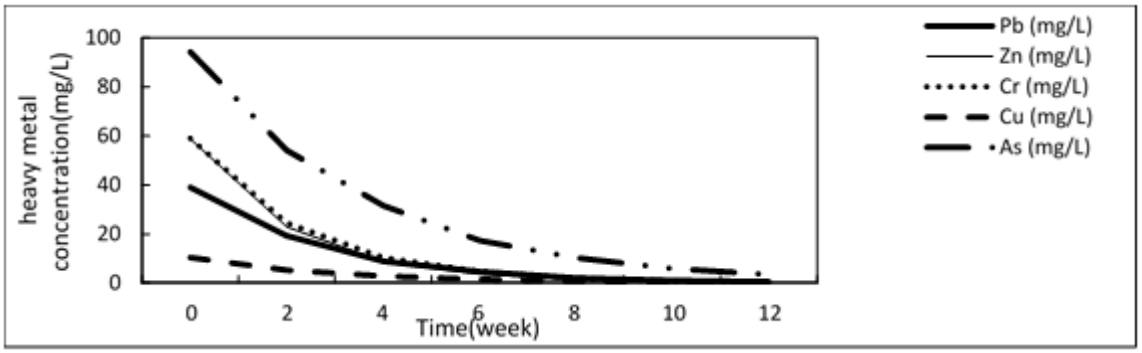



Figure 3*:* Treatment response of Sample-A with 15g nZVI

**Rate of heavy metal removal by 5, 10 and 15g doses of nZVI**

The concentration of heavy metals in the spent drilling mud was brought down to 90%, 95% and 99% by 5,10 and 15g nZVI treatment, respectively in twelve weeks (Figure 4). The rate of mercury removal in the spent mud, using 5,10 and 15g doses of nZVI is shown in Figure 4. It can be seen from the Figure that for the period of treatment,15g nZVI treatment proved to be more effective than 5 and 10 g treatment. The same trend was observed with other metals. Iron based technologies for remediation of contaminated groundwater and soil has been documented [9]. nZVI has been proven to be a strong chemical reductant and is able to convert many mobile oxidized oxyanions e.g $CrO^{2}_{4}$ and oxycations e.g $UO_2^{2+}$ into immobile forms [9].

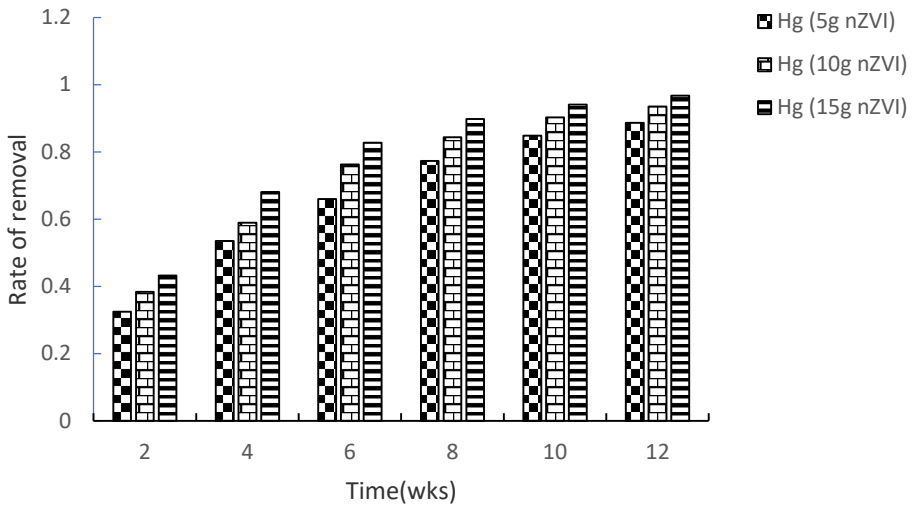



Figure 4: Rate of mercury removal by 5,10 and 15 g treatment

## 4. Conclusion

Based on this study, it can be concluded that spent drilling mud from different fields in the Niger Delta have different concentrations of heavy metals, and nZVI can effectively treat spent synthetic based mud laden with heavy metals. A reduction of over 99% in 12 weeks was recorded. The heavy metal concentrations in the treated spent mud, for the five mud samples tested complied with Nigerian NUPRC and other international prescribed limits (Table 2).

## References

[1] M. Liu, G. Chen, L. Xu, Z. He, and Y. Ye, "Environmental remediation approaches by nanoscale zero valent iron (nZVI) based on its reductivity: A review," *RSC Advances*, vol. 14, pp. 21118–21138, 2024. doi: 10.1039/D4RA02789B.

[2] National Population Commission, "2023/2024 Nigeria Demographic and Health Survey," 2024. Available: NPC Nigeria Demographic Survey. Accessed: May 26, 2026.

[3] Organization of the Petroleum Exporting Countries, "Annual Statistical Bulletin 2025," 2025. Available: OPEC Official Website. Accessed: May 26, 2026.

[4] Z. Yan, J. Ouyang, B. Wu, C. Liu, H. Wang, A. Wang, and Z. Li, "Nonmetallic modified zero-valent iron for remediating halogenated organic compounds and heavy metals: A comprehensive review," *Environmental Science and Ecotechnology*, vol. 21, p. 100417, 2024. doi: 10.1016/j.ese.2024.100417.

[5] C. Kamunda, M. Mathuthu, and M. Madhuku, "An assessment of radiological hazards from gold mine tailings in the province of Gauteng in South Africa," *International Journal of Environmental Research and Public Health*, vol. 13, no. 1, p. 138, 2016, doi: 10.3390/ijerph13010138.

[6] K. Clements, J. A. Veil, and A. J. Leuterman, "Global practices and regulations for land application and disposal of drill cuttings and fluids," in *Proceedings of the SPE International Conference on Health, Safety and Environment in Oil and Gas Exploration and Production*, Rio de Janeiro, Brazil, 2010, Paper SPE-126565-MS, doi: 10.2118/126565-MS.

[7] M. Namakka, M. R. Rahman, K. A. B. Mohamad Said, and A. Muhammad, "Insights into micro-and nano-zero valent iron materials: Synthesis methods and multifaceted applications," *RSC Advances*, vol. 14, pp. 30411–30439, 2024. doi: 10.1039/D4RA03507K.

[8] M. Liu, G. Chen, L. Xu, Z. He, and Y. Ye, "Environmental remediation approaches by nanoscale zero valent iron (nZVI) based on its reductivity: A review," *RSC Advances*, vol. 14, pp. 21118–21138, 2024. doi: 10.1039/D4RA02789B.

[9] M. Komárek, "Perspectives of soil nanoremediation: The case of nano zerovalent iron and metal(loid) contaminants," *npj Materials Sustainability*, vol. 2, no. 8, pp. 1–14, 2024. doi: 10.1038/s44296-024-00013-z.

# GEOPHYSICAL ASSESSMENT OF GEOTHERMAL ENERGY POTENTIAL IN THE SOKOTO BASIN, NORTHWESTERN NIGERIA

**Aliyu, A[1*]., Sonloye, A. S[1]., Amusat, R. O[1]., Hassan, M[1]., Joseph, A, A[2]., Usman, A[3]., Aliyu, M. L[4]., Balarabe, B[5]., Umar, M[5].**

*[1]Department of Physics, University of Maiduguri, P. M. B 1069.*
*[2]Modibbo Adamawa University, Yola*
*[3]Department of Physics, Kebbi State University of Science and Technology, Aliero. [4]Department of Geology, Aliko Dangote University of Science and Technology.*
*[5]Department of Physics, Ahmadu Bello University, Zaria.*
*Corresponding author: aliyu@unimaid.edu.ng*

**Abstract**

The growing global demand for sustainable and low-carbon energy sources has intensified interest in geothermal resources, particularly within sedimentary basins characterized by favourable thermal regimes. This study presents a geophysical assessment of geothermal energy potential within the Sokoto Basin, a major intracratonic basin in northwestern Nigeria. The investigation integrates aeromagnetic data analysis, spectral depth estimation, and geothermal gradient modelling to evaluate subsurface thermal structures and heat flow characteristics. Curie Point Depth (CPD) estimation derived from magnetic spectral analysis range between 34.11 and 124.01 km with an average value of 66.07 km while the heat flow ranges from 11.69 to 42.51 $mWm^{-2}$ with an average value of 21.95 $mWm^{-2}$which infer the depth to the bottom of magnetized crust, which serves as a proxy for geothermal gradient distribution. Results indicate spatial variations in CPD ranging from shallow to moderately deep depths, suggesting localized zones of elevated geothermal gradient and enhanced heat flow. These thermal anomalies are structurally controlled by basement lineaments and fault systems that may facilitate heat transfer from deeper crustal levels. The findings highlight several prospective geothermal zones with significant implications for renewable energy development and regional energy diversification. The study has demonstrated that integrated geophysical techniques provide an effective framework for preliminary geothermal resource assessment in sedimentary environments and underscores the potential of the Sokoto Basin as a viable target for geothermal exploration in Nigeria.

**Keywords:** Geothermal, Renewable Energy, Curie Point, Heat flow, Sokoto Basin

## 1. Introduction

The global transition toward low-carbon energy systems has intensified interest in geothermal resources as a reliable, baseload renewable energy option. Geothermal energy, derived from subsurface heat stored within the Earth's crust, offers continuous power generation potential with minimal greenhouse gas emissions compared to fossil-based alternatives. In sedimentary basins, geothermal prospectivity is typically controlled by variations in Curie point depth (CPD), geothermal gradient, heat flow, and subsurface thermal conductivity, all of which can be effectively constrained using geophysical data such as aeromagnetic data analysis [1]. In Nigeria, increasing energy demand and persistent electricity deficits have motivated the exploration of alternative renewable resources beyond hydropower and gas-fired generation. The Sokoto Basin, part of the larger Iullemmeden Basin in northwestern Nigeria, has emerged as a significant geological province of interest due to its sedimentary thickness, tectonic evolution, and evidence of elevated subsurface thermal regimes [2]. Previous studies have demonstrated that sedimentary basins such as Sokoto can exhibit moderate to high geothermal gradients, particularly in zones where crustal thinning and radiogenic heat production influence thermal structure [3].

Despite these advances, geothermal exploration in Nigeria remains underdeveloped, with limited systematic characterization of deep thermal structures across most basins, including Sokoto. Existing studies are often localized and lack modern and international techniques of analysing and interpreting geophysical frameworks of CPD estimation, heat flow modelling, and structural interpretation at basin scale. Consequently, there is a need for more comprehensive geophysical assessments to refine the understanding of geothermal potential and to support future exploration and energy development strategies in the region.

## 2. Materials and Method

This study utilized high-resolution aeromagnetic data (Sheets 10, 11, 29, and 30) covering parts of the Sokoto Basin, Northwestern Nigeria. The dataset comprises total magnetic intensity (TMI) measurements acquired from airborne geophysical surveys conducted over the region. The data were obtained from Nigerian Geological Survey Agency (NGSA) with uniform flight line spacing and corrected for diurnal variations, IGRF (International Geomagnetic Reference Field), and other regional effects to ensure consistency and reliability for subsurface interpretation. Other materials used were software; Oasis-Montaj, Geothermal Plotter, Sufer, Msc Excel and Arc-GIS.

**Reduction to Equator (RTE) Transformation:** The TMI data were first transformed into the RTE magnetic field using standard reduction techniques. This correction compensates for inclination and declination effects, ensuring that magnetic anomalies are symmetrically aligned with their geological sources, thereby improving spectral depth estimation accuracy [4], [5]. The RTE map of the Sokoto Basin reveals a heterogeneous magnetic signature characterized by alternating high and low magnetic intensity zones, indicating variations in basement depth, lithological contrasts, and structural discontinuities [4], [5].

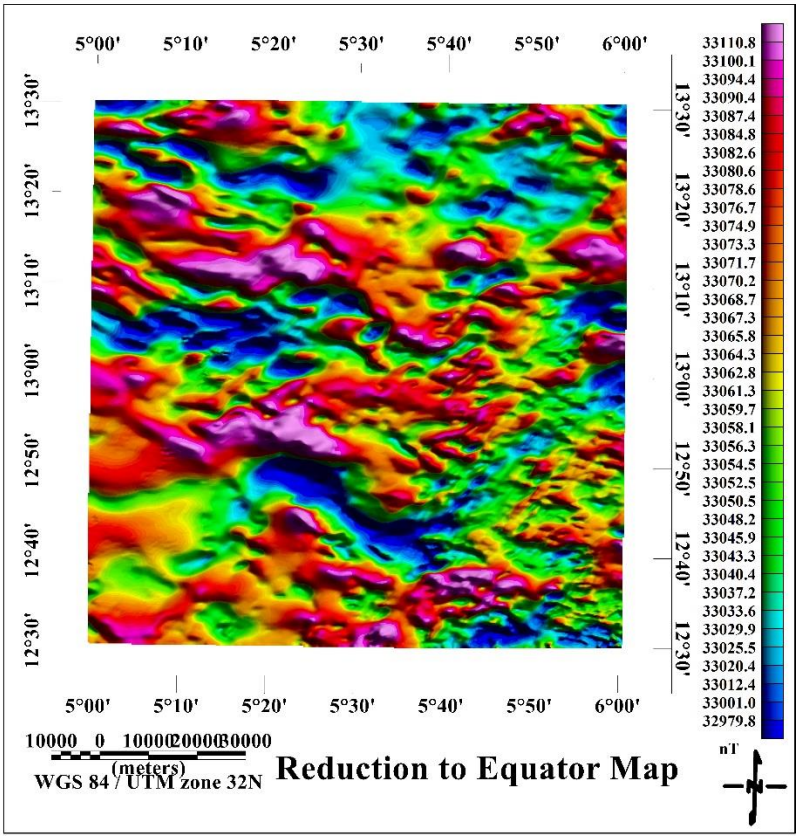



Figure 1: Reductio-to-Equator (RTE) Magnetic Anomaly Map of the Sokoto Basin

**Spectral Depth Estimation (Zo, Zt, Zb):** Spectral analysis of the RTE magnetic data was performed using the radial power spectrum method (Fast Fourier Transform)**.** This technique is widely used for estimating Curie point depth and related thermal parameters [6], [7]. Three key depths were derived using slope relationships of power spectrum:

**$Z_o$ (Centroid depth)** – average depth of magnetic sources

$$Zo = -\frac{1}{2} \quad \text{Slope of low frequency segment} \qquad 1$$

**Zt (Top boundary depth)** – depth to the top of magnetic layer

$$Zt = -\frac{1}{2} \quad \text{Slope of high frequency segment} \qquad 2$$

**Zb (Bottom boundary / Curie point depth)** – depth at which ferromagnetic minerals lose magnetization (~580°C)

$$Zb = 2Zo - Zt \qquad 3$$

The Curie point depth (Zb) is a fundamental geothermal parameter widely used in regional heat flow estimation [7], [8].

**Geothermal Gradient (dT/dZ) Estimation:** The geothermal gradient was derived from Curie point depth assuming a Curie isotherm temperature of approximately 580°C:

$$\frac{dT}{dZ} = \frac{T_c - T_s}{Zb} = \frac{580^0C - T_s}{Z_b} \quad 4$$

where Tc is the Curie Temperature, Ts surface temperature and Zb curie point depth (km)

**Surface Heat Flow (q) Estimation:** Heat flow was calculated using Fourier law of heat conduction

$$q = k\left(\frac{dT}{dZ}\right) = k\frac{580^oC - T_s}{Zb} \quad 5$$

where q is the heat flow and k are the coefficient of thermal conductivity which varied within the study area due to different rock units.

This approach is standard in geothermal exploration in Nigerian sedimentary basins for assessing subsurface heat potential [6], [8].

### 3. Results and Discussion

The entire study area was segmented into sixteen (16) blocks, spectral plots were extracted from each block (fig. 2) to display depth to top (Zt) and to centroid (Zo). Complete determined and calculated data shown in table 1 were harnessed to produced maps of top, centroid, bottom, GTG, and heat flow as shown in fig. 3a-e

The depth to top depth (Zt) (fig. 3a) ranges from shallow levels (6 km to 26 km) in structurally disturbed zones around eastern, central and northern regions associated with near-surface volcanic or basement uplift features to deeper depth values of (30 to 60 km) in stable sedimentary regions. This implies that accessibility of geothermal energy is cost effective at shallower depths and capital intensive at greater depths by the virtue of cost of drilling.

Spectral analysis of the RTE magnetic data yielded spatially varying estimates of magnetic source depths. The centroid depth (Zo) (fig. 3b) shows moderate to high depth variation ranging from 62 km to 90 km across the western and eastern part of the basin, indicating uneven distribution of magnetic sources within the crust, shallow to most shallow depth is recorded around central, northern and southern parts of the study area.

The most critical parameter, the **Curie point depth (Zb) (fig. 3c)**, exhibits significant spatial variation across the study area. Estimated Zb values range from relatively shallow depths (30 to 65 km) in the NNE, SS and SW portions of the basin to deeper levels (100 to 125) toward the NW and E margins. These variations suggest strong lateral changes in crustal thermal structure and also indicated elevated geothermal condition. Shallow Curie depths indicate elevated geothermal conditions, while deeper Curie depths correspond to cooler crustal regimes. Similar variations in CPD have been reported in other sedimentary basins in West Africa and are often linked to crustal thinning, tectonic reactivation, and radiogenic heat concentration [4], [5].

Table 1: Results of Spectral Depth Estimates (Centroid Depth Zo; Top Depth, Zt; Curie point Depth, Zb), Geothermal Gradient (dT/dZ), and Surface Heat Flow (q) values across the sixteen (16) Blocks within the Sokoto Basin

| Blocks | Long/deg | Lat/deg | Zo/km | Zt/km | Zb/km | dT/dz (C/km) | q (mW/m^2) |
|---|---|---|---|---|---|---|---|
| 1 | 5.24639 | 13.25338 | 45.99 | 8.09 | 83.89 | 6.91 | 17.2845393 |
| 2 | 5.40211 | 13.25567 | 37.83 | 9.33 | 66.33 | 8.74 | 21.860395 |
| 3 | 5.58531 | 13.25796 | 42.72 | 19.47 | 65.97 | 8.79 | 21.9796877 |
| 4 | 5.749045 | 13.26025 | 31.39 | 11.15 | 51.63 | 11.23 | 28.084447 |
| 5 | 5.249825 | 13.0885 | 88.65 | 53.29 | 124.01 | 4.68 | 11.6926054 |
| 6 | 5.405545 | 13.09193 | 49.25 | 21.07 | 77.43 | 7.49 | 18.7265918 |
| 7 | 5.5876 | 13.09422 | 36.14 | 16.68 | 55.6 | 10.43 | 26.0791367 |
| 8 | 5.751335 | 13.09651 | 39.81 | 18.64 | 60.98 | 9.51 | 23.778288 |
| 9 | 5.24868 | 12.91102 | 37.56 | 29.61 | 45.51 | 12.74 | 31.8611294 |
| 10 | 5.407835 | 12.91446 | 50.68 | 16.9 | 84.46 | 6.87 | 17.1678901 |
| 11 | 5.588745 | 12.91675 | 32.31 | 23.38 | 41.24 | 14.06 | 35.1600388 |
| 12 | 5.75019 | 12.91904 | 57.34 | 17.37 | 97.31 | 5.96 | 14.9008324 |
| 13 | 5.25097 | 12.75072 | 33.19 | 32.27 | 34.11 | 17.00 | 42.509528 |
| 14 | 5.4093 | 12.75318 | 41.63 | 15.66 | 67.6 | 8.58 | 21.4497041 |
| 15 | 5.59398 | 12.75204 | 39.47 | 34 | 44.94 | 12.91 | 32.2652425 |
| 16 | 5.75244 | 12.75204 | 35.82 | 15.56 | 56.08 | 10.34 | 25.8559201 |

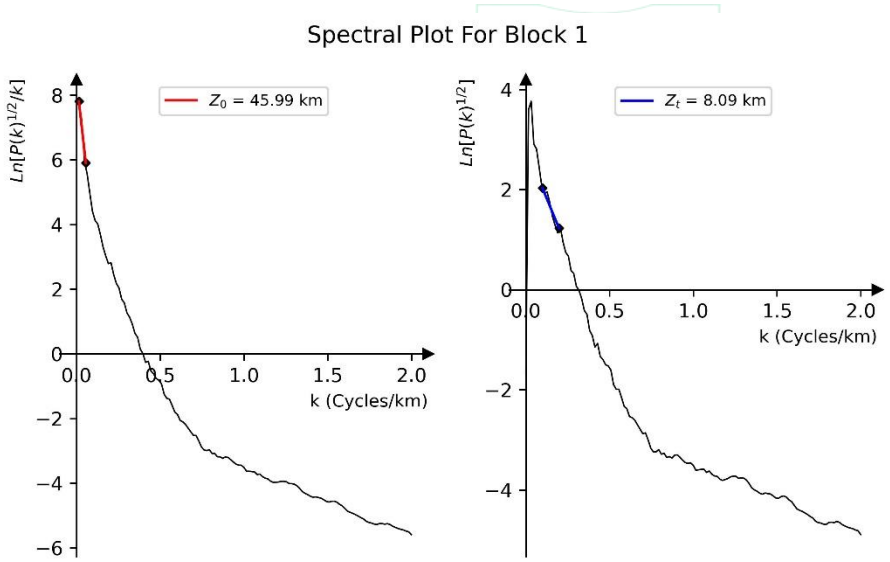
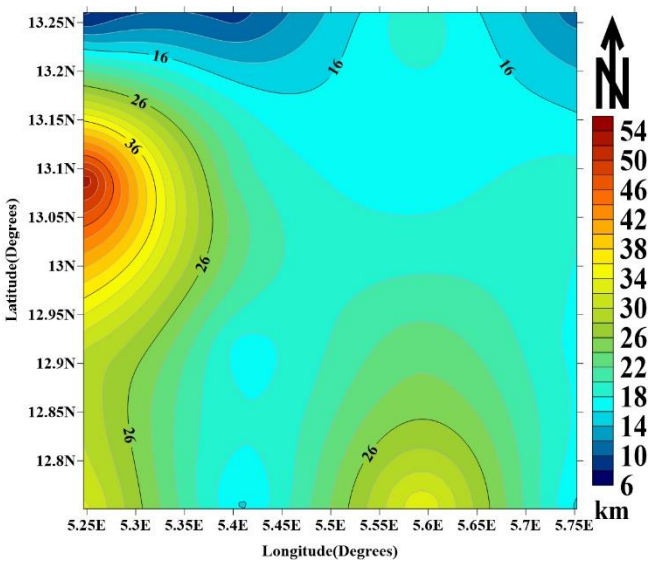
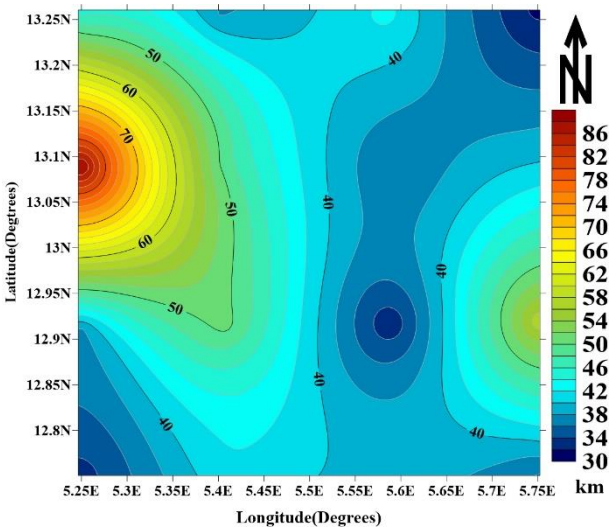
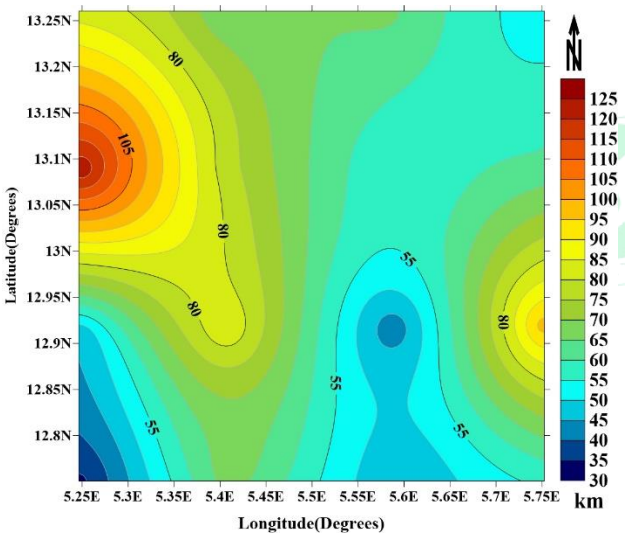


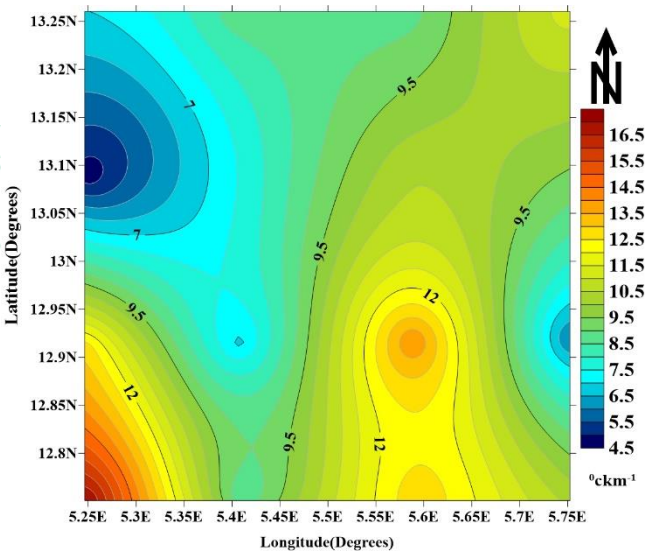

Figure 2: Radial power spectrum plot for spectral depth estimation in the Sokoto Basin

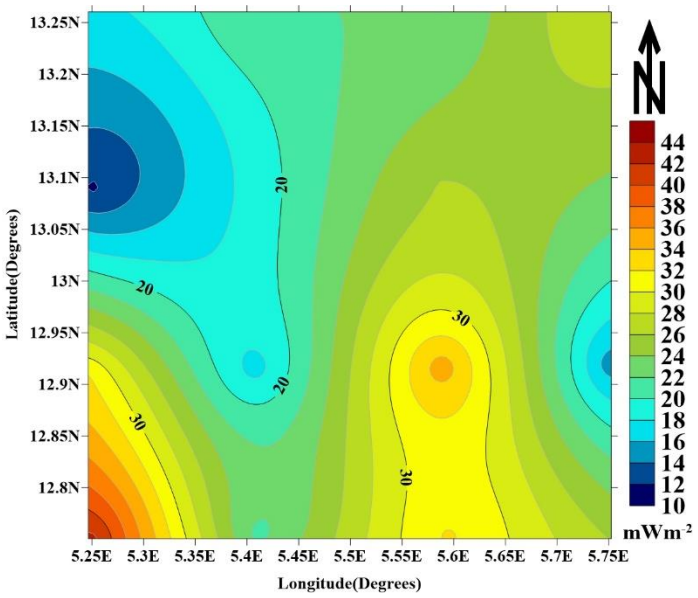

Latitude(Degrees)
Longitude(Degrees)
km


Latitude(Degtrees)
Longitude(Degrees)
km


Latitude(Degrees)
Longitude(Degrees)
km

(c)


Latitude(Degrees)
Longitude(Degrees)
°ckm⁻¹




**(e)**

Figure 3**:** Spatial distribution maps of geothermal parameters within the Sokoto Basin: (a) Depth to Top ($Z_t$), (b) Depth to Centroid ($Z_o$), (c) Curie Point Depth (Zp), (d) Geothermal Gradient, and (e) Surface Heat Flow Map

The geothermal gradient derived from Curie point depth shows an inverse relationship with Zb, as expected from thermal theory (Eq. 3 and 4). Zones with shallow Curie depths exhibit elevated geothermal gradients, reaching relatively high values compared to the basin average. Higher geothermal gradients are predominantly concentrated in structurally complex zones where basement faults and lineaments intersect (fig. 1). These zones SS, SW, Central regions likely represent areas of enhanced heat transfer due to increased crustal permeability and localized mantle heat upwelling [8]. Conversely, regions with deeper Curie depths show lower geothermal gradients, indicating thermally stable and less prospective geothermal conditions. This spatial variation confirms the non-uniform thermal regime of the Sokoto Basin.

Surface heat flow values computed from geothermal gradients reveal significant spatial variability across the basin. Elevated heat flow zones correspond closely with areas of shallow Curie point depth and high geothermal gradient. Estimated heat flow values indicate that parts of the Sokoto Basin fall within moderate to high geothermal heat flow regimes, suggesting potential for geothermal energy exploitation. These anomalous zones are primarily located in the central, south-south and southwestern sections of the basin.

## 4. Conclusion

The research covering part of Sokoto Basin has successfully revealed areas with prospects for geothermal energy resource potential. Regions with high geothermal gradient (14.5 $°Ckm-1$ to 20 $°Ckm-1$) and high heat flow (36 $mWm^{-2}$ to 50 $mWm^{-2}$) have high prospects for geothermal energy. If these areas are exploited can serve as an alternative source of energy that will reduce the effects of global warming posed by fossil fuel and other non-renewable energy resources.

## References

[1] S. Brown, L. R. William, G. Chen, F. Michael, F. James, M. "Bayesian neural networks for geothermal resource assessment: Prediction with uncertainty," *arXiv preprint arXiv:2209.15543*, 2022.

[2] N. G. Obaje, *Petroleum Geology for Geoscientists*, Xlibris/XULON Press, 2015.

[3] M. Yakubu, K. M. Lawal, B. B. M. Dewu, and I. E. Awajiokan, "Determination of heat flow and temperature variations for geothermal energy assessment over Sokoto Basin, Nigeria, using aeromagnetic and aero-radiometric data," *Journal of Applied Geophysics*, vol. 7, pp. 1217–1232, 2022.

[4] M. Telford, L. Geldart, and R. Sheriff, *Applied Geophysics*, 2nd ed., Cambridge University Press, 1990.

[5] B. Blakely, *Potential Theory in Gravity and Magnetic Applications*, Cambridge University Press, 1995.

[6] A. Salem, K. Ushijima, and T. H. Saibi, "Curie point depth estimation and heat flow analysis using aeromagnetic data," *Journal of Geophysical Research*, vol. 115, 2010.

[7] U. Z. Magawata, N. K. Olasunkanmi and T. A Issa. "Geothermal parameter estimation using centroid spectral method in sedimentary basins," *Journal of African Earth Sciences*, vol. 152, pp. 110–125, 2024. https://flayoophl.com/journals/index.php/rans

[8] S. Taufiq, F. N. Okeke, D. N. Obiora and J. C. Ibuot. "Assessment of geothermal potential of Sokoto Basin using aero-radiometric data," *Mediterranean Earth Sciences*, vol. 7, no. 1, 2021. DOI:10.1007/s40808-020-01013-3

# HEALTH RISK ASSESSMENT AND MOSQUITO REPELLENT FORMULATION FROM *TRIUMFETTA RHOMBOIDEA*: SENSORY EVALUATION AND GC-MS ANALYSIS

**Abdullahi Sahal[1*], Opeyemi John[1], Fatima Idris Adam[1], Abdulazeez Abubakar Umar[1], Ishaq Shehu[1], Umar Sa'ad[1]**

*[1]Department of Chemistry/Biochemistry, School of Applied Science, Nuhu Bamalli Polytechnic, Zaria, Nigeria*
**Corresponding Author: abuhanifa25@gmail.com*

**Abstract**

*Triumfetta rhomboidea* (Burback) is a tropical plant traditionally used as a mosquito repellent. However, its safety concerning potentially toxic elements and its formulation into standardized products have not been adequately studied. This study assessed the health risks associated with potentially toxic elements (Pb, Cd, Cr, Ni, Fe) in *T. rhomboidea* and formulated a mosquito repellent cream from its oil, followed by sensory evaluation and GC-MS analysis. Samples (extracted oil, dried plant material, and a commercial repellent) were digested and analyzed for toxic elements using Atomic Absorption Spectrophotometry. Health risk was evaluated via Estimated Daily Intake (EDI), Hazard Quotient (HQ), and Hazard Index (HI). Oil was extracted by Soxhlet extraction (ethanol) and incorporated into creams at 10%, 30%, and 50% concentrations. Sensory evaluation was conducted using a 9-point hedonic scale, and the oil was analyzed by GC-MS. All metal concentrations were within WHO permissible limits. HI values were 0.00187 (extracted oil), 0.16372 (dried sample), and 0.20376 (commercial repellent), all <1, indicating no significant non-carcinogenic risk. GC-MS revealed oleic acid as the major component (peak area up to 16.54%), with minor terpenoids such as p-menth-3-en-9-ol. Sensory evaluation showed that the 10% formulation had the highest overall acceptability (8.8 ± 0.63). *T. rhomboidea* is relatively safe regarding toxic elements, and its oil can be formulated into an acceptable mosquito repellent cream, though higher concentrations reduce sensory appeal.

**Keywords:** *Triumfetta rhomboidea*; mosquito repellent; health risk assessment; heavy metals; GC-MS;

## 1. Introduction

Mosquito-borne diseases such as malaria, dengue fever, and yellow fever remain major public health challenges, especially in sub-Saharan Africa. Nigeria bears a substantial burden of malaria, contributing significantly to morbidity and mortality [1]. Personal protection using mosquito repellents is a key prevention strategy. Synthetic repellents like DEET are effective but have been associated with skin irritation, allergic reactions, and potential neurotoxicity [2], [3]. Additionally, they persist in the environment and may affect non-target organisms [4]. Consequently, there is growing interest in plant-based repellents, which are biodegradable, affordable, and culturally acceptable [5]. *Triumfetta rhomboidea* (family Malvaceae) is a tropical shrub used traditionally in Africa for wound healing, skin infections, and as an insect repellent [6], [7]. However, plants grown in contaminated environments can accumulate potentially toxic elements (PTEs) such as lead (Pb), cadmium (Cd), chromium (Cr), nickel (Ni), and iron (Fe), which pose health risks to users [8]. This study therefore assesses the health risk of PTEs in the plant and develops a mosquito repellent cream from its oil, evaluating its chemical composition (GC-MS) and consumer acceptability.

## 2. Materials and Methods

### Sample Collection and Preparation

Fresh leaves of *Triumfetta rhomboidea* were collected from Nuhu Bamalli Polytechnic, Zaria, Nigeria, and authenticated. The plant material was divided into two portions: one for oil extraction (fresh leaves) and

one for heavy metal analysis (dried, ground). A commercial mosquito repellent was purchased for comparison.

**Oil Extraction**

Fresh chopped leaves (200 g) were extracted by Soxhlet apparatus using 2.5 L n hexan for 6–8 h. The solvent was evapourated in a water bath, and the crude oil was stored.

**Health Risk Assessment**

**Digestion and Metal Analysis**

Samples (extracted oil, dried plant, commercial repellent) were digested using wet acid digestion (7.5 mL conc. $HNO_3$ + 2.5 mL HCl). Metals (Cd, Cr, Fe, Ni, Pb) were determined using an Atomic Absorption Spectrophotometer (AAS) following APHA (2017) methods.

**Estimated Daily Intake (EDI)**

$$EDI = \frac{Conc\ metals\ x\ IR}{BW}$$

Where C = metal concentration (mg/kg), IR = intake rate (0.01 kg/day), BW = average body weight (60 kg).

**Hazard Quotient (HQ) and Hazard Index (HI)**

$$HQ = \frac{EDI}{RfD}$$

RfD refers to reference dose (mg/kg/day) : Cd 0.001, Cr 0.003, Fe 0.70, Ni 0.02, Pb 0.0035 mg/kg/day). HI = ΣHQ. HI < 1 indicates no significant non-carcinogenic risk (USEPA, 2011).

**Formulation of Mosquito Repellent Creams**

Three creams were prepared with oil concentrations: F1 (10%), F2 (30%), F3 (50%). The cream base contained emulsifying wax, liquid paraffin, glycerol, distilled water, and methyl paraben. Oil and aqueous phases were heated separately to 70 °C, mixed with stirring, and then plant oil and preservative were added.

**Sensory Evaluation**

Ten volunteer panelists assessed colour, odour, texture, spreadability, skin feel, absorption, and overall acceptability using a 9-point hedonic scale (1 = dislike extremely, 9 = like extremely). Results expressed as mean ± SD.

**Data Analysis**

Descriptive statistics were used for sensory scores; health risk indices were calculated according to USEPA formulas.

**3. Results**

**Health Risk Assessment**

**Table 1: Instrumental concentration of potentially toxic elements (ppm)**

| Element | Sample A (extracted oil) | Sample B (dried plant) | Sample C (commercial) |
|---|---|---|---|
| Cd | ND | 0.055± 0.003 | 0.009± 0.0005 |
| Cr | 0.023± 0.001 | 0.081± 0.004 | 0.350± 0.018 |
| Fe | 1.081± 0.054 | 5.622± 0.281 | 8.442± 0.422 |
| Ni | ND | 0.028± 0.001 | ND |

| Element | Sample A (extracted oil) | Sample B (dried plant) | Sample C (commercial) |
|---|---|---|---|
| Pb | 0.007± 0.0004 | 3.118± 0.156 | 3.797± 0.190 |

ND = not detected

**Table 2: Estimated Daily Intake (EDI, mg/kg/day)**

| Sample | Cd | Cr | Fe | Ni | Pb |
|---|---|---|---|---|---|
| A | ND | $3.83 \times 10^{-6}$ | $1.80 \times 10^{-4}$ | ND | $1.17 \times 10^{-6}$ |
| B | $9.17 \times 10^{-6}$ | $1.35 \times 10^{-5}$ | $9.37 \times 10^{-4}$ | $4.67 \times 10^{-6}$ | $5.20 \times 10^{-4}$ |
| C | $1.50 \times 10^{-6}$ | $5.83 \times 10^{-5}$ | $1.41 \times 10^{-3}$ | ND | $6.33 \times 10^{-4}$ |

**Table 3: Hazard Quotient and Hazard Index**

| Sample | Cd | Cr | HQ Fe H | Ni | Pb | HI |
|---|---|---|---|---|---|---|
| **A** | 0.00 | 0.00128 | 0.00026 | 0.00 | 0.00033 | 0.00187 |
| **B** | 0.00917 | 0.00450 | 0.00134 | 0.00023 | 0.14848 | 0.16372 |
| **C** | 0.00150 | 0.01944 | 0.00201 | 0.00 | 0.18081 | 0.20376 |

All HI values $< 1 \rightarrow$ no significant non-carcinogenic risk.

**Table 4: Selected compounds from GC-MS of *T. rhomboidea* oil**

| RT (min) | Compound | Peak area (%) | Quality (%) |
|---|---|---|---|
| 22.189 | p-Menth-3-en-9-ol | 16.54 | 38 |
| 25.777 | Oleic acid | 11.51 | 93 |
| 25.816 | Oleic acid | 2.22 | 93 |
| 25.893 | Cis-vaccenic acid | 4.69 | 45 |
| 26.008 | Oleic acid | 6.96 | 87 |
| 26.141 | Oleic acid | 4.99 | 83 |
| 26.217 | 9-Octadecenoic acid | 5.06 | 70 |
| 30.495 | Phenylephrine | 0.41 | 38 |

Oleic acid was the predominant component. Trace terpenoids (p-menth-3-en-9-ol) were present but with lower match quality.

**Table 5: Physical Characteristics of Formulated Creams**

| Formulation | Colour | Odour | Texture | Appearance |
|---|---|---|---|---|
| F1 (10%) | Creamy white | Mild herbal | Smooth | Homogeneous |
| F2 (30%) | Greenish cream | Moderate herbal | Slightly thick | Homogeneous |
| F3 (50%) | Greenish cream | Very strong | Watery | Homogeneous |

**Table 6: Sensory Evaluation (Sensory scores)**

| Parameter | F1 (10%) | F2 (30%) | F3 (50%) |
|---|---|---|---|
| Colour | 9.0 ± 0.00 | 7.6 ± 1.17 | 2.2 ± 1.23 |
| Odour | 9.0 ± 0.00 | 3.0 ± 1.20 | 5.9 ± 1.97 |
| Texture | 9.0 ± 0.00 | 8.6 ± 0.97 | 8.7 ± 0.67 |
| Spreadability | 8.6 ± 0.84 | 5.9 ± 2.51 | 8.5 ± 0.85 |
| Skin feel | 8.5 ± 1.60 | 8.0 ± 1.49 | 8.1 ± 1.45 |
| Absorption | 8.1 ± 1.52 | 5.2 ± 1.62 | 7.6 ± 0.97 |

| Parameter | F1 (10%) | F2 (30%) | F3 (50%) |
|---|---|---|---|
| Overall acceptability | 8.8 ± 0.63 | 5.6 ± 1.89 | 6.3 ± 2.45 |

F1 (10% oil) had the highest overall acceptability (8.8 ± 0.63), while higher oil concentrations reduced colour and odour acceptability.

**4. Discussion**

**Health Risk Assessment**

The concentrations of potentially toxic elements (Cd, Cr, Fe, Ni, and Pb) in the extracted oil (Sample A), dried plant material (Sample B), and commercial sample (Sample C) revealed notable variations in elemental accumulation and transfer during processing. The results indicate that the extracted oil generally contained lower concentrations of toxic metals than the dried plant and commercial samples, suggesting that the extraction process reduced the transfer of certain metallic contaminants into the oil fraction. The concentrations of Cd, Cr, Fe, Ni, and Pb in the extracted oil, dried plant, and commercial repellent were all below WHO permissible limits. The HI values for all samples were <1 (maximum 0.20376 for commercial repellent), indicating no significant non-carcinogenic risk. Lead contributed the highest HQ values in samples B and C, yet remained below the threshold. These findings suggest that *T. rhomboidea* used as a mosquito repellent is relatively safe regarding elemental contamination, consistent with reports that plants from non-industrial areas often have low metal burdens [11]. The extracted oil (Sample A) had the lowest HI (0.00187), making it the safest of the three.

**GC-MS and Chemical Composition**

The dominance of oleic acid (a monounsaturated fatty acid) in the oil is notable. While oleic acid is not a classical volatile repellent, it serves as a good emollient and may enhance skin retention of active compounds. The presence of p-menth-3-en-9-ol (a terpenoid) is promising because terpenoids are known to interfere with mosquito olfactory receptors [4]. The low match quality (38%) suggests that other terpenoids may be present below detection thresholds or that extraction parameters need optimization for volatile compound recovery. The absence of highly volatile repellents like citronellal or eucalyptol may be due to loss during solvent evapouration.

**Formulation and Sensory Evaluation**

All formulations were homogeneous and stable. The 10% formulation (F1) was rated highest for colour, odour, texture, spreadability, skin feel, absorption, and overall acceptability. Higher oil concentrations (30%, 50%) produced darker green colour and stronger herbal odour, which reduced consumer appeal despite acceptable functional properties (texture, skin feel). This trade-off between efficacy (often higher at higher concentrations) and sensory acceptability is well documented for plant-based topical products [12]. The lower SD values for F1 indicate good panelist agreement, while higher SD for F2 and F3 reflect mixed individual preferences.

**5. Conclusion**

This study demonstrates that *Triumfetta rhomboidea* used as a mosquito repellent contains low levels of potentially toxic elements (Pb, Cd, Cr, Ni, Fe) and poses no significant non-carcinogenic health risk (HI < 1). The extracted oil is rich in oleic acid and contains minor terpenoids that may contribute to repellent activity. A 10% oil-in-cream formulation (F1) was the most sensorially acceptable and stable. Future work should combine efficacy testing with formulation optimization to develop a marketable, safe, and affordable natural mosquito repellent.

**References**

[1] World Health Organization, "World malaria report 2023," WHO, Geneva, Switzerland, 2023.

[2] A. Singhamahapatra, L. Sahoo, and S. Sahoo, "Mosquito repellent: a novel approach for human protection," in *Molecular Identification of Mosquito Vectors and Their Management*, Singapore: Springer, 2021, pp. 149–178.

[3] T. M. Katz, J. H. Miller, and A. A. Hebert, "Insect repellents: Historical perspectives and new developments," *Journal of the American Academy of Dermatology*, vol. 58, no. 5, pp. 865–871, 2008.

[4] M. B. Isman, "Botanical insecticides, deterrents and repellents," *Annual Review of Entomology*, vol. 51, pp. 45–66, 2006.

[5] A. L. Souto, M. Sylvestre, E. D. Tölke, J. F. Tavares, J. M. Barbosa-Filho, and G. Cebrián-Torrejón, "Plant-derived pesticides as an alternative to pest management and sustainable agricultural production: Prospects, applications and challenges," *Molecules*, vol. 26, no. 16, art. no. 4835, 2021.

[6] A. Sofowora, *Medicinal Plants and Traditional Medicine in Africa*, 3rd ed. Ibadan, Nigeria: Spectrum Books, 2008.
[7] H. M. Burkill, *The Useful Plants of West Tropical Africa*, vol. 2, 2nd ed. Kew, UK: Royal Botanic Gardens, 2004.

[8] M. Jaishankar, T. Tseten, N. Anbalagan, B. B. Mathew, and K. N. Beeregowda, "Toxicity, mechanism and health effects of some heavy metals," *Interdisciplinary Toxicology*, vol. 7, no. 2, pp. 60–72, 2014.

[9] APHA, *Standard Methods for the Examination of Water and Wastewater*, 23rd ed. Washington, DC, USA: American Public Health Association, 2017.

[10] USEPA, "Risk assessment guidance for superfund," United States Environmental Protection Agency, Washington, DC, USA, 2011.

[11] B. J. Alloway, *Heavy Metals in Soils*, 3rd ed. Dordrecht, Netherlands: Springer, 2013.

[12] H. T. Lawless and H. Heymann, *Sensory Evaluation of Food: Principles and Practices*, 2nd ed. New York, NY, USA: Springer, 2010.

# SYNTHESIS AND CHARCTERIZATION OF (2E)-1-(4-BROMOPHENYL)-3-(4-NITROPHENYL)PROP-2-EN-1-ONE CHALCONE

**Aliyu Ahmad Aliyu[1*], AbdulRazaq Tukur[2], Haruna Aliyu Agum[3]Muhammad Ali Uthman[4] and Ummusalma Muhammad Salisu[5]**

*[1]Department of Pure and Industrial Chemistry, Bayero University, Kano*
*[2]Department of Chemistry, Al-Qalam University, Katsina*
*[3]Department of Pure and Industrial Chemistry, Bayero University, Kano*
*[4]Department Industrial Pharmacy and Pharmaceutical Technology, University of Jos*
*[5]Department of Pure and Industrial Chemistry, Bayero University, Kano*
**Corresponding Author: aleeuahmerd@gmail.com*

**Abstract**

Chalcones (benzylidene acetophenones) are important intermediates in organic synthesis with notable pharmaceutical potential due to their simple structure and ease of preparation. In this study, (2E)-3-(4-bromophenyl)-1-(4-nitrophenyl)prop-2-en-1-one was synthesized via Claisen–Schmidt condensation of 4-bromoacetophenone and 4-nitrobenzaldehyde using 10% NaOH in ethanol. The product was recrystallized from n-hexane to obtain a yellow crystalline solid (58% yield; m.p. 58 °C). Thin layer chromatography showed a single spot (Rf = 0.52), confirming purity. The compound was soluble in n-hexane, ethyl acetate, and ethanol but insoluble in water. UV analysis gave a λmax at 306 nm, while FT-IR confirmed key functional groups, including α,β-unsaturated C=O (1674 $cm^{-1}$), C=C, C–Br, C–H, C–N, and N–O. GC–MS analysis further confirmed the molecular weight, purity, and fragmentation pattern. A single dominant peak at ~18.2 min indicated high purity, while the molecular ion peak at m/z 318/320 with a characteristic 1:1 isotopic pattern verified the presence of bromine. Antimicrobial studies showed moderate activity. Overall, the results confirm successful synthesis and characterization, highlighting its potential as a scaffold for drug development.

**Keywords:** Chalcone, Claisen–Schmidt condensation, Acetophenone, Benzaldehyde, GC–MS analysis

## 1. Introduction

Synthesis and biological activities of chalcones have attracted significant attention in recent years. Chalcones are important constituents of natural sources (1) and were first isolated from Chinese liquorice (*Glycyrrhizae inflata*) (2). Structurally, chalcones possess a 1,3-diaryl-2-propen-1-one framework, which serves as the main pharmacophore.

Chalcones are a major class of flavonoids widely distributed in the plant kingdom (3) (4). They act as open-chain precursors in the biosynthesis of flavonoids and exist mainly as polyphenolic compounds (5). Structurally, chalcones occur in trans (E) and cis (Z) isomeric forms, with the E-isomer being more stable (6). The conjugated α,β-unsaturated carbonyl system enables π-electron delocalization, making chalcones valuable intermediates for synthesizing biologically active heterocycles (7).

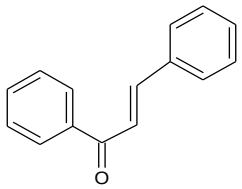



Fig :1: Structure of Chalcone

Chalcones are naturally abundant in edible and medicinal plants (8) (9) (10) (11). Their formation is mediated by chalcone synthase, producing compounds such as naringenin chalcone (12) (13). Various synthetic methods have been reported, including Claisen–Schmidt condensation, which remains the most widely used due to its simplicity and efficiency (14)(15)(16)(17).

Chalcones exhibit a broad spectrum of biological activities, including antioxidant, antibacterial, antifungal, antiviral, anti-inflammatory, anticancer, and antidiabetic properties (18). Their activity is largely attributed to the reactive α,β-unsaturated keto group. Despite existing antimicrobial agents, antibiotic resistance remains a serious global challenge, necessitating new therapeutic agents.

Therefore, this study aims to synthesize and characterize chalcone derivatives via base-catalyzed Claisen–Schmidt condensation and evaluate their physicochemical properties using chromatographic and spectroscopic techniques, contributing to the search for novel bioactive compounds.

**2. Methodology**

All reagents, including sodium hydroxide (10%), 4-nitrobenzaldehyde, 4-bromoacetophenone, ethanol, n-hexane, and distilled water, were obtained from Sigma–Aldrich and used without further purification. Standard laboratory equipment and analytical instruments (UV–Vis, FT-IR, GC–MS, melting point apparatus, and TLC plates) were employed.

Synthesis of Chalcone: A mixture of 4-nitrobenzaldehyde (1.2 g) and 4-bromoacetophenone (1.2 g) in rectified spirit (25 mL) was stirred for 30 min. Sodium hydroxide solution (10 mL, 10%) was added dropwise, and the reaction was maintained at 20–25 °C with continuous stirring for 4–5 h. Reaction progress was monitored by TLC. The mixture was refrigerated overnight to yield a precipitate, which was filtered, dried, and recrystallized from n-hexane.

Characterization: TLC was performed on silica gel plates and visualized under UV light. Melting point was determined using an SM-P10 apparatus. UV–Vis (200–400 nm), FT-IR (KBr disc), and GC–MS analyses were carried out using standard procedures.

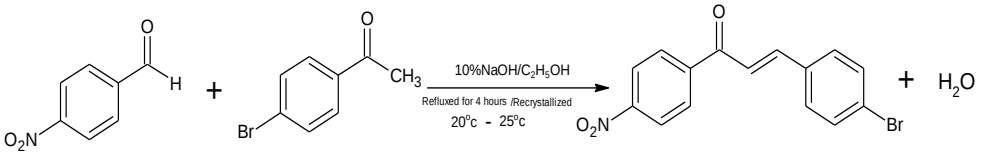
Antibacterial Activity: Antimicrobial activity was evaluated using the agar well diffusion method. Samples (25–100 µg/mL) were tested against microbial cultures, with ciprofloxacin and fluconazole as standards. Zones of inhibition were measured after incubation.

**3. Results and Discussion**

(2E)-1-(4-bromophenyl)-3-(4-nitrophenyl)prop-2-en-1-one chalcone was obtained as a yellow solid with a percentage yield of 58%. The melting point of the synthesized compound was found to be 58 °C. The compound exhibited an Rf value of 0.52 using n-hexane and ethyl acetate (3:7 v/v) solvent system, indicating good purity.

The FTIR spectrum showed characteristic absorption peaks ($cm^{-1}$) at 2921 (C–H stretching), 1674 (C=O stretching of α,β-unsaturated ketone), 1625 (C=C stretching), 1499 (aromatic C=C stretching), 1242 (C–N stretching), 1309 (N–O symmetric stretching), and 750 (C–Br stretching), confirming the presence of the expected functional groups. These values are consistent with reported literature for chalcone derivatives (19)(20)(21).

The UV–visible spectrum of the compound showed a maximum absorption (λmax) at 306 nm, which is characteristic of chalcone chromophores and corresponds to π⟶π* electronic transitions. This falls within the expected range for chalcone derivatives, where band I typically appears between 340–390 nm with minor absorption around 300–320 nm (22).




Scheme 1. Synthesis of Chalcones

Thin layer chromatography analysis revealed a single spot under UV light (254 nm and 366 nm), confirming the purity of the synthesized compound with no detectable impurities.

The synthesized chalcone was found to be soluble in n-hexane, ethyl acetate, and ethanol, but insoluble in water, consistent with its non-polar aromatic structure.

**Table 1: Description of the Synthesized Compound**

| Tests | Inference |
|---|---|

| | |
|---|---|
| Color | Yellow |
| State | Solid |
| Melting point | 58 °C |
| Yield | 58% |
| Rf value | 0.52 |

**Table 2: Solubility**

| Solvent(s) | Influence |
|---|---|
| n-hexane | Soluble |
| Ethyl acetate | Soluble |
| $H_2O$ | Insoluble |
| Ethanol | Soluble |

**Table 3: FTIR Numeric Data Obtained From the Analysis of Synthesized Substituted Chalcone**

| Functional group | Wave number ($cm^{-1}$) |
|---|---|
| C=C Stretch | 1625 |
| C=O Stretch | 1674 |
| C-C Stretch | 1499 |
| C-Br Stretch | 750 |
| C-H Stretch | 2921 |
| C-N Stretch | 1242 |
| N-O Symmetric Stretch | 1309 |

**GC–MS Analysis**

The GC chromatogram revealed a single dominant peak, indicating high purity of the synthesized compound. The retention time (Rt) was observed at ~18.2 min, suggesting a relatively non-polar compound consistent with chalcone derivatives.

The mass spectrum exhibited a molecular ion peak ($M^+$) at m/z = 318/320, corresponding to the presence of bromine (Br), which shows a characteristic isotopic pattern (M and M+2 peaks in ~1:1 ratio). This confirms the incorporation of the bromophenyl moiety.

The fragmentation pattern showed major ions arising from Cleavage of the α,β-unsaturated, arbonyl system, Loss of $NO_2$ group and Benzoyl and phenyl fragment formations. These fragmentation pathways strongly support the proposed chalcone structure.

**Table 4: GC–MS Data of Synthesized Chalcone**

| Parameter | Observation | Interpretation |
|---|---|---|
| Retention Time (Rt) | 18.2 min | Indicates non-polar aromatic compound |
| Molecular Ion Peak ($M^+$) | m/z = 318/320 | Confirms molecular weight with Br isotopic pattern |
| Base Peak | m/z = 183 | Stable benzoyl fragment |
| Fragment Ion 1 | m/z = 165 | Aromatic ring cleavage |
| Fragment Ion 2 | m/z = 135 | Loss of $NO_2$ group |
| Fragment Ion 3 | m/z = 77 | Phenyl cation |
| Purity | Single major peak | High purity |

The synthesized chalcone exhibited moderate antimicrobial activity, with activity increasing with concentration. The presence of electron-withdrawing groups (Br and $NO_2$) enhances biological activity by improving interaction with microbial enzymes and cell membranes.

**Table 5: Antibacterial Activity (Zone of Inhibition in mm)**

| Organism | 25 µg/mL | 50 µg/Ml | 100 µg/mL | Standard (Ciprofloxacin) |
|---|---|---|---|---|
| *E. coli* | 8 mm | 11 mm | 15 mm | 24 mm |
| *S. aureus* | 9 mm | 13 mm | 17 mm | 26 mm |

**Table 6: Antifungal Activity (Zone of Inhibition in mm)**

| Organism | 25 µg/mL | 50 µg/mL | 100 µg/Ml | Standard (Fluconazole) |
|---|---|---|---|---|
| *C. albicans* | 7 mm | 10 mm | 14 mm | 22 mm |

**Minimum Inhibitory Concentration (MIC)**

The Minimum Inhibitory Concentration (MIC) was determined using the broth dilution method.

**Table 7: MIC Values of Synthesized Chalcone**

| Organism | MIC (µg/mL) |
|---|---|
| *E. coli* | 50 |
| *S. aureus* | 50 |
| *C. albicans* | 100 |

The compound shows better activity against Gram-positive bacteria compared to Gram-negative bacteria due to simpler cell wall structure. Moderate antifungal activity was observed, activity is attributed to α,β-unsaturated carbonyl system, electron-withdrawing substituents (Br, $NO_2$) and enhanced lipophilicity.

## 4. Conclusion

A novel chalcone, (2E)-1-(4-bromophenyl)-3-(4-nitrophenyl)prop-2-en-1-one chalcone, was synthesized via Claisen–Schmidt condensation of 4-nitrobenzaldehyde and 4-bromoacetophenone in alkaline ethanol (10% NaOH). The compound was soluble in n-hexane and ethyl acetate but insoluble in water. Structural formation proceeded through enolate nucleophilic addition to the carbonyl carbon, yielding a C–C bond. Spectroscopic characterization (UV–Vis and FT-IR) confirmed the structure, with key FT-IR absorptions at 1674 $cm^{-1}$ (α,β-unsaturated C=O), 750 $cm^{-1}$ (C–Br), and 1625 $cm^{-1}$ (aromatic C=C). The melting point was 58 °C. GC–MS analysis supported the molecular structure via fragmentation patterns. Antimicrobial evaluation showed moderate activity, indicating potential as a lead compound for drug development.

## References

[1] M. Shailendra *et al.*, "Synthesis and characterization of some chalcone derivatives," vol. 2, no. 1, pp. 52–56, 2017.

[2] K. R. Yerra, S. Fang, and Y. M. Tzeng, "Synthesis of 2-oxygenated chalcones," *Bioorg. Med. Chem.*, vol. 12, pp. 2679–2686, 2004.

[3] L. Ni, C. Q. Meng, and J. A. Sikorski, "Recent advances in therapeutic chalcones," *Expert Opin. Ther. Pat.*, vol. 14, pp. 1669–1691, 2004.

[4] N. K. Sahu *et al.*, "Exploring pharmacological significance of chalcone scaffold: A review," *Curr. Med. Chem.*, vol. 19, pp. 209–225, 2012

[5] E. Wong, "The role of chalcones and flavanones in flavonoid biosynthesis," *Phytochemistry*, vol. 7, pp. 1751–1758, 1968.

[6] A. B. Evranos and R. Ertan, "Chemical and structural properties of chalcones I," *FABAD J. Pharm. Sci.*, vol. 36, pp. 223–242, 2011.

[7] Koo, "Journal of Pharmaceutical Science," *J. Pharm. Sci.*, vol. 26, pp. 41–85, 1961.

[8] C. Lei *et al.*, "Macdentichalcone, a unique polycyclic dimeric chalcone from *Macaranga denticulata*," *Tetrahedron Lett.*, vol. 57, no. 49, pp. 54–75, 2016.

[9] A. W. Salae *et al.*, "Antiplasmodial dimeric chalcone derivatives from the roots of *Uvaria siamensis*," *Phytochemistry*, vol. 135, pp. 135–143, 2017.

[10] P. Morales *et al.*, "2',3,4-trihydroxychalcone, phloretin and calomelanone from *Stevia lucida*," *Biochem. Syst. Ecol.*, vol. 77, pp. 57–60, 2018.

[11] R. Wen *et al.*, "Anti-inflammatory flavone and chalcone derivatives from the roots of *Pongamia pinnata*," *Phytochemistry*, vol. 149, pp. 56–63, 2018.

[12] U. Koca *et al.*, "Decreasing unpalatable flavonoid components in citrus: The effect of transformation construct," *Physiol. Plant.*, vol. 137, pp. 101–114, 2009.

[13] J. L. Ferrer *et al.*, "Structure of chalcone synthase and the molecular basis of plant polyketide biosynthesis," *Nat. Struct. Biol.*, vol. 6, pp. 775–784, 1999.

[14] D. N. Dhar, *Chemistry of Chalcones and Related Compounds*. New York, NY, USA: Wiley, 1981.

[15] S. Eddarir, N. Cotelle, Y. Bakkour, and C. Rolando, "Tetrahedron Letters," *Tetrahedron Lett.*, vol. 44, pp. 53–59, 2003.

[16] G. Romanelli *et al.*, "Journal of Molecular Catalysis A: Chemical," *J. Mol. Catal. A Chem.*, vol. 340, pp. 24–, 2011.

[17] S. N. A. Bukhari, M. Jasamai, and I. Jantan, "Synthesis and biological evaluation of chalcone derivatives (mini review)," *Mini Rev. Med. Chem.*, vol. 12, pp. 1394–1403, 2012.

[18] B. B. Chavan *et al.*, "Synthesis and medicinal significance of chalcones – A review," *Asian J. Biomed. Pharm. Sci.*, vol. 6, no. 56, pp. 1–7, 2016.

[19] N. Harmastuti *et al.*, "Synthesis and cytotoxic activity of chalcone derivatives on human breast cancer cell lines," *Indones. J. Chem.*, vol. 12, pp. 261–267, 2012.

[20] B. M. Sahoo *et al.*, "Green expedient synthesis of pyrimidine derivatives via chalcones and evaluation of their anthelmintic activity," *Indian J. Pharm. Educ. Res.*, vol. 51, no. 4S, pp. S700–S706, 2017.

[21] S. A. Hasan, A. N. Elias, and M. S. Farhan, "Synthesis, characterization and antimicrobial evaluation of a series of chalcone derivatives," *Der Pharma Chemica*, vol. 7, no. 2, pp. 39–42, 2015.

[22] P. Kumar *et al.*, "Optical and structural properties of chalcone NLO single crystals," *J. Mol. Struct.*, vol. 1005, pp. 1–7, 2011.

# MODIFIED SYNTHESIS AND CHARACTERIZATION OF GRAPHENE OXIDE

**Sha'aban Sallau[1*], Muhammad Babati[1], Abbas Abubakar[2]**, Joy Yohana Ishaya[1] , **Babagana Shuaibu[3]**

[1]*Department of Chemistry, Faculty of Science, Air Force Institute of Technology, Kaduna, Nigeria.*
[2]*Department of Chemical and Biomolecular Engineering, Tulane University, USA.*
[3]*School of Water, Energy and Environment (SWEE), Cranfield University, UK.*
**Corresponding Author: sallaushaaban@gmail.com*

**Abstract**

Graphene is a two-dimensional monolayer of carbon, one atom thick, known for its exceptional thermal, mechanical, electronic, and optical properties. In this study, graphene oxide (GO) was successfully produced using the modified Hummer method. The GO was characterized with FT-IR spectroscopy and SEM imaging. FT-IR analysis identified C=O stretching vibrations at 1732 $cm^{-1}$ and C=C stretching vibrations at 1620 $cm^{-1}$, confirming the successful synthesis of GO. SEM images showed GO's characteristic two-dimensional sheet structure. These results provide valuable insights into the structural features of graphene oxide produced via the modified Hummers method.

**Keywords:** Nanomaterials, hybridization, graphene oxide, 2-D materials

## 1. Introduction

Graphene is an extraordinary single-layer form of graphite composed of $SP^2$ hybridized carbon atoms arranged in a distinctive honeycomb pattern. It exhibits high electrical conductivity, excellent thermal stability, and exceptional mechanical strength, making it particularly suitable for a range of electronic applications [1-5]. The name "graphene" was attributed to this two-dimensional $SP^2$-carbon sheet because of its expansive honeycomb structure, which constitutes the fundamental unit of other significant allotropes [6]. These outstanding properties of graphene are vital at the nanoscale and need to be utilized for larger-scale applications. To comprehensively understand the advanced characteristics of a single graphene sheet, it is crucial to incorporate 2D graphene materials into 3D architectures [7]. Graphene oxide is a widely studied and promoted nanomaterial in scientific research. It features a distinctive single-layer, two-dimensional C-C $SP^2$-bonded structure and has excellent mechanical, thermal, and electrical properties [8]. Additionally, its surface contains functional groups such as epoxide, hydroxyl, and carboxylic acid [9-11, 21]. As the first discovered two-dimensional material [12,13], graphene shows outstanding electrical, thermal, and mechanical properties [14-16]. Since its discovery, it has been utilized in areas such as biology, chemistry, medical science, and communication [17–20].

Graphene features a hexagonal structure composed of two sublattice atoms connected by σ bonds. Each carbon atoms π orbitals are partially filled on both sides of the plane [22]. When graphene undergoes oxidation, it forms graphene oxide, which is functionalized with oxygen-containing groups, thereby enhancing its hydrophilicity and facilitating dispersion in polar solvents [23]. Over the past few years, graphene has been widely studied and promoted as a nanomaterial because of its unique single-layer, two-dimensional C − C sp2-bonded structure and exceptional mechanical, thermal, and electrical properties [25 - 27]. Furthermore, graphene's high specific surface area enables it to serve as an efficient acceptor for nanoparticles [28], and engineered graphene-based two-dimensional carbon nanostructures function as catalyst nanoparticles [29]. During the COVID-19 pandemic, graphene oxide served as an air-filtering material in face masks [30]. Graphite, a material used extensively throughout history, consists of fundamental units: carbon atoms arranged in a honeycomb pattern on a single plane, known as graphene [6]. To date, numerous hybrid nanocomposites have been developed for diverse applications by combining graphene with various nanomaterials. At the same time, noble metal nanoparticles such as Ag, Pt, and Au

have attracted interest in catalysis owing to their distinctive physical and chemical properties [24]. The research focuses on synthesizing and characterizing Graphene oxide.

## 2. Material and Methods

All reagents/chemicals used in this research were of analytical grade, including graphite, $NaNO_3$, $H_2SO_4$, $H_3PO_4$, KMnO4, $H_2O_2$, and HCl.

Synthesis of Graphene Oxide (GO)

The approach from [31, 6, 32], with slight adjustments, was utilized. Graphene oxide was produced through the modified Hummers method. Specifically, 5.0 g of graphite and 2.50 g of $NaNO_3$ were mixed with 108.0 $cm^3$ of $H_2SO_4$ and 12.0 $cm^3$ of $H_3PO_4$, then stirred in an ice bath for 10 minutes. Next, 15.0 g of $KMnO_4$ was added slowly to maintain the temperature below 5 °C. The mixture was stirred for 2 hours in an ice bath, then for 60 hours at 40 °C in a water bath. The temperature was maintained at 98 °C for 60 hours with continuous water addition. Deionized water was added until the suspension volume reached 400 $cm^3$, and 15 $cm^3$ of $H_2O_2$ was then added after 5 minutes. The product was then centrifuged and washed multiple times with deionized water and 5.0 % HCl. It was finally dried at 60 °C.

Compared with the classical Hummers method, the present procedure incorporates several key modifications. First, a mixed-acid system ($H_2SO_4$ /$H_3PO_4$ ) was employed instead of concentrated $H_2SO_4$ alone, which helps to moderate the oxidation process, suppress excessive defect formation, and improve the oxidation efficiency of graphite. Second, the amount of $KMnO_4$ was carefully controlled and added gradually under strict temperature regulation (< 5 °C) to minimize violent reactions and prevent overheating.

Unlike the traditional method, which typically involves shorter oxidation durations, this modified approach used prolonged stirring at moderate (40 °C) and high (98 °C) temperatures, allowing more complete intercalation and oxidation of graphite layers. Additionally, extended water addition and controlled dilution to a fixed volume (400 $cm^3$) were applied to ensure uniform exfoliation and safe termination of the reaction. Finally, the product was thoroughly purified using repeated washing with dilute HCl (5.0 %) and deionized water, enhancing the removal of residual metal ions and acid impurities before drying. Overall, these modifications improve oxidation uniformity, structural integrity, and safety relative to the conventional Hummers method.

Analytical Techniques

The synthesized materials were characterized using various analytical techniques: Fourier Transform Infrared (FT-IR) Spectroscopy was employed to analyze the composition and chemical structure, focusing on functional groups, within the range of 4000 to 650 $cm^{-1}$. The surface morphology of the composite was analyzed with scanning electron microscopy. The samples were examined using an electron microscope operated at a specific accelerating voltage with a focused electron beam. One limitation of the study was the lack of X-ray Diffraction (XRD) analysis, due to the unavailability of sample material remaining.

## 3. Result and Discussion

The FT-IR absorption bands of graphene oxide display distinctive features. The peak at 3738 $cm^{-1}$ indicates O-H stretching, while the one at 2925 $cm^{-1}$ signifies C-H stretching vibration. The band at 1732 $cm^{-1}$ points to C=O stretching in carboxyl groups. Peaks at 1230 and 1280 $cm^{-1}$ correspond to epoxy (C-O) stretching. Around 1620 $cm^{-1}$, it shows aromatic C=C bond vibrations in graphene sheets. The

peak at 1459 $cm^{-1}$ is attributed to C-O stretching in carboxyl and epoxy groups. These findings align with the work of [9, 33-37].

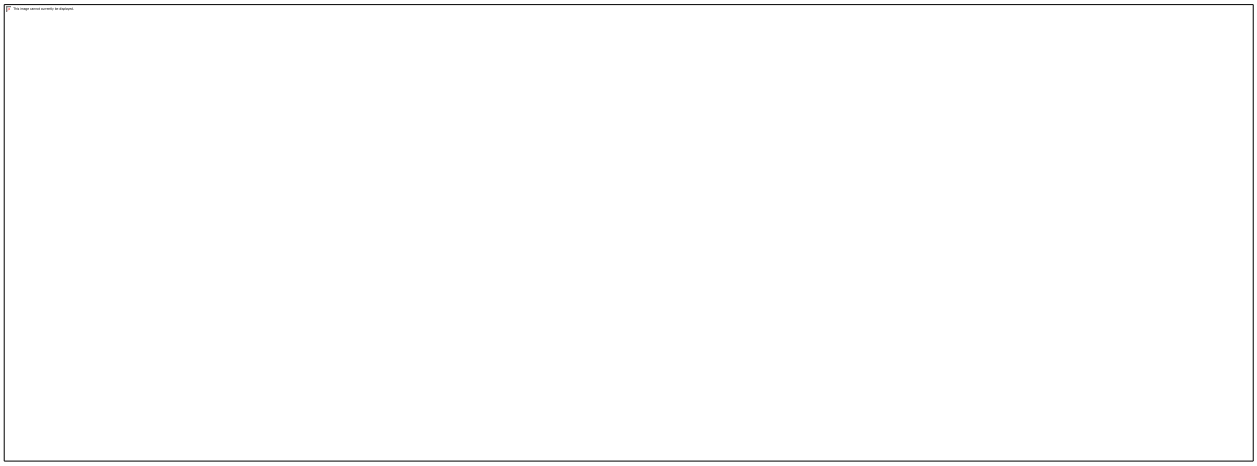


**Figure 1: FTIR Spectrum**

The SEM micrograph (Figure 2) displays GO synthesized using a modified Hummers method. Multiple layers of GO are visible, clearly indicating its two-dimensional sheet-like structure. The SEM image reveals numerous lamellar layers and allows identification of the edges of individual sheets; comparable findings have been reported [38]. Additionally, the SEM image definitively confirms GO's planar structure, as also reported by [39].



**Figure 2: SEM Image**

## 4. Conclusion

GO was successfully synthesized using the modified Hummer method. SEM analysis confirmed the formation of GO films, as evidenced by the observed microscopic morphology. Additionally, the FT-IR peaks indicating the presence of C-O bonds verified the successful preparation of GO.

## References

[1] Rasmeet, S., Sajid, U., Nikita, R., Mandeep, S., Indrajit, P., Daniel, A. D. C., Prince, J. I., Keyvan, E.S., Rahul, K. &Vijayan, V. (2022). Synthesis of Three-Dimensional Reduced-Graphene Oxide from Graphene Oxide. *Journal of Nanomaterial*, 8731429, 1-18.

[2] Novoselov, K. S., Geim, A. K., & Morozov, S. V. (2004). Electric field effect in atomically thin carbon films, *Science*, vol. 306, no. 5696, 666–669, 2004.

[3] Balandin, A., Ghosh, S., & W. Bao, W. (2008). Superior thermal conductivity of single-layer graphene, *Nano Letters*, vol. 8(3), 902–907, 2008.

[4] Lee, C., Wei, X., Kysar, J., & Hone, J. (2008). Measurement of the elastic properties and intrinsic strength of monolayer graphene, *Science*, 321(5887), 385–388, 2008.

5. Magne, T. M., de Oliveira, V. T., Alencar, L. M. R., Junior, F. F. M., Gemini-Piperni, S., Carneiro, S. V., Fechine, L. M. U. D., Freire, R. M., Golokhvast, K., Metrangolo, P., Fechine, P. B. A., & Santos-Oliveira, R. (2022). Graphene and its derivatives: understanding the main chemical and medicinal chemistry roles for biomedical applications. *Journal of Nanostructure in Chemistry*, 12(5), 693–727. https://doi.org/10.1007/s40097-021-00444-3.

6. Mbayachi, V. B., Ndayiragije, E., Sammani, T., Taj, S., Mbuta, E. R., & Khan, A.U. (2021). Graphene synthesis, characterization and its applications: *A review. Results in Chemistry*, 3, 100163. https://doi.org/10.1016/j.rechem.2021.100163.

[7] Zeng, M., Wang, W., & X. Bai, X. (2013). Preparing three-dimensional graphene architectures: review of recent developments, *Chinese Physics B*, 22 (9), 098105, 2013.

8. Akarsh, P. K., Shrinidhi, D., Marathe, S., & Bhat, A. K. (2022). Graphene oxide as nano-material in developing sustainable concrete – A brief review. *Materials Today*: *Proceedings*, 60, 234–246. https://doi.org/10.1016/j.matpr.2021.12.510.

9. Somayeh, S., & Manijeh, T. (2023). Synthesis, Characterization, and Dye Removal Applications of Graphene Oxide-Gold Nanocomposite. *Biointerface Research in Applied Chemistry*, 13(4), 385.

10. Chen, D., Feng, H., & Li, J. (2012). Graphene oxide: preparation, functionalization, and electrochemical applications. *Chemical reviews*, 112, 6027-6053, https://doi.org/10.1021/cr300115g.
11. Jian, M., Zhang, Y., & Liu, Z. (2022). Graphene fibers: Preparation, properties, and applications. *Acta Phys. Chim. Sin*. 38, 2007093, https://doi.org/10.3866/PKU.WHXB202007093.

12. Shaoqiu, J., Rongguo, S., Zelong, H., Yitong, X., Guan-Long, H., & Daping, H. (2022). Millimeter wave phased array antenna based on highly conductive graphene-assembled film for 5G applications. Carbon, 1-6.

13. Novoselov, K.S., Geim, A.K., Morozov, S.V., Jiang, D., Zhang, Y., & Dubonos, S.V. (2004). Electric field effect in atomically thin carbon films, *Science,* 306, 666–669.

14. Lee, C., Wei, X., Kysar, J.W., & Hone, J. (2008). Measurement of the elastic properties and intrinsic strength of monolayer graphene, *Science*, 321, 385–388.

[15] Du, X., Skachko, I., Barker, A., Andrei, E.Y. (2008). Approaching ballistic transport in suspended graphene, *Nat. Nanotechnol.* 3, 491–495.

[16] Balandin, A.S., Bao, W., Calizo, I., Teweldebrhan, D., Miao, F. (2008). Superior thermal conductivity of single-layer graphene, *Nano Lett*. 8 (2008), 902–907.

17. Kamalakar, M.V., Groenveld, C., Dankert, A., & Dash, S.P. (2015). Long distance spin communication in chemical vapour deposited graphene, *Nat. Commun.* 6, 1–8.
[18] Pospischil, A., Humer, M., Furchi, M.M., Bachmann, D., Guider, R., & Fromherz, T. (2013). CMOS-compatible graphene photodetector covering all optical communication bands, *Nat. Photonics* 7,892–896.

[19] Kostarelos, K., &Novoselov, K.S. (2014). Exploring the interface of graphene and biology, *Science* 344,261–263.
[20] Yao, J., Sun, Y., Yang, M., & Duan, Y. (2012). Chemistry, physics and biology of graphene-based nanomaterials: new horizons for sensing, imaging and medicine, *J. Mater.Chem.* 22, 14313–14329.

21. Mahdi, S., Soheila, K., Seyed, M. N., Fateme, H., Davood, T. (2022). An Efficient Electrochemical Biosensor Based on Pencil Graphite Electrode Mediated by 2D Functionalized Graphene Oxide to Detect HER2 Breast Cancer Biomarker. *International Journal of Electrochemical Science.* 17, 1-15.

22. Armano, A., & Agnello, S. (2019). Two-Dimensional Carbon: A Review of Synthesis Methods, and Electronic, Optical, and Vibrational Properties of Single-Layer Graphene. *Journal of Carbon Research,* 5(4), 67. https://doi.org/10.3390/c5040067.

23. Yu, W., Sisi, L., Haiyan, Y., & Jie, L. (2020). Progress in the functional modification of graphene/graphene oxide: a review. *RSC Advances*, 10(26), 15328–15345. https://doi.org/10.1039/D0RA01068E.

24. Piu, D., Bapan, B., Sanjukta, G., Raktim, G., Somasri, D., & Moni, B. (Sen) (2022). Green Synthesis of recyclable reduced graphene oxide-gold nanocatalyst using Alstonia scholaris: Applications in waste water purification and microbial field. *Research Square,* 1-13.

25. Papageorgiou, D.G., Kinloch, I.A., & Young, R.J. (2017). Mechanical properties of graphene and graphene-based nanocomposites. *Prog Mater Sci,*90:75-127. https://doi.org/10.1016/j.pmatsci.2017.07.004.

26. Phiri, J., Johansson, L.S., Gane, P., & Maloney, T. (2018). A comparative study of mechanical, thermal and electrical properties of graphene-, graphene oxide- and reduced graphene oxide-doped microfi brillated cellulose nanocomposites. *Compos B Eng,* 147, 104-113. https://doi.org/10.1016/j.compositesb.2018.04.018.

27. Liu, Y., Zheng, J., Zhang, X., Li, K., Du, Y., Yu, G., Jia, Y., & Zhang, Y. (2021). Recent advances on graphene microstructure engineering for propellant-related applications. *J Appl Polym* Sci, 1-22. https://doi.org/10.1002/app.50474.

28. Wang, K., Hui, K.N., Hui, K.S., Peng, S., & Xu, Y. (2021). Recent progress in metal–organic framework/graphene-derived materials for energy storage and conversion: design, preparation, and application. *Chem Sci*, 12, 5737-5766. https://doi.org/10.1039/D1SC00095K.

29. Wang, C., & Astruc, D. (2018). Recent developments of metallic nanoparticle-graphene nanocatalysts. *Prog Mater Sci,* 94,306-383.https://doi.org/10.1016/j.pmatsci.2018.01.003.

30. De, M., Palmieri, F., Babini, V., Augello, G., Palucci, A., Perini, I., Salustri, G., Spilman, A., De, P., Spirito, M., Sanguinetti, M., Delogu, G., Rizzi, L. G., Cesareo, G., Soon-Shiong, P., Sali, M., & Papi, M. (2021). Graphene nanoplatelet and graphene oxide functionalization of face mask materials inhibits infectivity of trapped SARS-CoV-2. *IScience,* 24(7), 102788. https://doi.org/10.1016/j.isci.2021.102788.

31. Song, J., Wang, X., & Chang, C.T. (2014). Preparation and Characterization of Graphene Oxide. *Journal of Nanomaterials*, 2014, 1–6. https://doi.org/10.1155/2014/276143.

32. Saqezi, A.S., Kermanian, M., Ramazani, A., Sadighian, S. (2022). Synthesis of Graphene Oxide/Iron Oxide/Au Nanocomposite for Quercetin Delivery. Journal of Inorganic and Organometallic Polymers and Materials, 32, 1541-1550, https://doi.org/10.1007/s10904-022-02259-3.

33. Sahoo, P., Shubhadarshinee, L., Jali, B. R., Mohapatra, P., & Barick, A. K. (2022). Synthesis and characterization of graphene oxide and graphene from coal. Materials Today: Proceedings, 56, 2421–2427. https://doi.org/10.1016/j.matpr.2021.08.206.

34. Reza, E.- K., Farkhondeh. A., Hooman, Aghamirza, M. A., Ehsan, B. N., Ali, R. A., Ali, Maleki, H. M., & Mohammad, M. (2022). Functionalized graphene oxide nanosheets with folic acid and silk fibroin as a novel nanobiocomposite for biomedical applications. *Scientific Research*, 12, 6205.

35. Mohammad, B. H., Lamia, V. M., Mohammad, R. R. L. K., & Amir, S. (2022). Mollifying Salt Depression on Anethum graveolens L. by the Foliar Prescription of Nano-Zn, $KNO_3$, Methanol, and Graphene Oxide. Journal of Soil Science and Plant Nutrition, X, 1-12.

36. Shahriary, L., & Athawale, A. (2014). Graphene oxide synthesized by using modifed hummers approach. *Int J Energy Environ Eng*, 2:58–63 https://www.researchgate.net/publication/303044105.

37. Abubakar, A., Mahmoud, A. A., Ajiya, D. A., Hassan, U. F., Muhammad, K. Y., Ishaq, A. M., Abubakar, H. Sallau, S., Usman, A., Lawal, A. I. (2023). Synthesis of Biodiesel from *Jatropha curcas* Seed Oil Using $CaTiO_3$ Catalyst and Optimization of Process Parameters to Improve the Biodiesel Conversation. *Journal of Chemistry Letters,* 3,189- 196.

38. Zhang, E., Yang, M., Zhou, Y., Ke, X., Tang, J., Guo, J., & Li, Z. (2023). Silicon-oxy-carbide intercalated three-dimensional graphene hybrid membrane for all-solid-state supercapacitors. *Applied Surface Science*, 646, 158915. https://doi.org/10.1016/j.apsusc.2023.158915.

39. Marso, T.M.M., Kalpage, C.S., & Udugala-Ganehenege, M.Y. (2017). Metal-modified graphene oxide composite catalyst for the production of biodiesel via pre-esterification of Calophyllum inophyllum oil. *Fuel*, 199, 47-64.

# GREEN SYNTHESIS OF GRASSHOPPER CHITOSAN USING WOOD ASH AQUEOUS EXTRACT AS AN ECO-FRIENDLY ALTERNATIVE MEDIUM FOR ALKALINE DEACETYLATION OF CHITIN

**Bashir, U. G.[1*], Sani, M. G.[2],Umar A.[3], Auwal A.S.[4] , Zaharddeen N.[5] and Bawa A.A.[5]**

*[1]Science Department Jigawa State College of Remedial and Advanced Studies (JICORAS), Babura.*
*[2]Department of Pure and Industrial Chemistry, College of Natural and Pharmaceutical Sciences, Bayero University, Kano.*
*[3]Chemistry Department Sule Lamido University, Kafin Hausa. Jigawa State.*
*[4]Chemistry Department Ahmadu Bello University Zaria.*
*[5]Science Department Kano state College of Education And Preliminary Studies.*
**Corresponding Author:bashirgumel69@gmail.com*

**Abstract**

The importance of chitosan has grown significantly over the last years due to its medicinal, agricultural, and industrial applications. Conventional production of chitosan from crustaceans employs harsh chemicals, prompting the search for greener alternatives. The present study aimed to describe for the preparation of chitosan from chitin using wood ash aqueous extract as an alkaline medium. This study reports the extraction of chitin from the exoskeletons of short-horned grasshopper (*Schistocerca gregaria*, Orthoptera: Acrididae) and its conversion to chitosan using wood ash aqueous extract (pH =12.4) as a sustainable alkaline medium. The yield of the obtained chitosan was found to be 11.5%. The degree of acetylation was found to be 83.2%. The solubility of the sample in 1% acetic acid was found to be 77.8%. The SEM analysis of the sample showed an amorphous morphology comparable to commercial samples. FTIR characterization confirmed the deacetylation through reduced amide bands and emergence of amino group signals of the absorption bands at 3456 and 1636 $cm^{-1}$. This eco-friendly protocol valorizes abundant agricultural pest biomass and reduces reliance on concentrated NaOH, aligning with circular economy principles. The resulting chitosan shows promise for agricultural and environmental applications.

**Keywords**: chitosan, green synthesis, *Schistocerca gregaria*, wood ash, chitin deacetylation

## 1. Introduction

Chitin is considered the second most abundant biopolymer found in nature after cellulose. This biopolymer has been produced by an enormous number of living organisms and is found in the exoskeleton shells of crustaceans and arthropods or the cell walls of fungi and yeast. Chitosan usually refers to a group of polymers that are obtained after deacetylation of chitin[1], by changing the number of degrees of deacetylation, which reflects the balance between the two types (Figure 1) and differentiates chitin from chitosan.

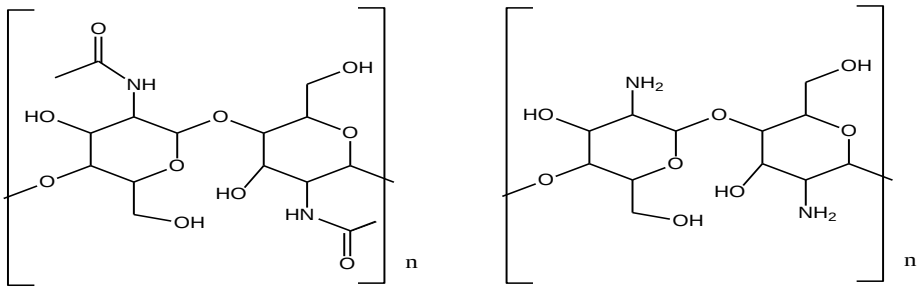



Fig. 1 (a) Chitin (b) Chitason

Figure1. Structures of (a) Chitin (b). Chitosan

The extraction of chitin from crude materials requires the removal of two significant constituents: proteins by deproteinization and inorganic mineral (calcium carbonate) by demineralization, along with small amounts of pigments and lipids that are in general eliminated during these two steps and or decolouration process, [2]**.** Both deproteinization and demineralization steps could be carried out utilizing chemical and enzymatic or biological treatments. The order of the two steps mentioned above might be reversed with some advantages, particularly when enzymatic or biological treatment is used[3]. Microbial fermentations are also employed, in this situation, the deproteinization and demineralization steps are achieved at the same time. The extraction by chemical treatments has numerous disadvantages to the environment [4]

The improvement of green extraction techniques based on the concept of "Green Chemistry" is gaining more attention, favoring the use of enzymes and microorganisms for chitosan extraction. The biological or enzymatic extraction of chitin and chitosan offers high reproducibility in a short period, simple to control, smaller solvent consumption, and low energy input. However, this method is yet restricted to laboratory-scale researches. In the biological process, chitin extraction requires the utilization of proteases. Crude proteases are mainly derived from bacteria and fish viscera. In several of the major fish-producing countries, these by-products might represent about 45% of the seafood harvest. These materials are to a great extend underutilized and disposed as waste, consequently harming the environment.

Hence, the utilization of these crude enzymes in chitin extraction could be interesting in decreasing the cost of the processes.

Alternative methods to obtain chitosan from chitin without utilization of environmentally unsafe reagents, for example, the highly concentrated sodium hydroxide have been investigated. However, in spite of the numerous investigations on the issue, it is still far from being solved.

This study aimed extraction of chitin and use it to prepare chitosan from the exoskeletons of short-horned grasshopper using an eco-friendly method. The study will report the greener method of chitin deacetylation using a strongly basic aqueous extract prepared from wood ash as an alternative to strong sodium hydroxide solution, in an eco-friendly, low-cost, and innovative method by applying "Green Chemistry" approach.

## 2. Materials and Methods

The exoskeletons of the grasshopper were procured from Maigatari International Market, Jigawa state. 500g of the insect was size reduced, washed in running tap water and rinsed with distilled water. The pasty mass was oven dried at 50C for 24h. The dried mass was then milled into a fine powder, stored in a cool and dried place.

The sweet potatoes (0.5 Kg), fish (source of fish viscera, 1.0 Kg); vinegar (as the source of acetic acid, 1.0 L), and sugar (100 g) were purchased from local vendors at Kabuga, Cooperative fish market and Galadima Market Kano. The wood ash (1.0 Kg) was obtained from the local households.

### Extraction of Chitin by Biological Method

150 g of dried and milled exoskeletons of the grasshopper were mixed with an aqueous extract of sweet potatoes, (0.5 Kg of pilled and milled were extracted with 0.5 L of water) in a 5L mud pot, and then 100 g of fish viscera was added. The mixture was left at room temperature for 48 h for fermentation (aerobic at daytime and anaerobic at night time), with occasional stirring. During this period, the pH of the reaction mixture was kept under control (3.5 to 4.2) [5]. After fermentation, 50 g of sugar was added to complete the deproteinization and demineralization processes. The whole process is recommended to be done in a

well-ventilated laboratory due to the strong odour. 48 h later, the demineralized and deproteinazed chitin was washed with a running tap water and rinsed with distilled water and dried for 2 h at 50°C in a hot air oven to obtain 34.1 g of a sample.

**Chitosan Preparation Using an Aqueous Extract of Wood Ash**

An aqueous wood ash extract was prepared by dissolving 200g of the ash in 800mL of water by boiling for 1 hour and allowed to cool overnight and filtered. The pH of filtrate was measured (pH=12.4). 200 ml of the wood ash solution was added to 20 g of prepared chitin in a 1L Conical flask and shake in an incubator shaker operating at 40 rpm for 4hrs at 30°C[5,6]. The reaction mixture was then cooled to room temperature and filtered. The extract was washed and dried in a hot air oven for 2h at 50°C to obtain (19.1g) of chitosan. The obtained chitosan was purified by dissolving in 500 mL of 5% vinegar and heated at 120°C for 2 h with periodic stirring. Then, the mixture was cooled at room temperature and precipitated by adding 660 mL of vinegar. The precipitate was filtered and dried in an oven at 50°C for 4 h. The pure chitosan (16.5 g) was obtained as a white amorphous solid.

Wood Ash Alkalinity (Simplified): $K_2CO_3 + H_2O \rightleftharpoons 2KOH + CO_2$ (partial hydrolysis).

**Physicochemical and characterization of extracted chitosan:**

**Yield of chitosan**

The chitosan yield (%) was calculated as a ratio of the dry weight of the chitosan flakes relative to the wet weight of the Crustacean's waste.

$$Chitosan\ Yeild(\%) = \frac{Extracted\ Chitosan\ (g)}{Extarcted\ Chitin\ (g)}\ x\ 100 \quad (1)$$

**Degree of Deacetylation**

The degree of deacetylation of the chitosan samples were determined from the spectral data of FTIR results

The DD% of chitosan could be calculated using the following equation (2).

$DD\%$ = 118.883 – (1.33 $X$ (A1655/A3450). (2)

Where, A1655 and A3450 are the absorbance at 1655 cm-1 of the amide-I band as a measure of the N-acetyl group content and 3450 cm-1 of the hydroxyl group band as an internal standard to correct film thickness or for differences in chitosan concentration powder form. The factor 1.33 denotes the value of the ratio between A1655/A3450 for full N-acetylated chitosan.

It was assumed that the value of this ratio was zero for full-deacetylated chitosan and that there was a rectilinear relationship between the N-acetyl group content and the absorbance of the amide-I band.

**Solubility of Chitosan**

The chitosan samples obtained from short horned grasshopper was tested for solubility in aqueous solution of acetic acid as follows;

In a beaker, 0.2 g of sample was dissolved in 1% acetic acid (20 ml) for 30 minutes on a magnetic stirrer at 250 rpm, the solution was filtered using filter paper and the insoluble fraction was cleaned with distilled water and dried to a constant weight.

Chitosan solubility was calculated using equation (3)

Percentage solubility **= 100 –** (weight of insoluble fraction/initial weight of the sample) x 100 (3)

**4. Results and Disscussion**

**Chitosan Yield:** The yielding proportion of Chitosan obtained from the sample at various stages of extraction and other physicochemical properties are depicted in Table 1.

Table1:Physicochemcal Properties of Chitosan samples obtained from short-horned grasshopper.

| **Physicochemical properties** | **Grasshopper Chitosan** |
|---|---|
| Yield | 49.70 |
| DD | 96.80 |
| Solubility in 1% acetic Acid | 67.53 |
| SEM analysis | Amorphous |

**Demineralization and Deproteinization of Chitin**

The mass analysis showed that the exoskeletons of the grasshopper used consisted of 34.1 g (23.7%) and 33.2 g (23.2%) of dry weight chitin. Hence, insects are considered a good source of chitin (20-30%). The values obtained were in agreement with those reported by [6]. The authors reported using fish viscera as a source of enzymes for deproteinization and demineralization of chitin.

The demineralization process was achieved using lactic acid produced by bacteria derived from fish viscera, through the converting the carbohydrates present in sweet potatoes aqueous extracts as a source of carbon. The deproteinization was carried out using proteases secreted by bacteria into the fermentation medium. The lactic acid is formed from the breakdown of glucose at low pH (measured, 3 to 4) thereby reacting with calcium carbonate present in the chitin, leading to the formation of calcium lactate, which precipitates and removed by washing with water [6].

**Deacetylation of Chitin Using an Aqueous Extract of Wood Ash**

Wood ash consists mainly of inorganic minerals and organic compounds remaining in the ash due to incomplete combustion. Besides these chemicals, all the major macronutrients are also found in the ash. The significant extent of the minerals in the ash is combination of oxides, hydroxides, silicates, and carbonates of the base-forming cations [7]. A portion of the oxides and hydroxides in the ash dissolve easily in water and produce a strongly alkaline solution. From the literature, the pH of the aqueous extract of wood ash was found to be12.6 [8]. The measured pH value of the solution was found to be 12.4. This pH value is in some way very close to a pH of a solution of NaOH 50% w/v (pH 13.7) normally used for the chemical deacetylation of chitin.

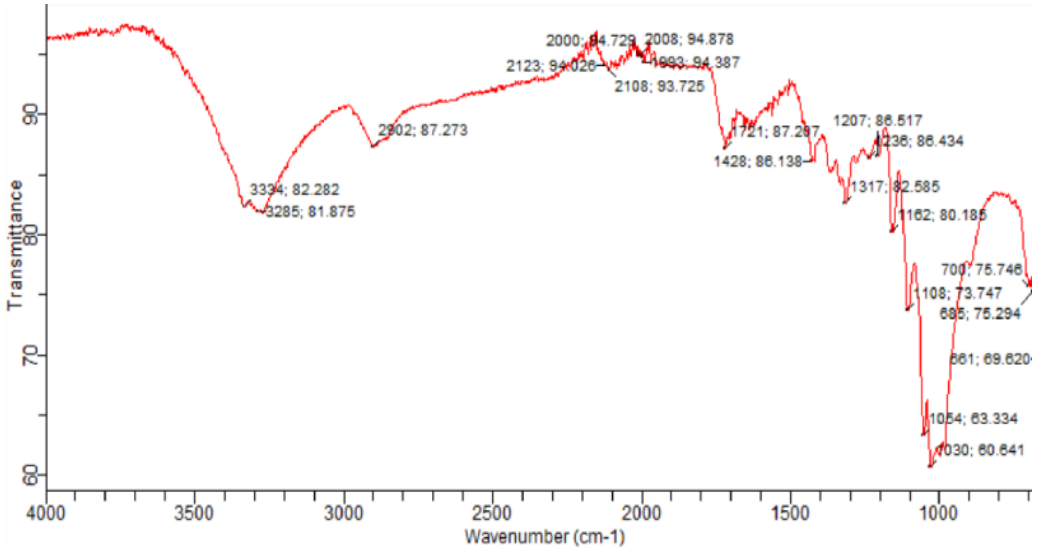
The yield of chitosan was obtained by comparing the weight of the raw material and the weighed chitosan, which was obtained after the treatment. The yield of the purified sample was 16.5 g (11.5%). The results is in conformity that reported by[6]. The authors reported yield of chitosan extracted from crab shells to be in the range of 30 – 36%. The differences in the yield could be due to the reaction time, which has a positive effect on the yield. The yield of the obtained chitosan samples could also be affected by the loss of sample mass from excessive removal of the acetyl groups from the polymer during deacetylation, i.e., the conversion of chitin to chitosan.

**Fourier Transform Infrared Spectroscopy**

FT-IR spectroscopy is a technique that is used to determine the vibrational functional groups of samples. The FT-IR spectra of the sample was examined and the results are presented in Table 2. The –OH stretching band was depicted at 3495 $cm^{-1}$, which showed the alcohol group in the chitosan . According to the literature, the vibration identified as the alcohol group (-OH band) is found between 3650-3200 $cm^{-1}$[9]. The stretching band for C-O was found at 1076 $cm^{-1}$. Also, the stretching band for NH was observed at 3440 $cm^{-1}$. As mentioned in the literature, the band identified as amine group (N-H stretching bands) absorbs infrared from 3500 to 3100 $cm^{-1}$. Moreover, the bending band of N-$H_2$ in the chitosan was 1622 $cm^{-1}$. The appearance of these bands depends on the DD.

Table 2: FTIR spectra of the extracted chitosan sample with its absorption band

| **Functional group** | **Characteristics absorption band ($cm^{-1}$)** | **Types of vibration** |
|---|---|---|
| OH alcoholic group | 3334 | Stretching |
| $NH_2$ Amino group | 3285 | Stretching |
| C-O-C, Glucosamine group | 1162 | Stretching vibration |
| $CH_2$ | 2902 | Stretching |
| C-O,NH | 1428 | Stretching vibration |
| CH | 13 | Stretching in the ring |
| C=O | 1721 | Stretching vibration |




**F**igure 2; FTIR spectra of the Chitosan sample

**Determination of Degree of Deacetylation (DD)**

The DD influences the physical, chemical, and biological properties of chitosan, such as acid-base characteristics, biodegradability, self-aggregation, as well as the ability to chelate metal ions. In addition, the DD determines the content of free anime groups in the polysaccharide that can be used to differentiate chitin and chitosan.

**Scanning Electron Microscopic Analysis**

Figure 3 shows the SEM photographs examined at 50 X magnification of chitosan prepared from the exoskeleton of short-horned grasshopper. The sample exhibited amorphous morphological structure. Since sample for further purified, it is reasonable to state that the purity of chitosan could affect the changes in its morphological structure. Crystalline and amorphous structures of chitosan have been reported,[10]

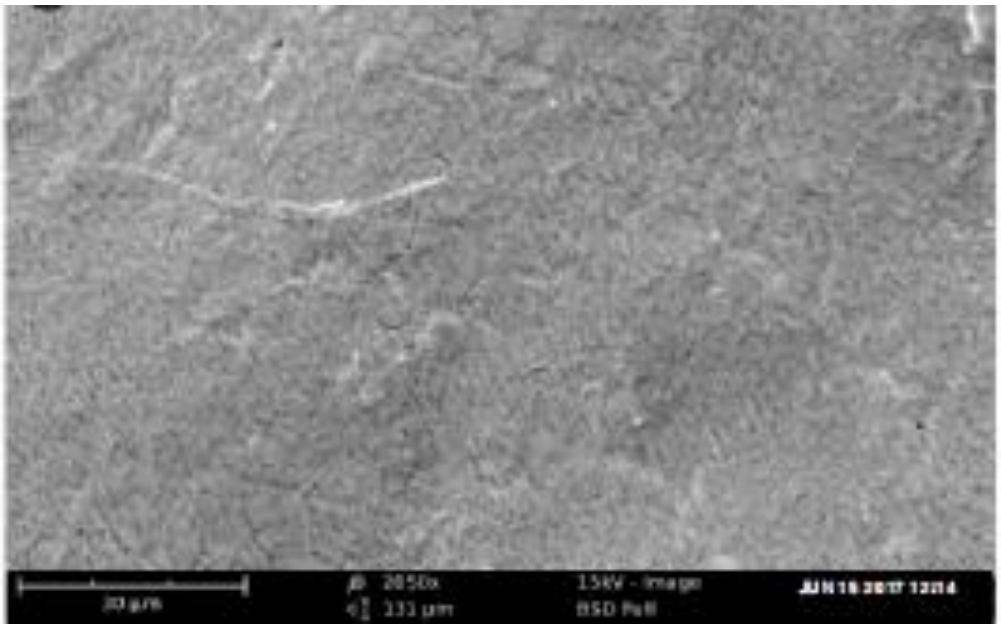


Figure 3: Micrograph of extracted grasshopper chitosan

**4. Conclusion**

Crab shells waste produced by the seafood industry is one of the important problems contributing to significant environmental and health hazards. Biopolymers like chitin and chitosan are important due to their biological and physiological properties. These properties offer many potential applications in various fields like environmental protection, agriculture, medicine, pharmaceutics, and biotechnology. The current study demonstrated an effective method for the extraction of high purity chitosan from the exoskeletons of short-horned grasshopper. The produced chitosan samples had low viscosity, low molecular weight, and high DD.

**References**

*1.* A. Ewais., A. Abdel Ghany., R.A Sabir.,Mahmoud Sitohy, (2023). Fully deacetylated Chitosan from Shrinp and Crab using minimum Heat imput. *Egyptian Journal of Chemistry. Vol.66. No. 2 pp;231-237.*

*2.* H. AudiaTriani Olii, A. Najib,(2024). The Effect Of Temperature Variations On The Deacetylation Process Of Chitosan Characteristics From Mud Crab (Scylla Serrata) Shell Waste. *Universal Journal of Pharmaceutical Research 2024; 9(4): 28-31.*

*3.* V.Ilakkiya,. B. Dhanalakshmi and V. Kaviya,(2021). Comparative Study on the Extraction, Physico Chemical Properties and Antibacterial activity of Chitosan from different crustacean shell wastes. *International Journal of Creative Research Thoughts. Volume 9, Issue 4. Pp:4682-4691.*

*4.* M. sathiyabama, R.V.Boojima.,S. Muthukumar, M. Ghandi, S. Salma., T. Kokila Prinsha and B. Rengasamy,(2024).Green Synthesis of Chitosan nanoparticles Using tea extract and its antimicrobial activity against economically important phytopathogens of Rice. *Scientific Reports. (2024)14:7381. www.nature.com/scientificreports.*

5. *S.Abirami., D.Nagaraja.,V.Antony,. S.Mini A.varsini.,Sugashi A.,Daniel Alex anand.* (2021). Production of chitosan from crab shells using an aqueous extract of wood ash. *American Journal of Polymer Science and Technology, 7(2), 29–37. https://doi.org/10.11648/j.ajpst.20210702.12.*

6. B. U. Gumel,. S. M. Gumel,. A. A. Bawa., and A. S. Auwal. (2019). Experimental Assessments of Chitosan Foliar Applications on growth and Yield Attributes of Sesame. 16th Annual Technical Conference and AGM of Polymer Institute of Nigeria Ibadan (2019. *Proceedings of the 30th Annual Technical Conference/AGM "IBADAN" – 2019 of Polymer Institute of Nigeria (PIN) 23rd – 26th October 2019.*

*7.* Mostafa et al.,(2019). Current trends in fungal biosynthesis of chitin and chitosan. *Bulletin of the National Research Centre (2019) 43:59. https://doi.org/10.1186/s42269-019-0105-y*

*8.* S.M. Gumel., B.U.Gumel and A.A. Bawa. (2017). Comparative study... short-horned grasshopper. *Bayero Journal of Pure and Applied Sciences.*

*9.* Z. Mei., et al. (2024). Update on chitin and chitosan from insects. Biomimetics. *(Recent review).*

*10.* K. Murat ., L.Evaldas Radvile N., S.Idris .,A.Gulsin ., M.Abas ., B.Talat ., Esran C. and B.Betal. (2015). Differentiations of chitin content and surface morphologies of chitins extracted from male and female grasshopper species. *PLOS ONE, 10(1), Article e0115531. https://doi.org/10.1371/journal.pone.0115531*